

# **MULTIPLE LIGHT SCATTERING** **Tables, Formulas, and Applications**

**Volume 2**

***H. C. VAN DE HULST***

*Astronomical Observatory  
University of Leiden  
Leiden, The Netherlands*



1980

**ACADEMIC PRESS**

A Subsidiary of Harcourt Brace Jovanovich, Publishers

**New York London Toronto Sydney San Francisco**

COPYRIGHT © 1980, BY ACADEMIC PRESS, INC.

ALL RIGHTS RESERVED.

NO PART OF THIS PUBLICATION MAY BE REPRODUCED OR TRANSMITTED IN ANY FORM OR BY ANY MEANS, ELECTRONIC OR MECHANICAL, INCLUDING PHOTOCOPY, RECORDING, OR ANY INFORMATION STORAGE AND RETRIEVAL SYSTEM, WITHOUT PERMISSION IN WRITING FROM THE PUBLISHER.

ACADEMIC PRESS, INC.

111 Fifth Avenue, New York, New York 10003

*United Kingdom Edition published by*  
ACADEMIC PRESS, INC. (LONDON) LTD.  
24/28 Oval Road, London NW1 7DX

#### Library of Congress Cataloging in Publication Data

Hulst, Hendrik Christoffel van de.

Multiple light scattering

Includes bibliographies and index.

1. Light--Scattering--Handbooks, manuals, etc.
2. Radiative transfer--Handbooks, manuals, etc.

1. Title.

QC427.6.H84 535'.4 79-26581

ISBN 0-12-710702-9 (v. 2)

PRINTED IN THE UNITED STATES OF AMERICA

80 81 82 83 9 8 7 6 5 4 3 2 1

# Contents

PREFACE	ix
CONTENTS OF VOLUME 1	xi

## Part III ANISOTROPIC SCATTERING

### 10 Phase Functions

10.1 Phase Functions in Common Use	303
10.2 Phase Functions of Air, Clouds, and Haze	310
10.3 Expansion Coefficients of Phase Function and Phase Matrix	317
References	329

### 11 Results for the Henyey–Greenstein Phase Function, Unbounded and Semi-Infinite Medium

11.1 The Unbounded Medium: Diffusion Pattern and Diffusion Length	331
11.2 The Milne Problem: Escape Function	339
11.3 The Reflection Function	339
References	344

### 12 Other Phase Functions, Semi-Infinite Atmospheres

12.1 Comments and Comparisons, Conservative Scattering	355
12.2 Comments and Comparisons, Nonconservative Scattering	364
12.3 The Spectrum of the Anisotropic Transfer Equation	376
12.4 Asymptotic Expressions for High-Order Terms	388
References	394

**13 Henyey–Greenstein Functions, Results for Finite Layers**

13.1	Reflection and Transmission	396
13.2	Fate of Incident Energy	400
13.3	Point–Direction Gain and Internal Flux	405
13.4	Convergence of the Successive Scattering Method and of the Doubling Method	406
	References	411

**14 Results for Other Phase Functions, Finite Layers**

14.1	Similarity Relations	477
14.2	Truncation Tests	481
14.3	Strictly Forward and Backward Scattering	489
	References	492

**15 Polarization and Azimuth-Dependent Terms**

15.1	The Formalism	493
15.2	Some Results	506
15.3	Successive Scattering in the Azimuth-Dependent Terms	514
15.4	Behavior of Fourier Terms for Large $m$ ; a Practice Example	523
	References	530

**16 Rayleigh Scattering**

16.1	The Phase Matrix	531
16.2	Exact Solutions	536
16.3	Some Results for a Semi-Infinite Atmosphere	539
16.4	Rayleigh Scattering in Atmospheres of Finite Depth	555
	References	567

**Part IV SAMPLE APPLICATIONS****17 Photon Optical Paths and Absorption Lines**

17.1	General Theory	573
17.2	Photon Optical Paths	577
17.3	Absorption Lines in Diffuse Reflection	592
	References	598

**18 Planets**

18.1	Integration over the Planet's Disk	599
18.2	Practical Use of the Reciprocity Principle	614
18.3	A Planet in Opposition	617
18.4	Partially Transparent Atmospheres	625
18.5	Interpretation of Planetary Absorption Spectra	634
18.6	Thermal Emission of the Planets	642
	References	646



**19 Scattered Light in the Earth's Atmosphere**

19.1	Looking at the Daylight Sky	651
19.2	The Natural Aerosols	661
19.3	Lidar Reflection from Clouds	675
19.4	Elements of the Earth Radiation Budget	682
	References	688

**20 Miscellaneous Applications**

20.1	Other Geometries	691
20.2	Layered Structures	698
20.3	Heat Transfer; Radiation Hydrodynamics	706
20.4	Light Scattering in the Oceans	707
20.5	Interstellar Scattering	713
	References	720

**INDEX****723**

## □ Preface

The play of radiation by repeated scattering in a cloud layer or any other slab of particles poses a problem that is common to atmospheric physics, astronomy, ocean optics, and branches of industrial research. Methods for solving this problem in diverse situations have been known for decades but their complexity has given the subject the reputation of being accessible only to specialists.

This book is aimed at the nonspecialist, e.g., an expert in an applied field, who needs a result from multiple scattering theory but does not wish to spend excessive time in solving it himself or searching the very extensive literature.

Numerical results form the core of these two volumes. Since users from diverse fields should be served, the tabulated quantities are named by their physical meaning, e.g., reflection function, gain, diffusion pattern, net flux, but are presented in the form of functions of a few dimensionless parameters. Most tables have five-figure accuracy in order to enable readers to use them for checking their own computer programs. The graphical illustrations have been chosen to serve as a quick orientation and also to highlight key phenomena such as asymptotic behavior.

Special cases such as the limits adopted for each quantity for conservative scattering ( $a = 1$ ), or in a semi-infinite atmosphere ( $b = \infty$ ), or at large depth ( $\tau \gg 1$ ) have been included in each tabulation. The same is true for moments and bimoments of the functions of the angles of incidence and emergence.

The formulas expressing these results show a similar ramification of special cases and asymptotic forms. For clarity and ease of access, they have been arranged, where possible, in a "Display," which is a collection of formulas in tabular form. Derivations have been kept to a minimum. They are presented in

a form emphasizing the physical content and the use of certain intermediate results. Only rarely does an intricate derivation require the use of numbered equations.

Although the author's prime intention is to present known results, new discoveries or new light shed on the meaning and use of known forms was unavoidable. The major findings have been published in scientific journals and several have come into general use. Subjects like doubling, similarity relations, reduction to  $H$  functions, and, generally, the interpretation of mathematical results in physical terms, are presented here in their proper context.

The volumes have a strict organization: Part I on general relations and Part II on isotropic scattering (Volume 1), Part III on anisotropic scattering and Part IV on applications to selected fields (Volume 2). The division of parts into chapters again follows a strictly logical scheme as the table of contents for each volume shows.

What I started as a sideline has become a major project. This would not have been possible without the help and encouragement of a great many people. Among this long list I wish to record my special gratitude to K. G. Grossman and J. W. Hovenier for their support throughout the work and to W. M. Irvine and V. V. Ivanov, whose enthusiasm helped the project gain momentum in the early years.

# **□ Contents of Volume I**

## **Part I GENERAL THEORY**

- 1 Concepts, Terms, Notation**
- 2 Exponential Integrals and Related Functions**
- 3 Reciprocity**
- 4 Methods**
- 5 Very Thick Layers with Arbitrary Anisotropic Scattering**
- 6 Results Obtained by Expanding the Phase Function  
in Legendre Polynomials**

## **Part II ISOTROPIC SCATTERING**

- 7 Isotropic Scattering; Solutions by Use  
of the Milne Operator**
- 8 Isotropic Scattering, Semi-Infinite Atmospheres**
- 9 Isotropic Scattering, Finite Slabs**

# **MULTIPLE LIGHT SCATTERING**

## **Tables, Formulas, and Applications**

**Volume 2**

## **Part III ○ ANISOTROPIC SCATTERING**

## 10 Phase Functions

### 10.1 PHASE FUNCTIONS IN COMMON USE

#### 10.1.1 Definitions

The choice of phase function is a decision of importance in any calculation on multiple scattering. Strictly, in a well defined physical problem the phase function is given, not chosen. As a historical curiosity we show in Fig. 10.1 an original illustration of the backward part of the exact scattering pattern of a medium sized sphere based on the Mie theory (Blumer, 1925). Such complicated phase functions are quite normal for large spheres. In practice they would lead to very time consuming computations or force an author to employ very approximate methods in his multiple-scattering calculation. Instead, he often prefers to adopt at once a phase function which preserves the main characteristics of the actual function, e.g., its degree of anisotropy, and yet renders the multiple-scattering computations manageable.

The errors made in replacing one phase function by another, and the characteristics to be maintained in order to minimize these errors, will be examined in Chapters 12 and 14 with the help of actual examples. This is the general *similarity problem*. It will be seen that it is often possible, without loss of practical accuracy, to replace a phase function by a simpler one. The main single-scattering characteristics undoubtedly are the albedo  $a$  and the asymmetry parameter  $g$  defined below.

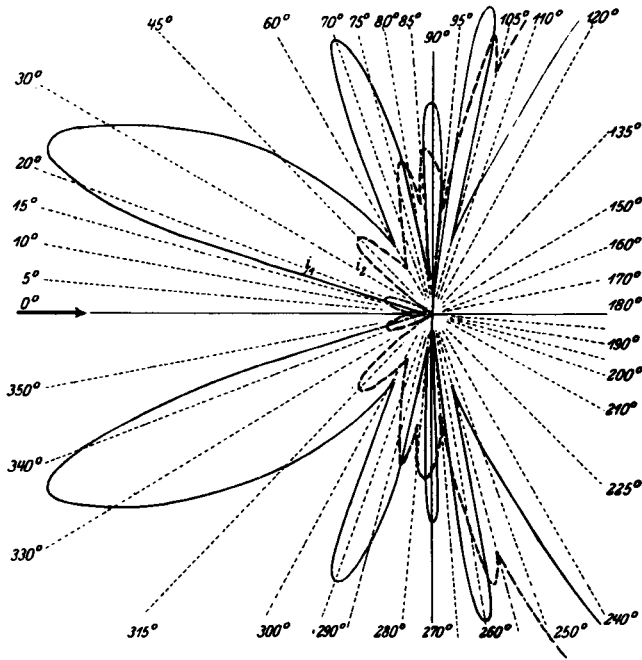


Fig. 10.1. Early diagram of the lobe pattern of radiation in two polarizations scattered into backward hemisphere from a sphere with refractive index  $m = 1.25$ , size parameter  $x = 8$  (after Blumer, 1925).

The product of the albedo and any unpolarized phase function can be expanded (Section 6.1) as:

$$a\Phi(\cos \alpha) = \omega_0 + \omega_1 P_1(\cos \alpha) + \omega_2 P_2(\cos \alpha) + \dots$$

where  $P_n(\cos \alpha)$  is a Legendre polynomial of order  $n$ . Conversely, we can obtain  $\omega_n$  from

$$\omega_n = \frac{(2n+1)a}{2} \int_{-1}^1 \Phi(\cos \alpha) P_n(\cos \alpha) d(\cos \alpha)$$

In particular,  $\omega_0 = a$ , the albedo, and  $\omega_1 = 3ag$ , so that

$$\frac{1}{2} \int_{-1}^1 \Phi(\cos \alpha) d(\cos \alpha) = 1 \quad (\text{normalization integral})$$

$$\frac{1}{2} \int_{-1}^1 \Phi(\cos \alpha) \cos \alpha d(\cos \alpha) = g \quad (\text{asymmetry parameter})$$



The fraction scattered into the forward hemisphere is

$$f = \frac{1}{2} \int_0^1 \Phi(\cos \alpha) d(\cos \alpha)$$

A collection of phase functions used in the literature as practicing examples is given in Display 10.1. All of these phase functions are normalized. The numerical examples in Display 10.1, with the exception of phase function 23 (Section 18.1.4), are limited to  $g \geq 0$  (scattering symmetric or predominantly in the forward directions). They can be changed into predominantly backward scattering functions by changing the signs of  $\cos \alpha$ ,  $g$ ,  $\omega_n$  ( $n$  odd), and by replacing  $f$  by  $1 - f$ . Display 10.1 lists  $\omega_0 - \omega_3$ , the values  $\Phi(1)$  reached at  $\alpha = 0^\circ$  (forward direction) and  $\Phi(-1)$  reached at  $\alpha = 180^\circ$  (backscatter), and any value of  $\alpha$  at which  $\Phi(\cos \alpha)$  has a zero. The final columns give asymmetry factor  $g$ , and the fraction  $f$  scattered into the forward hemisphere.

10.1.2 Phase Functions with Finite Expansions

The functions 1–15 have finite  $N$ , where  $N$  is the order of the highest Legendre function occurring in the expansion.

$N = 0$ . Isotropic scattering, requires no comment.

$N = 1$ . Many authors have used this linearly anisotropic scattering function as a practicing example. Its use is limited because even in the extreme case  $g$  becomes only  $\frac{1}{3}$ , if one wishes to avoid negative values of the phase function.

$N = 2$ . This choice permits more variation. Only one subcase, the Rayleigh phase function, has a resemblance to a physical problem. It is the correct phase function for Rayleigh scattering without the correct polarization.

10.1.3 Sets of Functions Permitting a Smooth Transition from Isotropic to Strictly Forward Scattering

In some studies it is useful to have sets of functions going all the way from isotropic to a sharply forward directed peak. The list contains the sets shown in the accompanying enumeration.

Number in Display 10.1	Character	Parameters to be varied	Functions belonging to this set
12	$N$ finite	$N$	1, 3, 11, 13, 29
14	$N$ finite	$N$	1, 3, 10, 15, 29
16	$N = \infty$	$g$	1, 17, 18, 19, 20, 29
21	$N = \infty$	$b$	1, 29
22	$N = \infty$	$\alpha_0$	1, 29
24	$N = \infty$	$g$	1, 29

# 306

**DISPLAY 10.1**  
Some Phase Functions in Common Use

Number and name	Formula $\Phi(\cos \alpha)$	Legendre coefficients				Special values			Further form parameters	
		$\omega_0$	$\omega_1$	$\omega_2$	$\omega_3$	$\Phi(1)$	$\Phi(-1)$	Zeroes ( $\alpha$ )	$g$	$f$
1. Isotropic scattering	1	1	0	0	0	1	1	none	0	0.500
2. $N = 1$ , general	$1 + \omega_1 \cos \alpha$	1	$\omega_1$	0	0	$1 + \omega_1$	$1 - \omega_1$	—	$\frac{1}{3}\omega_1$	$\frac{1}{2} + \frac{1}{4}\omega_1$
3. Extreme case of 2	$1 + \cos \alpha$	1	1	0	0	2	0	$180^\circ$	0.333	0.750
4. $N = 2$ , general	$1 + \omega_1 \cos \alpha$ $+ \omega_2(-\frac{1}{2} + \frac{3}{2} \cos^2 \alpha)$	1	$\omega_1$	$\omega_2$	0	$1 + \omega_1 + \omega_2$	$1 - \omega_1 + \omega_2$	—	$\frac{1}{3}\omega_1$	$\frac{1}{2} + \frac{1}{4}\omega_1$
5. Rayleigh phase function	$\frac{3}{2}(1 + \cos^2 \alpha)$	1	0	$\frac{1}{2}$	0	1.500	1.500	none	0	0.500
6. Another subcase of 4	see set 4	1	1	1.0490	0	3.049	1.049	none	0.333	0.750
7. $N = 2$ with a zero point	$\frac{(\cos \alpha + x)^2}{x^2 + \frac{1}{3}}$	1	$\frac{2x}{x^2 + \frac{1}{3}}$	$\frac{\frac{2}{3}}{x^2 + \frac{1}{3}}$	0	$\frac{(1+x)^2}{x^2 + \frac{1}{3}}$	$\frac{(1-x)^2}{x^2 + \frac{1}{3}}$	$\cos \alpha = -x$	$\frac{\frac{2}{3}x}{x^2 + \frac{1}{3}}$	$\frac{1}{2} + \frac{1}{4}\omega_1$
8. Case 7, $x = 0$	$3 \cos^2 \alpha$	1	0	2	0	3	3	$90^\circ$	0	0.500
9. Case 7, $x = 0.1835$	$2.725(\cos \alpha + 0.1835)^2$	1	1	1.8165	0	3.816	1.816	$101^\circ$	0.333	0.750
10. Case 7, $x = 0.5773$	$1.5(\cos \alpha + 0.5773)^2$	1	1.7320	1	0	3.732	0.268	$125^\circ$	0.577	0.933
11. Case 7, $x = 1$	$0.75(\cos \alpha + 1)^2$	1	1.5000	0.5000	0	3	0	$180^\circ$	0.500	0.875
12. Sets of power functions	$\frac{N+1}{2^N} (1 + \cos \alpha)^N$	1	$\frac{3N}{N+2}$	$\frac{5N(N-1)}{(N+2)(N+3)}$	...	$N+1$	0	$180^\circ$	$\frac{N}{N+2}$	$1 - 2^{-(N+1)}$
13. Case 12, $N = 3$	$\frac{1}{2}(1 + \cos \alpha)^3$	1	1.8	1	0.2	4	0	$180^\circ$	0.600	0.937
14. Set of functions with maximum $g$ for given $N$	not worked out	—	—	—	—	—	—	—	—	—
15. Case 14, $N = 3$	$1.638(\cos \alpha + 1) \times (\cos \alpha + 0.2899)^2$	1	2.070	1.725	0.655	5.449	0	$\begin{cases} 180^\circ \\ 107^\circ \end{cases}$	0.690	0.976

16. Henry-Greenstein functions	$\frac{1-g^2}{(1+g^2-2g\cos\alpha)^{3/2}}$	1	3g	5g <sup>2</sup>	7g <sup>3</sup>	$\frac{1+g}{(1-g)^2}$	$\frac{1-g}{(1+g)^2}$	none	g	$\frac{1+g}{2g} \left[ 1 - \frac{1-g}{(1+g^2)^{1/2}} \right]$
17. Case 16, g = 0.25	see set 16			see set 16		2.222	0.480	none	0.250	0.681
18. Case 16, g = 1/3	see set 16			see set 16		3.000	0.375	none	0.333	0.735
19. Case 16, g = 0.5	see set 16			see set 16		6.000	0.222	none	0.500	0.829
20. Case 16, g = 0.75	see set 16			see set 16		28.000	0.082	none	0.750	0.933
21. Inverse linear phase function	$k/(b-\cos\alpha)$ with $\frac{1}{k} = \frac{1}{2} \ln \frac{b+1}{b-1}$	1	3(b-k)	—	—	$\frac{k}{b-1}$	$\frac{k}{b+1}$	none	b-k	$\frac{k}{2} \ln \left( \frac{1-\frac{1}{b}}{1+\frac{1}{b}} \right)$
22. Isotropic sector	c for $\alpha < \alpha_0$ 0 for $\alpha > \alpha_0$ with $c = 2/(1-x)$ , $x = \cos \alpha_0$	1	$\frac{3}{2}(1+x)$	$\frac{5}{2}x(1+x)$	$\frac{7}{8}(5x^2-1)(1+x)$	c	0	all $\alpha > \alpha_0$	$\frac{1}{2}(1+x)$	1 for $\alpha_0 < 90^\circ$ $\frac{1}{2}c$ for $\alpha_0 > 90^\circ$
23. White sphere	$\frac{8}{3\pi}(\sin\alpha - \alpha\cos\alpha)$	1	$-\frac{4}{3}$	$\frac{1}{15}$	0	0	2.667	none	-0.444	0.167
24. Isotropic scattering combined with forward peak	$1-g+2g\delta(1-\cos\alpha)$	1	3g	5g	7g	$\infty$	1-g	none	g	$\frac{1}{2}(1+g)$
25. One-angle scattering	$2\delta(\cos\alpha - x)$ with $x = \cos \alpha_0$	1	3x	$5P_2(x)$	$7P_3(x)$	0	0	all $\alpha \neq \alpha_0$	x	1 for $\alpha_0 < 90^\circ$ 0 for $\alpha_0 > 90^\circ$
26. Case 25, with $\alpha_0 = 90^\circ$	$2\delta(\cos\alpha)$	1	0	$-\frac{5}{2}$	0	0	0	all $\alpha \neq 90^\circ$	0	undetermined
27. Combined forward and backward peaks	$(1+g)\delta(1-\cos\alpha) + (1-g)\delta(1+\cos\alpha)$	1	3g	5	7g	$\infty$	$\infty$	all $\alpha \neq 0^\circ$ or $180^\circ$	g	$\frac{1}{2}(1+g)$
28. Equal forward and backward peaks	$\delta(1-\cos\alpha) + \delta(1+\cos\alpha)$	1	0	5	0	$\infty$	$\infty$	all $\alpha \neq 0^\circ$ or $180^\circ$	0	0.500
29. Forward peak	$2\delta(1-\cos\alpha)$	1	3	5	7	$\infty$	0	all $\alpha \neq 0^\circ$	1	1

Set 12 is the simplest one with finite  $N$  and has been used, for instance, by Kaper *et al.* (1970) and Chang and Shultis (1976). The general expansion coefficient is

$$\omega_n = (2n + 1) \frac{N}{N + 2} \cdot \frac{N - 1}{N + 3} \cdot \dots \cdot \frac{N - n + 1}{N + n + 1}$$

Set 14 contains for each  $N$  the function with maximum  $g$  consistent with the condition that  $\Phi \geq 0$  in the interval  $-1 \leq \cos \alpha \leq 1$ . This set has not been used; we have not worked out the details for  $N > 3$ .

Set 16 appears in the astronomical literature in 1941 (Henye and Greenstein, 1941). It varies smoothly from isotropic ( $g = 0$ ) to a narrow forward peak ( $g = 1$ , function 29) or to a narrow backward peak,  $g = -1$ . At each  $g > 0$  the function increases uniformly from the backward direction to the forward direction. This makes the function ideal for test calculations on multiple scattering in which one wishes to examine the influence of anisotropy with a continuous one-parameter family. The function has been used by many authors. Its expansion coefficients have the very simple form

$$\omega_n = (2n + 1)g^n$$

The occasionally used inverse linear or elliptical phase function, set 21, has similar properties. It has a somewhat simpler form than set 16, but the fact that set 16 has a far simpler expression for the general Legendre coefficient  $\omega_n$  makes the Henye–Greenstein functions preferable in practice.

Set 22, the isotropic sector, has occasionally been used because it permits a simple visualization (e.g., Sobolev, 1967; Caroll, as cited in Section 12.1.2). Its properties are not very attractive, except that the exact expression for  $\omega_n$  is simple:

$$\omega_n = [P_{n-1}(x) - P_{n+1}(x)]/(1 - x), \quad x = \cos \alpha_0, \quad n \geq 1$$

#### 10.1.4 Miscellaneous and Singular Phase Functions

Number 23, the first of the remaining functions in Display 10.1, has a different origin. It appears in the literature as a plausible phase function of a large body, e.g., an entire planet, not as referring to a single atmospheric particle. But there is no reason why we should not give it the same treatment (Section 18.1.4). It should not be a bad approximation for the phase function of coarse dust (e.g., chalk dust).

Number 24 is the first example of a singular function. It is often useful to introduce a phase function of this type as a thought experiment, because it can be strictly reduced to isotropic scattering alone (Section 14.1.3).

Number 25, with 26 as a particular case, has some rather attractive properties but has very rarely been used in transfer computations.

More importance must be attached to set 27 and in particular to its symmetric version, function 28. Many (but not all) of the so-called "two-stream approximations", that have appeared extensively in literature about the approximate solution of transfer problems, can be regarded as giving the exact solutions for such a phase function. For that reason I have devoted a separate section (Section 18.3) to the exact results obtained with phase function 27 and Sections 20.2.1 and 20.2.2 to its wide, but not very accurate, use in some applications.

The  $\delta$  functions used in describing the singular functions (numbers 24–29) are the ordinary  $\delta$  functions. They are to be read in such a way that a peak at one of the ends of the integration interval  $(-1, 1)$  is assumed to fall fully within that interval, and that the integral over this peak with respect to  $d(\cos \alpha)$  is 1.

### 10.1.5 General Comments

The collection presented here offers ample opportunity to mathematical experiments and numerical comparisons. The list contains five different functions with  $g = 0$  (numbers 1, 5, 8, 26, 28). Four functions with  $g = \frac{1}{3}$  have been explicitly listed (3, 6, 9, 18), and more may be taken from sets 21, 22, 24, 25, and 27. Besides the six sets already listed, which present (by sign reversal) a smooth transition from a backward peak through isotropic scattering to a forward peak, there are two sets (numbers 25 and 27) that go from fully backward to fully forward *without* going through isotropic scattering.

In order to dispel any overly optimistic idea that  $g$  might be the only parameter which counts in choosing the phase function, we present Fig. 10.2, where the fraction  $f$  in the forward hemisphere is plotted against  $g$  for several sets of functions. This figure shows that the Henyey–Greenstein functions form a good

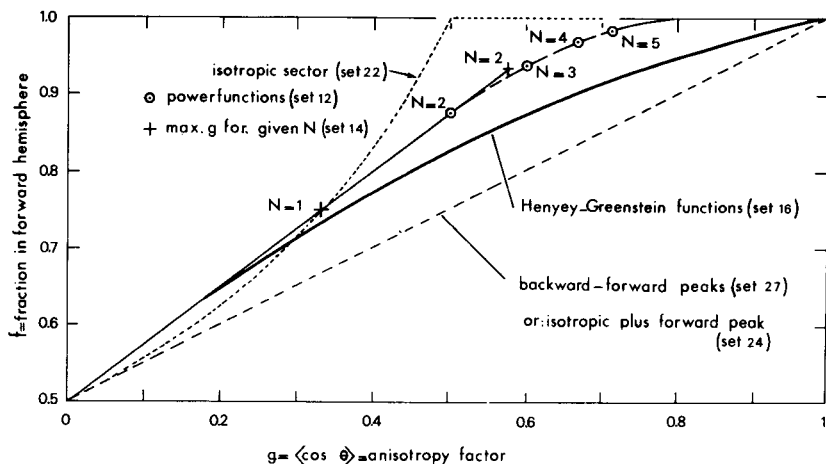


Fig. 10.2. The two rival parameters  $f$  and  $g$ , which may serve to characterize the asymmetry of commonly used phase functions, are not uniquely linked. The Henyey–Greenstein functions form an intermediate choice.

middle-of-the-road choice, and that the sets 22 and 27 deviate strongly in opposite directions. This knowledge may be useful in comparing numerical results of multiple-scattering calculations in later chapters.

In assessing whether in a particular problem the choice of a phase function with finite  $N$  or with infinite  $N$  is more appropriate, the following advantages of either choice may be considered.

In favor of finite  $N$ :

- (1) The programming is simpler *if* the method is based on such an expansion.
- (2) Many rigorous proofs have been presented only for finite  $N$ .
- (3) Examples for  $N \leq 3$  are available in the work of Chandrasekhar, Busbridge, and others (Chapters 6 and 12).

In favor of infinite  $N$ :

- (1) The choice is wider.
- (2) It contains a variety of continuous sets going all the way to the highest asymmetry,  $g = 1$ .
- (3) Detailed examples are available for several such phase functions, and very extensive results for the Henyey–Greenstein phase functions (Chapters 11 and 13).

## 10.2 PHASE FUNCTIONS OF AIR, CLOUDS, AND HAZE

It is not the purpose of this book to review in any detail the scattering properties of diffusing media encountered in nature and in the laboratory. Yet a few words may be devoted to the familiar phenomena in the earth's atmosphere, which have in so many ways served as the prototype for all multiple scattering problems.

### 10.2.1 Air

A brief summary, based on an earlier review (van de Hulst, 1949a) may suffice. Rayleigh's recognition, over a century ago, of molecular scattering as the cause of the blue daylight sky initiated a classical area of research. Typical values for the optical depth  $b$  from sea level through the entire atmosphere (reduced height  $\sim 8$  km) are 1.2 in the ultraviolet near 300 nm, 0.35 near 400 nm, 0.14 near 500 nm, and 0.035 near 700 nm.

On a typical mountain station, say at 1.8 km height, those numbers must be reduced by 20%. The astronomical experience at such a station is that on days considered clear, the excess extinction over the value for pure air ranges from some 3% in the near ultraviolet to a factor of 2 in the red.

The values of  $b$  show that at no wavelength in visible light can the atmosphere be considered as optically very thin. Hence, the distribution of light and polarization over the blue sky must contain a considerable contribution arising from multiple scattering. The challenge of this problem formed a strong motivation behind the work reported in Chandrasekhar's book (1950) and has again inspired later authors.

Many of the multiple scattering exercises for this purpose have been made with pure Rayleigh scattering, the polarization of which is 100% at  $90^\circ$ . It is common knowledge that the Rayleigh phase function (Display 10.1, No. 5) cannot serve as a substitute for true Rayleigh scattering, even if only the total intensity is sought. Section 14.2.1 gives a quantitative illustration of this point. However, even full Rayleigh scattering is unrealistic in two respects.

(a) Pure air has, as a consequence of the asymmetry of the air molecules, a certain depolarization. A beam of unpolarized light scattered by  $90^\circ$  in a horizontal plane gives a scattered beam with the intensity ratio  $I_H/I_V = \delta$  between the horizontally and vertically polarized components. If we adopt the value  $\delta = 0.031$  (van de Hulst, 1957), the degree of polarization of this scattered beam is  $(1 - \delta)/(1 + \delta) = 94.0\%$ . The full scattering process can then be correctly described, except for the effect on circular polarization, by writing the scattering matrix as 0.046 times isotropic scattering plus 0.954 times Rayleigh scattering (Section 16.1.1).

Zuev (1974) quotes  $\delta = 0.035$  from Elterman (1964) as the best value for air. However, the most careful recent studies by Bridge and Buckingham (1966), Alms *et al.* (1975), and Baas and van den Hout (1979) give, near 600 nm,  $\delta = 0.020$  for  $N_2$  and 0.058 for  $O_2$ , leading to 0.027 for dry air.

(b) Pure air does not exist, and haze scattering is virtually always predominant in the range of small scattering angles, as the white "aureole" around the sun shows.

### 10.2.2 Spheres of a Single Size

The scattering diagram of a sphere for incident light with a single wavelength is given by the Mie theory. Extensive reviews of this subject are available (van de Hulst, 1957; Deirmendjian, 1969; Kerker, 1969). The amplitudes of the scattered light in two planes of polarization according to this theory are series of functions related to the Legendre functions, the coefficients of which are complicated functions of two parameters: the refractive index  $m$  and the size parameter  $x = 2\pi r/\lambda$ , where  $r$  is the radius and  $\lambda$  the wavelength.

As long as the wavelengths near absorption bands are avoided,  $m$  varies only slowly with  $\lambda$ , so that a (downward) variation in  $\lambda$  has about the same effect on the scattering patterns as an (upward) variation in  $r$ , since both variations increase  $x$ . Most of the lobes in the scattering patterns shift rapidly with changing

$x$  so that, in fact, the pattern integrated over a range of sizes and/or wavelengths is much smoother. Hence it is not advisable to go from the Mie formulas directly into multiple scattering theory.

With the smoothing of the lobes, the wild fluctuations in polarization (see, e.g., Fig. 10.1) also are smoothed, and a moderate degree of polarization remains. An exception is formed in the rainbow and glory angles, where the remaining polarization is strong.

For many purposes it suffices to take the total intensity pattern (i.e., the intensities in the two polarizations summed at each scattering angle) and to develop this function in the usual manner (Sections 6.1. and 10.1) in a series of Legendre functions

$$a\Phi(\cos \alpha) = \sum_{n=0}^{\infty} \omega_n P_n(\cos \alpha)$$

In any case the most important quantities remain albedo  $a = \omega_0$  and asymmetry factor  $g = \omega_1/3\omega_0 = \langle \cos \alpha \rangle$ .

Much information about the values of  $g$  following from the rigorous Mie theory has been compiled in Fig. 10.3. The data were taken from some 5 or 6 different figures presented by Irvine (1963, 1965) and check well with the results given by Hansen and Travis (1974). The following details may be noted.

*Nonabsorbing spheres* are characterized by a real refractive index  $m = n$ . The data are presented in three size ranges, in each of which  $x = 2\pi r/\lambda$  and  $\rho = 2x(n - 1) = 4\pi r(n - 1)/\lambda$ . The physical significance of  $\rho$  is the phase shift of a ray passing through the sphere along a diameter with respect to a ray traveling the same distance in vacuum.

It is well known that the main maximum in the curve of the extinction efficiency  $Q_{\text{ext}}$  against  $\rho$  or  $x$  occurs near  $\rho = 4.0$  because the waves passing through the sphere then have the correct phase to reinforce the diffraction peak arising from the incomplete wavefront passing along the sphere. As expected, this reinforced peak shows up also as a maximum in the  $g$  values. Figure 10.3a shows the rise towards this maximum on an expanded  $\rho$  scale. Some  $x$  values are shown for convenience. Figure 10.3b shows that also the first minimum (near  $\rho = 8$ ) and the next maximum (near  $\rho = 11$ ) are well visible in the  $g(\rho)$  plots. Again some values of  $x$  have been written in for convenience. The fine ripple, which is particularly striking in the exact curves for  $m = 1.33$  and  $1.50$  has been smoothed out in these graphs. It arises from an interference effect with a wave traveling along the surface of the sphere and has no practical consequences.

Figure 10.3c sketches the approach to the limiting value for very large spheres ( $x = \infty$ ). Here we have drawn  $g$  for water drops ( $m = 1.33$ ), the bars indicating the approximate amplitude from minimum to maximum in the main wiggle. The bars for  $x = 20$  and  $25$  correspond to the wiggles shown in the central graph; those for  $x = 50$  and  $x = 100$  were read from sample figures in Irvine's paper. The limiting value for  $x = \infty$ , read by van de Hulst (1957) from a graph computed by Debye (in 1909!), was  $g = 0.87$ , in good agreement with the newly computed values  $g = 0.884$  (Irvine, 1963).



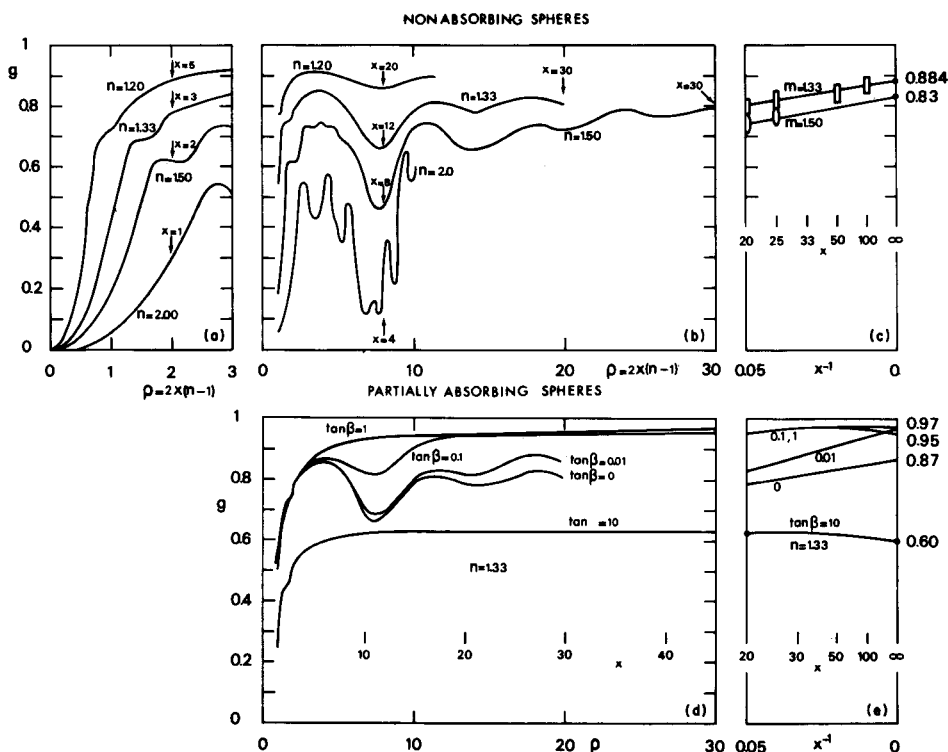


Fig. 10.3. Condensed information about the asymmetry factor  $g$  obtained from the Mie theory for (a)–(c), nonabsorbing spheres of any size and (d), (e), absorbing spheres. Consult text for further explanation.

The appearance that the average  $g$  increases as  $x^{-1}$ , and that the amplitude of the wiggles remains constant is probably misleading. The exact theory of the interference of the diffracted wave with the grazingly reflected waves is well understood and leads to terms proportional to  $x^{-2/3}$ , but for practical purposes the straight line drawn in Fig. 10.3 should suffice. A similar graph is given for  $m = 1.50$  (glass beads).

It should be noted that all data in Fig. 10.3 include the diffraction peak as part of the scattering pattern, even for large spheres, for in the exact Mie theory these parts are inseparable. However, an author performing a multiple-scattering calculation certainly has the option (see Sections 13.2.2 and 15.1.2) to regard the diffraction peak as essentially nonscattered light and accordingly, to exclude it from the scattering pattern. The consequence is that the extinction cross section, and hence the optical depth of the layer, must be halved, and that  $g$  must be replaced by  $g' = 2g - 1$ . For large water drops,  $g' = 0.77$ .

Since  $gQ_{\text{sca}}$  is proportional to the forward carried momentum in the scattered light, the radiation pressure exerted on the sphere (in the absence of absorption) is proportional to

$$Q_{\text{pr}} = (1 - g)Q_{\text{ext}}$$

This prompted Debye's interest in the factor  $g$ . Irvine's curves show that  $Q_{pr}$  shows less pronounced wiggles than either  $Q_{ext}$  or  $g$ .

*Absorbing spheres* are characterized by a complex refractive index

$$m = 1 + (n - 1)(1 - i \tan \beta)$$

where  $\beta$  represents a loss angle for a wave traveling through the bulk medium. The results obtained by Irvine for four values of  $\tan \beta$  and one value  $n = 1.33$  are shown in Figs. 10.3d,e. The abscissas correspond with those in the upper part, so that the curves for  $\tan \beta = 0$  are simply repeated. The effect of the absorption is to reduce the intensity of the light which passes with two refractions through the sphere. This has two consequences. First, the main maxima and minima tend to vanish, because there is a less intense refracted wave to interfere with the diffracted wave. Second, the value of  $g$  rises because the diffraction peak and the grazing reflection assume relatively more prominence. This is seen particularly well in the run of  $g$  against  $x^{-1}$  for large particles, sketched in (e). The functional dependence may be wrong in detail, but the values at  $x = \infty$  computed by Irvine (1965) and the general behavior of the curves should be correct.

When the absorption becomes so strong that  $\tan \beta \geq 1$ , the material starts to show metallic optical properties. As a consequence, the radiation which hits the sphere fullface is no longer refracted into the sphere but reflected back.

This backscatter results in a much lower value of  $g$ . In the limit of perfect reflection, corresponding to  $|m| = \infty$ , the radiation reflected from a large sphere gives an isotropic scattering pattern. Hence  $g' = 0$  (without the diffraction peak) and  $g = 0.5$  (with the diffraction peak). The curve computed by Irvine for  $\tan \beta = 10$  approaches this limit.

*Nonspherical particles* are abundant in nature: falling rain drops are elongated, many hailstones have nonconcentric cores, hexagonal ice crystals give rise to beautiful halo phenomena, and snowflakes are well known for their intricate forms.

The scattering law of nonspherical particles that are much smaller than the wavelength is governed by their polarizability tensor. The theory is well known (e.g., van de Hulst, 1957) but of little interest in this book. Particles of simple shape that are much larger than the wavelength may be treated by a combination of geometrical optics and Fraunhofer diffraction. An example is Jacobowitz' (1971) computation of the halo caused by randomly oriented ice crystals. At intermediate sizes, fancy theoretical methods and relatively simple shapes are needed to solve the problem at all. For those sizes empirical knowledge must be relied upon. This may be obtained in two ways. The most complete and reliable data have been obtained from microwave analog measurements (Greenberg *et al.*, 1961; Lind *et al.*, 1965; Zerull and Giese, 1973; Zerull and Weiss, 1977). Size distributions of nonspherical particles have been examined by Heintzenberg (1977).

A promising new method is to study scattering of a laser beam by individual particles (Blau *et al.*, 1970).

Additional references, both on the theoretical and on the experimental methods to determine light scattering and polarization from nonspherical particles may be found in the review of Coffeen and Hansen (1974).

### 10.2.3 Polydisperse Collections of Waterdrops

It is obvious that integrations over the drop size with a suitable distribution function have to be made in order to obtain a match with experimental data. Such integrations have been made for application in interstellar astronomy (e.g., van de Hulst, 1949b; Greenberg and Hanner, 1970), in planetary physics (Hansen and Travis, 1974; Coffeen and Hansen, 1974), in meteorology (Deirmendjian, 1969; Yanovitskii and Dumanskii, 1972), and in chemistry (Kerker, 1969). They may refer to extinction (i.e., turbidity), to scattered intensity, to the degree of polarization (or polarization ratio) of the scattered light, or to all of these.

Of these properties, the polarization carries the most specific information. This is illustrated in Fig. 10.4 by an example from Coffeen and Hansen (1974), where the refractive index is 1.33, the mean size parameter  $x = 2\pi a/\lambda$  is varied, and the distribution function of actual radii  $r$  is

$$N(r) = \text{const} \cdot r^{(1-3b)/b} e^{-r/(ab)}$$

with  $b = 0.05$ . Graphs of this kind are very important in interpreting the observed polarization of Venus (Section 18.1.5). Computations of this type form the only reliable basis for judging to what extent the effects of rainbow and glory

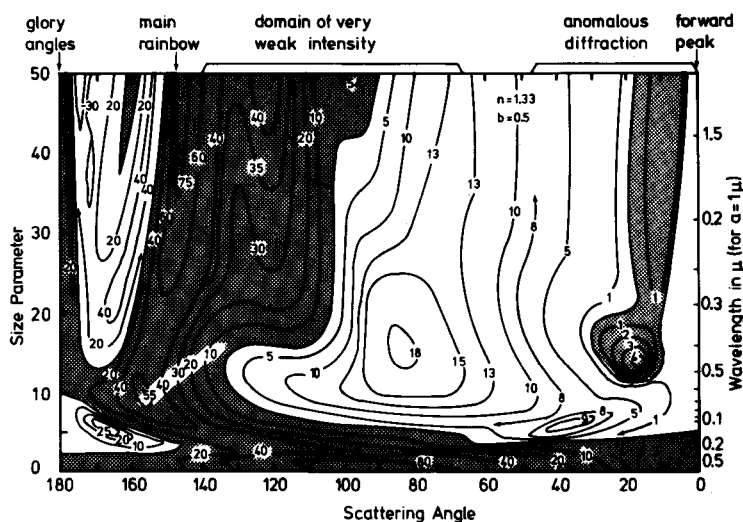


Fig. 10.4. Degree of polarization (in percent) of light scattered from a polydisperse collection of water spheres with dominant size parameter as shown (adapted from Coffeen and Hansen, 1974).

are still visible in a polydisperse cloud. The glory theory is reviewed and extended by Bryant and Jarmie (1974) and Shipley and Weinman (1978).

We now turn to the scattered intensity. A striking difference may be noticed between the treatment of these subjects in the books by Deirmendjian and by Kerker. This difference is fully justified by the different applications considered. Kerker (1969) deals at length with a variety of possible distribution laws and shows by experimental examples how the parameters describing the dominant size and the spread in sizes in the distribution can be determined from accurate measurements of the turbidity spectrum or polarization ratio on controlled samples with first-order scattering only.

Similarly precise conclusions cannot be expected for meteorological objects (clouds and haze) or for clouds on the planets or in interstellar space. In these natural objects, where the experimental conditions are less well defined, coarser parameters suffice for an adequate description. For instance, if we are told to expect waterdrops in the size range 2–10  $\mu\text{m}$  diameter, then for green light it suffices to compute

$$x = \frac{2\pi r}{\lambda} = \frac{2r}{\lambda/\pi} = \frac{(2-10) \mu\text{m}}{0.16 \mu\text{m}} = 13-63$$

From Fig. 10.3 we may then read that the value of  $g$  should be somewhere between 0.77 and 0.87, with the most probable value near 0.83. An accurate integration may improve this result by 1–2%, but observational data for which such an improvement would pay off are hard to find.

Deirmendjian (1969) presents accurately integrated data for ten selected size distributions of water drops, all represented by the same four parameter function on the interval  $(0, \infty)$  in  $r$ :

$$n(r) dr = ar^\alpha \exp(-br^\gamma) dr$$

The maximum, or mode, is reached at the mode radius  $r_c$  given by

$$\gamma r_c^\gamma = \alpha/b$$

For the three selected haze models,  $r_c$  ranges from 0.05 to 0.10  $\mu\text{m}$ . The four cloud models have  $r_c = 2$  or 4  $\mu\text{m}$ . Two rain models have  $r_c = 50$  and 70  $\mu\text{m}$ . Finally, the hailstones have  $r_c = 1000 \mu\text{m} = 1 \text{ mm}$ . Accurate refractive indices varying with the wavelength  $\lambda$  were used. The scattering patterns of these 10 model distributions for a variety of wave lengths from 0.44 to 16.6  $\mu\text{m}$  is presented for all four Stokes parameters separately in 125 tables of the same format. Unfortunately, the calculation of important derived constants, such as the factor  $g = \langle \cos \alpha \rangle$ , is left to the reader.

Yanovitskii and Dumanskii (1972) present a booklet with 110 pages of tables referring to real refractive indices  $m = 1.33$  and 1.55. Gaussian distributions in  $\log$  (particle size) were used throughout. Intensity and polarization are computed in four decimals at thirty angles; the extinction coefficient is also given.

Abundant references to computed and measured properties of the natural aerosols known as atmospheric haze, fog, and clouds of various types may be found in Chapter 6 of McCartney (1976). His review refers mostly to optical and infrared wavelengths, from 0.4 to 15  $\mu\text{m}$ . Rozenberg (1972) reviews in a similar manner the scattering and attenuation of millimeter and centimeter waves.

### 10.3 EXPANSION COEFFICIENTS OF PHASE FUNCTION AND PHASE MATRIX

#### 10.3.1 Expansion of the Phase Function

We have emphasized the importance of the asymmetry factor  $g$  with good reason. In many problems the knowledge of this factor alone suffices to obtain solutions of multiple scattering problems accurate to some 5%. However, further parameters are required for a complete description. Many authors use for this purpose the numerical values of the phase function at certain angles. This is, of course, correct, but it is likely to lead to an uneconomic computing program.

An equally feasible alternative is to compute a small number of coefficients  $\omega_1, \omega_2, \omega_3, \dots, \omega_j$  directly from the Mie theory.  $\omega_1$ , which enters into the expression for the radiation pressure exerted on a sphere, has been computed in this manner as early as 1908. The concept of similarity, and the tests performed on it in Chapters 12 and 14, lead us to think that the influence of  $\omega_1$  on the numerical results is large, that of  $\omega_2$  smaller, that of  $\omega_3$  still smaller, etc.

Although this suggestion was made early, by Hartel (1940), the follow-up in published numerical work on multiple scattering and radiative transfer has been slow. This is the more surprising since the same expansion in terms of Legendre polynomials has always been a prominent device in the corresponding theoretical work (Chapter 6). Only with the advent of the fast computers of the 1960s did this approach become practical.

Values of the coefficients  $\omega_n$  for spheres with refractive indices  $m = 1.33$  were computed by Chu and Churchill (1955) and Clark *et al.* (1957). A graph of the numbers  $\omega_n/(2n + 1)$  is reproduced in Fig. 10.5. A separate report (Chu *et al.*, 1957) gives the coefficients  $\omega_n$  for  $m = 0.9, 0.93, 1.05, 1.10, 1.15, 1.20, 1.25, 1.30, 1.33, 1.40, 1.44, 1.50, 1.60, 2.00$ , and  $\infty$ .

Table 20 gives a selection of numbers based on this report. They have been arranged in blocks of approximately equal phase shift  $|\rho|$ . For instance, all points corresponding to the maximum of the extinction curve near  $\rho = 4$  are shown together. The table shows, however, that the higher coefficients for different  $m$  agree better when  $x$  is equal than when  $\rho$  is equal.

A very similar method is described by Kattawar *et al.* (1973). Hunt (1970, 1971) prefers to find the coefficients by a least-square fit to the phase function.

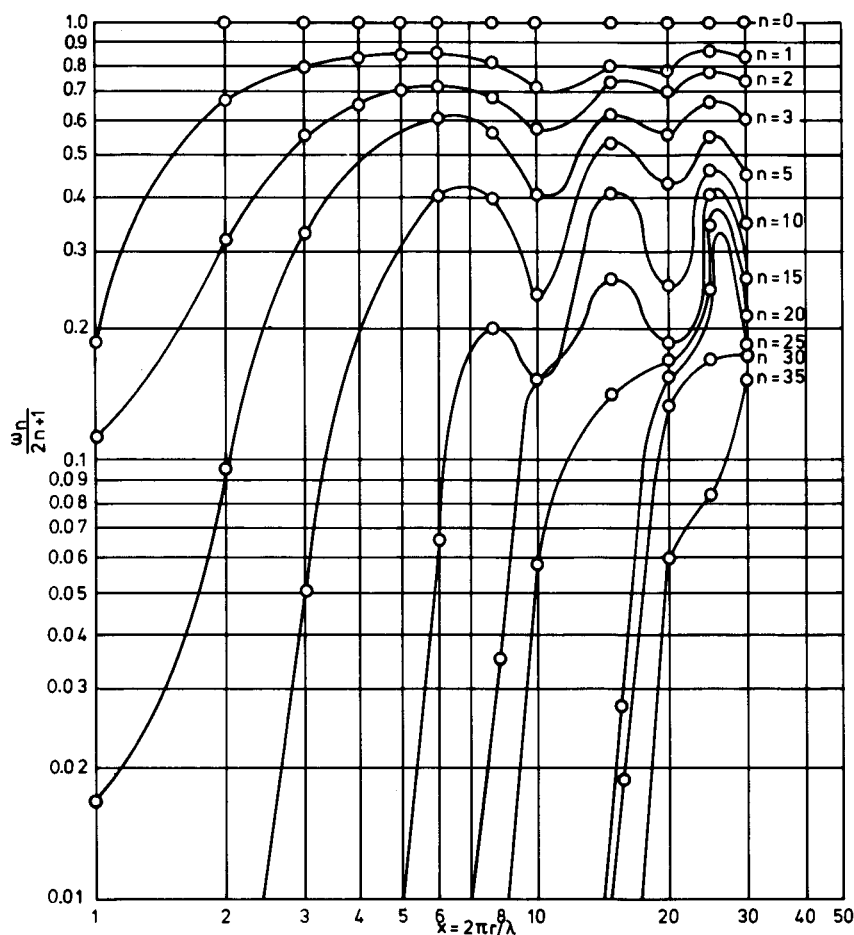


Fig. 10.5. Coefficients  $\omega_n$  in the Legendre expansion of the phase function for spheres of refractive index 1.33 and varying size parameter (from Clark *et al.*, 1957).

The same method is applied by Kolesov and Smoktii (1971), who fit expansions with  $N = 2$  and  $N = 3$  to thirteen exact phase functions based on Mie scattering with a certain size distribution. The influence of a distribution of sizes on the asymmetry parameter  $g$  is nicely illustrated in Figs. 11–13 of Hansen and Travis (1974).

As a first illustration of the use of such expansions, Fig. 10.6 (van de Hulst and Irvine, 1962) shows two exact scattering patterns, in the two polarizations combined, for water spheres of one size ( $m = 1.33$ ,  $x = 2.4$  and  $3.6$ ). For comparison, the Henyey–Greenstein curves for the two parameters  $g = 0.5$  and  $g = 0.75$  are given, all properly normalized to  $\omega_0 = 1$ . It is obvious that we are

TABLE 20

A Selection of Values of  $\omega_1$  through  $\omega_5$  for Mie Scattering<sup>a</sup>

$\rho$	$m$	$x$	$\omega_1/3$	$\omega_2/5$	$\omega_3/7$	$\omega_4/9$	$\omega_5/11$	$Q_{\text{ext}}$
-0.4	0.90	2	0.577	0.259	0.096	0.027	0.005	0.052
-0.42	0.93	3	0.799	0.534	0.281	0.121	0.043	0.065
0.4	1.05	4	0.875	0.693	0.498	0.313	0.163	0.073
0.4	1.10	2	0.638	0.286	0.100	0.027	0.005	0.058
0.4	1.20	1	0.176	0.111	0.017	0.002	0.000	0.034
-1.0	0.90	5	0.907	0.766	0.600	0.481	0.286	0.385
1.0	1.10	5	0.906	0.775	0.625	0.469	0.328	0.477
1.0	1.25	2	0.668	0.308	0.099	0.026	0.005	0.387
1.0	1.50	1	0.199	0.113	0.016	0.001	0.000	0.215
-2.0	0.90	10	0.966	0.911	0.841	0.773	0.679	1.377
-2.1	0.93	15	0.983	0.953	0.915	0.870	0.820	1.560
2.0	1.20	5	0.893	0.762	0.614	0.471	0.336	1.770
2.0	1.25	4	0.846	0.682	0.495	0.333	0.193	1.781
1.98	1.33	3	0.783	0.548	0.331	0.155	0.050	1.753
2.0	1.50	2	0.626	0.295	0.086	0.023	0.004	1.798
2.0	2.00	1	0.276	0.118	0.014	0.001	0.000	0.797
3.0	1.15	10	0.951	0.889	0.819	0.744	0.670	3.017
3.0	1.25	6	0.896	0.784	0.662	0.546	0.437	3.189
3.0	1.30	5	0.860	0.728	0.582	0.455	0.363	3.257
3.0	1.50	3	0.734	0.516	0.314	0.150	0.051	3.418
-4.0	0.90	20	0.980	0.947	0.905	0.858	0.809	2.776
4.0	1.20	10	0.927	0.852	0.770	0.666	0.613	3.685
4.0	1.25	8	0.898	0.805	0.703	0.610	0.526	3.785
3.96	1.33	6	0.848	0.731	0.602	0.497	0.402	3.889
4.0	1.40	5	0.806	0.672	0.531	0.414	0.320	3.972
4.0	1.50	4	0.750	0.595	0.433	0.306	0.199	4.052
4.0	2.00	2	0.506	0.289	0.166	0.065	0.006	4.769
6.0	1.20	15	0.874	0.777	0.668	0.569	0.485	2.489
6.0	1.50	6	0.644	0.520	0.342	0.294	0.253	2.904
6.0	1.60	5	0.572	0.466	0.275	0.227	0.103	2.961
6.0	2.00	3	0.391	0.325	0.180	0.188	0.081	3.035
8.0	1.20	20	0.816	0.709	0.571	0.456	0.364	1.733
8.0	1.40	10	0.571	0.458	0.249	0.236	0.171	1.688
8.0	1.50	8	0.453	0.377	0.166	0.209	0.130	1.778
8.0	2.00	4	0.324	0.365	0.023	0.087	-0.036	1.747
10.0	1.20	25	0.866	0.813	0.728	0.665	0.613	2.586
9.9	1.33	15	0.795	0.738	0.619	0.574	0.530	2.709
10.0	1.50	10	0.743	0.677	0.540	0.530	0.470	2.882
10.0	2.00	5	0.606	0.537	0.368	0.355	0.219	2.853

<sup>a</sup> Based on data from Chu-Clark-Churchill (1957).

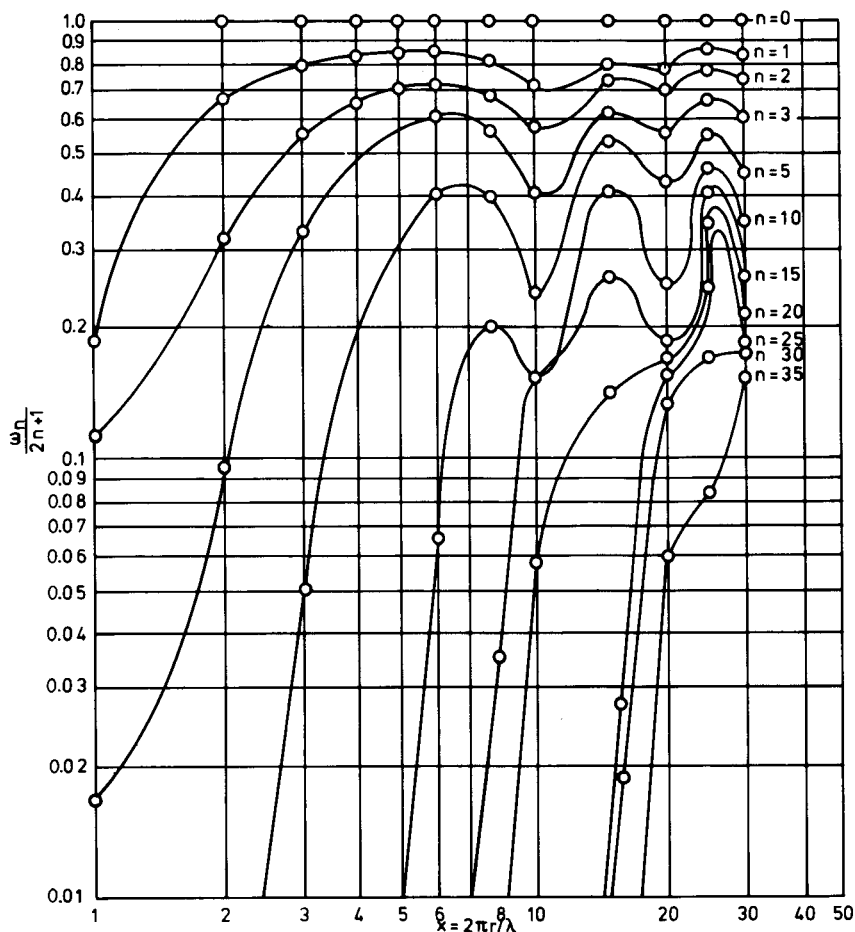


Fig. 10.5. Coefficients  $\omega_n$  in the Legendre expansion of the phase function for spheres of refractive index 1.33 and varying size parameter (from Clark *et al.*, 1957).

The same method is applied by Kolesov and Smoktii (1971), who fit expansions with  $N = 2$  and  $N = 3$  to thirteen exact phase functions based on Mie scattering with a certain size distribution. The influence of a distribution of sizes on the asymmetry parameter  $g$  is nicely illustrated in Figs. 11–13 of Hansen and Travis (1974).

As a first illustration of the use of such expansions, Fig. 10.6 (van de Hulst and Irvine, 1962) shows two exact scattering patterns, in the two polarizations combined, for water spheres of one size ( $m = 1.33$ ,  $x = 2.4$  and  $3.6$ ). For comparison, the Henyey–Greenstein curves for the two parameters  $g = 0.5$  and  $g = 0.75$  are given, all properly normalized to  $\omega_0 = 1$ . It is obvious that we are



**TABLE 20**  
A Selection of Values of  $\omega_1$  through  $\omega_5$  for Mie Scattering<sup>a</sup>

$\rho$	$m$	$x$	$\omega_1/3$	$\omega_2/5$	$\omega_3/7$	$\omega_4/9$	$\omega_5/11$	$Q_{\text{ext}}$
-0.4	0.90	2	0.577	0.259	0.096	0.027	0.005	0.052
-0.42	0.93	3	0.799	0.534	0.281	0.121	0.043	0.065
0.4	1.05	4	0.875	0.693	0.498	0.313	0.163	0.073
0.4	1.10	2	0.638	0.286	0.100	0.027	0.005	0.058
0.4	1.20	1	0.176	0.111	0.017	0.002	0.000	0.034
-1.0	0.90	5	0.907	0.766	0.600	0.481	0.286	0.385
1.0	1.10	5	0.906	0.775	0.625	0.469	0.328	0.477
1.0	1.25	2	0.668	0.308	0.099	0.026	0.005	0.387
1.0	1.50	1	0.199	0.113	0.016	0.001	0.000	0.215
-2.0	0.90	10	0.966	0.911	0.841	0.773	0.679	1.377
-2.1	0.93	15	0.983	0.953	0.915	0.870	0.820	1.560
2.0	1.20	5	0.893	0.762	0.614	0.471	0.336	1.770
2.0	1.25	4	0.846	0.682	0.495	0.333	0.193	1.781
1.98	1.33	3	0.783	0.548	0.331	0.155	0.050	1.753
2.0	1.50	2	0.626	0.295	0.086	0.023	0.004	1.798
2.0	2.00	1	0.276	0.118	0.014	0.001	0.000	0.797
3.0	1.15	10	0.951	0.889	0.819	0.744	0.670	3.017
3.0	1.25	6	0.896	0.784	0.662	0.546	0.437	3.189
3.0	1.30	5	0.860	0.728	0.582	0.455	0.363	3.257
3.0	1.50	3	0.734	0.516	0.314	0.150	0.051	3.418
-4.0	0.90	20	0.980	0.947	0.905	0.858	0.809	2.776
4.0	1.20	10	0.927	0.852	0.770	0.666	0.613	3.685
4.0	1.25	8	0.898	0.805	0.703	0.610	0.526	3.785
3.96	1.33	6	0.848	0.731	0.602	0.497	0.402	3.889
4.0	1.40	5	0.806	0.672	0.531	0.414	0.320	3.972
4.0	1.50	4	0.750	0.595	0.433	0.306	0.199	4.052
4.0	2.00	2	0.506	0.289	0.166	0.065	0.006	4.769
6.0	1.20	15	0.874	0.777	0.668	0.569	0.485	2.489
6.0	1.50	6	0.644	0.520	0.342	0.294	0.253	2.904
6.0	1.60	5	0.572	0.466	0.275	0.227	0.103	2.961
6.0	2.00	3	0.391	0.325	0.180	0.188	0.081	3.035
8.0	1.20	20	0.816	0.709	0.571	0.456	0.364	1.733
8.0	1.40	10	0.571	0.458	0.249	0.236	0.171	1.688
8.0	1.50	8	0.453	0.377	0.166	0.209	0.130	1.778
8.0	2.00	4	0.324	0.365	0.023	0.087	-0.036	1.747
10.0	1.20	25	0.866	0.813	0.728	0.665	0.613	2.586
9.9	1.33	15	0.795	0.738	0.619	0.574	0.530	2.709
10.0	1.50	10	0.743	0.677	0.540	0.530	0.470	2.882
10.0	2.00	5	0.606	0.537	0.368	0.355	0.219	2.853

<sup>a</sup> Based on data from Chu-Clark-Churchill (1957).

somewhere near a correct fit. The accompanying tabulation shows that the next coefficients in the expansion are also of the right order of magnitude.

	$\omega_0$	$g = \omega_1/3$	$\omega_2/5$	$\omega_3/7$
Mie curve, $m = 1.33$ , $x = 2.4$	1	0.74	0.42	0.20
Mie curve, $m = 1.33$ , $x = 3.6$	1	0.81	0.60	0.42
Henyeý-Greenstein curve, $g = 0.5$	1	0.50	0.25	0.12
Henyeý-Greenstein curve, $g = 0.75$	1	0.75	0.56	0.42

Those for the Mie curves were found (by interpolation) from the tables presented by Clark *et al.* (1957). Casual inspection of the curves in Fig. 10.6 seems to show that the Mie patterns require a higher value of  $\omega_2$ , because there is a dip in the middle. This is misleading for two reasons: The differences are easily misjudged on a logarithmic scale, and the dip is not centered at  $90^\circ$ .

Figure 10.7 shows as a further example the phase function for Deirmendjian's haze M at  $\lambda = 0.7 \mu\text{m}$ . Irvine (1965) has chosen as a reasonable fit to this curve a combination of two Henyeý-Greenstein functions: a strong forward one with weight  $b = 0.9724$  and  $g_1 = 0.824$ , and a weaker backward one with weight  $1 - b = 0.0276$  and  $g_2 = -0.550$ .

This idea has been systematically explored by Kattawar (1975). He shows that the three free parameters  $b$ ,  $g_1$ , and  $g_2$  can be so chosen that the three coefficients  $g = \omega_1/3\omega_0$ ,  $h = \omega_2/5\omega_0$ , and  $t = \omega_3/7\omega_0$  are matched exactly. Generally, this gives a much improved fit to the phase function. The following examples are worked out:

Size distribution	Refractive index	$b$	$g_1$	$g_2$	$g$	$h$	$t$
Haze L	1.55	0.962	0.713	-0.760	0.657	0.511	0.332
Same	1.55-0.001 $i$	0.963	0.714	-0.761	0.660	0.513	0.335
Same	1.55-0.0127 $i$	0.975	0.728	-0.764	0.691	0.532	0.365
Cloud	1.33 match 1	0.983	0.879	-0.984	0.848	0.776	0.652
	1.33 match 2	0.978	0.884	-0.749	0.848	0.776	0.666
Rayleigh phase function		0.500	0.316	-0.316	0	0.100	0

Here haze L has the size distribution  $n(r) \propto r^2 \exp(-15.119r^{1/2})$  and the cloud has  $n(r) \propto r^6 \exp(-1.5r)$ . Match 1 reproduces the expansion coefficients  $g$ ,  $h$ ,  $t$  exactly; match 2 with a slight change, shows a reduced glory peak and a better match to the phase function.

A more pedestrian way to adopt an analytic curve is to take a combination of exponentials

$$\Phi(\cos \alpha) = \sum_i c_i e^{-r_i \alpha}$$

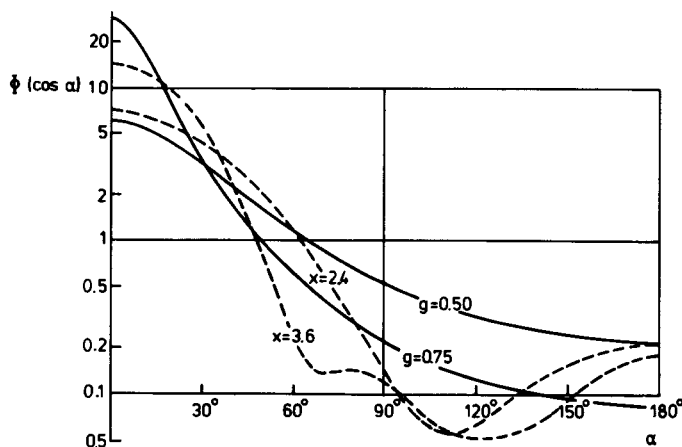


Fig. 10.6. Comparison between Mie phase functions,  $m = 1.33$ , two size parameters, and the Henyey-Greenstein phase functions for two values of the asymmetry parameter  $g$ .

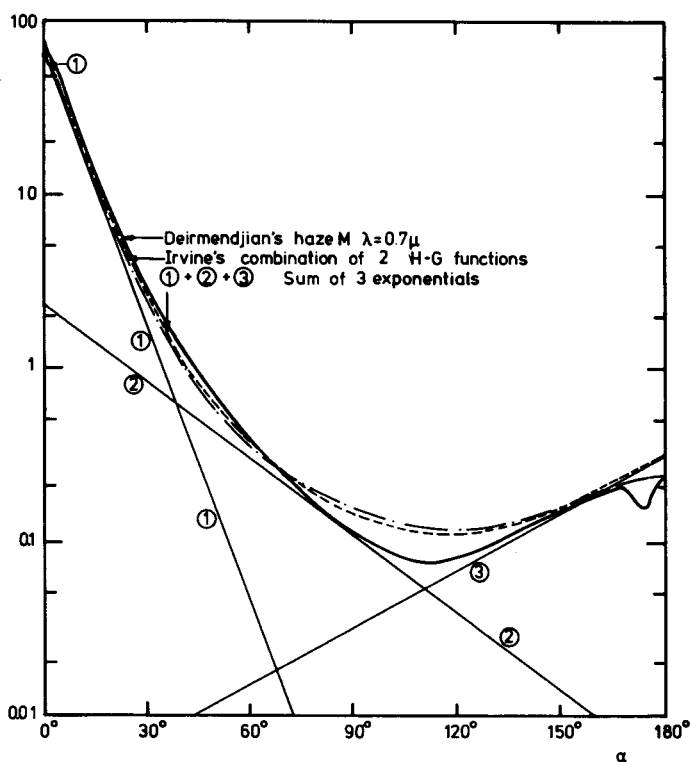


Fig. 10.7. Two ways of approximately representing the phase function for Deirmendjian's haze by a sum of simple phase functions. See specifications in text.

each of which is represented by a straight line on the logarithmic graph. Straight integration then gives, if  $\alpha$  is expressed in radians,

$$\omega_0 = \sum_i \frac{c_i(1 + e^{-\pi r_i})}{2(r_i^2 + 1)}$$

$$\frac{\omega_1}{3} = \sum_i \frac{c_i(1 - e^{-\pi r_i})}{2(r_i^2 + 4)}$$

$$\frac{\omega_2}{5} = -\frac{\omega_0}{8} + \sum_i \frac{9c_i(1 + e^{-\pi r_i})}{16(r_i^2 + 9)}$$

In Fig. 10.7, such an adaptation is shown with  $c_1 = 70.0$ ,  $c_2 = 2.30$ ,  $c_3 = 0.0033$ ,  $r_1 = 6.96$ ,  $r_2 = 1.94$ , and  $r_3 = -1.45$ .

Numerical results for this example are shown in the accompanying tabulation.

	$\omega_0$	$\omega_1/3$	$\omega_2/5$
Deirmendjian's table numerically integrated	1.00	0.81	—
Irvine's approximation by two Henyey-Greenstein functions	0.9724	0.801	0.660
	0.0276	-0.015	0.008
	1.0000	0.786	0.668
Approximation by three exponentials:			
$i = 1$	0.707	0.665	0.595
$i = 2$	0.242	0.148	0.072
$i = 3$	0.051	-0.025	0.010
	1.000	0.788	0.677

The match could be improved, if desired. However, the example suffices to show that the  $\omega_n$  may be obtained in various ways from simple formulas. It is seen that the value of  $\omega_1/3$  corresponds approximately to single particles with size parameter  $x = 3.6$  (see above), but that  $\omega_2/5$  is relatively larger owing to the influence of the peaked diagram of the larger particles in the distribution.

Finally, Fig. 10.8 shows Deirmendjian's phase function (Table T.35 of his book) in the separate polarizations, for his cloud model C1 at  $\lambda = 0.45 \mu\text{m}$ . The large size and short wavelength combine to make  $x \sim 55$  at the mode radius. For reason of this large value, the diffraction peak near  $\alpha = 0^\circ$ , the strongly polarized rainbows, and the glory near  $\alpha = 180^\circ$  are clearly seen.

Quite probably, hardly any of this detail survives the smoothing which is caused by more than one scattering in succession. It is therefore useful to know the first Legendre coefficients. The shape of the curve invites again the adaptation of a few exponentials as done with Fig. 10.7. With ruler and slide rule, one quickly

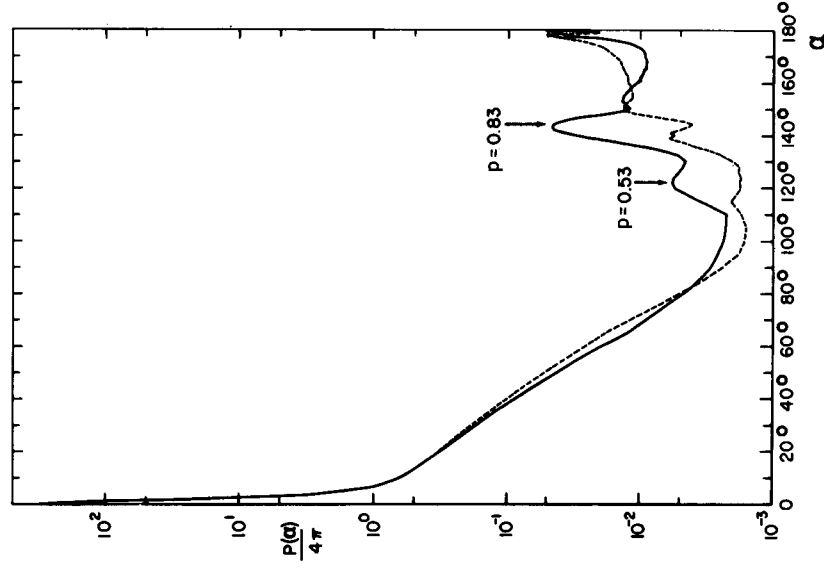


Fig. 10.8. Phase functions for Deirmendjian's cloud model C1, shown in the separate polarizations. The maximum of the size distribution occurs at drop radius  $r_c = 4 \mu\text{m}$ ; adopted wavelength  $\lambda = 0.45 \mu\text{m}$ .

finds the numbers in the accompanying tabulation, referring to  $\Phi(\cos \alpha)$  itself, i.e., after multiplying all numbers plotted in Fig. 10.8 by  $4\pi$ .

	$\omega_0$	$\omega_1/3$	$\omega_2/5$
Peak	0.452	0.449	0.443
First term, $c_1 = 16.6$ , $r_1 = 3.90$	0.512	0.432	0.322
Second term, $c_2 = 2.2 \times 10^{-4}$ , $r_2 = -2.46$	0.036	-0.025	0.014
	1.000	0.856	0.779

If the peak corresponds exactly to the diffraction peak, its contribution to  $\omega_0$  should be exactly 0.5. The graphical separation amounts to a somewhat arbitrary division, in which we have used the peak to make up the total  $\omega_0 = 1$ .

It is gratifying to see that  $g = 0.856$  comes out precisely where it should be according to Fig. 10.3 in the size range  $x = 50\text{--}60$ , and the value  $\omega_2/5 = 0.78$  checks well with the value obtained by a slight extrapolation of the curve in Fig. 10.5.

The conclusion of this section is the following. If the phase function is sought for use in multiple scattering of light in clouds, use Mie theory, but do not make this job too elaborate. The most relevant numbers generally are the first few Legendre coefficients, which can be found simply from the literature. Be careful, however, in problems that are particularly sensitive to the rainbow or glory angles (e.g., lidar).

### 10.3.2 Expansion of Element 12 (or 21) of the Phase Matrix

In radiative transfer with polarization (Chapter 15), the phase function is replaced by the phase matrix, and the expansion of the phase function in Legendre polynomials is replaced by expansions of each of the elements of the phase matrix. It is logical to treat those expansions here.

Finding these expansions from the Mie theory for a collection of particles with a given size distribution is a somewhat tedious job, but poses no problems of principle. Various methods have been used.

The most elegant treatment is to employ the CP representation of polarized light combined with generalized spherical functions (discussion and references in Section 15.1.2). In order to avoid the introduction of yet another set of functions and symbols, the more pedestrian method based on the traditional Stokes parameters and the classical associated Legendre functions is chosen here. This method requires a little more algebra, but leads to the same result. The main steps are spelled out, since this derivation had not been published elsewhere. Since then Bugayenko (1976) used a similar method.

Since the phase function is element  $Z_{11}^0$  of the azimuth dependent part of the phase matrix, its expansion, described in Section 10.3.1, does not have to be repeated. The element  $Z_{12}^0$  is expanded in this section, and  $Z_{22}^0$  in Section 10.3.3. Comparison with results obtained by other methods and reference to published numerical values of the coefficients is made in Section 15.2.3.

It is necessary to look at the detailed form of the scattering amplitudes. By the Mie theory for spherical particles, the function  $b_1(v)$ , introduced in Section 15.1.4, is composed of contributions  $|S_1|^2 - |S_2|^2$ . Here  $S_1$  and  $S_2$  are the complex scattering amplitudes given for spheres of any size by

$$S_1 = \sum_{n=1}^{\infty} (a_n^\dagger \pi_n + b_n^\dagger \tau_n)$$

$$S_2 = \sum_{n=1}^{\infty} (b_n^\dagger \pi_n + a_n^\dagger \tau_n)$$

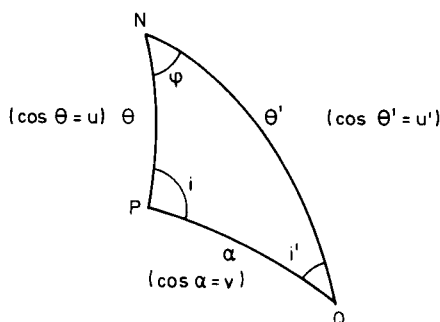


Fig. 10.9. Notations used in expanding the elements of the phase matrix.

The coefficients  $a_n^\dagger$  and  $b_n^\dagger$  depend on the size parameter  $x$  and the complex refractive index  $m$ . The  $b_n^\dagger$  should not be confused with the function  $b_1(v)$  we are seeking to expand. Further,  $\pi_n$  and  $\tau_n$  are functions of  $v = \cos \alpha$ , where  $\alpha$  is the scattering angle (Fig. 10.9), defined in terms of the Legendre function  $P_n(v)$  by means of

$$\pi_n = dP_n/dv, \quad \tau_n = v\pi_n - (1 - v^2) d\pi_n/dv$$

Writing \* for the complex conjugate and

$$|S_1|^2 - |S_2|^2 = \text{Re}[(S_1 - S_2)(S_1^* + S_2^*)]$$

and observing that

$$\pi_n \pm \tau_n = (1 \pm v)\pi_n \mp (1 - v^2) d\pi_n/dv$$

we find that  $\pi_n \pm \tau_n$ , and hence  $S_1 \pm S_2$ , has a factor  $(1 \pm v)$ , so that  $|S_1|^2 - |S_2|^2$ , and hence  $b_1(v)$ , must have a factor  $1 - v^2$ . It is therefore possible to expand (the superscript 2 of the  $P$  denotes the associated Legendre polynomial and is not a square!)

$$b_1(v) = \sum_{n=2}^{\infty} \beta_n P_n^2(v)$$

This can evidently be made into a procedure for computing  $\beta_n$  if the refractive index and size distribution are given.

Now consider the matrix element  $Z_{21}^0$ , which, in full analogy with  $Z_{11}^0$  (cf. Sections 10.3.1 and 15.1.3), may be written as

$$Z_{21}^0(u, u') = \frac{1}{2\pi} \int_0^{2\pi} b_1(v) \cos 2i \, d\varphi$$

where  $v$  and  $i$  are functions of  $u, u'$ , and  $\varphi$ . In order to write this in the form

$$Z_{21}^0(u, u') = \sum_{j=0}^{\infty} C_j(u) P_j(u')$$

we may proceed by the standard procedure based on the orthogonality of the Legendre functions:

$$C_j(u) = \int_{-1}^1 \frac{2j+1}{2} Z_{21}^0(u, u') P_j(u') du'$$

Replacing  $Z_{21}^0$  by its defining integral, this takes the form of a double integral over  $u'$  and  $\varphi$ , which geometrically means (Fig. 10.9) that an average is taken for  $Q$  covering the entire sphere, while  $N$  and  $P$  are kept fixed. The same average can be found by a double integral over  $v$  and  $i$ :

$$C_j(u) = (2j+1) \int_{-1}^1 \frac{dv}{2} \int_0^{2\pi} \frac{di}{2\pi} b_1(v) \cos 2i P_j(u')$$

Inserting the expansion of  $b_1(v)$  and the well known expression

$$P_j(u') = P_j(u)P_j(v) + 2 \sum_{m=1}^j \frac{(j-m)!}{(j+m)!} P_j^m(u)P_j^m(v)$$

we obtain

$$C_j(u) = \beta_j P_j^2(u)$$

so that the expansion sought is

$$Z_{21}^0(u, u') = \sum_{j=0}^{\infty} \beta_j P_j^2(u) P_j(u')$$

The element  $Z_{12}^0(u, u')$  is obtained in quite the same way, replacing  $i$  by  $i'$ , which means interchanging  $u$  and  $u'$ .

### 10.3.3 Expansion of Element 22 of the Phase Matrix

From Section 15.2.3 we obtain the defining equation

$$\begin{aligned} Z_{22}^0(u, u') &= \frac{1}{2\pi} \int_0^{2\pi} [a_2(v) \cos 2i \cos 2i' - a_3(v) \sin 2i \sin 2i'] d\varphi \\ &= \frac{1}{2\pi} \int_0^{2\pi} [\tfrac{1}{2}(a_2 + a_3) \cos 2(i + i') + \tfrac{1}{2}(a_2 - a_3) \cos 2(i - i')] d\varphi \end{aligned}$$

where  $a_2$  consists of contributions  $S_1 S_1^* + S_2 S_2^*$ , and  $a_3$  of contributions  $S_1 S_2^* + S_2 S_1^*$ , so that  $a_2 + a_3$  consists of contributions  $|S_1 + S_2|^2$ , and  $a_2 - a_3$  of contributions  $|S_1 - S_2|^2$ , all contributions being integrated over the assumed size distribution of spherical particles. It follows at once that  $a_2 + a_3$  contains a factor  $(1 + v)^2$ , and  $a_2 - a_3$  a factor  $(1 - v)^2$ . Therefore it is possible to expand

$$\tfrac{1}{2}(a_2 + a_3) = (1 + v)^2 \sum_{n=0}^{\infty} \gamma_n P_n(v)$$

$$\tfrac{1}{2}(a_2 - a_3) = (1 - v)^2 \sum_{n=0}^{\infty} \delta_n P_n(v)$$



Actual values of the expansion coefficients  $\gamma_n$  and  $\delta_n$  for a given size distribution may, in principle, be found from the Mie theory. The fact that  $a_2$  (used here) and  $a_1$  (defined in Section 15.1.4 and expanded in Section 10.3.1) are by the Mie theory identical does *not* introduce a simplification.

In the spherical triangle (Fig. 10.9), we have the identities

$$\sin(i \pm i') = (u \pm u') \sin \varphi / (1 \pm v)$$

which can be derived by combining the expressions

$$\cos i = (\cos \theta' - \cos \theta \cos \alpha) / \sin \theta \sin \alpha, \quad \sin i = \sin \theta' \sin \varphi / \sin \alpha$$

with the corresponding expressions for  $\cos i'$  and  $\sin i'$ . Writing  $\cos 2(i \pm i') = 1 - 2 \sin^2(i \pm i')$ , we obtain

$$\begin{aligned} Z_{22}^0(u, u') = \frac{1}{2\pi} \int_0^{2\pi} \sum_n P_n(v) \{ \gamma_n [(1+v)^2 - 2(u+u')^2 \sin^2 \varphi] \\ + \delta_n [(1-v)^2 - 2(u-u')^2 \sin^2 \varphi] \} d\varphi \end{aligned}$$

where  $v = uu' + ss' \cos \varphi$ , and the notation  $s = (1 - u^2)^{1/2}$ ,  $s' = (1 - u'^2)^{1/2}$  has been introduced.

The transformation of this integral into an expansion in products of associated Legendre functions may be made as follows. The help of Dr. J. W. Hovenier in tracing an error in the first try is acknowledged.

Write  $\langle \rangle$  for the average over  $\varphi$ . Let

$$k = 1 + v^2 - 2(u^2 + u'^2) \sin^2 \varphi$$

$$l = v - 2uu' \sin^2 \varphi$$

Make a Fourier expansion of  $k$  and  $l$ :

$$k = \frac{3}{2}s^2s'^2 + 2uu'ss' \cos \varphi + \frac{1}{2}(1+u^2)(1+u'^2) \cos 2\varphi$$

$$l = ss' \cos \varphi + uu' \cos 2\varphi$$

and expand  $P_n(v)$  in the usual manner as

$$P_n(v) = P_n(u)P_n(u') + 2 \sum_{m=1}^n \frac{(n-m)!}{(n+m)!} P_n^m(u)P_n^m(u') \cos m\varphi$$

Integration now gives for  $n \geq 2$

$$\langle kP_n(v) \rangle = \frac{3}{2}s^2s'^2 P_n(u)P_n(u') + \frac{2uu'ss'}{n(n+1)} P_n^1(u)P_n^1(u')$$

$$+ \frac{\frac{1}{2}(1+u^2)(1+u'^2)}{(n-1)n(n+1)(n+2)} P_n^2(u)P_n^2(u')$$

$$\langle lP_n(v) \rangle = \frac{ss'}{n(n+1)} P_n^1(u)P_n^1(u') + \frac{uu'}{(n-1)n(n+1)(n+2)} P_n^2(u)P_n^2(u')$$

and for  $n = 0$  or  $n = 1$ , the same expression with omission of the terms in which the upper index would exceed  $n$ . The rest is algebra. Not writing the argument  $u$  we have the identities:

$$(1) \quad (2n + 1)sP_n = P_{n+1}^1 - P_{n-1}^1$$

$$(2) \quad (2n + 1)sP_n^1 = P_{n+1}^2 - P_{n-1}^2$$

$$(3) \quad (2n - 1)(2n + 1)(2n + 3)s^2P_n \\ = (2n - 1)P_{n+2}^2 - 2(2n + 1)P_n^2 + (2n + 3)P_{n-2}^2$$

$$(4) \quad (2n + 1)uP_n^1 = nP_{n+1}^1 + (n + 1)P_{n-1}^1$$

$$(5) \quad (2n + 1)uP_n^2 = (n - 1)P_{n+1}^2 + (n + 2)P_{n-1}^2$$

$$(6) \quad (2n - 1)(2n + 1)(2n + 3)usP_n^1 \\ = n(2n - 1)P_{n+2}^2 + 3(2n + 1)P_n^2 - (n + 1)(2n + 3)P_{n-2}^2$$

$$(7) \quad (2n - 1)(2n + 1)(2n + 3)(1 + u^2)P_n^2 \\ = n(n - 1)(2n - 1)P_{n+2}^2 \\ + 6(n - 1)(n + 2)(2n + 1)P_n^2 + (n + 1)(n + 2)(2n + 3)P_{n-2}^2$$

Upon substitution of expressions (3), (6), and (7) into  $\langle kP_n(v) \rangle$ , and of expressions (2) and (5) into  $\langle lP_n(v) \rangle$ , we obtain

$$\langle kP_n(v) \rangle = \frac{P_{n-2}^2(u)P_{n-2}^2(u')}{(n - 1)n(2n - 1)(2n + 1)} \\ + \frac{6P_n^2(u)P_n^2(u')}{n(n + 1)(2n - 1)(2n + 3)} + \frac{P_{n+2}^2(u)P_{n+2}^2(u')}{(n + 1)(n + 2)(2n + 1)(2n + 3)}$$

and

$$\langle lP_n(v) \rangle = \frac{P_{n-1}^2(u)P_{n-1}^2(u')}{(n - 1)n(n + 1)(2n + 1)} + \frac{P_{n+1}^2(u)P_{n+1}^2(u')}{n(n + 1)(n + 2)(2n + 1)}$$

where (for small  $n$ ) terms in which the associated Legendre functions would have a lower index  $< 2$  should be omitted. Substitution of these forms into the equation

$$Z_{22}^0(u, u') = \sum_{n=0}^{\infty} (\gamma_n + \delta_n) \langle kP_n(v) \rangle + 2 \sum_{n=0}^{\infty} (\gamma_n - \delta_n) \langle lP_n(v) \rangle$$

gives the expression to be used in calculations on radiative transfer:

$$Z_{22}^0(u, u') = \sum_{j=2}^{\infty} \varepsilon_j P_j^2(u) P_j^2(u')$$

The equations derived above contain an implicit procedure to compute the expansion coefficients  $\varepsilon_j$  from the coefficients  $\gamma_n$  and  $\delta_n$  obtained earlier. In particular,

$$\begin{aligned}\varepsilon_2 &= \frac{1}{6}(\gamma_0 + \delta_0) + \frac{1}{9}(\gamma_1 - \delta_1) + \frac{1}{21}(\gamma_2 + \delta_2) + \cdots \\ \varepsilon_3 &= \frac{1}{90}(\gamma_1 + \delta_1) + \frac{1}{60}(\gamma_2 - \delta_2) + \cdots\end{aligned}$$

## REFERENCES

- Alms, G. R., Burnham, A. K., and Flygare, W. H. (1975). *J. Chem. Phys.* **63**, 3321.  
 Baas, F., and van den Hout, K. D. (1979). *Physica* **95A**, 597.  
 Blau, H. H., McCleese, D. J., and Watson, D. (1970). *Appl. Opt.* **9**, 2522.  
 Blumer, H. (1925). *Z. Phys.* **32**, 119.  
 Bridge, N. J., and Buckingham, A. D. (1966). *Proc. R. Soc. London Ser. A* **295**, 334.  
 Bryant, H. C., and Jarmie, N. (1974). *Sci. Am.* **231**, July; 60.  
 Bugayenko, O. I. (1976). *Fiz. Atmosf. Okeana* **12**, 603.  
 Chandrasekhar, S. (1950). "Radiative Transfer." Oxford Univ. Press (Clarendon), London and New York. Also Dover, New York, 1960.  
 Chang, Sin-Chung, and Shultis, J. K. (1976). *J. Comput. Phys.* **20**, 336.  
 Chu, C. M., and Churchill, S. W. (1955). *J. Opt. Soc. Am.* **45**, 958.  
 Chu, C. M., Clark, G. C., and Churchill, S. W. (1957). "Tables of Angular Distribution Coefficients for Light Scattering by Spheres." Univ. of Michigan Press, Eng. Res. Inst. Publ., Ann Arbor, Michigan.  
 Clark, G. C., Chu, C. M., and Churchill, S. W. (1957). *J. Opt. Soc. Am.* **47**, 81.  
 Coffeen, D. L., and Hansen, J. E. (1974). In "Planets, Stars and Nebulae Studied with Spectrophotopolarimetry," (T. Gehrels, ed.), p. 518. Univ. of Arizona Press, Tucson, Arizona.  
 Deirmendjian, D. (1969). "Electromagnetic Scattering on Spherical Polydispersions." Elsevier, Amsterdam.  
 Elterman, L. (1964). Environmental Research Papers, No. 46. AFCRL, Massachusetts.  
 Greenberg, J. M., and Hanner, M. (1970). *Astrophys. J.* **161**, 947.  
 Greenberg, J. M., Pederson, N. E., and Pederson, J. C. (1961). *J. Appl. Phys.* **32**, 233.  
 Hansen, J. E., and Travis, L. D. (1974). *Space Sci. Rev.* **16**, 527.  
 Hartel, W. (1940). *Das Licht* **40**, 141, 165, 190, 214, 232.  
 Heintzenberg, J. (1977). In *Proc. Symp. Radiat. Atmos. Garmisch-Partenkirchen 1976* (H. J. Bolle, ed.), p. 157. Science Press, Princeton, New Jersey.  
 Henyey, L. G., and Greenstein, J. L. (1941). *Astrophys. J.* **93**, 76.  
 Hunt, G. E. (1970). *J. Quant. Spectrosc. Radiat. Transfer* **10**, 857.  
 Hunt, G. E. (1971). *J. Quant. Spectrosc. Radiat. Transfer* **11**, 655.  
 Irvine, W. M. (1963). *Bull. Astron. Inst. Neth.* **17**, 176.  
 Irvine, W. M. (1965). *J. Opt. Soc. Am.* **55**, 16.  
 Jacobowitz, H. (1971). *J. Quant. Spectrosc. Radiat. Transfer* **11**, 691.  
 Kaper, H. G., Shultis, J. K., and Veninga, J. G. (1970). *J. Computational. Phys.* **6**, 288.  
 Kattawar, G. W. (1975). *J. Quant. Spectrosc. Radiat. Transfer* **15**, 839.  
 Kattawar, G. W., Hirtzfelder, S. J., and Binstock, J. (1973). *J. Atmos. Sci.* **30**, 289.  
 Kerker, M. (1969). "The Scattering of Light and Other Electromagnetic Radiation." Academic Press, New York.  
 Kolesov, A. K., and Smoktii, O. I. (1971). *Astron. Zh.* **48**, 1013 [English transl.: *Sov. Astron.-AJ* **15**, 802].  
 Lind, A. C., Wang, R. T. and Greenberg, J. M. (1965). *Appl. Opt.* **4**, 1555.

- McCartney, E. J. (1976). "Optics of the Atmosphere; Scattering by Molecules and Particles." Wiley, New York.
- Rozenberg, V. I. (1972). "Scattering and Attenuation of Electromagnetic Radiation by Atmospheric Particles" (Russian). Leningrad Gidrometeoizdat, [English transl.: NASA Tech. Translation, NASA TT F-771. National Technical Information Service (1974).
- Shipley, S. T., and Weinman J. A. (1978). *J. Opt. Soc. Am.* **68**, 130.
- Sobolev, V. V. (1967). *Dokl. Akad. Nauk* **177**, 812.
- van de Hulst, H. C. (1949a). In "The Atmospheres of the Earth and Planets" (G. P. Kuiper, ed.), p. 49. Univ. of Chicago Press, Chicago, Illinois.
- van de Hulst, H. C. (1949b). *Rech. Astron. Observ. Utrecht* **11**, part 2.
- van de Hulst, H. C. (1957). "Light Scattering by Small Particles." Wiley, New York. Also Dover, New York, 1980.
- van de Hulst, H. C., and Irvine, W. M. (1962). In *La physique des planètes, Congr. Colloq. Univ. Liège* **24**, 78.
- Yanovitskii, E. G., and Dumanskii, Z. O. (1972). "Tables of Light Scattering by Polydisperse Systems of Spherical Particles." Izdatelstvo Naykova Dymka, Kiev (in Russian).
- Zerull, R., and Giese, R. H. (1973). In "Planets, Stars and Nebulae Studied with Spectrophotopolarimetry" p. 901 Univ. of Arizona Press, Tucson, Arizona.
- Zerull, R., and Weiss, K. (1977). In *Proc. Symp. Radiat. Atmos. Garmisch-Partenkirchen, 1976* (H. J. Bolle, ed.), p. 110. Science Press, Princeton, New Jersey.
- Zuev, V. E. (1974). "Propagation of Visible and Infrared Radiation in the Atmosphere." Wiley, New York (orig. Russian, 1970).

- McCartney, E. J. (1976). "Optics of the Atmosphere; Scattering by Molecules and Particles." Wiley, New York.
- Rozenberg, V. I. (1972). "Scattering and Attenuation of Electromagnetic Radiation by Atmospheric Particles" (Russian). Leningrad Gidrometeoizdat, [English transl.: NASA Tech. Translation, NASA TT F-771. National Technical Information Service (1974).
- Shipley, S. T., and Weinman J. A. (1978). *J. Opt. Soc. Am.* **68**, 130.
- Sobolev, V. V. (1967). *Dokl. Akad. Nauk* **177**, 812.
- van de Hulst, H. C. (1949a). In "The Atmospheres of the Earth and Planets" (G. P. Kuiper, ed.), p. 49. Univ. of Chicago Press, Chicago, Illinois.
- van de Hulst, H. C. (1949b). *Rech. Astron. Observ. Utrecht* **11**, part 2.
- van de Hulst, H. C. (1957). "Light Scattering by Small Particles." Wiley, New York. Also Dover, New York, 1980.
- van de Hulst, H. C., and Irvine, W. M. (1962). In *La physique des planètes, Congr. Colloq. Univ. Liège* **24**, 78.
- Yanovitskii, E. G., and Dumanskii, Z. O. (1972). "Tables of Light Scattering by Polydisperse Systems of Spherical Particles." Izdatelstvo Naykova Dymka, Kiev (in Russian).
- Zerull, R., and Giese, R. H. (1973). In "Planets, Stars and Nebulae Studied with Spectrophotopolarimetry" p. 901 Univ. of Arizona Press, Tucson, Arizona.
- Zerull, R., and Weiss, K. (1977). In *Proc. Symp. Radiat. Atmos. Garmisch-Partenkirchen, 1976* (H. J. Bolle, ed.), p. 110. Science Press, Princeton, New Jersey.
- Zuev, V. E. (1974). "Propagation of Visible and Infrared Radiation in the Atmosphere." Wiley, New York (orig. Russian, 1970).

## 11 ☐ Results for the Henyey-Greenstein Phase Function, Unbounded and Semi-Infinite Medium

### 11.1 THE UNBOUNDED MEDIUM: DIFFUSION PATTERN AND DIFFUSION LENGTH

In this chapter and in Chapter 13 numerical results and some comments for the phase function listed as set 16 in Display 10.1 are presented. That function is characterized by

$$\text{phase function: } \Phi(\cos \alpha) = (1 - g^2)/(1 + g^2 - 2g \cos \alpha)^{3/2}$$

$$\text{Legendre coefficients: } \omega_n = a(2n + 1)g^n$$

Table 21 gives this function for eight values of  $g$ .

All results reported in this chapter depend on the two parameters albedo  $a$  and asymmetry factor  $g$ . At  $g = 0$ , the results for isotropic scattering reappear. The presentation is arranged by the optical thickness of the layer as shown in the accompanying tabulation.

	Isotropic scattering	Henyey-Greenstein phase function	Other anisotropic phase functions
Unbounded and semi-infinite medium	Chapter 8	Chapter 11	Chapter 12
Finite slabs	Chapter 9	Chapter 13	Chapter 14

TABLE 21

Henyey–Greenstein Phase Functions

The tabulated value is  $\Phi(g, \cos \alpha)$ . The bottom line gives  $f$ , the fraction scattered into the forward hemisphere. For negative values of  $g$  take opposite signs of  $\cos \alpha$  and  $f$ .

	$g=0$	$g=0.125$	$g=0.250$	$g=0.375$	$g=0.500$	$g=0.625$	$g=0.750$	$g=0.875$
$\cos \alpha = -1.0$	1	0.6914	0.4800	0.3306	0.2222	0.1420	0.0816	0.0356
-0.9	1	0.7124	0.5040	0.3513	0.2379	0.1527	0.0880	0.0384
-0.8	1	0.7345	0.5301	0.3742	0.2555	0.1649	0.0953	0.0416
-0.7	1	0.7577	0.5585	0.3998	0.2754	0.1787	0.1036	0.0453
-0.6	1	0.7822	0.5895	0.4284	0.2981	0.1946	0.1132	0.0496
-0.5	1	0.8081	0.6235	0.4606	0.3240	0.2129	0.1244	0.0546
-0.4	1	0.8354	0.6609	0.4970	0.3539	0.2344	0.1376	0.0605
-0.3	1	0.8643	0.7022	0.5385	0.3887	0.2597	0.1532	0.0676
-0.2	1	0.8949	0.7480	0.5861	0.4295	0.2900	0.1721	0.0762
-0.1	1	0.9273	0.7990	0.6412	0.4781	0.3266	0.1952	0.0867
0	1	0.9617	0.8560	0.7055	0.5367	0.3716	0.2240	0.0999
0.1	1	0.9984	0.9202	0.7812	0.6081	0.4280	0.2606	0.1168
0.2	1	1.0374	0.9928	0.8716	0.6971	0.5002	0.3084	0.1392
0.3	1	1.0790	1.0755	0.9809	0.8100	0.5954	0.3728	0.1696
0.4	1	1.1235	1.1704	1.1150	0.9570	0.7250	0.4633	0.2131
0.5	1	1.1712	1.2801	1.2828	1.1547	0.9096	0.5974	0.2788
0.6	1	1.2223	1.4080	1.4973	1.4312	1.1884	0.8113	0.3872
0.7	1	1.2772	1.5588	1.7791	1.8387	1.6458	1.1924	0.5896
0.8	1	1.3364	1.7386	2.1619	2.4845	2.4960	2.0045	1.0601
0.9	1	1.4002	1.9557	2.7048	3.6221	4.4512	4.4662	2.8161
1.0	1	1.4694	2.2222	3.5200	6.0000	11.5556	28.0000	120.0000
$f$	0.5000	0.5929	0.6810	0.7605	0.8292	0.8866	0.9333	0.9706

11.1.1 The Redistribution Function

The redistribution function  $h(u, v)$  occurring in the transfer equations of the azimuth-independent part of the radiation (Display 4.4) can be found numerically from the defining equations

$$h(u, v) = \frac{1}{2\pi} \int_0^{2\pi} a\Phi[uv + (1 - u^2)^{1/2}(1 - v^2)^{1/2} \cos \varphi] d\varphi$$

or

$$h(u, v) = \sum_{n=0}^{\infty} \omega_n P_n(u)P_n(v)$$

TABLE 22

Redistribution Function  $h(u, v)$  for Henyey–Greenstein Phase Function with  $g = 0.5$

$u =$	1.0	0.9	0.7	0.5	0.3	0.1	0.0
$v = 1.0$	6.0000	3.6221	1.8387	1.1547	0.8100	0.6082	0.5367
0.9	3.6221	3.1201	2.0196	1.3285	0.9317	0.6916	0.6062
0.7	1.8387	2.0196	1.9936	1.6082	1.2012	0.8951	0.7790
0.5	1.1547	1.3285	1.6082	1.6431	1.4291	1.1339	0.9966
0.3	0.8100	0.9317	1.2012	1.4291	1.4885	1.3460	1.2294
0.1	0.6082	0.6916	0.8951	1.1339	1.3460	1.4254	1.3942
0.0	0.5367	0.6062	0.7790	0.9966	1.2294	1.3942	1.4181
-0.1	0.4781	0.5365	0.6827	0.8745	1.1041	1.3213	1.3942
-0.3	0.3887	0.4305	0.5357	0.6781	0.8679	1.1041	1.2294
-0.5	0.3240	0.3548	0.4315	0.5353	0.6781	0.8745	0.9966
-0.7	0.2754	0.2986	0.3555	0.4315	0.5357	0.6827	0.7790
-0.9	0.2379	0.2557	0.2986	0.3548	0.4305	0.5365	0.6062
-1.0	0.2222	0.2379	0.2754	0.3240	0.3887	0.4781	0.5367

For the Henyey–Greenstein phase function, it can also be expressed in known functions (van de Hulst and Davis, 1961) by

$$h(u, v) = [(1 - g^2)/(\alpha + \beta)^{1/2}(\alpha - \beta)](2/\pi)E(k^2)$$

where  $u = \cos \theta$ ,  $v = \cos \theta_1$ ,  $\alpha = 1 + g^2 - 2guv$ ,  $\beta = 2g \sin \theta \sin \theta_1$ ,  $k^2 = 2\beta/(\alpha + \beta)$ , and  $E(k^2)$  is the complete elliptical integral tabulated by Jahnke–Emde (1945) on p. 80. This representation is practical only for hand computation. Table 22 gives for reference the value of  $h(u, v)$  for  $g = 0.50$ . The lines  $u = 1$  or  $v = 1$  represent the phase function itself.

### 11.1.2 Diffusion Length and Pattern

The modes of propagation through an unbounded homogeneous medium follow from the integral equation presented in Section 6.2.1. The fundamental mode is the one which is least damped, i.e., the one for which the diffusion exponent  $k$  is smallest, and the diffusion length  $k^{-1}$  largest. This mode persists far from source layers or boundaries.

Values of  $k$  for the Henyey–Greenstein phase function are given in Table 23. In addition to these numerical data, the following properties of the function  $k(a, g)$  or of the inverse function  $a(k, g)$  may be noted.

$$\begin{aligned} (g = 0) \quad & \frac{1}{a} = \frac{1}{2k} \ln \frac{1+k}{1-k} \\ (g = -1) \quad & a = (1 - k^2)^{1/2} \\ (g = 1) \quad & a = 1 - k \\ (a = 0) \quad & k = 1 \\ (a = 1) \quad & k = 0 \end{aligned}$$



TABLE 23

First Characteristic Exponent  $k$  for Henyey-Greenstein Functions

	a=0	a=0.2	a=0.4	a=0.6	a=0.8	a=0.9	a=0.95	a=0.99	a=1
$g = -1$	1	.9798	.9165	.8000	.6000	.4359	.3122	.1411	0
-.975	1		.9466	.8543	.6851	.5399	.4237	.2259	0
-.950	1		.9604	.8802	.7242	.5812	.4563	.2321	0
-.925	1		.9700	.8990	.7513	.6060	.4717	.2334	0
-.900	1	.9994	.9773	.9136	.7714	.6219	.4798	.2333	0
-.875	1		.9828	.9254	.7867	.6323	.4841	.2327	0
-.850	1		.9871	.9350	.7983	.6392	.4862	.2317	0
-.825	1		.9904	.9429	.8072	.6435	.4868	.2306	0
-.800	1	1	.9929	.9494	.8139	.6461	.4866	.2293	0
-.775	1		.9949	.9547	.8189	.6474	.4857	.2280	0
-.75	1		.9964	.9590	.8224	.6477	.4843	.2266	0
-.70	1		.9982	.9652	.8262	.6460	.4804	.2236	0
-.65	1		.9992	.9690	.8266	.6423	.4756	.2205	0
-.60	1		.9997	.9708	.8245	.6370	.4701	.2173	0
-.55	1		1	.9712	.8205	.6307	.4641	.2140	0
-.50	1		1	.9703	.8150	.6236	.4577	.2106	0
-.45	1		.9999	.9684	.8082	.6158	.4510	.2072	0
-.40	1		.9997	.9654	.8003	.6074	.4440	.2037	0
-.35	1		.9993	.9615	.7916	.5986	.4367	.2001	0
-.30	1		.9987	.9566	.7820	.5893	.4292	.1964	0
-.25	1		.9979	.9508	.7716	.5796	.4215	.1926	0
-.20	1		.9966	.9440	.7606	.5695	.4136	.1888	0
-.15	1		.9949	.9363	.7490	.5590	.4054	.1849	0
-.10	1	1	.9926	.9276	.7367	.5482	.3970	.1808	0
-.05	1		.9896	.9180	.7239	.5370	.3884	.1767	0
0	1	.9999	.9858	.9074	.7104	.5254	.3795	.1725	0
.05	1	.9999	.9811	.8959	.6964	.5135	.3704	.1682	0
.10	1	.9996	.9754	.8834	.6818	.5012	.3610	.1637	0
.15	1		.9687	.8701	.6666	.4885	.3513	.1592	0
.20	1	.9987	.9609	.8559	.6508	.4753	.3413	.1545	0
.25	1	.9971	.9520	.8407	.6344	.4618	.3310	.1496	0
.30	1	.9949	.9421	.8247	.6174	.4477	.3203	.1446	0
.35	1	.9921	.9310	.8078	.5997	.4331	.3093	.1394	0
.40	1	.9882	.9188	.7899	.5812	.4179	.2978	.1340	0
.45	1	.9835	.9056	.7710	.5620	.4021	.2858	.1283	0
.50	1	.9777	.8911	.7512	.5418	.3856	.2733	.1224	0
.55	1		.8754	.7301	.5207	.3683	.2602	.1162	0
.60	1	.9627	.8585	.7079	.4986	.3501	.2464	.1097	0
.65	1		.8401	.6843	.4751	.3308	.2317	.1027	0
.70	1	.9424	.8201	.6591	.4502	.3102	.2160	.0952	0
.75	1		.7983	.6319	.4234	.2881	.1990	.0871	0
.775	1		.7865	.6175	.4093	.2763	.1899	.0827	0
.800	1	.9155	.7740	.6023	.3944	.2639	.1804	.0781	0
.825	1		.7608	.5864	.3789	.2509	.1703	.0732	0
.850	1		.7467	.5695	.3624	.2371	.1595	.0680	0
.875	1		.7315	.5514	.3448	.2224	.1480	.0623	0
.900	1	.8783	.7149	.5318	.3258	.2064	.1354	.0560	0
.925	1		.6964	.5102	.3049	.1887	.1214	.0490	0
.950	1		.6750	.4855	.2812	.1686	.1054	.0407	0
.975	1		.6487	.4552	.2523	.1441	.0857	.0302	0
1	1	.8000	.6000	.4000	.2000	.1000	.0500	.0100	0

Expansion useful near  $a = 1$ :

$$a = 1 - \frac{1}{3(1-g)} k^2 - \frac{4-5g-5g^3}{45(1-g)^4(1+g)} k^4 + O(k^6)$$

Expansion useful near  $g = 0$ :

$$k = k(0) - [12a(1-a)^2/mk^2(0)]g + O(g^2)$$

where  $k(0)$  is the value of  $k$  at  $g = 0$ . The complete set of curves for this fundamental mode is presented in Fig. 11.1. A derived quantity, the diffusion constant

$$D = (1-a)(1-ag)/k^2$$

(Display 5.2) is tabulated separately (Table 24). Its variation with  $g$  is seen to be small.

The corresponding eigenfunctions  $P(u)$  are shown in Table 25. As shown in Section 6.2.1, the intensity pattern in the fundamental mode is proportional to  $P(u)$ , and the source function to  $(1 - ku)P(u)$ . The same table shows the derived constant  $m$  (Section 5.2.1). Values of  $ma^{-2} = M$  (Sobolev's notation) for additional values of  $g$  and  $a$  are found in Table 16 of Dlugach and Yanovitskii (1974). The data in Table 25 were obtained by the asymptotic fitting process, and not by the direct solution of the integral equation. This has introduced inaccuracies, mainly at  $a = 0.4$  and  $a = 0.6$ , in comparison with the accurate  $k$  values in Table 23.

TABLE 24  
Diffusion Constant  $D$  for Henyey-Greenstein Phase Functions

	$g = 0$	$g = 0.25$	$g = 0.5$	$g = 0.75$	$g = 0.875$
$a = 0.60$	0.4858	0.4810	0.4962	0.5509	0.6248
0.80	0.3963	0.3975	0.4087	0.4462	0.5047
0.90	0.3622	0.3635	0.3699	0.3916	0.4298
0.95	0.3472	0.3480	0.3513	0.3631	0.3854
0.99	0.3360	0.3362	0.3369	0.3394	0.3446
1.00	0.3333	0.3333	0.3333	0.3333	0.3333

The function  $k(a, g)$  discussed and tabulated above is the smallest eigenvalue of an integral equation introduced in Sections 5.2.2 and 6.2.1. The properties of the higher eigenvalues are discussed and illustrated in Section 12.3. Knowledge of these higher eigenvalues is essential in the Case method (Section 6.5) and is helpful in assessing at what depth the asymptotic formulas for thick layers become practical.

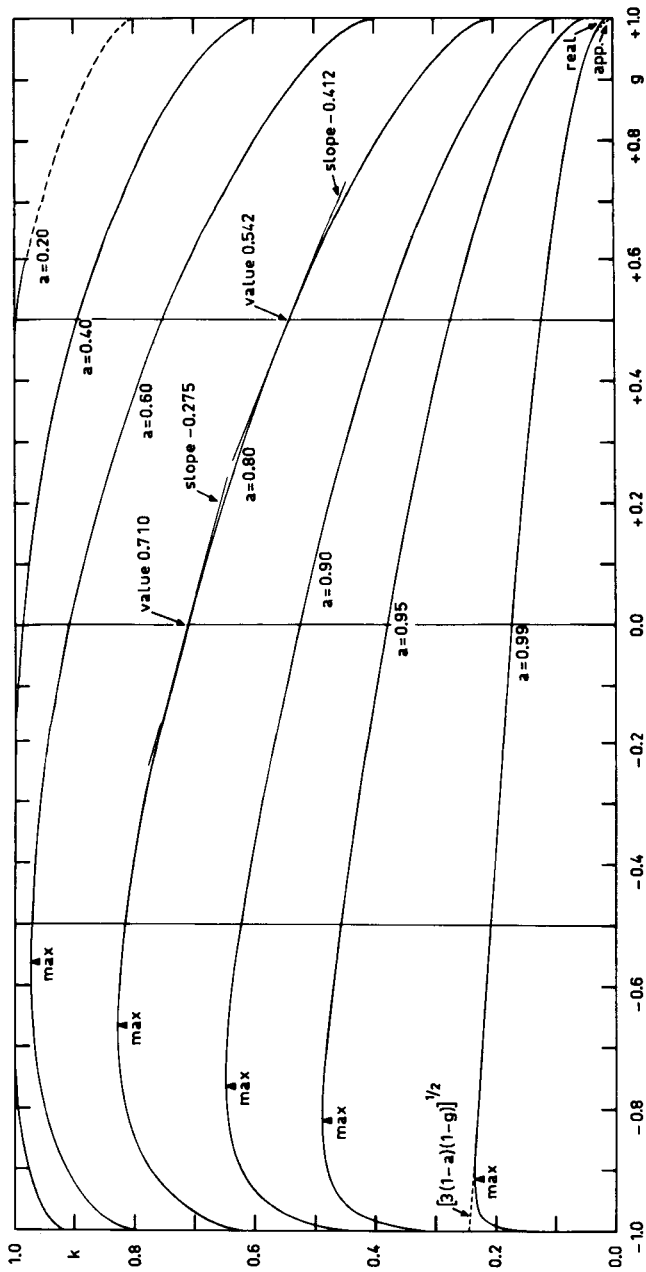


Fig. 11.1. Diffusion exponent  $k$  for Henyey–Greenstein phase functions in the full domain of asymmetry parameter  $g$  and single-scattering albedo  $a$ .

**TABLE 25**  
Diffusion Pattern in Unbounded Medium

	a=	THIS BLOCK		g=-0.25		1.00
		0.60	0.80	0.90	0.95	
u=-1.0	0.43462	0.55644	0.65277	0.73276	0.86357	1.00000
-0.9	0.43537	0.56680	0.66700	0.74747	0.87412	1.00000
-0.7	0.44381	0.59347	0.70026	0.78037	0.89642	1.00000
-0.5	0.46247	0.62975	0.74121	0.81869	0.92044	1.00000
-0.3	0.49385	0.67865	0.79195	0.86357	0.94637	1.00000
-0.1	0.54282	0.74502	0.85550	0.91654	0.97443	1.00000
0.0	0.57658	0.78712	0.89342	0.94669	0.98933	1.00000
0.1	0.61894	0.83707	0.93643	0.97969	1.00486	1.00000
0.3	0.74256	0.96974	1.04186	1.05591	1.03795	1.00000
0.5	0.96448	1.17312	1.18361	1.14932	1.07402	1.00000
0.7	1.45762	1.51792	1.38275	1.26602	1.11348	1.00000
0.9	3.39062	2.21816	1.68078	1.41545	1.15679	1.00000
1.0	7.14580	2.90622	1.89205	1.50688	1.18006	1.00000
k	0.95098	0.77164	0.57955	0.42151	0.19263	0
m	6.86237	2.64135	1.52631	0.99382	0.41892	0
	a=	THIS BLOCK		g= 0.0		1.00
		0.60	0.80	0.90	0.95	
u=-1.0	0.31434	0.46772	0.59000	0.68866	0.84434	1.00000
-0.9	0.33005	0.48799	0.61104	0.70814	0.85695	1.00000
-0.7	0.36671	0.53429	0.65799	0.75061	0.88333	1.00000
-0.5	0.41254	0.59031	0.71275	0.79849	0.91139	1.00000
-0.3	0.47146	0.65945	0.77745	0.85290	0.94129	1.00000
-0.1	0.55031	0.74693	0.85507	0.91527	0.97321	1.00000
0.0	0.60000	0.80000	0.90000	0.95000	0.99000	1.00000
0.1	0.65999	0.86118	0.94991	0.98747	1.00738	1.00000
0.3	0.82498	1.01669	1.06841	1.07205	1.04403	1.00000
0.5	1.10013	1.24075	1.22070	1.17247	1.08345	1.00000
0.7	1.65277	1.59152	1.42361	1.29364	1.12597	1.00000
0.9	3.33525	2.21893	1.70742	1.44275	1.17196	1.00000
1.0	5.93064	2.75760	1.89635	1.53098	1.19639	1.00000
k	0.90736	0.71041	0.52543	0.37949	0.17251	0
m	6.21443	2.77038	1.66646	1.09974	0.46751	0
	a=	THIS BLOCK		g= 0.25		1.00
		0.60	0.80	0.90	0.95	
u=-1.0	0.22892	0.38700	0.52379	0.63754	0.81912	1.00000
-0.9	0.24700	0.41107	0.54896	0.66079	0.83398	1.00000
-0.7	0.29007	0.46649	0.60520	0.71141	0.86499	1.00000
-0.5	0.34528	0.53407	0.67083	0.76835	0.89787	1.00000
-0.3	0.41787	0.61789	0.74822	0.83277	0.93277	1.00000
-0.1	0.51640	0.72396	0.84056	0.90614	0.96989	1.00000
0.0	0.57967	0.78807	0.89367	0.94675	0.98934	1.00000
0.1	0.65584	0.86162	0.95231	0.99034	1.00942	1.00000
0.3	0.86485	1.04610	1.08983	1.08780	1.05159	1.00000
0.5	1.20575	1.30401	1.26257	1.20174	1.09667	1.00000
0.7	1.84409	1.68641	1.48515	1.33646	1.14495	1.00000
0.9	3.40908	2.30489	1.78146	1.49793	1.19677	1.00000
1.0	5.29588	2.77827	1.96917	1.59119	1.22413	1.00000
k	0.84071	0.63445	0.46176	0.33101	0.14961	0
m	6.27814	3.08711	1.90033	1.26325	0.53934	0

TABLE 25 (continued)

a=	THIS BLOCK		g= 0.50			
	0.60	0.80	0.90	0.95	0.99	1.00
u=-1.0	0.14873	0.29253	0.43595	0.56435	0.77961	1.00000
-0.9	0.16502	0.31755	0.46415	0.59145	0.79756	1.00000
-0.7	0.20534	0.37660	0.52811	0.65100	0.83513	1.00000
-0.5	0.25975	0.45092	0.60415	0.71869	0.87508	1.00000
-0.3	0.33502	0.54582	0.69529	0.79600	0.91760	1.00000
-0.1	0.44242	0.66914	0.80559	0.88472	0.96292	1.00000
0.0	0.51381	0.74492	0.86955	0.93405	0.98670	1.00000
0.1	0.60165	0.83268	0.94049	0.98713	1.01126	1.00000
0.3	0.84977	1.05499	1.10754	1.10604	1.06291	1.00000
0.5	1.26358	1.36664	1.31736	1.24508	1.11814	1.00000
0.7	2.02605	1.82111	1.58542	1.40887	1.17730	1.00000
0.9	3.68072	2.51974	1.93486	1.60351	1.24074	1.00000
1.0	5.34101	3.01894	2.15065	1.71481	1.27420	1.00000
k	0.75114	0.54183	0.38562	0.27334	0.12243	0
m	7.14941	3.71867	2.31684	1.54493	0.66045	0
a=	THIS BLOCK		g= 0.75			
	0.60	0.80	0.90	0.95	0.99	1.00
u=-1.0	0.06788	0.16503	0.29286	0.43027	0.69724	1.00000
-0.9	0.07787	0.18559	0.32116	0.46111	0.72067	1.00000
-0.7	0.10418	0.23685	0.38795	0.53077	0.77027	1.00000
-0.5	0.14290	0.30621	0.47163	0.61288	0.82381	1.00000
-0.3	0.20172	0.40152	0.57726	0.71003	0.88166	1.00000
-0.1	0.29443	0.53481	0.71172	0.82545	0.94420	1.00000
0.0	0.36085	0.62120	0.79258	0.89123	0.97737	1.00000
0.1	0.44705	0.72488	0.88443	0.96317	1.01188	1.00000
0.3	0.71186	1.00196	1.10846	1.12824	1.08519	1.00000
0.5	1.20231	1.41625	1.40221	1.32708	1.16465	1.00000
0.7	2.19009	2.05422	1.79198	1.56785	1.25086	1.00000
0.9	4.41049	3.07078	2.31592	1.86098	1.34449	1.00000
1.0	6.54962	3.80242	2.64471	2.03122	1.39431	1.00000
k	0.63191	0.42344	0.28808	0.19898	0.08710	0
m	9.86722	5.29064	3.30283	2.19681	0.93528	0
a=	THIS BLOCK		g= 0.875			
	0.60	0.80	0.90	0.95	0.99	1.00
u=-1.0	0.03012	0.08260	0.17216	0.29391	0.59365	1.00000
-0.9	0.03499	0.09544	0.19480	0.32376	0.62228	1.00000
-0.7	0.04834	0.12939	0.25125	0.39411	0.68412	1.00000
-0.5	0.06930	0.17935	0.32742	0.48188	0.75266	1.00000
-0.3	0.10378	0.25460	0.43123	0.59182	0.82864	1.00000
-0.1	0.16373	0.37084	0.57421	0.73018	0.91294	1.00000
0.0	0.21035	0.45218	0.66541	0.81246	0.95851	1.00000
0.1	0.27487	0.55533	0.77332	0.90509	1.00653	1.00000
0.3	0.49708	0.85681	1.05379	1.12726	1.11051	1.00000
0.5	0.98278	1.36500	1.45342	1.41074	1.22611	1.00000
0.7	2.15992	2.24928	2.02898	1.77378	1.35464	1.00000
0.9	5.32150	3.82926	2.96352	2.23910	1.49732	1.00000
1.0	8.64134	5.04368	3.41144	2.51777	1.57412	1.00000
k	0.55143	0.34478	0.22235	0.14798	0.06230	0
m	14.08599	7.67067	4.76768	3.14847	1.32705	0

## 11.2 THE MILNE PROBLEM: ESCAPE FUNCTION

The escape function  $K(\mu)$  was defined in Section 5.2.1 as the intensity distribution of the radiation emerging at the surface from a radiation field which, at deep layers, corresponds to an outward diffusion stream of strength 1. The problem of determining this function (and the radiation field at all depths) is usually called the Milne problem. The conservative case of a constant net outward flux has intrigued generations of research workers from the studies by Chwolson and by Lommel around 1890 (see start of Chapter 7). The corresponding problem for a nonconservative atmosphere was solved by Chandrasekhar (Appendix to his 1950 book) for a linearly anisotropic phase function, and the general solution in terms of  $H$  functions is given in Display 6.11.

The results for Henyey–Greenstein phase functions presented below were all obtained by means of asymptotic fitting. Table 26 gives the escape functions, together with the moments and derived constants defined in Section 6.4.3. These results check quite well with those tabulated for  $g = 0.5, 0.75, 0.8, 0.85$ , and  $0.9$  by Dlugach and Yanovitskii (1974). Their Tables 4, 6, 8, 10, 12, and 14 give  $aK(\mu)$ , and their Table 17 gives  $l$ .

A selection of these functions has been plotted in Fig. 11.2. A striking feature is that the curves for conservative scattering ( $a = 1$ ) almost coincide. This remains true if we choose conservative phase functions from different sets, as will be shown more fully in Section 12.1.2 (Table 30). The curves for nonconservative scattering also run closely together, but it is clear that an even closer match could be obtained by making not only the values of  $g$ , but also the values of  $a$  different. This question is taken up in a wider context as the similarity problem in Section 12.2.

## 11.3 THE REFLECTION FUNCTION

The azimuth independent part of the reflection function of a semi-infinite layer with Henyey–Greenstein phase function, again obtained by the asymptotic fitting method, is presented in Table 27.† The moments and the three bi-moments obtained with the operators  $N$  and  $U$  are also given. In most entries of Table 27 the last decimal is significant but errors up to 0.00018 occur in the pages referring to  $g = 0.875$ , where it was necessary to start the asymptotic fitting process with  $b = 32$ .

As explained in Section 6.1, there is no way to represent this function of the two variables  $\mu$  and  $\mu_0$  in a simple manner in terms of functions of one variable,  $\mu$  or  $\mu_0$ . It is nevertheless interesting to make an empirical check if a formula of

† Table 27 is placed at the end of the chapter, beginning on page 345.

TABLE 26  
Escape Function and Derived Constants

THIS BLOCK $g = -0.25$						
	$\alpha = 0.60$	0.80	0.90	0.95	0.99	1.00
FUNCTION $k(\alpha, g, \mu)$						
$\mu = 0.0$	0.05629	0.16080	0.24413	0.30178	0.37324	0.42392
0.1	0.06632	0.19645	0.30289	0.37707	0.46885	0.53320
0.3	0.08730	0.26324	0.40508	0.50246	0.62218	0.70672
0.5	0.12046	0.35083	0.52099	0.63258	0.76899	0.86933
0.7	0.18979	0.48896	0.66936	0.77956	0.91697	1.02822
0.9	0.44478	0.75945	0.87918	0.95500	1.06935	1.18543
1.0	1.17723	1.02920	1.02415	1.05826	1.14796	1.26368
MOMENTS						
KN	0.19940	0.41678	0.55717	0.64983	0.76890	0.86394
KU	0.28805	0.53378	0.67677	0.77008	0.89411	0.99996
KW	0.23648	0.40479	0.49605	0.55573	0.63767	0.71113
DERIVED CONSTANTS						
$l$	0.12789	0.31504	0.47296	0.60054	0.80107	1.00000
$q$	1.07955	0.74843	0.64597	0.60488	0.57575	0.56892
$(1-g)q$	1.34944	0.93553	0.80747	0.75610	0.71969	0.71115
THIS BLOCK $g = 0.0$						
	$\alpha = 0.60$	0.80	0.90	0.95	0.99	1.00
FUNCTION $k(\alpha, g, \mu)$						
$\mu = 0.0$	0.07102	0.17030	0.24877	0.30482	0.37762	0.43301
0.1	0.08525	0.20877	0.30776	0.37870	0.47065	0.54012
0.3	0.11573	0.28148	0.41089	0.50237	0.62072	0.71123
0.5	0.16198	0.37327	0.52502	0.62893	0.76396	0.87156
0.7	0.25098	0.50799	0.66475	0.76828	0.90733	1.02796
0.9	0.51297	0.74072	0.84987	0.92886	1.05361	1.18238
1.0	1.00721	0.93987	0.96981	1.02036	1.12844	1.25912
MOMENTS						
KN	0.23674	0.42575	0.55282	0.64173	0.76286	0.86603
KU	0.33000	0.53603	0.66542	0.75626	0.88442	0.99995
KW	0.26401	0.40176	0.48493	0.54400	0.62987	0.71041
DERIVED CONSTANTS						
$l$	0.11628	0.28279	0.43617	0.56687	0.78068	1.00000
$q$	1.18511	0.88896	0.78957	0.74788	0.71762	0.71044
$(1-g)q$	1.18511	0.88896	0.78957	0.74788	0.71762	0.71044
THIS BLOCK $g = 0.25$						
	$\alpha = 0.60$	0.80	0.90	0.95	0.99	1.00
FUNCTION $k(\alpha, g, \mu)$						
$\mu = 0.0$	0.07132	0.15995	0.23350	0.28847	0.36349	0.42419
0.1	0.08820	0.19970	0.29280	0.36248	0.45747	0.53407
0.3	0.12565	0.27540	0.39625	0.48565	0.60787	0.70816
0.5	0.18230	0.36942	0.50922	0.61051	0.75063	0.87055
0.7	0.28522	0.50105	0.64375	0.74582	0.89271	1.02850
0.9	0.53333	0.70742	0.81395	0.89814	1.03675	1.18409
1.0	0.85506	0.86384	0.91899	0.98299	1.11005	1.26130
MOMENTS						
KN	0.24977	0.41292	0.53204	0.62069	0.74865	0.86440
KU	0.34333	0.51814	0.64038	0.73224	0.86946	0.99994
KW	0.27081	0.38665	0.46609	0.52663	0.61952	0.71086
DERIVED CONSTANTS						
$l$	0.09465	0.23813	0.38579	0.51997	0.75131	1.00000
$q$	1.40194	1.13086	1.03135	0.98787	0.95561	0.94786
$(1-g)q$	1.05145	0.84815	0.77351	0.74090	0.71671	0.71090

TABLE 26 (continued)

THIS BLOCK $g = 0.50$						
FUNCTION	$\alpha = 0.60$	0.80	0.90	0.95	0.99	1.00
$k(\alpha, g, \mu)$						
$\mu = 0.0$	0.05681	0.13063	0.19747	0.25068	0.32802	0.39508
0.1	0.07361	0.16992	0.25735	0.32703	0.42829	0.51597
0.3	0.11201	0.24447	0.35980	0.45069	0.58347	0.70090
0.5	0.17181	0.33725	0.47059	0.57395	0.72738	0.86914
0.7	0.27951	0.46562	0.60130	0.70620	0.86867	1.03029
0.9	0.51132	0.65798	0.76384	0.85375	1.01077	1.18760
1.0	0.74938	0.79421	0.86194	0.93527	1.08279	1.26533
MOMENTS						
KN	0.23435	0.37692	0.49127	0.58238	0.72313	0.85990
KU	0.32512	0.47807	0.59659	0.69209	0.84460	0.99993
KW	0.25642	0.35792	0.43557	0.49899	0.60284	0.71190
DERIVED CONSTANTS						
$l$	0.06259	0.17659	0.31311	0.44933	0.70430	1.00000
$q$	1.84458	1.60005	1.50564	1.46339	1.43160	1.42391
$(1-g)q$	0.92229	0.80002	0.75282	0.73169	0.71580	0.71195
THIS BLOCK $g = 0.75$						
FUNCTION	$\alpha = 0.60$	0.80	0.90	0.95	0.99	1.00
$k(\alpha, g, \mu)$						
$\mu = 0.0$	0.02874	0.07737	0.13052	0.17842	0.25656	0.33261
0.1	0.04101	0.11154	0.18903	0.25905	0.37330	0.48421
0.3	0.06996	0.17478	0.28304	0.37900	0.53607	0.69212
0.5	0.12032	0.25809	0.38594	0.49603	0.67852	0.86862
0.7	0.22041	0.38148	0.51285	0.62416	0.81627	1.03306
0.9	0.44578	0.57554	0.67774	0.77162	0.95503	1.19166
1.0	0.66790	0.71506	0.77986	0.85498	1.02576	1.26967
MOMENTS						
KN	0.18386	0.30231	0.41050	0.50596	0.67088	0.85244
KU	0.26738	0.39835	0.51206	0.61268	0.79218	0.99970
KW	0.21554	0.30366	0.37845	0.44520	0.56728	0.71315
DERIVED CONSTANTS						
$l$	0.02512	0.09100	0.19622	0.32353	0.60875	1.00000
$q$	2.91479	2.83015	2.82654	2.83566	2.84924	2.85322
$(1-g)q$	0.72870	0.70754	0.70664	0.70892	0.71231	0.71330
THIS BLOCK $g = 0.875$						
FUNCTION	$\alpha = 0.60$	0.80	0.90	0.95	0.99	1.00
$k(\alpha, g, \mu)$						
$\mu = 0.0$	0.01126	0.03768	0.07477	0.11424	0.18889	0.27219
0.1	0.01792	0.06218	0.12527	0.19280	0.32070	0.46285
0.3	0.03418	0.10684	0.20114	0.29815	0.48054	0.68796
0.5	0.06797	0.17445	0.29177	0.40483	0.61612	0.86886
0.7	0.14943	0.28997	0.41617	0.53045	0.74882	1.03478
0.9	0.37456	0.49818	0.59487	0.68618	0.88557	1.19363
1.0	0.62961	0.66267	0.71339	0.77895	0.95665	1.27130
MOMENTS						
KN	0.13411	0.22906	0.32708	0.42264	0.60903	0.84724
KU	0.20775	0.31906	0.42457	0.52541	0.72702	0.99645
KW	0.17324	0.25036	0.32023	0.38672	0.52268	0.71163
DERIVED CONSTANTS						
$l$	0.00861	0.03855	0.10393	0.20497	0.49557	1.00000
$q$	4.30793	4.71993	5.09060	5.35543	5.63707	5.70662
$(1-g)q$	0.53849	0.58999	0.63632	0.66943	0.70463	0.71333



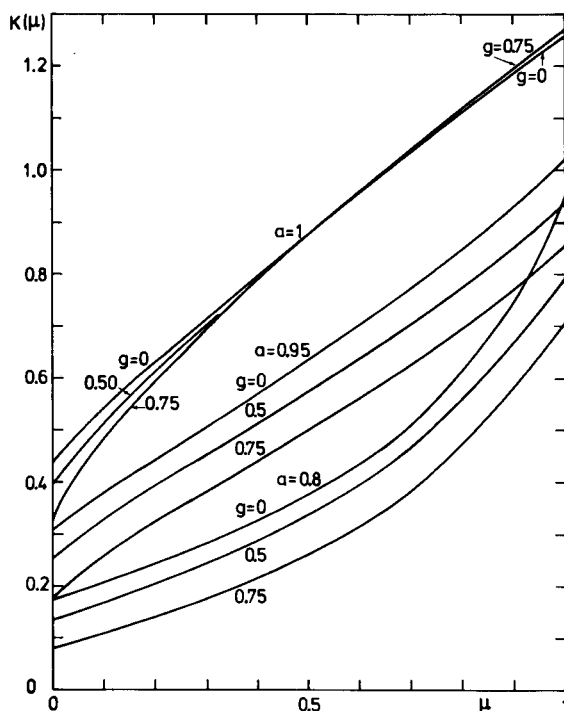


Fig. 11.2. Escape function  $K(a, \mu)$  for Henyey-Greenstein phase functions with three values of  $a$  and three values of  $g$ .

the type valid for isotropic scattering may be used here too. If  $R(a, g, \mu, \mu_0)$  were expressible in the form

$$f(a, g, \mu)f(a, g, \mu_0)/(\mu + \mu_0)$$

then the ratio

$$R(1, 1)R(0.1, 0.1)/[R(1, 0.1)]^2 = Q(1, 0.1)$$

should be  $121/40 = 3.025$ , independently of  $a$  and  $g$ . The numbers in Table 28 show that this is not the case.

TABLE 28

Ratios  $Q(1, 0.1)$  as Defined in Text for a Check on the Reflection Formula for Semi-Infinite Atmospheres

	$g = 0$	$g = 0.25$	$g = 0.50$	$g = 0.75$
$a = 0.6$	3.025	3.221	5.598	14.68
$a = 0.8$	3.025	3.504	6.300	16.85
$a = 0.95$	3.025	3.653	6.397	16.55
$a = 1$	3.025	3.574	5.585	11.48

We may, of course, go further in the search to represent the reflection function by an empirical formula of limited accuracy. In one example ( $g = 0.5$ ;  $a = 1$ ) we chose

$$R_{\text{approx}}(\mu, \mu_0) = g(\mu)g(\mu_0)/[c(\mu) + c(\mu_0)]$$

The numbers shown in the accompanying tabulation gave a difference  $R_{\text{exact}} - R_{\text{approx}}$  of at most 10%. A more precise fit over a limited domain of variables is possible.

$\mu = 0$	0.1	0.3	0.5	1
$c(\mu) = 0$	0.05	0.17	0.35	1.00
$g(\mu) = 0.39$	0.50	0.66	0.85	1.48

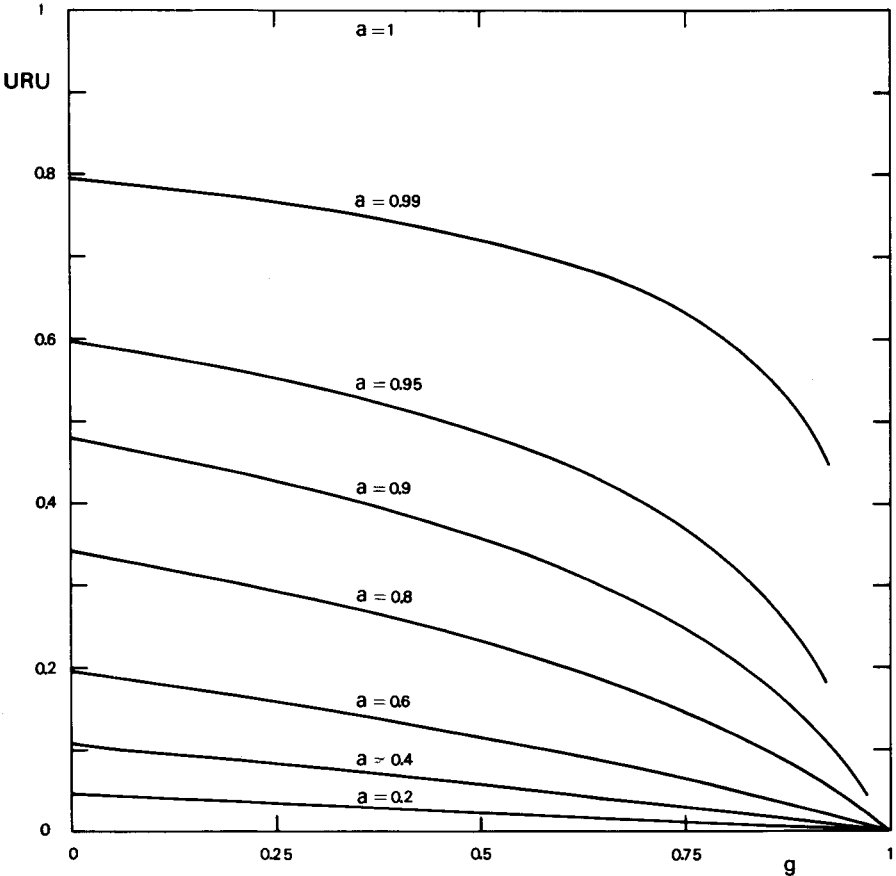


Fig. 11.3. Bimoment of reflection function  $URU$ , or spherical albedo, of a semi-infinite atmosphere with Henyey–Greenstein phase function and varying  $a$  and  $g$ .

The numbers presented in Table 27 may be used to find numbers for intermediate values of  $a$  and  $g$  by graphical interpolation. Figure 11.3 presents as an example the values of the important bimoment  $URU$ , which is the albedo for uniform incidence, also called the spherical albedo  $A^*$ .

In many cases, the interpolation may be eased by arranging the graphs in such a way that the numbers plotted should be approximately constant in virtue of the similarity law discussed in Section 12.2.

#### REFERENCES

- Dlugach, J. M., and Yanovitskii, E. G. (1974). *Icarus* **22**, 66.  
Jahnke, E., and Emde, F. (1945). "Tables of Functions." Dover, New York.  
van de Hulst, H. C., and Davis, M. M. (1961). *Proc. Koninkl. Nederl. Akad. Wet.* **B64**, 220.

TABLE 27

Reflection Function  $R(\mu, \mu_0)$  with Its Moments and Bi-Moments for Semi-Infinite Atmosphere,  
 $b = \infty$

$\mu_0$	$\mu=0.0$	0.100	0.300	0.500	0.700	0.900	1.000	N	FLUX
$g=0.0 \quad a=0.20$									
0.1	0.51281	0.26297							
0.3	0.17472	0.13439	0.09158						
0.5	0.10612	0.09070	0.06953	0.05630					
0.7	0.07642	0.06858	0.05607	0.04730	0.04088				
0.9	0.05978	0.05518	0.04700	0.04078	0.03598	0.03217			
1.0	0.05393	0.05029	0.04349	0.03815	0.03394	0.03055	0.02909		
N		0.12809	0.08049	0.06118	0.04987	0.04228	0.03932	0.07561	
FLUX	0.10557	0.08266	0.06238	0.05085	0.04312	0.03751	0.03523	0.05573	0.04626
$g=0.0 \quad a=0.40$									
0.1	1.05536	0.55689							
0.3	0.36930	0.29231	0.20457						
0.5	0.22784	0.20038	0.15776	0.12978					
0.7	0.16583	0.15313	0.12860	0.11020	0.09625				
0.9	0.13076	0.12420	0.10865	0.09576	0.08538	0.07694			
1.0	0.11834	0.11354	0.10085	0.08987	0.08080	0.07330	0.07002		
N		0.27680	0.17983	0.13919	0.11486	0.09823	0.09169	0.16818	
FLUX	0.22540	0.18252	0.14183	0.11759	0.10085	0.08845	0.08336	0.12702	0.10733
$g=0.0 \quad a=0.60$									
0.1	1.63702	0.89328							
0.3	0.59293	0.48532	0.35157						
0.5	0.37374	0.33990	0.27701	0.23281					
0.7	0.27619	0.26374	0.22926	0.20071	0.17798				
0.9	0.22028	0.21637	0.19592	0.17642	0.15970	0.14557			
1.0	0.20031	0.19874	0.18272	0.16637	0.15187	0.13934	0.13375		
N		0.45674	0.30978	0.24581	0.20634	0.17872	0.16770	0.28895	
FLUX	0.36754	0.30977	0.24999	0.21208	0.18485	0.16408	0.15541	0.22515	0.19472
$g=0.0 \quad a=0.80$									
0.1	2.27762	1.29688							
0.3	0.86706	0.74056	0.56384						
0.5	0.56531	0.53648	0.45952	0.39946					
0.7	0.42844	0.42692	0.39006	0.35321	0.32123				
0.9	0.34857	0.35725	0.34000	0.31668	0.29401	0.27337			
1.0	0.31964	0.33092	0.31979	0.30116	0.28195	0.26388	0.25543		
N		0.69404	0.50098	0.41326	0.35681	0.31586	0.29911	0.46851	
FLUX	0.55279	0.49071	0.41836	0.36797	0.32939	0.29853	0.28525	0.38197	0.34187



TABLE 27 (continued)

$\mu_0$	$\mu=0.0$	0.100	0.300	0.500	0.700	0.900	1.000	N	FLUX
$g=0.25$		$a=0.20$							
0.1	0.55371	0.28080							
0.3	0.18403	0.13800	0.08823						
0.5	0.10691	0.08803	0.06216	0.04615					
0.7	0.07242	0.06207	0.04619	0.03549	0.02800				
0.9	0.05260	0.04613	0.03552	0.02801	0.02256	0.01851			
1.0	0.04554	0.04028	0.03145	0.02508	0.02039	0.01687	0.01542		
N		0.12924	0.07490	0.05228	0.03902	0.03024	0.02689	0.06867	
FLUX	0.10471	0.07803	0.05366	0.03987	0.03085	0.02452	0.02204	0.04588	0.03468
$g=0.25$		$a=0.40$							
0.1	1.13854	0.59464							
0.3	0.38732	0.30019	0.19854						
0.5	0.22787	0.19463	0.14312	0.10937					
0.7	0.15571	0.13894	0.10833	0.08609	0.06981				
0.9	0.11389	0.10431	0.08465	0.06933	0.05759	0.04849			
1.0	0.09892	0.09153	0.07550	0.06265	0.05260	0.04469	0.04136		
N		0.27896	0.16859	0.12102	0.09237	0.07297	0.06546	0.15378	
FLUX	0.22184	0.17236	0.12399	0.09514	0.07555	0.06142	0.05577	0.10658	0.08340
$g=0.25$		$a=0.60$							
0.1	1.76402	0.95338							
0.3	0.61923	0.49853	0.34407						
0.5	0.37151	0.33088	0.25568	0.20262					
0.7	0.25770	0.24065	0.19841	0.16433	0.13781				
0.9	0.19092	0.18366	0.15846	0.13579	0.11700	0.10158			
1.0	0.16683	0.16219	0.14278	0.12416	0.10826	0.09492	0.08909		
N		0.45991	0.29320	0.21839	0.17176	0.13928	0.12645	0.26683	
FLUX	0.35931	0.29317	0.22293	0.17813	0.14621	0.12230	0.11248	0.19368	0.15801
$g=0.25$		$a=0.80$							
0.1	2.45051	1.38267							
0.3	0.90199	0.76132	0.55780						
0.5	0.56007	0.52515	0.43397	0.36219					
0.7	0.39991	0.39471	0.35020	0.30684	0.26964				
0.9	0.30423	0.31036	0.28961	0.26340	0.23831	0.21565			
1.0	0.26926	0.27834	0.26522	0.24508	0.22454	0.20530	0.19632		
N		0.69916	0.48095	0.37855	0.31170	0.26309	0.24330	0.44009	
FLUX	0.53848	0.46767	0.38362	0.32457	0.27939	0.24350	0.22818	0.34086	0.29409



TABLE 27 (continued)

$\mu_0$	$\mu=0.0$	0.100	0.300	0.500	0.700	0.900	1.000	N	FLUX
g=0.50    o=0.20									
0.1	0.71439	0.34869							
0.3	0.21300	0.14928	0.08159						
0.5	0.10435	0.08012	0.04923	0.03228					
0.7	0.05862	0.04753	0.03181	0.02227	0.01620				
0.9	0.03569	0.03021	0.02167	0.01601	0.01216	0.00945			
1.0	0.02852	0.02459	0.01818	0.01375	0.01064	0.00840	0.00752		
N		0.13952	0.06797	0.04042	0.02618	0.01798	0.01517	0.06310	
FLUX	0.10408	0.07031	0.04161	0.02721	0.01888	0.01370	0.01182	0.03499	0.02315
g=0.50    o=0.40									
0.1	1.46856	0.74070							
0.3	0.44635	0.32678	0.18754						
0.5	0.22130	0.17918	0.11725	0.08036					
0.7	0.12567	0.10826	0.07791	0.05733	0.04326				
0.9	0.07732	0.06990	0.05426	0.04228	0.03337	0.02671			
1.0	0.06210	0.05731	0.04594	0.03669	0.02953	0.02402	0.02175		
N		0.30159	0.15504	0.09599	0.06428	0.04538	0.03873	0.14173	
FLUX	0.21904	0.15644	0.09885	0.06780	0.04883	0.03646	0.03185	0.08285	0.05779
g=0.50    o=0.60									
0.1	2.27391	1.19074							
0.3	0.71029	0.54633	0.33285						
0.5	0.35941	0.30892	0.21785	0.15777					
0.7	0.20822	0.19189	0.15033	0.11759	0.09300				
0.9	0.13072	0.12707	0.10806	0.08983	0.07451	0.06203			
1.0	0.10605	0.10541	0.09278	0.07914	0.06700	0.05672	0.05224		
N		0.49770	0.27410	0.17912	0.12559	0.09224	0.08011	0.24743	
FLUX	0.35231	0.26852	0.18388	0.13403	0.10137	0.07877	0.07002	0.15482	0.11523
g=0.50    o=0.80									
0.1	3.15377	1.72929							
0.3	1.02906	0.84032	0.55519						
0.5	0.54159	0.50000	0.38868	0.30392					
0.7	0.32717	0.32641	0.28462	0.24155	0.20426				
0.9	0.21469	0.22687	0.21574	0.19504	0.17315	0.15262			
1.0	0.17815	0.19267	0.18984	0.17620	0.15969	0.14314	0.13523		
N		0.75700	0.46014	0.32616	0.24567	0.19222	0.17184	0.41400	
FLUX	0.52488	0.43465	0.33172	0.26339	0.21400	0.17681	0.16153	0.28560	0.23184





TABLE 27 (continued)

$\mu_0$	$\mu=0.0$	0.100	0.300	0.500	0.700	0.900	1.000	N	FLUX
$g=0.75$		$a=0.20$							
0.1	1.20610	0.48260							
0.3	0.22366	0.13118	0.05354						
0.5	0.07214	0.05060	0.02642	0.01530					
0.7	0.03095	0.02424	0.01486	0.00963	0.00658				
0.9	0.01594	0.01341	0.00918	0.00645	0.00469	0.00352			
1.0	0.01201	0.01038	0.00742	0.00539	0.00402	0.00308	0.00272		
N		0.15734	0.04903	0.02210	0.01212	0.00749	0.00608	0.05840	
FLUX	0.10372	0.05408	0.02374	0.01303	0.00810	0.00545	0.00457	0.02192	0.01158
$g=0.75$		$a=0.40$							
0.1	2.48627	1.04969							
0.3	0.46995	0.30036	0.13300						
0.5	0.15413	0.11922	0.06819	0.04125					
0.7	0.06709	0.05804	0.03907	0.02650	0.01853				
0.9	0.03497	0.03242	0.02434	0.01794	0.01339	0.01018			
1.0	0.02649	0.02518	0.01970	0.01501	0.01150	0.00894	0.00793		
N		0.34559	0.11653	0.05524	0.03122	0.01966	0.01606	0.13113	
FLUX	0.21730	0.12396	0.05978	0.03452	0.02207	0.01509	0.01271	0.05299	0.03004
$g=0.75$		$a=0.60$							
0.1	3.86294	1.73217							
0.3	0.75221	0.52874	0.25850						
0.5	0.25397	0.21890	0.14007	0.09021					
0.7	0.11349	0.10966	0.08293	0.06018	0.04389				
0.9	0.06049	0.06249	0.05272	0.04167	0.03254	0.02548			
1.0	0.04625	0.04891	0.04296	0.03514	0.02822	0.02262	0.02028		
N		0.58025	0.21702	0.11067	0.06577	0.04285	0.03545	0.22927	
FLUX	0.34737	0.22017	0.11977	0.07448	0.04993	0.03521	0.03001	0.10243	0.06369
$g=0.75$		$a=0.80$							
0.1	5.37740	2.58884							
0.3	1.10202	0.86534	0.48237						
0.5	0.39461	0.38550	0.28584	0.20328					
0.7	0.18711	0.20533	0.18100	0.14589	0.11503				
0.9	0.10527	0.12321	0.12122	0.10680	0.09049	0.07547			
1.0	0.08249	0.09863	0.10097	0.09211	0.08040	0.06875	0.06332		
N		0.89871	0.39136	0.22510	0.14688	0.10291	0.08772	0.38689	
FLUX	0.51314	0.37229	0.23990	0.16808	0.12315	0.09296	0.08147	0.20190	0.14362



TABLE 27 (continued)

$\mu_0$	$\mu=0.0$	0.100	0.300	0.500	0.700	0.900	1.000	N	FLUX
$g=0.875 \quad a=0.20$									
0.1	1.70381	0.45776							
0.3	0.15198	0.08043	0.02800						
0.5	0.03801	0.02617	0.01268	0.00700					
0.7	0.01480	0.01162	0.00681	0.00428	0.00286				
0.9	0.00729	0.00619	0.00410	0.00282	0.00202	0.00150			
1.0	0.00542	0.00473	0.00329	0.00234	0.00172	0.00131	0.00115		
N		0.14743	0.02802	0.01082	0.00557	0.00334	0.00269	0.05644	
FLUX	0.10367	0.03606	0.01206	0.00605	0.00361	0.00238	0.00198	0.01352	0.00578
$g=0.875 \quad a=0.40$									
0.1	3.53373	1.05937							
0.3	0.32413	0.19821	0.07476						
0.5	0.08265	0.06531	0.03439	0.01940					
0.7	0.03261	0.02907	0.01847	0.01190	0.00803				
0.9	0.01621	0.01549	0.01108	0.00782	0.00567	0.00422			
1.0	0.01210	0.01184	0.00885	0.00648	0.00483	0.00368	0.00324		
N		0.33551	0.07009	0.02805	0.01466	0.00885	0.00713	0.12656	
FLUX	0.21698	0.08677	0.03187	0.01645	0.00992	0.00656	0.00546	0.03315	0.01527
$g=0.875 \quad a=0.60$									
0.1	5.53997	1.87715							
0.3	0.53167	0.38250	0.16146						
0.5	0.14010	0.12959	0.07691	0.04534					
0.7	0.05652	0.05837	0.04170	0.02823	0.01946				
0.9	0.02855	0.03129	0.02501	0.01861	0.01383	0.01043			
1.0	0.02144	0.02398	0.01996	0.01539	0.01179	0.00912	0.00806		
N		0.58799	0.14036	0.05973	0.03217	0.01972	0.01596	0.22094	
FLUX	0.34624	0.16345	0.06875	0.03749	0.02317	0.01548	0.01293	0.06559	0.03351
$g=0.875 \quad a=0.80$									
0.1	7.81657	3.05499							
0.3	0.81477	0.70847	0.35383						
0.5	0.23042	0.25685	0.18273	0.11843					
0.7	0.09797	0.12074	0.10340	0.07768	0.05695				
0.9	0.05144	0.06666	0.06351	0.05263	0.04192	0.03300			
1.0	0.03923	0.05166	0.05107	0.04390	0.03614	0.02926	0.02628		
N		0.96135	0.28342	0.13658	0.07944	0.05111	0.04206	0.37259	
FLUX	0.50928	0.29840	0.15571	0.09550	0.06335	0.04420	0.03746	0.13577	0.08194

TABLE 27 (continued)

$\mu_0$	$\mu=0.0$	0.100	0.300	0.500	0.700	0.900	1.000	N	FLUX
<b>g=0.875    <math>\alpha=0.90</math></b>									
0.1	9.11958	3.88141							
0.3	1.02468	0.99743	0.56578						
0.5	0.31397	0.39133	0.31871	0.22699					
0.7	0.14330	0.19654	0.19272	0.15978	0.12628				
0.9	0.07986	0.11466	0.12473	0.11429	0.09847	0.08245			
1.0	0.06249	0.09101	0.10253	0.09746	0.08692	0.07501	0.06916		
N		1.24767	0.43843	0.23980	0.15330	0.10602	0.08986	0.51509	
FLUX	0.62546	0.42689	0.26578	0.18364	0.13307	0.09934	0.08655	0.22562	0.15681
<b>g=0.875    <math>\alpha=0.95</math></b>									
0.1	9.84172	4.40365							
0.3	1.17401	1.22176	0.75961						
0.5	0.38869	0.51736	0.46299	0.35702					
0.7	0.19199	0.28023	0.30104	0.26975	0.22836				
0.9	0.11527	0.17558	0.20833	0.20567	0.18934	0.16818			
1.0	0.09338	0.14410	0.17667	0.18066	0.17191	0.15721	0.14887		
N		1.45580	0.58717	0.35887	0.25147	0.18795	0.16490	0.64962	
FLUX	0.71293	0.54252	0.38652	0.29538	0.23259	0.18640	0.15755	0.33182	0.25720
<b>g=0.875    <math>\alpha=0.99</math></b>									
0.1	10.49104	4.93838							
0.3	1.36301	1.52293	1.07200						
0.5	0.51701	0.73715	0.74446	0.64781					
0.7	0.29814	0.46299	0.55405	0.55236	0.51976				
0.9	0.20895	0.33647	0.43838	0.47433	0.47818	0.46463			
1.0	0.18235	0.29669	0.39680	0.44156	0.45689	0.45402	0.44802		
N		1.73831	0.85993	0.62549	0.50959	0.43560	0.40677	0.91684	
FLUX	0.85009	0.75082	0.64554	0.57201	0.51272	0.46235	0.43968	0.59027	0.52992
<b>g=0.875    <math>\alpha=1.00</math></b>									
0.1	10.71578	5.17768							
0.3	1.49664	1.74590	1.36420						
0.5	0.65346	0.97024	1.07612	1.04258					
0.7	0.44430	0.71262	0.91774	0.99564	1.02609				
0.9	0.36546	0.60343	0.83059	0.95823	1.03724	1.08767			
1.0	0.34388	0.57207	0.80225	0.94371	1.03944	1.10574	1.13090		
N		1.98767	1.17883	1.00122	0.93236	0.89897	0.88853	1.28083	
FLUX	1.00004	1.00006	1.00010	1.00012	1.00015	1.00018	1.00014	1.00012	1.00014

## 12 ☐ Other Phase Functions, Semi-Infinite Atmospheres

### 12.1 COMMENTS AND COMPARISONS, CONSERVATIVE SCATTERING

We shall later (Section 14.1.1) formulate similarity rules which serve to transform the albedo  $a$  and the depth  $b$  of the layer in such a manner that a problem solved for two different phase functions is likely to give similar results.

These similarity rules are not rigorous, so only numerical tests can show how well they are obeyed. In this chapter and Chapter 14 we present such tests based on our own results for Henyey–Greenstein phase functions and results found scattered in the literature for many different phase functions.

In the present section the similarity concept is completely degenerated; everything is similar. For instance, in the reflection problem the complete incident flux comes back out, because nothing is lost by transmission from the bottom ( $b = \infty$ ) nor by absorption inside ( $a = 1$ ). We should not be surprised, therefore, to find that the reflection function of the total atmosphere has only a weak signature of the particular phase function employed. Similarly, for any phase function, the radiation in the Milne problem will escape from the atmosphere with roughly the same angular distribution. What is surprising is how well these statements are fulfilled.

### 12.1.1 Worked Examples

An example of an accurately worked out solution for a quite different phase function (Busbridge and Orchard, 1968) is presented in Table 29. It refers to a phase function with a finite Legendre expansion with  $N = 3$ . This example provides the opportunity for many numerical checks. An alternative expression for the characteristic function (Display 6.8) is

$$2\Psi(\mu) = \sum_{n=0}^N \omega_n (-1)^n q_n(\mu) q_n(-\mu)$$

Substitution gives literal and numerical values as follows

$$\text{coefficient of } \mu^0: 1 + \omega_2/4 = 1.25$$

$$\text{coefficient of } \mu^2: 2c_{01} - \omega_2 c_{21} - c_{00}^2 - \omega_2 c_{20}^2 + \omega_3 c_{30}^2 = 0.25000$$

$$\text{coefficient of } \mu^4: c_{01}^2 + \omega_2 c_{21}^2 - \omega_3 c_{31}^2 = -1.66667$$

agreeing with the coefficients given in Table 29. Further checks follow from

$$b_0 = 2l_0 - \omega_2 l_2$$

$$b_1 = 2(l_0 c_{00} + \omega_2 l_2 c_{20} + \omega_3 l_3 c_{30})$$

$$0 = l_0 c_{01} + \omega_2 l_2 c_{21} + \omega_3 l_3 c_{31}$$

One detail may be mentioned. In the course of the computation it was desirable to know  $\alpha_4$ , which was not tabulated by Busbridge and Orchard. Instead of returning to a numerical integration of the  $H$  function, it appeared faster to extrapolate from  $\alpha_n$ ,  $n = 0-3$ , by considering that the product  $(n+2)\alpha_n$  must reach a finite limit for  $n \rightarrow \infty$ , and that this limit is  $H(1) = 3.29006$  by exactly the same reasoning as in isotropic scattering (Section 8.3.3). Differentially,

$$\lim_{n \rightarrow \infty} (n+2)(\alpha_{n, \text{this example}} - \alpha_{n, \text{isotropic}}) = 3.29006 - 2.90780 = 0.38226$$

A simple linear interpolation with respect to  $n^{-1}$  then gives  $\alpha_n$  for any  $n \geq 4$  with the desired accuracy.

Numerical results fully comparable to the example just shown are presented by Kolesov and Smoktii (1971) for 13 phase functions with  $N = 2$  and  $N = 3$  chosen to give a close fit to certain Mie scattering functions (Section 10.3.1). The Rayleigh phase function, for which many transfer computations have been published (Section 16.2.2), is another example of a phase function with  $N = 2$ . Solutions for the  $N = 2$  phase functions have been derived quite early (Mark, 1943, as quoted by Kuščer, 1958).

An example quite different from anything we have treated so far is Rayleigh scattering, because it involves polarization. For instance, in the Milne problem for Rayleigh scattering the flux  $\pi$ , carried through the atmosphere to its surface,

**TABLE 29**  
A Worked Example with a Four-Term Phase Function<sup>a</sup>

Given:

$$\begin{aligned}\omega_0 &= \omega_2 = \omega_3 = 1, \quad \omega_1 \text{ is arbitrary} \\ \omega_n &= 0 \text{ for } n \geq 4 \quad (N = 3)\end{aligned}$$

Characteristic function:

$$2\Psi(\mu) = \frac{5}{4} + \frac{1}{4}\mu^2 - \frac{5}{3}\mu^4$$

$H$  function:

$H(0) = 1$		$H(1) = 3.29006$	
$\alpha_0 = 2.19861$		$\gamma_{00} = \alpha_1 - \frac{5}{3}\alpha_3 = 0.09302$	
$\alpha_1 = 1.28506$		$\gamma_{01} = 1 - \frac{3}{4}\alpha_0 + \frac{3}{4}\alpha_2 = -0.06017$	
$\alpha_2 = 0.91747$		$\delta_{02} = -\frac{5}{4}\alpha_1 + \frac{3}{4}\alpha_3 = -1.06991$	
$\alpha_3 = 0.71522$			
$\alpha_4 = 0.5865$			
$D = 1.31969$	$D^{-1} = 0.75775$	$l_0 = 0.86194$	
$b_0 = 1.62145$	$b_1 = -0.09118$	$l_1 = 0.50000$	
$c_0 = 0.69521$	$c_1 = 0.97376$	$l_2 = 0.10244$	
$c_{00} = -0.22569$	$c_{01} = 0.09964$	$l_3 = -0.05862$	
$c_{20} = 0.92357$	$c_{21} = -0.09541$		
$c_{30} = -0.92695$	$c_{31} = 1.29834$		

<sup>a</sup> For notation see Section 6.4.2, Displays 6.9 and 6.10.

escapes at the surface ( $\tau = 0$ ) with partial linear polarization. The intensity and polarization of the emerging radiation in any direction may be read from Table 53 (Section 16.3.2).

### 12.1.2 An Accurate Numerical Comparison of Results for Different $\omega_2, \omega_3$

Accurate solutions as sketched above are available for many phase functions with  $N \leq 3$ . The accuracy chiefly depends on the care with which the  $H$  function has been solved. Most authors have followed Chandrasekhar's example of presenting results with about 5 figure accuracy. The asymptotic fitting results for the Henyey-Greenstein phase functions presented in the tables of Chapter 11 have a similar accuracy.

A detailed comparison of some key quantities for each of these phase functions is made in Table 30. The similarity is striking. In spite of the enormous variations in the shape of the scattering diagram, the total spread in  $K(1)$  remains  $< 2\%$ , and in the reduced extrapolation length  $q'$  remains below  $1\%$ . The spread in  $K(0)$  is larger, illustrating the well known sensitivity of the intensity in grazing directions to changes in the model.



TABLE 30  
Numerical Comparison of Results for Various Conservative Phase Functions

Part I Specification of Phase Function ( $\omega_0 = 1$ , $\omega_1$ arbitrary)					Reference
Code	$\omega_2$	$\omega_3$	$N$	Name	
Unpolarized					
$I$	0	0	0 or 1	Isotropic or linearly anisotropic	Chandrasekhar (1950)
$P$	0.5	0	2	Rayleigh phase function	Chandrasekhar (1950)
$C$	1	0	2	—	Horak and Janousek (1965)
$D$	1.5	0	2	—	Horak and Janousek (1965)
$E$	1	0.5	3	—	Busbridge and Orchard (1968)
$E'$	1	1	3	—	Busbridge and Orchard (1968)
$H(\frac{1}{4})$	0.3125	0.1094	$\infty$	Henryey-Greenstein function with $g = \frac{1}{4}$	Chapter 11
$H(\frac{1}{3})$	0.5556	0.2593	$\infty$	Henryey-Greenstein function with $g = \frac{1}{3}$	Chapter 11
$H(\frac{1}{2})$	1.2500	0.8750	$\infty$	Henryey-Greenstein function with $g = \frac{1}{2}$	Chapter 11
$H(\frac{2}{3})$	2.8125	2.9531	$\infty$	Henryey-Greenstein function with $g = \frac{2}{3}$	Chapter 11
$H(\frac{3}{4})$	3.8281	4.6895	$\infty$	Henryey-Greenstein function with $g = \frac{3}{4}$	Chapter 11
Same, combined with forward peak $F$					
$(1-g)I + gF$	$5g$	$7g$	$\infty$		
$(1-g)C + gF$	$1 + 4g$	$7g$	$\infty$		
$(1-g)E' + gF$	$1 + 4g$	$1 + 6g$	$\infty$		
$F$	$\frac{5}{7}$	$7$	$\infty$		
Polarized					
$R$	—	—	2	Rayleigh scattering	Chandrasekhar (1950)
$cR + (1-c)I$	—	—	2	Mixed isotropic and Rayleigh scattering	Bond and Siewert (1971)

Part II Computed Quantities<sup>a</sup> ( $l_1$  is always  $\frac{1}{2}$ )

Code	$K(0)$	$K(1)$	$q_0(1 - g)$	$l_0$	$l_2$	$l_3$	$l_4$
$I$	0.4330	1.2591	0.7104	0.8660	0.0998	-0.0596	-0.0178
$P$	0.4188	1.2646	0.7114	0.8630	0.1020	—	—
$C$	0.4037	1.2708	0.7125	0.8597	0.1045	—	—
$D$	0.3878	1.2779	0.7137	0.8560	0.1072	—	—
$E$	0.3933	1.2649	0.7119	—	—	—	—
$E'$	0.3826	1.2587	0.7112	0.8619	0.1024	-0.0586	—
$H(\frac{1}{4})$	0.4242	1.2613	0.7109	0.8644	0.1010	—	—
$H(\frac{1}{3})$	0.4171	1.2625	0.7112	0.8632	0.1018	—	—
$H(\frac{1}{2})$	0.3951	1.2653	0.7120	0.8599	0.1040	-0.0574	-0.0159
$H(\frac{3}{4})$	0.3326	1.2697	0.7134	0.8524	0.1088	—	—
$H(\frac{7}{8})$	0.2722	1.2713	0.7140	0.8427	0.1118	—	—
(1 - g)X + gF All values are the same as for phase function X, X arbitrary, 0 ≤ g < 1							
$F$	Undetermined						
$R$	0.4144	1.2694	0.7121	0.8612	0.1035	—	—
$0.8R + 0.2I$	—	—	0.7116	—	—	—	—
$0.6R + 0.4I$	—	—	0.7112	—	—	—	—
$0.4R + 0.6I$	—	—	0.7109	—	—	—	—

<sup>a</sup> Numbers are probably correct to the last digit given.

We can even go a step further by examining whether these data permit interpolation in an  $(\omega_2, \omega_3)$  plane. The question has to be put in this form because  $\omega_0 = 1$  is constant and  $\omega_1$  irrelevant. A detailed test of this idea was carried out for the extrapolation length. This test, presented below, greatly extends results published earlier (van de Hulst, 1971). Figure 12.1 shows a plot in the  $(\omega_2, \omega_3)$  plane of all the information on precisely computed extrapolation lengths for conservative, unpolarized phase functions that was available to the author. Encircled numbers are the 3rd and 4th digit of each computed value. The total spread is from  $q' = 0.7092$  (extreme left) to  $q' = 0.7150$  (extreme right). This spread is already less than 1 %, and yet the variation within it, both with  $\omega_2$  and with  $\omega_3$ , is seen to be very systematic. By interpolation, the value of  $q'$  can be predicted to one or two units in the fourth decimal. In practice the values of  $\omega_n$  with  $n \geq 4$  do not seem to matter much.

The following material has been used:

- (1) Codes *I, P, C, D, E, E'*: Simple phase functions listed in Table 30.
- (2) Code *H*: Henyey–Greenstein phase functions with the value of  $g$  written in parentheses. For values of  $g$  not shown in Table 30, the  $q'$  value was obtained by interpolation.
- (3) Axis  $\omega_3 = 0$ : Additional values from the Horak–Janousek tables, in agreement with Table 6.7 of Case and Zweifel (1967).
- (4) Code *S*: The isotropic sector phase function (Display 10.1, number 22) again with  $g$  written in parentheses. Values of  $q'$  for this phase function were made available to the author by Dr. R. Aronson (private communication) from an unpublished thesis at New York University (1969) of G. Carroll. This is a quite unrealistic type of phase function, as shown also by the strange locus of the points in Fig. 12.1, but the values fit the pattern quite well.

These data amply suffice for the following discussion, but even more values are probably available in journals of nuclear physics (e.g., Su and McCormick, 1971) and possibly also in the literature of atmospheric physics. Vanmassenhove (1969) adopts the phase function ( $N = 2$ ) with  $\omega_0 = 1$ ,  $\omega_1 = 0$ , and  $\omega_2 = 2$ , which would follow at equal distance the sequence *I, P, C, D*, in Table 30. He does not give enough decimals to make the result [ $\frac{1}{2}$  scalar density =  $l_0$ ,  $\frac{1}{4}$  angular density =  $K(\mu)$ ] better than that obtained from a straight extrapolation in Table 30. This statement refers to conservative scattering; the same paper presents results for  $a = 0.3, 0.5$ , and  $0.9$ .

More about the dependence on  $\omega_2, \omega_3$  can be found in two ways.

First, on the basis of the theory of Section 14.1.3, we can combine any phase function with a forward peak  $F$  and still obtain the same exact solutions and hence the same value of  $q'$ . The points for which this is true lie on straight lines in Fig. 12.1. All these lines converge to the point  $F(\omega_2 = 5, \omega_3 = 7)$ , which is far off scale. Starting from known points on the  $\omega_2$  axis, these lines have been drawn in at intervals of 0.0008 in  $q'$ .

Second, we may postulate expansions and with some effort find several exact coefficients. This will be illustrated for  $l_n$ . In the bottom relation in Display 6.12,

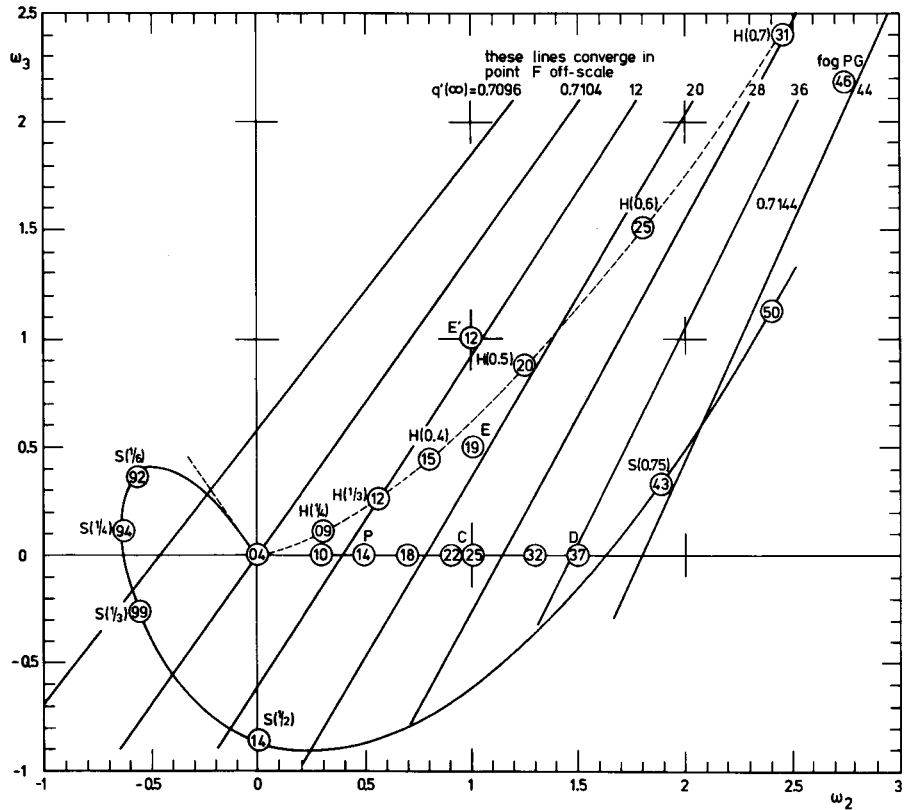


Fig. 12.1. Precise extrapolation lengths  $q'$  for conservative scattering computed for many phase functions and plotted in the  $\omega_2, \omega_3$  plane. The encircled numbers show the 3rd and 4th decimals, the first two being 0.70 or 0.71. See further explanation in text.

which is exact, we expand:

$$\begin{aligned} l_0 &= a + b\omega_2 + c\omega_2^2 + b'\omega_3 + b''\omega_4 + \dots \\ l_2 &= d + e\omega_2 + \dots \\ l_3 &= d' + \dots \\ l_4 &= d'' + \dots \end{aligned}$$

and now match the coefficients

of 1: $\frac{3}{4} = a^2$	well known for isotropic scattering
of $\omega_2$ : $0 = 2ab + d^2$	gives $b$
of $\omega^3$ : $0 = 2ab' + d'^2$	gives $b'$
of $\omega^4$ : $0 = 2ab'' + d''^2$	gives $b''$
of $\omega_2^2$ : $0 = b^2 + 2ac + 2de$	gives relation between $c$ and $e$

Starting from the known values of  $l_0-l_3$  for isotropic scattering (see Table 30), we can thus find at once

$$b = -0.00575, \quad b' = +0.00193, \quad b'' = -0.00018$$

and, upon using the empirical value  $e = 0.0043$ ,

$$c = -0.00052$$

The agreement with the empirical coefficients that may be derived from Table 30 is very gratifying. As final formulas, we suggest

$$K(1) = 1.259 + 0.012\omega_2 - 0.012\omega_3 + \dots$$

$$K(0) = 0.433 - 0.028\omega_2 - 0.021\omega_3 + \dots$$

$$l_0 = 0.8660 - 0.0057\omega_2 + 0.0020\omega_3 + \dots$$

$$l_2 = 0.0998 + 0.0043\omega_2 - 0.0021\omega_3 + \dots$$

$$q' = \frac{2}{3}l_0 + \frac{4}{3}l_2 = 0.7104 + 0.0019\omega_2 - 0.0014\omega_3 + \dots$$

The coefficients of  $\omega_2$  and  $\omega_3$  in most of these quantities are not in the ratio  $-7$  to  $5$ , as would result from adding a forward peak. This points to a real difference arising from the different values of  $\omega_4, \dots$ . Apparently  $q'$  is less sensitive to this difference than other quantities.

The significance of this analysis is that using only well known numbers from isotropic scattering, we have made a sensitive check on the accuracy of the numbers in Table 30. The fact that this check is simple and matches data obtained by entirely different methods (the reduction to  $H$  functions and asymptotic fitting) gives great confidence in the correct numerical execution of both methods.

Rayleigh scattering is seen in Table 30 to give deviations from the results for isotropic scattering which are nearly twice the deviations produced by the Rayleigh phase function.

### 12.1.3 Rapid-Guess Formulas

The practical man's comment on the preceding conclusion is "Reflection and escape for conservative semi-infinite atmospheres are largely independent of the assumed phase function. How can I rapidly arrive at reasonable estimates of these functions and of all related quantities?" The following treatment may please him.

Assume that  $R(\mu, \mu_0)$  depends linearly on  $\mu$  and  $\mu_0$ . In order that all incident energy be reflected ( $UR = 1$ ), and that  $R$  be symmetric in  $\mu$  and  $\mu_0$ , we must write

$$R(\mu, \mu_0) = 1 + c(1 - \frac{3}{2}\mu)(1 - \frac{3}{2}\mu_0)$$

where  $c$  is still undetermined. We can now glance through the various integrations of Chapter 5 in which  $R(\mu, \mu_0)$  appears and find its moments and bimo-  
ments, and the escape function  $K(\mu)$ , and their moments, the constants  $l_n$ . The  
results are in Display 12.1. In the same display we have tabulated, whenever

**DISPLAY 12.1**

Rapid-Guess Formulas for Conservative Scattering, Semi-Infinite Atmospheres

Rapid-guess formula	Value of $c$ that will give exact match <sup>a</sup>	
	For isotropic scattering $g = 0$	For Henyey-Greenstein phase function $g = 0.75$
$R(\mu, \mu_0) = 1 + c(1 - 3\mu/2)(1 - 3\mu_0/2)$	—	—
$R(1, 1) = 1 + c/4$	0.23	0.48
$K(\mu) = 1 - (\frac{1}{2} + c/16)(1 - 3\mu/2)$	—	—
$K(1) = \frac{5}{4} + c/24$	0.29	0.63
$NR = \int_0^1 R d\mu_0 = 1 + (c/4)(1 - 3\mu/2)$	0.37†	0.79†
$UR = \int_0^1 R 2\mu_0 d\mu_0 = 1$	—	—
$WR = \int_0^1 R 2\mu_0^2 d\mu_0 = \frac{2}{3} - (c/12)(1 - 3\mu/2)$	0.29†	0.63†
$VR = \int_0^1 R 2\mu_0^3 d\mu_0 = \frac{1}{2} - (c/10)(1 - 3\mu/2)$	N.C.	N.C.
$NRN = 1 + c/16$	1.08	2.98*
$WRN = \frac{2}{3} - c/48$	0.58	1.44
$VRN = \frac{1}{2} - c/40$	N.C.	N.C.
$WRW = \frac{4}{9} - c/144$	0.40	0.98
$WRV = \frac{1}{3} - c/120$	N.C.	N.C.
$NK = l_0 = \frac{7}{8} - c/64$	0.58	1.44
$UK = 2l_1 = 1$	—	—
$WK = q' = \frac{17}{24} + c/192$	0.40	0.98
$VK = \frac{11}{20} + c/160$	N.C.	N.C.
$l_2 = \frac{3}{32}(1 + c/8)$	0.52	N.C.
$l_3 = -\frac{1}{16}(1 - c/8)$	0.38	N.C.
Recommended value	0.4	0.8

<sup>a</sup> †, Match made at  $\mu = 1$ ; \*, accuracy not guaranteed; —, not defined; N.C., not computed.

available, the value of  $c$  that should be chosen to match the exact value. The fact that  $c$  varies shows that the rapid guess is not correct, but it is also clear that we cannot go far wrong by taking the recommended values of  $c$  at the bottom. An error of 0.4 is then exceptional, and with a divisor 40 this gives an error of 0.01 in the quantity sought.

These formulas may be useful whenever integrations over  $R(\mu, \mu_0)$  or  $K(\mu)$  should be made and a 1% error does not matter. Note, however, that the function represented here is only the azimuth-independent part of the reflection function.

It should be stressed that the approximate equations just quoted are not unique. Simple, yet fairly accurate expressions exist in great variety. Kolesov and Smoktii (1971) cite in their Eqs. (50) and (51) simple expressions due to Sobolev, but their examples show that deviations of 10% are not uncommon.

## 12.2 COMMENTS AND COMPARISONS, NONCONSERVATIVE SCATTERING

In this section we treat results for semi-infinite atmospheres in the nonconservative case. The recommended similarity rule for this case is to keep  $(1 - a)/(1 - ag)$  constant (Section 14.1.1, Eq. 6).

We shall examine how well the similarity holds by using material from the tables for the Henyey-Greenstein function in the preceding chapter and published exact results for different phase functions.

### 12.2.1 A Numerical Example of the Solution for $N = 1$

In order to permit a detailed comparison with the exact solution for linearly anisotropic scattering ( $N = 1$ ), a typical example is shown. The calculations were made for  $\omega_0 = \omega_1 = 0.9$ , all further  $\omega_n = 0$ . This corresponds to a characteristic function  $\Psi(\mu) = a' + b'\mu^2$  with  $a' = 0.45$ ,  $b' = 0.045$ . The  $H$  function is tabulated by Chandrasekhar (1950, p. 139) and so are its moments (p. 141)  $\alpha_0 = 1.57449$ , and  $\alpha_1 = 0.86228$  as well as the constants  $p = +0.34308$  and  $x = -0.13312$  appearing in the Busbridge polynomials  $q_0(\mu) = 1 + x\mu$  and  $q_1(\mu) = p\mu$ . We find  $\alpha_2 = 0.5978$  from the exact relation  $a'\alpha_0 + b'\alpha_2 = 1 - A$ , where  $A = (1 - 2a' - \frac{2}{3}b')^{1/2} = 0.26458$ . Further moments  $\alpha_n$  can be obtained approximately from an interpolation graph (Fig. 12.2) in which  $(n + 2)\alpha_n$  is plotted against  $(n + 1)^{-1}$ . In a manner analogous to the derivation in Section 8.3.3 for isotropic scattering, we can show that the limit of this quantity for  $n \rightarrow \infty$  is  $H(1) = 1.9610$ . With sufficient precision we read  $\alpha_3 = 0.4580 \pm 0.0002$ . An even safer interpolation may be made if the multiplier  $n + 1.25$  is used.

Many of these quantities appear in Fig. 12.3, where  $f(s) = [H(\mu)]^{-1}$  is plotted against  $s = \mu^{-1}$ . The zero point is reached at  $s = -k$ , equivalent to  $\mu = -\gamma$ ,

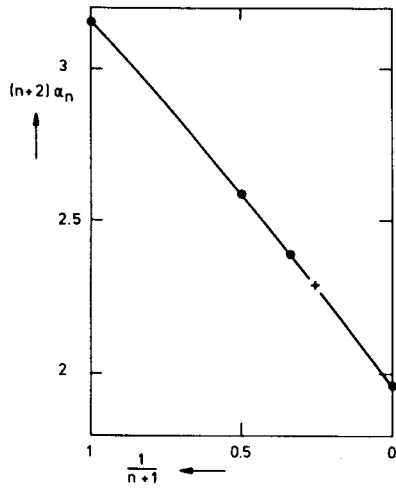


Fig. 12.2. Graphical method to find higher moments of the  $H$  function.

where, as before,  $k$  is the characteristic root and  $\gamma = k^{-1}$ . The slope at this zero point may be found by starting from the relation on line 8 of Display 6.7, which for our purpose we write as

$$f(s)f(-s) = T(s^{-1})$$

Differentiating with respect to  $s$  and then taking  $s = k$ , we obtain

$$f(k)f'(-k) = \gamma^2 T'(\gamma)$$

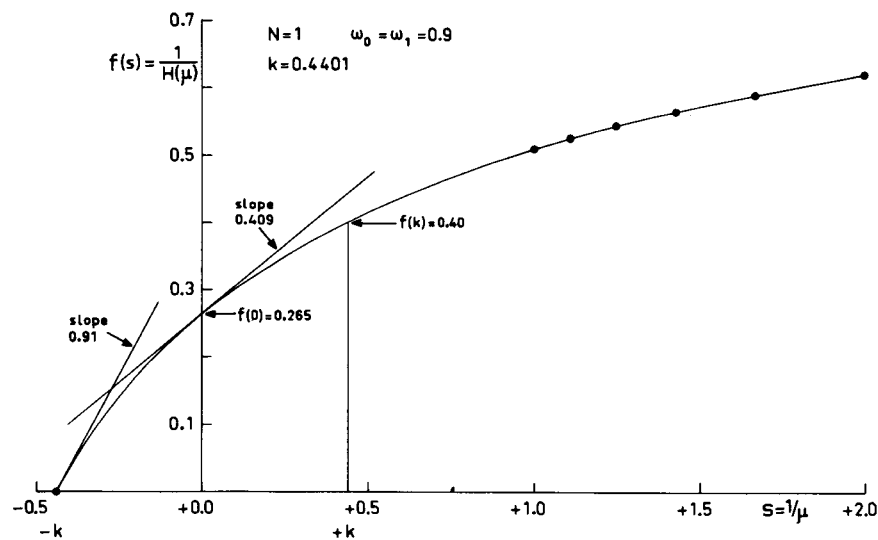


Fig. 12.3. Inverse  $H$  function plotted against  $\mu^{-1}$  for a particular example with anisotropic scattering. Values and/or slopes at three points of special importance are shown.



We readily find that the dispersion function defined in Display 6.7, line 1, and its derivative are ( $z > 1$ )

$$T(z) = 1 - 2(a' + b'z^2)zQ_0(z) + 2b'z^2$$

and

$$T'(z) = -2(a' + 3b'z^2)Q_0(z) + 2z(a' + b'z^2)/(z^2 - 1) + 4b'z$$

where  $Q_0(z)$  is the Legendre function of the second kind (see end of Section 6.2.3).

Numerically, we first obtain from the characteristic equation  $T(\gamma) = 0$  the root  $\gamma = 2.2724$ ,  $k = 0.44006$ . As an alternative, we may use the method explained in Section 12.3.1 (Table 33, third example). Subsequent substitution gives

$$\Psi(\gamma) = 0.68238, \quad \gamma^{-1}Q_0(\gamma) = 0.20784, \quad \gamma^2T'(\gamma) = 0.3627$$

Multiplication of the last quantity by  $8\Psi(\gamma)$  gives by Display 6.11 the value  $m = 1.980$ , in good agreement with the value found directly in Table 33 (Section 12.3.1). Division by  $f(k) = 0.400$ , which we have read (within 1%) from the graph, gives  $f'(-k) = 0.914$ ; this tangent has been drawn in. The graph has further been drawn through the values tabulated by Chandrasekhar for  $s \geq 1$ . At  $s = 0$  we have the value  $f(0) = A$  and the slope  $f'(0) = a'\alpha_1 + b'\alpha_3 = 0.4086$ .

The further quantities of Display 6.11 read in this example:

$$l = 0.3570 \quad l_0 = 0.5221$$

$$q = -\frac{1}{2}\gamma \ln l = 1.170 \quad l_1 = 0.3125$$

$$(1 - g)q = 0.7803$$

and a useful check is provided by the last relation in Display 6.11, which becomes

$$l = \frac{1}{2}m\gamma(\omega_0 l_0^2 - \omega_1 l_1^2) = 0.3570$$

This completes one numerical example. Probably a host of further data is scattered in the literature since linearly anisotropic scattering has often been used as a practice example. We mention only a few. Fricke (1975) presents  $H$  functions of improved accuracy for  $\omega_0 = 0.8$  and 1, adopting for  $\omega_1$  the extreme values  $\pm\omega_0$  of forward and backward scattering compatible with a nonnegative phase function. Yanovitskii (1968) derives the expansions of the  $H$  function and its moments in powers of  $t = (1 - \omega_0)^{1/2}$  up to  $t^3$ .

## 12.2.2 The Influence of Truncation

A simple similarity test can be made by comparing the reflection function or any other quantity for two phase functions with the same  $\omega_0$  and  $\omega_1$  (i.e., the same  $a$  and  $g$ ). The expansion of one phase function is supposed to end at  $N = 1$ , and the other continues with coefficients  $\omega_n = (2n + 1)ag^n$  (the Henyey-Greenstein function,  $N = \infty$ ). The first function may be said to be truncated at  $N = 1$ .

TABLE 31

Comparison of Results for Nonconservative Scattering, with the Same Values  $\omega_0 = 0.9$ ,  $g = \frac{1}{3}$ , between the Henyey-Greenstein Function ( $N = \infty$ ) and the phase Function with  $N = 1$

	(1)	(2)	(1) - (2)	Difference in	
	H-G function ( $N = \infty$ )	$\omega_0(1 + \cos \alpha)$ ( $N = 1$ )	Difference	First order	Higher orders
Basic constants					
$k$	0.4380	0.4401	-0.0021		
$m$	2.0108	1.9804	+0.0304		
$(1 - \omega_0)(1 - g)k^{-2}$	0.3475	0.3443	+0.0032		
$m(1 - g)k^{-1}$	3.0604	3.0003	+0.0601		
$(1 - g)q$	0.7682	0.7803	-0.0121		
$l_0 = NK$	0.5211	0.5221	-0.0010		
$l_1 = \frac{1}{2}UK$	0.3142	0.3125	+0.0017		
$l$	0.3644	0.3570	+0.0074		
Reflected fraction of incident flux $UR$					
For $\mu_0 = 1$	0.332	0.327	+0.005		
For $\mu_0 = 0.5$	0.445	0.447	-0.002		
For $\mu_0 = 0.1$	0.595	0.594	+0.001		
For $\mu_0 = 0$	0.662	0.657	+0.005		
For distributed incidence: $URU =$	0.4090	0.4083	+0.0007		
Reflection function for perpendicular incidence					
$R(1, 1)$	0.301	0.274	+0.027	+0.042	-0.015
$R(1, 0.5)$	0.347	0.356	-0.009	+0.001	-0.010
$R(1, 0.1)$	0.355	0.400	-0.045	-0.042	-0.003
$R(1, 0)$	0.327	0.382	-0.055	-0.054	-0.001

We choose the example  $\omega_0 = \omega_1 = 0.9$ . By the technique of asymptotic fitting (Section 5.6), we found for  $\omega_0 = 0.9$ ,  $g = \omega_1/3\omega_0 = \frac{1}{3}$  the values given in the column  $N = \infty$  in Table 31. The quantities in the column  $N = 1$  are based on the formulas and numbers cited in Section 12.2.1. Note that  $UR$  or twice the first moment of  $R(\mu, \mu_0)$  is, by Display 6.11, generally expressible as

$$UR = 1 - \mu^{-1}q_1(\mu)H(\mu)$$

which in the particular case  $N = 1$  reduces to

$$UR = 1 - pH(\mu) = 1 - [(1 - \omega_0)/(1 - \frac{1}{2}\omega_0\alpha_0)]H(\mu)$$

Upon further integration this yields

$$URU = 1 - 2p\alpha_1$$

It was fully expected that the reflection function itself should show larger differences between the results obtained by means of the two phase functions. These differences, shown in the last four lines of Table 31, rise to 10 or 15%. The expectation was that these differences would be most pronounced in the first few orders of scattering and would be small in the higher orders. A check was made by subtracting the exact first-order term of the reflection function. The equation

$$R_1(\mu, 1) = \omega_0 \Phi(-\mu)/4(1 + \mu)$$

where  $\Phi(\cos \alpha)$  is the phase function, follows most simply from that of isotropic scattering (Display 9.1) by putting the phase function in as an extra factor.

The differences in these first-order terms are large. For instance, the H-G phase function in straight backward reflection ( $\mu = 1$ ) for  $g = \frac{1}{3}$  has  $\Phi(-1) = \frac{3}{8}$ , but the  $N = 1$  function  $\Phi = 1 + \cos \alpha$  has no first order scattering at all in this direction. The sign and magnitude of the differences thus computed and shown in the last column of Table 31 compare quite well with those in the preceding column, which shows that our hunch was roughly correct. The remaining difference, which is still 5% in  $R(1, 1)$ , must be attributed to the second- and higher-order terms.

The findings presented in Table 31 can have significant implications for numerical work. Separately computing only one or two low-order scattering terms is not very demanding on machine time. Hence a method in which this is made the basis of the entire computation may be very attractive. This idea is by no means new. It has been proposed and used in various forms by a number of authors. A comparison as made in Table 31 permits a more detailed examination of the merits of such a method than the usual graphs in which a match within 5% looks very good.

The truncation test just presented can be extended by employing accurate data for still more functions with the same  $\omega_0$  and  $\omega_1$ . It generally takes a fair amount of computing to reach the desired accuracy. However, phase functions made up from other ones by adding or subtracting a forward peak do not have this drawback. With relative ease six examples were thus collected (van de Hulst, 1974a), extending the two treated above, as shown in the accompanying tabulation.

	Phase function	$\omega_0$	$\omega_1$	$\omega_2$	$\omega_3$	UR(1)
(a)	Linearly anisotropic $0.9(1 + \cos \alpha)$	0.9	0.9	0	0	0.327
(b)	$1.2 \text{ H-G}(\frac{1}{2}) - 0.3 \text{ forward peak}$	0.9	0.9	0	-1.05	0.326
(c)	$0.9 \text{ H-G}(\frac{1}{3})$	0.9	0.9	0.50	0.27	0.332
(d)	$0.8 \text{ H-G}(\frac{1}{4}) + 0.1 \text{ forward peak}$	0.9	0.9	0.75	0.79	0.336
(e)	$0.6 \text{ isotropic} + 0.3 \text{ forward peak}$	0.9	0.9	1.50	2.10	0.349
(f)	$0.6 \text{ forward peak} + 0.3 \text{ backward peak}$	0.9	0.9	4.50	2.10	0.451

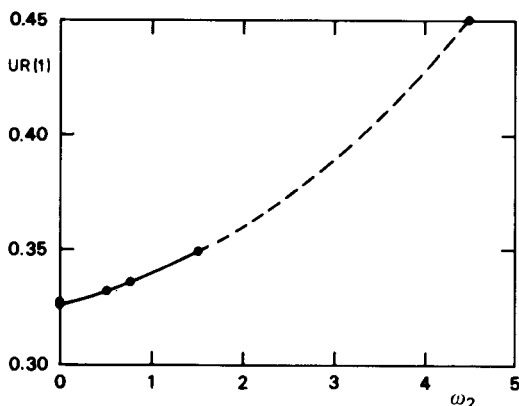


Fig. 12.4. Albedo of a semi-infinite atmosphere with perpendicular incidence shown in 6 situations with the same single scattering albedo  $a = 0.9$  and the same asymmetry parameter  $g = \frac{1}{3}$  but different values of  $\omega_2$ .

The last column gives  $UR(1)$ , i.e., the reflected fraction of flux for perpendicular incidence. This quantity is plotted against  $\omega_2$  in Fig. 12.4. It is a pleasant surprise that the points fit a smooth curve within 1%.

The asymmetry factor  $g = \frac{1}{3}$  in these examples is too low to be representative for haze or clouds (see Section 10.3.1). Additional tests are thus necessary to see if smooth curves like Fig. 12.4 would still be obtained for realistic asymmetries.

### 12.2.3 Approximation Formula for Spherical Albedo

The bimoment of the reflection function  $URU$ , which is also the spherical albedo  $A^*$  (Section 18.1.2), is a much needed quantity. Strictly, it depends on all expansion coefficients  $\omega_0, \omega_1, \omega_2, \dots$ . By the similarity rule we may hope that in a fair approximation it would depend on  $a$  and  $g$  only. Van de Hulst (1974b) examined this question and found that for all practical purposes, the spherical albedo may be computed from the simple approximation:

$$A_{\text{approx}}^* = (1 - 0.139s)(1 - s)/(1 + 1.170s)$$

where

$$s = [(1 - a)/(1 - ag)]^{1/2}$$

The choice of  $s$  as a similarity parameter is explained in Section 14.1.1. The rationale behind this form of approximation was that by a two-parameter formula we can match the coefficients of  $s$  and  $s^2$  in the expansion

$$A^* = 1 - (4/\sqrt{3})s + 4q's^2 + \dots = 1 - 2.309s + 2.842s^2 + \dots$$

which may be derived from Eq. (39) in Section 5.4.1. The factor  $1 - s$  assures that the function vanishes at  $a = 0, s = 1$ , and it so happens that a function of this form also gives nearly the correct slope at  $s = 1$ .

The numerical comparison with the exact values for Henyey–Greenstein phase functions is illustrated in Fig. 12.5. With the abscissa  $t = (1 - a)^{1/2}$  chosen in (a), the points for various  $g$  and  $a$  neatly form a two-dimensional grid. However, with the abscissa  $s$  chosen in (b), this grid virtually collapses into one smooth curve. The deviations are quite invisible on this scale. In order to study the deviations nevertheless, we subtracted the smooth curve defined by  $A_{\text{approx}}^*$ . The differences  $A_{\text{exact}}^* - A_{\text{approx}}^*$  blown up to a scale  $100 \times$  larger than the main figure are shown in (c). It is seen that perfect similarity is not reached, but the maximum difference between extreme curves ( $g = 0$  and  $g = 0.875$ ) is only 0.0030, i.e., 0.3% of the incident flux. The example worked out in Table 31 has  $s = 0.3780$ ,  $z(s) = 0.4085$ , and  $\Delta = +0.0005$  for the Henyey–Greenstein function, and  $\Delta = -0.0002$  for the corresponding  $N = 1$  function.

The theoretical tangents at  $s = 1$  are also shown in Fig. 12.5c. They were computed by observing that the quantity  $URU$  for  $a \ll 1$  equals  $a$  times  $UR_1U$  for  $a = 1$ , where the index 1 signifies first-order reflection. The latter quantity itself is not presented in the previous tables, but its inverse equals the ratio of total to first-order scattering for  $a = 1$ , which can be read for various values of  $g$  from Table 38 (Section 13.1).

Tests with more realistic phase functions gave similarly encouraging results. An approximation producing a less perfect collapse into one curve has been suggested by Wang (1972). Irvine (1974) shows by several examples that the Eddington approximation gives a fine match to the plane albedo  $UR(\mu)$ . Presumably this means that by integration over  $\mu$  a good match to  $URU = A^*$  can also be obtained.

We have also examined the alternative of plotting  $A^*$  against  $u = [(1 - a)/(1 - g)]^{1/2}$  instead of  $s$ . The expansion in terms of powers of  $u$  has the same coefficients as the expansion of  $A_{\text{approx}}^*$  in terms of powers of  $s$  in the terms proportional to  $u$  and  $u^2$  (Sobolev, 1969, 1975), but the coefficient of  $u^3$  (Yanovitskii, 1972) is different from that of  $s^3$ ; nor do the curves against  $u$  reach a common end point at  $a = 0$ .

Numerical values of  $A^*$  for isotropic scattering may be read for some values of  $a$  from Table 12 (Section 9.1.1) or Table 9 (Section 8.4) and for 50 values of  $a$  from Chamberlain and Smith (1970). Values of  $A^*$  for 7 phase functions (isotropic, Rayleigh phase function, and Henyey–Greenstein phase function with  $g = 0.5, 0.75, 0.8, 0.85$ , and  $0.9$ ) and 9 values of  $a$  from 0.7 to 1 are presented in Table 20 of Dlugach and Yanovitskii (1974).

### 12.2.4 Further Similarity Tests

Without claiming completeness, we shall now discuss some further quantities to which similarity tests have been applied.

*Planetary absorption spectra.* In a symposium discussion in 1967 the following question was raised: If someone has made a long computation, of absorption

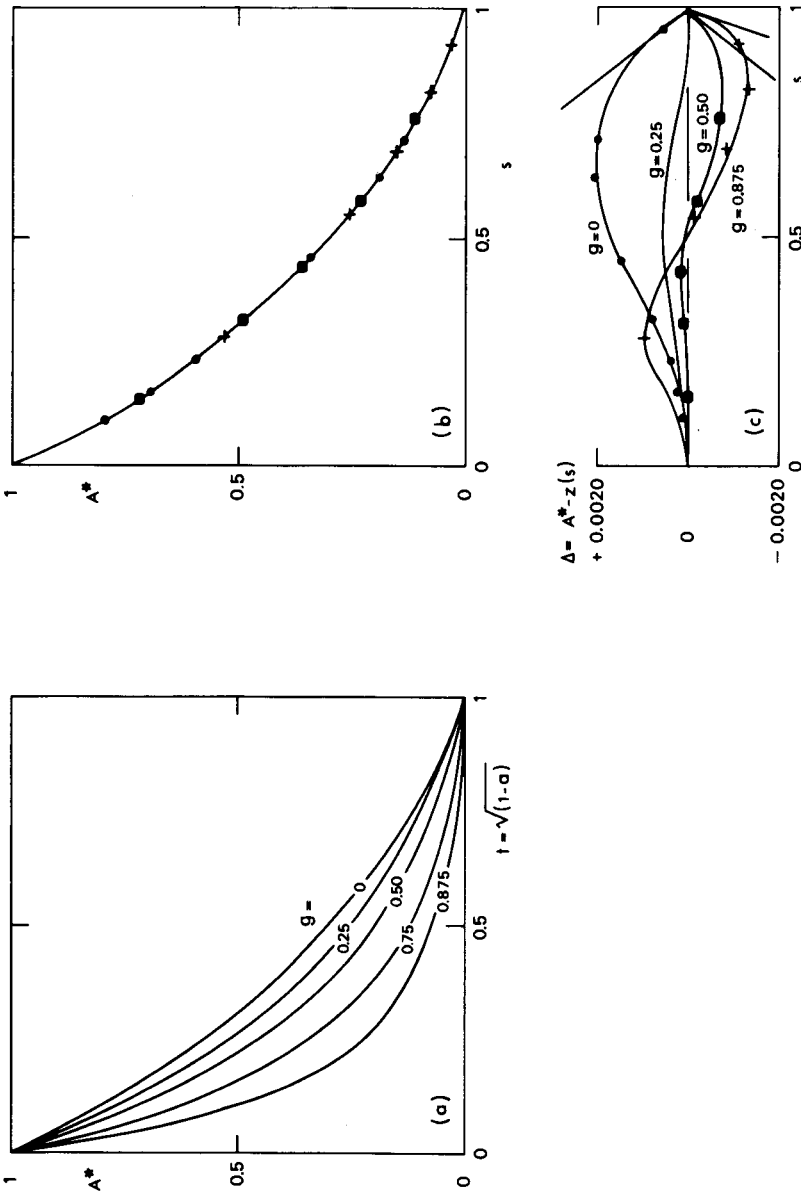


Fig. 12.5. (a) The spherical albedo  $A^*$  of a semi-infinite atmosphere as a function of the single scattering albedo  $a$  follows a different curve for each value of the asymmetry parameter  $g$  of the single scattering pattern. (b) These curves can be made to virtually coincide by choosing  $s = [(1 - a)/(1 - ag)]^{1/2}$  as the abscissa (●,  $g = 0$ ; ■,  $g = 0.50$ ; +,  $g = 0.875$ ). (c) The remaining differences stay within  $\pm 0.002$ .

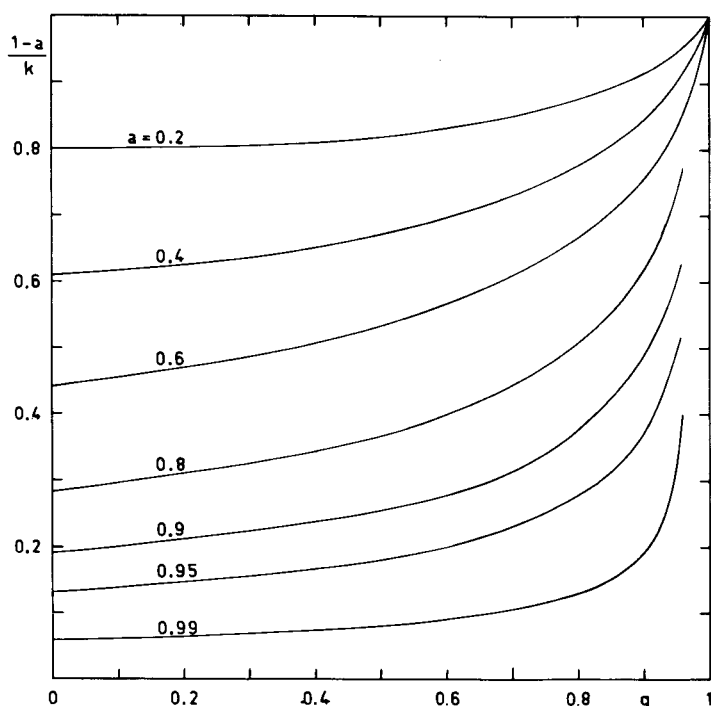


Fig. 12.6. Graph of the similarity parameter  $y = (1 - a)/k$  for varying single-scattering albedo  $a$  and asymmetry parameter  $g$ , based on Henyey–Greenstein phase functions.

lines in reflection against a thick planetary atmosphere, assuming isotropic scattering, should someone else, who wishes to assume a different scattering pattern, repeat the entire computation or can he apply a similarity rule? Van de Hulst and Grossman (1968) answered that the albedo  $a$  should be transformed at the same time as the asymmetry factor  $g$  in such a way that the quantity  $y = (1 - a)/k$  is preserved (cf. Section 5.2.3). An interpolation graph for  $y$  is given in Fig. 12.6.

Figure 12.7 shows the comparison made on that basis in the 1968 paper for the (diffuse) perpendicular reflection  $R(1, 1)$ . It shows that from  $R(1, 1) \approx 1.10$ , which holds in the absence of absorption, down to  $R(1, 1) \approx 0.30$ , which already corresponds to a deep absorption line, the extreme curves when plotted against  $y$  do not differ by more than 7%. In practice the assumptions about  $g$  made by different authors should not vary so widely, and the agreement will be correspondingly closer. Between  $g = 0.75$  and  $g = 0.875$  differences should not exceed 2%. The same figure shows that  $R(0.5, 0.5)$  has an equally striking similarity. This function should, however, be completed by the azimuth dependent terms before it represents an observable intensity.

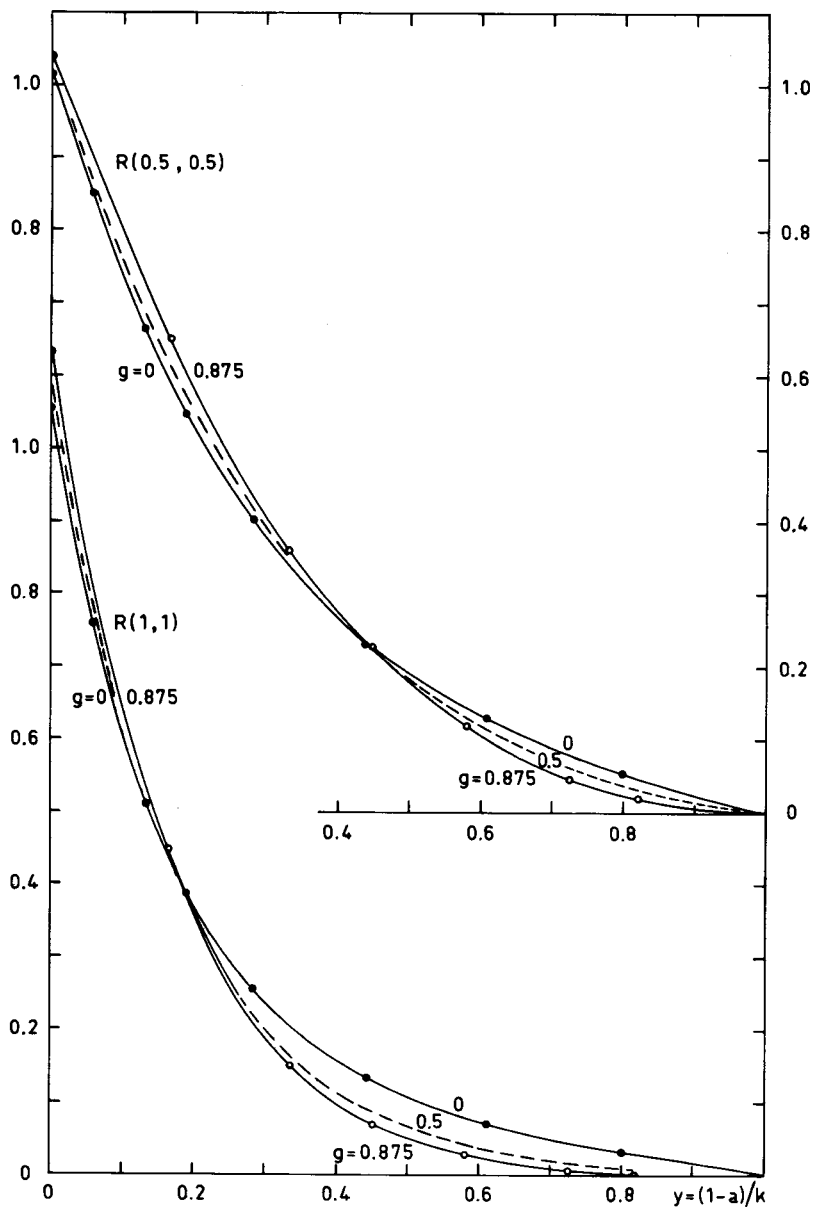


Fig. 12.7. Similarity test: It is shown by two examples with  $b = \infty$ ,  $\mu = \mu_0$  (fixed) that plotting the reflection function against the variable  $y$  brings the curves for various asymmetry parameters  $g$  very close together. Only  $a$  and  $g$  vary (from van de Hulst and Grossman, 1968).



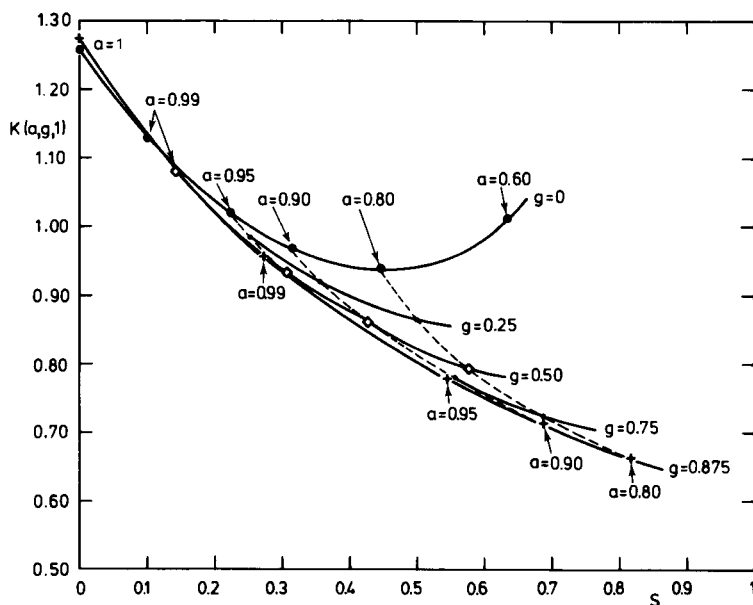


Fig. 12.8. Similarity test of the escape function for varying  $a$  and  $g$ . Mutual differences remain quite small for  $s < 0.3$ .

It was later realized (Section 14. 1.1) that probably  $s = [(1 - a)/(1 - ag)]^{1/2}$  is a slightly better similarity parameter than  $y$ . An additional test in which  $R(1, 1)$  was plotted against  $s$  did not show much improvement over Fig. 12.7.

*The escape function.* The escape function in perpendicular direction  $K(a, g, 1)$  is plotted against  $s$  in Fig. 12.8. The precise numbers are in Table 26 (Section 11.2). The graph shows fine coincidence for small values of  $a$ , but strangely enough, at larger  $s$ , the curve for  $g = 0$  deviates most, while those for  $g = 0.5-0.875$  stick closely together.

*Extrapolation length.* As a further example we wish to examine the behavior of the extrapolation length  $q$ . Since  $q$  is by definition an optical depth, we may hope that in similar problems the values of  $kq$  are about equal. As an equivalent we have plotted in Fig. 12.9 the negative internal reflection coefficient  $l = e^{-2kq}$  against  $s$ . Precise values are in Table 26 (Section 11.2). The similarity is very close. For practical purposes we may assume coincidence with one smooth curve. This counts the more since the only situation in which the return diffusion stream of negative strength has numerical significance (Section 5.3) is when  $l$  is not too far from 1.

Aronson (private communication) has compared the behavior of  $l$  with two different sets of phase functions, namely, the Henyey-Greenstein function and the isotropic sector (set 22 of Display 10.1). Choosing (in our notation)

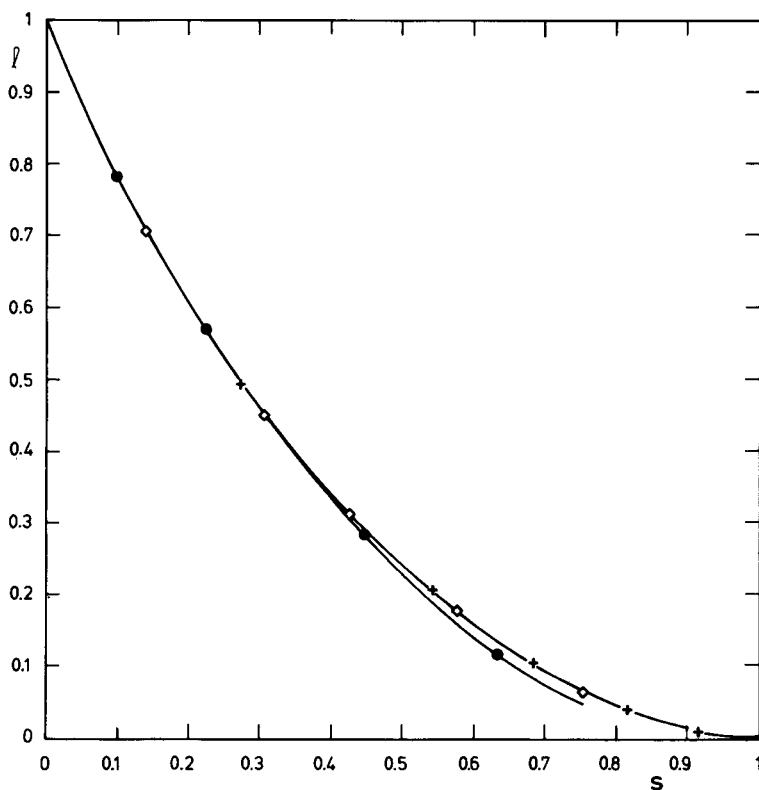


Fig. 12.9. Similarity test of the negative internal reflection coefficient  $l$ . For all practical purposes  $l$  can be considered a function of  $s$  only (●,  $g = 0$ ; ◇,  $g = 0.5$ ; +,  $g = 0.875$ ).

$a(1 - ag)q$  as a convenient quantity for comparison, Aronson finds the numbers given in Table 32. This table, in which we have entered also the values of  $s$ , shows that at each  $g$  value the difference between the two phase functions is small. Only for  $s \geq 0.8$ , which by Fig. 12.9 corresponds to  $l < 0.05$ , do larger differences appear. Owing to the somewhat arbitrary multiplication factor  $a(1 - ag)$  the columns with different  $g$  in Table 32 are not directly comparable at the same  $s$ .

*The diffusion pattern.* Kattawar (1975) compared a realistic phase function to a simpler one consisting of one or two Henyey–Greenstein functions (numbers in Section 10.3.1). In testing the similarity, he paid particular attention to the diffusion pattern. This pattern,  $P(u)$ , is the intensity distribution deep inside the atmosphere in the presence of a one-way diffusion stream (Sections 5.2.1 and 6.2.1). The approximation of very slightly absorbing haze ( $m = 1.55 - 0.001i$ ) gave a fit well within 1%. With greater absorption ( $m = 1.55 - 0.013i$ ), the difference with the diffusion pattern of the fitted one-term H–G function was 10%, but a two-term fit reduced these differences substantially.

**TABLE 32**  
Extrapolation Length  $q$  for Two Sets of phase functions<sup>a</sup>

$a$	$g = 0$		$g = 0.25$			$g = 0.50$		
	$s$	HG = LA = IS	$s$	HG	IS	$s$	HG	IS
1.0	0	0.7104	0	0.7109	0.7094	0	0.7120	0.7114
0.9	0.316	0.7106	0.359	0.7193	0.7136	0.426	0.7453	0.7350
0.8	0.447	0.7112	0.500	0.7238	0.7166	0.577	0.7681	0.7519
0.7	0.548	0.7127	0.603	0.7231	0.7187	0.679	0.7786	0.7614
0.5	0.707	0.7205	0.756	0.7006	0.7219	0.816	0.7547	0.7551

$a$	$g = 0.75$			$g = 0.80$		
	$s$	HG	IS	$s$	HG	IS
1.0	0	0.7134	0.7143	0	0.7137	0.7150
0.9	0.555	0.8268	0.8114	0.598	0.8657	0.8687
0.8	0.707	0.9058	0.8851	0.745	0.9687	0.9494
0.7	0.795	0.9512	0.9361	0.826	1.0268	1.0197
0.5	0.894	0.9395	0.9654	0.913	1.0151	1.0627

<sup>a</sup> The values tabulated in the columns HG (Henyey–Greenstein scattering) and IS (isotropic sector) are  $a(1 - ag)q$ . For reference also  $s = [(1 - a)/(1 - ag)]^{1/2}$ .

## 12.3 THE SPECTRUM OF THE ANISOTROPIC TRANSFER EQUATION

This section, largely following van de Hulst (1970a), is more technical than most others. The integral equation detailing the propagation in an unbounded medium for an arbitrary phase function (Section 6.2.1) may have a number of discrete roots  $\pm k_j$ , where  $k_j$  is defined to be positive. Very often we need only the smallest value,  $k_0 = k$ , which describes the dominant mode of propagation. We have consistently called this the diffusion mode and  $k$  the diffusion exponent. Yet it is sometimes useful to know also the higher eigenvalues,  $k_1, k_2$  etc., if they exist. The set of all eigenvalues is called the spectrum. Some of its properties are discussed below.

### 12.3.1 Convergence of the Kuščer Polynomials

The Kuščer polynomials  $g_n(x)$  are defined (Section 6.2.2 with  $m = 0$ ) by

$$(n+1)!g_{n+1}(x) = \begin{vmatrix} h_0 x & 1 & & & \\ 1 & h_1 x & 2 & & \\ & 2 & & \ddots & \\ & & \ddots & \ddots & n \\ & & & n & h_n x \end{vmatrix}$$

If  $k_j$  is one of the eigenvalues, then by Section 6.2.3 the characteristic root or diffusion length  $\gamma_j = k_j^{-1}$  satisfies

$$\lim_{n \rightarrow \infty} g_n(\gamma_j) = 0$$

We shall henceforth omit the index  $j$  except when it is needed to avoid confusion. We shall first explore by means of actual examples how  $g_n(\gamma)$  approaches 0 if the root  $\gamma$  is correctly chosen, and also how  $g_n(x)$  diverges if  $x$  is slightly different from  $\gamma$ . Four examples, all referring to the main eigenvalue, are shown in Table 33.

Define the ratio

$$r_n(x) = g_n(x)/g_{n-1}(x)$$

The recurrence relation (Display 6.2),

$$h_n x g_n(x) = (n+1)g_{n+1}(x) + n g_{n-1}(x)$$

then gives

$$r_{n+1}(x) = h_n x / (n+1) - n / (n+1) r_n(x)$$

The examples in Table 33 show that for  $x = \gamma$ ,  $n \rightarrow \infty$ ,  $r_n(\gamma)$  approaches a finite limit  $r$ , and hence  $g_n(\gamma)$  converges to zero approximately as a geometric series with ratio  $r$ . Observing that  $h_n = 2n + 1 - \omega_n$  and that  $\omega_n \rightarrow 0$ , we find the asymptotic expression

$$r_n(\gamma) = r[1 - (2n)^{-1} + O(n^{-2})]$$

with

$$r = \gamma - (\gamma^2 - 1)^{1/2}$$

The actual ratios in the four examples of Table 33 are illustrated in Fig. 12.10. For  $n \geq 10$ , all four curves very nicely fit the asymptotic expression shown by the value and tangent at  $n^{-1} = 0$ . In the isotropic examples, the ratio increases all the way. The two other examples show a marked bend near the value of  $n$  where  $\omega_n$  becomes negligible.

Table 33 further shows, by way of illustration, the computation of  $m$  by the infinite series in Display 6.11. The tendency in the literature is not to bother with such infinite series if  $N$  is finite. Yet the numbers show an attractively fast convergence for finite and infinite  $N$  alike, so the possible use of such series in practical computations should not be forgotten.

The behavior of  $g_n(x)$  and  $r_n(x)$  if  $x$  is not exactly the desired root is quite different. The tendency for  $r_n$  is again to approach a fixed limit for  $n \rightarrow \infty$ , but now this limit is the other root of the quadratic equation, namely  $r = x + (x^2 - 1)^{1/2}$ . This is  $> 1$  (for  $x > 1$ ) so that from a certain  $n$  onwards,  $g_n(x)$  diverges as a geometric series.

This peculiar behavior can be most easily understood if  $N$  is finite. We observe in Display 6.2 ( $m = 0$ ) that for  $n > N$ , we have  $\omega_n = 0$ ,  $h_n = 2n + 1$ , so

**TABLE 33**  
Some Examples Showing the Convergence of  $g_n(\gamma)$

Phase function	$N = 0$ , isotropic		$N = 1$	$N = \infty$
	$\omega_0 = 0.8$	$\omega_0 = 0.95$	$\omega_0 = \omega_1 = 0.9$	H-G function $\omega_0 = 0.8, g = 0.5$
$k$	0.7104118	0.3794852	0.4400561	0.5418337
$\gamma = k^{-1}$	1.4076343	2.6351488	2.2724377	1.8455848
$h_0$	0.2	0.05	0.1	0.2
$h_1$	3	3	2.1	1.8
$h_2$	5	5	5	4.0
$h_3$	7	7	7	6.3
$h_4$	9	9	9	8.55
$h_5$	11	11	11	10.725
$g_0(\gamma)$	1.00000	1.00000	1.00000	1.00000
$r_1$	0.282	0.132	0.227	0.369
$g_1(\gamma)$	0.28153	0.13176	0.22724	0.36912
$r_2$	0.335	0.158	0.186	0.306
$g_2(\gamma)$	0.09443	0.02080	0.04222	0.11311
$r_3$	0.359	0.169	0.199	0.285
$g_3(\gamma)$	0.03385	0.00352	0.00840	0.03227
$r_4$	0.371	0.175	0.206	0.278
$g_4(\gamma)$	0.01257	0.00062	0.00173	0.00896
$r_5$	0.380	0.179	0.211	0.276
$g_5(\gamma)$	0.00477	0.00011	0.00036	0.00247
$r_6$	0.385	0.182	0.214	0.276
$g_6(\gamma)$	0.00184	0.00002	0.00008	0.00068
$r_7$	0.389	0.184	0.216	0.277
$g_7(\gamma)$	0.00072	—	0.00002	0.00019
$r_8$	0.393	0.186	0.218	0.278
$g_8(\gamma)$	0.00028	—	—	0.00005
$r$	0.417	0.197	0.232	0.294
$g_0 g_1$	0.281527	0.131757	0.227244	0.369117
$2g_1 g_2$	0.053169	0.005481	0.019187	0.083504
$3g_2 g_3$	0.009591	0.000219	0.001064	0.010950
$4g_3 g_4$	0.001702	0.000009	0.000058	0.001157
$5g_4 g_5$	0.000300	—	0.000003	0.000111
$6g_5 g_6$	0.000053	—	—	0.000010
$7g_6 g_7$	0.000009	—	—	0.000001
$8g_7 g_8$	0.000002	—	—	—
Sum	0.346353	0.137467	0.247556	0.464849
$m = 8 \times \text{sum}$	2.770826	1.099737	1.980449	3.718795

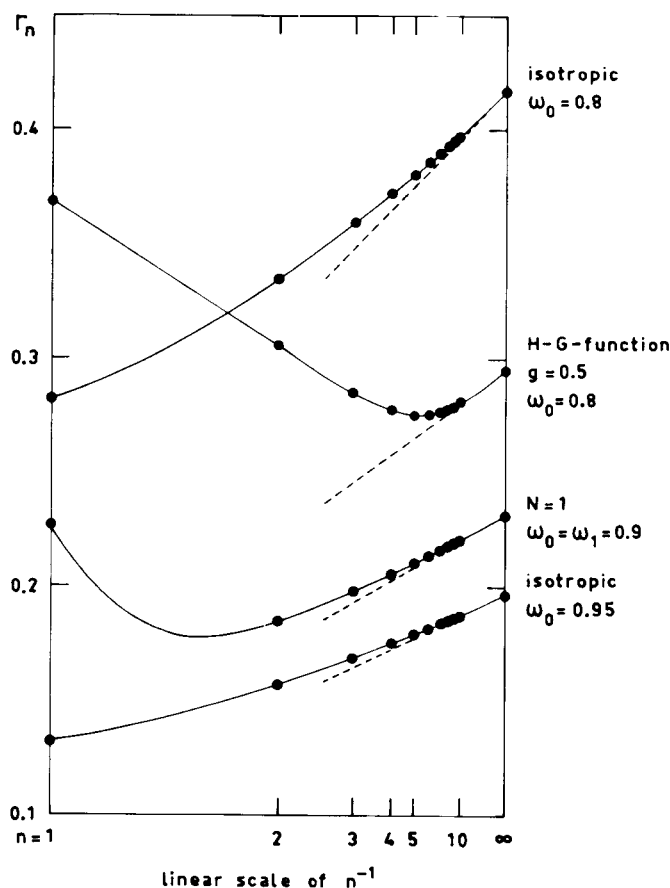


Fig. 12.10. Ratios of Kušcer polynomials of successive orders computed for the correctly converging solutions belonging to 4 combinations of single-scattering albedo and phase function.

that the recurrence relation is identical to that for the Legendre functions. If, for a fixed argument  $x > 1$ , the values  $g_m(x)$  and  $g_{m+1}(x)$  are given, these can always be written as a linear combination of the Legendre functions of the first kind  $P_n(x)$  and of the second kind  $Q_n(x)$ , of the corresponding orders  $m$  and  $m + 1$ . The recurrence relation then states that this must be true for all  $n \geq N$ , and hence we have

$$g_n(x) = A(x)P_n(x) + B(x)Q_n(x) \quad (n \geq N)$$

Since only  $Q_n(x) \rightarrow 0$  for  $n \rightarrow \infty$ , we must have  $A(\gamma) = 0$  and

$$g_n(\gamma) = BQ_n(\gamma)$$

where  $B$  is a constant. At any other value  $x$ , the coefficient  $A(x)$  is nonzero. Since  $P_n(x)$  diverges, this term will then dominate the values of  $g_n(x)$  for  $n \rightarrow \infty$ .

Numerical experimentation both in Groningen (Dr. Kaper, private communication) and in our institute (by Mr. Zorn) confirmed this behavior. An error  $|x - \gamma|$  even in the tenth decimal place may make  $g_n(x)$  diverge before the fifth decimal has become 0.

The pleasant counterpart of this statement is that it is possible to obtain  $\gamma$  with very great accuracy if we can devise a means by which  $r_j(x)$  or  $g_j(x)$  are kept within reasonable bounds for a certain moderately large  $j$ , e.g.,  $j = 10$ . Several numerical or analytic tricks may be devised to exploit this idea. A simple but not necessarily the best method is to solve the equation  $g_j(x) = 0$  and to call its root  $x_j$ . Then we should have

$$\lim_{j \rightarrow \infty} x_j = \gamma$$

and we can vary  $j$  until no further change occurs in the desired decimal place. This method worked well in practice. It was used by Dr. Grossman in computing the roots shown in Table 23 (Section 11.1.2).

In this connection, particular interest must be attached to the idea of considering not  $\omega_0$  (the albedo), but  $k$  (the diffusion exponent) as the independent variable. In the simplest form, in which Busbridge (1967) poses this problem, we consider  $\omega_n$  and hence  $h_n = 2n + 1 - \omega_n$  as given constants for  $n \geq 1$ , and wish to find  $\omega_0$  or  $h_0 = 1 - \omega_0$  for a given  $k$ .

Numerically this problem can be solved by taking  $x = k^{-1}$  and starting at some not too small  $j$  (e.g.,  $j = 10$ ) with any guess for  $r_j(x)$ . This guess may be 0, better  $r$ , or still better  $r(1 - 1/2n)$ , as shown above. The recurrence relation then is run backwards in the form

$$r_n(x) = [(h_n x/n) - (n + 1)r_{n+1}(x)/n]^{-1}$$

until we arrive at  $r_1(x)$ , which must be equated to  $h_0 x$  so that

$$1 - \omega_0 = h_0 = r_1(x)/x$$

gives the unique value  $\omega_0$  that is the solution of the problem posed.

Exactly the same procedure may be followed if we aim for a series expansion of  $\omega_0$  in  $k$ . The result is a continued fraction of the form

$$1 - \omega_0 = h_0 = \frac{k^2}{h_1 - \frac{4k^2}{h_2 - \frac{9k^2}{\ddots \frac{h_{j-1} - j^2 k^2}{h_j - (j+1)r_{j+1}k}}}}$$

This form makes clear at once that the constant  $h_n$  enters only in the terms of order  $k^{2n}$  and beyond. Upon terminating the fraction by putting  $r_{j+1} = 0$ , i.e.,

upon solving the equation  $g_{j+1}(x) = 0$ , we obtain the correct coefficients of the power series in  $k^2$  up to the power  $k^{2j}$  inclusive. For instance, setting  $r_3 = 0$ , we obtain

$$1 - \omega_0 = \frac{k^2}{h_1 - 4k^2/h_2} = \frac{k^2}{h_1} + \frac{4k^4}{h_1^2 h_2} + \dots$$

where the written coefficients are exact and will not change any further if we take  $j > 2$  or go to the limit  $j \rightarrow \infty$ .

### 12.3.2 The Function $a(k)$ for Patterns of Constant Form; Nonuniqueness

In a quite similar manner, we may also solve a slightly different problem: What is the expansion of albedo  $a$  in powers of  $k^2$  if the phase function is kept constant and the albedo is varied? Then

$$\omega_n = (2n + 1)ab_n$$

where  $b_n = \text{const}$ ,  $b_0 = 1$ ,  $b_1 = g$  is the asymmetry factor,  $b_2 = h$ ,  $b_3 = t$ , etc. The solution is again that coefficients up to the power  $k^{2j}$ , inclusive, are obtained by putting  $g_{j+1} = 0$ .

By starting with an arbitrary guess about  $r_{j+1}$ , e.g., at  $j = 10$ , we can again work rapidly towards lower  $r_n$  by backwards recurrence, which is a numerically stable process if  $k < 1$ . In contrast to the problem discussed in Section 12.3.1, we have to assume a value of  $a$  from the beginning, because it appears in every  $h_n$ . If the final value of  $a$  obtained from  $r_1$  does not check with the assumed value, we have to repeat until agreement is reached.

In this process, multiple roots exist. This is most easily demonstrated if  $N$  is finite.

The results for  $N = 1$  are first reviewed briefly. Here  $a$  follows from the quadratic equation

$$x(1 - a)^2 + [3 - x - 2kQ_2(\gamma)/Q_1(\gamma)](1 - a) - k^2 = 0$$

in the traditional notation with  $\omega_0 = a$ ,  $\omega_1 = ax$ , and  $\gamma = k^{-1}$ . It is seen that the two roots  $a_0$  and  $a_1$  belonging to the same value of  $k$  are related by

$$(1 - a_0)(1 - a_1) = -k^2/x$$

Figure 12.11 shows these roots for  $x = 1$ , i.e., for the extreme case of linearly anisotropic scattering, which has often been used as a practice example. The values of the lower root  $a_0$  were taken from Kaper *et al.* (1970). They define a curve rather similar to that for  $N = 0$ . The values  $a_1$  then follow from the equation just given. The curve starts at  $k = 0$ ,  $a_1 = 3$  and finishes at  $k = 1$ ,  $a_1 = 2$  with a vertical tangent.

The obvious generalization of this result for any finite  $N$  is that  $N + 1$  real, nonnegative values of  $a$  correspond to one  $k$ . We shall discuss only the general



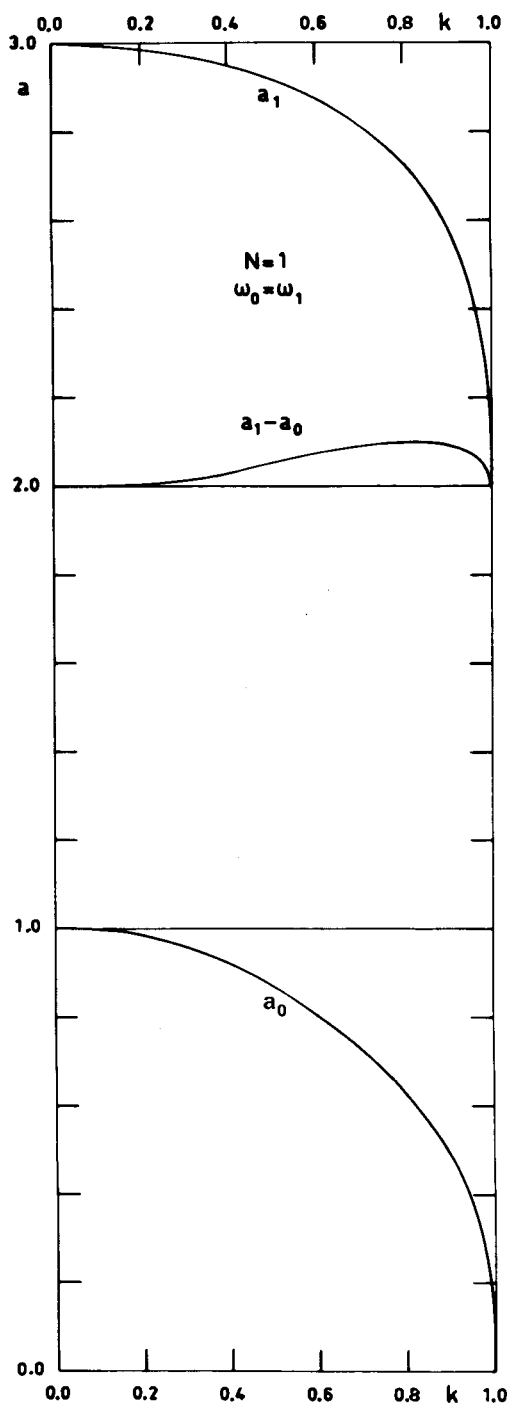


Fig. 12.11. Two values of the albedo,  $a_0$  and  $a_1$ , satisfy the characteristic equation for any given value of  $k$  for the linearly anisotropic phase function with  $\omega_0 = \omega_1$  ( $N = 1$ ).

properties of these solutions at and near  $k = 0$ . At  $k = 0$  the  $N + 1$  nontrivial solutions of the characteristic equation are defined by

$$h_j = 0 \quad (j = 0, 1, \dots, N)$$

which gives  $a_j = b_j^{-1}$  and  $g_j = 1, g_n = 0$  for  $n \neq j$ .

From here on we may find the series expansion in  $k^2$ , to be used near  $k = 0$ . It seems simplest to start from the continued fraction (Section 12.3.1). If this is cut off after  $h_2$ , the equation for  $a$  is

$$1 - a = k^2/[3(1 - ag) - 4k^2/5(1 - ah)]$$

This is an equation of the third degree having the roots

$$(j = 0) \quad a = 1 - \frac{k^2}{3(1 - g)} - \frac{(4 - 9g + 5gh)k^4}{45(1 - g)^3(1 - h)} + \dots$$

$$(j = 1) \quad a = \frac{1}{g} - \frac{(4 - 9g + 5h)k^2}{15(1 - g)(g - h)} + \dots$$

$$(j = 2) \quad a = \frac{1}{h} + \dots$$

The dots signify terms containing the next higher power of  $k^2$ , with a coefficient dependent also on the next higher Legendre coefficient  $b_3$ .

It is not too difficult to find a general procedure for computing the coefficients. Postulate expansions of the form

$$g_n(\gamma) = \sum_{l=0}^{\infty} g_{nl} k^{n+2l}, \quad a = \sum_{l=0}^{\infty} a_l k^{2l}$$

Then the roots ( $j = 0, 1, 2, \dots$ ) are defined by  $a_0 = b_j^{-1}$  and  $g_{nl} = 0$  for  $n + l < j$ . The normalization of  $g_n(\gamma)$  can still be an arbitrary function of  $k$ ; it seems simplest to adopt  $g_j(\gamma) = 1$  by which  $g_{j0} = 1, g_{jl} = 0$  for  $l \geq 1$ . The recurrence formula for  $g_n(\gamma)$  then leads to relations between the coefficients which permit their computation one by one.

We do not spell out all equations because we also found by some practical examples that the convergence of these expansions for the higher roots is very poor, so the use of a few terms only is of little use.

It is also possible to make the inverse expansion, of  $k^2$  in powers of  $1 - a$ , which has somewhat simpler coefficients. Grosjean (1963) gives the expansion for the main root up to terms proportional to  $(1 - a)^3$ .

Still pursuing the solution near  $k = 0$ , we may also express the diffusion pattern in a series expansion. Limiting the discussion to the main root ( $j = 0$ ), we find the ratios  $r_n = g_n(\gamma)/g_{n-1}(\gamma)$  as follows:

$$r_1 = (1 - a)/k = bk + ck^3 + \dots$$

$$2r_2 = fk + \dots$$

$$3r_3 = pk + \dots$$

with

$$\begin{aligned} b &= 1/3(1 - g), & f &= 4/5(1 - h), & p &= 9/7(1 - t) \\ c &= b^2(f - 3gb) = (4 - 9g + 5gh)/45(1 - g)^3(1 - h) \end{aligned}$$

from which  $g_n(\gamma)$  follows by multiplication, and the diffusion pattern  $P(u)$  by Eq. (1a) of Section 6.2.3:

$$\begin{aligned} P(u) &= \sum_{n=0}^{\infty} (2n + 1)g_n(\gamma)P_n(u) \\ &= 1 + \frac{1}{1 - g} P_1(u)k + \frac{2}{3(1 - g)(1 - h)} P_2(u)k^2 \\ &\quad + \left[ \frac{4 - 9g + 5gh}{15(1 - g)^3(1 - h)} P_1(u) + \frac{2}{5(1 - g)(1 - h)(1 - t)} P_3(u) \right] k^3 + \dots \end{aligned}$$

The terms proportional to  $k$  and  $k^2$  were given by van de Hulst (1968). The extension to the  $k^3$  term was first given by Kattawar (1975) with omission of the  $P_1(u)$  term and later corrected by Kattawar (1977).

We now proceed with some detailed results on the multiple solution for one particular example with  $N = \infty$ , namely, the Henyey–Greenstein phase function.

Figure 12.12 shows the next smallest values  $k_1$ ,  $k_2$ , which for a given combination  $(a, g)$  follow the main root  $k_0$  given in Fig. 11.1. A variety of numerical methods has been used. All three roots go to the limit  $k = 1 - a$  for  $g \rightarrow 1$ . For any  $a \leq 1$ , the root  $k_1$  exists only if  $g > 0.50$  (approximately), and the root  $k_2$ , if  $g > 0.71$  (approximately). A similar situation exists for  $g < 0$ , i.e., for predominantly backward scattering. All roots go to  $k = (1 - a^2)^{1/2}$  for  $g \rightarrow -1$ . Further details are not presented because these values of  $g$  do not find much application.

The three roots are jointly shown for the value  $g = 0.75$  in Fig. 12.13 and for two more values of  $g$  in Fig. 12.14. The starting points at  $k = 0$  are at  $a = 1$ ,  $a = g^{-1}$ , and  $a = g^{-2}$ ; and the downward curvature from those points illustrates the series expansions just given.

A quite different problem is what happens at  $k = 1$ . By analogy with Fig. 12.11 we expect that each root reaches a finite value  $a$  in the limit  $k = 1$ . These values are found along the top of Fig. 12.12 and along the right edges of the drawings in Figs. 12.13 and 12.14. To find these limits precisely we may observe that in the limit  $k = 1$  the characteristic equation takes the form

$$2\Psi(1) = \sum_n \omega_n g_n(1) = 0$$

which fixes the relation between  $a$  and  $g$  for each root at  $k = 1$ . Vanmassenhove (1967, Table 4) has computed a few values. Let  $a_j(g)$  be the  $j$ th root belonging to a value of  $g$ ; the main root is  $a_0 = 0$ . We find it convenient to use the products  $a_j g^j$  because it can be shown that for  $g \rightarrow 0$  these approach the finite limit

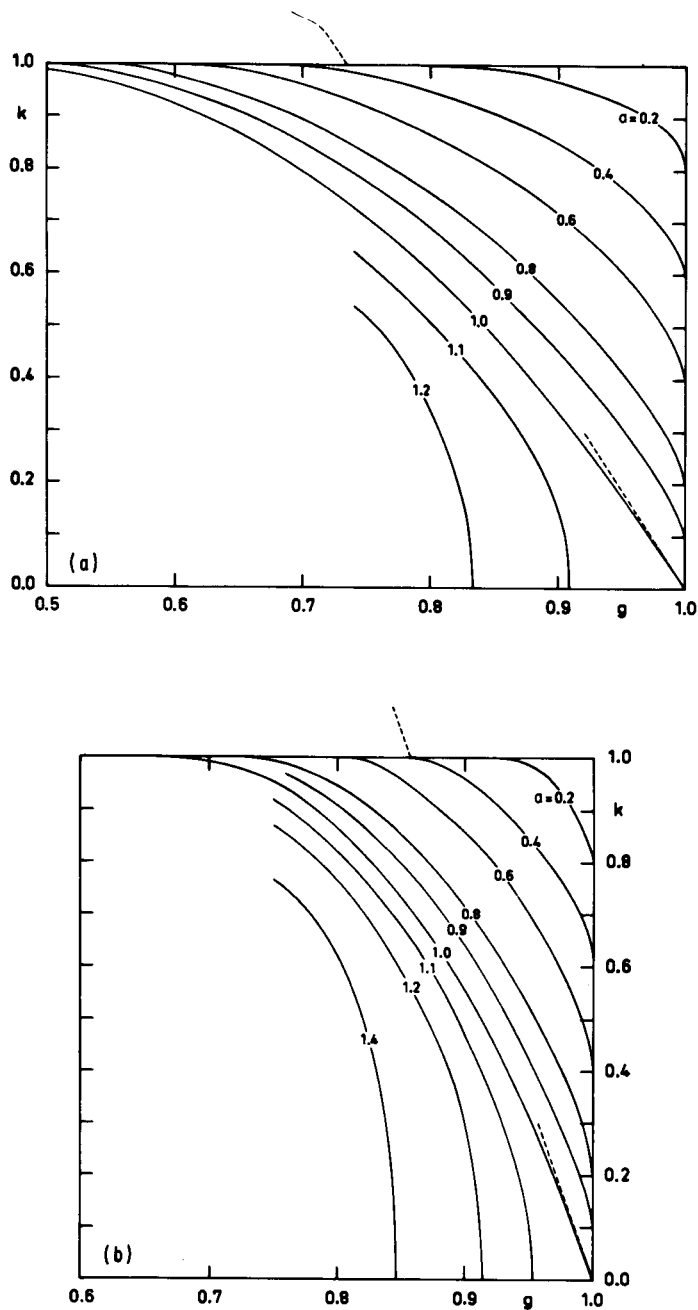


Fig. 12.12. Relations between  $a$  and  $k$  in the second root (a) and third root (b), both for Henyey-Greenstein phase functions in the range of strong asymmetry parameters.

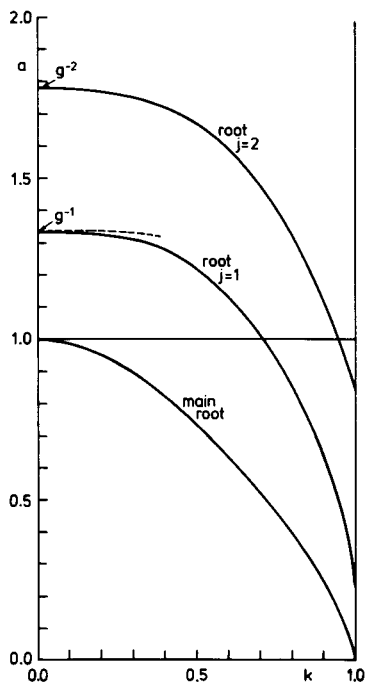


Fig. 12.13. Relations between  $a$  and  $k$  in the first three roots for a Henyey-Greenstein phase function with asymmetry parameter  $g = 0.75$ ; same format as Fig. 12.11.

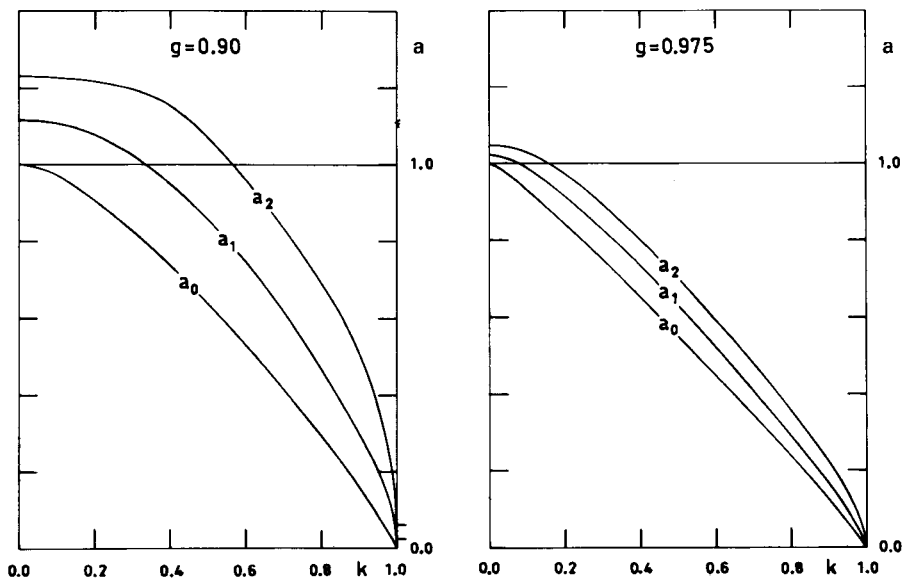
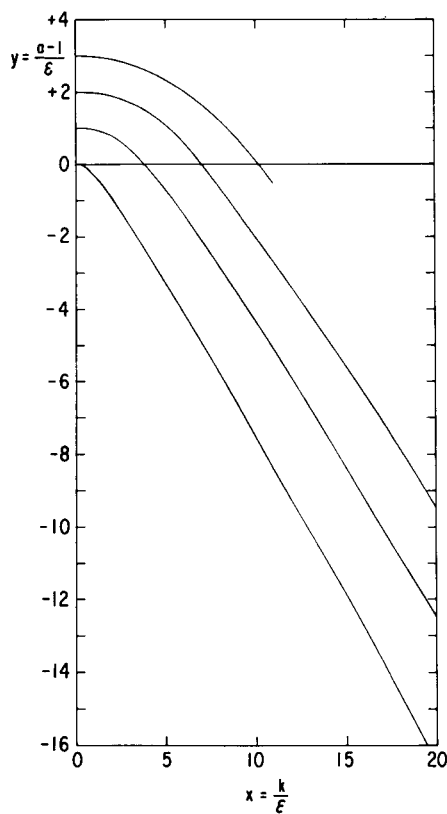


Fig. 12.14. Relation between  $a$  and  $k$  in the first three roots for a Henyey-Greenstein phase function with two values of  $g$ ; same format as Figs. 12.11 and 12.13.

$j/(2j + 1)$ . The combined available values are shown in the accompanying tabulation.

	<i>g</i>				
	0	0.1	0.3	0.5	0.7
$a_1g$	0.333	0.374	0.411	0.33	0.15
$a_2g^2$	0.400	0.412	0.439	0.46	0.33
$a_3g^3$	0.429	—	—	0.47	0.45

It appears likely that near  $g = 1$  the approximate behavior is  $a_1 = 2.4(1 - g)^2$ , and similarly for  $a_2$ , but the coefficient is uncertain, and the matter has not been pursued. It should be noted that knowledge of the exact  $a_j(g)$  relations for  $k = 1$  would not help much in drawing the curves in Fig. 12.12 because of the horizontal tangents.



**Fig. 12.15.** Limiting form of the curves shown in the preceding figures if  $g \rightarrow 1$ . See explanation in text.

The behavior of the main root near the point  $k = 1$ ,  $a = 0$  for an arbitrary phase function has been studied in detail by Maslennikov and Sushkevich (1964).

*The limit  $g \rightarrow 1$ .* What happens to the curves in Figs. 12.13 and 12.14 if we let  $g \rightarrow 1$ ? The answer, again limited to Henyey–Greenstein phase functions, is shown in Fig. 12.15. If we define

$$y = (a - 1)/(1 - g), \quad x = k/(1 - g)$$

and then let  $g \rightarrow 1$ , the curves from Fig. 12.14 approach those of Fig. 12.15. In this limit we may compute  $x$  as an eigenvalue for which the set of equations

$$(2n + 1)(n - y)x^{-1}g_n = (n + 1)g_{n+1} + ng_{n-1}$$

has a solution satisfying  $g_n \rightarrow 0$  for  $n \rightarrow \infty$ . This equation and this condition follow from those for arbitrary  $g$  defined earlier. A computation showed that the value  $y = 0$  is reached for  $x = 3.7900$ ,  $6.9830$ ,  $10.1466$ , etc. These zeros differ little from the zeros of the Bessel function  $J_1(x)$ . The precise value of the first root, found by an inverse recursion technique similar to that explained in Section 12.3.1, is  $3.79000743$ .

## 12.4 ASYMPTOTIC EXPRESSIONS FOR HIGH-ORDER TERMS

### 12.4.1 General Expressions

We are still dealing with semi-infinite atmospheres ( $b = \infty$ ). If the scattering in such an atmosphere is conservative ( $a = 1$ ), every photon entering it must sooner or later emerge again. Before doing so, it may have traveled a very long optical path  $\lambda$  and may have been scattered  $n$  times. For any  $n$ , the average  $\lambda$  is  $n$ , and the root-mean-square deviation is  $\sqrt{n}$ . For any chosen  $\lambda$ , the average value of  $n$  is  $\lambda + 1$ , and the root-mean-square deviation is  $\sqrt{\lambda}$ . At large  $n$  or  $\lambda$ , both distributions are approximately Gaussian (Section 17.2.2).

It is clear that a very slight deviation from the assumption  $a = 1$  will eliminate the contribution from large  $n$  and thus cause a substantial reduction in the reflection function. (The assumption that the layer is finite will be similarly disastrous but is not considered in this section.) This makes it interesting to consider more closely the transition from  $a < 1$  to  $a = 1$ . The best way to deal with this problem is to derive the expansions in  $k$  valid for the nearly conservative case (e.g., Section 5.4.1).

These expansions may be put to the following use.

- (a) In some applications, e.g., terrestrial clouds, the simplest nearly conservative approximation with only one power of  $k$  suffices (Section 19.4.2).
- (b) A computation scheme based on power expansions in  $k$  may be attractive even in circumstances where the absorption is considerable and many terms of the power series are required.

**DISPLAY 12.2**

Asymptotic Expressions for High-Order Scattering in a Semi-Infinite Atmosphere

Let  $a$  be the albedo in single scattering,  $k$  the diffusion exponent, and  $f$  any physical quantity (e.g., reflection function for fixed  $\mu, \mu_0$ )

$$\begin{aligned} (0) \quad & t = (1 - a)^{1/2} \\ (1) \quad & f = f_1 a + f_2 a^2 + f_3 a^3 + \dots \quad (\text{expansion in successive orders}) \\ (2) \quad & f = F_0 + F_1 k + F_2 k^2 + \dots \\ (3) \quad & f = G_0 + G_1 t + G_2 t^2 + \dots \\ (4) \quad & a = 1 - Ak^2 + Bk^4 + \dots \end{aligned} \quad \left. \vphantom{\begin{aligned} (1) \\ (2) \\ (3) \\ (4) \end{aligned}} \right\} \text{(near-conservative expansions)}$$

Interrelations:

$$\begin{aligned} (5) \quad & k^2 = t^2/A + Bt^4/A^3 + \dots \\ (6) \quad & \begin{cases} G_0 = F_0, & G_1 = F_1/A^{1/2}, & G_2 = F_2/A \\ G_3 = F_3/A^{3/2} + \frac{1}{2}BF_1/A^{5/2}, & G_4 = F_4/A^2 + BF_2/A^3 \end{cases} \end{aligned}$$

Asymptotic expressions:

$$\begin{aligned} (7) \quad & f_n \sim (4\pi n^3)^{-1/2} [-G_1 + \frac{3}{2}(G_3 - \frac{1}{4}G_1)n^{-1} + \dots] \\ (8) \quad & f_n \sim -G_1[4\pi(n+c)^3]^{-1/2}[1 + sn^{-2} + O(n^{-3})] \quad \text{with } c = G_3/G_1 - \frac{1}{4} \\ (9) \quad & f_n \sim (4\pi n^3 A)^{-1/2} \{-F_1 + \frac{3}{2}[(-\frac{1}{4} + \frac{1}{2}B/A^2)F_1 + F_3/A]n^{-1} + \dots\} \end{aligned}$$

(c) Series in  $k$  can be transformed into power series of  $a$  and thereby yield the asymptotic behavior of the higher order terms for  $n \rightarrow \infty$ . This particular possibility will be explored in the present section.

We make the same assumption as in Section 12.3.2, namely, that the scattering pattern has an arbitrary fixed form but that the albedo  $a$  is variable. The Legendre coefficients of  $a\Phi(\cos \alpha)$  then are

$$\omega_n = ab_n$$

where  $b_n$  is fixed,  $a$  variable. In principle, any physical quantity based on this scattering law is a function of  $a$ ; so is the diffusion exponent  $k$ . The relationship between  $k$  and  $a$  has been derived in Section 12.3.2. Since  $k$  grows if  $a$  decreases, starting from the conservative case  $k = 0$  for  $a = 1$ , we are entitled to choose  $k$  instead of  $a$  as the variable on which every quantity depends.

Let  $f$  be any such quantity; refer to Display 12.2 for the resulting expansions. We simply assume that expansions of the form (1) and (2) exist. A link between the low-order terms in (2) and the asymptotic form of the high-order terms in (1) must exist on the basis of relation (4), which has been derived earlier (Section 5.4.1 and 12.3.2).

The simplest procedure for finding the actual relations is to transform (2) to (3) by the straightforward relations (5) and (6). Then use the binomial expansion

$$-t = -(1 - a)^{1/2} = \sum_{n=0}^{\infty} y_n a^n$$



where  $y_0 = -1$ ,  $y_1 = \frac{1}{2}$ , and for  $n \geq 2$

$$y_n = \frac{1 \cdot 3 \cdot 5 \cdot \dots \cdot (2n-3)}{2 \cdot 4 \cdot 6 \cdot \dots \cdot (2n-2)2n}$$

exactly. By the Wallis formula (Abromowitz and Stegun, 1965, p. 258)  $y_n$  has the asymptotic form

$$y_n \sim (4\pi n^3)^{-1/2} [1 + \frac{3}{8}n^{-1} + \dots]$$

and consequently

$$y_n - y_{n-1} \sim (4\pi n^3)^{-1/2} [-\frac{3}{2}n^{-1} + \dots]$$

The even terms in (3) do not contribute to the asymptotic forms, but the odd terms give

$$f_n = -G_1 y_n - G_3 (y_n - y_{n-1}) - G_5 (y_n - 2y_{n-1} + y_{n-2}) - \dots$$

which leads at once to (7). Expression (8) is an obvious equivalent of (7). Finally, by means of (6), we can transform (7) into (9).

The derivation followed above (van de Hulst, 1970b) is simpler than that first followed by Uesugi and Irvine (1970a) where only the coefficient of  $n^{-3/2}$  was obtained. An alternative form, as accurate as (7), is to replace the factor in brackets in (7) by  $-G_1 \exp(-d/n)$ . This form has been used by Uesugi and Irvine but does not lead to simpler summations.

### 12.4.2 Numerical Examples

The asymptotic expression in the form (8) of Display 12.2 has been tested in five examples in Fig. 12.16, for which Table 34 provides the numerical data. The choice of  $(n+4)^{-2}$  as abscissa has been made because the average value of  $c$  is about 4. Unfortunately, in some of the examples we had numerical data available only for the terms of order  $n = 1, 2, 3$ . The values of  $G_n$  were taken as much as possible from the exact equations available in Section 5.4.1 using the numerical data on escape function, etc., in Chapter 11. We then started from the values of  $f$  available for  $a = 1, 0.99, 0.95, 0.9$ , and  $0.8$ , subtracted the known value for  $a = 1$ ,  $t = 0$ , divided by  $t$ , and repeated this process. The additional values  $G_n$  were found by extrapolating the graphs thus obtained to  $t = 0$ . An estimated error is shown with these extrapolated values. The value of  $c$  obtained from  $G_3$  and  $G_1$  is not much affected by these uncertainties.

In the case of the bimoments for isotropic scattering, all coefficients were known. For instance, from  $URU = 1 - 2\alpha_1 t$  we find by reference to the moment equations in Section 8.3.3 (details are omitted!):  $G_1 = -4/\sqrt{3}$ ,  $G_2 = 4q_\infty$ , and  $G_3 = -28/(5\sqrt{3})$ .

The curves in Fig. 12.16 behave exactly as expected. Those for  $URU$ , where we start with a diffuse radiation field, are flatter than those for  $1R1$ , and those for

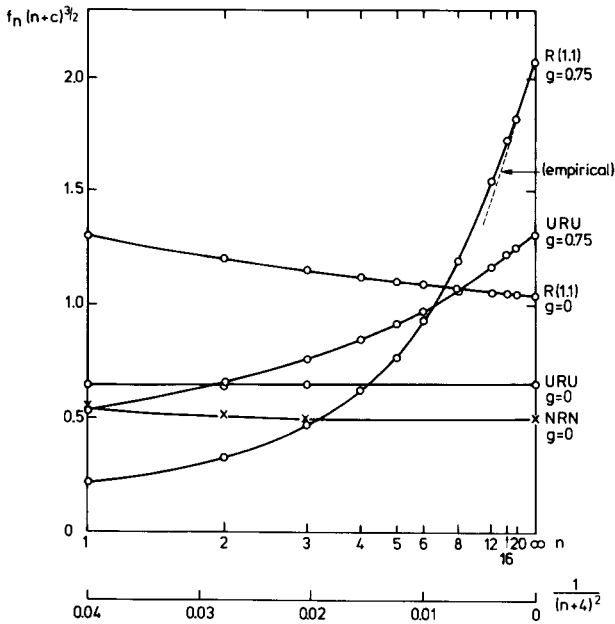


Fig. 12.16. In reflection from a semi-infinite atmosphere with conservative scattering the terms of high-order  $n$  converge very slowly as  $n^{-3/2}$ . Nevertheless, an accurate interpolation of all orders is possible by using the exact asymptotic behavior.

isotropic scattering are flatter than those for the highly anisotropic scattering with  $g = 0.75$ . The fact that the plotted product for  $URU$ ,  $g = 0$ , starts off at  $n = 1$  at less than 1% from the asymptotic value is far better than expected. On the other hand, in the worst example,  $1R1$  for  $g = 0.75$ , the radiation after only three scatterings still is mainly going down into the atmosphere. The corresponding reflection terms must therefore be quite small, and we cannot expect at all that an approach to the asymptotic formulas has already set in at  $n = 3$ .

The fact that all five curves in Fig. 12.16 permit a smooth interpolation between the points at small  $n$  and the asymptotic point at  $n = \infty$  suggests that we have here a potentially powerful method to obtain all terms of intermediate and high orders with good accuracy. By summing these, with the proper factor  $a^n$ , we can then find the entire reflection function. This may be particularly attractive if the albedo  $a$  is to be varied, as in the case of absorption lines.

The practical execution of this method may be performed in a variety of ways. We mention a few without a claim of completeness.

(a) For  $n \geq j$ , replace the sum by an integral. This possibility has been exploited in some detail by Uesugi and Irvine (1969, 1970a,b), by Fouquart and Lenoble (1973), and by Appleby and Irvine (1973). Uesugi and Irvine take  $j = 51$  and use only the dominant asymptotic term. The author's preference would be to take  $j$  much smaller, e.g.,  $j = 11$ , and to integrate not only the

TABLE 34  
Examples of Asymptotic Expressions for High-Order Terms<sup>a</sup>

Quantity $f$	$R(1, 1)$		$URU$		$NRN$
	$g = 0$	$g = 0.75$	$g = 0$	$g = 0.75$	$g = 0$
Coefficients of expansion in $t$	$G_0$	1.057	1.119	1	1.067
	$G_1$	-3.661	-7.329	-2.309	-4.619
	$G_2$	7.84	$23.6 \pm 0.1$	+2.842	11.414
	$G_3$	$-14.8 \pm 0.2$	$-51 \pm 3$	-3.233	$-19.7 \pm 0.2$
	$c$	3.76	6.75	1.15 (exact!)	4.00
Low-order terms	$f_1$	0.1250	0.0102	0.2046	0.0470
	$f_2$	0.0866	0.0129	0.1158	0.0446
	$f_3$	0.0653	0.0155	0.0767	0.0409
	$f_4$	0.0517	0.0176	—	0.0372
	$f_5$	0.0423	0.0192	—	0.0338
$f_n(n + c)^{3/2}$	$n = 1$	1.298	0.220	0.645	0.525
	$n = 2$	1.197	0.335	0.647	0.656
	$n = 3$	1.147	0.471	0.648	0.758
	$n = 4$	1.118	0.620	—	0.842
	$n = 5$	1.097	0.773	—	0.913
	$n = \infty$	1.033	2.068	0.651	1.303

<sup>a</sup> Refer to Display 12.2.

dominant asymptotic term but one or two more. If necessary, an Euler–MacLaurin correction term may be added. In any case, the integral is expressible in an error integral, tables of which are available.

(b) Subtract a series with known sum that has the same asymptotic expansion. This seems rather simpler, in principle. We know, after all, the values of  $G_1 t$  and  $G_3 t^3$  and the exact power expansions

$$G_1 t = \sum_{n=0}^{\infty} -G_1 y_n a^n, \quad G_3 t^3 = (1-a) \sum_{n=0}^{\infty} -G_3 y_n a^n$$

that correspond to these terms. To this we must add corrections that can be computed individually for terms  $n < j$  and that can be neglected (or still replaced by an integral) for  $n \geq j$ . The convergence is fast since we have taken out the least convergent terms. The practical execution is left to the reader.

The need for a summation formula occurs not only if the reflection function is sought, but also if we wish to determine the probability distribution of photon optical paths. Here, again, it is mostly a matter of convenience to represent the numbers  $f_n$  in such a manner that the summation can be readily performed (Section 17.2.2).

### 12.4.3 Asymptotic Expansion of Green's Function

An interesting extension to the preceding results was derived by Ivanov (1974). He analyzes Green's function  $G(\tau, u; \tau_0, u_0)$ , which is the intensity at depth  $\tau$  in direction  $u$  caused by a source layer at depth  $\tau_0$  shining in direction  $u_0$ , with the source density  $\delta(\tau - \tau_0) \delta(u - u_0)$ , i.e., the same source layer as considered at the end of Section 5.5. Expanding in a power series

$$G(\tau, u; \tau_0, u_0) = \sum_{n=0}^{\infty} a^n G_n(\tau, u; \tau_0, u_0)$$

he finds the asymptotic expression ( $n \rightarrow \infty$ )

$$G_n \sim 4[3\pi(1-g)]^{-1/2} n^{-3/2} I_M^0(\tau, u) I_M^0(\tau_0, -u_0)$$

We have written this result in a notation consistent with ours, except for  $G$ ,  $G_n$ , which take the place of  $f, f_n$  in Display 12.2. The function  $I_M^0(\tau, u)$  is the intensity at depth  $\tau$  in direction  $u$  in the conservative Milne problem. The particular forms of this function for  $\tau \gg 1$  and for  $\tau = 0$  are given in Section 5.4.3, Eqs. (43) and (44), if we put  $F = 1$ .

The physics behind this remarkable factorization is that the photons, after very many scattering events, simply "forget" at what depth and in what direction they were injected. Their distribution in  $\tau$  and  $u$  thus becomes independent of  $\tau_0$  and  $u_0$ . The other factor then follows by reciprocity. The factor in front may be verified by returning to reflection in taking  $\tau = \tau_0 = 0$ ,  $u_0 = \mu_0 > 0$ ,  $-u = \mu > 0$ ,  $I_M^0(0, -\mu) = K(1, \mu)$ ,  $G(0, -\mu; 0, \mu_0) = 2R(\mu, \mu_0)$ , and applying

line 9 of Display 12.2 with the constants taken from Eqs. (31) and (35) of Section 5.4.1.

Yet this is not the complete story. The radiation field  $I_n(\tau, u)$  of photons that have gone through  $n$  scattering events has, for  $n \gg 1$ , a broad maximum at depths of the order of  $n^{1/2}$ . Near this maximum the radiation is approximately isotropic. Further up, for  $\tau \ll n^{1/2}$ , the radiation diffuses outward, and Ivanov's asymptotic formula (which is based on  $\tau$  fixed,  $n \rightarrow \infty$ ) refers to this realm. Further down, for  $\tau \gg n^{1/2}$ , the radiation diffuses inward as set forth at the end of Section 5.5. At each succeeding scattering, the maximum imperceptibly flattens and shifts downward.

A good illustration with isotropic scattering is provided by Fig. 7.1a. Here, at  $n = 5$ , the maximum has barely reached  $\tau = 1$ . For very much larger  $n$ , the curve of  $J_n$  near the surface will more and more resemble the Hopf solution shown in Fig. 8.12 with a proportionality factor that can be derived from the formula above. At the same time the curve near the maximum and further down will start to resemble the curves  $F_n(x)$  shown in Fig. 8.1.

## REFERENCES

- Abramowitz, M., and Stegun, I. A. (1965). "Handbook of Mathematical Functions." Dover, New York.
- Appleby, J. F., and Irvine, W. M. (1973). *Astrophys. J.* **183**, 337.
- Bond, G. R., and Siewert, C. E. (1971). *Astrophys. J.* **164**, 97.
- Busbridge, I. W. (1967). *Astrophys. J.* **149**, 195.
- Busbridge, I. W., and Orchard, S. E. (1968). *Astrophys. J.* **154**, 729.
- Case, K. M., and Zweifel, P. F. (1967). "Linear Transport Theory." Addison-Wesley, Reading, Massachusetts.
- Chamberlain, J. W., and Smith, G. R. (1970). *Astrophys. J.* **160**, 755.
- Chandrasekhar, S. (1950). "Radiative Transfer." Oxford Univ. Press (Clarendon), London and New York. Also Dover, New York, 1960.
- Dlugach, J. M. and Yanovitskii, E. G. (1974). *Icarus* **22**, 66.
- Fouquart, Y., and Lenoble, J. (1973). *J. Quant. Spectrosc. Radiat. Transfer* **13**, 447.
- Fricke, C. L. (1975). An Improved Technique for Determining Reflection from Semi-infinite Atmospheres with Linearly Anisotropic phase Functions. NASA Tech. Note TN D-8011.
- Grosjean, C. C. (1963). Verhandelingen Kon. Vlaamse Acad. voor Wetenschappen, letteren en schone kunsten van België, Klasse der Wetenschappen, No. 70.
- Horak, H. G., and Janousek, A. L. (1965). *Astrophys. J. Suppl.* **11**, 277.
- Irvine, W. M. (1974). *Icarus* **25**, 175.
- Ivanov, V. V. (1974). *Astrofizika* **10**, 193 [English transl.: **10**, 117].
- Kaper, H. G., Shultis, J. K., and Veninga, J. G. (1970). *J. Comput. Phys.* **6**, 288.
- Kattawar, G. W. (1975). *J. Quant. Spectrosc. Radiat. Transfer* **15**, 839.
- Kattawar, G. W. (1977). *J. Quant. Spectrosc. Radiat. Transfer* **18**, 143.
- Kolesov, A. K., and Smoktii, O. I. (1971). *Astron. Zh.* **48**, 1013 [English transl.: *Sov. Astron. AJ* **15**, 802].
- Kuščer, I. (1958). *J. Math. Phys.* **37**, 52.
- Mark, J. C. (1943). Nat. Res. Council, Canada, Publ. No. 1561 (MT-26).
- Maslennikov, M. V., and Sushkevich, T. A. (1964). *Comput. Math. Math. Phys. USSR* **4**, 29.

- Sobolev, V. V. (1969). *Dok. Akad. Nauk* **184**, 318 [English transl.: *Sov. Phys. Dokl.* **14**, 1].
- Sobolev, V. V. (1975). "Light Scattering in Planetary Atmospheres." Pergamon, Oxford. Orig. Russian, 1972.
- Su, S. F., and McCormick, N. J. (1971). *J. Nucl. Energy* **25**, 657.
- Uesugi, A., and Irvine, W. M. (1969). *J. Atmos. Sci.* **26**, 973.
- Uesugi, A., and Irvine, W. M. (1970a). *Astrophys. J.* **159**, 127.
- Uesugi, A., and Irvine, W. M. (1970b). *Astrophys. J.* **161**, 243.
- van de Hulst, H. C. (1968). *Bull. Astron. Inst. Neth.* **20**, 77.
- van de Hulst, H. C. (1970a). *Astron. Astrophys.* **9**, 366.
- van de Hulst, H. C. (1970b). *Astron. Astrophys.* **9**, 374.
- van de Hulst, H. C. (1971). In "Planetary Atmospheres" (C. Sagan *et al.*, eds.), Inter. Astron. Union Symp. 40, p. 177. Reidel, Dordrecht.
- van de Hulst, H. C. (1974a). In *UCLA Int. Conf. Radiat. Remote Probing Atmos.* (J. G. Kuriyan, ed.), p. 162. Western Periodicals Co., North Hollywood, California.
- van de Hulst, H. C. (1974b). *Astron. Astrophys.* **35**, 209.
- van de Hulst, H. C., and Grossman, K. (1968). In "The Atmospheres of Venus and Mars" (J. C. Brandt and M. B. McElroy, eds.), p. 35. Gordon and Breach, New York.
- Vanmassenhove, F. R. (1967). *Simon Stevin* **41**, 1.
- Vanmassenhove, F. R. (1969). *Physica* **42**, 179.
- Wang, L. (1972). *Astrophys. J.* **174**, 671.
- Yanovitskii, E. G. (1968). *Astromet. Astrofiz. (Kiev)* **1**, 165.
- Yanovitskii, E. G. (1972). *Astron. Zh.* **49**, 844 [English transl.: *Sov. Astron. AJ* **16**, 687 (1973)].

## 13 ☐ Henyey-Greenstein Functions, Results for Finite Layers

This chapter contains an account of computations with one set of phase functions (the same as in Chapter 11) now varying not only albedo  $a$ , anisotropy  $g$ , cosines of angles  $\mu$  and  $\mu_0$ , but also optical thickness  $b$  of the layer. It is clearly impossible to present functions of so many variables in any detail. A selection of tables and figures has been made, all based on computations made by Dr. K. Grossman at the NASA Institute for Space Studies, New York, N.Y., and virtually all done by the doubling method. Comparisons with results for other phase functions are made in the next chapter.

### 13.1 REFLECTION AND TRANSMISSION

The reflection and transmission functions for two anisotropies  $g = 0.50$  and  $g = 0.75$  are presented in Table 35<sup>‡</sup> using the same format as Table 12 (Section 9.1.1), which contains the corresponding numbers for isotropic scattering ( $g = 0$ ). The choice of values of the optical thickness has been limited to  $b = \frac{1}{2}, 1, 2, 4$  for  $g = 0.5$  and  $b = 1, 2, 4, 8$  for  $g = 0.75$  in such a way that the range of reduced optical depths  $b(1 - g)$  is in either case 0.25–2, which forms a fair middle range between very thin and very thick atmospheres. Some individual entries for a more complete grid of  $b$  and  $g$  values can be found in Tables 37–39 later in this chapter.

<sup>‡</sup> Table 35 is placed at the end of this chapter, beginning on page 412.

The use of Table 35 may be extended toward higher values of  $b$  by referring first to Table 27 (Section 11.3) which gives the corresponding arrays for  $b = \infty$  and second, to the thick-layer formulas in Section 5.3 combined with the constants and escape function found in Tables 23 and 26 (Sections 11.1–2).

The extension of Table 35 toward lower values of  $b$  can best be made starting from single scattering. The single term in reflection, if no integration over azimuth is made, is

$$R_1(\mu, \varphi; \mu_0, \varphi_0) = [a\Phi(\cos \alpha)/4(\mu + \mu_0)](1 - e^{-b/\mu - b/\mu_0})$$

where  $\alpha$  is the angle between directions  $(-\mu, \varphi)$  and  $(\mu_0, \varphi_0)$ , and  $\Phi(\cos \alpha)$  may be read from Table 21 (Section 11.1). This is simply the equation for isotropic scattering (Display 9.1) with the phase function put in as an extra factor. The first-order term of the transmission function can be obtained similarly. The corresponding term averaged over azimuth is found by replacing  $\Phi(\cos \alpha)$  by  $h(u, v)$ , the redistribution function presented in Table 22 (Section 11.1).

The range of  $b$  values for which these first-order formulas can be used without any correction is very small indeed. A quick assessment of the correction required may be taken from Table 38, where the ratio of total to first-order reflection is presented for a representative set of angles and moments and for a wider range of  $b$  and  $g$  values than available in Table 35.

#### NUMERICAL EXAMPLE

Find from the tables here presented an estimate of  $R(a, g, b, \mu, \mu_0)$  for  $a = 0.9$ ,  $g = 0.75$ ,  $b = 0.25$ ,  $\mu = 1$ ,  $\mu_0 = 0.5$ . This is a case of bad luck, for the  $b$  value is below the range of Table 35 and well above the range where single scattering suffices. Table 38 shows that for  $a = 1$ , the ratio  $R/R_1$  would be 1.88. The actual ratio for  $a = 0.9$  should be somewhat smaller, and a fair estimate can be made by simply assuming a geometric series for all orders so that  $1.88 = (1 - r)^{-1}$ , from which we find  $r = 0.469$  and  $(1 - 0.9r)^{-1} = 1.73$ . Furthermore, since  $\mu = 1$ , averaging over azimuth does not occur, and we have, without including albedo,  $\Phi(\cos \alpha) = 0.1244$ . Finally, starting from the first-order value for isotropic scattering and not writing  $\mu$  and  $\mu_0$ , we have  $R(0.9, 0.75, 0.25) = 1.73 \times 0.1244 \times 0.9 \times 0.0879 = 0.0170$ , which differs less than 1% from the correct value 0.01714.

For further illustration, we show in Table 36 the values of  $R$  in this example in the full range of  $b$  (obtained from the same computer output as Table 35 but not reproduced in toto there because we must make a selection). The same table also shows a comparison with an approximately similar case of isotropic scattering. Roughly 4 scatterings at  $g = 0.75$  correspond to one at  $g = 0$ , so that  $b$  has to be reduced by a factor of 4, and  $a$  has to be taken  $(0.9)^4 = 0.66$ . More precisely, Fig. 12.6 shows that similarity for thick layers would require a choice of  $a$



TABLE 36

Reflection Function for a Sample Problem with Anisotropic Scattering, Compared with an Approximately Similar Problem with Isotropic Scattering

Column	(1)	(2)	(3)	(4)	(5)
	$R(0.9, 0.75, b)$			$R(0.6, 0, \frac{1}{4}b)$	
$b$	Total	1st order	Ratio (1)/(2)	Total	Ratio (1)/(4)
0	0	0	1	0	0.747
$\frac{1}{128}$	0.00045	0.00043	1.031	0.00059	0.760
$\frac{1}{64}$	0.00090	0.00086	1.058	0.00117	0.770
$\frac{1}{32}$	0.00185	0.00167	1.106	0.00235	0.787
$\frac{1}{16}$	0.00382	0.00319	1.199	0.00469	0.815
$\frac{1}{8}$	0.00804	0.00584	1.378	0.00933	0.862
$\frac{1}{4}$	0.01714	0.00984	1.740	0.01838	0.933
$\frac{1}{2}$	0.03618	0.01450	2.496	0.03529	1.025
1	0.0713	0.01773	4.022	0.0642	1.111
2	0.1196	0.01861	6.423	0.1050	1.139
4	0.1606	0.01866	8.605	0.1444	1.112
8	0.1776	0.01866	9.516	0.1634	1.087
16	0.1795	0.01866	9.618	0.1663	1.079
32	0.1795	0.01866	9.619	0.1664	1.079
$\infty$	0.1795	0.01866	9.619	0.1664	1.079

slightly above 0.7. We have chosen from the  $a$  values for which results are available in Table 12 the value  $a = 0.6$ , and the correction factors then required to get the function we seek are shown in column (5) of the table and in Fig. 13.1. It should be noted that the change sets in already at very small  $b$ .

The methods used in this example cannot, of course, replace a good computer run, but in situations where a quick estimate with a 1% accuracy is required, they may prove useful.

Conservative scattering ( $a = 1$ ) takes such a prominent place in the applications that we have selected more complete data for this case in Table 37.† They are in the form of reflection and transmission functions arranged in matrix form with all moments and bimoments obtained with the operators  $U$  and  $N$ . The layer thickness ranges from  $\frac{1}{2}$  to 8 for  $g = 0.25, 0.75, 0.875$  but has been extended to the wider range  $\frac{1}{16}$ –32 for  $g = 0.50$ . Corresponding values for isotropic scattering,  $g = 0$ , may again be obtained from Table 12.

Finally, we present for quick reference in Table 38‡ the ratios of total to first-order reflection in a format very similar to that in which these ratios were

† Tables 37 and 38 are placed at the end of this chapter, beginning on pages 444 and 454, respectively.

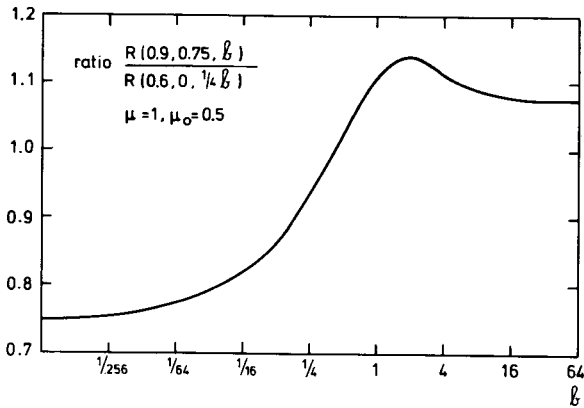


**Fig. 13.1.** Ratio of reflection values in two roughly similar situations as a function of optical thickness.

given for isotropic scattering (Table 13, Section 9.1.2). As expected, these ratios reach very much higher values than for isotropic scattering, particularly when  $g$  is large. Again, grazing incidence gives low factors, and perpendicular incidence, higher factors. Generally, the order in which the factors increase with changing assumptions about the directions of incidence is 0,  $N$ ,  $U$ , 1. The unidirectional incidence  $\mu_0 = 0.5$  gives factors not too different from those corresponding to the uniform incidence  $U$ .

The inverse value of the ratio in Table 38, namely, the fraction contributed to the total reflection by the first-order term, has been plotted in Fig. 13.2 for the

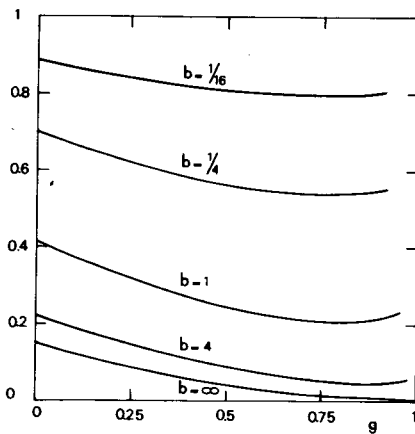


**Fig. 13.2.** Fraction of first-order scattering contained in the plane albedo of a conservative slab of varying optical thickness  $b$  and asymmetry parameter  $g$ .

combination  $1RU$ , which is the albedo of the slab for perpendicular incidence. With this particular set of phase functions, the fraction appears to reach a finite limit if  $b$  is fixed,  $g \rightarrow 1$ . We have not derived this limit. Only the following simple result may be mentioned. If  $g \rightarrow 1$  and  $b \rightarrow 0$ , then both  $UR_1$  and  $UR_1 1$  approach the limit  $(1/\sqrt{2} - \frac{1}{2})(1 - g)b = 0.207(1 - g)b$ . This also fits reasonably with the limits suggested empirically in Fig. 13.7.

### 13.2 FATE OF INCIDENT ENERGY

Among the numbers that may be read from Tables 35 and 36, the moments with "vector"  $U$  are particularly important because they tell us what happens to the incident energy. If the radiation is incident from direction  $\mu_0$ , a fraction  $UR(\mu_0)$  is reflected, a fraction  $UT(\mu_0)$  is transmitted, and the remainder is absorbed. These three fractions have been separately tabulated in Table 39<sup>‡</sup> for four assumptions about the incident radiation, eight values of the albedo, ten values of the optical depth  $b$ , and three anisotropies. This table has the same

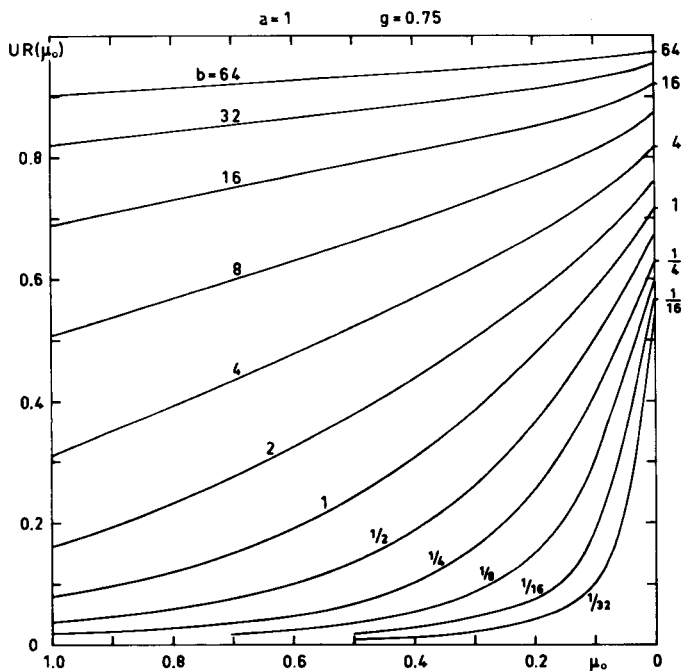
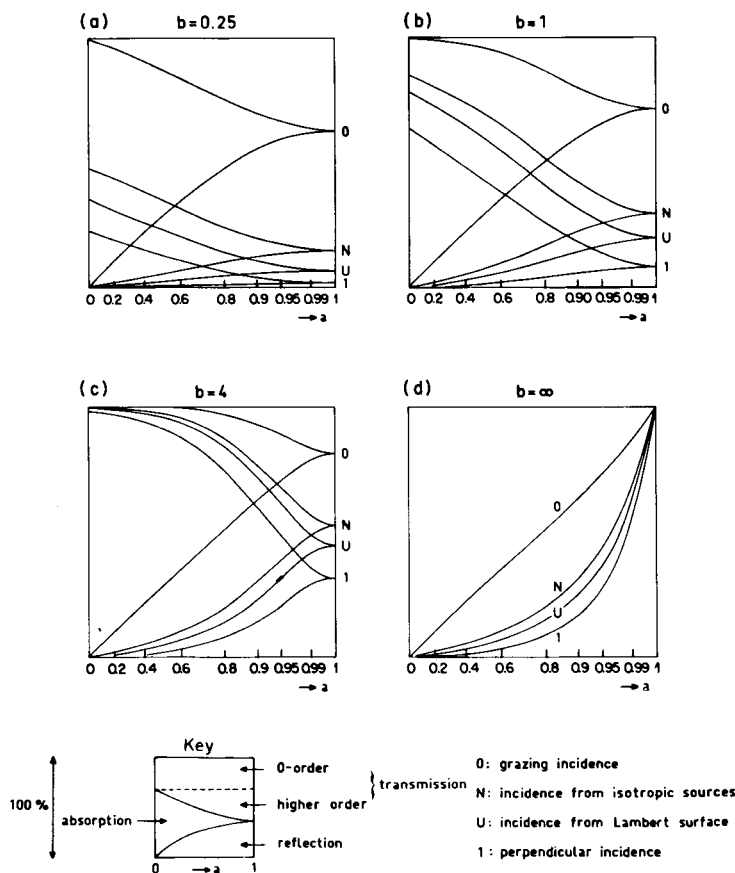


Fig. 13.3. Plane albedo for incidence from direction  $\mu_0$  of slabs of varying thickness with conservative scattering and asymmetry parameter  $g = 0.75$ .

<sup>‡</sup> Table 39 is placed at the end of this chapter, beginning on page 456.



**Fig. 13.4.** Fate of incident energy for a slab with Henyey-Greenstein scattering with  $g = 0.75$ . By choosing the optical thickness  $b$ , the albedo for single scattering  $a$ , and the angular distribution of incident radiation 0,  $N$ ,  $U$ , or 1, a vertical line with two intersection points is defined. The key shows how these points divide the 100% of available energy into its transmitted, absorbed, and reflected parts (same format as Fig. 9.4).

format as Table 15 for isotropic scattering. Figure 13.3 illustrates for one combination,  $g = 0.75$ ,  $a = 1$ , how the reflected fraction gradually goes from 0 for thin layers to 1 for very thick layers. At grazing incidence, the reflected fraction is always  $> \frac{1}{2}$  because half of the radiation escapes upon the first scattering.

For the same value of  $g$ , we can see in Fig. 13.4 how the reflected, transmitted, and absorbed fractions of the incident flux vary with albedo  $a$ . The format is identical to that of Fig. 9.4, which shows these fractions for isotropic scattering. The bimoments  $URU$  and  $URN$  are again seen to fit neatly between the extreme values  $UR(0)$  and  $UR(1)$ . Only the detailed numbers are different. Comparison with Fig. 9.4 shows that for the same value of  $b$ , the forward scattering pattern

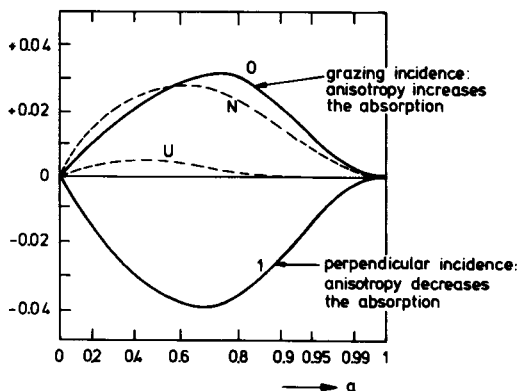


Fig. 13.5. Difference between the fractions of energy absorbed inside a slab with optical thickness  $b$  for anisotropic scattering ( $g = 0.75$ ) and isotropic scattering ( $g = 0$ ). The directions of incident radiation are varied and so is the individual scattering albedo  $a$ .

( $g = 0.75$ ) yields a relatively weaker reflection and stronger transmission. It is not so obvious how the absorbed fraction is affected. The differences for  $b = 1$  are shown in a separate graph (Fig. 13.5). It is seen that anisotropy increases the absorbed fraction for grazing incidence but reduces it for perpendicular incidence. The difference is important only in the middle range of the albedos, and even there reaches at most 3 or 4%.

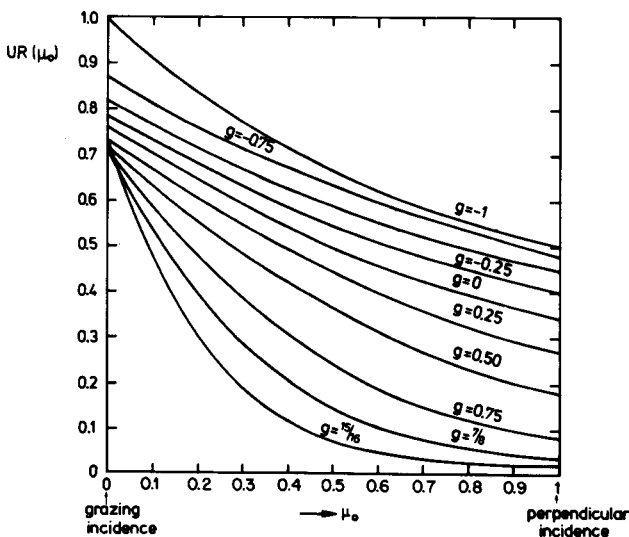


Fig. 13.6. Plane albedo of a slab with optical thickness 1 and conservative scattering. The direction of incidence and the asymmetry parameter are varied.

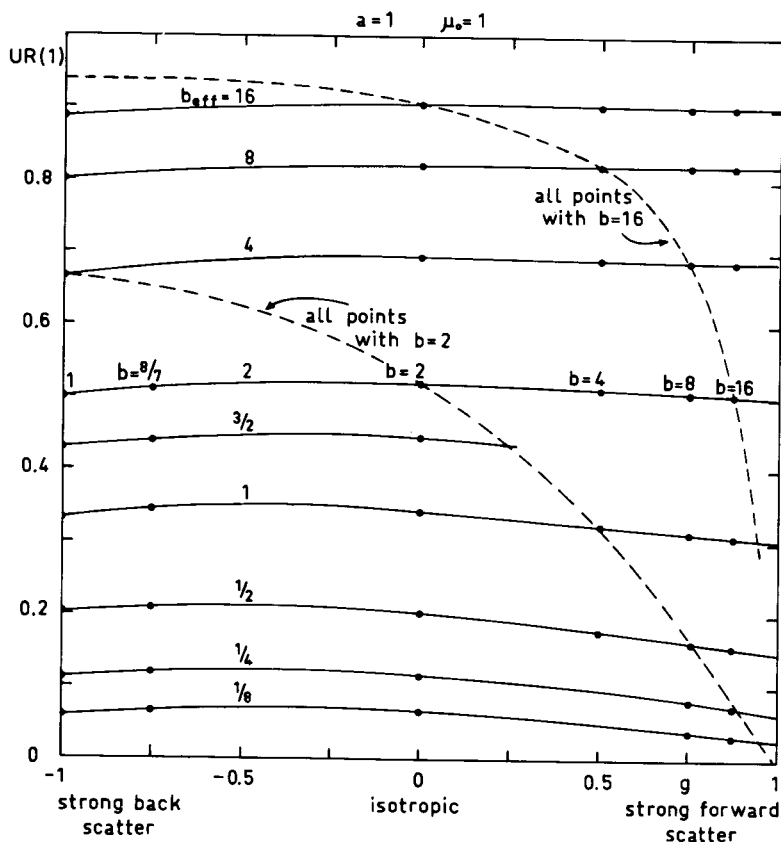


Fig. 13.7. Plane albedo of slabs of varying thickness  $b$  for conservative scattering with varying asymmetry parameter  $g$  and perpendicular incidence. The similarity rule is demonstrated by the fact that curves with constant  $b_{\text{eff}} = b(1 - g)$  are nearly horizontal.

The variation of the reflected fraction with  $g$  and  $\mu_0$  is shown for one combination:  $b = 1$ ,  $a = 1$ , in Fig. 13.6. In this graph we have included results for values of  $g$  for which no tables are presented in this book. These values are  $g = -0.25$ ,  $-0.50$ , and  $-0.75$ , corresponding to predominant backscatter, and  $g = \frac{15}{16}$ , corresponding to extreme forward scatter. Furthermore, we have included the limiting curve for  $g = -1$ , corresponding to the reflected fraction  $1/(1 + \mu_0)$ , which may be read from Display 14.2, column 7.

We can now proceed to look at some figures where both  $b$  and  $g$  are varied. These are Figs. 13.7 and 13.8, very similar in format, both referring to the conservative case. The curves of constant  $b$  are seen to link up smoothly with the points at  $g = -1$ , for which the formulas are

$$UR(1) = b/(b + 1)$$

$$URU = 1 - UTU = 2b[1 - b \ln(1 + b^{-1})]$$

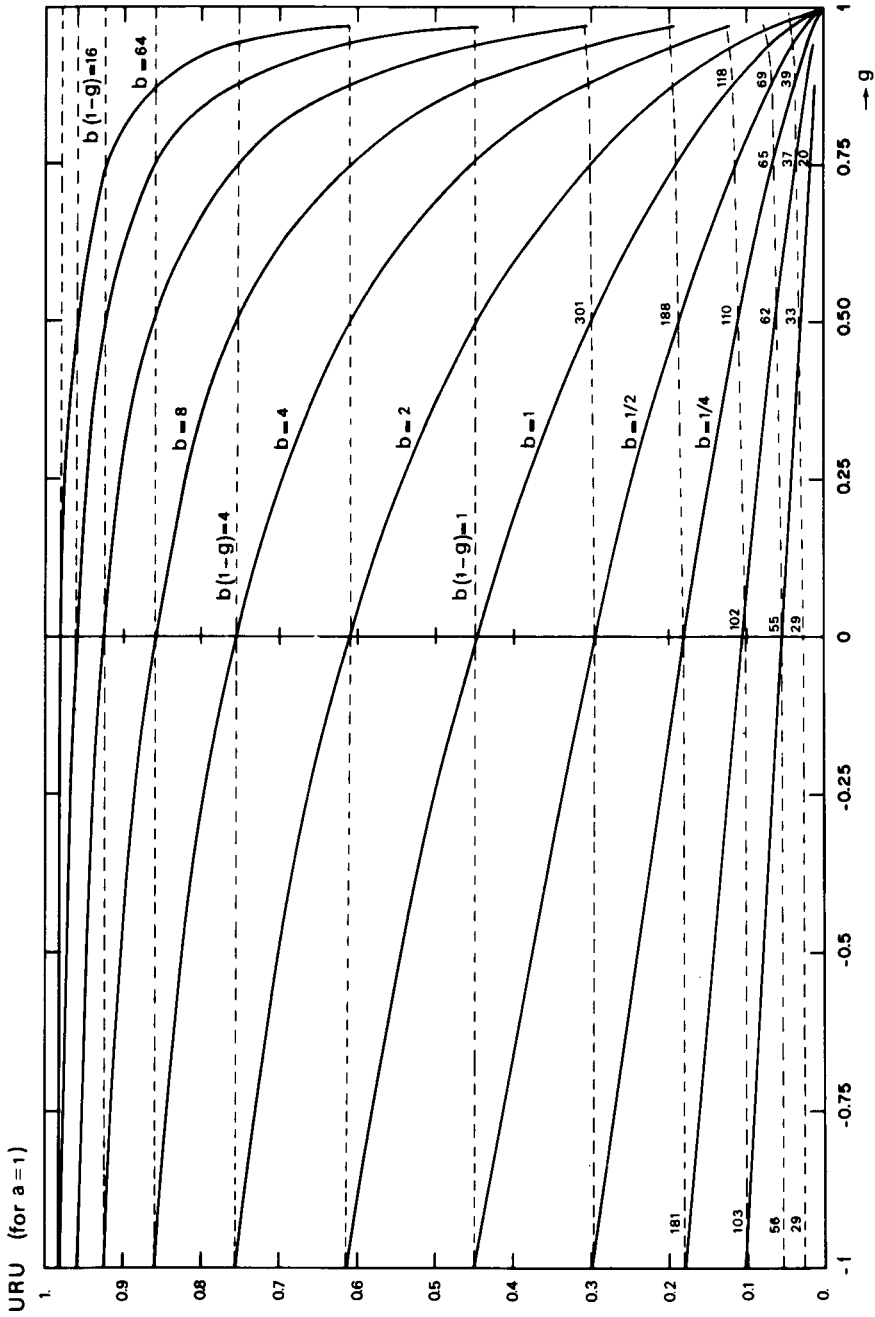


Fig. 13.8. Spherical albedo, or bimonent  $URU$ , for conservative scattering in slabs of varying thickness and varying asymmetry parameter. The format is as in Fig. 13.7, and the similarity rule is followed even more closely.

All curves are seen to vanish to 0 in the limit  $g \rightarrow 1$ , because no scattering at all automatically implies no reflection at all.

However, the most striking feature of both Figs. 13.7 and 13.8 is that the curves of constant  $b_{\text{reduced}} = b(1 - g)$  are almost horizontal. This came as a surprise when it was first discovered (van de Hulst and Grossman, 1968). It is now recognized as an illustration of the similarity principle for finite layers, which will be discussed in Chapter 14. We have also tried to prove that these almost horizontal curves should reach a finite limit at  $g \rightarrow 1$ ,  $b \rightarrow \infty$ , if  $b_{\text{reduced}}$  is kept fixed. This effort has been unsuccessful; it is likely that the behavior in this limit depends on the precise set of scattering patterns chosen. The complications of this problem can also be gathered from Section 12.3.2, where it is shown that if we were to work by means of an eigenfunction expansion, i.e., by the Case method, a great many discrete eigenvalues would have to be taken into account precisely in this limit (Fig. 12.15).

### 13.3 POINT-DIRECTION GAIN AND INTERNAL FLUX

The doubling method, which was employed in obtaining the numerical data for this chapter, does not give the radiation field at an arbitrary depth inside the layer. It may be modified to do so, and Display 4.6 contains the relevant formulas.

In our routine we obtained automatically the full radiation field at the mid-layer depth. For illustration, Table 40<sup>‡</sup> presents this midlayer field for three total thicknesses ( $b = 0.5$ ,  $b = 2$ , and  $b = 8$ ), employing the same anisotropic phase function,  $g = 0.5$ , and assuming nonconservative scattering ( $a = 0.9$ ) or conservative scattering ( $a = 1.0$ ).

Some graphs of the midlayer intensity obtained in this manner are found in Fig. 9.15b. These combinations of  $g$ ,  $b$ , and  $a$  have been chosen to provide approximate similarity (see Section 14.1) with those for isotropic scattering in Fig. 9.15a.

Table 41 of gain, gain moments, and internal fluxes, which is an extension of Table 17 to anisotropic scattering patterns, has accordingly been restricted to the values at top, bottom, and midlayer depth. The organization of the table is identical to that of Table 17, and the reader may refer to Section 9.3.1 for a full explanation.

One quantity of interest to be obtained from this table is the *escape probability*. Generally, quanta emitted from an isotropic source at depth  $\tau$  in a layer of thickness  $b$  have a probability  $\frac{1}{2}g_0(a, b, \tau)$  to escape with or without scattering from the top surface of the layer. The zero-order gain moment  $g_0$  is the quantity given in the left part of Table 41 on the pages with input  $U$ . The probability for

<sup>‡</sup> Tables 40 and 41 are placed at the end of this chapter, beginning on pages 462 and 465, respectively.



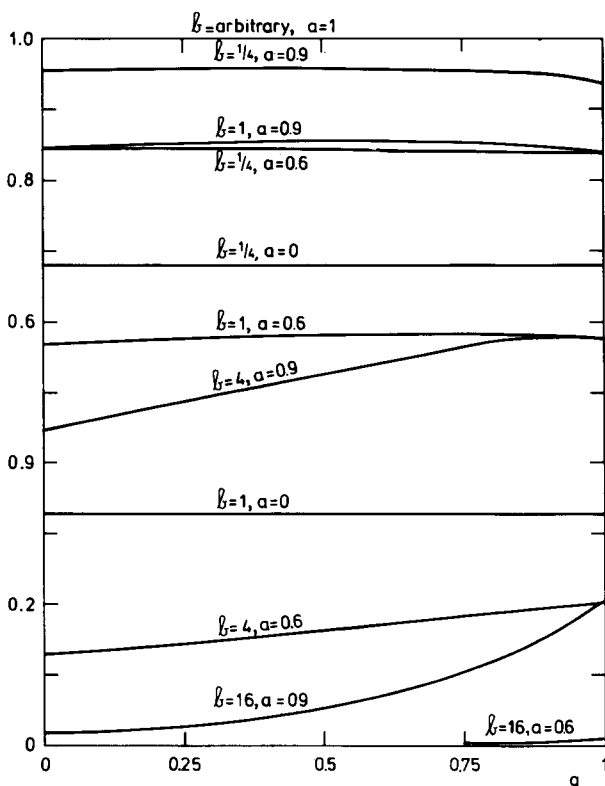
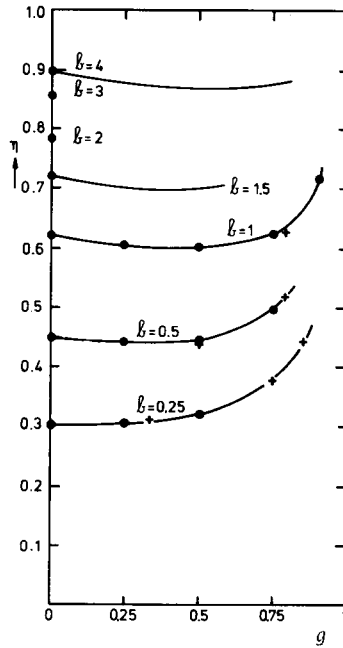


Fig. 13.9. Escape probability from a slab of thickness  $b$  for an isotropic source at midlayer through both surfaces combined. Thickness and single-scattering albedo are varied by steps and the asymmetry parameter is varied continuously.

escape from a midlayer point is  $\frac{1}{2}g_0$  through top or bottom surface, i.e.,  $g_0$  combined. This quantity has been plotted for some combinations of  $a$  and  $b$  in Fig. 13.9. The variation with the asymmetry factor  $g$  is surprisingly small, even though we knew from the start that this escape probability is independent of  $g$  for the two limiting albedos: if  $a = 1$  it is simply 1, and if  $a = 0$  it is  $E_2(\frac{1}{2}b)$ . The graphs in Fig. 13.9 have been completed by the exact points at  $g = 1$ , which have the escape probability  $E_2[(1 - a)\frac{1}{2}b]$ .

#### 13.4 CONVERGENCE OF THE SUCCESSIVE SCATTERING METHOD AND OF THE DOUBLING METHOD

The following numerical data may be helpful in assessing the rapidity by which the successive scattering method and the doubling method converge. Corresponding data for isotropic scattering have been presented in Sections



**Fig. 13.10.** The eigenvalue  $\eta$ , to which the ratio of successive orders of scattering in any slab problem converges, is shown for Henyey–Greenstein scattering as a function of asymmetry parameter  $g$  and slab thickness  $b$  (● and drawn curves). Some points read from graphs of other authors (+) are in good agreement.

7.4.1 and 9.6.4. Our main concern is to see what changes occur if the scattering pattern is anisotropic.

The orders in the *successive scattering method* converge as a geometric series with ratio  $a\eta_1$ , where  $a$  is the albedo and  $\eta_1$  the eigenvalue presented in Fig. 7.2 for isotropic scattering. Figure 13.10 shows how this eigenvalue varies with  $g$ . The graph is incomplete because the dots are based on early computer runs; in later runs we have not used this method. Some values read from graphs presented by other authors, notably Irvine (1968, Fig. 5), have been added as crosses. They fit well, though the points at  $g = 0.79$  do not refer to Henyey–Greenstein scattering. The general conclusion is that convergence is about equally fast for all reasonable values of the asymmetry factor.

Figure 13.11 shows for one value,  $g = 0.5$ , the dependence of the eigenvalue on  $b$ . The thick curve in the middle range shows hardly any deviation from the corresponding  $g = 0$  curve (thin dashed curve). The approximate formula for large  $b$ ,

$$\eta_1 = 1 - 20/[3(b + 3)^2]$$

again represented by a thick curve, links up satisfactorily.

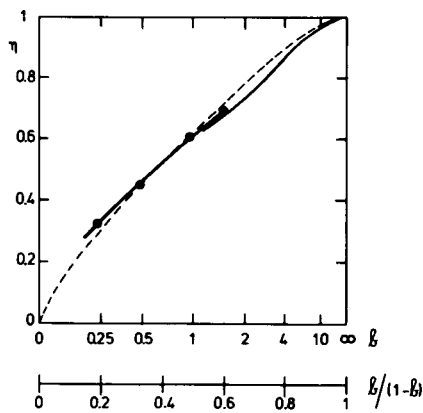


**Fig. 13.11.** The eigenvalue  $\eta$  of a slab of thickness  $b$  in the successive-order method for Henye y–Greenstein scattering with  $g = 0.5$  (● and drawn curves) differs little from the corresponding value for isotropic scattering (dashed curve).

The *doubling method* converges as a geometric series whose ratio is the eigenvalue  $\zeta_1(a, b, g)$ . It was presented for isotropic scattering ( $g = 0$ ) in Table 19 and Fig. 9.18. In seeing how this value varies with the assumed asymmetry factor  $g$ , we have confined our attention to the conservative case ( $a = 1$ ). The values are shown in Table 42 and Fig. 13.12. It is seen that  $\zeta_1$  is smaller, hence the convergence, faster, for the same value of  $b$  if a forward scattering pattern is introduced. But the difference becomes small if we compare situations with the same reduced thickness  $b(1 - g)$  according to the similarity principle.

**TABLE 42**  
Eigenvalues in Doubling Method for Conservative Scattering;  
Henye y–Greenstein Phase Functions

Doubling from $\frac{1}{2}b$ to $b$		$g = 0$	$g = 0.25$	$g = 0.50$	$g = 0.75$
		Value of $\zeta_1$			
$\frac{1}{2}$	1	0.1065	—	—	0.0489
1	2	0.2168	0.1687	0.1213	0.0796
2	4	0.3825	0.3100	0.2251	0.1432
4	8	0.5730	0.4947	0.3853	0.2354
8	16	0.7385	0.6754	0.5738	0.4040
16	32	0.8534	0.8119	0.7387	0.6276
$\infty$	$\infty$	1	1	1	1
		Value of $\zeta_2$ (asymptote only)			
$\infty$	$\infty$	0.0026	0.0038	0.0077	0.0149

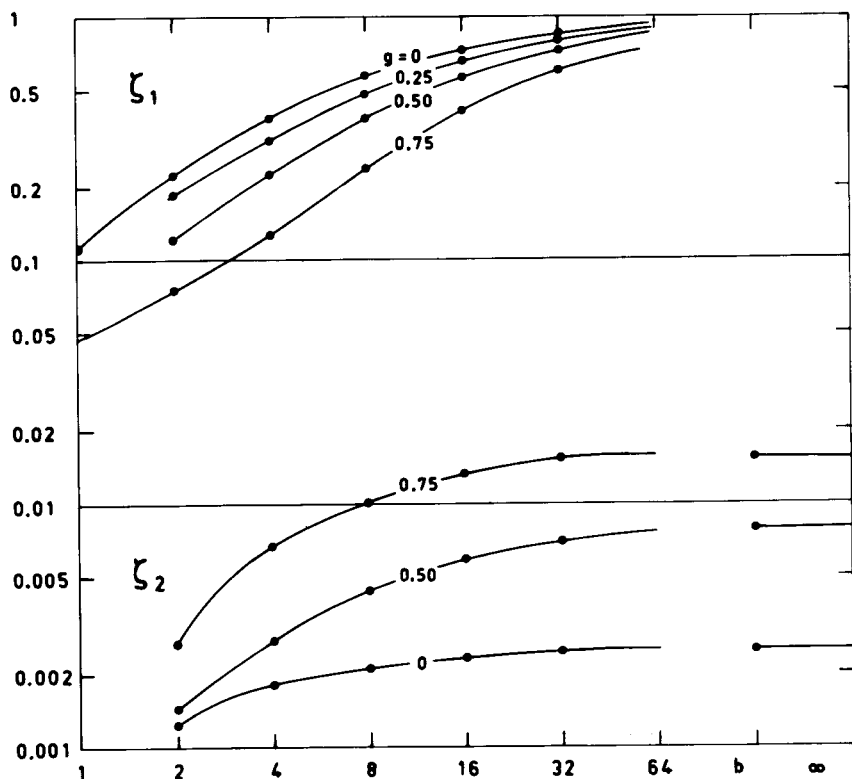


Fig. 13.12. The eigenvalue  $\zeta_1$ , to which the ratio of successive terms in doubling from  $\frac{1}{2}b$  to  $b$  converges, is shown as a function of  $b$  and  $g$ . The second eigenvalue  $\zeta_2$ , plotted on the same scale, is comfortably lower.

The same graph also gives the second eigenvalue  $\zeta_2(1, b, g)$ . These values were obtained from the same computer runs, but may have considerable errors, because no attempt at a precise determination was made. The enormous ratio between the first and second eigenvalue, which we had noticed for  $g = 0$ , is reduced but remains larger than a factor  $\sim 20$ . This large factor explains why the method is so attractive in practical computations. At  $b \rightarrow \infty$ , the second eigenvalue approaches a limit which may be approximated by the surprisingly simple formula (derived below):

$$\zeta_2(1, \infty, g) = [24(1 - g)q_0 - 17]^2$$

where  $q_0$ , the extrapolation length for conservative scattering, may be taken from Table 26 (Section 11.2). The resulting numbers are given in the bottom line of Table 42 and are shown as asymptotes in Fig. 13.12. They match the data for large  $b$  very well. Corresponding values for many more scattering functions

may be read from Table 30 (Section 12.1.2). Isotropic scattering gives  $q_0 = 0.7104$ ,  $\lambda_2 = 0.0507$ ,  $\zeta_2 = 0.0026$ . See a better estimate below.

We shall now briefly derive this formula. Returning to the “vector” and “matrix” notation of Chapter 5, we can state that the quantities  $\zeta_1$  and  $\zeta_2$  are the squares of the two largest eigenvalues in the equation

$$RI = \lambda I \quad (1)$$

Let the phase function be arbitrary, with asymmetry  $g$ , and let the albedo  $a$  be close to 1. Then, employing the notation of Display 5.1 and Eq. (35) from Section 5.4.1, we may write

$$\begin{aligned} UR &= U - cK_0 + O(k^2) \\ WR &= \frac{4}{3}K_0 - W - cq'K_0 + O(k^2) \end{aligned} \quad (2)$$

where  $c = 4k/3(1 - g)$  and  $q' = (1 - g)q_0$ . Empirically, we know that  $K_0$  is a nearly linear function of  $\mu$ , i.e., a linear combination of  $U$  and  $W$ . Fixing the coefficients to satisfy the exact relations  $UK_0 = 1$  and  $WK_0 = q'$ , we have (with  $UU = 1$ ,  $UW = \frac{2}{3}$ ,  $WW = \frac{1}{2}$ ):

$$K_0 = (9 - 12q')U + (18q' - 12)W$$

We adopt this approximation and take the trial function

$$I = U + zW$$

With omission of the terms  $O(k^2)$ , Eq. (1) can then be satisfied, because both sides form a linear combination of  $U$  and  $W$ . The resulting quadratic equation has the solutions

$$\begin{aligned} \lambda_1 &= 1, & z_1 &= 0 \\ \lambda_2 &= 24q' - 17, & z_2 &= -\frac{3}{2} \end{aligned}$$

The first root corresponds to the known relation  $U = RU$  for conservative scattering with any anisotropy. It can be refined to the first order in  $k$  by taking  $\lambda_1 = 1 - c$ . The corresponding tangent (for isotropic scattering) has been drawn in Fig. 9.18. The square of the second root,  $\zeta_2 = \lambda_2^2$ , provides the limiting value we set out to derive.

The procedure outlined above may be refined as desired. For isotropic scattering with arbitrary  $a$ , an appropriate trial function is  $I = A_1 + pA_2 + qA_3$ , where  $A_i$  is the vector defined in Section 8.4. In conservative scattering we know the first eigenvalue 1 and the first eigenfunction  $A_1 = U$ , and may therefore take at once the trial function  $I = (A_1 - A_2) + p(A_2 - A_3)$ , which is orthogonal to  $A_1$ . The ratio  $IRI/II$  then has for  $p = 0$  the value 0.0507, already

given; but the maximum 0.0566 reached near  $p = -0.66$ , is a better estimate. The improved value of  $\zeta_2$  is  $0.0566^2 = 0.0032$ .

## REFERENCES

- Irvine, W. M. (1968). *J. Quant. Spectrosc. Radiat. Transfer* **8**, 471.  
van de Hulst, H. C., and Grossman, K. (1968). In "The Atmospheres of Venus and Mars" (J. C. Brandt and M. B. McElroy, eds.), p. 35. Gordon and Breach, New York.

TABLE 35

Reflection and Transmission by Finite Layer with Henyey-Greenstein Scattering,  
 $g = 0.50$ ,  $b = 0.50$ , Reflection

VECTOR	$\mu = 0.0$	$\mu = 0.1$	$\mu = 0.3$	$\mu = 0.5$	$\mu = 0.7$	$\mu = 0.9$	$\mu = 1.0$	AVERAGE N	FLUX U
$b = 0.50$ $\mu_0 = 0.1$									
FIRST ORDER	3.48549	1.65151	0.68918	0.36348	0.21264	0.13360	0.10823	0.65197	0.32072
SECOND ORDER	0.40591	0.42543	0.24661	0.15093	0.09768	0.06602	0.05502	0.19690	0.12587
THIRD ORDER	0.11604	0.14376	0.10281	0.06858	0.04685	0.03291	0.02785	0.07802	0.05616
SUMS $a = 0.20$	0.71434	0.34857	0.14860	0.07934	0.04685	0.02965	0.02409	0.13896	0.06967
$a = 0.40$	1.46795	0.73967	0.32314	0.17493	0.10440	0.06662	0.05431	0.29836	0.15284
$a = 0.60$	2.27031	1.18529	0.53264	0.29296	0.17692	0.11395	0.09326	0.48505	0.25456
$a = 0.80$	3.13571	1.70367	0.79119	0.44319	0.27129	0.17657	0.14512	0.70965	0.38280
$a = 0.90$	3.59869	1.99869	0.94560	0.53508	0.32999	0.21601	0.17795	0.84125	0.46073
$a = 0.95$	3.83940	2.15728	1.03077	0.58642	0.36306	0.23837	0.19661	0.91314	0.50411
$a = 0.99$	4.03695	2.29019	1.10331	0.63048	0.39160	0.25774	0.21280	0.97402	0.54128
$a = 1.00$	4.08707	2.32431	1.12211	0.64194	0.39904	0.26280	0.21704	0.98975	0.55094
$b = 0.50$ $\mu_0 = 0.3$									
FIRST ORDER	1.02453	0.68918	0.34873	0.19717	0.12153	0.07997	0.06618	0.29395	0.16833
SECOND ORDER	0.17774	0.24661	0.17782	0.11756	0.07952	0.05537	0.04669	0.13329	0.09588
THIRD ORDER	0.07606	0.10281	0.08285	0.05804	0.04091	0.02938	0.02508	0.06192	0.04730
SUMS $a = 0.20$	0.21269	0.14860	0.07759	0.04465	0.02785	0.01847	0.01533	0.06467	0.03792
$a = 0.40$	0.44420	0.32314	0.17443	0.10224	0.06456	0.04317	0.03593	0.14376	0.08640
$a = 0.60$	0.70132	0.53264	0.29789	0.17799	0.11384	0.07678	0.06410	0.24281	0.14968
$a = 0.80$	0.99467	0.79119	0.45953	0.28011	0.18155	0.12356	0.10349	0.37048	0.23449
$a = 0.90$	1.16003	0.94560	0.56021	0.34500	0.22514	0.15393	0.12915	0.44922	0.28820
$a = 0.95$	1.24868	1.03077	0.61690	0.38190	0.25008	0.17139	0.14392	0.49337	0.31869
$a = 0.99$	1.32290	1.10331	0.66577	0.41390	0.27178	0.18662	0.15682	0.53133	0.34510
$a = 1.00$	1.34195	1.12211	0.67852	0.42227	0.27747	0.19061	0.16020	0.54122	0.35201
$b = 0.50$ $\mu_0 = 0.5$									
FIRST ORDER	0.49828	0.36348	0.19717	0.11571	0.07370	0.04999	0.04195	0.16244	0.09827
SECOND ORDER	0.09699	0.15093	0.11756	0.07946	0.05442	0.03827	0.03242	0.08653	0.06446
THIRD ORDER	0.04886	0.06858	0.05804	0.04136	0.02943	0.02128	0.01821	0.04311	0.03364
SUMS $a = 0.20$	0.10397	0.07934	0.04465	0.02668	0.01718	0.01172	0.00985	0.03633	0.02253
$a = 0.40$	0.21871	0.17493	0.10224	0.06225	0.04051	0.02780	0.02341	0.08222	0.05228
$a = 0.60$	0.34875	0.29296	0.17799	0.11044	0.07268	0.05020	0.04235	0.14156	0.09228
$a = 0.80$	0.50135	0.44319	0.28011	0.17715	0.11790	0.08199	0.06932	0.22051	0.14737
$a = 0.90$	0.58964	0.53508	0.34500	0.22028	0.14746	0.10290	0.08710	0.27030	0.18288
$a = 0.95$	0.63768	0.58642	0.38190	0.24501	0.16448	0.11498	0.09738	0.29853	0.20321
$a = 0.99$	0.67830	0.63048	0.41390	0.26655	0.17935	0.12555	0.10639	0.32296	0.22092
$a = 1.00$	0.68878	0.64194	0.42227	0.27220	0.18326	0.12833	0.10876	0.32935	0.22556
$b = 0.50$ $\mu_0 = 0.7$									
FIRST ORDER	0.27821	0.21264	0.12153	0.07370	0.04827	0.03356	0.02848	0.09904	0.06246
SECOND ORDER	0.05853	0.09768	0.07952	0.05442	0.03759	0.02663	0.02265	0.05803	0.04409
THIRD ORDER	0.03256	0.04685	0.04091	0.02943	0.02105	0.01527	0.01309	0.03026	0.02390
SUMS $a = 0.20$	0.05827	0.04685	0.02785	0.01718	0.01134	0.00791	0.00672	0.02240	0.01447
$a = 0.40$	0.12326	0.10440	0.06456	0.04051	0.02699	0.01889	0.01605	0.05129	0.03393
$a = 0.60$	0.19806	0.17692	0.11384	0.07268	0.04885	0.03435	0.02921	0.08945	0.06056
$a = 0.80$	0.28772	0.27129	0.18155	0.11790	0.07999	0.05650	0.04811	0.14125	0.09782
$a = 0.90$	0.34060	0.32999	0.22514	0.14746	0.10050	0.07117	0.06063	0.17439	0.12210
$a = 0.95$	0.36969	0.36306	0.25008	0.16448	0.11237	0.07966	0.06789	0.19330	0.13607
$a = 0.99$	0.39444	0.39160	0.27178	0.17935	0.12275	0.08712	0.07426	0.20974	0.14828
$a = 1.00$	0.40086	0.39904	0.27747	0.18326	0.12549	0.08908	0.07594	0.21405	0.15148

TABLE 35 (continued)  
 $g = 0.50, b = 0.50$ , Transmission

VECTOR	$\mu = 0.0$	$\mu = 0.1$	$\mu = 0.3$	$\mu = 0.5$	$\mu = 0.7$	$\mu = 0.9$	$\mu = 1.0$	AVERAGE N	FLUX U
<b>b = 0.50</b>									
ZERO ORDER	$\mu_0 = 0.1$ 0.0	PEAK	0.0	0.0	0.0	0.0	0.0	0.03369	0.00674
FIRST ORDER	0.02349	0.12005	0.30644	0.25593	0.18006	0.12254	0.10132	0.19712	0.18765
SECOND ORDER	0.10148	0.16602	0.20412	0.16865	0.13043	0.09904	0.08612	0.15227	0.13670
THIRD ORDER	0.08025	0.10982	0.10428	0.08031	0.06072	0.04611	0.04030	0.07939	0.06623
SUMS $\alpha = 0.20$	0.00947	0.03163	0.07037	0.05864	0.04176	0.02887	0.02406	0.07990	0.05032
$\alpha = 0.40$	0.03212	0.08336	0.16340	0.13559	0.09758	0.06841	0.05740	0.14312	0.10881
$\alpha = 0.60$	0.07567	0.16550	0.28834	0.23781	0.17264	0.12250	0.10342	0.23036	0.18795
$\alpha = 0.80$	0.15270	0.29455	0.45963	0.37604	0.27487	0.19708	0.16725	0.35263	0.29656
$\alpha = 0.90$	0.20992	0.38469	0.56955	0.46372	0.33990	0.24481	0.20824	0.43213	0.36609
$\alpha = 0.95$	0.24476	0.43820	0.63230	0.51347	0.37680	0.27197	0.23160	0.47778	0.40570
$\alpha = 0.99$	0.27616	0.48575	0.68683	0.55653	0.40875	0.29551	0.25185	0.51758	0.44006
$\alpha = 1.00$	0.28455	0.49836	0.70111	0.56778	0.41711	0.30166	0.25715	0.52802	0.44906
<b>b = 0.50</b>									
ZERO ORDER	$\mu_0 = 0.3$ 0.0	0.0	PEAK	0.0	0.0	0.0	0.0	0.31479	0.18888
FIRST ORDER	0.19351	0.30644	0.39048	0.31977	0.22573	0.14941	0.12082	0.27604	0.23917
SECOND ORDER	0.14767	0.20412	0.19446	0.15085	0.11435	0.08635	0.07501	0.14837	0.12411
THIRD ORDER	0.08039	0.10428	0.08884	0.06546	0.04825	0.03605	0.03134	0.06780	0.05404
SUMS $\alpha = 0.20$	0.04532	0.07037	0.08665	0.07056	0.05014	0.03365	0.02744	0.37653	0.24215
$\alpha = 0.40$	0.10734	0.16340	0.19421	0.15711	0.11231	0.07636	0.06274	0.45422	0.30858
$\alpha = 0.60$	0.19324	0.28834	0.33043	0.26530	0.19064	0.13117	0.10855	0.55375	0.39284
$\alpha = 0.80$	0.31422	0.45963	0.50731	0.40384	0.29145	0.20278	0.16893	0.68425	0.50207
$\alpha = 0.90$	0.39323	0.56955	0.61670	0.48860	0.35328	0.24708	0.20647	0.76545	0.56944
$\alpha = 0.95$	0.43870	0.63230	0.67806	0.53589	0.38778	0.27190	0.22755	0.81111	0.60716
$\alpha = 0.99$	0.47839	0.68683	0.73082	0.57642	0.41737	0.29322	0.24568	0.85044	0.63956
$\alpha = 1.00$	0.48881	0.70111	0.74457	0.58695	0.42506	0.29877	0.25041	0.86069	0.64799
<b>b = 0.50</b>									
ZERO ORDER	$\mu_0 = 0.5$ 0.0	0.0	0.0	PEAK	0.0	0.0	0.0	0.36788	0.36788
FIRST ORDER	0.18331	0.25593	0.31977	0.30224	0.24458	0.17094	0.13779	0.25685	0.23797
SECOND ORDER	0.13335	0.16865	0.15085	0.11783	0.09161	0.07133	0.06290	0.11891	0.09917
THIRD ORDER	0.06447	0.08031	0.06546	0.04767	0.03506	0.02626	0.02288	0.05041	0.03957
SUMS $\alpha = 0.20$	0.04256	0.05864	0.07056	0.06558	0.05289	0.03727	0.03027	0.42445	0.41979
$\alpha = 0.40$	0.09965	0.13559	0.15711	0.14343	0.11519	0.08180	0.06693	0.49354	0.48198
$\alpha = 0.60$	0.17681	0.23781	0.26530	0.23763	0.18987	0.13580	0.11188	0.57948	0.55784
$\alpha = 0.80$	0.28253	0.37604	0.40384	0.35444	0.28147	0.20260	0.16801	0.68891	0.65253
$\alpha = 0.90$	0.35009	0.46372	0.48860	0.42428	0.33575	0.24238	0.20164	0.75557	0.70936
$\alpha = 0.95$	0.38854	0.51347	0.53589	0.46279	0.36554	0.26425	0.22017	0.79266	0.74076
$\alpha = 0.99$	0.42187	0.55653	0.57642	0.49558	0.39083	0.28284	0.23594	0.82441	0.76751
$\alpha = 1.00$	0.43059	0.56778	0.58695	0.50407	0.39737	0.28764	0.24003	0.83266	0.77444
<b>b = 0.50</b>									
ZERO ORDER	$\mu_0 = 0.7$ 0.0	0.0	0.0	0.0	PEAK	0.0	0.0	0.34967	0.48954
FIRST ORDER	0.13619	0.18006	0.22573	0.24458	0.24897	0.21259	0.17926	0.22095	0.22841
SECOND ORDER	0.10865	0.13043	0.11435	0.09161	0.07448	0.06135	0.05575	0.09369	0.07979
THIRD ORDER	0.05037	0.06072	0.04825	0.03506	0.02591	0.01959	0.01718	0.03753	0.02931
SUMS $\alpha = 0.20$	0.03202	0.04176	0.05014	0.05289	0.05300	0.04514	0.03823	0.39794	0.53867
$\alpha = 0.40$	0.07573	0.09758	0.11231	0.11519	0.11349	0.09634	0.08193	0.45593	0.59592
$\alpha = 0.60$	0.13533	0.17264	0.19064	0.18987	0.18363	0.15522	0.13250	0.52683	0.66375
$\alpha = 0.80$	0.21723	0.27487	0.29145	0.28147	0.26672	0.22420	0.19205	0.61549	0.74593
$\alpha = 0.90$	0.26950	0.33990	0.35328	0.33575	0.31467	0.26363	0.22618	0.66875	0.79415
$\alpha = 0.95$	0.29920	0.37680	0.38778	0.36554	0.34062	0.28485	0.24458	0.69818	0.82049
$\alpha = 0.99$	0.32492	0.40875	0.41737	0.39083	0.36247	0.30265	0.26002	0.72327	0.84277
$\alpha = 1.00$	0.33164	0.41711	0.42506	0.39737	0.36809	0.30723	0.26399	0.72977	0.84852



TABLE 35 (continued)  
 $g = 0.50, b = 0.50$ , Reflection

VECTOR	$\mu = 0.0$	$\mu \pm 0.1$	$\mu = 0.3$	$\mu = 0.5$	$\mu = 0.7$	$\mu = 0.9$	$\mu = 1.0$	AVERAGE N	FLUX U
$b = 0.50$ $\mu_0 = 0.9$									
FIRST ORDER	0.16838	0.13360	0.07997	0.04999	0.03356	0.02382	0.02041	0.06473	0.04232
SECOND ORDER	0.03790	0.06602	0.05537	0.03827	0.02663	0.01901	0.01622	0.04025	0.03101
THIRD ORDER	0.02248	0.03291	0.02938	0.02128	0.01527	0.01111	0.00954	0.02167	0.01726
SUMS $\alpha = 0.20$	0.03539	0.02565	0.01847	0.01172	0.00791	0.00562	0.00482	0.01475	0.00986
$\alpha = 0.40$	0.07523	0.06662	0.04317	0.02780	0.01889	0.01345	0.01152	0.03405	0.02326
$\alpha = 0.60$	0.12170	0.11395	0.07678	0.05020	0.03435	0.02451	0.02099	0.05990	0.04178
$\alpha = 0.80$	0.17839	0.17657	0.12356	0.08199	0.05650	0.04043	0.03463	0.09548	0.06795
$\alpha = 0.90$	0.21235	0.21601	0.15393	0.10290	0.07117	0.05100	0.04369	0.11845	0.08511
$\alpha = 0.95$	0.23119	0.23837	0.17139	0.11498	0.07966	0.05714	0.04895	0.13163	0.09502
$\alpha = 0.99$	0.24731	0.25774	0.18662	0.12555	0.08712	0.06252	0.05356	0.14311	0.10369
$\alpha = 1.00$	0.25150	0.26280	0.19061	0.12833	0.08908	0.06394	0.05478	0.14612	0.10597
$b = 0.50$ $\mu_0 = 1.0$									
FIRST ORDER	0.13416	0.10823	0.06618	0.04195	0.02848	0.02041	0.01756	0.05343	0.03551
SECOND ORDER	0.03115	0.05502	0.04669	0.03242	0.02265	0.01622	0.01387	0.03391	0.02628
THIRD ORDER	0.01891	0.02785	0.02508	0.01821	0.01309	0.00954	0.00819	0.01849	0.01477
SUMS $\alpha = 0.20$	0.02825	0.02409	0.01533	0.00985	0.00672	0.00482	0.00414	0.01221	0.00828
$\alpha = 0.40$	0.06018	0.05431	0.03593	0.02341	0.01605	0.01152	0.00989	0.02827	0.01958
$\alpha = 0.60$	0.09765	0.09326	0.06410	0.04235	0.02921	0.02099	0.01802	0.04989	0.03525
$\alpha = 0.80$	0.14372	0.14512	0.10349	0.06932	0.04811	0.03463	0.02973	0.07979	0.05744
$\alpha = 0.90$	0.17149	0.17795	0.12915	0.08710	0.06063	0.04369	0.03751	0.09917	0.07204
$\alpha = 0.95$	0.18695	0.19661	0.14392	0.09738	0.06789	0.04895	0.04203	0.11030	0.08047
$\alpha = 0.99$	0.20021	0.21280	0.15682	0.10639	0.07426	0.05356	0.04600	0.12002	0.08786
$\alpha = 1.00$	0.20366	0.21704	0.16020	0.10876	0.07594	0.05478	0.04704	0.12257	0.08980
$b = 0.5$ NARROW SURFACE LAYER AT TOP									
FIRST ORDER	INFINITE	0.65198	0.29395	0.16244	0.09904	0.06473	0.05343	0.27863	0.14188
SECOND ORDER	0.13931	0.19690	0.13329	0.08653	0.05803	0.04025	0.03391	0.10225	0.07107
THIRD ORDER	0.05892	0.07802	0.06192	0.04311	0.03026	0.02167	0.01849	0.04638	0.03515
SUMS $\alpha = 0.20$	INFINITE	0.13896	0.06467	0.03633	0.02240	0.01475	0.01221	0.06022	0.03153
$\alpha = 0.40$	INFINITE	0.29836	0.14376	0.08222	0.05129	0.03405	0.02827	0.13145	0.07089
$\alpha = 0.60$	INFINITE	0.48505	0.24281	0.14156	0.08945	0.05990	0.04989	0.21782	0.12127
$\alpha = 0.80$	INFINITE	0.70965	0.37048	0.22051	0.14125	0.09548	0.07979	0.32587	0.18769
$\alpha = 0.90$	INFINITE	0.84125	0.44922	0.27030	0.17439	0.11845	0.09917	0.39115	0.22931
$\alpha = 0.95$	INFINITE	0.91314	0.49337	0.29853	0.19330	0.13163	0.11030	0.42740	0.25290
$\alpha = 0.99$	INFINITE	0.97402	0.53133	0.32296	0.20974	0.14311	0.12002	0.45840	0.27321
$\alpha = 1.00$	INFINITE	0.98975	0.54122	0.32935	0.21405	0.14612	0.12257	0.46645	0.27851
$b = 0.5$ LAMBERT SURFACE ON TOP									
FIRST ORDER	0.50000	0.32072	0.16833	0.09827	0.06246	0.04232	0.03551	0.14188	0.08399
SECOND ORDER	0.08513	0.12587	0.09588	0.06446	0.04409	0.03101	0.02628	0.07107	0.05244
THIRD ORDER	0.04024	0.05616	0.04730	0.03364	0.02390	0.01726	0.01477	0.03515	0.02731
SUMS $\alpha = 0.20$	0.10376	0.06967	0.03792	0.02253	0.01447	0.00986	0.00828	0.03153	0.01911
$\alpha = 0.40$	0.21681	0.15284	0.08640	0.05228	0.03393	0.02326	0.01958	0.07089	0.04411
$\alpha = 0.60$	0.34286	0.25456	0.14968	0.09228	0.06056	0.04178	0.03525	0.12127	0.07744
$\alpha = 0.80$	0.48785	0.38280	0.23449	0.14737	0.09782	0.06795	0.05744	0.18769	0.12301
$\alpha = 0.90$	0.57035	0.46073	0.28820	0.18288	0.12210	0.08511	0.07204	0.22935	0.15241
$\alpha = 0.95$	0.61483	0.50411	0.31869	0.20321	0.13607	0.09502	0.08047	0.25290	0.16911
$\alpha = 0.99$	0.65222	0.54128	0.34510	0.22092	0.14828	0.10369	0.08786	0.27325	0.18371
$\alpha = 1.00$	0.66184	0.55094	0.35201	0.22556	0.15148	0.10597	0.08980	0.27857	0.18751

TABLE 35 (continued)

 $g = 0.50, b = 0.50$ , Transmission

VECTOR	$\mu = 0.0$	$\mu = 0.1$	$\mu = 0.3$	$\mu = 0.5$	$\mu = 0.7$	$\mu = 0.9$	$\mu = 1.0$	AVERAGE N	FLUX U
<b>b = 0.50</b>									
	$\mu_0 = 0.9$								
ZERO ORDER	0.0	0.0	0.0	0.0	0.0	PEAK	0.0	0.31875	0.57375
FIRST ORDER	0.09661	0.12254	0.14941	0.17094	0.21259	0.27626	0.29681	0.18601	0.21706
SECOND ORDER	0.08531	0.09904	0.08635	0.07133	0.06135	0.05496	0.05269	0.07414	0.06533
THIRD ORDER	0.03929	0.04611	0.03605	0.02626	0.01959	0.01504	0.01332	0.02835	0.02215
SUMS									
$\alpha = 0.20$	0.02308	0.02887	0.03365	0.03727	0.04514	0.05758	0.06158	0.35917	0.61997
$\alpha = 0.40$	0.05529	0.06841	0.07636	0.08180	0.09634	0.12044	0.12816	0.40719	0.67272
$\alpha = 0.60$	0.09988	0.12250	0.13117	0.13580	0.15522	0.18978	0.20078	0.46520	0.73384
$\alpha = 0.80$	0.16170	0.19708	0.20278	0.20260	0.22420	0.26743	0.28104	0.53679	0.80612
$\alpha = 0.90$	0.20130	0.24481	0.24708	0.24238	0.26363	0.31021	0.32476	0.57936	0.84774
$\alpha = 0.95$	0.22381	0.27197	0.27190	0.26425	0.28485	0.33280	0.34770	0.60276	0.87024
$\alpha = 0.99$	0.24332	0.29551	0.29322	0.28284	0.30265	0.35151	0.36663	0.62263	0.88916
$\alpha = 1.00$	0.24842	0.30166	0.29877	0.28764	0.30723	0.35629	0.37144	0.62777	0.89403
<b>b = 0.50</b>									
	$\mu_0 = 1.0$								
ZERO ORDER	0.0	0.0	0.0	0.0	0.0	0.0	PEAK	0.30327	0.60653
FIRST ORDER	0.08137	0.10132	0.12082	0.13779	0.17926	0.29681	0.45490	0.17030	0.21121
SECOND ORDER	0.07510	0.08612	0.07501	0.06290	0.05575	0.05269	0.05257	0.06614	0.05950
THIRD ORDER	0.03475	0.04030	0.03134	0.02288	0.01718	0.01332	0.01186	0.02479	0.01940
SUMS									
$\alpha = 0.20$	0.01958	0.02406	0.02744	0.03027	0.03823	0.06158	0.09318	0.34019	0.65132
$\alpha = 0.40$	0.04721	0.05740	0.06274	0.06693	0.08193	0.12816	0.19126	0.38387	0.70201
$\alpha = 0.60$	0.08574	0.10342	0.10855	0.11188	0.13250	0.20078	0.29516	0.43636	0.76020
$\alpha = 0.80$	0.13940	0.16725	0.16893	0.16801	0.19205	0.28104	0.40627	0.50080	0.82831
$\alpha = 0.90$	0.17385	0.20824	0.20647	0.20164	0.22618	0.32476	0.46516	0.53896	0.86720
$\alpha = 0.95$	0.19345	0.23160	0.22755	0.22017	0.24458	0.34770	0.49559	0.55988	0.88814
$\alpha = 0.99$	0.21044	0.25185	0.24568	0.23594	0.26002	0.36663	0.52047	0.57763	0.90569
$\alpha = 1.00$	0.21488	0.25715	0.25041	0.24003	0.26399	0.37144	0.52677	0.58221	0.91020
<b>b = 0.5</b> NARROW SURFACE LAYER AT TOP									
ZERO ORDER	0.0	0.03369	0.31479	0.36788	0.34967	0.31875	0.30327	0.27989	0.32664
FIRST ORDER	0.12863	0.19712	0.27604	0.25685	0.22095	0.18601	0.17030	0.22634	0.22104
SECOND ORDER	0.11475	0.15227	0.14837	0.11891	0.09369	0.07414	0.06614	0.11642	0.10016
THIRD ORDER	0.06237	0.07939	0.06780	0.05041	0.03753	0.02835	0.02479	0.05214	0.04183
SUMS									
$\alpha = 0.20$	0.03087	0.07990	0.37653	0.42445	0.39794	0.35917	0.34019	0.33027	0.37523
$\alpha = 0.40$	0.07470	0.14312	0.45422	0.49354	0.45593	0.40719	0.38387	0.39309	0.43432
$\alpha = 0.60$	0.13702	0.23036	0.55375	0.57948	0.52683	0.46520	0.43636	0.47287	0.50749
$\alpha = 0.80$	0.22644	0.35263	0.68425	0.68891	0.61549	0.53679	0.50080	0.57657	0.60022
$\alpha = 0.90$	0.28540	0.43213	0.76545	0.75557	0.66875	0.57936	0.53896	0.64069	0.65651
$\alpha = 0.95$	0.31947	0.47778	0.81111	0.79266	0.69818	0.60276	0.55988	0.67663	0.68777
$\alpha = 0.99$	0.34928	0.51758	0.85044	0.82441	0.72327	0.62263	0.57763	0.70753	0.71449
$\alpha = 1.00$	0.35711	0.52802	0.86069	0.83266	0.72977	0.62777	0.58221	0.71557	0.72143
<b>b = 0.5</b> LAMBERT SURFACE ON TOP									
ZERO ORDER	0.0	0.00674	0.18888	0.36788	0.48954	0.57375	0.60653	0.32664	0.44321
FIRST ORDER	0.13412	0.18765	0.23917	0.23797	0.22841	0.21706	0.21121	0.22104	0.22604
SECOND ORDER	0.10943	0.13670	0.12411	0.09917	0.07979	0.06533	0.05950	0.10016	0.08565
THIRD ORDER	0.05377	0.06623	0.05404	0.03957	0.02931	0.02215	0.01940	0.04183	0.03299
SUMS									
$\alpha = 0.20$	0.03167	0.05032	0.24215	0.41979	0.53867	0.61997	0.65132	0.37523	0.49213
$\alpha = 0.40$	0.07531	0.10881	0.30858	0.48198	0.59592	0.67272	0.70201	0.43432	0.54987
$\alpha = 0.60$	0.13552	0.18795	0.39284	0.55784	0.66375	0.73384	0.76020	0.50749	0.61921
$\alpha = 0.80$	0.21934	0.29656	0.50207	0.65253	0.74593	0.80612	0.82831	0.60022	0.70442
$\alpha = 0.90$	0.27341	0.36609	0.56944	0.70936	0.79415	0.84774	0.86720	0.65651	0.75498
$\alpha = 0.95$	0.30430	0.40570	0.60716	0.74076	0.82049	0.87024	0.88814	0.68777	0.78275
$\alpha = 0.99$	0.33113	0.44006	0.63956	0.76751	0.84277	0.88916	0.90569	0.71449	0.80633
$\alpha = 1.00$	0.33816	0.44906	0.64799	0.77444	0.84852	0.89403	0.91020	0.72143	0.81242

TABLE 35 (continued)

 $g = 0.50, b = 1$ , Reflection

VECTOR	$\mu = 0.0$	$\mu = 0.1$	$\mu = 0.3$	$\mu = 0.5$	$\mu = 0.7$	$\mu = 0.9$	$\mu = 1.0$	AVERAGE N	FLUX U
$b = 1.00 \quad \mu_0 = 0.1$									
FIRST ORDER	3.48549	1.65159	0.69006	0.36438	0.21335	0.13411	0.10867	0.65260	0.32139
SECOND ORDER	0.40621	0.42638	0.25439	0.15961	0.10499	0.07179	0.06013	0.20305	0.13270
THIRD ORDER	0.11895	0.14860	0.11755	0.08471	0.06080	0.04423	0.03797	0.09025	0.06933
SUMS $\alpha = 0.20$	0.71439	0.34868	0.14924	0.08003	0.04743	0.03010	0.02449	0.13945	0.07022
$\alpha = 0.40$	1.46845	0.74054	0.32636	0.17841	0.10734	0.06897	0.05640	0.30095	0.15563
$\alpha = 0.60$	2.27294	1.18943	0.54364	0.30466	0.18691	0.12201	0.10045	0.49405	0.26407
$\alpha = 0.80$	3.14638	1.71946	0.82402	0.47720	0.30041	0.20020	0.16627	0.73673	0.41081
$\alpha = 0.90$	3.61926	2.02844	1.00135	0.59198	0.37865	0.25557	0.21339	0.88734	0.50780
$\alpha = 0.95$	3.86780	2.19797	1.10344	0.65997	0.42591	0.28949	0.24243	0.97325	0.56510
$\alpha = 0.99$	4.07368	2.34243	1.19324	0.72088	0.46877	0.32053	0.26910	1.04842	0.61636
$\alpha = 1.00$	4.12625	2.37992	1.21698	0.73715	0.48030	0.32892	0.27632	1.06824	0.63004
$b = 1.00 \quad \mu_0 = 0.3$									
FIRST ORDER	1.02453	0.69006	0.36117	0.21087	0.13277	0.08864	0.07376	0.30344	0.17888
SECOND ORDER	0.18223	0.25439	0.20255	0.14454	0.10272	0.07407	0.06335	0.15363	0.11779
THIRD ORDER	0.08586	0.11755	0.11261	0.08920	0.06791	0.05148	0.04492	0.08686	0.07319
SUMS $\alpha = 0.20$	0.21297	0.14924	0.08136	0.04877	0.03128	0.02116	0.01770	0.06762	0.04116
$\alpha = 0.40$	0.44604	0.32636	0.18629	0.11504	0.07536	0.05176	0.04354	0.15326	0.09662
$\alpha = 0.60$	0.70829	0.54364	0.32723	0.20904	0.14023	0.09797	0.08297	0.26666	0.17486
$\alpha = 0.80$	1.01682	0.82402	0.52792	0.35070	0.24172	0.17221	0.14695	0.42663	0.29245
$\alpha = 0.90$	1.19852	1.00135	0.66488	0.45146	0.31585	0.22745	0.19491	0.53540	0.37605
$\alpha = 0.95$	1.29934	1.10344	0.74691	0.51308	0.36179	0.26199	0.22501	0.60049	0.42719
$\alpha = 0.99$	1.38606	1.19324	0.82084	0.56932	0.40405	0.29395	0.25292	0.65916	0.47389
$\alpha = 1.00$	1.40870	1.21698	0.84064	0.58449	0.41550	0.30263	0.26051	0.67488	0.48649
$b = 1.00 \quad \mu_0 = 0.5$									
FIRST ORDER	0.49828	0.36438	0.21087	0.13137	0.08697	0.06054	0.05131	0.17336	0.11061
SECOND ORDER	0.10211	0.15961	0.14454	0.10937	0.08048	0.05950	0.05142	0.10916	0.08897
THIRD ORDER	0.05973	0.08471	0.08920	0.07406	0.05797	0.04480	0.03939	0.06949	0.06099
SUMS $\alpha = 0.20$	0.10429	0.08003	0.04877	0.03133	0.02115	0.01490	0.01268	0.03967	0.02624
$\alpha = 0.40$	0.22073	0.17841	0.11504	0.07639	0.05267	0.03762	0.03218	0.09274	0.06372
$\alpha = 0.60$	0.35625	0.30466	0.20904	0.14387	0.10149	0.07361	0.06331	0.16729	0.11965
$\alpha = 0.80$	0.52445	0.47720	0.35070	0.25088	0.18139	0.13375	0.11574	0.27923	0.20830
$\alpha = 0.90$	0.62911	0.59198	0.45146	0.32960	0.24139	0.17955	0.15588	0.35889	0.27359
$\alpha = 0.95$	0.68918	0.65997	0.51308	0.37851	0.27904	0.20848	0.18130	0.40765	0.31419
$\alpha = 0.99$	0.74203	0.72088	0.56932	0.42356	0.31391	0.23537	0.20497	0.45220	0.35162
$\alpha = 1.00$	0.75602	0.73715	0.58449	0.43578	0.32339	0.24270	0.21142	0.46423	0.36177
$b = 1.00 \quad \mu_0 = 0.7$									
FIRST ORDER	0.27821	0.21335	0.13277	0.08697	0.05984	0.04298	0.03693	0.10836	0.07314
SECOND ORDER	0.06287	0.10499	0.10272	0.08048	0.06049	0.04544	0.03954	0.07773	0.06556
THIRD ORDER	0.04199	0.06080	0.06791	0.05797	0.04610	0.03600	0.03178	0.05328	0.04786
SUMS $\alpha = 0.20$	0.05854	0.04743	0.03128	0.02115	0.01481	0.01075	0.00926	0.02527	0.01769
$\alpha = 0.40$	0.12500	0.10734	0.07536	0.05267	0.03762	0.02761	0.02388	0.06038	0.04389
$\alpha = 0.60$	0.20452	0.18691	0.14023	0.10149	0.07401	0.05500	0.04779	0.11169	0.08436
$\alpha = 0.80$	0.30759	0.30041	0.24172	0.18139	0.13515	0.10182	0.08889	0.19190	0.15062
$\alpha = 0.90$	0.37448	0.37865	0.31585	0.24139	0.18183	0.13796	0.12074	0.25061	0.20045
$\alpha = 0.95$	0.41384	0.42591	0.36179	0.27904	0.21134	0.16092	0.14101	0.28705	0.23175
$\alpha = 0.99$	0.44903	0.46877	0.40405	0.31391	0.23879	0.18234	0.15995	0.32061	0.26076
$\alpha = 1.00$	0.45842	0.48030	0.41550	0.32339	0.24628	0.18819	0.16512	0.32971	0.26866

TABLE 35 (continued)  
 $g = 0.50, b = 1$ , Transmission

VECTOR	$\mu = 0.0$	$\mu = 0.1$	$\mu = 0.3$	$\mu = 0.5$	$\mu = 0.7$	$\mu = 0.9$	$\mu = 1.0$	AVERAGE N	FLUX U
<b>b = 1.00</b>									
ZERO ORDER	$\mu_0 = 0.0$	0.0	0.0	0.0	0.0	0.0	0.0	0.00023	0.00005
FIRST ORDER	0.00016	0.00162	0.05994	0.09588	0.08936	0.07113	0.06214	0.06350	0.07692
SECOND ORDER	0.02840	0.04181	0.09041	0.11172	0.10843	0.09535	0.08767	0.08935	0.09950
THIRD ORDER	0.04218	0.05761	0.08294	0.08616	0.07867	0.06823	0.06292	0.07443	0.07598
SUMS	$\alpha = 0.20$	0.00157	0.00255	0.01638	0.02443	0.02292	0.01866	0.01650	0.01719
	$\alpha = 0.40$	0.00860	0.01273	0.04577	0.06361	0.05973	0.04941	0.04412	0.04638
	$\alpha = 0.60$	0.02737	0.03893	0.09864	0.12759	0.11920	0.09967	0.08962	0.09678
	$\alpha = 0.80$	0.07146	0.09911	0.19612	0.23591	0.21802	0.18328	0.16556	0.18613
	$\alpha = 0.90$	0.11168	0.15339	0.27456	0.31840	0.29201	0.24563	0.22220	0.25614
	$\alpha = 0.95$	0.13912	0.19024	0.32527	0.37035	0.33814	0.28438	0.25738	0.30081
	$\alpha = 0.99$	0.16575	0.22591	0.37304	0.41852	0.38066	0.32001	0.28971	0.34256
	$\alpha = 1.00$	0.17317	0.23583	0.38615	0.43163	0.39219	0.32965	0.29845	0.35396
<b>b = 1.00</b>									
ZERO ORDER	$\mu_0 = 0.0$	0.0	0.0	0.0	0.0	0.0	0.0	0.05946	0.03567
FIRST ORDER	0.03655	0.05994	0.14750	0.17803	0.15314	0.11395	0.09610	0.13012	0.13926
SECOND ORDER	0.06287	0.09041	0.13980	0.14768	0.13438	0.11459	0.10431	0.12487	0.12863
THIRD ORDER	0.06158	0.08294	0.10359	0.09861	0.08565	0.07198	0.06562	0.08809	0.08517
SUMS	$\alpha = 0.20$	0.01040	0.01638	0.03604	0.04241	0.03678	0.02802	0.02398	0.09128
	$\alpha = 0.40$	0.03015	0.04577	0.09025	0.10316	0.08991	0.06938	0.06056	0.13897
	$\alpha = 0.60$	0.06715	0.09864	0.17478	0.19333	0.16876	0.13330	0.11670	0.21263
	$\alpha = 0.80$	0.13740	0.19612	0.31335	0.33413	0.29101	0.23268	0.20539	0.33176
	$\alpha = 0.90$	0.19484	0.27456	0.41720	0.43612	0.37881	0.30428	0.26950	0.42004
	$\alpha = 0.95$	0.23223	0.32527	0.48220	0.49890	0.43256	0.34811	0.30878	0.47496
	$\alpha = 0.99$	0.26757	0.37304	0.54231	0.55636	0.48159	0.38808	0.34462	0.52555
	$\alpha = 1.00$	0.27729	0.38615	0.55863	0.57189	0.49481	0.39886	0.35428	0.53926
<b>b = 1.00</b>									
ZERO ORDER	$\mu_0 = 0.0$	0.0	0.0	0.0	0.0	0.0	0.0	0.13534	0.13534
FIRST ORDER	0.06744	0.09588	0.17803	0.22237	0.20971	0.16097	0.13426	0.17267	0.18571
SECOND ORDER	0.08311	0.11172	0.14768	0.14880	0.13525	0.11712	0.10763	0.13151	0.13175
THIRD ORDER	0.06578	0.08616	0.09861	0.09007	0.07681	0.06410	0.05838	0.08267	0.07766
SUMS	$\alpha = 0.20$	0.01742	0.02443	0.04241	0.05124	0.04804	0.03745	0.03168	0.17588
	$\alpha = 0.40$	0.04592	0.06361	0.10316	0.12027	0.11188	0.08839	0.07570	0.23237
	$\alpha = 0.60$	0.09320	0.12759	0.19333	0.21692	0.19969	0.15950	0.13811	0.31392
	$\alpha = 0.80$	0.17419	0.23591	0.33413	0.35978	0.32680	0.26320	0.23006	0.43783
	$\alpha = 0.90$	0.23626	0.31840	0.43612	0.45951	0.41407	0.33450	0.29358	0.52752
	$\alpha = 0.95$	0.27544	0.37035	0.49890	0.51981	0.46638	0.37721	0.33170	0.57960
	$\alpha = 0.99$	0.31182	0.41852	0.55636	0.57444	0.51352	0.41567	0.36605	0.62849
	$\alpha = 1.00$	0.32172	0.43163	0.57189	0.58912	0.52614	0.42597	0.37524	0.64165
<b>b = 1.00</b>									
ZERO ORDER	$\mu_0 = 0.0$	0.0	0.0	0.0	0.0	0.0	0.0	0.17118	0.23965
FIRST ORDER	0.06667	0.08936	0.15314	0.20971	0.24376	0.22605	0.19648	0.18356	0.21282
SECOND ORDER	0.08442	0.10843	0.13438	0.13525	0.12686	0.11534	0.10897	0.12354	0.12442
THIRD ORDER	0.06161	0.07867	0.08565	0.07681	0.06532	0.05481	0.05017	0.07183	0.06661
SUMS	$\alpha = 0.20$	0.01727	0.02292	0.03678	0.04804	0.05441	0.05031	0.04410	0.21348
	$\alpha = 0.40$	0.04536	0.05973	0.08991	0.11188	0.12315	0.11332	0.10008	0.27032
	$\alpha = 0.60$	0.09109	0.11920	0.16876	0.19969	0.21301	0.19459	0.17296	0.34939
	$\alpha = 0.80$	0.16734	0.21802	0.29101	0.32680	0.33656	0.30428	0.27190	0.46508
	$\alpha = 0.90$	0.22444	0.29201	0.37881	0.41407	0.41830	0.37567	0.33641	0.54507
	$\alpha = 0.95$	0.26003	0.33814	0.43256	0.46638	0.46638	0.41730	0.37402	0.59318
	$\alpha = 0.99$	0.29282	0.38066	0.48159	0.51352	0.50923	0.45416	0.40733	0.63661
	$\alpha = 1.00$	0.30170	0.39219	0.49481	0.52614	0.52063	0.46394	0.41617	0.64826

TABLE 35 (continued)

 $g = 0.50, b = 1$ , Reflection

VECTOR	$\mu = 0.0$	$\mu = 0.1$	$\mu = 0.3$	$\mu = 0.5$	$\mu = 0.7$	$\mu = 0.9$	$\mu = 1.0$	AVERAGE N	FLUX U
$b = 1.00$ $\mu_0 = 0.9$									
FIRST ORDER	0.16838	0.13411	0.08864	0.06054	0.04298	0.03167	0.02751	0.07219	0.05096
SECOND ORDER	0.04134	0.07179	0.07407	0.05950	0.04544	0.03457	0.03025	0.05630	0.04860
THIRD ORDER	0.03014	0.04423	0.05148	0.04480	0.03600	0.02831	0.02507	0.04062	0.03705
SUMS $a = 0.20$	0.03561	0.03010	0.02116	0.01490	0.01075	0.00798	0.00695	0.01706	0.01248
$a = 0.40$	0.07663	0.06897	0.05176	0.03762	0.02761	0.02068	0.01805	0.04142	0.03139
$a = 0.60$	0.12694	0.12201	0.09797	0.07361	0.05500	0.04163	0.03645	0.07802	0.06127
$a = 0.80$	0.19459	0.20020	0.17221	0.13375	0.10182	0.07792	0.06846	0.13684	0.11124
$a = 0.90$	0.23998	0.25557	0.22745	0.17955	0.13796	0.10617	0.09346	0.18073	0.14934
$a = 0.95$	0.26720	0.28949	0.26199	0.20848	0.16092	0.12419	0.10943	0.20822	0.17344
$a = 0.99$	0.29183	0.32053	0.29395	0.23537	0.18234	0.14104	0.12437	0.23369	0.19585
$a = 1.00$	0.29845	0.32892	0.30263	0.24270	0.18819	0.14564	0.12846	0.24061	0.20197
$b = 1.00$ $\mu_0 = 1.0$									
FIRST ORDER	0.13416	0.10867	0.07376	0.05131	0.03693	0.02751	0.02402	0.06007	0.04324
SECOND ORDER	0.03420	0.06013	0.06335	0.05142	0.03954	0.03025	0.02654	0.04829	0.04206
THIRD ORDER	0.02575	0.03797	0.04492	0.03939	0.03178	0.02507	0.02223	0.03554	0.03261
SUMS $a = 0.20$	0.02844	0.02449	0.01770	0.01268	0.00926	0.00695	0.00607	0.01427	0.01063
$a = 0.40$	0.06143	0.05640	0.04354	0.03218	0.02388	0.01805	0.01581	0.03486	0.02688
$a = 0.60$	0.10234	0.10045	0.08297	0.06331	0.04779	0.03645	0.03201	0.06612	0.05275
$a = 0.80$	0.15824	0.16627	0.14695	0.11574	0.08889	0.06846	0.06032	0.11691	0.09636
$a = 0.90$	0.19628	0.21339	0.19491	0.15588	0.12074	0.09346	0.08248	0.15509	0.12979
$a = 0.95$	0.21927	0.24243	0.22501	0.18130	0.14101	0.10943	0.09665	0.17909	0.15098
$a = 0.99$	0.24018	0.26910	0.25292	0.20497	0.15995	0.12437	0.10992	0.20136	0.17073
$a = 1.00$	0.24581	0.27632	0.26051	0.21142	0.16512	0.12846	0.11355	0.20743	0.17612
$b = 1.0$ NARROW SURFACE LAYER AT TOP									
FIRST ORDER	INFINITE	0.65260	0.30344	0.17336	0.10836	0.07219	0.06007	0.28626	0.15053
SECOND ORDER	0.14313	0.20305	0.15363	0.10916	0.07773	0.05630	0.04829	0.11928	0.08958
THIRD ORDER	0.06708	0.09025	0.08686	0.06949	0.05328	0.04062	0.03554	0.06747	0.05716
SUMS $a = 0.20$	INFINITE	0.13945	0.06762	0.03967	0.02527	0.01706	0.01427	0.06264	0.03421
$a = 0.40$	INFINITE	0.30095	0.15326	0.09274	0.06038	0.04142	0.03486	0.13930	0.07944
$a = 0.60$	INFINITE	0.49405	0.26666	0.16729	0.11169	0.07802	0.06612	0.23765	0.14238
$a = 0.80$	INFINITE	0.73673	0.42663	0.27923	0.19190	0.13684	0.11691	0.37267	0.23629
$a = 0.90$	INFINITE	0.88734	0.53540	0.35889	0.25061	0.18073	0.15509	0.46297	0.30293
$a = 0.95$	INFINITE	0.97325	0.60049	0.40765	0.28705	0.20822	0.17909	0.51663	0.34369
$a = 0.99$	INFINITE	1.04842	0.65916	0.45220	0.32061	0.23369	0.20136	0.56482	0.38092
$a = 1.00$	INFINITE	1.06824	0.67488	0.46423	0.32971	0.24061	0.20743	0.57770	0.39097
$b = 1.0$ LAMBERT SURFACE ON TOP									
FIRST ORDER	0.50000	0.32139	0.17888	0.11061	0.07314	0.05096	0.04324	0.15053	0.09377
SECOND ORDER	0.08917	0.13270	0.11779	0.08897	0.06556	0.04860	0.04206	0.08958	0.07259
THIRD ORDER	0.04911	0.06933	0.07319	0.06099	0.04786	0.03705	0.03261	0.05716	0.05027
SUMS $a = 0.20$	0.10402	0.07022	0.04116	0.02624	0.01769	0.01248	0.01063	0.03421	0.02212
$a = 0.40$	0.21845	0.15563	0.09662	0.06372	0.04389	0.03139	0.02688	0.07944	0.05346
$a = 0.60$	0.34899	0.26407	0.17486	0.11965	0.08436	0.06127	0.05275	0.14238	0.10001
$a = 0.80$	0.50693	0.41081	0.29245	0.20830	0.15062	0.11124	0.09636	0.23629	0.17368
$a = 0.90$	0.60308	0.50780	0.37605	0.27359	0.20045	0.14934	0.12979	0.30293	0.22795
$a = 0.95$	0.65762	0.56510	0.42719	0.31419	0.23175	0.17344	0.15098	0.34369	0.26173
$a = 0.99$	0.70526	0.61636	0.47389	0.35162	0.26076	0.19585	0.17073	0.38092	0.29288
$a = 1.00$	0.71781	0.63004	0.48649	0.36177	0.26866	0.20197	0.17611	0.39097	0.30133

TABLE 35 (continued)  
 $g = 0.50, b = 1$ , Transmission

VECTOR	$\mu = 0.0$	$\mu = 0.1$	$\mu = 0.3$	$\mu = 0.5$	$\mu = 0.7$	$\mu = 0.9$	$\mu = 1.0$	AVERAGE N	FLUX U
<b>b = 1.00</b>									
	$\mu_0 = 0.9$								
ZERO ORDER	0.0	0.0	0.0	0.0	0.0	PEAK	0.0	0.18288	0.32919
FIRST ORDER	0.05543	0.07113	0.11395	0.16097	0.22605	0.31701	0.35031	0.17798	0.22788
SECOND ORDER	0.07655	0.09535	0.11459	0.11712	0.11534	0.11363	0.11311	0.11087	0.11429
THIRD ORDER	0.05463	0.06823	0.07198	0.06410	0.05481	0.04664	0.04311	0.06081	0.05616
SUMS									
$\alpha = 0.20$	0.01464	0.01866	0.02802	0.03745	0.05031	0.06836	0.07497	0.22346	0.37984
$\alpha = 0.40$	0.03896	0.04941	0.06988	0.08839	0.11332	0.14872	0.16166	0.27681	0.44321
$\alpha = 0.60$	0.07879	0.09967	0.13330	0.15950	0.19459	0.24567	0.26423	0.34928	0.52503
$\alpha = 0.80$	0.14493	0.18328	0.23268	0.26320	0.30428	0.36746	0.39013	0.45262	0.63586
$\alpha = 0.90$	0.19408	0.24563	0.30428	0.33450	0.37567	0.44240	0.46608	0.52268	0.70826
$\alpha = 0.95$	0.22454	0.28438	0.34811	0.37721	0.41730	0.48481	0.50858	0.56438	0.75055
$\alpha = 0.99$	0.25250	0.32001	0.38808	0.41567	0.45416	0.52170	0.54527	0.60177	0.78807
$\alpha = 1.00$	0.26006	0.32965	0.39886	0.42597	0.46394	0.53139	0.55487	0.61176	0.79803
<b>b = 1.00</b>									
	$\mu_0 = 1.0$								
ZERO ORDER	0.0	0.0	0.0	0.0	0.0	0.0	PEAK	0.18394	0.36788
FIRST ORDER	0.04936	0.06214	0.09610	0.13426	0.19648	0.35031	0.55182	0.17215	0.23233
SECOND ORDER	0.07122	0.08767	0.10431	0.10763	0.10897	0.11311	0.11714	0.10412	0.10909
THIRD ORDER	0.05087	0.06292	0.06562	0.05838	0.05017	0.04311	0.04012	0.05573	0.05149
SUMS									
$\alpha = 0.20$	0.01318	0.01650	0.02398	0.03168	0.04410	0.07497	0.11540	0.22303	0.41917
$\alpha = 0.40$	0.03534	0.04412	0.06056	0.07570	0.10008	0.16166	0.24264	0.27402	0.48244
$\alpha = 0.60$	0.07187	0.08962	0.11670	0.13811	0.17296	0.26423	0.38552	0.34266	0.56290
$\alpha = 0.80$	0.13257	0.16556	0.20539	0.23006	0.27190	0.39013	0.55076	0.43953	0.67004
$\alpha = 0.90$	0.17762	0.22220	0.26950	0.29358	0.33641	0.46608	0.64557	0.50467	0.73909
$\alpha = 0.95$	0.20551	0.25738	0.30878	0.33170	0.37402	0.50858	0.69718	0.54327	0.77915
$\alpha = 0.99$	0.23107	0.28971	0.34462	0.36605	0.40733	0.54527	0.74094	0.57780	0.81452
$\alpha = 1.00$	0.23797	0.29845	0.35428	0.37524	0.41617	0.55487	0.75227	0.58701	0.82389
<b>b = 1.0</b> NARROW SURFACE LAYER AT TOP									
ZERO ORDER	0.0	0.00023	0.05946	0.13534	0.17118	0.18288	0.18394	0.10969	0.14850
FIRST ORDER	0.04507	0.06350	0.13012	0.17267	0.18356	0.17798	0.17215	0.14529	0.16837
SECOND ORDER	0.06691	0.08935	0.12487	0.13151	0.12354	0.11087	0.10412	0.11559	0.11927
THIRD ORDER	0.05694	0.07443	0.08809	0.08267	0.07183	0.06081	0.05573	0.07517	0.07191
SUMS									
$\alpha = 0.20$	0.01222	0.01719	0.09128	0.17588	0.21348	0.22346	0.22303	0.14406	0.18759
$\alpha = 0.40$	0.03368	0.04638	0.13897	0.23237	0.27032	0.27681	0.27402	0.19263	0.24092
$\alpha = 0.60$	0.07127	0.09678	0.21263	0.31392	0.34939	0.34928	0.34266	0.26381	0.31628
$\alpha = 0.80$	0.13853	0.18613	0.33176	0.43783	0.46508	0.45262	0.43953	0.37363	0.42840
$\alpha = 0.90$	0.19149	0.25614	0.42004	0.52590	0.54507	0.52268	0.50467	0.45253	0.50690
$\alpha = 0.95$	0.22534	0.30081	0.47496	0.57960	0.59318	0.56438	0.54327	0.50091	0.55441
$\alpha = 0.99$	0.25700	0.34256	0.52555	0.62849	0.63661	0.60177	0.57780	0.54509	0.59746
$\alpha = 1.00$	0.26566	0.35396	0.53926	0.64165	0.64826	0.61176	0.58701	0.55701	0.60903
<b>b = 1.0</b> LAMBERT SURFACE ON TOP									
ZERO ORDER	0.0	0.00005	0.03567	0.13534	0.23965	0.32919	0.36788	0.14850	0.21938
FIRST ORDER	0.05640	0.07692	0.13926	0.18571	0.21282	0.22788	0.23233	0.16837	0.19928
SECOND ORDER	0.07648	0.09950	0.12863	0.13175	0.12442	0.11429	0.10909	0.11927	0.12169
THIRD ORDER	0.05909	0.07598	0.08817	0.07766	0.06661	0.05616	0.05149	0.07191	0.06747
SUMS									
$\alpha = 0.20$	0.01488	0.02010	0.06945	0.17845	0.28779	0.37984	0.41917	0.18759	0.26471
$\alpha = 0.40$	0.03982	0.05320	0.11912	0.23715	0.35016	0.44321	0.48244	0.24092	0.32414
$\alpha = 0.60$	0.08156	0.10806	0.19415	0.31982	0.43376	0.52503	0.56290	0.31628	0.40481
$\alpha = 0.80$	0.15301	0.20144	0.31257	0.44219	0.55156	0.63586	0.67004	0.42840	0.52010
$\alpha = 0.90$	0.20751	0.27255	0.39870	0.52752	0.63087	0.70826	0.73909	0.50690	0.59855
$\alpha = 0.95$	0.24180	0.31727	0.45178	0.57906	0.67794	0.75055	0.77915	0.55441	0.64536
$\alpha = 0.99$	0.27356	0.35870	0.50038	0.62571	0.72009	0.78807	0.81452	0.59746	0.68742
$\alpha = 1.00$	0.28219	0.36996	0.51351	0.63823	0.73134	0.79803	0.82389	0.60903	0.69867

TABLE 35 (continued)  
 $g = 0.50, b = 2$ , Reflection

VECTOR	$\mu = 0.0$	$\mu = 0.1$	$\mu = 0.3$	$\mu = 0.5$	$\mu = 0.7$	$\mu = 0.9$	$\mu = 1.0$	AVERAGE N	FLUX U
$b = 2.00 \quad \mu_0 = 0.1$									
FIRST ORDER	3.48549	1.65159	0.69006	0.36438	0.21335	0.13411	0.10867	0.65260	0.32140
SECOND ORDER	0.40621	0.42638	0.25482	0.16066	0.10624	0.07301	0.06129	0.20384	0.13376
THIRD ORDER	0.11928	0.14906	0.11937	0.08823	0.06493	0.04828	0.04186	0.09304	0.07289
SUMS $\alpha = 0.20$	0.71439	0.34869	0.14928	0.08011	0.04752	0.03020	0.02459	0.13952	0.07030
$\alpha = 0.40$	1.46855	0.74068	0.32676	0.17913	0.10817	0.06978	0.05718	0.30153	0.15635
$\alpha = 0.60$	2.27377	1.19055	0.54603	0.30838	0.19109	0.12607	0.10435	0.49713	0.26779
$\alpha = 0.80$	3.15180	1.72671	0.83650	0.49447	0.31911	0.21822	0.18355	0.75143	0.42778
$\alpha = 0.90$	3.63298	2.04670	1.03033	0.62982	0.41882	0.29397	0.25015	0.91996	0.54466
$\alpha = 0.95$	3.88988	2.22728	1.14829	0.71689	0.48566	0.34636	0.29680	1.02261	0.62025
$\alpha = 0.99$	4.10629	2.38566	1.25758	0.80072	0.55180	0.39924	0.34426	1.11800	0.69336
$\alpha = 1.00$	4.16226	2.42766	1.28754	0.82422	0.57063	0.41446	0.35797	1.14420	0.71391
$b = 2.00 \quad \mu_0 = 0.3$									
FIRST ORDER	1.02453	0.69006	0.36163	0.21189	0.13390	0.08968	0.07473	0.30417	0.17983
SECOND ORDER	0.18254	0.25482	0.20457	0.14848	0.10726	0.07844	0.06750	0.15668	0.12168
THIRD ORDER	0.08718	0.11937	0.11742	0.09733	0.07719	0.06053	0.05360	0.09366	0.08134
SUMS $\alpha = 0.20$	0.21300	0.14928	0.08158	0.04922	0.03180	0.02165	0.01815	0.06796	0.04159
$\alpha = 0.40$	0.44633	0.32676	0.18750	0.11715	0.07774	0.05403	0.04570	0.15493	0.09869
$\alpha = 0.60$	0.71006	0.54603	0.33235	0.21697	0.14903	0.10644	0.09106	0.27318	0.18268
$\alpha = 0.80$	1.02614	0.83650	0.54953	0.38048	0.27380	0.20295	0.17635	0.45189	0.32156
$\alpha = 0.90$	1.22029	1.03033	0.71103	0.51158	0.37943	0.28801	0.25278	0.58710	0.43439
$\alpha = 0.95$	1.33310	1.14829	0.81570	0.60024	0.45299	0.34854	0.30764	0.67593	0.51138
$\alpha = 0.99$	1.43457	1.25758	0.91679	0.68823	0.52738	0.41057	0.36415	0.76260	0.58827
$\alpha = 1.00$	1.46192	1.28754	0.94515	0.71330	0.54878	0.42854	0.38058	0.78706	0.61026
$b = 2.00 \quad \mu_0 = 0.5$									
FIRST ORDER	0.49828	0.36438	0.21189	0.13377	0.08979	0.06323	0.05386	0.17514	0.11298
SECOND ORDER	0.10286	0.16066	0.14848	0.11684	0.08920	0.06802	0.05957	0.11508	0.09649
THIRD ORDER	0.06229	0.08823	0.09733	0.08713	0.07284	0.05937	0.05341	0.08030	0.07415
SUMS $\alpha = 0.20$	0.10435	0.08011	0.04922	0.03225	0.02222	0.01593	0.01367	0.04038	0.02716
$\alpha = 0.40$	0.22126	0.17913	0.11715	0.08012	0.05695	0.04178	0.03615	0.09573	0.06745
$\alpha = 0.60$	0.35900	0.30838	0.21697	0.15624	0.11532	0.08702	0.07615	0.17752	0.13194
$\alpha = 0.80$	0.53736	0.49447	0.38048	0.29204	0.22590	0.17655	0.15673	0.31422	0.24869
$\alpha = 0.90$	0.65754	0.62982	0.51158	0.40805	0.32455	0.25894	0.23181	0.42644	0.34989
$\alpha = 0.95$	0.73204	0.71689	0.60024	0.48906	0.39495	0.31867	0.28658	0.50346	0.42118
$\alpha = 0.99$	0.80224	0.80072	0.68823	0.57105	0.46713	0.38048	0.34346	0.58064	0.49372
$\alpha = 1.00$	0.82170	0.82422	0.71330	0.59465	0.48805	0.39848	0.36006	0.60274	0.51467
$b = 2.00 \quad \mu_0 = 0.7$									
FIRST ORDER	0.27821	0.21335	0.13390	0.08979	0.06328	0.04637	0.04019	0.11051	0.07602
SECOND ORDER	0.06376	0.10624	0.10726	0.08920	0.07083	0.05567	0.04939	0.08473	0.07448
THIRD ORDER	0.04500	0.06493	0.07719	0.07284	0.06314	0.05282	0.04802	0.06569	0.06296
SUMS $\alpha = 0.20$	0.05862	0.04752	0.03180	0.02222	0.01609	0.01201	0.01048	0.02611	0.01878
$\alpha = 0.40$	0.12560	0.10817	0.07774	0.05695	0.04261	0.03252	0.02861	0.06384	0.04823
$\alpha = 0.60$	0.20761	0.19109	0.14903	0.11532	0.08964	0.07031	0.06252	0.12321	0.09825
$\alpha = 0.80$	0.32160	0.31911	0.27380	0.22590	0.18361	0.14869	0.13390	0.22991	0.19459
$\alpha = 0.90$	0.40469	0.41882	0.37943	0.32455	0.27040	0.22291	0.20215	0.32244	0.28173
$\alpha = 0.95$	0.45885	0.48566	0.45299	0.39495	0.33337	0.27737	0.25247	0.38776	0.34438
$\alpha = 0.99$	0.51166	0.55180	0.52738	0.46713	0.39852	0.33410	0.30502	0.45433	0.40890
$\alpha = 1.00$	0.52659	0.57063	0.54878	0.48805	0.41750	0.35068	0.32039	0.47357	0.42764

TABLE 35 (continued)  
 $g = 0.50, b = 2$ , Transmission

VECTOR	$\mu = 0.0$	$\mu = 0.1$	$\mu = 0.3$	$\mu = 0.5$	$\mu = 0.7$	$\mu = 0.9$	$\mu = 1.0$	AVERAGE N	FLUX U
<b>b = 2.00</b>									
ZERO ORDER	$\mu_0 = 0.1$ 0.0	PEAK	0.0	0.0	0.0	0.0	0.0	0.00000	0.00000
FIRST ORDER	0.00000	0.00000	0.00214	0.01298	0.02142	0.02342	0.02286	0.01198	0.01733
SECOND ORDER	0.00463	0.00631	0.01440	0.02997	0.04291	0.04909	0.04992	0.02851	0.03782
THIRD ORDER	0.01191	0.01585	0.02731	0.04094	0.05022	0.05422	0.05465	0.03765	0.04582
SUMS									
$a = 0.20$	0.00031	0.00042	0.00129	0.00420	0.00649	0.00717	0.00709	0.00391	0.00543
$a = 0.40$	0.00221	0.00294	0.00622	0.01421	0.02036	0.02240	0.02230	0.01321	0.01753
$a = 0.60$	0.00916	0.01214	0.02132	0.03805	0.05035	0.05442	0.05419	0.03519	0.04447
$a = 0.80$	0.03252	0.04289	0.06641	0.09831	0.11953	0.12540	0.12417	0.09029	0.10819
$a = 0.90$	0.06110	0.08043	0.11823	0.16170	0.18813	0.19351	0.19061	0.14799	0.17237
$a = 0.95$	0.08451	0.11118	0.15954	0.21028	0.23920	0.24330	0.23887	0.19213	0.22052
$a = 0.99$	0.11045	0.14524	0.20459	0.26208	0.29272	0.29488	0.28866	0.23915	0.27120
$a = 1.00$	0.11826	0.15550	0.21806	0.27739	0.30840	0.30989	0.30311	0.25304	0.28609
<b>b = 2.00</b>									
ZERO ORDER	$\mu_0 = 0.3$ 0.0	0.0	PEAK	0.0	0.0	0.0	0.0	0.00212	0.00127
FIRST ORDER	0.00130	0.00214	0.01052	0.03045	0.04216	0.04158	0.03878	0.02530	0.03423
SECOND ORDER	0.01039	0.01440	0.03028	0.05216	0.06710	0.07254	0.07239	0.04723	0.05972
THIRD ORDER	0.02047	0.02731	0.04439	0.06051	0.06928	0.07148	0.07084	0.05447	0.06378
SUMS									
$a = 0.20$	0.00089	0.00129	0.00376	0.00877	0.01178	0.01190	0.01132	0.00960	0.01112
$a = 0.40$	0.00449	0.00622	0.01371	0.02651	0.03422	0.03492	0.03367	0.02518	0.03066
$a = 0.60$	0.01577	0.02132	0.03892	0.06396	0.07854	0.08000	0.07764	0.05853	0.07048
$a = 0.80$	0.04981	0.06641	0.10541	0.15008	0.17373	0.17447	0.16942	0.13576	0.15823
$a = 0.90$	0.08911	0.11823	0.17705	0.23597	0.26431	0.26227	0.25415	0.21302	0.24308
$a = 0.95$	0.12049	0.15954	0.23257	0.30026	0.33053	0.32559	0.31499	0.27092	0.30559
$a = 0.99$	0.15472	0.20459	0.29215	0.36789	0.39921	0.39069	0.37735	0.33188	0.37072
$a = 1.00$	0.16496	0.21806	0.30982	0.38774	0.41922	0.40957	0.39541	0.34979	0.38974
<b>b = 2.00</b>									
ZERO ORDER	$\mu_0 = 0.5$ 0.0	0.0	0.0	PEAK	0.0	0.0	0.0	0.01832	0.01832
FIRST ORDER	0.00913	0.01298	0.03045	0.06019	0.07864	0.07477	0.06756	0.05122	0.06507
SECOND ORDER	0.02210	0.02997	0.05216	0.07610	0.09116	0.09617	0.09556	0.06897	0.08302
THIRD ORDER	0.03096	0.04094	0.06051	0.07517	0.08142	0.08145	0.07996	0.06770	0.07615
SUMS									
$a = 0.20$	0.00302	0.00420	0.00877	0.01580	0.02015	0.01957	0.01808	0.03197	0.03537
$a = 0.40$	0.01039	0.01421	0.02651	0.04341	0.05359	0.05272	0.04955	0.05628	0.06474
$a = 0.60$	0.02824	0.03805	0.06396	0.09494	0.11263	0.11116	0.10566	0.10220	0.11810
$a = 0.80$	0.07379	0.09831	0.15008	0.20176	0.22799	0.22343	0.21360	0.19803	0.22496
$a = 0.90$	0.12189	0.16170	0.23597	0.30186	0.33172	0.32253	0.30854	0.28812	0.32254
$a = 0.95$	0.15879	0.21028	0.30026	0.37468	0.40565	0.39238	0.37525	0.35374	0.39258
$a = 0.99$	0.19816	0.26208	0.36789	0.45004	0.48123	0.46327	0.44281	0.42171	0.46449
$a = 1.00$	0.20980	0.27739	0.38774	0.47198	0.50309	0.48369	0.46224	0.44150	0.48533
<b>b = 2.00</b>									
ZERO ORDER	$\mu_0 = 0.7$ 0.0	0.0	0.0	0.0	PEAK	0.0	0.0	0.04102	0.05743
FIRST ORDER	0.01598	0.02142	0.04216	0.07864	0.11683	0.12858	0.11937	0.07722	0.10054
SECOND ORDER	0.03272	0.04291	0.06710	0.09116	0.10782	0.11626	0.11762	0.08490	0.10034
THIRD ORDER	0.03859	0.05022	0.06928	0.08142	0.08570	0.08480	0.08316	0.07405	0.08121
SUMS									
$a = 0.20$	0.00488	0.00649	0.01178	0.02015	0.02848	0.03116	0.02935	0.06057	0.08232
$a = 0.40$	0.01542	0.02036	0.03422	0.05359	0.07175	0.07758	0.07391	0.09236	0.12110
$a = 0.60$	0.03829	0.05035	0.07854	0.11263	0.14201	0.15078	0.14473	0.14754	0.18549
$a = 0.80$	0.09118	0.11953	0.17373	0.22799	0.26895	0.27809	0.26775	0.25395	0.30417
$a = 0.90$	0.14361	0.18813	0.26431	0.33172	0.37742	0.38359	0.36917	0.34895	0.40687
$a = 0.95$	0.18263	0.23920	0.33053	0.40565	0.45287	0.45580	0.43831	0.41645	0.47875
$a = 0.99$	0.22349	0.29272	0.39921	0.48123	0.52893	0.52786	0.50713	0.48533	0.55145
$a = 1.00$	0.23546	0.30840	0.41922	0.50309	0.55077	0.54843	0.52675	0.50524	0.57236



TABLE 35 (continued)

 $g = 0.50, b = 2$ , Reflection

VECTOR	$\mu = 0.0$	$\mu = 0.1$	$\mu = 0.3$	$\mu = 0.5$	$\mu = 0.7$	$\mu = 0.9$	$\mu = 1.0$	AVERAGE N	FLUX U
$b = 2.00$ $\mu_0 = 0.9$									
FIRST ORDER	0.16838	0.13411	0.08968	0.06323	0.04637	0.03510	0.03084	0.07429	0.05382
SECOND ORDER	0.04220	0.07301	0.07844	0.06802	0.05567	0.04481	0.04016	0.06320	0.05744
THIRD ORDER	0.03310	0.04828	0.06053	0.05937	0.05282	0.04503	0.04125	0.05284	0.05196
SUMS $a = 0.20$	0.03568	0.03020	0.02165	0.01593	0.01201	0.00925	0.00818	0.01789	0.01356
$a = 0.40$	0.07722	0.06978	0.05403	0.04178	0.03252	0.02559	0.02280	0.04482	0.03567
$a = 0.60$	0.12996	0.12607	0.10644	0.08702	0.07031	0.05674	0.05105	0.08925	0.07487
$a = 0.80$	0.20809	0.21822	0.20295	0.17655	0.14869	0.12351	0.11235	0.17353	0.15377
$a = 0.90$	0.26888	0.29397	0.28801	0.25894	0.22291	0.18799	0.17203	0.24952	0.22730
$a = 0.95$	0.31007	0.34636	0.34854	0.31867	0.27737	0.23573	0.21636	0.30420	0.28093
$a = 0.99$	0.35124	0.39924	0.41057	0.38048	0.33410	0.28570	0.26285	0.36059	0.33661
$a = 1.00$	0.36303	0.41446	0.42854	0.39848	0.35068	0.30033	0.27648	0.37699	0.35285
$b = 2.00$ $\mu_0 = 1.0$									
FIRST ORDER	0.13416	0.10867	0.07473	0.05386	0.04019	0.03084	0.02727	0.06209	0.04599
SECOND ORDER	0.03503	0.06129	0.06750	0.05957	0.04939	0.04016	0.03615	0.05491	0.05058
THIRD ORDER	0.02859	0.04186	0.05360	0.05341	0.04802	0.04125	0.03791	0.04731	0.04700
SUMS $a = 0.20$	0.02851	0.02458	0.01815	0.01367	0.01048	0.00818	0.00727	0.01507	0.01167
$a = 0.40$	0.06200	0.05718	0.04570	0.03615	0.02861	0.02280	0.02042	0.03813	0.03100
$a = 0.60$	0.10524	0.10435	0.09106	0.07615	0.06252	0.05105	0.04614	0.07693	0.06585
$a = 0.80$	0.17118	0.18355	0.17635	0.15673	0.13390	0.11235	0.10262	0.15211	0.13721
$a = 0.90$	0.22395	0.25015	0.25278	0.23181	0.20215	0.17203	0.15798	0.22097	0.20451
$a = 0.95$	0.26026	0.29680	0.30764	0.28658	0.25247	0.21636	0.19924	0.27089	0.25386
$a = 0.99$	0.29691	0.34426	0.36415	0.34346	0.30502	0.26285	0.24257	0.32261	0.30527
$a = 1.00$	0.30746	0.35797	0.38058	0.36006	0.32039	0.27648	0.25529	0.33768	0.32030
$b = 2.0$ NARROW SURFACE LAYER AT TOP									
FIRST ORDER	INFINITE	0.65260	0.30417	0.17514	0.11051	0.07429	0.06209	0.28761	0.15234
SECOND ORDER	0.14381	0.20384	0.15668	0.11508	0.08473	0.06320	0.05491	0.12400	0.09561
THIRD ORDER	0.06911	0.09304	0.09346	0.08030	0.06569	0.05284	0.04731	0.07641	0.06811
SUMS $a = 0.20$	INFINITE	0.13952	0.06796	0.04038	0.02611	0.01789	0.01507	0.06319	0.03493
$a = 0.40$	INFINITE	0.30153	0.15493	0.09573	0.06384	0.04482	0.03813	0.14171	0.08246
$a = 0.60$	INFINITE	0.49713	0.27318	0.17752	0.12321	0.08925	0.07693	0.24615	0.15261
$a = 0.80$	INFINITE	0.75143	0.45189	0.31422	0.22991	0.17353	0.15211	0.40250	0.27078
$a = 0.90$	INFINITE	0.91996	0.58710	0.42644	0.32244	0.24952	0.22097	0.52126	0.36885
$a = 0.95$	INFINITE	1.02261	0.67593	0.50346	0.38776	0.30420	0.27089	0.59979	0.43665
$a = 0.99$	INFINITE	1.11800	0.76260	0.58064	0.45433	0.36059	0.32261	0.67681	0.50494
$a = 1.00$	INFINITE	1.14420	0.78706	0.60274	0.47357	0.37699	0.33768	0.69863	0.52455
$b = 2.0$ LAMBERT SURFACE ON TOP									
FIRST ORDER	0.50000	0.32140	0.17983	0.11298	0.07602	0.05382	0.04599	0.15234	0.09620
SECOND ORDER	0.08991	0.13376	0.12168	0.09649	0.07448	0.05744	0.05058	0.09561	0.08030
THIRD ORDER	0.05170	0.07289	0.08134	0.07415	0.06296	0.05196	0.04700	0.06811	0.06364
SUMS $a = 0.20$	0.10408	0.07030	0.04159	0.02716	0.01878	0.01356	0.01167	0.03493	0.02306
$a = 0.40$	0.21897	0.15635	0.09869	0.06745	0.04823	0.03567	0.03100	0.08246	0.05724
$a = 0.60$	0.35174	0.26779	0.18268	0.13194	0.09825	0.07487	0.06585	0.15261	0.11235
$a = 0.80$	0.51964	0.42778	0.32156	0.24869	0.19459	0.15377	0.13721	0.27078	0.21357
$a = 0.90$	0.63080	0.54466	0.43439	0.34989	0.28173	0.22730	0.20451	0.36885	0.30254
$a = 0.95$	0.69917	0.62025	0.51138	0.42118	0.34438	0.28093	0.25386	0.43665	0.36569
$a = 0.99$	0.76335	0.69336	0.58827	0.49372	0.40890	0.33661	0.30527	0.50494	0.43026
$a = 1.00$	0.78111	0.71391	0.61026	0.51467	0.42764	0.35285	0.32030	0.52455	0.44896

TABLE 35 (continued)

 $g = 0.50, b = 2$ , Transmission

VECTOR	$\mu = 0.0$	$\mu = 0.1$	$\mu = 0.3$	$\mu = 0.5$	$\mu = 0.7$	$\mu = 0.9$	$\mu = 1.0$	AVERAGE N	FLUX U
$b = 2.00$									
$\mu_0 = 0.9$									
ZERO ORDER	0.0	0.0	0.0	0.0	0.0	PEAK	0.0	0.06020	0.10837
FIRST ORDER	0.01825	0.02342	0.04158	0.07477	0.12858	0.20872	0.24419	0.09581	0.13376
SECOND ORDER	0.03843	0.04909	0.07254	0.09617	0.11626	0.13355	0.14150	0.09348	0.11113
THIRD ORDER	0.04233	0.05422	0.07148	0.08145	0.08480	0.08420	0.08309	0.07500	0.08118
SUMS									
$a = 0.20$	0.00559	0.00717	0.01190	0.01957	0.03116	0.04786	0.05526	0.08381	0.14032
$a = 0.40$	0.01748	0.02240	0.03492	0.05272	0.07758	0.11220	0.12749	0.12030	0.18690
$a = 0.60$	0.04240	0.05442	0.08000	0.11116	0.15078	0.20382	0.22708	0.18035	0.25923
$a = 0.80$	0.09739	0.12540	0.17447	0.22343	0.27809	0.34780	0.37783	0.28996	0.38383
$a = 0.90$	0.14994	0.19351	0.26227	0.32253	0.38359	0.45892	0.49076	0.38401	0.48668
$a = 0.95$	0.18826	0.24330	0.32559	0.39238	0.45580	0.53236	0.56422	0.44951	0.55699
$a = 0.99$	0.22788	0.29488	0.39069	0.46327	0.52786	0.60414	0.63532	0.51555	0.62713
$a = 1.00$	0.23941	0.30989	0.40957	0.48369	0.54843	0.62441	0.65529	0.53451	0.64715
$b = 2.00$									
$\mu_0 = 1.0$									
ZERO ORDER	0.0	0.0	0.0	0.0	0.0	0.0	PEAK	0.06767	0.13534
FIRST ORDER	0.01816	0.02286	0.03878	0.06756	0.11937	0.24419	0.40601	0.10206	0.14864
SECOND ORDER	0.03951	0.04992	0.07239	0.09556	0.11762	0.14150	0.15565	0.09548	0.11456
THIRD ORDER	0.04299	0.05465	0.07084	0.07996	0.08316	0.08309	0.08244	0.07412	0.07998
SUMS									
$a = 0.20$	0.00562	0.00709	0.01132	0.01808	0.02935	0.05526	0.08818	0.09259	0.17039
$a = 0.40$	0.01763	0.02230	0.03367	0.04955	0.07391	0.12749	0.19434	0.13044	0.22021
$a = 0.60$	0.04268	0.05419	0.07764	0.10566	0.14473	0.22708	0.32850	0.19156	0.29549
$a = 0.80$	0.09724	0.12417	0.16942	0.21360	0.26775	0.37783	0.51326	0.30071	0.42148
$a = 0.90$	0.14874	0.19061	0.25415	0.30854	0.36917	0.49076	0.64192	0.39288	0.52327
$a = 0.95$	0.18603	0.23887	0.31499	0.37525	0.43831	0.56422	0.72246	0.45652	0.59210
$a = 0.99$	0.22440	0.28866	0.37735	0.44281	0.50713	0.63532	0.79860	0.52035	0.66030
$a = 1.00$	0.23553	0.30311	0.39541	0.46224	0.52675	0.65529	0.81971	0.53862	0.67970
$b = 2.0$ NARROW SURFACE LAYER AT TOP									
ZERO ORDER	0.0	0.00000	0.00212	0.01832	0.04102	0.06020	0.06767	0.02445	0.03753
FIRST ORDER	0.00893	0.01198	0.02530	0.05122	0.07722	0.09581	0.10206	0.05235	0.07036
SECOND ORDER	0.02165	0.02851	0.04723	0.06897	0.08490	0.09348	0.09548	0.06453	0.07832
THIRD ORDER	0.02881	0.03765	0.05447	0.06770	0.07405	0.07500	0.07412	0.06161	0.06942
SUMS									
$a = 0.20$	0.00294	0.00391	0.00960	0.03197	0.06057	0.08381	0.09259	0.03809	0.05540
$a = 0.40$	0.00999	0.01321	0.02518	0.05628	0.09236	0.12030	0.13044	0.06157	0.08468
$a = 0.60$	0.02673	0.03519	0.05853	0.10220	0.14754	0.18035	0.19156	0.10479	0.13598
$a = 0.80$	0.06879	0.09029	0.13576	0.19803	0.25395	0.28996	0.30071	0.19338	0.23606
$a = 0.90$	0.11284	0.14799	0.21302	0.28812	0.34895	0.38401	0.39288	0.27592	0.32619
$a = 0.95$	0.14652	0.19213	0.27092	0.35374	0.41645	0.44951	0.45652	0.33582	0.39053
$a = 0.99$	0.18239	0.23915	0.33188	0.42171	0.48533	0.51555	0.52035	0.39775	0.45639
$a = 1.00$	0.19299	0.25304	0.34979	0.44150	0.50524	0.53451	0.53862	0.41576	0.47545
$b = 2.0$ LAMBERT SURFACE ON TOP									
ZERO ORDER	0.0	0.00000	0.00127	0.01832	0.05743	0.10837	0.13534	0.03753	0.06027
FIRST ORDER	0.01308	0.01733	0.03423	0.06507	0.10054	0.13376	0.14864	0.07036	0.09505
SECOND ORDER	0.02899	0.03782	0.05972	0.08302	0.10034	0.11113	0.11456	0.07832	0.09377
THIRD ORDER	0.033529	0.04582	0.06378	0.07615	0.08121	0.08118	0.07998	0.06942	0.07677
SUMS									
$a = 0.20$	0.00412	0.00543	0.01112	0.03537	0.08232	0.14032	0.17039	0.05540	0.08375
$a = 0.40$	0.01337	0.01753	0.03066	0.06474	0.12110	0.18690	0.22021	0.08468	0.12032
$a = 0.60$	0.03401	0.04447	0.07048	0.11810	0.18549	0.25923	0.29549	0.13598	0.18118
$a = 0.80$	0.08284	0.10819	0.15823	0.22496	0.30417	0.38383	0.42148	0.23606	0.29400
$a = 0.90$	0.13196	0.17237	0.24308	0.32254	0.40687	0.48668	0.52327	0.32619	0.39217
$a = 0.95$	0.16879	0.22052	0.30559	0.39258	0.47875	0.55699	0.59210	0.39053	0.46108
$a = 0.99$	0.20753	0.27120	0.37072	0.46449	0.55145	0.62713	0.66030	0.45639	0.53093
$a = 1.00$	0.21889	0.28609	0.38974	0.48533	0.57236	0.64715	0.67970	0.47545	0.55104

TABLE 35 (continued)

 $g = 0.50, b = 4$ , Reflection

VECTOR	$\mu = 0.0$	$\mu = 0.1$	$\mu = 0.3$	$\mu = 0.5$	$\mu = 0.7$	$\mu = 0.9$	$\mu = 1.0$	AVERAGE N	FLUX U
$b = 4.00 \quad \mu_0 = 0.1$									
FIRST ORDER	3.48549	1.65159	0.69006	0.36438	0.21335	0.13411	0.10867	0.65260	0.32140
SECOND ORDER	0.40621	0.42638	0.25483	0.16069	0.10630	0.07309	0.06138	0.20387	0.13381
THIRD ORDER	0.11929	0.14908	0.11941	0.08839	0.06524	0.04870	0.04231	0.09323	0.07317
SUMS									
$a = 0.20$	0.71439	0.34869	0.14928	0.08012	0.04753	0.03021	0.02459	0.13952	0.07031
$a = 0.40$	1.46856	0.74070	0.32678	0.17918	0.10826	0.06989	0.05730	0.30159	0.15643
$a = 0.60$	2.27391	1.19073	0.54632	0.30890	0.19186	0.12702	0.10536	0.49767	0.26849
$a = 0.80$	3.15357	1.72903	0.83995	0.49948	0.32569	0.22590	0.19156	0.75643	0.43393
$a = 0.90$	3.64000	2.05589	1.04341	0.64743	0.44060	0.31853	0.27552	0.93717	0.56514
$a = 0.95$	3.90477	2.24677	1.17552	0.75228	0.52813	0.39336	0.34504	1.05686	0.66032
$a = 0.99$	4.13499	2.42324	1.30929	0.86614	0.62845	0.48270	0.42944	1.18082	0.76588
$a = 1.00$	4.19644	2.47240	1.34889	0.90132	0.66043	0.51182	0.45720	1.21811	0.79894
$b = 4.00 \quad \mu_0 = 0.3$									
FIRST ORDER	1.02453	0.69006	0.36163	0.21189	0.13391	0.08969	0.07474	0.30417	0.17984
SECOND ORDER	0.18254	0.25483	0.20458	0.14855	0.10741	0.07864	0.06772	0.15677	0.12181
THIRD ORDER	0.08721	0.11941	0.11753	0.09767	0.07782	0.06136	0.05449	0.09385	0.08189
SUMS									
$a = 0.20$	0.21300	0.14928	0.08159	0.04923	0.03181	0.02167	0.01818	0.06797	0.04161
$a = 0.40$	0.44635	0.32678	0.18754	0.11725	0.07791	0.05425	0.04594	0.15504	0.09885
$a = 0.60$	0.71028	0.54632	0.33283	0.21782	0.15029	0.10799	0.09270	0.27407	0.18383
$a = 0.80$	1.02878	0.83995	0.55465	0.38793	0.28357	0.21434	0.18824	0.45932	0.33068
$a = 0.90$	1.23028	1.04341	0.72968	0.53669	0.41046	0.32298	0.28890	0.61162	0.46356
$a = 0.95$	1.35390	1.17552	0.85375	0.64970	0.51234	0.41419	0.37501	0.72378	0.56737
$a = 0.99$	1.47407	1.30929	0.98796	0.77827	0.63287	0.52539	0.48133	0.84905	0.68807
$a = 1.00$	1.50878	1.34889	1.02928	0.81902	0.67191	0.56201	0.51659	0.88840	0.72683
$b = 4.00 \quad \mu_0 = 0.5$									
FIRST ORDER	0.49828	0.36438	0.21189	0.13382	0.08989	0.06336	0.05399	0.17520	0.11306
SECOND ORDER	0.10288	0.16069	0.14855	0.11711	0.08971	0.06870	0.06030	0.11540	0.09695
THIRD ORDER	0.06241	0.08839	0.09767	0.08797	0.07430	0.06127	0.05544	0.08123	0.07546
SUMS									
$a = 0.20$	0.10435	0.08012	0.04923	0.03228	0.02227	0.01601	0.01375	0.04042	0.02721
$a = 0.40$	0.22130	0.17918	0.11725	0.08035	0.05733	0.04227	0.03668	0.09598	0.06779
$a = 0.60$	0.35940	0.30890	0.21782	0.15773	0.11752	0.08971	0.07901	0.17906	0.13395
$a = 0.80$	0.54119	0.49948	0.38793	0.30287	0.24010	0.19308	0.17398	0.32501	0.26194
$a = 0.90$	0.67099	0.64743	0.53669	0.44185	0.36633	0.30601	0.28041	0.45947	0.38917
$a = 0.95$	0.75907	0.75228	0.64970	0.55336	0.47209	0.40396	0.37410	0.56565	0.49395
$a = 0.99$	0.85221	0.86614	0.77827	0.68497	0.60058	0.52570	0.49164	0.69000	0.61996
$a = 1.00$	0.88059	0.90132	0.81902	0.72753	0.64278	0.56617	0.53092	0.73008	0.66114
$b = 4.00 \quad \mu_0 = 0.7$									
FIRST ORDER	0.27821	0.21335	0.13391	0.08989	0.06348	0.04666	0.04050	0.11063	0.07621
SECOND ORDER	0.06380	0.10630	0.10741	0.08971	0.07180	0.05698	0.05081	0.08533	0.07536
THIRD ORDER	0.04524	0.06524	0.07782	0.07430	0.06559	0.05603	0.05147	0.06730	0.06520
SUMS									
$a = 0.20$	0.05862	0.04753	0.03181	0.02227	0.01620	0.01216	0.01064	0.02618	0.01888
$a = 0.40$	0.12567	0.10826	0.07791	0.05733	0.04325	0.03335	0.02951	0.06427	0.04882
$a = 0.60$	0.20820	0.19186	0.15029	0.11752	0.09289	0.07432	0.06678	0.12550	0.10124
$a = 0.80$	0.32662	0.32569	0.28357	0.24010	0.20224	0.17044	0.15661	0.24407	0.21199
$a = 0.90$	0.42132	0.44060	0.41046	0.36633	0.32207	0.28117	0.26235	0.36329	0.33032
$a = 0.95$	0.49130	0.52813	0.51234	0.47209	0.42596	0.37982	0.35763	0.46242	0.43174
$a = 0.99$	0.57022	0.62845	0.63287	0.60058	0.55489	0.50436	0.47880	0.58249	0.55685
$a = 1.00$	0.59518	0.66043	0.67191	0.64278	0.59772	0.54610	0.51956	0.62190	0.59828

TABLE 35 (continued)  
 $g = 0.50, b = 4$ , Transmission

VECTOR	$\mu = 0.0$	$\mu = 0.1$	$\mu = 0.3$	$\mu = 0.5$	$\mu = 0.7$	$\mu = 0.9$	$\mu = 1.0$	AVERAGE N	FLUX U
$b = 4.00$									
ZERO ORDER	$\mu_0 = 0.0$	PEAK	0.0	0.0	0.0	0.0	0.0	0.00000	0.00000
FIRST ORDER	0.00000	0.00000	0.00000	0.00024	0.00123	0.00254	0.00309	0.00081	0.00133
SECOND ORDER	0.00027	0.00036	0.00070	0.00181	0.00446	0.00809	0.00990	0.00311	0.00471
THIRD ORDER	0.00116	0.00151	0.00264	0.00501	0.00900	0.01384	0.01623	0.00643	0.00901
SUMS	$a = 0.20$	0.00003	0.00003	0.00006	0.00018	0.00052	0.00098	0.00118	0.00036
	$a = 0.40$	0.00026	0.00034	0.00057	0.00114	0.00239	0.00398	0.00472	0.00170
	$a = 0.60$	0.00165	0.00216	0.00334	0.00544	0.00903	0.01328	0.01526	0.00667
	$a = 0.80$	0.00979	0.01276	0.01850	0.02602	0.03602	0.04656	0.05129	0.02800
	$a = 0.90$	0.02571	0.03355	0.04711	0.06223	0.07950	0.09612	0.10321	0.06368
	$a = 0.95$	0.04387	0.05729	0.07919	0.10150	0.12481	0.14582	0.15442	0.10162
	$a = 0.99$	0.07033	0.09189	0.12544	0.15706	0.18742	0.21296	0.22287	0.15472
	$a = 1.00$	0.07984	0.10433	0.14199	0.17675	0.20936	0.23621	0.24646	0.17344
$b = 4.00$									
ZERO ORDER	$\mu_0 = 0.0$	0.0	PEAK	0.0	0.0	0.0	0.0	0.00000	0.00000
FIRST ORDER	0.00000	0.00000	0.00003	0.00060	0.00248	0.00456	0.00530	0.00154	0.00249
SECOND ORDER	0.00053	0.00070	0.00139	0.00347	0.00776	0.01315	0.01570	0.00533	0.00793
THIRD ORDER	0.00202	0.00264	0.00459	0.00841	0.01428	0.02086	0.02398	0.01020	0.01402
SUMS	$a = 0.20$	0.00005	0.00006	0.00012	0.00035	0.00096	0.00166	0.00194	0.00064
	$a = 0.40$	0.00044	0.00057	0.00097	0.00198	0.00403	0.00636	0.00736	0.00280
	$a = 0.60$	0.00256	0.00334	0.00521	0.00858	0.01408	0.02007	0.02268	0.01029
	$a = 0.80$	0.01418	0.01850	0.02689	0.03800	0.05235	0.06661	0.07264	0.04049
	$a = 0.90$	0.03609	0.04711	0.06625	0.08772	0.11177	0.13378	0.14269	0.08927
	$a = 0.95$	0.06062	0.07919	0.10957	0.14069	0.17267	0.20020	0.21090	0.14030
	$a = 0.99$	0.09599	0.12544	0.17138	0.21485	0.25602	0.28921	0.30144	0.21104
	$a = 1.00$	0.10863	0.14199	0.19338	0.24100	0.28509	0.31992	0.33253	0.23586
$b = 4.00$									
ZERO ORDER	$\mu_0 = 0.0$	0.0	0.0	PEAK	0.0	0.0	0.0	0.00034	0.00034
FIRST ORDER	0.00017	0.00024	0.00060	0.00220	0.00596	0.00947	0.01038	0.00370	0.00565
SECOND ORDER	0.00136	0.00181	0.00347	0.00736	0.01403	0.02176	0.02534	0.00974	0.01392
THIRD ORDER	0.00382	0.00501	0.00841	0.01421	0.02201	0.03011	0.03382	0.01599	0.02127
SUMS	$a = 0.20$	0.00013	0.00018	0.00035	0.00089	0.00198	0.00307	0.00343	0.00164
	$a = 0.40$	0.00086	0.00114	0.00198	0.00388	0.00721	0.01061	0.01188	0.00531
	$a = 0.60$	0.00415	0.00544	0.00858	0.01401	0.02212	0.03023	0.03343	0.01644
	$a = 0.80$	0.01991	0.02602	0.03800	0.05363	0.07285	0.09075	0.09780	0.05659
	$a = 0.90$	0.04762	0.06223	0.08772	0.11611	0.14681	0.17343	0.18353	0.11749
	$a = 0.95$	0.07765	0.10150	0.14069	0.18062	0.22048	0.25316	0.26508	0.17938
	$a = 0.99$	0.12012	0.15706	0.21485	0.26933	0.31971	0.35852	0.37193	0.26376
	$a = 1.00$	0.13517	0.17675	0.24100	0.30034	0.35404	0.39461	0.40838	0.29313
$b = 4.00$									
ZERO ORDER	$\mu_0 = 0.0$	0.0	0.0	0.0	PEAK	0.0	0.0	0.00236	0.00330
FIRST ORDER	0.00092	0.00123	0.00248	0.00596	0.01342	0.02132	0.02301	0.00889	0.01307
SECOND ORDER	0.00339	0.00446	0.00776	0.01403	0.02359	0.03468	0.04005	0.01697	0.02330
THIRD ORDER	0.00690	0.00900	0.01428	0.02201	0.03140	0.04072	0.04496	0.02352	0.03019
SUMS	$a = 0.20$	0.00040	0.00052	0.00096	0.00198	0.00395	0.00606	0.00665	0.00506
	$a = 0.40$	0.00182	0.00239	0.00403	0.00721	0.01261	0.01837	0.02027	0.01129
	$a = 0.60$	0.00691	0.00903	0.01408	0.02212	0.03390	0.04605	0.05041	0.02742
	$a = 0.80$	0.02759	0.03602	0.05235	0.07285	0.09780	0.12158	0.13037	0.07846
	$a = 0.90$	0.06087	0.07950	0.11177	0.14681	0.18447	0.21777	0.22976	0.15026
	$a = 0.95$	0.09552	0.12481	0.17267	0.22048	0.26800	0.30766	0.32146	0.22075
	$a = 0.99$	0.14339	0.18742	0.25602	0.31971	0.37839	0.42434	0.43955	0.31495
	$a = 1.00$	0.16015	0.20936	0.28509	0.35404	0.41622	0.46397	0.47950	0.34742

TABLE 35 (continued)  
 $g = 0.50, b = 4$ , Reflection

VECTOR	$\mu = 0.0$	$\mu = 0.1$	$\mu = 0.3$	$\mu = 0.5$	$\mu = 0.7$	$\mu = 0.9$	$\mu = 1.0$	AVERAGE N	FLUX U
<b>b = 4.00</b>									
	$\mu_0 = 0.9$								
FIRST ORDER	0.16838	0.13411	0.08969	0.06336	0.04666	0.03551	0.03130	0.07446	0.05408
SECOND ORDER	0.04226	0.07309	0.07864	0.06870	0.05698	0.04660	0.04211	0.06401	0.05862
THIRD ORDER	0.03341	0.04870	0.06136	0.06127	0.05603	0.04924	0.04580	0.05495	0.05490
SUMS									
$a = 0.20$	0.03569	0.03021	0.02167	0.01601	0.01216	0.00945	0.00840	0.01798	0.01369
$a = 0.40$	0.07731	0.06989	0.05425	0.04227	0.03335	0.02668	0.02397	0.04537	0.03644
$a = 0.60$	0.13068	0.12702	0.10799	0.08971	0.07432	0.06174	0.05637	0.09210	0.07858
$a = 0.80$	0.21395	0.22590	0.21434	0.19308	0.17044	0.14897	0.13900	0.19007	0.17411
$a = 0.90$	0.28764	0.31853	0.32298	0.30601	0.28117	0.25383	0.24013	0.29559	0.28213
$a = 0.95$	0.34597	0.39336	0.41419	0.40396	0.37982	0.34926	0.33300	0.38683	0.37764
$a = 0.99$	0.41499	0.48270	0.52539	0.52570	0.50436	0.47129	0.45240	0.50016	0.49776
$a = 1.00$	0.43741	0.51182	0.56201	0.56617	0.54610	0.51244	0.49278	0.53784	0.53794
<b>b = 4.00</b>									
	$\mu_0 = 1.0$								
FIRST ORDER	0.13416	0.10867	0.07474	0.05399	0.04050	0.03130	0.02777	0.06227	0.04627
SECOND ORDER	0.03509	0.06138	0.06772	0.06030	0.05081	0.04211	0.03828	0.05580	0.05186
THIRD ORDER	0.02893	0.04231	0.05449	0.05544	0.05147	0.04580	0.04283	0.04959	0.05016
SUMS									
$a = 0.20$	0.02852	0.02459	0.01818	0.01375	0.01064	0.00840	0.00751	0.01517	0.01182
$a = 0.40$	0.06210	0.05730	0.04594	0.03668	0.02951	0.02397	0.02169	0.03872	0.03182
$a = 0.60$	0.10601	0.10536	0.09270	0.07901	0.06678	0.05637	0.05182	0.07994	0.06979
$a = 0.80$	0.17730	0.19156	0.18824	0.17398	0.15661	0.13900	0.13053	0.16940	0.15847
$a = 0.90$	0.24333	0.27552	0.28890	0.28041	0.26235	0.24013	0.22846	0.26857	0.26118
$a = 0.95$	0.29712	0.34504	0.37501	0.37410	0.35763	0.33300	0.31913	0.35572	0.35317
$a = 0.99$	0.36198	0.42944	0.48133	0.49164	0.47880	0.45240	0.43624	0.46507	0.46980
$a = 1.00$	0.38327	0.45720	0.51659	0.53092	0.51956	0.49278	0.47593	0.50162	0.50897
<b>b = 4.0</b> <b>NARROW SURFACE LAYER AT TOP</b>									
FIRST ORDER	INFINITE	0.65260	0.30417	0.17520	0.11063	0.07446	0.06227	0.28768	0.15244
SECOND ORDER	0.14384	0.20387	0.15677	0.11540	0.08533	0.06401	0.05580	0.12437	0.09615
THIRD ORDER	0.06925	0.09323	0.09385	0.08123	0.06730	0.05495	0.04959	0.07746	0.06957
SUMS									
$a = 0.20$	INFINITE	0.13952	0.06797	0.04042	0.02618	0.01798	0.01517	0.06324	0.03499
$a = 0.40$	INFINITE	0.30159	0.15504	0.09598	0.06427	0.04537	0.03872	0.14199	0.08284
$a = 0.60$	INFINITE	0.49767	0.27407	0.17906	0.12550	0.09210	0.07994	0.24777	0.15473
$a = 0.80$	INFINITE	0.75643	0.45932	0.32501	0.24407	0.19007	0.16940	0.41328	0.28402
$a = 0.90$	INFINITE	0.93717	0.61162	0.45947	0.36329	0.29559	0.26857	0.55355	0.40726
$a = 0.95$	INFINITE	1.05686	0.72378	0.56565	0.46242	0.38683	0.35572	0.65999	0.50710
$a = 0.99$	INFINITE	1.18082	0.84905	0.69000	0.58249	0.50016	0.46507	0.78186	0.62620
$a = 1.00$	INFINITE	1.21811	0.88840	0.73008	0.62190	0.53784	0.50162	0.82070	0.66499
<b>b = 4.0</b> <b>LAMBERT SURFACE ON TOP</b>									
FIRST ORDER	0.50000	0.32140	0.17984	0.11306	0.07621	0.05408	0.04627	0.15244	0.09636
SECOND ORDER	0.08995	0.13381	0.12181	0.09695	0.07536	0.05862	0.05186	0.09615	0.08109
THIRD ORDER	0.05191	0.07317	0.08189	0.07546	0.06520	0.05490	0.05016	0.06957	0.06568
SUMS									
$a = 0.20$	0.10408	0.07031	0.04161	0.02721	0.01888	0.01369	0.01182	0.03499	0.02314
$a = 0.40$	0.21904	0.15643	0.09885	0.06779	0.04882	0.03644	0.03182	0.08284	0.05778
$a = 0.60$	0.35228	0.26849	0.18383	0.13395	0.10124	0.07858	0.06979	0.15473	0.11511
$a = 0.80$	0.52433	0.43393	0.33068	0.26194	0.21199	0.17411	0.15847	0.28402	0.22984
$a = 0.90$	0.64644	0.56514	0.46356	0.38917	0.33032	0.28213	0.26118	0.40726	0.34824
$a = 0.95$	0.72978	0.66032	0.56737	0.49395	0.43174	0.37764	0.35317	0.50710	0.44813
$a = 0.99$	0.81875	0.76588	0.68807	0.61996	0.55685	0.49776	0.46980	0.62620	0.57026
$a = 1.00$	0.84605	0.79894	0.72683	0.66114	0.59828	0.53794	0.50897	0.66499	0.61053

TABLE 35 (continued)  
 $g = 0.50, b = 4$ , Transmission

VECTOR	$\mu = 0.0$	$\mu = 0.1$	$\mu = 0.3$	$\mu = 0.5$	$\mu = 0.7$	$\mu = 0.9$	$\mu = 1.0$	AVERAGE N	FLUX U
<b>b = 4.00</b>									
	$\mu_0 = 0.9$								
ZERO ORDER	0.0	0.0	0.0	0.0	0.0	PEAK	0.0	0.00652	0.01174
FIRST ORDER	0.00198	0.00254	0.00456	0.00947	0.02132	0.04524	0.05951	0.01685	0.02546
SECOND ORDER	0.00628	0.00809	0.01315	0.02176	0.03468	0.05134	0.06079	0.02594	0.03496
THIRD ORDER	0.01072	0.01384	0.02086	0.03011	0.04072	0.05123	0.05615	0.03138	0.03924
SUMS									
$\alpha = 0.20$	0.00076	0.00098	0.00166	0.00307	0.00606	0.01160	0.01488	0.01125	0.01862
$\alpha = 0.40$	0.00309	0.00398	0.00636	0.01061	0.01837	0.03149	0.03910	0.02080	0.03164
$\alpha = 0.60$	0.01027	0.01328	0.02007	0.03023	0.04605	0.06992	0.08338	0.04260	0.05948
$\alpha = 0.80$	0.03587	0.04656	0.06661	0.09075	0.12158	0.16165	0.18309	0.10412	0.13317
$\alpha = 0.90$	0.07387	0.09612	0.13378	0.17343	0.21777	0.26943	0.29581	0.18466	0.22588
$\alpha = 0.95$	0.11193	0.14582	0.20020	0.25316	0.30766	0.36659	0.39556	0.26107	0.31221
$\alpha = 0.99$	0.16328	0.21296	0.28921	0.35852	0.42434	0.49015	0.52110	0.36115	0.42408
$\alpha = 1.00$	0.18106	0.23621	0.31992	0.39461	0.46397	0.53171	0.56311	0.39531	0.46206
<b>b = 4.00</b>									
	$\mu_0 = 1.0$								
ZERO ORDER	0.0	0.0	0.0	0.0	0.0	0.0	PEAK	0.00916	0.01832
FIRST ORDER	0.00246	0.00309	0.00530	0.01038	0.02301	0.05951	0.10989	0.02137	0.03324
SECOND ORDER	0.00776	0.00990	0.01570	0.02534	0.04005	0.06079	0.07412	0.03056	0.04115
THIRD ORDER	0.01264	0.01623	0.02398	0.03382	0.04496	0.05615	0.06155	0.03506	0.04343
SUMS									
$\alpha = 0.20$	0.00093	0.00118	0.00194	0.00343	0.00665	0.01488	0.02554	0.01501	0.02704
$\alpha = 0.40$	0.00370	0.00472	0.00736	0.01188	0.02027	0.03910	0.06180	0.02630	0.04267
$\alpha = 0.60$	0.01188	0.01526	0.02268	0.03343	0.05041	0.08338	0.11996	0.05092	0.07435
$\alpha = 0.80$	0.03966	0.05129	0.07264	0.09780	0.13037	0.18309	0.23597	0.11711	0.15388
$\alpha = 0.90$	0.07954	0.10321	0.14269	0.18353	0.22976	0.29581	0.35781	0.20103	0.25053
$\alpha = 0.95$	0.11878	0.15442	0.21090	0.26508	0.32146	0.39556	0.46225	0.27939	0.33905
$\alpha = 0.99$	0.17117	0.22287	0.30144	0.37193	0.43955	0.52110	0.59143	0.38105	0.45265
$\alpha = 1.00$	0.18921	0.24646	0.33253	0.40838	0.47950	0.56311	0.63431	0.41558	0.49103
<b>b = 4.0 NARROW SURFACE LAYER AT TOP</b>									
ZERO ORDER	0.0	0.00000	0.00000	0.00034	0.00236	0.00652	0.00916	0.00189	0.00320
FIRST ORDER	0.00062	0.00081	0.00154	0.00370	0.00889	0.01685	0.02137	0.00643	0.00973
SECOND ORDER	0.00239	0.00311	0.00533	0.00974	0.01697	0.02594	0.03056	0.01229	0.01709
THIRD ORDER	0.00495	0.00643	0.01020	0.01599	0.02352	0.03138	0.03506	0.01754	0.02278
SUMS									
$\alpha = 0.20$	0.00028	0.00036	0.00064	0.00164	0.00506	0.01125	0.01501	0.00385	0.00606
$\alpha = 0.40$	0.00130	0.00170	0.00280	0.00531	0.01129	0.02080	0.02630	0.00847	0.01239
$\alpha = 0.60$	0.00513	0.00667	0.01029	0.01644	0.02742	0.04260	0.05092	0.02080	0.02824
$\alpha = 0.80$	0.02149	0.02800	0.04049	0.05659	0.07846	0.10412	0.11711	0.06163	0.07749
$\alpha = 0.90$	0.04881	0.06368	0.08927	0.11749	0.15026	0.18466	0.20103	0.12108	0.14634
$\alpha = 0.95$	0.07784	0.10162	0.14030	0.17938	0.22075	0.26107	0.27939	0.18049	0.21382
$\alpha = 0.99$	0.11845	0.15472	0.21104	0.26376	0.31495	0.36115	0.38105	0.26079	0.30395
$\alpha = 1.00$	0.13276	0.17344	0.23586	0.29313	0.34742	0.39531	0.41558	0.28862	0.33501
<b>b = 4.0 LAMBERT SURFACE ON TOP</b>									
ZERO ORDER	0.0	0.00000	0.00000	0.00034	0.00330	0.01174	0.01832	0.00320	0.00552
FIRST ORDER	0.00103	0.00133	0.00249	0.00565	0.01307	0.02546	0.03324	0.00973	0.01469
SECOND ORDER	0.00363	0.00471	0.00793	0.01392	0.02330	0.03496	0.04115	0.01705	0.02336
THIRD ORDER	0.00695	0.00901	0.01402	0.02127	0.03019	0.03924	0.04343	0.02278	0.02913
SUMS									
$\alpha = 0.20$	0.00043	0.00055	0.00097	0.00225	0.00715	0.01862	0.02704	0.00606	0.00969
$\alpha = 0.40$	0.00189	0.00245	0.00401	0.00731	0.01558	0.03164	0.04267	0.01239	0.01832
$\alpha = 0.60$	0.00692	0.00899	0.01379	0.02165	0.03611	0.05948	0.07435	0.02824	0.03862
$\alpha = 0.80$	0.02694	0.03507	0.05059	0.07020	0.09733	0.13317	0.15388	0.07749	0.09784
$\alpha = 0.90$	0.05889	0.07678	0.10746	0.14086	0.18019	0.22588	0.25053	0.14634	0.17738
$\alpha = 0.95$	0.09209	0.12016	0.16569	0.21124	0.26003	0.31221	0.33905	0.21382	0.25384
$\alpha = 0.99$	0.13791	0.18008	0.24538	0.30605	0.36555	0.42408	0.45265	0.30395	0.35485
$\alpha = 1.00$	0.15395	0.20106	0.27317	0.33886	0.40172	0.46206	0.49103	0.33501	0.38947

TABLE 35 (continued)  
 $g = 0.75, b = 1$ , Reflection

VECTOR	$\mu = 0.0$	$\mu = 0.1$	$\mu = 0.3$	$\mu = 0.5$	$\mu = 0.7$	$\mu = 0.9$	$\mu = 1.0$	AVERAGE N	FLUX U
<b>b = 1.00</b>									
	$\mu_0 = 0.1$								
FIRST ORDER	5.87169	2.23714	0.58248	0.21991	0.10429	0.05742	0.04437	0.72518	0.24068
SECOND ORDER	0.74008	0.80818	0.32643	0.14362	0.07216	0.04060	0.03153	0.27749	0.13066
THIRD ORDER	0.24636	0.32213	0.17718	0.09012	0.04885	0.02862	0.02250	0.13075	0.07464
SUMS									
$a = 0.20$	1.20610	0.48260	0.13116	0.05056	0.02420	0.01338	0.01035	0.15731	0.05405
$a = 0.40$	2.48622	1.04962	0.30010	0.11880	0.05761	0.03204	0.02483	0.34528	0.12359
$a = 0.60$	3.86246	1.73141	0.52681	0.21607	0.10677	0.05994	0.04656	0.57807	0.21761
$a = 0.80$	5.37253	2.58140	0.85106	0.36649	0.18608	0.10592	0.08259	0.88332	0.35487
$a = 0.90$	6.19887	3.10000	1.07476	0.47761	0.24681	0.14175	0.11081	1.08033	0.45192
$a = 0.95$	6.63626	3.39207	1.21018	0.54752	0.28579	0.16497	0.12913	1.19551	0.51164
$a = 0.99$	7.00045	3.64536	1.33334	0.61271	0.32259	0.18703	0.14656	1.29808	0.56658
$a = 1.00$	7.09374	3.71179	1.36653	0.63053	0.33272	0.19311	0.15137	1.32540	0.58148
<b>b = 1.00</b>									
	$\mu_0 = 0.3$								
FIRST ORDER	1.07503	0.58248	0.22144	0.10584	0.05870	0.03605	0.02908	0.21173	0.09736
SECOND ORDER	0.19157	0.32643	0.19496	0.10460	0.05939	0.03620	0.02895	0.14045	0.08555
THIRD ORDER	0.10754	0.17718	0.14004	0.08443	0.05013	0.03089	0.02468	0.09445	0.06528
SUMS									
$a = 0.20$	0.22365	0.13116	0.05338	0.02614	0.01459	0.00895	0.00721	0.04884	0.02350
$a = 0.40$	0.46980	0.30010	0.13202	0.06665	0.03754	0.02303	0.01852	0.11542	0.05845
$a = 0.60$	0.75100	0.52681	0.25352	0.13289	0.07583	0.04660	0.03741	0.21158	0.11348
$a = 0.80$	1.09272	0.85106	0.45472	0.24946	0.14482	0.08929	0.07160	0.36220	0.20714
$a = 0.90$	1.30257	1.07476	0.60910	0.34291	0.20112	0.12428	0.09961	0.47410	0.28071
$a = 0.95$	1.42262	1.21018	0.70766	0.40390	0.23818	0.14738	0.11809	0.54456	0.32828
$a = 0.99$	1.52825	1.33334	0.80019	0.46191	0.27363	0.16950	0.13580	0.61024	0.37331
$a = 1.00$	1.55622	1.36653	0.82557	0.47794	0.28345	0.17564	0.14070	0.62818	0.38571
<b>b = 1.00</b>									
	$\mu_0 = 0.5$								
FIRST ORDER	0.34316	0.21991	0.10584	0.05868	0.03596	0.02373	0.01970	0.09137	0.05076
SECOND ORDER	0.07517	0.14362	0.10460	0.06327	0.03893	0.02512	0.02055	0.07320	0.05031
THIRD ORDER	0.05136	0.09012	0.08443	0.05577	0.03503	0.02242	0.01817	0.05650	0.04247
SUMS									
$a = 0.20$	0.07212	0.05056	0.02614	0.01479	0.00908	0.00596	0.00493	0.02173	0.01256
$a = 0.40$	0.15388	0.11880	0.06665	0.03869	0.02384	0.01557	0.01284	0.05334	0.03222
$a = 0.60$	0.25217	0.21607	0.13289	0.07954	0.04927	0.03203	0.02629	0.10245	0.06485
$a = 0.80$	0.38218	0.36649	0.24946	0.15461	0.09647	0.06239	0.05097	0.18569	0.12342
$a = 0.90$	0.46938	0.47761	0.34291	0.21649	0.13563	0.08752	0.07131	0.25116	0.17104
$a = 0.95$	0.52206	0.54752	0.40390	0.25739	0.16160	0.10415	0.08476	0.29356	0.20233
$a = 0.99$	0.57011	0.61271	0.46191	0.29657	0.18653	0.12009	0.09763	0.33375	0.23221
$a = 1.00$	0.58311	0.63053	0.47794	0.30743	0.19344	0.12452	0.10120	0.34482	0.24048
<b>b = 1.00</b>									
	$\mu_0 = 0.7$								
FIRST ORDER	0.14589	0.10429	0.05870	0.03596	0.02361	0.01639	0.01389	0.04860	0.03043
SECOND ORDER	0.03715	0.07216	0.05939	0.03893	0.02533	0.01703	0.01416	0.04162	0.03075
THIRD ORDER	0.02754	0.04885	0.05013	0.03503	0.02285	0.01504	0.01233	0.03384	0.02663
SUMS									
$a = 0.20$	0.03092	0.02420	0.01459	0.00908	0.00595	0.00410	0.00346	0.01170	0.00757
$a = 0.40$	0.06682	0.05761	0.03754	0.02384	0.01560	0.01066	0.00895	0.02918	0.01953
$a = 0.60$	0.11164	0.10677	0.07583	0.04927	0.03222	0.02180	0.01819	0.05714	0.03965
$a = 0.80$	0.17445	0.18608	0.14482	0.09647	0.06306	0.04220	0.03497	0.10602	0.07622
$a = 0.90$	0.21890	0.24681	0.20112	0.13563	0.08863	0.05897	0.04867	0.14530	0.10621
$a = 0.95$	0.24658	0.28579	0.23818	0.16160	0.10557	0.07004	0.05769	0.17101	0.12600
$a = 0.99$	0.27232	0.32259	0.27363	0.18653	0.12182	0.08062	0.06630	0.19553	0.14494
$a = 1.00$	0.27936	0.33272	0.28345	0.19344	0.12633	0.08355	0.06868	0.20232	0.15019

TABLE 35 (continued)

 $g = 0.75, b = 1$ , Transmission

VECTOR	$\mu = 0.0$	$\mu = 0.1$	$\mu = 0.3$	$\mu = 0.5$	$\mu = 0.7$	$\mu = 0.9$	$\mu = 1.0$	AVERAGE N	FLUX U
$b = 1.00$									
ZERO ORDER	$\mu_0 = 0.0$	PEAK	0.0	0.0	0.0	0.0	0.0	0.00023	0.00005
FIRST ORDER	0.00027	0.00299	0.08038	0.07818	0.05127	0.03285	0.02663	0.04926	0.05138
SECOND ORDER	0.01990	0.04024	0.13266	0.13795	0.09848	0.06392	0.05127	0.09452	0.09545
THIRD ORDER	0.04183	0.07221	0.13650	0.12935	0.09394	0.06228	0.05018	0.09842	0.09356
SUMS $a = 0.20$	0.00128	0.00293	0.02267	0.02236	0.01506	0.00970	0.00784	0.01479	0.01501
$a = 0.40$	0.00780	0.01512	0.06590	0.06477	0.04449	0.02881	0.02324	0.04402	0.04419
$a = 0.60$	0.02817	0.05014	0.14874	0.14357	0.09977	0.06491	0.05232	0.10145	0.09957
$a = 0.80$	0.08407	0.14119	0.31209	0.29169	0.20361	0.13284	0.10703	0.21573	0.20556
$a = 0.90$	0.14090	0.23114	0.45042	0.41213	0.28748	0.18766	0.15116	0.31261	0.29269
$a = 0.95$	0.18194	0.29530	0.54242	0.49043	0.34172	0.22306	0.17965	0.37698	0.34963
$a = 0.99$	0.22323	0.35940	0.63070	0.56447	0.39280	0.25637	0.20646	0.43869	0.40364
$a = 1.00$	0.23497	0.37755	0.65518	0.58483	0.40682	0.26550	0.21380	0.45578	0.41852
$b = 1.00$									
ZERO ORDER	$\mu_0 = 0.0$	0.0	PEAK	0.0	0.0	0.0	0.0	0.05946	0.03567
FIRST ORDER	0.03835	0.08038	0.27255	0.23059	0.11536	0.05936	0.04424	0.15108	0.13529
SECOND ORDER	0.07576	0.13266	0.24418	0.22650	0.15172	0.09082	0.06986	0.16828	0.15452
THIRD ORDER	0.08586	0.13650	0.18517	0.15654	0.10925	0.07034	0.05580	0.13055	0.11439
SUMS $a = 0.20$	0.01152	0.02267	0.06598	0.05660	0.03013	0.01614	0.01215	0.09760	0.06996
$a = 0.40$	0.03549	0.06590	0.16410	0.14165	0.07954	0.04416	0.03355	0.15806	0.12420
$a = 0.60$	0.08444	0.14874	0.31657	0.27261	0.16010	0.09170	0.07031	0.25634	0.21132
$a = 0.80$	0.18574	0.31209	0.56769	0.48287	0.29410	0.17307	0.13388	0.42315	0.35621
$a = 0.90$	0.27385	0.45042	0.75762	0.63777	0.39432	0.23488	0.18246	0.55114	0.46529
$a = 0.95$	0.33315	0.54242	0.87743	0.73395	0.45682	0.27367	0.21303	0.63230	0.53370
$a = 0.99$	0.39042	0.63070	0.98890	0.82253	0.51449	0.30957	0.24137	0.70801	0.59706
$a = 1.00$	0.40635	0.65518	1.01930	0.84654	0.53013	0.31933	0.24908	0.72868	0.61429
$b = 1.00$									
ZERO ORDER	$\mu_0 = 0.0$	0.0	0.0	PEAK	0.0	0.0	0.0	0.13534	0.13534
FIRST ORDER	0.04644	0.07818	0.23059	0.41114	0.25154	0.10388	0.06946	0.21412	0.21992
SECOND ORDER	0.08882	0.13795	0.22650	0.24359	0.18840	0.11450	0.08568	0.18109	0.17456
THIRD ORDER	0.08802	0.12935	0.15654	0.13510	0.10010	0.06715	0.05359	0.11667	0.10263
SUMS $a = 0.20$	0.01366	0.02236	0.05660	0.09318	0.05873	0.02595	0.01779	0.18646	0.18722
$a = 0.40$	0.04062	0.06477	0.14165	0.21442	0.13876	0.06522	0.04577	0.25966	0.25959
$a = 0.60$	0.09216	0.14357	0.27261	0.37747	0.24975	0.12421	0.08906	0.36754	0.36288
$a = 0.80$	0.19111	0.29169	0.48287	0.60730	0.40871	0.21404	0.15660	0.53372	0.51606
$a = 0.90$	0.27244	0.41213	0.63777	0.76179	0.51581	0.27675	0.20445	0.65267	0.62234
$a = 0.95$	0.32553	0.49043	0.73395	0.85339	0.57919	0.31442	0.23341	0.72548	0.68629
$a = 0.99$	0.37585	0.56447	0.82253	0.93544	0.63582	0.34837	0.25960	0.79193	0.74403
$a = 1.00$	0.38969	0.58483	0.84654	0.95734	0.65092	0.35746	0.26663	0.80986	0.75952
$b = 1.00$									
ZERO ORDER	$\mu_0 = 0.0$	0.0	0.0	0.0	PEAK	0.0	0.0	0.17118	0.23965
FIRST ORDER	0.03496	0.05127	0.11536	0.25154	0.45325	0.22569	0.12742	0.21746	0.27165
SECOND ORDER	0.06819	0.09848	0.15172	0.18840	0.19927	0.15252	0.11620	0.15701	0.16947
THIRD ORDER	0.06709	0.09394	0.10925	0.10010	0.08407	0.06452	0.05403	0.08967	0.08324
SUMS $a = 0.20$	0.01034	0.01506	0.03013	0.05873	0.09936	0.05180	0.03060	0.22175	0.30149
$a = 0.40$	0.03078	0.04449	0.07954	0.13876	0.21969	0.11959	0.07367	0.29058	0.38201
$a = 0.60$	0.06955	0.09977	0.16010	0.24975	0.36839	0.20877	0.13369	0.38673	0.48897
$a = 0.80$	0.14280	0.20361	0.29410	0.40871	0.55772	0.32793	0.21777	0.52659	0.63580
$a = 0.90$	0.20205	0.28748	0.39432	0.51581	0.67425	0.40325	0.27251	0.62235	0.73165
$a = 0.95$	0.24033	0.34172	0.45682	0.57919	0.73994	0.44615	0.30411	0.67957	0.78743
$a = 0.99$	0.27637	0.39280	0.51449	0.63582	0.79685	0.48349	0.33183	0.73102	0.83674
$a = 1.00$	0.28624	0.40682	0.53013	0.65092	0.81176	0.49329	0.33914	0.74478	0.84981



TABLE 35 (continued)

 $g = 0.75, b = 1$ , Reflection

VECTOR	$\mu = 0.0$	$\mu = 0.1$	$\mu = 0.3$	$\mu = 0.5$	$\mu = 0.7$	$\mu = 0.9$	$\mu = 1.0$	AVERAGE N	FLUX U
$b = 1.00$ $\mu_0 = 0.9$									
FIRST ORDER	0.07457	0.05742	0.03605	0.02373	0.01639	0.01182	0.01018	0.02939	0.01996
SECOND ORDER	0.02124	0.04060	0.03620	0.02512	0.01703	0.01181	0.00995	0.02564	0.01986
THIRD ORDER	0.01628	0.02862	0.03089	0.02242	0.01504	0.01011	0.00836	0.02111	0.01710
SUMS $a = 0.20$	0.01592	0.01338	0.00895	0.00596	0.00410	0.00293	0.00251	0.00710	0.00495
$a = 0.40$	0.03473	0.03204	0.02303	0.01557	0.01066	0.00754	0.00642	0.01779	0.01273
$a = 0.60$	0.05884	0.05994	0.04660	0.03203	0.02180	0.01522	0.01287	0.03502	0.02574
$a = 0.80$	0.09384	0.10592	0.08929	0.06239	0.04220	0.02902	0.02433	0.06537	0.04929
$a = 0.90$	0.11934	0.14175	0.12428	0.08752	0.05897	0.04022	0.03356	0.08990	0.06855
$a = 0.95$	0.13547	0.16497	0.14738	0.10415	0.07004	0.04756	0.03958	0.10599	0.08123
$a = 0.99$	0.15061	0.18703	0.16950	0.12009	0.08062	0.05456	0.04531	0.12136	0.09336
$a = 1.00$	0.15476	0.19311	0.17564	0.12452	0.08355	0.05649	0.04689	0.12562	0.09672
$b = 1.00$ $\mu_0 = 1.0$									
FIRST ORDER	0.05600	0.04437	0.02908	0.01970	0.01389	0.01018	0.00882	0.02365	0.01657
SECOND ORDER	0.01669	0.03153	0.02895	0.02055	0.01416	0.00995	0.00843	0.02064	0.01628
THIRD ORDER	0.01289	0.02250	0.02468	0.01817	0.01233	0.00836	0.00694	0.01698	0.01389
SUMS $a = 0.20$	0.01199	0.01035	0.00721	0.00493	0.00346	0.00251	0.00217	0.00572	0.00410
$a = 0.40$	0.02626	0.02483	0.01852	0.01284	0.00895	0.00642	0.00550	0.01431	0.01050
$a = 0.60$	0.04474	0.04656	0.03741	0.02629	0.01819	0.01287	0.01095	0.02817	0.02115
$a = 0.80$	0.07186	0.08259	0.07160	0.05097	0.03497	0.02433	0.02051	0.05256	0.04033
$a = 0.90$	0.09181	0.11081	0.09961	0.07131	0.04867	0.03356	0.02814	0.07226	0.05595
$a = 0.95$	0.10447	0.12913	0.11809	0.08476	0.05769	0.03958	0.03310	0.08518	0.06622
$a = 0.99$	0.11639	0.14656	0.13580	0.09763	0.06630	0.04531	0.03780	0.09751	0.07603
$a = 1.00$	0.11967	0.15137	0.14070	0.10120	0.06868	0.04689	0.03909	0.10093	0.07874
$b = 1.0$ NARROW SURFACE LAYER AT TOP									
FIRST ORDER	INFINITE	0.72518	0.21173	0.09137	0.04860	0.02939	0.02365	0.26648	0.09332
SECOND ORDER	0.13324	0.27749	0.14045	0.07320	0.04162	0.02564	0.02064	0.11164	0.06212
THIRD ORDER	0.09103	0.13075	0.09445	0.05650	0.03384	0.02111	0.01698	0.06616	0.04441
SUMS $a = 0.20$	INFINITE	0.15731	0.04884	0.02173	0.01170	0.00710	0.00572	0.05837	0.02156
$a = 0.40$	INFINITE	0.34528	0.11542	0.05334	0.02918	0.01779	0.01431	0.13019	0.05122
$a = 0.60$	INFINITE	0.57807	0.21158	0.10245	0.05714	0.03502	0.02817	0.22359	0.09482
$a = 0.80$	INFINITE	0.88332	0.36220	0.18569	0.10602	0.06537	0.05256	0.35555	0.16496
$a = 0.90$	INFINITE	1.08033	0.47410	0.25116	0.14530	0.08990	0.07226	0.44702	0.21831
$a = 0.95$	INFINITE	1.19551	0.54456	0.29356	0.17101	0.10599	0.08518	0.50278	0.25234
$a = 0.99$	INFINITE	1.29808	0.61024	0.33375	0.19553	0.12136	0.09751	0.55379	0.28432
$a = 1.00$	INFINITE	1.32540	0.62818	0.34482	0.20232	0.12562	0.10093	0.56759	0.29310
$b = 1.0$ LAMBERT SURFACE ON TOP									
FIRST ORDER	0.50000	0.24068	0.09736	0.05076	0.03043	0.01996	0.01657	0.09332	0.04594
SECOND ORDER	0.08210	0.13066	0.08555	0.05031	0.03075	0.01986	0.01628	0.06212	0.04074
THIRD ORDER	0.04534	0.07464	0.06528	0.04247	0.02663	0.01710	0.01389	0.04441	0.03266
SUMS $a = 0.20$	0.10370	0.05405	0.02350	0.01256	0.00757	0.00495	0.00410	0.02156	0.01112
$a = 0.40$	0.21707	0.12359	0.05845	0.03222	0.01953	0.01273	0.01050	0.05122	0.02784
$a = 0.60$	0.34573	0.21761	0.11348	0.06485	0.03965	0.02574	0.02115	0.09482	0.05462
$a = 0.80$	0.50169	0.35487	0.20714	0.12342	0.07622	0.04929	0.04033	0.16496	0.10119
$a = 0.90$	0.59785	0.45192	0.28071	0.17104	0.10621	0.06855	0.05595	0.21831	0.13836
$a = 0.95$	0.65317	0.51164	0.32828	0.20233	0.12600	0.08123	0.06622	0.25234	0.16258
$a = 0.99$	0.70208	0.56658	0.37331	0.23221	0.14494	0.09336	0.07603	0.28432	0.18561
$a = 1.00$	0.71507	0.58148	0.38571	0.24048	0.15019	0.09672	0.07874	0.29310	0.19197

TABLE 35 (continued)  
 $g = 0.75, b = 1$ , Transmission

VECTOR	$\mu = 0.0$	$\mu = 0.1$	$\mu = 0.3$	$\mu = 0.5$	$\mu = 0.7$	$\mu = 0.9$	$\mu = 1.0$	AVERAGE N	FLUX U
$b = 1.00$									
	$\mu_0 = 0.9$								
ZERO ORDER	0.0	0.0	0.0	0.0	0.0	PEAK	0.0	0.18288	0.32919
FIRST ORDER	0.02455	0.03285	0.05936	0.10388	0.22569	0.62841	0.43196	0.19714	0.29655
SECOND ORDER	0.04667	0.06392	0.09082	0.11450	0.15252	0.20946	0.21409	0.12571	0.15459
THIRD ORDER	0.04593	0.06228	0.07034	0.06715	0.06452	0.06411	0.06329	0.06532	0.06550
SUMS									
$a = 0.20$	0.00720	0.00970	0.01614	0.02595	0.05180	0.13461	0.09549	0.22792	0.39526
$a = 0.40$	0.02130	0.02881	0.04416	0.06522	0.11959	0.28958	0.21162	0.28708	0.47761
$a = 0.60$	0.04786	0.06491	0.09170	0.12421	0.20877	0.46971	0.35293	0.36667	0.58195
$a = 0.80$	0.09763	0.13284	0.17307	0.21404	0.32793	0.68200	0.52580	0.47777	0.71772
$a = 0.90$	0.13760	0.18766	0.23488	0.27675	0.40325	0.80359	0.62708	0.55136	0.80246
$a = 0.95$	0.16331	0.22306	0.27367	0.31442	0.44615	0.86918	0.68221	0.59454	0.85052
$a = 0.99$	0.18744	0.25637	0.30957	0.34837	0.48349	0.92430	0.72878	0.63292	0.89231
$a = 1.00$	0.19404	0.26550	0.31933	0.35746	0.49329	0.93848	0.74080	0.64312	0.90328
$b = 1.00$									
	$\mu_0 = 1.0$								
ZERO ORDER	0.0	0.0	0.0	0.0	0.0	0.0	PEAK	0.18394	0.36788
FIRST ORDER	0.02060	0.02663	0.04424	0.06946	0.12742	0.43196	2.57516	0.18446	0.30222
SECOND ORDER	0.03823	0.05127	0.06986	0.08568	0.11620	0.21409	0.38627	0.11118	0.14600
THIRD ORDER	0.03746	0.05018	0.05580	0.05359	0.05403	0.06329	0.07539	0.05537	0.05795
SUMS									
$a = 0.20$	0.00600	0.00784	0.01215	0.01779	0.03060	0.09549	0.53111	0.22577	0.43467
$a = 0.40$	0.01763	0.02324	0.03355	0.04577	0.07367	0.21162	1.09720	0.27991	0.51656
$a = 0.60$	0.03942	0.05232	0.07031	0.08906	0.13369	0.35293	1.70324	0.35162	0.61846
$a = 0.80$	0.08009	0.10703	0.13388	0.15660	0.21777	0.52580	2.35589	0.44999	0.74832
$a = 0.90$	0.11266	0.15116	0.18246	0.20445	0.27251	0.62708	2.70260	0.51424	0.82792
$a = 0.95$	0.13358	0.17965	0.21303	0.23341	0.30411	0.68221	2.88178	0.55165	0.87260
$a = 0.99$	0.15319	0.20646	0.24137	0.25960	0.33183	0.72878	3.02819	0.58473	0.91118
$a = 1.00$	0.15855	0.21380	0.24908	0.26663	0.33914	0.74080	3.06524	0.59350	0.92126
$b = 1.0$ NARROW SURFACE LAYER AT TOP									
ZERO ORDER	0.0	0.00023	0.05946	0.13534	0.17118	0.18288	0.18394	0.10969	0.14850
FIRST ORDER	0.02883	0.04926	0.15108	0.21412	0.21746	0.19714	0.18446	0.16546	0.19485
SECOND ORDER	0.05971	0.09452	0.16828	0.18109	0.15701	0.12571	0.11118	0.14469	0.14914
THIRD ORDER	0.06547	0.09842	0.13055	0.11667	0.08967	0.06532	0.05537	0.09944	0.09122
SUMS									
$a = 0.20$	0.00878	0.01479	0.09760	0.18646	0.22175	0.22792	0.22577	0.14948	0.19425
$a = 0.40$	0.02711	0.04402	0.15806	0.25966	0.29058	0.28708	0.27991	0.20745	0.25784
$a = 0.60$	0.06419	0.10145	0.25634	0.36754	0.38673	0.36667	0.35162	0.29491	0.34894
$a = 0.80$	0.13960	0.21573	0.42315	0.53372	0.52659	0.47777	0.44999	0.43373	0.48558
$a = 0.90$	0.20427	0.31261	0.55114	0.65267	0.62235	0.55136	0.51424	0.53565	0.58160
$a = 0.95$	0.24744	0.37698	0.63230	0.72548	0.67957	0.59454	0.55165	0.59892	0.63983
$a = 0.99$	0.28894	0.43869	0.70801	0.79193	0.73102	0.63292	0.58473	0.65720	0.69268
$a = 1.00$	0.30045	0.45578	0.72868	0.80986	0.74478	0.64312	0.59350	0.67300	0.70690
$b = 1.0$ LAMBERT SURFACE ON TOP									
ZERO ORDER	0.0	0.00005	0.03567	0.13534	0.23965	0.32919	0.36788	0.14850	0.21938
FIRST ORDER	0.03239	0.05138	0.13529	0.21992	0.27165	0.29655	0.30222	0.19485	0.24613
SECOND ORDER	0.06336	0.09545	0.15452	0.17456	0.16947	0.15459	0.14600	0.14914	0.16038
THIRD ORDER	0.06470	0.09356	0.11439	0.10263	0.08324	0.06550	0.05795	0.09122	0.08461
SUMS									
$a = 0.20$	0.00962	0.01501	0.06996	0.18722	0.30149	0.39526	0.43467	0.19425	0.27578
$a = 0.40$	0.02888	0.04419	0.12420	0.25959	0.38201	0.47761	0.51656	0.25784	0.35030
$a = 0.60$	0.06616	0.09957	0.21132	0.36288	0.48897	0.58195	0.61846	0.34894	0.45126
$a = 0.80$	0.13848	0.20556	0.35621	0.51606	0.63580	0.71772	0.74832	0.48558	0.59349
$a = 0.90$	0.19832	0.29269	0.46529	0.62234	0.73165	0.80246	0.82792	0.58160	0.68855
$a = 0.95$	0.23750	0.34963	0.53370	0.68629	0.78743	0.85052	0.87260	0.63983	0.74464
$a = 0.99$	0.27469	0.40364	0.59706	0.74403	0.83674	0.89231	0.91118	0.69268	0.79469
$a = 1.00$	0.28493	0.41852	0.61429	0.75952	0.84981	0.90328	0.92126	0.70690	0.80803

TABLE 35 (continued)  
 $g = 0.75, b = 2$ , Reflection

VECTOR	$\mu = 0.0$	$\mu = 0.1$	$\mu = 0.3$	$\mu = 0.5$	$\mu = 0.7$	$\mu = 0.9$	$\mu = 1.0$	AVERAGE N	FLUX U
<b>b = 2.00</b> <span style="margin-left: 100px;"><math>\mu_0 = 0.1</math></span>									
FIRST ORDER	5.87169	2.23714	0.58248	0.21991	0.10429	0.05742	0.04437	0.72518	0.24069
SECOND ORDER	0.74008	0.80818	0.32662	0.14399	0.07257	0.04097	0.03187	0.27776	0.13101
THIRD ORDER	0.24644	0.32226	0.17812	0.09177	0.05055	0.03010	0.02385	0.13193	0.07609
SUMS $\alpha = 0.20$	1.20610	0.48260	0.13118	0.05060	0.02424	0.01341	0.01038	0.15734	0.05408
$\alpha = 0.40$	2.48626	1.04968	0.30035	0.11919	0.05800	0.03237	0.02513	0.34556	0.12392
$\alpha = 0.60$	3.86288	1.73208	0.52856	0.21856	0.10918	0.06195	0.04836	0.57993	0.21974
$\alpha = 0.80$	5.37615	2.58700	0.86225	0.38078	0.19933	0.11670	0.09211	0.89429	0.36686
$\alpha = 0.90$	6.20944	3.11619	1.10365	0.51241	0.27837	0.16710	0.13304	1.10754	0.48089
$\alpha = 0.95$	6.65455	3.41995	1.25735	0.60270	0.33524	0.20440	0.16362	1.23908	0.55737
$\alpha = 0.99$	7.02910	3.68886	1.40403	0.69343	0.39421	0.24378	0.19610	1.36235	0.63325
$\alpha = 1.00$	7.12584	3.76049	1.44492	0.71948	0.41144	0.25540	0.20571	1.39638	0.65489
<b>b = 2.00</b> <span style="margin-left: 100px;"><math>\mu_0 = 0.3</math></span>									
FIRST ORDER	1.07503	0.58248	0.22172	0.10635	0.05920	0.03648	0.02946	0.21208	0.09779
SECOND ORDER	0.19167	0.32662	0.19639	0.10703	0.06180	0.03824	0.03079	0.14215	0.08762
THIRD ORDER	0.10808	0.17812	0.14384	0.09038	0.05592	0.03574	0.02901	0.09869	0.07032
SUMS $\alpha = 0.20$	0.22366	0.13118	0.05354	0.02641	0.01485	0.00917	0.00741	0.04902	0.02373
$\alpha = 0.40$	0.46995	0.30035	0.13297	0.06813	0.03897	0.02422	0.01958	0.11647	0.05970
$\alpha = 0.60$	0.75209	0.52856	0.25814	0.13939	0.08198	0.05165	0.04189	0.21638	0.11893
$\alpha = 0.80$	1.09993	0.86225	0.47718	0.27789	0.17093	0.11034	0.09011	0.38394	0.23081
$\alpha = 0.90$	1.32140	1.10365	0.66078	0.40484	0.25690	0.16879	0.13856	0.52239	0.33197
$\alpha = 0.95$	1.45353	1.25735	0.78768	0.49709	0.32124	0.21325	0.17560	0.61801	0.40518
$\alpha = 0.99$	1.57476	1.40403	0.91533	0.59290	0.38931	0.26077	0.21531	0.71437	0.48110
$\alpha = 1.00$	1.60784	1.44492	0.95195	0.62087	0.40938	0.27487	0.22710	0.74207	0.50325
<b>b = 2.00</b> <span style="margin-left: 100px;"><math>\mu_0 = 0.5</math></span>									
FIRST ORDER	0.34316	0.21991	0.10635	0.05975	0.03713	0.02479	0.02068	0.09212	0.05174
SECOND ORDER	0.07539	0.14399	0.10703	0.06761	0.04342	0.02905	0.02413	0.07630	0.05416
THIRD ORDER	0.05235	0.09177	0.09038	0.06511	0.04431	0.03030	0.02525	0.06330	0.05054
SUMS $\alpha = 0.20$	0.07214	0.05060	0.02641	0.01529	0.00960	0.00642	0.00535	0.02208	0.01300
$\alpha = 0.40$	0.15412	0.11919	0.06813	0.04109	0.02625	0.01765	0.01471	0.05508	0.03431
$\alpha = 0.60$	0.25374	0.21856	0.13939	0.08891	0.05837	0.03965	0.03310	0.10944	0.07289
$\alpha = 0.80$	0.39141	0.38078	0.27789	0.19111	0.13048	0.09016	0.07550	0.21375	0.15416
$\alpha = 0.90$	0.49211	0.51241	0.40484	0.29140	0.20385	0.14244	0.11956	0.30979	0.23357
$\alpha = 0.95$	0.55828	0.60270	0.49709	0.36677	0.25999	0.18278	0.15362	0.38002	0.29322
$\alpha = 0.99$	0.62330	0.69343	0.59290	0.44656	0.32004	0.22614	0.19028	0.45329	0.35638
$\alpha = 1.00$	0.64177	0.71948	0.62087	0.47009	0.33784	0.23903	0.20119	0.47474	0.37502
<b>b = 2.00</b> <span style="margin-left: 100px;"><math>\mu_0 = 0.7</math></span>									
FIRST ORDER	0.14589	0.10429	0.05920	0.03713	0.02497	0.01768	0.01512	0.04946	0.03157
SECOND ORDER	0.03739	0.07257	0.06180	0.04342	0.03018	0.02142	0.01822	0.04492	0.03489
THIRD ORDER	0.02857	0.05055	0.05592	0.04431	0.03233	0.02326	0.01978	0.04071	0.03486
SUMS $\alpha = 0.20$	0.03095	0.02424	0.01485	0.00960	0.00652	0.00462	0.00395	0.01208	0.00805
$\alpha = 0.40$	0.06706	0.05800	0.03897	0.02625	0.01813	0.01290	0.01101	0.03097	0.02171
$\alpha = 0.60$	0.11317	0.10918	0.08198	0.05837	0.04131	0.02960	0.02523	0.06402	0.04764
$\alpha = 0.80$	0.18304	0.19933	0.17093	0.13048	0.09534	0.06900	0.05882	0.13238	0.10532
$\alpha = 0.90$	0.23957	0.27837	0.25690	0.20385	0.15166	0.11039	0.09411	0.19901	0.16385
$\alpha = 0.95$	0.27911	0.33524	0.32124	0.25999	0.19518	0.14248	0.12147	0.24916	0.20860
$\alpha = 0.99$	0.31960	0.39421	0.38931	0.32004	0.24199	0.17705	0.15093	0.30239	0.25646
$\alpha = 1.00$	0.33137	0.41144	0.40938	0.33784	0.25590	0.18733	0.15969	0.31811	0.27066

TABLE 35 (continued)  
 $g = 0.75, b = 2$ , Transmission

VECTOR	$\mu = 0.0$	$\mu = 0.1$	$\mu = 0.3$	$\mu = 0.5$	$\mu = 0.7$	$\mu = 0.9$	$\mu = 1.0$	AVERAGE N	FLUX U
$b = 2.00$									
ZERO ORDER	$\mu_0 = 0.1$ 0.0	PEAK	0.0	0.0	0.0	0.0	0.0	0.00000	0.00000
FIRST ORDER	0.00000	0.00000	0.00287	0.01058	0.01229	0.01081	0.00980	0.00729	0.00980
SECOND ORDER	0.00187	0.00309	0.01327	0.03210	0.03770	0.03313	0.02964	0.02378	0.03059
THIRD ORDER	0.00702	0.01113	0.02931	0.05190	0.05787	0.05083	0.04546	0.04006	0.04878
SUMS $a = 0.20$	0.00016	0.00026	0.00143	0.00393	0.00455	0.00400	0.00360	0.00282	0.00368
$a = 0.40$	0.00141	0.00221	0.00696	0.01510	0.01705	0.01492	0.01338	0.01121	0.01408
$a = 0.60$	0.00726	0.01117	0.02576	0.04539	0.04930	0.04269	0.03815	0.03472	0.04174
$a = 0.80$	0.03176	0.04805	0.08875	0.12990	0.13356	0.11356	0.10092	0.10227	0.11663
$a = 0.90$	0.06590	0.09903	0.16659	0.22325	0.22193	0.18621	0.16486	0.17846	0.19738
$a = 0.95$	0.09564	0.14330	0.23075	0.29604	0.28885	0.24043	0.21237	0.23856	0.25949
$a = 0.99$	0.12976	0.19401	0.30201	0.37422	0.35934	0.29698	0.26176	0.30357	0.32561
$a = 1.00$	0.14023	0.20957	0.32351	0.39740	0.38002	0.31347	0.27614	0.32292	0.34511
$b = 2.00$									
ZERO ORDER	$\mu_0 = 0.3$ 0.0	0.0	PEAK	0.0	0.0	0.0	0.0	0.00212	0.00127
FIRST ORDER	0.00137	0.00287	0.01945	0.03943	0.03176	0.02166	0.01785	0.02297	0.02699
SECOND ORDER	0.00772	0.01327	0.04221	0.07577	0.07657	0.05931	0.05010	0.05320	0.06338
THIRD ORDER	0.01835	0.02931	0.06461	0.09426	0.09518	0.07817	0.06782	0.07198	0.08238
SUMS $a = 0.20$	0.00079	0.00143	0.00624	0.01185	0.01034	0.00747	0.00624	0.00956	0.01002
$a = 0.40$	0.00415	0.00696	0.02162	0.03741	0.03429	0.02579	0.02180	0.02724	0.03045
$a = 0.60$	0.01614	0.02576	0.06087	0.09410	0.08799	0.06799	0.05801	0.06917	0.07737
$a = 0.80$	0.05750	0.08875	0.16778	0.22852	0.21238	0.16624	0.14274	0.17398	0.18950
$a = 0.90$	0.10927	0.16659	0.28559	0.36347	0.33350	0.26132	0.22473	0.28267	0.30155
$a = 0.95$	0.15215	0.23075	0.37772	0.46417	0.42210	0.33039	0.28424	0.36505	0.38471
$a = 0.99$	0.19990	0.30201	0.47699	0.56960	0.51360	0.40136	0.34531	0.45214	0.47144
$a = 1.00$	0.21433	0.32351	0.50648	0.60045	0.54017	0.42189	0.36297	0.47775	0.49675
$b = 2.00$									
ZERO ORDER	$\mu_0 = 0.5$ 0.0	0.0	0.0	PEAK	0.0	0.0	0.0	0.01832	0.01832
FIRST ORDER	0.00629	0.01058	0.03943	0.11128	0.09432	0.04826	0.03495	0.06051	0.07092
SECOND ORDER	0.02024	0.03210	0.07577	0.12759	0.13464	0.10048	0.08112	0.09365	0.10935
THIRD ORDER	0.03398	0.05190	0.09426	0.12514	0.12585	0.10385	0.08951	0.09968	0.11073
SUMS $a = 0.20$	0.00242	0.00393	0.01185	0.02856	0.02544	0.01465	0.01108	0.03512	0.03793
$a = 0.40$	0.00955	0.01510	0.03741	0.07673	0.07075	0.04480	0.03511	0.06704	0.07449
$a = 0.60$	0.02940	0.04539	0.09410	0.16386	0.15369	0.10473	0.08448	0.13010	0.14449
$a = 0.80$	0.08576	0.12990	0.22852	0.33727	0.31509	0.22643	0.18682	0.26438	0.28720
$a = 0.90$	0.14851	0.22325	0.36347	0.49323	0.45573	0.33375	0.27785	0.39001	0.41589
$a = 0.95$	0.19759	0.29604	0.46417	0.60361	0.55320	0.40815	0.34113	0.48054	0.50671
$a = 0.99$	0.25037	0.37422	0.56960	0.71561	0.65068	0.48246	0.40440	0.57336	0.59859
$a = 1.00$	0.26602	0.39740	0.60045	0.74784	0.67850	0.50364	0.42244	0.60021	0.62498
$b = 2.00$									
ZERO ORDER	$\mu_0 = 0.7$ 0.0	0.0	0.0	0.0	PEAK	0.0	0.0	0.04102	0.05743
FIRST ORDER	0.00838	0.01229	0.03176	0.09432	0.21724	0.12838	0.07741	0.09586	0.12893
SECOND ORDER	0.02555	0.03770	0.07657	0.13464	0.18379	0.16746	0.13623	0.11928	0.14858
THIRD ORDER	0.03962	0.05787	0.09518	0.12585	0.13844	0.12827	0.11532	0.10858	0.12359
SUMS $a = 0.20$	0.00310	0.00455	0.01034	0.02544	0.05208	0.03355	0.02198	0.06599	0.09031
$a = 0.40$	0.01164	0.01705	0.03429	0.07075	0.12832	0.08904	0.06255	0.10836	0.14370
$a = 0.60$	0.03375	0.04930	0.08799	0.15369	0.24576	0.18117	0.13482	0.18353	0.23357
$a = 0.80$	0.09168	0.13356	0.21238	0.31509	0.44051	0.33953	0.26488	0.32718	0.39495
$a = 0.90$	0.15242	0.22193	0.33350	0.45573	0.59233	0.46346	0.36889	0.45149	0.52772
$a = 0.95$	0.19835	0.28885	0.42210	0.55320	0.69167	0.54406	0.43706	0.53746	0.61699
$a = 0.99$	0.24669	0.35934	0.51360	0.65068	0.78753	0.62136	0.50265	0.62335	0.70460
$a = 1.00$	0.26086	0.38002	0.54017	0.67850	0.81436	0.64290	0.52095	0.64786	0.72934

TABLE 35 (continued)  
 $g = 0.75, b = 2$ , Reflection

VECTOR	$\mu = 0.0$	$\mu = 0.1$	$\mu = 0.3$	$\mu = 0.5$	$\mu = 0.7$	$\mu = 0.9$	$\mu = 1.0$	AVERAGE N	FLUX U
<b>b = 2.00</b> $\mu_0 = 0.9$									
FIRST ORDER	0.07457	0.05742	0.03648	0.02479	0.01768	0.01310	0.01141	0.03020	0.02105
SECOND ORDER	0.02145	0.04097	0.03824	0.02905	0.02142	0.01589	0.01377	0.02859	0.02361
THIRD ORDER	0.01718	0.03010	0.03574	0.03030	0.02326	0.01738	0.01501	0.02703	0.02423
SUMS $\alpha = 0.20$	0.01594	0.01341	0.00917	0.00642	0.00462	0.00343	0.00298	0.00745	0.00539
$\alpha = 0.40$	0.03494	0.03237	0.02422	0.01765	0.01290	0.00959	0.00832	0.01936	0.01466
$\alpha = 0.60$	0.06012	0.06195	0.05165	0.03965	0.02960	0.02205	0.01911	0.04086	0.03259
$\alpha = 0.80$	0.10084	0.11670	0.11034	0.09016	0.06900	0.05161	0.04459	0.08707	0.07339
$\alpha = 0.90$	0.13597	0.16710	0.16879	0.14244	0.11039	0.08270	0.07132	0.13340	0.11548
$\alpha = 0.95$	0.16145	0.20440	0.21325	0.18278	0.14248	0.10679	0.09200	0.16876	0.14789
$\alpha = 0.99$	0.18814	0.24378	0.26077	0.22614	0.17705	0.13271	0.11423	0.20660	0.18271
$\alpha = 1.00$	0.19598	0.25540	0.27487	0.23903	0.18733	0.14042	0.12083	0.21782	0.19306
<b>b = 2.00</b> $\mu_0 = 1.0$									
FIRST ORDER	0.05600	0.04437	0.02946	0.02068	0.01512	0.01141	0.01002	0.02441	0.01760
SECOND ORDER	0.01689	0.03187	0.03079	0.02413	0.01822	0.01377	0.01202	0.02336	0.01974
THIRD ORDER	0.01372	0.02385	0.02901	0.02525	0.01978	0.01501	0.01305	0.02233	0.02036
SUMS $\alpha = 0.20$	0.01201	0.01038	0.00741	0.00535	0.00395	0.00298	0.00261	0.00604	0.00451
$\alpha = 0.40$	0.02645	0.02513	0.01958	0.01471	0.01101	0.00832	0.00728	0.01575	0.01228
$\alpha = 0.60$	0.04588	0.04836	0.04189	0.03310	0.02523	0.01911	0.01666	0.03342	0.02734
$\alpha = 0.80$	0.07806	0.09211	0.09011	0.07550	0.05882	0.04459	0.03873	0.07181	0.06178
$\alpha = 0.90$	0.10641	0.13304	0.13856	0.11956	0.09411	0.07132	0.06180	0.11058	0.09739
$\alpha = 0.95$	0.12722	0.16362	0.17560	0.15362	0.12147	0.09200	0.07960	0.14028	0.12487
$\alpha = 0.99$	0.14917	0.19610	0.21531	0.19028	0.15093	0.11423	0.09871	0.17213	0.15440
$\alpha = 1.00$	0.15564	0.20571	0.22710	0.20119	0.15969	0.12083	0.10438	0.18159	0.16318
<b>b = 2.0</b> NARROW SURFACE LAYER AT TOP									
FIRST ORDER	INFINITE	0.72518	0.21208	0.09212	0.04946	0.03020	0.02441	0.26704	0.09404
SECOND ORDER	0.13352	0.27776	0.14215	0.07630	0.04492	0.02859	0.02336	0.11389	0.06494
THIRD ORDER	0.09174	0.13193	0.09869	0.06330	0.04071	0.02703	0.02233	0.07114	0.05037
SUMS $\alpha = 0.20$	INFINITE	0.15734	0.04902	0.02208	0.01208	0.00745	0.00604	0.05863	0.02189
$\alpha = 0.40$	INFINITE	0.34556	0.11647	0.05508	0.03097	0.01936	0.01575	0.13147	0.05277
$\alpha = 0.60$	INFINITE	0.57993	0.21638	0.10944	0.06402	0.04086	0.03342	0.22884	0.10088
$\alpha = 0.80$	INFINITE	0.89429	0.38394	0.21375	0.13238	0.08707	0.07181	0.37721	0.18876
$\alpha = 0.90$	INFINITE	1.10754	0.52239	0.30979	0.19901	0.13340	0.11058	0.49304	0.26750
$\alpha = 0.95$	INFINITE	1.23908	0.61801	0.38002	0.24916	0.16876	0.14028	0.57127	0.32449
$\alpha = 0.99$	INFINITE	1.36235	0.71437	0.45329	0.30239	0.20660	0.17213	0.64924	0.38364
$\alpha = 1.00$	INFINITE	1.39638	0.74207	0.47474	0.31811	0.21782	0.18159	0.67153	0.40091
<b>b = 2.0</b> LAMBERT SURFACE ON TOP									
FIRST ORDER	0.50000	0.24069	0.09779	0.05174	0.03157	0.02105	0.01760	0.09404	0.04689
SECOND ORDER	0.08229	0.13101	0.08762	0.05416	0.03489	0.02361	0.01974	0.06494	0.04428
THIRD ORDER	0.04621	0.07609	0.07032	0.05054	0.03486	0.02423	0.02036	0.05037	0.03980
SUMS $\alpha = 0.20$	0.10372	0.05408	0.02373	0.01300	0.00805	0.00539	0.00451	0.02189	0.01154
$\alpha = 0.40$	0.21727	0.12392	0.05970	0.03431	0.02171	0.01466	0.01228	0.05277	0.02973
$\alpha = 0.60$	0.34708	0.21974	0.11893	0.07289	0.04764	0.03259	0.02734	0.10088	0.06166
$\alpha = 0.80$	0.50945	0.36686	0.23081	0.15416	0.10532	0.07339	0.06178	0.18876	0.12744
$\alpha = 0.90$	0.61681	0.48089	0.33197	0.23357	0.16385	0.11548	0.09739	0.26750	0.19109
$\alpha = 0.95$	0.68324	0.55737	0.40518	0.29322	0.20860	0.14789	0.12487	0.32449	0.23876
$\alpha = 0.99$	0.74607	0.63325	0.48110	0.35638	0.25646	0.18271	0.15440	0.38364	0.28918
$\alpha = 1.00$	0.76355	0.65489	0.50325	0.37502	0.27066	0.19306	0.16318	0.40091	0.30404

TABLE 35 (continued)  
 $g = 0.75, b = 2$ , Transmission

VECTOR	$\mu = 0.0$	$\mu = 0.1$	$\mu = 0.3$	$\mu = 0.5$	$\mu = 0.7$	$\mu = 0.9$	$\mu = 1.0$	AVERAGE N	FLUX U
$b = 2.00$									
$\mu_0 = 0.9$									
ZERO ORDER	C.0	0.0	0.0	0.0	0.0	PEAK	0.0	0.06020	0.10837
FIRST ORDER	0.00808	0.01081	0.02166	0.04826	0.12838	0.41374	0.30110	0.11627	0.18354
SECOND ORDER	C.02378	0.03313	0.05931	0.10048	0.16746	0.26916	0.29213	0.12572	0.17323
THIRD ORDER	C.03608	0.05083	0.07817	0.10385	0.12827	0.15271	0.16165	0.10263	0.12372
SUMS									
$a = 0.20$	0.00293	0.00400	0.00747	0.01465	0.03355	0.09487	0.07333	0.08944	0.15313
$a = 0.40$	0.01079	0.01492	0.02579	0.04480	0.08904	0.22085	0.17995	0.13591	0.22002
$a = 0.60$	C.03058	0.04269	0.06799	0.10473	0.18117	0.39291	0.33485	0.21294	0.32339
$a = 0.80$	C.08069	0.11356	0.16624	0.22643	0.33953	0.63817	0.56392	0.34976	0.49254
$a = 0.90$	0.13171	0.18621	0.26132	0.33375	0.46346	0.80492	0.72155	0.46162	0.62182
$a = 0.95$	C.16961	0.24043	0.33039	0.40815	0.54406	0.90522	0.81636	0.53657	0.70519
$a = 0.99$	C.20902	0.29698	0.40136	0.48246	0.62136	0.99654	0.90245	0.60994	0.78480
$a = 1.00$	C.22049	0.31347	0.42189	0.50364	0.64290	1.02124	0.92569	0.63063	0.80694
$b = 2.00$									
$\mu_0 = 1.0$									
ZERO ORDER	C.0	0.0	0.0	0.0	0.0	0.0	PEAK	0.06767	0.13534
FIRST ORDER	0.00758	0.00980	0.01785	0.03495	0.07741	0.30110	1.89469	0.12132	0.20698
SECOND ORDER	C.02179	0.02964	0.05010	0.08112	0.13623	0.29213	0.55889	0.12387	0.18036
THIRD ORDER	C.03277	0.04546	0.06782	0.08951	0.11532	0.16165	0.20668	0.09667	0.12074
SUMS									
$a = 0.20$	0.00272	0.00360	0.00624	0.01108	0.02198	0.07333	0.40309	0.09778	0.18504
$a = 0.40$	0.00991	0.01338	0.02180	0.03511	0.06255	0.17995	0.86302	0.14447	0.25710
$a = 0.60$	C.02785	0.03815	0.05801	0.08448	0.13482	0.33485	1.39695	0.21985	0.36489
$a = 0.80$	0.07278	0.10092	0.14274	0.18682	0.26488	0.56392	2.03218	0.34993	0.53494
$a = 0.90$	0.11811	0.16486	0.22473	0.27785	0.36889	0.72155	2.40270	0.45383	0.66096
$a = 0.95$	0.15159	0.21237	0.28424	0.34113	0.43706	0.81636	2.60601	0.52253	0.74076
$a = 0.99$	0.18626	0.26176	0.34531	0.40440	0.50265	0.90245	2.77961	0.58920	0.81604
$a = 1.00$	0.19633	0.27614	0.36297	0.42244	0.52095	0.92569	2.82478	0.60791	0.83682
$b = 2.0$ NARROW SURFACE LAYER AT TOP									
ZERO ORDER	C.0	0.00000	0.00212	0.01832	0.04102	0.06020	0.06767	0.02445	0.03753
FIRST ORDER	0.00481	0.00729	0.02297	0.06051	0.09586	0.11627	0.12132	0.06061	0.08436
SECOND ORDER	C.01579	0.02378	0.05320	0.09365	0.11928	0.12572	0.12387	0.08296	0.10498
THIRD ORDER	0.02692	0.04006	0.07198	0.09968	0.10858	0.10263	0.09667	0.08427	0.09754
SUMS									
$a = 0.20$	0.00187	0.00282	0.00956	0.03512	0.06599	0.08944	0.09778	0.04070	0.05953
$a = 0.40$	0.00748	0.01121	0.02724	0.06704	0.10836	0.13591	0.14447	0.07002	0.09709
$a = 0.60$	C.02334	0.03472	0.06917	0.13010	0.18353	0.21294	0.21985	0.12600	0.16457
$a = 0.80$	0.06916	0.10227	0.17938	0.26438	0.32718	0.34976	0.34993	0.24292	0.29621
$a = 0.90$	C.12095	0.17846	0.28267	0.39001	0.45149	0.46162	0.45383	0.35166	0.41238
$a = 0.95$	0.16180	0.23856	0.36505	0.48054	0.53746	0.53657	0.52253	0.42998	0.49370
$a = 0.99$	C.20600	0.30357	0.45214	0.57336	0.62335	0.60994	0.58920	0.51031	0.57561
$a = 1.00$	C.21915	0.32292	0.47775	0.60021	0.64786	0.63063	0.60791	0.53356	0.59909
$b = 2.0$ LAMBERT SURFACE ON TOP									
ZERO ORDER	0.0	0.00000	0.00127	0.01832	0.05743	0.10837	0.13534	0.03753	0.06027
FIRST ORDER	C.00669	0.00980	0.02699	0.07092	0.12893	0.18354	0.20698	0.08436	0.12139
SECOND ORDER	C.02076	0.03059	0.06338	0.10935	0.14858	0.17323	0.18036	0.10498	0.13539
THIRD ORDER	C.03334	0.04878	0.08238	0.11073	0.12359	0.12372	0.12074	0.09754	0.11329
SUMS									
$a = 0.20$	0.00251	0.00368	0.01002	0.03793	0.09031	0.15313	0.18504	0.05953	0.09102
$a = 0.40$	0.00961	0.01408	0.03045	0.07449	0.14370	0.22002	0.25710	0.09709	0.14060
$a = 0.60$	0.02855	0.04174	0.07737	0.14449	0.23357	0.32339	0.36489	0.16457	0.22413
$a = 0.80$	0.07994	0.11663	0.18950	0.28720	0.39495	0.49254	0.53494	0.29621	0.37559
$a = 0.90$	0.13532	0.19738	0.30155	0.41589	0.52772	0.62182	0.66096	0.41238	0.50182
$a = 0.95$	C.17787	0.25949	0.38471	0.50671	0.61699	0.70519	0.74076	0.49370	0.58744
$a = 0.99$	0.22311	0.32561	0.47144	0.59859	0.70460	0.78480	0.81604	0.57561	0.67199
$a = 1.00$	0.23645	0.34511	0.49675	0.62498	0.72934	0.80694	0.83682	0.59909	0.69596

TABLE 35 (continued)  
 $g = 0.75, b = 4$ , Reflection

VECTOR	$\mu = 0.0$	$\mu = 0.1$	$\mu = 0.3$	$\mu = 0.5$	$\mu = 0.7$	$\mu = 0.9$	$\mu = 1.0$	AVERAGE N	FLUX U
<b>b = 4.00      <math>\mu_0 = 0.1</math></b>									
FIRST ORDER	5.87169	2.23714	0.58248	0.21991	0.10429	0.05742	0.04437	0.72518	0.24069
SECOND ORDER	0.74008	0.80818	0.32662	0.14400	0.07258	0.04099	0.03189	0.27776	0.13102
THIRD ORDER	0.24644	0.32226	0.17813	0.09183	0.05065	0.03022	0.02398	0.13198	0.07618
SUMS $a = 0.20$	1.20610	0.48260	0.13118	0.05060	0.02424	0.01341	0.01038	0.15734	0.05408
$a = 0.40$	2.48627	1.04969	0.30036	0.11922	0.05804	0.03242	0.02517	0.34559	0.12396
$a = 0.60$	3.86294	1.73217	0.52873	0.21889	0.10964	0.06246	0.04886	0.58024	0.22015
$a = 0.80$	5.37723	2.58860	0.86495	0.38493	0.20450	0.12211	0.09741	0.89809	0.37148
$a = 0.90$	6.21451	3.12366	1.11540	0.52876	0.29756	0.18652	0.15185	1.12232	0.49825
$a = 0.95$	6.66613	3.43699	1.28326	0.63706	0.37427	0.24319	0.20094	1.26999	0.59296
$a = 0.99$	7.05251	3.72329	1.45499	0.75849	0.46615	0.31415	0.26341	1.42064	0.69925
$a = 1.00$	7.15398	3.80188	1.50576	0.79643	0.49594	0.33771	0.28433	1.46527	0.73254
<b>b = 4.00      <math>\mu_0 = 0.3</math></b>									
FIRST ORDER	1.07503	0.58248	0.22172	0.10635	0.05920	0.03648	0.02947	0.21208	0.09780
SECOND ORDER	0.19167	0.32662	0.19639	0.10707	0.06186	0.03831	0.03087	0.14218	0.08768
THIRD ORDER	0.10809	0.17813	0.14388	0.09055	0.05622	0.03609	0.02938	0.09887	0.05057
SUMS $a = 0.20$	0.22366	0.13118	0.05354	0.02642	0.01486	0.00918	0.00742	0.04903	0.02374
$a = 0.40$	0.46995	0.30036	0.13300	0.06819	0.03907	0.02434	0.01970	0.11653	0.05978
$a = 0.60$	0.75221	0.52873	0.25849	0.14004	0.08289	0.05265	0.04289	0.21699	0.11973
$a = 0.80$	1.10176	0.86495	0.48176	0.28493	0.17967	0.11946	0.09903	0.39036	0.23862
$a = 0.90$	1.32937	1.11540	0.67930	0.43060	0.28707	0.19927	0.16804	0.54564	0.35926
$a = 0.95$	1.47113	1.28326	0.82710	0.54937	0.38055	0.27211	0.23217	0.66497	0.45923
$a = 0.99$	1.60940	1.45499	0.99076	0.68921	0.49570	0.36472	0.31469	0.80060	0.57869
$a = 1.00$	1.64920	1.50576	1.04142	0.73403	0.53352	0.39566	0.34243	0.84329	0.61732
<b>b = 4.00      <math>\mu_0 = 0.5</math></b>									
FIRST ORDER	0.34316	0.21991	0.10635	0.05977	0.03717	0.02484	0.02073	0.09215	0.05178
SECOND ORDER	0.07539	0.14400	0.10707	0.06776	0.04368	0.02936	0.02446	0.07645	0.05438
THIRD ORDER	0.05238	0.09183	0.09055	0.06564	0.04519	0.03133	0.02630	0.06383	0.05129
SUMS $a = 0.20$	0.07214	0.05060	0.02642	0.01530	0.00963	0.00645	0.00539	0.02210	0.01303
$a = 0.40$	0.15413	0.11922	0.06819	0.04125	0.02650	0.01793	0.01500	0.05523	0.03452
$a = 0.60$	0.25396	0.21889	0.14004	0.09016	0.06011	0.04156	0.03500	0.11062	0.07441
$a = 0.80$	0.39422	0.38493	0.28493	0.20191	0.14390	0.10416	0.08919	0.22361	0.16615
$a = 0.90$	0.50321	0.52876	0.43060	0.32724	0.24583	0.18486	0.16059	0.34214	0.27155
$a = 0.95$	0.58162	0.63706	0.54937	0.43609	0.33865	0.26086	0.22868	0.44230	0.36491
$a = 0.99$	0.66753	0.75849	0.68921	0.56954	0.45591	0.35891	0.31723	0.56340	0.48101
$a = 1.00$	0.69409	0.79643	0.73403	0.61321	0.49489	0.39186	0.34710	0.60278	0.51932
<b>b = 4.00      <math>\mu_0 = 0.7</math></b>									
FIRST ORDER	0.14589	0.10429	0.05920	0.03717	0.02505	0.01779	0.01524	0.04950	0.03165
SECOND ORDER	0.03740	0.07258	0.06186	0.04368	0.03066	0.02202	0.01885	0.04520	0.03530
THIRD ORDER	0.02863	0.05065	0.05622	0.04519	0.03378	0.02500	0.02157	0.04160	0.03611
SUMS $a = 0.20$	0.03095	0.02424	0.01486	0.00963	0.00658	0.00469	0.00402	0.01212	0.00810
$a = 0.40$	0.06709	0.05804	0.03907	0.02650	0.01853	0.01337	0.01149	0.03122	0.02206
$a = 0.60$	0.11348	0.10964	0.08289	0.06011	0.04376	0.03234	0.02798	0.06567	0.04980
$a = 0.80$	0.18654	0.20450	0.17967	0.14390	0.11215	0.08667	0.07617	0.14471	0.12036
$a = 0.90$	0.25259	0.29756	0.28707	0.24583	0.20104	0.16057	0.14277	0.23705	0.20857
$a = 0.95$	0.30564	0.37427	0.38055	0.33865	0.28473	0.23175	0.20747	0.32003	0.29027
$a = 0.99$	0.36851	0.46615	0.49570	0.45591	0.39248	0.32462	0.29227	0.42430	0.39459
$a = 1.00$	0.38883	0.49594	0.53352	0.49489	0.42863	0.35596	0.32097	0.45888	0.42945

TABLE 35 (continued)  
 $g = 0.75, b = 4$ , Transmission

VECTOR	$\mu = 0.0$	$\mu = 0.1$	$\mu = 0.3$	$\mu = 0.5$	$\mu = 0.7$	$\mu = 0.9$	$\mu = 1.0$	AVERAGE N	FLUX U
$b = 4.00$									
$\mu_0 = 0.1$									
ZERO ORDER	C.0	PEAK	0.0	0.0	0.0	0.0	0.0	0.00000	0.00000
FIRST ORDER	C.00000	0.00000	0.00000	0.00019	0.00071	0.00117	0.00133	0.00042	0.00067
SECOND ORDER	C.00007	0.00011	0.00030	0.00135	0.00361	0.00559	0.00618	0.00220	0.00337
THIRD ORDER	0.00045	0.00066	0.00158	0.00444	0.00934	0.01349	0.01469	0.00591	0.00865
SUMS									
$a = 0.20$	C.00001	0.00001	0.00004	0.00015	0.00040	0.00061	0.00068	0.00024	0.00037
$a = 0.40$	0.00015	C.00021	0.00044	0.00112	0.00230	0.00330	0.00359	0.00148	0.00214
$a = 0.60$	C.00126	0.00183	0.00335	0.00636	0.01067	0.01399	0.01486	0.00724	0.00983
$a = 0.80$	0.00976	0.01424	0.02308	0.03537	0.04922	0.05834	0.06016	0.03599	0.04539
$a = 0.90$	C.02842	0.04150	0.06349	0.08832	0.11218	0.12539	0.12683	0.08594	0.10381
$a = 0.95$	C.05023	0.07340	0.10915	0.14483	0.17558	0.18998	0.19000	0.13814	0.16294
$a = 0.99$	C.08170	0.11946	0.17369	0.22197	0.25899	0.27250	0.26976	0.20854	0.24105
$a = 1.00$	C.09282	0.13575	0.19628	0.24849	0.28713	0.29989	0.29606	0.23261	0.26746
$b = 4.00$									
$\mu_0 = 0.3$									
ZERO ORDER	C.0	0.0	PEAK	0.0	0.0	0.0	0.0	0.00000	0.00000
FIRST ORDER	0.00000	0.00000	0.00005	0.00077	0.00186	0.00237	0.00244	0.00101	0.00155
SECOND ORDER	0.00020	C.00030	0.00091	0.00366	0.00821	0.01097	0.01136	0.00481	0.00714
THIRD ORDER	C.00106	0.00158	0.00383	0.00992	0.01864	0.02459	0.02571	0.01171	0.01668
SUMS									
$a = 0.20$	0.00002	0.00004	0.00010	0.00042	0.00091	0.00119	0.00123	0.00053	0.00079
$a = 0.40$	C.00030	0.00044	0.00096	0.00250	0.00467	0.00598	0.00619	0.00291	0.00412
$a = 0.60$	C.00228	0.00335	0.00623	0.01202	0.01920	0.02347	0.02411	0.01284	0.01719
$a = 0.80$	0.01577	0.02308	0.03772	0.05811	0.07901	0.08991	0.09074	0.05743	0.07179
$a = 0.90$	0.04339	0.06349	0.09764	0.13621	0.17037	0.18497	0.18409	0.13013	0.15614
$a = 0.95$	0.07459	0.10915	0.16296	0.21666	0.25949	0.27417	0.27049	0.20375	0.23902
$a = 0.99$	0.11865	0.17369	0.25335	0.32421	0.37461	0.38643	0.37816	0.30125	0.34662
$a = 1.00$	0.13406	0.19628	0.28464	0.36081	0.41309	0.42343	0.41346	0.33427	0.38268
$b = 4.00$									
$\mu_0 = 0.5$									
ZERO ORDER	C.0	0.0	0.0	PEAK	0.0	0.0	0.0	0.00034	0.00034
FIRST ORDER	0.00012	0.00019	0.00077	0.00408	0.00714	0.00611	0.00537	0.00365	0.00511
SECOND ORDER	0.00088	0.00135	0.00366	0.01066	0.02032	0.02373	0.02283	0.01191	0.01688
THIRD ORDER	C.00297	0.00444	0.00992	0.02155	0.03598	0.04437	0.04497	0.02322	0.03185
SUMS									
$a = 0.20$	0.00010	0.00015	0.00042	0.00148	0.00263	0.00264	0.00247	0.00180	0.00238
$a = 0.40$	C.00074	0.00112	0.00250	0.00628	0.01055	0.01153	0.01116	0.00672	0.00906
$a = 0.60$	C.00430	0.00636	0.01202	0.02310	0.03510	0.03925	0.03867	0.02345	0.03069
$a = 0.80$	0.02410	0.03537	0.05811	0.08964	0.11955	0.13011	0.12825	0.08664	0.10718
$a = 0.90$	0.06028	0.08832	0.13621	0.19024	0.23540	0.24834	0.24313	0.17940	0.21389
$a = 0.95$	0.09887	0.14483	0.21666	0.28831	0.34270	0.35418	0.34485	0.26862	0.31360
$a = 0.99$	0.15151	0.22197	0.32421	0.41519	0.47710	0.48372	0.46834	0.38315	0.43922
$a = 1.00$	0.16960	0.24849	0.36081	0.45766	0.52133	0.52581	0.50828	0.42133	0.48069
$b = 4.00$									
$\mu_0 = 0.7$									
ZERO ORDER	C.0	0.0	0.0	0.0	PEAK	0.0	0.0	0.00236	0.00330
FIRST ORDER	C.00048	0.00071	0.00186	0.00714	0.02495	0.02129	0.01492	0.01109	0.01620
SECOND ORDER	0.00246	0.00361	0.00821	0.02032	0.04177	0.05370	0.05033	0.02540	0.03618
THIRD ORDER	C.00640	0.00934	0.01864	0.03598	0.05894	0.07602	0.07839	0.03974	0.05392
SUMS									
$a = 0.20$	C.00027	0.00040	0.00091	0.00263	0.00727	0.00717	0.00579	0.00601	0.00854
$a = 0.40$	C.00158	0.00230	0.00467	0.01055	0.02325	0.02520	0.02235	0.01548	0.02161
$a = 0.60$	C.00732	0.01067	0.01920	0.03510	0.06247	0.07046	0.06621	0.04178	0.05592
$a = 0.80$	C.03381	0.04922	0.07901	0.11955	0.17370	0.19304	0.18651	0.12482	0.15697
$a = 0.90$	0.07698	0.11218	0.17037	0.23540	0.30927	0.33389	0.32356	0.23368	0.28240
$a = 0.95$	0.12039	0.17558	0.25949	0.34270	0.42763	0.45222	0.43754	0.33252	0.39287
$a = 0.99$	C.17743	0.25899	0.37461	0.47710	0.57067	0.59147	0.57060	0.45495	0.52707
$a = 1.00$	C.19665	0.28713	0.41309	0.52133	0.61688	0.63581	0.61276	0.49502	0.57055



TABLE 35 (continued)  
 $g = 0.75, b = 4$ , Reflection

VECTOR	$\mu = 0.0$	$\mu = 0.1$	$\mu = 0.3$	$\mu = 0.5$	$\mu = 0.7$	$\mu = 0.9$	$\mu = 1.0$	AVERAGE N	FLUX U
<b>b = 4.00</b> $\mu_0 = 0.9$									
FIRST ORDER	0.07457	0.05742	0.03648	0.02484	0.01779	0.01326	0.01158	0.03027	0.02114
SECOND ORDER	0.02146	0.04099	0.03831	0.02936	0.02202	0.01667	0.01460	0.02895	0.02413
THIRD ORDER	0.01726	0.03022	0.03609	0.03133	0.02500	0.01952	0.01723	0.02811	0.02575
SUMS $\alpha = 0.20$	0.01594	0.01341	0.00918	0.00645	0.00469	0.00352	0.00308	0.00749	0.00545
$\alpha = 0.40$	0.03497	0.03242	0.02434	0.01793	0.01337	0.01015	0.00891	0.01965	0.01507
$\alpha = 0.60$	0.06046	0.06246	0.05265	0.04156	0.03234	0.02517	0.02225	0.04271	0.03501
$\alpha = 0.80$	0.10451	0.12211	0.11946	0.10416	0.08667	0.07039	0.06312	0.10003	0.08925
$\alpha = 0.90$	0.14916	0.18652	0.19927	0.18486	0.16057	0.13406	0.12132	0.17203	0.16099
$\alpha = 0.95$	0.18783	0.24319	0.27211	0.26086	0.23175	0.19632	0.17852	0.23938	0.22942
$\alpha = 0.99$	0.23600	0.31415	0.36472	0.35891	0.32462	0.27812	0.25386	0.32609	0.31828
$\alpha = 1.00$	0.25197	0.33771	0.39566	0.39186	0.35596	0.30582	0.27939	0.35520	0.34822
<b>b = 4.00</b> $\mu_0 = 1.0$									
FIRST ORDER	0.05600	0.04437	0.02947	0.02073	0.01524	0.01158	0.01020	0.02448	0.01770
SECOND ORDER	0.01690	0.03189	0.03087	0.02446	0.01885	0.01460	0.01291	0.02374	0.02030
THIRD ORDER	0.01380	0.02398	0.02938	0.02630	0.02157	0.01723	0.01536	0.02344	0.02192
SUMS $\alpha = 0.20$	0.01201	0.01038	0.00742	0.00539	0.00402	0.00308	0.00271	0.00608	0.00457
$\alpha = 0.40$	0.02648	0.02517	0.01970	0.01500	0.01149	0.00891	0.00789	0.01605	0.01270
$\alpha = 0.60$	0.04622	0.04886	0.04289	0.03500	0.02798	0.02225	0.01986	0.03528	0.02977
$\alpha = 0.80$	0.08165	0.09741	0.09903	0.08919	0.07617	0.06312	0.05706	0.08453	0.07736
$\alpha = 0.90$	0.11919	0.15185	0.16804	0.16059	0.14277	0.12132	0.11057	0.14804	0.14157
$\alpha = 0.95$	0.15260	0.20094	0.23217	0.22868	0.20747	0.17852	0.16335	0.20831	0.20346
$\alpha = 0.99$	0.19496	0.26341	0.31469	0.31723	0.29227	0.25386	0.23297	0.28655	0.28432
$\alpha = 1.00$	0.20914	0.28433	0.34243	0.34710	0.32097	0.27939	0.25658	0.31294	0.31164
<b>b = 4.0</b> NARROW SURFACE LAYER AT TOP									
FIRST ORDER	INFINITE	0.72518	0.21208	0.09215	0.04950	0.03027	0.02448	0.26706	0.09408
SECOND ORDER	0.13353	0.27776	0.14218	0.07645	0.04520	0.02895	0.02374	0.11406	0.06519
THIRD ORDER	0.09177	0.13198	0.09887	0.06383	0.04160	0.02811	0.02344	0.07169	0.05114
SUMS $\alpha = 0.20$	INFINITE	0.15734	0.04903	0.02210	0.01212	0.00749	0.00608	0.05865	0.02191
$\alpha = 0.40$	INFINITE	0.34559	0.11653	0.05523	0.03122	0.01965	0.01605	0.13163	0.05299
$\alpha = 0.60$	INFINITE	0.58024	0.21699	0.11062	0.06567	0.04271	0.03528	0.22996	0.10234
$\alpha = 0.80$	INFINITE	0.89809	0.39036	0.22361	0.14471	0.10003	0.08453	0.38625	0.19979
$\alpha = 0.90$	INFINITE	1.12232	0.54564	0.34214	0.23705	0.17203	0.14804	0.52234	0.30195
$\alpha = 0.95$	INFINITE	1.26999	0.66497	0.44230	0.32003	0.23938	0.20831	0.62737	0.38913
$\alpha = 0.99$	INFINITE	1.42064	0.80060	0.56340	0.42430	0.32609	0.28655	0.74800	0.49553
$\alpha = 1.00$	INFINITE	1.46527	0.84329	0.60278	0.45888	0.35520	0.31294	0.78627	0.53033
<b>b = 4.0</b> LAMBERT SURFACE ON TOP									
FIRST ORDER	0.50000	0.24069	0.09780	0.05178	0.03165	0.02114	0.01770	0.09408	0.04696
SECOND ORDER	0.08230	0.13102	0.08768	0.05438	0.03530	0.02413	0.02030	0.06519	0.04464
THIRD ORDER	0.04627	0.07618	0.07057	0.05129	0.03611	0.02575	0.02192	0.05114	0.04089
SUMS $\alpha = 0.20$	0.10372	0.05408	0.02374	0.01303	0.00810	0.00545	0.00457	0.02191	0.01158
$\alpha = 0.40$	0.21730	0.12396	0.05978	0.03452	0.02206	0.01507	0.01270	0.05299	0.03003
$\alpha = 0.60$	0.34735	0.22015	0.11973	0.07441	0.04980	0.03501	0.02977	0.10234	0.06356
$\alpha = 0.80$	0.51259	0.37148	0.23862	0.16615	0.12036	0.08925	0.07736	0.19979	0.14090
$\alpha = 0.90$	0.62859	0.49825	0.35926	0.27155	0.20857	0.16099	0.14157	0.30195	0.23161
$\alpha = 0.95$	0.70742	0.59296	0.45923	0.36491	0.29027	0.22942	0.20346	0.38913	0.31328
$\alpha = 0.99$	0.79095	0.69925	0.57869	0.48101	0.39459	0.31828	0.28432	0.49553	0.41598
$\alpha = 1.00$	0.81636	0.73254	0.61732	0.51932	0.42945	0.34822	0.31164	0.53033	0.45006

TABLE 35 (continued)  
 $g = 0.75, b = 4$ , Transmission

VECTOR	$\mu = 0.0$	$\mu = 0.1$	$\mu = 0.3$	$\mu = 0.5$	$\mu = 0.7$	$\mu = 0.9$	$\mu = 1.0$	AVERAGE N	FLUX U
$b = 4.00$									
	$\mu_0 = 0.9$								
ZERO ORDER	0.0	0.0	0.0	0.0	0.0	PEAK	0.0	0.00652	0.01174
FIRST ORDER	0.00088	0.00117	0.00237	0.00611	0.02129	0.08967	0.07338	0.02245	0.03705
SECOND ORDER	0.00403	0.00559	0.01097	0.02373	0.05370	0.11339	0.13827	0.04171	0.06316
THIRD ORDER	0.00954	0.01349	0.02459	0.04437	0.07602	0.11988	0.14296	0.05598	0.07800
SUMS									
$a = 0.20$	0.00045	0.00061	0.00119	0.00264	0.00717	0.02363	0.02157	0.01325	0.02246
$a = 0.40$	0.00235	0.00330	0.00598	0.01153	0.02520	0.06566	0.06493	0.02825	0.04476
$a = 0.60$	0.00986	0.01399	0.02347	0.03925	0.07046	0.14636	0.15217	0.06436	0.09449
$a = 0.80$	0.04072	0.05834	0.08991	0.13011	0.19304	0.31979	0.33871	0.16354	0.21953
$a = 0.90$	0.08708	0.12539	0.18497	0.24834	0.33389	0.49058	0.51724	0.28150	0.35857
$a = 0.95$	0.13157	0.18999	0.27417	0.35418	0.45222	0.62276	0.65217	0.38311	0.47396
$a = 0.99$	0.18825	0.27250	0.38643	0.48372	0.59147	0.77037	0.80008	0.50478	0.60893
$a = 1.00$	0.20703	0.29989	0.42343	0.52581	0.63581	0.81605	0.84536	0.54389	0.65178
$b = 4.00$									
	$\mu_0 = 1.0$								
ZERO ORDER	0.0	0.0	0.0	0.0	0.0	0.0	PEAK	0.00916	0.01832
FIRST ORDER	0.00103	0.00133	0.00244	0.00537	0.01492	0.07338	0.51284	0.02861	0.05053
SECOND ORDER	0.00456	0.00618	0.01136	0.02283	0.05033	0.13827	0.29439	0.04938	0.07796
THIRD ORDER	0.01055	0.01469	0.02571	0.04497	0.07839	0.14296	0.20458	0.06255	0.08921
SUMS									
$a = 0.20$	0.00051	0.00068	0.00123	0.00247	0.00579	0.02157	0.11624	0.01748	0.03242
$a = 0.40$	0.00261	0.00359	0.00619	0.01116	0.02235	0.06493	0.27028	0.03510	0.05998
$a = 0.60$	0.01062	0.01486	0.02411	0.03867	0.06621	0.15217	0.48866	0.07540	0.11769
$a = 0.80$	0.04236	0.06016	0.09074	0.12825	0.18651	0.33871	0.83155	0.18016	0.25356
$a = 0.90$	0.08869	0.12683	0.18409	0.24313	0.32356	0.51724	1.09786	0.29975	0.39732
$a = 0.95$	0.13236	0.19000	0.27049	0.34485	0.43754	0.65217	1.27803	0.40039	0.51333
$a = 0.99$	0.18730	0.26976	0.37816	0.46834	0.57060	0.80008	1.46161	0.51907	0.64651
$a = 1.00$	0.20539	0.29606	0.41346	0.50828	0.61276	0.84536	1.51553	0.55690	0.68836
$b = 4.0$ NARROW SURFACE LAYER AT TOP									
ZERO ORDER	0.0	0.00000	0.00000	0.00034	0.00236	0.00652	0.00916	0.00189	0.00320
FIRST ORDER	0.00030	0.00042	0.00101	0.00365	0.01109	0.02245	0.02861	0.00782	0.01235
SECOND ORDER	0.00153	0.00220	0.00481	0.01191	0.02540	0.04171	0.04938	0.01732	0.02558
THIRD ORDER	0.00410	0.00591	0.01171	0.02322	0.03974	0.05598	0.06255	0.02739	0.03796
SUMS									
$a = 0.20$	0.00017	0.00024	0.00053	0.00180	0.00601	0.01325	0.01748	0.00444	0.00709
$a = 0.40$	0.00103	0.00148	0.00291	0.00672	0.01548	0.02825	0.03510	0.01107	0.01660
$a = 0.60$	0.00501	0.00724	0.01284	0.02345	0.04178	0.06436	0.07540	0.03008	0.04198
$a = 0.80$	0.02480	0.03599	0.05743	0.08664	0.12482	0.16354	0.18016	0.09375	0.12051
$a = 0.90$	0.05908	0.08594	0.13013	0.17940	0.23368	0.28150	0.29975	0.18192	0.22303
$a = 0.95$	0.09483	0.13814	0.20375	0.26862	0.33252	0.38311	0.40039	0.26469	0.31620
$a = 0.99$	0.14298	0.20854	0.30125	0.38315	0.45495	0.50478	0.51907	0.36951	0.43180
$a = 1.00$	0.15943	0.23261	0.33427	0.42133	0.49502	0.54389	0.55690	0.40423	0.46967
$b = 4.0$ LAMBERT SURFACE ON TOP									
ZERO ORDER	0.0	0.00000	0.00000	0.00034	0.00330	0.01174	0.01832	0.00320	0.00552
FIRST ORDER	0.00048	0.00067	0.00155	0.00511	0.01620	0.03705	0.05053	0.01235	0.01975
SECOND ORDER	0.00237	0.00337	0.00714	0.01688	0.03618	0.06316	0.07796	0.02558	0.03799
THIRD ORDER	0.00603	0.00865	0.01668	0.03185	0.05392	0.07800	0.08921	0.03796	0.05253
SUMS									
$a = 0.20$	0.00026	0.00037	0.00079	0.00238	0.00854	0.02246	0.03242	0.00709	0.01153
$a = 0.40$	0.00149	0.00214	0.00412	0.00906	0.02161	0.04476	0.05998	0.01660	0.02529
$a = 0.60$	0.00684	0.00983	0.01719	0.03069	0.05592	0.09449	0.11769	0.04198	0.05944
$a = 0.80$	0.03138	0.04539	0.07179	0.10718	0.15697	0.21953	0.25356	0.12051	0.15673
$a = 0.90$	0.07155	0.10381	0.15614	0.21389	0.28240	0.35857	0.39732	0.22303	0.27618
$a = 0.95$	0.11210	0.16294	0.23902	0.31360	0.39287	0.47396	0.51333	0.31620	0.38114
$a = 0.99$	0.16558	0.24105	0.34662	0.43922	0.52707	0.60893	0.64651	0.43180	0.50863
$a = 1.00$	0.18364	0.26746	0.38268	0.48069	0.57055	0.65178	0.68836	0.46967	0.54994

TABLE 35 (continued)  
 $g = 0.75, b = 8$ , Reflection

VECTOR	$\mu=0.0$	$\mu=0.1$	$\mu=0.3$	$\mu=0.5$	$\mu=0.7$	$\mu=0.9$	$\mu=1.0$	AVERAGE N	FLUX U
<b>b = 8.00</b> <span style="margin-left: 100px;"><math>\mu_0 = 0.1</math></span>									
FIRST ORDER	5.87169	2.23714	0.58248	0.21991	0.10429	0.05742	0.04437	0.72518	0.24069
SECOND ORDER	0.74008	0.80818	0.32662	0.14400	0.07258	0.04099	0.03189	0.27776	0.13102
THIRD ORDER	0.24644	0.32226	0.17813	0.09183	0.05065	0.03022	0.02398	0.13198	0.07618
SUMS $\alpha = 0.20$	1.20610	0.48260	0.13118	0.05060	0.02424	0.01341	0.01038	0.15734	0.05408
$\alpha = 0.40$	2.48627	1.04969	0.30036	0.11922	0.05804	0.03242	0.02518	0.34559	0.12396
$\alpha = 0.60$	3.86294	1.73217	0.52874	0.21890	0.10966	0.06249	0.04890	0.58025	0.22017
$\alpha = 0.80$	5.37739	2.58883	0.86532	0.38549	0.20531	0.12318	0.09858	0.89869	0.37226
$\alpha = 0.90$	6.21609	3.12595	1.11887	0.53353	0.30380	0.19414	0.16002	1.12719	0.50424
$\alpha = 0.95$	6.67192	3.44542	1.29567	0.65339	0.39460	0.26697	0.22603	1.28621	0.61240
$\alpha = 0.99$	7.07159	3.75110	1.49508	0.80940	0.52693	0.38270	0.33463	1.47015	0.75729
$\alpha = 1.00$	7.18061	3.84070	1.56143	0.86649	0.57870	0.43014	0.37997	1.53304	0.81155
<b>b = 8.00</b> <span style="margin-left: 100px;"><math>\mu_0 = 0.3</math></span>									
FIRST ORDER	1.07503	0.58248	0.22172	0.10635	0.05920	0.03648	0.02947	0.21208	0.09780
SECOND ORDER	0.19167	0.32662	0.19639	0.10707	0.06186	0.03831	0.03087	0.14218	0.08768
THIRD ORDER	0.10809	0.17813	0.14388	0.09055	0.05622	0.03609	0.02938	0.09887	0.07057
SUMS $\alpha = 0.20$	0.22366	0.13118	0.05354	0.02642	0.01486	0.00918	0.00742	0.04903	0.02374
$\alpha = 0.40$	0.46995	0.30036	0.13300	0.06819	0.03907	0.02434	0.01970	0.11653	0.05978
$\alpha = 0.60$	0.75221	0.52874	0.25850	0.14007	0.08293	0.05272	0.04296	0.21702	0.11977
$\alpha = 0.80$	1.10201	0.86532	0.48235	0.28581	0.18096	0.12116	0.10090	0.39133	0.23986
$\alpha = 0.90$	1.33176	1.11887	0.68453	0.43780	0.29650	0.21078	0.18038	0.55300	0.36831
$\alpha = 0.95$	1.47965	1.29567	0.84536	0.57340	0.41046	0.30711	0.26909	0.68885	0.48785
$\alpha = 0.99$	1.63691	1.49508	1.04855	0.76260	0.58332	0.46353	0.41735	0.87196	0.66236
$\alpha = 1.00$	1.68739	1.56143	1.12126	0.83450	0.65223	0.52822	0.47958	0.94048	0.73062
<b>b = 8.00</b> <span style="margin-left: 100px;"><math>\mu_0 = 0.5</math></span>									
FIRST ORDER	0.34316	0.21991	0.10635	0.05977	0.03717	0.02484	0.02074	0.09215	0.05178
SECOND ORDER	0.07539	0.14400	0.10707	0.06776	0.04368	0.02936	0.02446	0.07646	0.05438
THIRD ORDER	0.05238	0.09183	0.09055	0.06564	0.04519	0.03134	0.02631	0.06383	0.05130
SUMS $\alpha = 0.20$	0.07214	0.05060	0.02642	0.01530	0.00963	0.00645	0.00539	0.02210	0.01303
$\alpha = 0.40$	0.15413	0.11922	0.06819	0.04125	0.02650	0.01794	0.01501	0.05524	0.03452
$\alpha = 0.60$	0.25397	0.21890	0.14007	0.09021	0.06018	0.04167	0.03513	0.11067	0.07448
$\alpha = 0.80$	0.39460	0.38549	0.28581	0.20324	0.14584	0.10671	0.09201	0.22506	0.16802
$\alpha = 0.90$	0.50649	0.53353	0.43780	0.33715	0.25881	0.20070	0.17758	0.35227	0.28400
$\alpha = 0.95$	0.59284	0.65339	0.57340	0.46772	0.37802	0.30691	0.27725	0.47373	0.40257
$\alpha = 0.99$	0.70246	0.80940	0.76260	0.66273	0.56718	0.48438	0.44757	0.65401	0.58726
$\alpha = 1.00$	0.74214	0.86649	0.83450	0.73967	0.64427	0.55868	0.51971	0.72509	0.66191
<b>b = 8.00</b> <span style="margin-left: 100px;"><math>\mu_0 = 0.7</math></span>									
FIRST ORDER	0.14589	0.10429	0.05920	0.03717	0.02505	0.01780	0.01524	0.04950	0.03165
SECOND ORDER	0.03740	0.07258	0.06186	0.04368	0.03066	0.02202	0.01886	0.04521	0.03531
THIRD ORDER	0.02863	0.05065	0.05622	0.04519	0.03379	0.02503	0.02161	0.04161	0.03613
SUMS $\alpha = 0.20$	0.03095	0.02424	0.01486	0.00963	0.00658	0.00469	0.00402	0.01212	0.00810
$\alpha = 0.40$	0.06709	0.05804	0.03907	0.02650	0.01853	0.01339	0.01150	0.03122	0.02207
$\alpha = 0.60$	0.11349	0.10966	0.08293	0.06018	0.04389	0.03254	0.02821	0.06577	0.04993
$\alpha = 0.80$	0.18710	0.20531	0.18096	0.14584	0.11495	0.09037	0.08025	0.14681	0.12307
$\alpha = 0.90$	0.25689	0.30380	0.29650	0.25881	0.21804	0.18133	0.16504	0.25032	0.22488
$\alpha = 0.95$	0.31960	0.39460	0.41046	0.37802	0.33374	0.28911	0.26797	0.35916	0.33716
$\alpha = 0.99$	0.41022	0.52693	0.58332	0.56718	0.52534	0.47446	0.44796	0.53250	0.52147
$\alpha = 1.00$	0.44560	0.57870	0.65223	0.64427	0.60512	0.55308	0.52493	0.60339	0.59793

TABLE 35 (continued)  
 $g = 0.75, b = 8$ , Transmission

VECTOR	$\mu = 0.0$	$\mu = 0.1$	$\mu = 0.3$	$\mu = 0.5$	$\mu = 0.7$	$\mu = 0.9$	$\mu = 1.0$	AVERAGE N	FLUX U
$b = 8.00$									
ZERO ORDER	$\mu_0 = 0.0$	PEAK	0.0	0.0	0.0	0.0	0.0	0.00000	0.00000
FIRST ORDER	0.00000	0.00000	0.00000	0.00000	0.00000	0.00001	0.00002	0.00000	0.00001
SECOND ORDER	0.00000	0.00000	0.00000	0.00000	0.00003	0.00011	0.00017	0.00003	0.00005
THIRD ORDER	0.00000	0.00001	0.00001	0.00004	0.00013	0.00041	0.00063	0.00012	0.00020
SUMS $a = 0.20$	0.00000	0.00000	0.00000	0.00000	0.00000	0.00001	0.00002	0.00000	0.00001
$a = 0.40$	0.00000	0.00001	0.00001	0.00002	0.00006	0.00013	0.00019	0.00005	0.00007
$a = 0.60$	0.00008	0.00011	0.00020	0.00034	0.00063	0.00117	0.00152	0.00050	0.00071
$a = 0.80$	0.00158	0.00228	0.00358	0.00532	0.00785	0.01142	0.01351	0.00611	0.00801
$a = 0.90$	0.00822	0.01192	0.01788	0.02443	0.03242	0.04200	0.04714	0.02575	0.03201
$a = 0.95$	0.02089	0.03035	0.04445	0.05825	0.07321	0.08934	0.09741	0.05908	0.07137
$a = 0.99$	0.04932	0.07178	0.10316	0.13066	0.15704	0.18226	0.19381	0.12875	0.15180
$a = 1.00$	0.06285	0.09152	0.13090	0.16438	0.19534	0.22377	0.23639	0.16085	0.18845
$b = 8.00$									
ZERO ORDER	$\mu_0 = 0.3$	0.0	PEAK	0.0	0.0	0.0	0.0	0.00000	0.00000
FIRST ORDER	0.00000	0.00000	0.00000	0.00000	0.00001	0.00003	0.00004	0.00001	0.00001
SECOND ORDER	0.00000	0.00000	0.00000	0.00001	0.00006	0.00021	0.00032	0.00006	0.00010
THIRD ORDER	0.00001	0.00001	0.00003	0.00008	0.00028	0.00080	0.00118	0.00025	0.00040
SUMS $a = 0.20$	0.00000	0.00000	0.00000	0.00000	0.00001	0.00003	0.00004	0.00001	0.00001
$a = 0.40$	0.00001	0.00001	0.00002	0.00004	0.00011	0.00025	0.00034	0.00009	0.00013
$a = 0.60$	0.00014	0.00020	0.00034	0.00059	0.00110	0.00199	0.00256	0.00085	0.00122
$a = 0.80$	0.00248	0.00358	0.00564	0.00838	0.01237	0.01787	0.02101	0.00960	0.01256
$a = 0.90$	0.01233	0.01788	0.02683	0.03668	0.04865	0.06282	0.07024	0.03860	0.04794
$a = 0.95$	0.03060	0.04445	0.06513	0.08536	0.10726	0.13058	0.14202	0.08649	0.10444
$a = 0.99$	0.07087	0.10316	0.14827	0.18782	0.22570	0.26153	0.27765	0.18496	0.21801
$a = 1.00$	0.08989	0.13090	0.18725	0.23516	0.27940	0.31963	0.33716	0.22999	0.26938
$b = 8.00$									
ZERO ORDER	$\mu_0 = 0.5$	0.0	0.0	PEAK	0.0	0.0	0.0	0.00000	0.00000
FIRST ORDER	0.00000	0.00000	0.00000	0.00000	0.00003	0.00007	0.00010	0.00002	0.00004
SECOND ORDER	0.00000	0.00000	0.00001	0.00004	0.00018	0.00051	0.00072	0.00015	0.00025
THIRD ORDER	0.00003	0.00004	0.00008	0.00022	0.00069	0.00175	0.00245	0.00057	0.00091
SUMS $a = 0.20$	0.00000	0.00000	0.00000	0.00001	0.00002	0.00006	0.00008	0.00002	0.00003
$a = 0.40$	0.00002	0.00002	0.00004	0.00009	0.00023	0.00049	0.00066	0.00018	0.00027
$a = 0.60$	0.00024	0.00034	0.00059	0.00105	0.00193	0.00342	0.00432	0.00148	0.00211
$a = 0.80$	0.00368	0.00532	0.00838	0.01245	0.01837	0.02634	0.03076	0.01422	0.01857
$a = 0.90$	0.01685	0.02443	0.03668	0.05015	0.06650	0.08556	0.09532	0.05269	0.06541
$a = 0.95$	0.04009	0.05825	0.08536	0.11190	0.14056	0.17075	0.18528	0.11327	0.13673
$a = 0.99$	0.08976	0.13066	0.18782	0.23794	0.28588	0.33081	0.35068	0.23418	0.27596
$a = 1.00$	0.11287	0.16438	0.23516	0.29535	0.35086	0.40090	0.42235	0.28872	0.33809
$b = 8.00$									
ZERO ORDER	$\mu_0 = 0.7$	0.0	0.0	0.0	PEAK	0.0	0.0	0.00001	0.00001
FIRST ORDER	0.00000	0.00000	0.00001	0.00003	0.00016	0.00032	0.00032	0.00010	0.00017
SECOND ORDER	0.00002	0.00003	0.00006	0.00018	0.00062	0.00158	0.00202	0.00050	0.00081
THIRD ORDER	0.00009	0.00013	0.00028	0.00069	0.00184	0.00425	0.00577	0.00146	0.00229
SUMS $a = 0.20$	0.00000	0.00000	0.00001	0.00002	0.00008	0.00018	0.00022	0.00007	0.00011
$a = 0.40$	0.00004	0.00006	0.00011	0.00023	0.00056	0.00114	0.00144	0.00043	0.00065
$a = 0.60$	0.00044	0.00063	0.00110	0.00193	0.00359	0.00626	0.00775	0.00273	0.00389
$a = 0.80$	0.00544	0.00785	0.01237	0.01837	0.02715	0.03896	0.04535	0.02101	0.02745
$a = 0.90$	0.02236	0.03242	0.04865	0.06650	0.08826	0.11379	0.12678	0.06997	0.08689
$a = 0.95$	0.05039	0.07321	0.10726	0.14056	0.17668	0.21507	0.23352	0.14245	0.17201
$a = 0.99$	0.10790	0.15704	0.22570	0.28588	0.34366	0.39833	0.42261	0.28161	0.33196
$a = 1.00$	0.13414	0.19534	0.27940	0.35086	0.41700	0.47721	0.50316	0.34325	0.40208

TABLE 35 (continued)  
 $g = 0.75$ ,  $b = 8$ , Reflection

VECTOR	$\mu = 0.0$	$\mu = 0.1$	$\mu = 0.3$	$\mu = 0.5$	$\mu = 0.7$	$\mu = 0.9$	$\mu = 1.0$	AVERAGE N	FLUX U
<b>b = 8.00</b>									
	$\mu_0 = 0.9$								
FIRST ORDER	0.07457	0.05742	0.03648	0.02484	0.01780	0.01326	0.01158	0.03027	0.02115
SECOND ORDER	0.02146	0.04099	0.03831	0.02936	0.02202	0.01669	0.01462	0.02896	0.02414
THIRD ORDER	0.01726	0.03022	0.03609	0.03134	0.02503	0.01958	0.01731	0.02813	0.02578
SUMS									
a = 0.20	0.01594	0.01341	0.00918	0.00645	0.00469	0.00352	0.00308	0.00749	0.00545
a = 0.40	0.03497	0.03242	0.02434	0.01794	0.01339	0.01018	0.00894	0.01966	0.01509
a = 0.60	0.06049	0.06249	0.05272	0.04167	0.03254	0.02548	0.02261	0.04285	0.03521
a = 0.80	0.10525	0.12318	0.12116	0.10671	0.09037	0.07529	0.06853	0.10281	0.09284
a = 0.90	0.15441	0.19414	0.21078	0.20070	0.18133	0.15946	0.14859	0.18825	0.18093
a = 0.95	0.20417	0.26697	0.30711	0.30691	0.28911	0.26351	0.24944	0.28518	0.28431
a = 0.99	0.28304	0.38270	0.46353	0.48438	0.47446	0.44722	0.42963	0.44814	0.46141
a = 1.00	0.31538	0.43014	0.52822	0.55868	0.55308	0.52609	0.50741	0.51661	0.53643
<b>b = 8.00</b>									
	$\mu_0 = 1.0$								
FIRST ORDER	0.05600	0.04437	0.02947	0.02074	0.01524	0.01158	0.01020	0.02448	0.01770
SECOND ORDER	0.01690	0.03189	0.03087	0.02446	0.01886	0.01462	0.01293	0.02374	0.02031
THIRD ORDER	0.01380	0.02398	0.02938	0.02631	0.02161	0.01731	0.01546	0.02347	0.02197
SUMS									
a = 0.20	0.01201	0.01038	0.00742	0.00539	0.00402	0.00308	0.00272	0.00608	0.00457
a = 0.40	0.02649	0.02518	0.01970	0.01501	0.01150	0.00894	0.00793	0.01606	0.01271
a = 0.60	0.04625	0.04890	0.04296	0.03513	0.02821	0.02261	0.02028	0.03545	0.03001
a = 0.80	0.08246	0.09858	0.10090	0.09201	0.08025	0.06853	0.06306	0.08760	0.08132
a = 0.90	0.12482	0.16002	0.18038	0.17758	0.16504	0.14859	0.13987	0.16544	0.16297
a = 0.95	0.16984	0.22603	0.26909	0.27725	0.26797	0.24944	0.23824	0.25662	0.26138
a = 0.99	0.24384	0.33463	0.41735	0.44757	0.44796	0.42963	0.41574	0.41338	0.43305
a = 1.00	0.27475	0.37997	0.47958	0.51971	0.52493	0.50741	0.49270	0.47998	0.50641
<b>b = 8.0</b> NARROW SURFACE LAYER AT TOP									
FIRST ORDER	INFINITE	0.72518	0.21208	0.09215	0.04950	0.03027	0.02448	0.26706	0.09408
SECOND ORDER	0.13353	0.27776	0.14218	0.07646	0.04521	0.02896	0.02374	0.11406	0.06519
THIRD ORDER	0.09177	0.13198	0.09887	0.06383	0.04161	0.02813	0.02347	0.07169	0.05115
SUMS									
a = 0.20	INFINITE	0.15734	0.04903	0.02210	0.01212	0.00749	0.00608	0.05865	0.02192
a = 0.40	INFINITE	0.34559	0.11653	0.05524	0.03122	0.01966	0.01606	0.13163	0.05299
a = 0.60	INFINITE	0.58025	0.21702	0.11067	0.06577	0.04285	0.03545	0.23002	0.10243
a = 0.80	INFINITE	0.89869	0.39133	0.22506	0.14681	0.10281	0.08760	0.38784	0.20183
a = 0.90	INFINITE	1.12719	0.55300	0.35227	0.25032	0.18825	0.16544	0.53270	0.31469
a = 0.95	INFINITE	1.28621	0.68885	0.47373	0.35916	0.28518	0.25662	0.65860	0.42656
a = 0.99	INFINITE	1.47015	0.87196	0.65401	0.53250	0.44814	0.41338	0.83613	0.59886
a = 1.00	INFINITE	1.53304	0.94048	0.72509	0.60339	0.51661	0.47998	0.90459	0.66828
<b>b = 8.0</b> LAMBERT SURFACE ON TOP									
FIRST ORDER	0.50000	0.24069	0.09780	0.05178	0.03165	0.02115	0.01770	0.09408	0.04696
SECOND ORDER	0.08230	0.13102	0.08768	0.05438	0.03531	0.02414	0.02031	0.06519	0.04464
THIRD ORDER	0.04627	0.07618	0.07057	0.05130	0.03613	0.02578	0.02197	0.05115	0.04091
SUMS									
a = 0.20	0.10372	0.05408	0.02374	0.01303	0.00801	0.00545	0.00457	0.02192	0.01158
a = 0.40	0.21730	0.12396	0.05978	0.03452	0.02207	0.01509	0.01271	0.05299	0.03004
a = 0.60	0.34737	0.22017	0.11977	0.07448	0.04993	0.03521	0.03001	0.10243	0.06369
a = 0.80	0.51312	0.37226	0.23986	0.16802	0.12307	0.09284	0.08132	0.20183	0.14353
a = 0.90	0.63272	0.50424	0.36831	0.28400	0.22488	0.18093	0.16297	0.31469	0.24727
a = 0.95	0.72078	0.61240	0.48785	0.40257	0.33716	0.28431	0.26138	0.42656	0.35815
a = 0.99	0.83078	0.75729	0.66236	0.58726	0.52147	0.46141	0.43305	0.59886	0.53715
a = 1.00	0.87055	0.81155	0.73062	0.66191	0.59793	0.53643	0.50641	0.66828	0.61089

TABLE 35 (continued)  
 $g = 0.75, b = 8$ , Transmission

VECTOR	$\mu = 0.0$	$\mu = 0.1$	$\mu = 0.3$	$\mu = 0.5$	$\mu = 0.7$	$\mu = 0.9$	$\mu = 1.0$	AVERAGE N	FLUX U
<b>b = 8.00</b>									
	$\mu_0 = 0.9$								
ZERO ORDER	0.0	0.0	0.0	0.0	0.0	PEAK	0.0	0.00008	0.00014
FIRST ORDER	0.00001	0.00001	0.00003	0.00007	0.00032	0.00211	0.00221	0.00048	0.00083
SECOND ORDER	0.00008	0.00011	0.00021	0.00051	0.00158	0.00521	0.00798	0.00157	0.00257
THIRD ORDER	0.00029	0.00041	0.00080	0.00175	0.00425	0.01034	0.01529	0.00360	0.00561
SUMS									
$a = 0.20$	0.00001	0.00001	0.00003	0.00006	0.00018	0.00075	0.00093	0.00028	0.00047
$a = 0.40$	0.00009	0.00013	0.00025	0.00049	0.00114	0.00319	0.00424	0.00112	0.00177
$a = 0.60$	0.00082	0.00117	0.00199	0.00342	0.00626	0.01265	0.01651	0.00522	0.00757
$a = 0.80$	0.00792	0.01142	0.01787	0.02634	0.03896	0.05950	0.07191	0.03103	0.04094
$a = 0.90$	0.02901	0.04200	0.06282	0.08556	0.11379	0.15214	0.17407	0.09146	0.11429
$a = 0.95$	0.06156	0.08934	0.13058	0.17075	0.21507	0.26858	0.29763	0.17490	0.21215
$a = 0.99$	0.12530	0.18226	0.26153	0.33081	0.39833	0.46991	0.50608	0.32817	0.38806
$a = 1.00$	0.15375	0.22377	0.31963	0.40090	0.47721	0.55473	0.59286	0.39464	0.46357
<b>b = 8.00</b>									
	$\mu_0 = 1.0$								
ZERO ORDER	0.0	0.0	0.0	0.0	0.0	0.0	PEAK	0.00017	0.00034
FIRST ORDER	0.00002	0.00002	0.00004	0.00010	0.00032	0.00221	0.01879	0.00088	0.00160
SECOND ORDER	0.00013	0.00017	0.00032	0.00072	0.00202	0.00798	0.02063	0.00254	0.00427
THIRD ORDER	0.00046	0.00063	0.00118	0.00245	0.00577	0.01529	0.02644	0.00530	0.00833
SUMS									
$a = 0.20$	0.00002	0.00002	0.00004	0.00008	0.00022	0.00093	0.00486	0.00051	0.00092
$a = 0.40$	0.00014	0.00019	0.00034	0.00066	0.00144	0.00424	0.01398	0.00175	0.00288
$a = 0.60$	0.00108	0.00152	0.00256	0.00432	0.00775	0.01651	0.03587	0.00710	0.01057
$a = 0.80$	0.00940	0.01351	0.02101	0.03076	0.04535	0.07191	0.10960	0.03739	0.04996
$a = 0.90$	0.03261	0.04714	0.07024	0.09532	0.12678	0.17407	0.22768	0.10371	0.13061
$a = 0.95$	0.06719	0.09741	0.14202	0.18528	0.23352	0.29763	0.36195	0.19207	0.23430
$a = 0.99$	0.13334	0.19381	0.27765	0.35068	0.42261	0.50608	0.58052	0.35068	0.41634
$a = 1.00$	0.16253	0.23639	0.33716	0.42235	0.50316	0.59286	0.67002	0.41869	0.49358
<b>b = 8.0</b> NARROW SURFACE LAYER AT TOP									
ZERO ORDER	0.0	0.00000	0.00000	0.00000	0.00001	0.00008	0.00017	0.00002	0.00003
FIRST ORDER	0.00000	0.00000	0.00001	0.00002	0.00010	0.00048	0.00088	0.00013	0.00023
SECOND ORDER	0.00002	0.00003	0.00006	0.00015	0.00050	0.00157	0.00254	0.00048	0.00079
THIRD ORDER	0.00009	0.00012	0.00025	0.00057	0.00146	0.00360	0.00530	0.00123	0.00193
SUMS									
$a = 0.20$	0.00000	0.00000	0.00001	0.00002	0.00007	0.00028	0.00051	0.00008	0.00014
$a = 0.40$	0.00003	0.00005	0.00009	0.00018	0.00043	0.00112	0.00175	0.00038	0.00060
$a = 0.60$	0.00035	0.00050	0.00085	0.00148	0.00273	0.00522	0.00710	0.00219	0.00316
$a = 0.80$	0.00424	0.00611	0.00960	0.01422	0.02101	0.03103	0.03739	0.01648	0.02163
$a = 0.90$	0.01777	0.02575	0.03860	0.05269	0.06997	0.09146	0.10371	0.05576	0.06942
$a = 0.95$	0.04068	0.05908	0.08649	0.11327	0.14245	0.17490	0.19207	0.11520	0.13932
$a = 0.99$	0.08848	0.12875	0.18496	0.23418	0.28161	0.32817	0.35068	0.23117	0.27276
$a = 1.00$	0.11048	0.16085	0.22999	0.28872	0.34325	0.39464	0.41869	0.28295	0.33172
<b>b = 8.0</b> LAMBERT SURFACE ON TOP									
ZERO ORDER	0.0	0.00000	0.00000	0.00000	0.00001	0.00014	0.00034	0.00003	0.00006
FIRST ORDER	0.00000	0.00001	0.00001	0.00004	0.00017	0.00083	0.00160	0.00023	0.00039
SECOND ORDER	0.00004	0.00005	0.00010	0.00025	0.00081	0.00257	0.00427	0.00079	0.00130
THIRD ORDER	0.00015	0.00020	0.00040	0.00091	0.00229	0.00561	0.00833	0.00193	0.00303
SUMS									
$a = 0.20$	0.00000	0.00001	0.00001	0.00003	0.00011	0.00047	0.00092	0.00014	0.00023
$a = 0.40$	0.00005	0.00007	0.00013	0.00027	0.00065	0.00177	0.00288	0.00060	0.00095
$a = 0.60$	0.00050	0.00071	0.00122	0.00211	0.00389	0.00757	0.01057	0.00316	0.00456
$a = 0.80$	0.00555	0.00801	0.01256	0.01857	0.02745	0.04094	0.04996	0.02163	0.02844
$a = 0.90$	0.02209	0.03201	0.04794	0.06541	0.08689	0.11429	0.13061	0.06942	0.08652
$a = 0.95$	0.04915	0.07137	0.10444	0.13673	0.17201	0.21215	0.23430	0.13932	0.16863
$a = 0.99$	0.10433	0.15180	0.21801	0.27596	0.33196	0.38806	0.41634	0.27276	0.32202
$a = 1.00$	0.12945	0.18845	0.26938	0.33809	0.40208	0.46357	0.49358	0.33172	0.38911

TABLE 37  
Reflection and Transmission by Slabs of Finite Thickness with Conservative Scattering  
Reflection Function  $R(\mu, \mu_0)$ ,  $g = 0.25$

$\mu_0$	$\mu = 0.0$	0.100	0.300	0.500	0.700	0.900	1.000	N	FLUX
<b>b = 0.50000</b>									
0.1	3.16608	1.83933							
0.3	1.16609	0.99622	0.66820						
0.5	0.70361	0.65911	0.46947	0.33454					
0.7	0.48622	0.47538	0.34836	0.24977	0.18702				
0.9	0.35809	0.35978	0.26864	0.19348	0.14525	0.11306			
1.0	0.31193	0.31687	0.23847	0.17213	0.12939	0.10083	0.08998		
N		0.89584	0.55249	0.38110	0.28051	0.21532	0.19082	0.48193	
FLUX	0.67014	0.57906	0.40405	0.28661	0.21361	0.16535	0.14707	0.33074	0.24601
<b>b = 1.00000</b>									
0.1	3.20721	1.89426							
0.3	1.23435	1.08746	0.81981						
0.5	0.77650	0.75637	0.63091	0.50694					
0.7	0.55367	0.56529	0.49749	0.40930	0.33481				
0.9	0.41803	0.43961	0.40097	0.33523	0.27669	0.23007			
1.0	0.36814	0.39171	0.36250	0.30506	0.25272	0.21066	0.19309		
N		0.97838	0.68948	0.52740	0.41590	0.33564	0.30367	0.60609	
FLUX	0.73500	0.66555	0.54754	0.44001	0.35568	0.29167	0.26558	0.46093	0.38259
<b>b = 2.00000</b>									
0.1	3.24678	1.94449							
0.3	1.29053	1.15877	0.92119						
0.5	0.84646	0.84517	0.75708	0.66399					
0.7	0.62920	0.66115	0.63354	0.57873	0.51783				
0.9	0.49360	0.53551	0.53691	0.50461	0.45989	0.41367			
1.0	0.44255	0.48614	0.49627	0.47178	0.43313	0.39158	0.37140		
N		1.05857	0.80333	0.66917	0.56898	0.48881	0.45449	0.73414	
FLUX	0.80576	0.75536	0.67498	0.59872	0.52714	0.46331	0.43462	0.60434	0.54321
<b>b = 4.00000</b>									
0.1	3.28247	1.98947							
0.3	1.33812	1.21875	1.00117						
0.5	0.90567	0.91980	0.85660	0.78783					
0.7	0.69861	0.74863	0.75018	0.72386	0.68794				
0.9	0.57039	0.63230	0.66596	0.66516	0.64809	0.62198			
1.0	0.52193	0.58619	0.62966	0.63771	0.62767	0.60695	0.59411		
N		1.13123	0.90020	0.78970	0.71027	0.64514	0.61609	0.85148	
FLUX	0.87206	0.83892	0.78640	0.73736	0.68963	0.64312	0.62050	0.73930	0.69845
<b>b = 8.00000</b>									
0.1	3.31011	2.02427							
0.3	1.37477	1.26491	1.06238						
0.5	0.95076	0.97657	0.93189	0.88044					
0.7	0.75190	0.81573	0.83918	0.83333	0.81735				
0.9	0.63157	0.70933	0.76811	0.79081	0.79662	0.79246			
1.0	0.58683	0.66789	0.73802	0.77099	0.78522	0.78779	0.78594		
N		1.18755	0.97490	0.88158	0.81887	0.76979	0.74831	0.94263	
FLUX	0.92379	0.90405	0.87278	0.84360	0.81523	0.78728	0.77341	0.84471	0.82035

TABLE 37 (continued)  
Transmission Function  $T(\mu, \mu_0)$ ,  $g = 0.25$

$\mu_0$	$\mu = 0.0$	0.100	0.300	0.500	0.700	0.900	1.000	N	FLUX
b = 0.50000									
0.1	0.23500	0.38444							
0.3	0.39705	0.54555	0.56762						
0.5	0.38378	0.48594	0.47222	0.39348					
0.7	0.33409	0.40749	0.38777	0.32876	0.28364				
0.9	0.28455	0.33944	0.32041	0.27741	0.24926	0.23329			
1.0	0.26220	0.31012	0.29194	0.25528	0.23443	0.22858	0.23123		
N	0.32719	0.46434	0.76970	0.75652	0.67889	0.60117	0.56610	0.65463	
FLUX	0.32986	0.42094	0.59595	0.71339	0.78639	0.83465	0.85293	0.66926	0.75399
b = 1.00000									
0.1	0.15322	0.19795							
0.3	0.23206	0.30773	0.43169						
0.5	0.27841	0.35787	0.45632	0.46336					
0.7	0.28237	0.35432	0.43128	0.43368	0.41051				
0.9	0.26734	0.32999	0.39137	0.39406	0.38144	0.36992			
1.0	0.25690	0.31505	0.37012	0.37339	0.36625	0.36586	0.37086		
N	0.24191	0.30892	0.46172	0.55477	0.57193	0.55507	0.54114	0.48905	
FLUX	0.26500	0.33445	0.45246	0.55999	0.64432	0.70833	0.73442	0.53907	0.61741
b = 2.00000									
0.1	0.10558	0.13333							
0.3	0.14224	0.18034	0.24713						
0.5	0.17906	0.22726	0.30767	0.37101					
0.7	0.20588	0.25971	0.34378	0.40444	0.43564				
0.9	0.21939	0.27474	0.35678	0.41353	0.44511	0.46175			
1.0	0.22206	0.27711	0.35699	0.41167	0.44415	0.46718	0.47918		
N	0.17007	0.21460	0.28856	0.36219	0.41776	0.44967	0.45831	0.34588	
FLUX	0.19424	0.24464	0.32502	0.40128	0.47286	0.53669	0.56538	0.39566	0.45679
b = 4.00000									
0.1	0.06843	0.08617							
0.3	0.09079	0.11435	0.15179						
0.5	0.11185	0.14090	0.18722	0.23099					
0.7	0.13229	0.16665	0.22130	0.27220	0.31885				
0.9	0.15083	0.18980	0.25124	0.30738	0.35791	0.40070			
1.0	0.15889	0.19978	0.26387	0.32189	0.37393	0.41908	0.43968		
N	0.11071	0.13941	0.18496	0.22778	0.26937	0.30753	0.32447	0.22557	
FLUX	0.12794	0.16108	0.21360	0.26264	0.31037	0.35688	0.37950	0.26070	0.30155
b = 8.00000									
0.1	0.04070	0.05124							
0.3	0.05397	0.06795	0.09010						
0.5	0.06634	0.08353	0.11076	0.13616					
0.7	0.07838	0.09869	0.13086	0.16088	0.19008				
0.9	0.09023	0.11361	0.15064	0.18517	0.21873	0.25159			
1.0	0.09608	0.12097	0.16038	0.19713	0.23280	0.26770	0.28484		
N	0.06587	0.08294	0.10997	0.13519	0.15973	0.18387	0.19581	0.13424	
FLUX	0.07621	0.09595	0.12722	0.15640	0.18477	0.21272	0.22659	0.15529	0.17965



TABLE 37 (continued)  
Reflection Function  $R(\mu, \mu_0, g = 0.50)$

$\mu_0$	$\mu = 0.0$	0.100	0.300	0.500	0.700	0.900	1.000	N	FLUX
<b>b = 0.06250</b>									
0.1	3.81750	1.35909							
0.3	1.13340	0.45640	0.14758						
0.5	0.55250	0.22763	0.07304	0.03650					
0.7	0.30933	0.13021	0.04228	0.02149	0.01288				
0.9	0.18782	0.08085	0.02678	0.01387	0.00847	0.00565			
1.0	0.14989	0.06523	0.02184	0.01142	0.00703	0.00473	0.00397		
N		0.51901	0.17005	0.08478	0.04882	0.03060	0.02482	0.20561	
FLUX	0.55138	0.21354	0.06972	0.03501	0.02056	0.01321	0.01085	0.08041	0.03334
<b>b = 0.12500</b>									
0.1	3.93617	1.88972							
0.3	1.19137	0.71977	0.27461						
0.5	0.58431	0.37214	0.14234	0.07460					
0.7	0.32864	0.21714	0.08434	0.04491	0.02749				
0.9	0.20035	0.13661	0.05416	0.02934	0.01825	0.01229			
1.0	0.16020	0.11077	0.04438	0.02425	0.01520	0.01031	0.00867		
N		0.71786	0.26706	0.13809	0.08127	0.05175	0.04223	0.27960	
FLUX	0.57859	0.33629	0.12927	0.06791	0.04082	0.02659	0.02194	0.12607	0.06166
<b>b = 0.25000</b>									
0.1	4.03058	2.20899							
0.3	1.26448	0.96633	0.46526						
0.5	0.62969	0.52442	0.26027	0.14809					
0.7	0.35806	0.31480	0.16064	0.09297	0.05926				
0.9	0.22030	0.20199	0.10582	0.06225	0.04024	0.02767			
1.0	0.17687	0.16503	0.08752	0.05189	0.03376	0.02335	0.01976		
N		0.88399	0.39589	0.21821	0.13336	0.08718	0.07188	0.36688	
FLUX	0.61527	0.45869	0.22459	0.12755	0.07992	0.05343	0.04450	0.19089	0.11006
<b>b = 0.50000</b>									
0.1	4.08707	2.32431							
0.3	1.34195	1.12211	0.67852						
0.5	0.68878	0.64194	0.42227	0.27220					
0.7	0.40086	0.39904	0.27747	0.18326	0.12549				
0.9	0.25150	0.26280	0.19061	0.12833	0.08908	0.06394			
1.0	0.20366	0.21704	0.16020	0.10876	0.07594	0.05478	0.04704		
N		0.98975	0.54122	0.32935	0.21405	0.14612	0.12257	0.46645	
FLUX	0.66184	0.55094	0.35201	0.22556	0.15148	0.10597	0.08980	0.27857	0.18758
<b>b = 1.00000</b>									
0.1	4.12625	2.37992							
0.3	1.40870	1.21698	0.84064						
0.5	0.75602	0.73715	0.58449	0.43578					
0.7	0.45842	0.48030	0.41550	0.32339	0.24628				
0.9	0.29845	0.32892	0.30263	0.24270	0.18819	0.14564			
1.0	0.24581	0.27632	0.26051	0.21142	0.16512	0.12846	0.11355		
N		1.06824	0.67488	0.46423	0.32971	0.24061	0.20743	0.57770	
FLUX	0.71781	0.63004	0.48649	0.36177	0.26866	0.20197	0.17611	0.39097	0.30133

TABLE 37 (continued)  
Transmission Function  $T(\mu, \mu_0)$ ,  $g = 0.50$

$\mu_0$	$\mu = 0.0$	0.100	0.300	0.500	0.700	0.900	1.000	N	FLUX
b = 0.06250									
0.1	2.19562	1.37472							
0.3	0.97054	0.53471	0.23616						
0.5	0.52057	0.28402	0.14069	0.09897					
0.7	0.30618	0.16479	0.08621	0.06987	0.06173				
0.9	0.19174	0.10117	0.05303	0.04552	0.04884	0.05813			
1.0	0.15476	0.08079	0.04189	0.03593	0.04026	0.06066	0.08974		
N	0.78127	3.20338	1.57891	1.01846	0.74429	0.58271	0.52476	1.34827	
FLUX	0.44862	0.78646	0.93028	0.96499	0.97944	0.98679	0.98915	0.91959	0.96666
b = 0.12500									
0.1	1.39414	1.64353							
0.3	0.88371	0.79685	0.41793						
0.5	0.51793	0.44779	0.25889	0.18716					
0.7	0.31924	0.26818	0.16230	0.13397	0.11882				
0.9	0.20618	0.16842	0.10177	0.08860	0.09462	0.11197			
1.0	0.16838	0.13573	0.08112	0.07053	0.07847	0.11677	0.17164		
N	0.61478	2.08674	1.44773	1.00352	0.75408	0.59759	0.53985	1.10859	
FLUX	0.42141	0.66371	0.87073	0.93209	0.95918	0.97341	0.97806	0.87393	0.93834
b = 0.25000									
0.1	0.65213	1.21535							
0.3	0.72066	0.90840	0.64093						
0.5	0.49455	0.57697	0.43063	0.33005					
0.7	0.33142	0.36992	0.28311	0.24369	0.21879				
0.9	0.22620	0.24367	0.18452	0.16612	0.17682	0.20745			
1.0	0.18870	0.20016	0.14965	0.13442	0.14842	0.21626	0.31398		
N	0.47287	1.05032	1.20490	0.95158	0.75569	0.61544	0.56052	0.89793	
FLUX	0.38473	0.54131	0.77541	0.87245	0.92008	0.94657	0.95550	0.80911	0.88994
b = 0.50000									
0.1	0.28455	0.49836							
0.3	0.48881	0.70111	0.74457						
0.5	0.43059	0.56778	0.58695	0.50407					
0.7	0.33164	0.41711	0.42506	0.39737	0.36809				
0.9	0.24842	0.30166	0.29877	0.28764	0.30723	0.35629			
1.0	0.21488	0.25715	0.25041	0.24003	0.26399	0.37144	0.52677		
N	0.35711	0.52802	0.86069	0.83266	0.72977	0.62777	0.58221	0.71557	
FLUX	0.33816	0.44906	0.64799	0.77444	0.84852	0.89403	0.91020	0.72143	0.81242
b = 1.00000									
0.1	0.17317	0.23583							
0.3	0.27729	0.38615	0.55863						
0.5	0.32172	0.43163	0.57189	0.58912					
0.7	0.30170	0.39219	0.49481	0.52614	0.52063				
0.9	0.26006	0.32965	0.39886	0.42597	0.46394	0.53139			
1.0	0.23797	0.29845	0.35428	0.37524	0.41617	0.55487	0.75227		
N	0.26566	0.35396	0.53926	0.64165	0.64826	0.61176	0.58701	0.55701	
FLUX	0.28219	0.36996	0.51351	0.63823	0.73134	0.79803	0.82389	0.60903	0.69867

TABLE 37 (continued)  
Reflection Function  $R(\mu, \mu_0)$ ,  $g = 0.50$

$\mu_0$	$\mu = 0.0$	0.100	0.300	0.500	0.700	0.900	1.000	N	FLUX
b = 2.00000									
0.1	4.16226	2.42766							
0.3	1.46192	1.28754	0.94515						
0.5	0.82170	0.82422	0.71330	0.59465					
0.7	0.52659	0.57063	0.54878	0.48805	0.41750				
0.9	0.36303	0.41446	0.42854	0.39848	0.35068	0.30033			
1.0	0.30746	0.35797	0.38058	0.36006	0.32039	0.27648	0.25529		
N		1.14420	0.78706	0.60274	0.47357	0.37699	0.33768	0.69863	
FLUX	0.78111	0.71391	0.61026	0.51467	0.42764	0.35285	0.32030	0.52455	0.44896
b = 4.00000									
0.1	4.19644	2.47240							
0.3	1.50878	1.34889	1.02928						
0.5	0.88059	0.90132	0.81902	0.72753					
0.7	0.59518	0.66043	0.67191	0.64278	0.59772				
0.9	0.43741	0.51182	0.56201	0.56617	0.54610	0.51244			
1.0	0.38327	0.45720	0.51659	0.53092	0.51956	0.44278	0.47593		
N		1.21811	0.88840	0.73008	0.62190	0.53784	0.50162	0.82070	
FLUX	0.84605	0.79894	0.72683	0.66114	0.59828	0.53794	0.50897	0.66499	0.61053
b = 8.00000									
0.1	4.22580	2.51076							
0.3	1.54869	1.40102	1.10012						
0.5	0.93012	0.96602	0.90695	0.83666					
0.7	0.65391	0.73713	0.77616	0.77217	0.75113				
0.9	0.50471	0.59973	0.68149	0.71445	0.72191	0.71393			
1.0	0.45448	0.55022	0.64300	0.68781	0.70558	0.70598	0.70152		
N		1.28199	0.97521	0.83783	0.74965	0.68425	0.65654	0.92709	
FLUX	0.90288	0.87316	0.82770	0.78634	0.74673	0.70806	0.68897	0.78861	0.75417
b = 16.00000									
0.1	4.24707	2.53854							
0.3	1.57758	1.43876	1.15138						
0.5	0.96595	1.01281	0.97051	0.91548					
0.7	0.69638	0.79261	0.85151	0.86561	0.86190				
0.9	0.55367	0.66367	0.76834	0.82215	0.84958	0.86109			
1.0	0.50663	0.61833	0.73552	0.80254	0.84159	0.86274	0.86852		
N		1.32828	1.03810	0.91582	0.84210	0.79080	0.77005	1.00425	
FLUX	0.94410	0.92700	0.90083	0.87703	0.85423	0.83197	0.82098	0.87834	0.85852
b = 32.00000									
0.1	4.26032	2.55583							
0.3	1.59557	1.46225	1.18330						
0.5	0.98826	1.04194	1.01009	0.96455					
0.7	0.72282	0.82714	0.89842	0.92378	0.93085				
0.9	0.58414	0.70347	0.82241	0.88920	0.92907	0.95271			
1.0	0.53911	0.66074	0.79313	0.87398	0.92627	0.96036	0.97252		
N		1.35710	1.07725	0.96437	0.89965	0.85714	0.84073	1.05228	
FLUX	0.96977	0.96052	0.94637	0.93349	0.92116	0.90912	0.90317	0.93420	0.92348

TABLE 37 (continued)  
Transmission Function  $T(\mu, \mu_0)$ ,  $g = 0.50$

$\mu_0$	$\mu = 0.0$	0.100	0.300	0.500	0.700	0.900	1.000	N	FLUX
b = 2.00000									
0.1	0.11826	0.15550							
0.3	0.16496	0.21806	0.30982						
0.5	0.20980	0.27739	0.38774	0.47198					
0.7	0.23546	0.30840	0.41922	0.50309	0.55077				
0.9	0.23941	0.30989	0.40957	0.48369	0.54843	0.62441			
1.0	0.23553	0.30311	0.39541	0.46224	0.52675	0.65529	0.81971		
N	0.19299	0.25304	0.34979	0.44150	0.50524	0.53451	0.53862	0.41576	
FLUX	0.21889	0.28609	0.38974	0.46533	0.57236	0.64715	0.67970	0.47545	0.55104
b = 4.00000									
0.1	0.07984	0.10433							
0.3	0.10863	0.14199	0.19338						
0.5	0.13517	0.17675	0.24100	0.30034					
0.7	0.16015	0.20936	0.28509	0.35404	0.41622				
0.9	0.18106	0.23621	0.31992	0.39461	0.46397	0.53171			
1.0	0.18921	0.24646	0.33253	0.40838	0.47950	0.56311	0.63431		
N	0.13276	0.17344	0.23586	0.29313	0.34742	0.39531	0.41558	0.28862	
FLUX	0.15395	0.20106	0.27317	0.33886	0.40172	0.46206	0.49103	0.33501	0.38947
b = 8.00000									
0.1	0.05012	0.06545							
0.3	0.06808	0.08891	0.12079						
0.5	0.08443	0.11026	0.14979	0.18575					
0.7	0.10008	0.13071	0.17757	0.22021	0.26106				
0.9	0.11533	0.15061	0.20459	0.25368	0.30067	0.34648			
1.0	0.12278	0.16034	0.21775	0.26994	0.31988	0.36900	0.39451		
N	0.08352	0.10908	0.14817	0.18374	0.21782	0.25102	0.26731	0.18178	
FLUX	0.09712	0.12684	0.17230	0.21366	0.25327	0.29194	0.31103	0.21139	0.24583
b = 16.00000									
0.1	0.02884	0.03767							
0.3	0.03918	0.05117	0.06951						
0.5	0.04858	0.06345	0.08619	0.10688					
0.7	0.05759	0.07521	0.10217	0.12669	0.15018				
0.9	0.06638	0.08670	0.11777	0.14604	0.17312	0.19955			
1.0	0.07073	0.09237	0.12548	0.15560	0.18445	0.21261	0.22653		
N	0.04807	0.06277	0.08527	0.10574	0.12535	0.14449	0.15394	0.10462	
FLUX	0.05590	0.07300	0.09917	0.12297	0.14577	0.16803	0.17902	0.12166	0.14148
b = 32.00000									
0.1	0.01560	0.02037							
0.3	0.02119	0.02767	0.03759						
0.5	0.02628	0.03432	0.04662	0.05781					
0.7	0.03115	0.04068	0.05526	0.06852	0.08123				
0.9	0.03590	0.04689	0.06370	0.07899	0.09363	0.10793			
1.0	0.03825	0.04996	0.06787	0.08416	0.09976	0.11499	0.12252		
N	0.02600	0.03395	0.04612	0.05719	0.06780	0.07815	0.08326	0.05658	
FLUX	0.03023	0.03948	0.05364	0.06651	0.07884	0.09088	0.09683	0.06580	0.07652

TABLE 37 (continued)  
Reflection Function  $R(\mu, \mu_0)$ ,  $g = 0.75$

$\mu_0$	$\mu = 0.0$	0.100	0.300	0.500	0.700	0.900	1.000	N	FLUX
B = 0.50000									
0.1	7.04962	3.63732							
0.3	1.48304	1.24327	0.62109						
0.5	0.52266	0.52970	0.31012	0.16640					
0.7	0.23756	0.26352	0.16818	0.09463	0.05581				
0.9	0.12679	0.14707	0.09897	0.05772	0.03508	0.02263			
1.0	0.09672	0.11369	0.07800	0.04618	0.02844	0.01856	0.01531		
N		1.24284	0.49103	0.23010	0.12211	0.07143	0.05628	0.47409	
FLUX	0.67077	0.50777	0.26310	0.13666	0.07682	0.04669	0.03734	0.20864	0.11519
b = 1.00000									
0.1	7.09374	3.71179							
0.3	1.55622	1.36653	0.82557						
0.5	0.58311	0.63053	0.47794	0.30743					
0.7	0.27936	0.33272	0.28345	0.19344	0.12633				
0.9	0.15476	0.19311	0.17564	0.12452	0.08355	0.05649			
1.0	0.11967	0.15137	0.14070	0.10120	0.06868	0.04689	0.03909		
N		1.32540	0.62818	0.34482	0.20232	0.12562	0.10093	0.56759	
FLUX	0.71507	0.58148	0.38571	0.24048	0.15019	0.09672	0.07874	0.29310	0.19197
b = 2.00000									
0.1	7.12584	3.76049							
0.3	1.60784	1.44492	0.95195						
0.5	0.64177	0.71948	0.62087	0.47009					
0.7	0.33137	0.41144	0.40938	0.33784	0.25590				
0.9	0.19598	0.25540	0.27487	0.23903	0.18733	0.14042			
1.0	0.15564	0.20571	0.22710	0.20119	0.15969	0.12083	0.10438		
N		1.39638	0.74207	0.47474	0.31811	0.21782	0.18159	0.67153	
FLUX	0.76355	0.65489	0.50325	0.37502	0.27066	0.19306	0.16318	0.40091	0.30404
b = 4.00000									
0.1	7.15398	3.80188							
0.3	1.64920	1.50576	1.04142						
0.5	0.69409	0.79643	0.73403	0.61321					
0.7	0.38883	0.49594	0.53352	0.49489	0.42863				
0.9	0.25197	0.33771	0.39566	0.39186	0.35596	0.30582			
1.0	0.20914	0.28433	0.34243	0.34710	0.32097	0.27939	0.25658		
N		1.46527	0.84329	0.60278	0.45888	0.35520	0.31294	0.78627	
FLUX	0.81636	0.73254	0.61732	0.51932	0.42945	0.34822	0.31164	0.53033	0.45006
b = 8.00000									
0.1	7.18061	3.84070							
0.3	1.68739	1.56143	1.12126						
0.5	0.74214	0.86649	0.83450	0.73967					
0.7	0.44560	0.57870	0.65223	0.64427	0.60512				
0.9	0.31538	0.43014	0.52822	0.55868	0.55308	0.52609			
1.0	0.27475	0.37997	0.47958	0.51971	0.52493	0.50741	0.49270		
N		1.53304	0.94048	0.72509	0.60339	0.51661	0.47998	0.90459	
FLUX	0.87055	0.81155	0.73062	0.66191	0.59793	0.53643	0.50641	0.66828	0.61089

TABLE 37 (continued)  
Transmission Function  $T(\mu, \mu_0)$ ,  $g = 0.75$

$\mu_0$	$\mu=0.0$	0.100	0.300	0.500	0.700	0.900	1.000	N	FLUX
b = 0.50000									
0.1	0.47704	0.99117							
0.3	0.71613	1.16906	1.36125						
0.5	0.46234	0.66606	0.80619	0.83844					
0.7	0.26776	0.35848	0.38839	0.47058	0.60842				
0.9	0.15747	0.20150	0.19846	0.21074	0.31228	0.66144			
1.0	0.12265	0.15443	0.14642	0.14574	0.19173	0.47707	2.30405		
N	0.41650	0.70406	1.08938	0.96053	0.77290	0.62305	0.56368	0.82773	
FLUX	0.32923	0.49223	0.73690	0.86334	0.92318	0.95331	0.96266	0.79136	0.88481
b = 1.00000									
0.1	0.23497	0.37755							
0.3	0.40635	0.65518	1.01930						
0.5	0.38969	0.58483	0.84654	0.95734					
0.7	0.28624	0.40682	0.53013	0.65092	0.81176				
0.9	0.19404	0.26550	0.31933	0.35746	0.49329	0.93848			
1.0	0.15855	0.21380	0.24908	0.26663	0.33914	0.74080	3.06524		
N	0.30045	0.45578	0.72868	0.80986	0.74478	0.64312	0.59350	0.67300	
FLUX	0.28493	0.41852	0.61429	0.75952	0.84981	0.90328	0.92126	0.70690	0.80803
b = 2.00000									
0.1	0.14023	0.20957							
0.3	0.21433	0.32351	0.50648						
0.5	0.26602	0.39740	0.60045	0.74784					
0.7	0.26086	0.38002	0.54017	0.67850	0.81436				
0.9	0.22049	0.31347	0.42189	0.50364	0.64290	1.02124			
1.0	0.19633	0.27614	0.36297	0.42244	0.52095	0.92569	2.82478		
N	0.21915	0.32292	0.47775	0.60021	0.64786	0.63063	0.60791	0.53356	
FLUX	0.23645	0.34511	0.49675	0.62498	0.72934	0.80694	0.83682	0.59909	0.69596
b = 4.00000									
0.1	0.09282	0.13575							
0.3	0.13406	0.19628	0.28464						
0.5	0.16960	0.24849	0.36081	0.45766					
0.7	0.19665	0.28713	0.41309	0.52133	0.61688				
0.9	0.20703	0.29989	0.42343	0.52581	0.63581	0.81605			
1.0	0.20539	0.29606	0.41346	0.50828	0.61276	0.84536	1.51553		
N	0.15943	0.23261	0.33427	0.42133	0.49502	0.54389	0.55690	0.40423	
FLUX	0.18364	0.26746	0.38268	0.48069	0.57055	0.65178	0.68836	0.46967	0.54994
b = 8.00000									
0.1	0.06285	0.09152							
0.3	0.08989	0.13090	0.18725						
0.5	0.11287	0.16438	0.23516	0.29535					
0.7	0.13414	0.19534	0.27940	0.35086	0.41700				
0.9	0.15375	0.22377	0.31963	0.40090	0.47721	0.55473			
1.0	0.16253	0.23639	0.33716	0.42235	0.50316	0.59286	0.67002		
N	0.11048	0.16085	0.22999	0.28872	0.34325	0.39464	0.41869	0.28295	
FLUX	0.12945	0.18845	0.26938	0.33809	0.40208	0.46357	0.49358	0.33172	0.38911

TABLE 37 (continued)  
Reflection Function  $R(\mu, \mu_0)$ ,  $g = 0.875$

$\mu_0$	$\mu = 0.0$	0.100	0.300	0.500	0.700	0.900	1.000	N	FLUX
<b>b = 0.50000</b>									
0.1	10.49928	4.77568							
0.3	1.17261	1.14843	0.46644						
0.5	0.32720	0.38571	0.18700	0.08264					
0.7	0.13349	0.16686	0.08839	0.04189	0.02248				
0.9	0.06724	0.08603	0.04812	0.02404	0.01351	0.00843			
1.0	0.05033	0.06482	0.03700	0.01890	0.01082	0.00686	0.00563		
N		1.45391	0.38370	0.14122	0.06515	0.03525	0.02709	0.50298	
FLUX	0.69236	0.45550	0.17564	0.07305	0.03610	0.02048	0.01605	0.15607	0.06910
<b>b = 1.00000</b>									
0.1	10.56302	4.91099							
0.3	1.26034	1.33267	0.72238						
0.5	0.37934	0.49354	0.34053	0.17936					
0.7	0.16146	0.22405	0.17104	0.09613	0.05413				
0.9	0.08300	0.11799	0.09475	0.05569	0.03264	0.02037			
1.0	0.06250	0.08940	0.07298	0.04367	0.02603	0.01650	0.01346		
N		1.55669	0.52756	0.22954	0.11385	0.06335	0.04900	0.58490	
FLUX	0.72932	0.53202	0.28420	0.14158	0.07482	0.04329	0.03399	0.21876	0.11786
<b>b = 2.00000</b>									
0.1	10.59902	4.97755							
0.3	1.32009	1.44317	0.90591						
0.5	0.43327	0.59283	0.50529	0.33073					
0.7	0.19812	0.29127	0.28234	0.20069	0.12820				
0.9	0.10627	0.16051	0.16496	0.12284	0.08130	0.05309			
1.0	0.08106	0.12326	0.12883	0.09748	0.06545	0.04328	0.03550		
N		1.63326	0.65455	0.34598	0.19434	0.11517	0.09060	0.67461	
FLUX	0.76720	0.60163	0.39954	0.24860	0.14974	0.09206	0.07334	0.30120	0.19411
<b>b = 4.00000</b>									
0.1	10.62435	5.02191							
0.3	1.36016	1.51337	1.01705						
0.5	0.48102	0.67644	0.63752	0.48842					
0.7	0.24197	0.36792	0.40327	0.34562	0.26294				
0.9	0.14058	0.22042	0.25923	0.23633	0.18808	0.13884			
1.0	0.11047	0.17460	0.20951	0.19481	0.15751	0.11771	0.10030		
N		1.69972	0.75952	0.47144	0.31030	0.20655	0.16920	0.77472	
FLUX	0.80708	0.67138	0.50960	0.38040	0.27212	0.18898	0.15689	0.40661	0.30531
<b>b = 8.00000</b>									
0.1	10.64609	5.05915							
0.3	1.39300	1.56962	1.10203						
0.5	0.52254	0.74756	0.74495	0.62424					
0.7	0.28862	0.44782	0.52392	0.49817	0.43451				
0.9	0.18699	0.29988	0.37916	0.38798	0.35909	0.31013			
1.0	0.15494	0.25072	0.32435	0.34002	0.32150	0.28243	0.25899		
N		1.76415	0.85682	0.59446	0.44865	0.34445	0.30144	0.88629	
FLUX	0.84999	0.74485	0.62053	0.52065	0.42997	0.34651	0.30807	0.53390	0.45058

TABLE 37 (continued)  
Transmission Function  $T(\mu, \mu_0)$ ,  $g = 0.875$

$\mu_0$	$\mu = 0.0$	0.100	0.300	0.500	0.700	0.900	1.000	N	FLUX
b = 0.50000									
0.1	0.91118	2.32902							
0.3	0.92240	1.70760	2.55747						
0.5	0.39611	0.62176	0.82802	1.51560					
0.7	0.17433	0.25302	0.26303	0.40514	1.12284				
0.9	0.08662	0.12064	0.10780	0.11810	0.22071	1.24793			
1.0	0.06378	0.08766	0.07424	0.07251	0.10390	0.34762	9.76635		
N	0.49337	1.01174	1.36901	1.03816	0.77116	0.59983	0.53796	0.95172	
FLUX	0.30764	0.54450	0.82436	0.92695	0.96390	0.97952	0.98394	0.84393	0.93090
b = 1.00000									
0.1	0.37814	0.76555							
0.3	0.60984	1.16691	1.98696						
0.5	0.40664	0.69359	1.04657	1.66000					
0.7	0.21625	0.34423	0.43564	0.62819	1.42207				
0.9	0.11572	0.17687	0.19878	0.22478	0.38585	1.72552			
1.0	0.08656	0.13050	0.14037	0.14488	0.20167	0.61216	12.81132		
N	0.34291	0.62633	1.00770	0.96323	0.78160	0.62549	0.56373	0.79532	
FLUX	0.27068	0.46798	0.71580	0.85842	0.92518	0.95672	0.96599	0.78124	0.88215
b = 2.00000									
0.1	0.18948	0.34305							
0.3	0.31394	0.57317	0.97414						
0.5	0.32910	0.57709	0.91667	1.24717					
0.7	0.24107	0.40348	0.57741	0.78015	1.29793				
0.9	0.15342	0.24793	0.32532	0.38808	0.58938	1.77220			
1.0	0.12063	0.19236	0.24363	0.27411	0.36839	0.93575	11.32448		
N	0.24336	0.42528	0.66935	0.78957	0.75089	0.64998	0.59772	0.65276	
FLUX	0.23280	0.39837	0.60046	0.75141	0.85027	0.90795	0.92664	0.69880	0.80590
b = 4.00000									
0.1	0.10979	0.19021							
0.3	0.16946	0.29455	0.45932						
0.5	0.21215	0.36763	0.56958	0.72542					
0.7	0.21621	0.36881	0.55190	0.71066	0.89039				
0.9	0.18257	0.30505	0.43533	0.54078	0.71627	1.27348			
1.0	0.15982	0.26437	0.36838	0.44579	0.57383	1.09060	5.15342		
N	0.17678	0.30305	0.45870	0.57858	0.64313	0.63875	0.61763	0.52161	
FLUX	0.19292	0.32863	0.49041	0.61961	0.72789	0.81105	0.84309	0.59340	0.69471
b = 8.00000									
0.1	0.07218	0.12311							
0.3	0.10797	0.18426	0.27607						
0.5	0.13665	0.23322	0.34951	0.44260					
0.7	0.15968	0.27208	0.40627	0.51439	0.60735				
0.9	0.17166	0.29105	0.42972	0.54136	0.65697	0.81845			
1.0	0.17176	0.29012	0.42471	0.53196	0.65111	0.88418	1.36920		
N	0.12902	0.21969	0.32753	0.41408	0.48897	0.54573	0.56391	0.39770	
FLUX	0.15002	0.25517	0.37949	0.47937	0.57006	0.65354	0.69194	0.46613	0.54945



TABLE 38  
Ratio of Total to First-Order Reflection;  $g = 0.250, 0.500$

$\mu_0$	1.0	1.0	1.0	0.5	0.5	U	U	U	N	N	U	U	N
$\mu$	1.0	0.5	0.0	0.5	0.0	1.0	0.5	0.0	1.0	0.5	U	N	N
<b>b = 1.00000 g = 0.250</b>													
$\alpha = 0.20$	1.23	1.18	1.06	1.14	1.05	1.18	1.15	1.05	1.15	1.12	1.15	1.12	1.09
$\alpha = 0.40$	1.53	1.42	1.14	1.33	1.12	1.43	1.34	1.10	1.36	1.28	1.34	1.28	1.21
$\alpha = 0.60$	1.97	1.76	1.26	1.59	1.21	1.78	1.60	1.18	1.64	1.50	1.61	1.49	1.37
$\alpha = 0.80$	2.63	2.26	1.43	1.97	1.33	2.30	1.99	1.29	2.07	1.81	2.01	1.81	1.59
$\alpha = 0.90$	3.10	2.62	1.56	2.24	1.42	2.67	2.27	1.37	2.37	2.03	2.29	2.03	1.75
$\alpha = 0.95$	3.39	2.84	1.63	2.40	1.47	2.89	2.43	1.42	2.55	2.16	2.46	2.16	1.84
$\alpha = 0.99$	3.65	3.04	1.70	2.54	1.52	3.10	2.58	1.46	2.72	2.28	2.62	2.28	1.93
$\alpha = 1.00$	3.72	3.09	1.72	2.58	1.53	3.15	2.62	1.47	2.76	2.31	2.66	2.31	1.95
<b>b = 16.00000 g = 0.250</b>													
$\alpha = 0.20$	1.29	1.21	1.06	1.15	1.05	1.22	1.16	1.05	1.18	1.13	1.17	1.13	1.10
$\alpha = 0.40$	1.72	1.51	1.16	1.37	1.12	1.54	1.38	1.11	1.43	1.31	1.40	1.31	1.23
$\alpha = 0.60$	2.47	1.99	1.30	1.69	1.22	2.07	1.73	1.20	1.84	1.57	1.77	1.59	1.42
$\alpha = 0.80$	4.09	2.95	1.57	2.26	1.38	3.15	2.36	1.35	2.66	2.05	2.47	2.10	1.76
$\alpha = 0.90$	6.01	3.99	1.86	2.83	1.52	4.37	3.00	1.48	3.56	2.50	3.21	2.62	2.08
$\alpha = 0.95$	8.04	5.02	2.13	3.33	1.64	5.60	3.59	1.60	4.45	2.92	3.91	3.10	2.37
$\alpha = 0.99$	12.18	6.94	2.62	4.18	1.82	7.99	4.64	1.80	6.14	3.62	5.19	3.95	2.88
$\alpha = 1.00$	15.23	8.27	2.94	4.71	1.93	9.67	5.32	1.92	7.31	4.07	6.06	4.51	3.20
<b>FOR <math>\alpha = 1.0</math> g = 0.250</b>													
$b = 0.0625$	1.21	1.19	1.10	1.17	1.10	1.18	1.16	1.10	1.16	1.15	1.16	1.15	1.13
$b = 0.1250$	1.39	1.34	1.17	1.29	1.17	1.33	1.29	1.15	1.29	1.26	1.29	1.26	1.22
$b = 0.2500$	1.72	1.61	1.28	1.52	1.26	1.61	1.52	1.23	1.53	1.46	1.52	1.46	1.37
$b = 0.5000$	2.37	2.13	1.46	1.94	1.39	2.14	1.94	1.34	1.97	1.80	1.94	1.79	1.61
$b = 1.0000$	3.72	3.09	1.72	2.58	1.53	3.15	2.62	1.47	2.76	2.31	2.66	2.31	1.95
<b>b = 2.0000</b>													
$b = 4.0000$	6.31	4.55	2.07	3.32	1.67	4.84	3.49	1.61	3.99	2.89	3.66	2.98	2.34
$b = 8.0000$	13.10	7.42	2.74	4.40	1.87	8.55	4.91	1.85	6.55	3.81	5.52	4.17	3.01
$b = 16.0000$	15.23	8.27	2.94	4.71	1.93	9.67	5.32	1.92	7.31	4.07	6.06	4.51	3.20
$b = \infty$	17.86	9.32	3.19	5.09	2.00	11.06	5.82	2.00	8.26	4.39	6.73	4.93	3.44
<b>b = 1.00000 g = 0.500</b>													
$\alpha = 0.20$	1.26	1.24	1.06	1.19	1.05	1.23	1.19	1.04	1.19	1.14	1.18	1.14	1.09
$\alpha = 0.40$	1.65	1.57	1.14	1.45	1.11	1.55	1.44	1.09	1.45	1.34	1.43	1.32	1.22
$\alpha = 0.60$	2.22	2.06	1.27	1.83	1.19	2.03	1.80	1.16	1.83	1.61	1.78	1.58	1.38
$\alpha = 0.80$	3.14	2.82	1.47	2.39	1.32	2.79	2.35	1.27	2.43	2.01	2.32	1.96	1.63
$\alpha = 0.90$	3.82	3.38	1.63	2.79	1.40	3.33	2.75	1.34	2.87	2.30	2.70	2.24	1.80
$\alpha = 0.95$	4.24	3.72	1.72	3.03	1.46	3.68	2.99	1.38	3.14	2.48	2.94	2.40	1.90
$\alpha = 0.99$	4.62	4.04	1.81	3.26	1.50	3.99	3.21	1.42	3.39	2.63	3.15	2.56	1.99
$\alpha = 1.00$	4.73	4.12	1.83	3.32	1.52	4.07	3.27	1.44	3.45	2.68	3.21	2.60	2.02
<b>b = 16.00000 g = 0.500</b>													
$\alpha = 0.20$	1.35	1.27	1.06	1.21	1.05	1.28	1.20	1.04	1.22	1.15	1.20	1.15	1.10
$\alpha = 0.40$	1.96	1.70	1.16	1.50	1.11	1.72	1.50	1.10	1.56	1.37	1.50	1.36	1.23
$\alpha = 0.60$	3.13	2.44	1.32	1.97	1.20	2.52	1.98	1.17	2.14	1.70	1.99	1.69	1.44
$\alpha = 0.80$	6.09	4.08	1.66	2.84	1.36	4.36	2.91	1.31	3.45	2.33	3.01	2.34	1.80
$\alpha = 0.90$	10.06	6.04	2.06	3.73	1.50	6.67	3.92	1.45	5.04	2.96	4.15	3.04	2.17
$\alpha = 0.95$	14.64	8.12	2.48	4.56	1.63	9.19	4.90	1.57	6.73	3.56	5.31	3.72	2.51
$\alpha = 0.99$	24.48	12.21	3.27	5.99	1.83	14.32	6.67	1.77	10.13	4.60	7.51	4.98	3.12
$\alpha = 1.00$	31.27	14.86	3.78	6.84	1.94	17.74	7.76	1.89	12.37	5.23	8.91	5.76	3.49
<b>FOR <math>\alpha = 1.0</math> g = 0.500</b>													
$b = 0.0625$	1.22	1.24	1.12	1.23	1.11	1.23	1.22	1.10	1.21	1.19	1.21	1.18	1.15
$b = 0.1250$	1.41	1.44	1.19	1.42	1.17	1.42	1.39	1.16	1.37	1.33	1.37	1.32	1.26
$b = 0.2500$	1.81	1.82	1.32	1.75	1.26	1.78	1.71	1.23	1.69	1.59	1.68	1.56	1.42
$b = 0.5000$	2.68	2.59	1.52	2.35	1.38	2.53	2.30	1.32	2.29	2.03	2.24	1.96	1.67
$b = 1.0000$	4.73	4.12	1.83	3.32	1.52	4.07	3.27	1.44	3.45	2.68	3.21	2.60	2.02
<b>b = 2.0000</b>													
$b = 4.0000$	9.36	6.68	2.29	4.45	1.65	6.96	4.56	1.56	5.44	3.44	4.67	3.44	2.43
$b = 8.0000$	17.14	9.83	2.86	5.44	1.77	11.00	5.85	1.69	8.06	4.17	6.34	4.36	2.85
$b = 16.0000$	25.25	12.74	3.39	6.25	1.87	14.89	6.95	1.81	10.54	4.78	7.83	5.17	3.22
$b = \infty$	31.27	14.86	3.78	6.84	1.94	17.74	7.76	1.89	12.37	5.23	8.91	5.76	3.49
$b = \infty$	39.42	17.74	4.30	7.64	2.04	21.61	8.84	2.00	14.84	5.83	10.38	6.56	3.86

TABLE 38 (continued)  
Ratio of Total to First-Order Reflection;  $g = 0.75$  and  $0.875$

$\mu_0$	1.0	1.0	1.0	0.5	0.5	U	U	U	N	N	U	U	N
$\mu$	1.0	0.5	0.0	0.5	0.0	1.0	0.5	0.0	1.0	0.5	U	U	N
<b>b = 1.00000 <math>g = 0.750</math></b>													
$\alpha = 0.20$	1.23	1.25	1.07	1.26	1.05	1.24	1.24	1.04	1.21	1.19	1.21	1.16	1.10
$\alpha = 0.40$	1.56	1.63	1.17	1.65	1.12	1.58	1.59	1.09	1.51	1.46	1.52	1.37	1.22
$\alpha = 0.60$	2.07	2.22	1.33	2.26	1.22	2.13	2.13	1.15	1.99	1.87	1.98	1.69	1.40
$\alpha = 0.80$	2.91	3.23	1.60	3.29	1.39	3.04	3.04	1.25	2.78	2.54	2.75	2.21	1.67
$\alpha = 0.90$	3.54	4.02	1.82	4.10	1.52	3.75	3.74	1.33	3.39	3.05	3.35	2.60	1.86
$\alpha = 0.95$	3.95	4.53	1.96	4.62	1.60	4.21	4.20	1.38	3.79	3.38	3.73	2.85	1.99
$\alpha = 0.99$	4.33	5.01	2.10	5.11	1.68	4.64	4.62	1.42	4.16	3.69	4.08	3.08	2.10
$\alpha = 1.00$	4.43	5.14	2.14	5.24	1.70	4.75	4.74	1.43	4.27	3.77	4.18	3.14	2.13
<b>b = 16.00000 <math>g = 0.750</math></b>													
$\alpha = 0.20$	1.33	1.30	1.07	1.28	1.05	1.29	1.26	1.04	1.24	1.20	1.23	1.16	1.10
$\alpha = 0.40$	1.94	1.81	1.18	1.73	1.12	1.80	1.67	1.09	1.64	1.50	1.60	1.41	1.23
$\alpha = 0.60$	3.31	2.82	1.38	2.52	1.23	2.82	2.40	1.16	2.41	2.00	2.26	1.81	1.44
$\alpha = 0.80$	7.76	5.55	1.84	4.25	1.44	5.75	4.06	1.28	4.48	3.05	3.82	2.68	1.82
$\alpha = 0.90$	15.64	9.62	2.49	6.29	1.64	10.39	6.12	1.41	7.60	4.26	5.89	3.73	2.22
$\alpha = 0.95$	26.68	14.68	3.27	8.36	1.83	16.42	8.36	1.52	11.56	5.49	8.27	4.87	2.62
$\alpha = 0.99$	53.54	25.85	4.97	12.13	2.13	30.24	12.71	1.73	20.45	7.77	13.17	7.11	3.37
$\alpha = 1.00$	70.83	32.68	5.99	14.19	2.28	38.86	15.19	1.84	25.93	9.02	16.06	8.40	3.78
<b>FOR <math>\alpha = 1.0</math> <math>g = 0.750</math></b>													
$b = 0.0625$	1.15	1.23	1.18	1.30	1.16	1.24	1.31	1.13	1.27	1.30	1.30	1.27	1.22
$b = 0.1250$	1.30	1.44	1.29	1.57	1.25	1.45	1.56	1.19	1.49	1.53	1.53	1.47	1.35
$b = 0.2500$	1.61	1.88	1.46	2.12	1.37	1.86	2.05	1.26	1.88	1.95	1.96	1.80	1.54
$b = 0.5000$	2.37	2.87	1.73	3.22	1.52	2.74	3.00	1.34	2.67	2.66	2.75	2.33	1.80
$b = 1.0000$	4.43	5.14	2.14	5.24	1.70	4.75	4.74	1.43	4.27	3.77	4.18	3.14	2.13
<b>b = 2.0000</b>													
$b = 4.0000$	10.42	9.73	2.78	7.87	1.87	9.27	7.25	1.53	7.44	5.15	6.48	4.26	2.51
$b = 8.0000$	25.15	16.74	3.73	10.26	2.02	17.60	10.03	1.63	12.78	6.54	9.58	5.64	2.94
$b = 16.0000$	48.28	25.06	4.91	12.37	2.16	28.60	12.78	1.74	19.61	7.87	13.01	7.10	3.39
$b = \infty$	70.83	32.68	5.99	14.19	2.28	38.86	15.19	1.84	25.93	9.02	16.06	8.40	3.78
$b = \infty$	109.52	45.75	7.84	17.29	2.49	56.48	19.31	2.00	36.79	11.00	21.30	10.63	4.46
<b>b = 1.00000 <math>g = 0.875</math></b>													
$\alpha = 0.20$	1.19	1.23	1.08	1.27	1.06	1.22	1.25	1.04	1.21	1.22	1.23	1.17	1.10
$\alpha = 0.40$	1.46	1.58	1.20	1.69	1.16	1.54	1.64	1.08	1.52	1.55	1.56	1.41	1.22
$\alpha = 0.60$	1.84	2.13	1.40	2.40	1.30	2.05	2.28	1.15	2.02	2.09	2.11	1.79	1.41
$\alpha = 0.80$	2.44	3.10	1.74	3.75	1.56	2.93	3.48	1.26	2.89	3.08	3.10	2.46	1.70
$\alpha = 0.90$	2.89	3.89	2.04	4.92	1.78	3.63	4.50	1.34	3.61	3.93	3.92	3.00	1.93
$\alpha = 0.95$	3.17	4.41	2.24	5.73	1.93	4.10	5.19	1.39	4.09	4.51	4.48	3.37	2.08
$\alpha = 0.99$	3.43	4.91	2.45	6.52	2.08	4.55	5.88	1.44	4.56	5.09	5.03	3.73	2.23
$\alpha = 1.00$	3.50	5.05	2.50	6.74	2.12	4.67	6.07	1.46	4.70	5.25	5.18	3.83	2.27
<b>b = 16.00000 <math>g = 0.875</math></b>													
$\alpha = 0.20$	1.29	1.28	1.08	1.29	1.06	1.28	1.27	1.04	1.24	1.23	1.25	1.18	1.10
$\alpha = 0.40$	1.82	1.78	1.21	1.79	1.16	1.76	1.73	1.08	1.65	1.59	1.65	1.44	1.23
$\alpha = 0.60$	3.02	2.82	1.43	2.79	1.31	2.77	2.63	1.15	2.46	2.26	2.41	1.90	1.43
$\alpha = 0.80$	7.39	6.03	1.96	5.46	1.61	6.03	5.02	1.27	4.87	3.87	4.42	2.95	1.81
$\alpha = 0.90$	17.24	11.89	2.78	9.31	1.95	12.36	8.59	1.39	9.24	6.04	7.51	4.36	2.22
$\alpha = 0.95$	34.45	20.68	3.91	13.83	2.29	22.40	13.03	1.50	15.90	8.55	11.60	6.06	2.65
$\alpha = 0.99$	82.60	42.94	6.70	22.83	2.86	48.80	22.55	1.69	33.01	13.53	20.94	9.66	3.46
$\alpha = 1.00$	112.98	56.46	8.38	27.64	3.14	65.08	27.87	1.79	43.48	16.22	26.34	11.67	3.88
<b>FOR <math>\alpha = 1.0</math> <math>g = 0.875</math></b>													
$b = 0.0625$	1.11	1.18	1.29	1.26	1.26	1.23	1.34	1.18	1.34	1.43	1.42	1.42	1.32
$b = 0.1250$	1.22	1.35	1.45	1.53	1.40	1.43	1.64	1.24	1.59	1.75	1.72	1.70	1.48
$b = 0.2500$	1.45	1.74	1.68	2.12	1.59	1.83	2.24	1.31	2.04	2.33	2.28	2.13	1.70
$b = 0.5000$	2.00	2.67	2.02	3.53	1.83	2.68	3.49	1.38	2.91	3.40	3.30	2.82	1.96
$b = 1.0000$	3.50	5.05	2.50	6.74	2.12	4.67	6.07	1.46	4.70	5.25	5.18	3.83	2.27
<b>b = 2.0000</b>													
$b = 4.0000$	8.14	10.73	3.25	12.21	2.43	9.50	10.47	1.53	8.41	7.85	8.38	5.24	2.61
$b = 8.0000$	22.58	21.40	4.42	18.02	2.69	20.20	16.01	1.61	15.67	10.69	13.16	7.08	3.00
$b = 16.0000$	58.27	37.35	6.20	23.04	2.93	39.65	21.91	1.70	27.92	13.49	19.42	9.29	3.43
$b = \infty$	112.98	56.46	8.38	27.64	3.14	65.08	27.87	1.79	43.48	16.22	26.34	11.67	3.88
$b = \infty$	254.24	103.33	13.74	38.50	3.66	128.71	42.09	2.00	82.19	22.72	43.11	17.41	4.98

TABLE 39

Table of Fluxes (Incident Flux = 10000)

ANISOTROPIC	g = 0.5				g = 0.75				g = 0.875				
	GRAZ	THIN	LAMB	PERP	GRAZ	THIN	LAMB	PERP	GRAZ	THIN	LAMB	PERP	
	b = 0.5	0	N	U	1	0	N	U	1	0	N	U	1
<hr/>													
σ=0.20													
REFLECTED	1038	315	191	83	1036	203	98	32	1036	128	50	14	
ABSORBED	8645	5933	4888	3404	8740	5976	4878	3351	8826	6015	4868	3323	
TRANSMITTED	317	3752	4921	6513	224	3821	5024	6617	138	3857	5082	6663	
σ=0.40													
REFLECTED	2168	709	441	196	2163	468	233	76	2166	301	121	33	
ABSORBED	7079	4948	4060	2784	7261	5029	4045	2690	7445	5106	4029	2640	
TRANSMITTED	753	4343	5499	7020	576	4503	5722	7234	389	4593	5850	7327	
σ=0.60													
REFLECTED	3429	1213	775	352	3423	826	426	139	3438	548	227	59	
ABSORBED	5216	3712	3033	2046	5455	3816	3018	1933	5727	3924	3002	1873	
TRANSMITTED	1355	5075	6192	7602	1122	5358	6556	7928	835	5528	6771	8068	
σ=0.80													
REFLECTED	4879	1877	1231	574	4891	1332	711	231	4952	927	397	98	
ABSORBED	2928	2121	1725	1143	3143	2213	1717	1053	3420	2319	1708	1003	
TRANSMITTED	2193	6002	7044	8283	1966	6455	7572	8716	1628	6754	7895	8899	
σ=0.90													
REFLECTED	5703	2293	1524	720	5743	1669	906	294	5858	1199	522	125	
ABSORBED	1563	1142	926	608	1704	1203	923	552	1902	1278	920	521	
TRANSMITTED	2734	6565	7550	8672	2553	7128	8171	9154	2240	7523	8558	9354	
σ=0.95													
REFLECTED	6148	2529	1692	805	6209	1866	1021	331	6367	1366	600	142	
ABSORBED	809	593	481	314	890	629	481	284	1008	674	479	265	
TRANSMITTED	3043	6878	7827	8881	2901	7505	8498	9385	2625	7960	8921	9593	
σ=0.99													
REFLECTED	6522	2733	1838	879	6605	2040	1125	365	6808	1519	672	157	
ABSORBED	167	122	99	64	185	131	99	57	212	141	99	54	
TRANSMITTED	3311	7145	8063	9057	3210	7829	8776	9578	2980	8340	9229	9789	
σ=1.00													
REFLECTED	6618	2786	1876	898	6708	2086	1152	373	6924	1561	691	160	
ABSORBED	0	0	0	0	0	0	0	0	0	0	0	0	1
TRANSMITTED	3382	7214	8124	9102	3292	7914	8848	9627	3076	8439	9309	9839	
ANY σ													
DIRECTLY TRANSMITTED	0	3266	4432	6065	0	3266	4432	6065	0	3266	4432	6065	

TABLE 39 (continued)

ANISOTROPIC	g = 0.5				g = 0.75				g = 0.875				
	GRAZ	THIN	LAMB	PERP	GRAZ	THIN	LAMB	PERP	GRAZ	THIN	LAMB	PERP	
	b = 1	0	N	U	1	0	N	U	1	0	N	U	1
a=0.20													
REFLECTED	1040	342	221	106	1037	216	111	41	1037	134	56	18	
ABSORBED	8811	7782	7132	5702	8867	7841	7131	5612	8909	7890	7125	5560	
TRANSMITTED	149	1876	2647	4192	96	1943	2758	4347	54	1976	2819	4422	
a=0.40													
REFLECTED	2184	794	535	269	2171	512	278	105	2169	323	142	45	
ABSORBED	7418	6797	6224	4907	7540	6910	6219	4729	7651	7008	6203	4622	
TRANSMITTED	398	2409	3241	4824	289	2578	3503	5166	180	2669	3655	5333	
a=0.60													
REFLECTED	3490	1424	1000	528	3457	948	546	212	3456	615	288	90	
ABSORBED	5694	5413	4952	3843	5881	5563	4941	3603	6078	5707	4916	3452	
TRANSMITTED	816	3163	4048	5629	662	3489	4513	6185	466	3678	4796	6458	
a=0.80													
REFLECTED	5069	2363	1737	964	5017	1650	1012	403	5031	1123	563	170	
ABSORBED	3401	3353	3062	2336	3598	3494	3053	2114	3850	3653	3033	1968	
TRANSMITTED	1530	4284	5201	6700	1385	4856	5935	7483	1119	5224	6404	7862	
a=0.90													
REFLECTED	6031	3029	2280	1298	5979	2183	1384	559	6027	1544	803	238	
ABSORBED	1894	1902	1735	1311	2038	2001	1731	1162	2243	2124	1721	1061	
TRANSMITTED	2075	5069	5985	7391	1983	5816	6885	8279	1730	6332	7476	8701	
a=0.95													
REFLECTED	6576	3437	2617	1510	6532	2523	1626	662	6616	1829	968	283	
ABSORBED	1006	1019	929	699	1093	1079	928	612	1225	1156	925	553	
TRANSMITTED	2418	5544	6454	7791	2375	6398	7446	8726	2159	7015	8107	9164	
a=0.99													
REFLECTED	7053	3809	2929	1707	7021	2843	1856	760	7149	2109	1132	327	
ABSORBED	211	216	197	148	232	230	197	128	265	249	197	115	
TRANSMITTED	2736	5975	6874	8145	2747	6927	7947	9112	2586	7642	8671	9558	
a=1.00													
REFLECTED	7178	3910	3013	1761	7151	2931	1920	787	7293	2188	1179	340	
ABSORBED	0	0	0	0	0	0	0	0	0	0	0	0	
TRANSMITTED	2822	6090	6987	8239	2849	7069	8080	9213	2707	7812	8821	9660	
ANY a													
DIRECTLY TRANSMITTED	0	1485	2194	3679	0	1485	2194	3679	0	1485	2194	3679	

TABLE 39 (continued)

ANISOTROPIC  b = 2	g = 0.5				g = 0.75				g = 0.875			
	GRAZ	THIN	LAMB	PERP	GRAZ	THIN	LAMB	PERP	GRAZ	THIN	LAMB	PERP
	0	N	U	1	0	N	U	1	0	N	U	1
$\alpha=0.20$												
REFLECTED	1041	349	231	117	1037	219	115	45	1037	135	58	20
ABSORBED	8918	9097	8931	8179	8938	9186	8975	8105	8950	9248	8990	8047
TRANSMITTED	41	554	838	1704	25	595	910	1850	13	617	952	1933
$\alpha=0.40$												
REFLECTED	2190	825	572	310	2173	528	297	123	2170	330	151	53
ABSORBED	7676	8328	8225	7488	7731	8501	8297	7306	7773	8630	8318	7160
TRANSMITTED	134	847	1203	2202	96	971	1406	2571	57	1040	1531	2787
$\alpha=0.60$												
REFLECTED	3517	1526	1123	658	3471	1009	617	273	3461	647	324	116
ABSORBED	6143	7114	7065	6387	6243	7345	7142	6078	6343	7535	7151	5817
TRANSMITTED	340	1360	1812	2955	286	1646	2241	3649	196	1818	2525	4067
$\alpha=0.80$												
REFLECTED	5196	2708	2136	1372	5095	1888	1274	618	5074	1269	712	264
ABSORBED	3976	4931	4924	4413	4106	5150	4970	4033	4280	5367	4959	3699
TRANSMITTED	828	2361	2940	4215	799	2962	3756	5349	646	3364	4329	6037
$\alpha=0.90$												
REFLECTED	6308	3688	3025	2045	6168	2675	1911	974	6150	1876	1126	422
ABSORBED	2372	3050	3053	2722	2479	3201	3071	2416	2650	3381	3060	2146
TRANSMITTED	1320	3262	3922	5233	1353	4124	5018	6610	1200	4743	5814	7432
$\alpha=0.95$												
REFLECTED	6992	4366	3657	2539	6832	3245	2388	1249	6828	2345	1458	550
ABSORBED	1320	1729	1732	1540	1389	1818	1738	1343	1513	1939	1733	1169
TRANSMITTED	1688	3905	4611	5921	1779	4937	5874	7408	1659	5716	6809	8281
$\alpha=0.99$												
REFLECTED	7634	5049	4303	3053	7461	3836	2892	1544	7486	2857	1828	691
ABSORBED	291	387	388	344	308	408	388	296	342	439	388	253
TRANSMITTED	2075	4564	5309	6603	2231	5756	6720	8160	2172	6704	7784	9056
$\alpha=1.00$												
REFLECTED	7811	5246	4490	3203	7636	4009	3040	1632	7672	3012	1941	733
ABSORBED	0	0	0	0	0	0	0	0	0	0	0	1
TRANSMITTED	2189	4754	5510	6797	2364	5991	6960	8368	2328	6988	8059	9266
ANY $\alpha$ DIRECTLY TRANSMITTED	0	375	603	1353	0	375	603	1353	0	375	603	1353

**TABLE 39** *(continued)*

ANISOTROPIC	g = 0.5				g = 0.75				g = 0.875				
	GRAZ	THIN	LAMB	PERP	GRAZ	THIN	LAMB	PERP	GRAZ	THIN	LAMB	PERP	
	b = 4	0	N	U	1	0	N	U	1	0	N	U	1
<hr/>													
a=0.20													
REFLECTED	1041	350	231	118	1037	219	116	46	1037	135	58	20	
ABSORBED	8955	9589	9672	9612	8960	9710	9769	9630	8962	9788	9815	9618	
TRANSMITTED	4	61	97	270	3	71	115	324	1	77	127	362	
<hr/>													
a=0.40													
REFLECTED	2190	828	578	318	2173	530	300	127	2170	331	153	55	
ABSORBED	7791	9048	9239	9255	7812	9304	9447	9273	7821	9476	9544	9212	
TRANSMITTED	19	124	183	427	15	166	253	600	9	193	303	733	
<hr/>													
a=0.60													
REFLECTED	3523	1547	1151	698	3474	1023	636	298	3462	655	334	128	
ABSORBED	6408	8171	8463	8558	6458	8557	8770	8525	6489	8827	8906	8333	
TRANSMITTED	69	282	386	744	68	420	594	1177	49	518	760	1539	
<hr/>													
a=0.80													
REFLECTED	5243	2840	2298	1585	5126	1998	1409	774	5090	1340	797	343	
ABSORBED	4488	6385	6724	6876	4560	6797	7024	6690	4638	7118	7133	6263	
TRANSMITTED	269	775	978	1539	314	1205	1567	2536	272	1542	2070	3394	
<hr/>													
a=0.90													
REFLECTED	6464	4073	3482	2612	6286	3020	2316	1416	6222	2123	1404	657	
ABSORBED	2947	4464	4744	4883	2999	4750	4922	4611	3094	5013	4973	4131	
TRANSMITTED	589	1463	1774	2505	715	2230	2762	3973	684	2864	3623	5212	
<hr/>													
a=0.95													
REFLECTED	7298	5071	4481	3532	7074	3891	3133	2035	6992	2837	1995	979	
ABSORBED	1781	2791	2981	3078	1805	2947	3056	2832	1884	3123	3073	2458	
TRANSMITTED	921	2138	2538	3390	1121	3162	3811	5133	1124	4040	4932	6563	
<hr/>													
a=0.99													
REFLECTED	8187	6262	5703	4698	7909	4955	4160	2843	7817	3756	2783	1417	
ABSORBED	434	699	749	775	435	727	754	692	459	773	754	582	
TRANSMITTED	1379	3039	3548	4527	1656	4318	5086	6465	1724	5471	6463	8001	
<hr/>													
a=1.00													
REFLECTED	8461	6650	6105	5090	8164	5303	4501	3116	8071	4066	3053	1569	
ABSORBED	0	0	0	0	0	0	0	0	0	0	0	0	
TRANSMITTED	1539	3350	3895	4910	1836	4697	5499	6884	1929	5934	6947	8431	
<hr/>													
ANY a DIRECTLY TRANSMITTED	0	32	55	183	0	32	55	183	0	32	55	183	

TABLE 39 (continued)

ANISOTROPIC	g = 0.5				g = 0.75				g = 0.875				
	GRAZ	THIN	LAMB	PERP	GRAZ	THIN	LAMB	PERP	GRAZ	THIN	LAMB	PERP	
	b = 8	0	N	U	1	0	N	U	1	0	N	U	1
<hr/>													
$\alpha=0.20$													
REFLECTED	1041	350	231	118	1037	219	116	46	1037	135	58	20	
ABSORBED	8959	9649	9767	9876	8963	9780	9882	9945	8963	9863	9939	9968	
TRANSMITTED	0	1	2	6	0	1	2	9	0	2	3	12	
<hr/>													
$\alpha=0.40$													
REFLECTED	2190	829	578	318	2173	530	300	127	2170	332	153	55	
ABSORBED	7810	9168	9417	9668	7826	9464	9691	9844	7830	9659	9833	9899	
TRANSMITTED	0	3	5	14	1	6	9	29	0	9	14	46	
<hr/>													
$\alpha=0.60$													
REFLECTED	3523	1548	1152	700	3474	1024	637	300	3462	656	335	129	
ABSORBED	6474	8438	8829	9259	6521	8944	9317	9594	6534	9293	9588	9674	
TRANSMITTED	3	14	19	41	5	32	46	106	4	51	77	197	
<hr/>													
$\alpha=0.80$													
REFLECTED	5249	2856	2318	1615	5131	2018	1435	813	5093	1357	818	372	
ABSORBED	4721	7056	7571	8201	4813	7766	8281	8687	4846	8278	8679	8669	
TRANSMITTED	30	88	111	184	56	216	284	500	61	365	503	959	
<hr/>													
$\alpha=0.90$													
REFLECTED	6502	4167	3596	2770	6327	3147	2473	1630	6250	2236	1542	826	
ABSORBED	3373	5522	6027	6686	3452	6159	6662	7064	3488	6631	6997	6839	
TRANSMITTED	125	311	377	544	221	694	865	1306	262	1133	1461	2335	
<hr/>													
$\alpha=0.95$													
REFLECTED	7422	5358	4822	3982	7208	4266	3581	2614	7092	3181	2403	1440	
ABSORBED	2276	3941	4345	4893	2300	4341	4733	5043	2319	4655	4918	4713	
TRANSMITTED	302	701	833	1125	492	1393	1686	2343	589	2164	2679	3847	
<hr/>													
$\alpha=0.99$													
REFLECTED	8588	7144	6731	6001	8308	5989	5371	4330	8130	4713	3884	2584	
ABSORBED	673	1227	1367	1561	649	1283	1409	1507	645	1350	1426	1335	
TRANSMITTED	739	1629	1902	2438	1043	2728	3220	4163	1225	3937	4690	6081	
<hr/>													
$\alpha=1.00$													
REFLECTED	9029	7886	7542	6890	8706	6683	6109	5064	8500	5339	4506	3081	
ABSORBED	0	0	0	0	0	0	0	0	0	0	-1	0	
TRANSMITTED	971	2114	2458	3110	1294	3317	3891	4936	1500	4661	5495	6919	
<hr/>													
ANY $\alpha$ DIRECTLY TRANSMITTED	0	0	1	3	0	0	1	3	0	0	1	3	

TABLE 39 (continued)

[illegible]



TABLE 40  
Sample Midlayer Intensity Distributions with Moments

q=0.50 b=0.5 a=0.9 DOWN THE D MATRIX IS									
$\mu_0$	$\mu = 0.0$	$\mu = 0.1$	$\mu = 0.3$	$\mu = 0.5$	$\mu = 0.7$	$\mu = 0.9$	$\mu = 1.0$	N	FLUX
0.0	0.24175	0.56510	0.62645	0.42832	0.28583	0.19437	0.16190	0.40997	0.33265
0.1	0.63877	1.09094	0.80539	0.50889	0.32493	0.21330	0.17497	0.97983	0.48733
0.3	0.75365	0.86195	0.59193	0.39392	0.25774	0.16754	0.13576	1.17216	0.74730
0.5	0.52594	0.55717	0.40181	0.30354	0.22257	0.15124	0.12228	0.93067	0.85171
0.7	0.35590	0.36107	0.26563	0.22426	0.19930	0.16029	0.13437	0.74017	0.93238
0.9	0.24484	0.23999	0.17411	0.15312	0.16077	0.18731	0.19491	0.60329	0.93074
1.0	0.20499	0.19797	0.14164	0.12408	0.13491	0.19501	0.28263	0.54966	0.96041
N	0.49249	1.01212	1.16409	0.91929	0.73053	0.59576	0.54305	0.86833	0.78222
FLUX	0.40831	0.52381	0.75162	0.85032	0.90006	0.92854	0.93838	0.78987	0.86988
q=0.5C b=0.5 a=0.9 UP THE A MATRIX IS									
$\mu_0$	$\mu = 0.0$	$\mu = 0.1$	$\mu = 0.3$	$\mu = 0.5$	$\mu = 0.7$	$\mu = 0.9$	$\mu = 1.0$	N	FLUX
0.0	0.24175	0.17355	0.08304	0.04656	0.02886	0.01912	0.01586	0.07129	0.04028
0.1	0.63877	0.39195	0.17917	0.09879	0.06029	0.03935	0.03242	0.15983	0.08596
0.3	0.75365	0.54176	0.25753	0.14346	0.08836	0.05816	0.04810	0.22121	0.12413
0.5	0.52594	0.40228	0.19554	0.11032	0.06882	0.04587	0.03817	0.16608	0.09532
0.7	0.35590	0.28307	0.14050	0.08031	0.05071	0.03418	0.02859	0.11841	0.06929
0.9	0.24484	0.20071	0.10161	0.05882	0.03756	0.02557	0.02149	0.08510	0.05068
1.0	0.20499	0.17020	0.08696	0.05065	0.03251	0.02224	0.01873	0.07265	0.04361
N	0.49249	0.36013	0.17351	0.09765	0.06075	0.04038	0.03355	0.14844	0.08444
FLUX	0.40831	0.31264	0.15313	0.08692	0.05452	0.03652	0.03045	0.12990	0.07506
q=0.50 b=0.5 a=1.0 DOWN THE D MATRIX IS									
$\mu_0$	$\mu = 0.0$	$\mu = 0.1$	$\mu = 0.3$	$\mu = 0.5$	$\mu = 0.7$	$\mu = 0.9$	$\mu = 1.0$	N	FLUX
0.0	0.33081	0.69597	0.74119	0.50600	0.33848	0.23084	0.19254	0.49085	0.39466
0.1	0.79981	1.30462	0.95009	0.60018	0.38421	0.25307	0.20793	1.08692	0.56145
0.3	0.91694	1.02917	0.69746	0.46214	0.30252	0.19729	0.16021	1.25442	0.80274
0.5	0.64151	0.66825	0.47343	0.35391	0.25840	0.17580	0.14243	0.98902	0.89314
0.7	0.43624	0.43550	0.31390	0.26087	0.22938	0.18379	0.15418	0.78259	0.93497
0.9	0.30156	0.29112	0.20682	0.17857	0.18450	0.21251	0.22044	0.63491	0.95737
1.0	0.25303	0.24078	0.16875	0.14509	0.15500	0.22059	0.31757	0.57719	0.96474
N	0.60571	1.13244	1.24337	0.97304	0.76891	0.62414	0.56771	0.93161	0.82771
FLUX	0.50000	0.61304	0.80905	0.89121	0.93164	0.95419	0.96180	0.83854	0.90621
q=0.50 b=0.5 a=1.0 UP THE A MATRIX IS									
$\mu_0$	$\mu = 0.0$	$\mu = 0.1$	$\mu = 0.3$	$\mu = 0.5$	$\mu = 0.7$	$\mu = 0.9$	$\mu = 1.0$	N	FLUX
0.0	0.33081	0.24068	0.11613	0.06541	0.04066	0.02697	0.02239	0.09933	0.05650
0.1	0.79981	0.50416	0.23336	0.12946	0.07936	0.05197	0.04288	0.20541	0.11239
0.3	0.91694	0.66736	0.31997	0.17915	0.11070	0.07302	0.06044	0.27387	0.15475
0.5	0.64151	0.49577	0.24290	0.13762	0.08605	0.05741	0.04778	0.20563	0.11870
0.7	0.43624	0.35020	0.17502	0.10037	0.06346	0.04277	0.03576	0.14707	0.08645
0.9	0.30156	0.24926	0.12691	0.07363	0.04703	0.03199	0.02687	0.10601	0.06334
1.0	0.25303	0.21173	0.10873	0.06343	0.04071	0.02782	0.02341	0.09061	0.05454
N	0.60571	0.44850	0.21785	0.12312	0.07678	0.05110	0.04247	0.18570	0.10629
FLUX	0.50000	0.38696	0.19095	0.10879	0.06836	0.04581	0.03820	0.16146	0.09379

TABLE 40 (continued)

g=0.50 b=2.0 a=0.9 DOWN THE D MATRIX IS									
$\mu_0$	$\mu = 0.0$	$\mu = 0.1$	$\mu = 0.3$	$\mu = 0.5$	$\mu = 0.7$	$\mu = 0.9$	$\mu = 1.0$	N	FLUX
0.0	0.12542	0.14427	0.21739	0.25216	0.23587	0.20248	0.18489	0.20985	0.22079
0.1	0.16881	0.19683	0.30460	0.33958	0.30723	0.25683	0.23188	0.28060	0.29023
0.3	0.28741	0.34443	0.46533	0.46999	0.40313	0.32215	0.28494	0.45926	0.42700
0.5	0.35536	0.40880	0.49857	0.50351	0.44569	0.35774	0.31367	0.57675	0.56427
0.7	0.34785	0.38650	0.44438	0.46036	0.45160	0.40018	0.35760	0.59842	0.66952
0.9	0.30958	0.33474	0.36636	0.37841	0.40730	0.46568	0.48622	0.57315	0.74491
1.0	0.28714	0.30697	0.32866	0.33546	0.36658	0.48830	0.66480	0.55275	0.77405
N	0.29266	0.33332	0.47350	0.56361	0.57220	0.54263	0.52192	0.49605	0.53840
FLUX	0.32085	0.35929	0.45889	0.57001	0.66144	0.73074	0.75854	0.55587	0.63402
g=0.50 b=2.0 a=0.9 UP THE A MATRIX IS									
$\mu_0$	$\mu = 0.0$	$\mu = 0.1$	$\mu = 0.3$	$\mu = 0.5$	$\mu = 0.7$	$\mu = 0.9$	$\mu = 1.0$	N	FLUX
0.0	0.12542	0.10982	0.08260	0.06041	0.04439	0.03312	0.02881	0.36628	0.05029
0.1	0.16881	0.14715	0.11016	0.08039	0.05898	0.04397	0.03822	0.08843	0.06692
0.3	0.28741	0.24447	0.17765	0.12768	0.09280	0.06874	0.05960	0.14293	0.10634
0.5	0.35536	0.30907	0.22961	0.16668	0.12186	0.09061	0.07867	0.18421	0.13872
0.7	0.34785	0.31081	0.23906	0.17674	0.13068	0.09795	0.08532	0.19150	0.14707
0.9	0.30958	0.28296	0.22447	0.16873	0.12608	0.09523	0.08321	0.17975	0.14046
1.0	0.28714	0.26501	0.21308	0.16135	0.12114	0.09181	0.08035	0.17067	0.13437
N	0.29266	0.25790	0.19548	0.14354	0.10572	0.07903	0.06878	0.15680	0.11948
FLUX	0.32085	0.28576	0.21938	0.16214	0.11990	0.08989	0.07832	0.17585	0.13496
g=0.50 b=2.0 a=1.0 DOWN THE D MATRIX IS									
$\mu_0$	$\mu = 0.0$	$\mu = 0.1$	$\mu = 0.3$	$\mu = 0.5$	$\mu = 0.7$	$\mu = 0.9$	$\mu = 1.0$	N	FLUX
0.0	0.22330	0.24883	0.33218	0.36142	0.33070	0.28161	0.25669	0.31013	0.31531
0.1	0.29872	0.33626	0.45897	0.48428	0.43065	0.35824	0.32327	0.41298	0.41389
0.3	0.46554	0.53592	0.66693	0.65010	0.55190	0.44127	0.39109	0.62707	0.57877
0.5	0.55175	0.61536	0.70500	0.68533	0.59639	0.47818	0.42057	0.74954	0.71850
0.7	0.53611	0.58069	0.63186	0.62534	0.59314	0.51786	0.46298	0.75926	0.81409
0.9	0.47844	0.50633	0.52773	0.51937	0.53227	0.58222	0.59902	0.71609	0.87595
1.0	0.44496	0.46635	0.47692	0.46419	0.48125	0.60331	0.79434	0.68627	0.89807
N	0.46421	0.51317	0.65485	0.72527	0.70935	0.65719	0.62645	0.65066	0.67879
FLUX	0.50000	0.54505	0.64079	0.73035	0.79867	0.84810	0.86736	0.71213	0.77552
g=0.50 b=2.0 a=1.0 UP THE A MATRIX IS									
$\mu_0$	$\mu = 0.0$	$\mu = 0.1$	$\mu = 0.3$	$\mu = 0.5$	$\mu = 0.7$	$\mu = 0.9$	$\mu = 1.0$	N	FLUX
0.0	0.22330	0.20034	0.15557	0.11581	0.08603	0.06468	0.05640	0.12476	0.09641
0.1	0.29872	0.26705	0.20658	0.15351	0.11392	0.08558	0.07461	0.16571	0.12780
0.3	0.46554	0.40833	0.30887	0.22699	0.16732	0.12513	0.10888	0.24811	0.18902
0.5	0.55175	0.49223	0.37847	0.28014	0.20734	0.15546	0.13541	0.30346	0.23316
0.7	0.53611	0.48913	0.38681	0.29044	0.21685	0.16358	0.14283	0.30983	0.24174
0.9	0.47844	0.44499	0.36105	0.27478	0.20689	0.15701	0.13743	0.28918	0.22880
1.0	0.44496	0.41728	0.34242	0.26218	0.19815	0.15080	0.13215	0.27431	0.21837
N	0.46421	0.41864	0.32708	0.24425	0.18179	0.13685	0.11940	0.26224	0.20334
FLUX	0.50000	0.45495	0.35921	0.26965	0.20133	0.15190	0.13264	0.28787	0.22448

TABLE 40 (continued)

g = 0.50 b = 8.0 a = 0.9 DOWN THE D MATRIX IS									
$\mu_0$	$\mu = 0.0$	$\mu = 0.1$	$\mu = 0.3$	$\mu = 0.5$	$\mu = 0.7$	$\mu = 0.9$	$\mu = 1.0$	N	FLUX
0.0	0.03665	0.03977	0.04717	0.05671	0.06847	0.08030	0.08546	0.05852	0.06700
0.1	0.04781	0.05190	0.06157	0.07409	0.08942	0.10450	0.11094	0.07633	0.08735
0.3	0.06706	0.07281	0.08651	0.10435	0.12567	0.14552	0.15351	0.10700	0.12227
0.5	0.08833	0.09599	0.11434	0.13795	0.16506	0.18884	0.19774	0.14078	0.16031
0.7	0.11296	0.12271	0.14583	0.17475	0.20783	0.23750	0.24795	0.18007	0.20509
0.9	0.13822	0.14958	0.17595	0.20805	0.24671	0.29390	0.31836	0.22158	0.25673
1.0	0.14986	0.16170	0.18887	0.22146	0.26148	0.32262	0.38253	0.24145	0.28433
N	0.09087	0.09858	0.11679	0.14007	0.16914	0.20061	0.21574	0.14516	0.16646
FLUX	0.10976	0.11901	0.14076	0.16819	0.20304	0.24519	0.26833	0.17548	0.20172
g = 0.50 b = 8.0 a = 0.9 UP THE A MATRIX IS									
$\mu_0$	$\mu = 0.0$	$\mu = 0.1$	$\mu = 0.3$	$\mu = 0.5$	$\mu = 0.7$	$\mu = 0.9$	$\mu = 1.0$	N	FLUX
0.0	0.03665	0.03383	0.02897	0.02492	0.02149	0.01857	0.01726	0.02558	0.02241
0.1	0.04781	0.04413	0.03778	0.03250	0.02803	0.02421	0.02251	0.03337	0.02922
0.3	0.06706	0.06188	0.05295	0.04553	0.03926	0.03390	0.03152	0.04676	0.04094
0.5	0.08833	0.08145	0.06962	0.05981	0.05154	0.04449	0.04136	0.06145	0.05377
0.7	0.11296	0.10419	0.08909	0.07655	0.06597	0.05694	0.05293	0.07864	0.06881
0.9	0.13822	0.12790	0.10992	0.09480	0.08193	0.07088	0.06595	0.09719	0.08533
1.0	0.14986	0.13902	0.11998	0.10382	0.08996	0.07798	0.07261	0.10625	0.09355
N	0.09087	0.08391	0.07188	0.06185	0.05336	0.04610	0.04287	0.06349	0.05563
FLUX	0.10976	0.10140	0.08693	0.07484	0.06460	0.05583	0.05192	0.07680	0.06732
g = 0.50 b = 8.0 a = 1.0 DOWN THE D MATRIX IS									
$\mu_0$	$\mu = 0.0$	$\mu = 0.1$	$\mu = 0.3$	$\mu = 0.5$	$\mu = 0.7$	$\mu = 0.9$	$\mu = 1.0$	N	FLUX
0.0	0.19804	0.20543	0.22030	0.23548	0.25021	0.26160	0.26526	0.23453	0.24631
0.1	0.25872	0.26838	0.28786	0.30778	0.32699	0.34142	0.34580	0.30638	0.32171
0.3	0.35177	0.36496	0.39162	0.41908	0.44496	0.46290	0.46753	0.41654	0.43714
0.5	0.43701	0.45353	0.48708	0.52138	0.55248	0.57208	0.57595	0.51740	0.54238
0.7	0.51802	0.53753	0.57686	0.61612	0.65151	0.67440	0.67819	0.61333	0.64302
0.9	0.59063	0.61196	0.65410	0.69484	0.73353	0.77280	0.79076	0.69988	0.73849
1.0	0.62201	0.64369	0.68591	0.72591	0.76461	0.81813	0.87512	0.73767	0.78341
N	0.43063	0.44664	0.47878	0.51135	0.54333	0.57053	0.58103	0.51002	0.53593
FLUX	0.50000	0.51847	0.55542	0.59240	0.62935	0.66565	0.68327	0.59224	0.62291
g = 0.50 b = 8.0 a = 1.0 UP THE A MATRIX IS									
$\mu_0$	$\mu = 0.0$	$\mu = 0.1$	$\mu = 0.3$	$\mu = 0.5$	$\mu = 0.7$	$\mu = 0.9$	$\mu = 1.0$	N	FLUX
0.0	0.19804	0.19067	0.17596	0.16127	0.14662	0.13224	0.12527	0.16136	0.14919
0.1	0.25872	0.24908	0.22986	0.21066	0.19152	0.17273	0.16362	0.21078	0.19487
0.3	0.35177	0.33862	0.31244	0.28631	0.26027	0.23473	0.22234	0.28649	0.26484
0.5	0.43701	0.42058	0.38792	0.35540	0.32302	0.29128	0.27590	0.35566	0.32872
0.7	0.51802	0.49859	0.45992	0.42138	0.38300	0.34537	0.32713	0.42168	0.38975
0.9	0.59063	0.56918	0.52601	0.48257	0.43904	0.39618	0.37536	0.48261	0.44656
1.0	0.62201	0.60005	0.55547	0.51023	0.46464	0.41957	0.39763	0.51000	0.47238
N	0.43063	0.41465	0.38273	0.35082	0.31898	0.28771	0.27254	0.35099	0.32454
FLUX	0.50000	0.48153	0.44458	0.40760	0.37065	0.33435	0.31673	0.40776	0.37709

TABLE 41

Point-Direction Gain and Net Flux in Finite Slabs with Henye-Greenstein Scattering  
 $g = 0.500$ , Incidence from  $\mu_0 = 0.1$

	$\alpha = 0.20$	0.60	0.90	0.99	1.00	0.20	0.60	0.90	0.99	1.00
	POINT DIRECTION GAIN X 10000					NET FLUX DOWN X 10000				
$b = 0.03125$										
$\tau = 0.0$	10127	10395	10609	10675	10683	9774	9296	8912	8793	8779
$\tau = 0.01562$	8711	9042	9305	9387	9396	8598	8688	8756	8777	8779
$\tau = 0.03125$	7451	7736	7962	8032	8040	7590	8164	8621	8763	8779
$b = 0.06250$										
$\tau = 0.0$	10185	10586	10920	11026	11038	9626	8803	8111	7890	7865
$\tau = 0.03125$	7547	8048	8463	8595	8609	7424	7642	7808	7859	7865
$\tau = 0.06250$	5540	5948	6287	6395	6407	5799	6771	7578	7836	7865
$b = 0.12500$										
$\tau = 0.0$	10238	10781	11260	11418	11436	9458	8198	7061	6681	6637
$\tau = 0.06250$	5643	6307	6895	7090	7112	5596	6102	6501	6623	6637
$\tau = 0.12500$	3077	3568	4010	4157	4173	3477	4894	6165	6589	6637
$b = 0.25000$										
$\tau = 0.0$	10270	10916	11530	11743	11768	9341	7697	6063	5481	5413
$\tau = 0.12500$	3151	3862	4563	4811	4840	3314	4300	5122	5384	5413
$\tau = 0.25000$	994	1444	1911	2081	2101	1449	3074	4741	5343	5413
$b = 0.50000$										
$\tau = 0.0$	10278	10970	11682	11948	11979	9303	7454	5393	4587	4491
$\tau = 0.25000$	1021	1594	2277	2552	2585	1383	2746	4014	4442	4491
$\tau = 0.50000$	160	461	864	1035	1056	503	1879	3661	4401	4491
$b = 1.00000$										
$\tau = 0.0$	10279	10988	11775	12097	12136	9298	7359	4922	3836	3700
$\tau = 0.50000$	165	525	1119	1417	1456	489	1720	3115	3638	3700
$\tau = 1.00000$	34	194	512	685	708	201	1081	2725	3587	3700
$b = 2.00000$										
$\tau = 0.0$	10279	10994	11840	12236	12288	9297	7322	4553	3066	2861
$\tau = 1.00000$	36	227	738	1103	1157	197	987	2233	2792	2861
$\tau = 2.00000$	8	70	296	478	506	54	445	1724	2712	2861
$b = 4.00000$										
$\tau = 0.0$	10279	10995	11874	12362	12436	9297	7315	4349	2341	2011
$\tau = 2.00000$	8	84	474	965	1060	53	405	1347	1931	2011
$\tau = 4.00000$	1	13	127	309	347	6	90	768	1801	2011
$b = 8.000$										
$\tau = 0.0$	10279	10995	11882	12451	12564	9297	7315	4299	1819	1268
$\tau = 4.000$	1	16	219	833	1034	5	82	581	1166	1268
$\tau = 8.000$	0	1	27	165	218	0	4	163	965	1268
$b = 16.000$										
$\tau = 0.0$	10279	10995	11883	12489	12657	9297	7315	4297	1597	730
$\tau = 8.000$	0	1	47	585	1032	0	4	122	583	730
$\tau = 16.000$	0	C	1	58	126	0	0	7	340	730
$b = 32.000$										
$\tau = 0.0$	10279	10995	11883	12495	12714	9297	7315	4297	1564	395
$\tau = 16.000$	0	C	2	238	1032	0	0	6	200	395
$\tau = 32.000$	0	0	0	8	68	0	0	0	48	395
$b = \infty$										
$\tau = 0.0$	10279	10995	11883	12495	12782	9297	7315	4297	1563	0

TABLE 41 (continued)  
 $g = 0.500$ , Incidence from  $\mu_0 = 1.0$

$a =$	0.20	0.60	0.90	0.99	1.00	0.20	0.60	0.90	0.99	1.00
	POINT DIRECTION GAIN X 10000					NET FLUX DOWN X 10000				
$b = 0.03125$										
$\tau = 0.0$	10053	10167	10258	10287	10290	9990	9969	9952	9947	9946
$\tau = 0.01562$	9941	10142	10301	10351	10356	9865	9906	9936	9945	9946
$\tau = 0.03125$	9807	10046	10233	10291	10297	9742	9843	9920	9944	9946
$b = 0.06250$										
$\tau = 0.0$	10085	10276	10438	10490	10496	9982	9940	9904	9893	9892
$\tau = 0.03125$	9861	10223	10521	10615	10625	9732	9812	9872	9890	9892
$\tau = 0.06250$	9597	10027	10374	10483	10495	9489	9685	9839	9886	9892
$b = 0.12500$										
$\tau = 0.0$	10130	10443	10734	10833	10845	9967	9886	9810	9784	9781
$\tau = 0.06250$	9681	10327	10891	11076	11097	9471	9626	9742	9777	9781
$\tau = 0.12500$	9167	9923	10566	10773	10797	9000	9372	9675	9770	9781
$b = 0.25000$										
$\tau = 0.0$	10187	10685	11217	11415	11438	9945	9792	9625	9562	9555
$\tau = 0.12500$	9291	10418	11500	11879	11923	8969	9261	9482	9548	9555
$\tau = 0.25000$	8326	9592	10764	11164	11210	8088	8758	9341	9533	9555
$b = 0.50000$										
$\tau = 0.0$	10244	10998	11983	12400	12451	9917	9648	9280	9121	9102
$\tau = 0.25000$	8489	10360	12446	13259	13356	8042	8566	8968	9089	9102
$\tau = 0.50000$	6804	8727	10779	11553	11644	6513	7602	8672	9057	9102
$b = 1.00000$										
$\tau = 0.0$	10285	11322	13102	14027	14149	9894	9472	8702	8293	8239
$\tau = 0.50000$	6980	9772	13679	15505	15738	6457	7314	8005	8215	8239
$\tau = 1.00000$	4461	6853	10093	11556	11740	4192	5629	7391	8145	8239
$b = 2.00000$										
$\tau = 0.0$	10301	11539	14419	16452	16754	9883	9342	7955	6947	6797
$\tau = 1.00000$	4597	7948	14468	18614	19212	4145	5305	6397	6756	6797
$\tau = 2.00000$	1852	3831	7858	10407	10772	1704	2955	5233	6603	6797
$b = 4.00000$										
$\tau = 0.0$	10303	11599	15371	19301	20032	9882	9302	7388	5302	4910
$\tau = 2.00000$	1912	4537	12687	21301	22907	1683	2739	4194	4832	4910
$\tau = 4.00000$	300	1018	4021	7621	8312	270	744	2505	4527	4910
$b = 8.000$										
$\tau = 0.0$	10303	11602	15633	21535	23131	9882	9300	7230	3999	3110
$\tau = 4.000$	310	1213	6954	20642	24953	267	684	1908	2944	3110
$\tau = 8.000$	7	58	894	4173	5346	6	41	544	2438	3110
$b = 16.000$										
$\tau = 0.0$	10303	11602	15646	22493	25401	9882	9300	7222	3439	1790
$\tau = 8.000$	7	69	1570	14788	25299	6	37	409	1475	1790
$\tau = 16.000$	0	0	41	1473	3079	0	0	25	860	1790
$b = 32.000$										
$\tau = 0.0$	10303	11602	15646	22637	26815	9882	9300	7222	3356	968
$\tau = 16.000$	0	0	72	6023	25307	0	0	19	506	968
$\tau = 32.000$	0	0	0	206	1665	0	0	0	120	968
$b = \infty$										
$\tau = 0.0$	10303	11602	15646	22640	28480	9882	9300	7222	3354	0

TABLE 41 (continued)  
 $g = 0.500$ , Incidence from Narrow Source Layer (N)

$\alpha =$	0.20	0.60	0.90	0.99	1.00	0.20	0.60	0.90	0.99	1.00
POINT DIRECTION GAIN X 10000						NET FLUX DOWN X 10000				
b = 0.03125										
$\tau = 0.0$	*****	*****	*****	*****	*****	9908	9714	9558	9509	9504
$\tau = 0.01562$	36358	37725	38812	39149	39187	9327	9415	9481	9502	9504
$\tau = 0.03125$	29828	31045	32012	32312	32346	8917	9202	9427	9496	9504
b = 0.06250										
$\tau = 0.0$	*****	*****	*****	*****	*****	9859	9550	9289	9205	9196
$\tau = 0.03125$	30146	32097	33713	34227	34284	8862	9028	9154	9192	9196
$\tau = 0.06250$	23352	25057	26467	26915	26965	8203	8675	9060	9182	9196
b = 0.12500										
$\tau = 0.0$	*****	*****	*****	*****	*****	9799	9328	8899	8756	8739
$\tau = 0.06250$	23726	26376	28721	29497	29585	8129	8429	8661	8731	8739
$\tau = 0.12500$	17216	19459	21442	22097	22172	7124	7864	8505	8715	8739
b = 0.25000										
$\tau = 0.0$	*****	*****	*****	*****	*****	9735	9060	8370	8120	8091
$\tau = 0.12500$	17602	20978	24293	25465	25602	7037	7546	7951	8077	8091
$\tau = 0.25000$	11532	14238	16905	17849	17959	5616	6679	7696	8050	8091
b = 0.50000										
$\tau = 0.0$	*****	*****	*****	*****	*****	9685	8787	7707	7267	7214
$\tau = 0.25000$	11866	15798	20335	22130	22346	5530	6314	6978	7190	7214
$\tau = 0.50000$	6605	9457	12814	14151	14311	3752	5075	6565	7145	7214
b = 1.00000										
$\tau = 0.0$	*****	*****	*****	*****	*****	9658	8576	6971	6191	6090
$\tau = 0.50000$	6831	10816	16704	19521	19882	3686	4723	5713	6051	6090
$\tau = 1.00000$	2881	5276	9051	10902	11140	1876	3163	5069	5975	6090
b = 2.00000										
$\tau = 0.0$	*****	*****	*****	*****	*****	9651	8474	6312	4951	4754
$\tau = 1.00000$	2986	6191	13057	17598	18258	1842	2906	4189	4694	4754
$\tau = 2.00000$	762	2096	5518	7955	8315	554	1360	3262	4564	4754
b = 4.00000										
$\tau = 0.0$	*****	*****	*****	*****	*****	9650	8453	5927	3738	3350
$\tau = 2.00000$	790	2493	8857	16082	17449	545	1242	2556	3258	3350
$\tau = 4.00000$	77	416	2422	5216	5772	61	282	1463	3039	3350
b = 8.000										
$\tau = 0.0$	*****	*****	*****	*****	*****	9650	8452	5833	2856	2114
$\tau = 4.000$	80	496	4173	14042	17220	60	258	1108	1969	2114
$\tau = 8.000$	1	20	512	2789	3636	1	14	311	1629	2114
b = 16.000										
$\tau = 0.0$	*****	*****	*****	*****	*****	9650	8452	5829	2483	1217
$\tau = 8.000$	1	23	898	9881	17198	1	12	233	985	1217
$\tau = 16.000$	0	0	23	984	2092	0	0	14	574	1217
b = 32.000										
$\tau = 0.0$	*****	*****	*****	*****	*****	9650	8452	5829	2427	658
$\tau = 16.000$	0	0	41	4022	17198	0	0	11	338	658
$\tau = 32.000$	0	0	0	137	1132	0	0	0	80	658
b = $\infty$										
$\tau = 0.0$	*****	*****	*****	*****	*****	9650	8452	5829	2426	0

TABLE 41 (continued)  
 $g = 0.500$ , Incidence from Lambert Surface (U)

$\alpha =$	0.20	0.60	0.90	0.99	1.00	0.20	0.60	0.90	0.99	1.00
	POINT DIRECTION GAIN X 10000					NET FLUX DOWN X 10000				
$b = 0.03125$										
$\tau = 0.0$	10092	10286	10442	10491	10496	9968	9899	9844	9826	9824
$\tau = 0.01562$	9417	9699	9923	9992	10000	9725	9775	9812	9823	9824
$\tau = 0.03125$	8917	9202	9427	9496	9504	9496	9657	9782	9820	9824
$b = 0.06250$										
$\tau = 0.0$	10141	10450	10711	10795	10804	9943	9815	9706	9671	9667
$\tau = 0.03125$	8999	9472	9862	9986	10000	9468	9567	9642	9664	9667
$\tau = 0.06250$	8203	8675	9060	9182	9196	9038	9340	9582	9658	9667
$b = 0.12500$										
$\tau = 0.0$	10201	10672	11101	11244	11261	9905	9676	9464	9392	9383
$\tau = 0.06250$	8319	9082	9753	9975	10000	8992	9187	9334	9378	9383
$\tau = 0.12500$	7124	7864	8505	8715	8739	8222	8763	9220	9367	9383
$b = 0.25000$										
$\tau = 0.0$	10265	10940	11630	11880	11909	9856	9474	9067	8917	8899
$\tau = 0.12500$	7269	8429	9557	9954	10000	8155	8523	8805	8890	8899
$\tau = 0.25000$	5616	6679	7696	8050	8091	6875	7767	8588	8867	8899
$b = 0.50000$										
$\tau = 0.0$	10315	11213	12293	12733	12786	9809	9225	8476	8162	8124
$\tau = 0.25000$	5768	7374	9198	9914	10000	6795	7436	7948	8107	8124
$\tau = 0.50000$	3752	5075	6565	7145	7214	4921	6192	7550	8063	8124
$b = 1.00000$										
$\tau = 0.0$	10342	11424	13029	13809	13910	9779	9000	7720	7071	6987
$\tau = 0.50000$	3875	5786	8535	9834	10000	4848	5817	6675	6955	6987
$\tau = 1.00000$	1876	3163	5069	5975	6090	2647	4048	5985	6874	6987
$b = 2.00000$										
$\tau = 0.0$	10349	11526	13688	15049	15246	9769	8877	6975	5697	5510
$\tau = 1.00000$	1943	3706	7317	9661	10000	2604	3739	4991	5456	5510
$\tau = 2.00000$	554	1360	3262	4564	4754	838	1812	3922	5309	5510
$b = 4.00000$										
$\tau = 0.0$	10350	11547	14073	16262	16650	9769	8849	6518	4297	3895
$\tau = 2.00000$	574	1617	5242	9247	10000	824	1659	3083	3802	3895
$\tau = 4.00000$	61	282	1463	3039	3350	97	386	1774	3548	3895
$b = 8.000$										
$\tau = 0.0$	10350	11548	14167	17144	17886	9769	8848	6404	3269	2458
$\tau = 4.000$	63	337	2523	8188	10000	95	353	1344	2299	2458
$\tau = 8.000$	1	14	311	1629	2114	2	19	377	1902	2458
$b = 16.000$										
$\tau = 0.0$	10350	11548	14171	17517	18783	9769	8848	6398	2832	1415
$\tau = 8.000$	1	16	545	5770	10000	2	17	283	1150	1415
$\tau = 16.000$	0	C	14	574	1217	0	0	17	671	1415
$b = 32.000$										
$\tau = 0.0$	10350	11548	14171	17573	19342	9769	8848	6398	2767	765
$\tau = 16.000$	0	C	25	2349	10000	0	0	13	395	765
$\tau = 32.000$	0	0	0	80	658	0	0	0	94	765
$b = \infty$										
$\tau = 0.0$	10350	11548	14171	17574	20000	9769	8848	6398	2766	0

TABLE 41 (continued)  
 $g = 0.750$ , Incidence from  $\mu_0 = 0.1$

$\alpha =$	0.20	0.60	0.90	0.99	1.00	0.20	0.60	0.90	0.99	1.00
	POINT DIRECTION GAIN X 10000					NET FLUX DOWN X 10000				
$b = 0.03125$										
$\tau = 0.0$	10161	10510	10798	10890	10900	9815	9407	9066	8957	8945
$\tau = 0.01562$	8783	9275	9676	9802	9817	8631	8788	8906	8941	8945
$\tau = 0.03125$	7523	7967	8328	8442	8455	7613	8248	8765	8927	8945
$b = 0.06250$										
$\tau = 0.0$	10224	10734	11179	11325	11341	9698	8997	8368	8159	8135
$\tau = 0.03125$	7645	8382	9016	9221	9245	7476	7802	8051	8127	8135
$\tau = 0.06250$	5631	6255	6792	6966	6986	5826	6889	7804	8102	8135
$b = 0.12500$										
$\tau = 0.0$	10279	10950	11584	11803	11828	9572	8497	7433	7057	7014
$\tau = 0.06250$	5758	6722	7621	7928	7964	5661	6313	6834	6996	7014
$\tau = 0.12500$	3164	3888	4575	4812	4840	3489	5009	6456	6956	7014
$b = 0.25000$										
$\tau = 0.0$	10307	11090	11900	12199	12234	9488	8085	6513	5911	5839
$\tau = 0.12500$	3252	4266	5324	5718	5765	3359	4490	5479	5802	5839
$\tau = 0.25000$	1042	1662	2366	2636	2668	1419	3107	5020	5752	5839
$b = 0.50000$										
$\tau = 0.0$	10314	11142	12072	12441	12486	9463	7889	5884	5028	4922
$\tau = 0.25000$	1073	1842	2838	3261	3313	1367	2823	4325	4860	4922
$\tau = 0.50000$	167	537	1112	1375	1408	438	1809	3875	4806	4922
$b = 1.00000$										
$\tau = 0.0$	10315	11156	12161	12596	12651	9460	7824	5481	4334	4185
$\tau = 0.50000$	171	597	1380	1796	1851	429	1691	3399	4101	4185
$\tau = 1.00000$	30	203	625	877	912	150	996	2927	4036	4185
$b = 2.00000$										
$\tau = 0.0$	10315	11160	12215	12725	12793	9459	7803	5191	3668	3451
$\tau = 1.00000$	30	226	813	1249	1314	148	940	2540	3348	3451
$\tau = 2.00000$	6	69	357	607	646	37	417	1974	3256	3451
$b = 4.00000$										
$\tau = 0.0$	10315	11160	12245	12841	12931	9459	7799	5017	3008	2675
$\tau = 2.00000$	6	77	490	988	1080	36	396	1675	2553	2675
$\tau = 4.00000$	0	14	172	417	465	4	98	1038	2410	2675
$b = 8.000$										
$\tau = 0.0$	10315	11161	12254	12940	13066	9459	7798	4958	2427	1885
$\tau = 4.000$	0	16	248	828	988	4	94	862	1740	1885
$\tau = 8.000$	0	1	51	258	322	0	7	320	1518	1885
$b = 16.000$										
$\tau = 0.0$	10315	11161	12255	13000	13185	9459	7798	4951	2073	1190
$\tau = 8.000$	0	1	76	647	969	0	7	263	1006	1190
$\tau = 16.000$	0	0	5	119	203	0	0	32	702	1190
$b = 32.000$										
$\tau = 0.0$	10315	11161	12255	13017	13271	9459	7798	4951	1973	685
$\tau = 16.000$	0	0	8	357	968	0	0	26	442	685
$\tau = 32.000$	0	0	0	29	117	0	0	0	171	685
$b = \infty$										
$\tau = 0.0$	10315	11161	12255	13018	13387	9459	7798	4951	1967	0



TABLE 41 (continued)  
 $g = 0.750$ , Incidence from  $\mu_0 = 1.0$

$a =$	0.20	0.60	0.90	0.99	1.00	0.20	0.60	0.90	0.99	1.00
	POINT DIRECTION GAIN X 10000					NET FLUX DOWN X 10000				
$b = 0.03125$										
$\tau = 0.0$	10022	10069	10108	10120	10122	9996	9988	9981	9979	9979
$\tau = 0.01562$	9905	10031	10130	10161	10164	9872	9925	9965	9978	9979
$\tau = 0.03125$	9781	9963	10105	10148	10153	9749	9863	9950	9976	9979
$b = 0.06250$										
$\tau = 0.0$	10035	10114	10185	10208	10211	9993	9977	9963	9958	9957
$\tau = 0.03125$	9802	10037	10229	10289	10296	9745	9851	9931	9955	9957
$\tau = 0.06250$	9557	9899	10174	10259	10269	9503	9726	9899	9951	9957
$b = 0.12500$										
$\tau = 0.0$	10053	10185	10314	10360	10366	9987	9956	9925	9914	9913
$\tau = 0.06250$	9591	10027	10400	10523	10536	9496	9703	9860	9908	9913
$\tau = 0.12500$	9115	9747	10276	10446	10465	9028	9455	9795	9901	9913
$b = 0.25000$										
$\tau = 0.0$	10075	10287	10531	10626	10637	9979	9919	9851	9824	9821
$\tau = 0.12500$	9165	9958	10694	10949	10979	9016	9411	9717	9811	9821
$\tau = 0.25000$	8273	9393	10406	10747	10787	8145	8926	9585	9797	9821
$b = 0.50000$										
$\tau = 0.0$	10098	10420	10887	11099	11126	9968	9861	9706	9635	9627
$\tau = 0.25000$	8339	9723	11179	11735	11801	8127	8849	9427	9607	9627
$\tau = 0.50000$	6784	8612	10496	11192	11274	6617	7928	9154	9578	9627
$b = 1.00000$										
$\tau = 0.0$	10114	10563	11445	11950	12019	9959	9788	9441	9240	9213
$\tau = 0.50000$	6856	9072	11895	13166	13328	6595	7806	8845	9176	9213
$\tau = 1.00000$	4515	7032	10285	11695	11870	4347	6185	8279	9112	9213
$b = 2.00000$										
$\tau = 0.0$	10121	10668	12212	13443	13632	9955	9727	9026	8456	8368
$\tau = 1.00000$	4572	7549	12617	15607	16030	4328	6034	7733	8304	8368
$\tau = 2.00000$	1956	4397	9077	11784	12158	1850	3649	6610	8160	8368
$b = 4.00000$										
$\tau = 0.0$	10122	10706	12961	15731	16259	9954	9702	8584	7157	6884
$\tau = 2.00000$	1982	4787	12203	18891	20050	1841	3528	5858	6777	6884
$\tau = 4.00000$	350	1508	5995	10381	11138	324	1177	3973	6465	6884
$b = 8.000$										
$\tau = 0.0$	10122	10709	13309	18268	19600	9954	9700	8370	5670	4936
$\tau = 4.000$	354	1653	8621	20755	23859	323	1132	3346	4747	4936
$\tau = 8.000$	10	142	2074	7014	8374	9	106	1306	4163	4936
$b = 16.000$										
$\tau = 0.0$	10122	10709	13349	19910	22697	9954	9700	8345	4700	3120
$\tau = 8.000$	10	156	3053	17661	25290	9	101	1076	2763	3120
$\tau = 16.000$	0	1	211	3269	5318	0	1	131	1930	3120
$b = 32.000$										
$\tau = 0.0$	10122	10709	13350	20375	24954	9954	9700	8345	4426	1796
$\tau = 16.000$	0	1	311	9814	25393	0	1	108	1215	1796
$\tau = 32.000$	0	0	2	794	3062	0	0	1	469	1796
$b = \infty$										
$\tau = 0.0$	10122	10709	13350	20404	28015	9954	9700	8345	4408	0

TABLE 41 (continued)  
 $g = 0.750$ , Incidence from Narrow Source Layer (N)

$\alpha =$	0.20	0.60	0.90	0.99	1.00	0.20	0.60	0.90	0.99	1.00
POINT DIRECTION GAIN X 10000					NET FLUX DOWN X 10000					
b = 0.03125										
$\tau = 0.0$	*****	*****	*****	*****	*****	9928	9771	9641	9600	9595
$\tau = 0.01562$	36546	38341	39803	40264	40315	9344	9469	9564	9592	9595
$\tau = 0.03125$	30025	31686	33035	33458	33506	8932	9252	9507	9586	9595
b = 0.06250										
$\tau = 0.0$	*****	*****	*****	*****	*****	9895	9654	9440	9369	9361
$\tau = 0.03125$	30354	32818	34931	35617	35694	8894	9124	9302	9355	9361
$\tau = 0.06250$	23583	25843	27771	28395	28465	8229	8762	9204	9345	9361
b = 0.12500										
$\tau = 0.0$	*****	*****	*****	*****	*****	9858	9505	9159	9038	9024
$\tau = 0.06250$	23924	27131	30097	31107	31223	8181	8592	8914	9013	9024
$\tau = 0.12500$	17456	20337	22992	23893	23996	7165	8005	8749	8996	9024
b = 0.25000										
$\tau = 0.0$	*****	*****	*****	*****	*****	9823	9336	8789	8578	8553
$\tau = 0.12500$	17763	21665	25698	27178	27352	7112	7797	8357	8533	8553
$\tau = 0.25000$	11750	15119	18613	19892	20042	5673	6890	8081	8504	8553
b = 0.50000										
$\tau = 0.0$	*****	*****	*****	*****	*****	9797	9174	8331	7960	7914
$\tau = 0.25000$	11979	16334	21604	23774	24038	5625	6661	7579	7879	7914
$\tau = 0.50000$	6773	10241	14553	16337	16555	3821	5358	7128	7829	7914
b = 1.00000										
$\tau = 0.0$	*****	*****	*****	*****	*****	9784	9052	7817	7157	7069
$\tau = 0.50000$	6908	11194	17692	20890	21304	3788	5145	6525	7013	7069
$\tau = 1.00000$	2990	5898	10713	13144	13460	1943	3489	5816	6927	7069
b = 2.00000										
$\tau = 0.0$	*****	*****	*****	*****	*****	9781	8991	7325	6164	5991
$\tau = 1.00000$	3046	6497	13777	18519	19206	1926	3335	5161	5902	5991
$\tau = 2.00000$	814	2520	7033	10206	10671	595	1646	4124	5756	5991
b = 4.00000										
$\tau = 0.0$	*****	*****	*****	*****	*****	9781	8977	6980	5045	4697
$\tau = 2.00000$	828	2783	9626	16590	17830	591	1571	3533	4564	4697
$\tau = 4.00000$	89	602	3638	7390	8085	71	420	2230	4318	4697
b = 8.000										
$\tau = 0.0$	*****	*****	*****	*****	*****	9781	8976	6853	4011	3317
$\tau = 4.000$	90	663	5242	14689	17195	70	401	1856	3124	3317
$\tau = 8.000$	2	44	1115	4623	5659	1	32	694	2728	3317
b = 16.000										
$\tau = 0.0$	*****	*****	*****	*****	*****	9781	8976	6840	3375	2094
$\tau = 8.000$	2	48	1641	11622	17056	1	30	571	1808	2094
$\tau = 16.000$	0	0	111	2138	3571	0	0	69	1262	2094
b = 32.000										
$\tau = 0.0$	*****	*****	*****	*****	*****	9781	8976	6839	3196	1206
$\tau = 16.000$	0	0	164	6419	17049	0	0	57	794	1206
$\tau = 32.000$	0	0	1	519	2056	0	0	1	307	1206
b = $\infty$										
$\tau = 0.0$	*****	*****	*****	*****	*****	9781	8976	6839	3184	0

TABLE 41 (continued)  
 $g = 0.750$ , Incidence from Lambert Surface (U)

$a =$	0.20	0.60	0.90	0.99	1.00	0.20	0.60	0.90	0.99	1.00
	POINT DIRECTION GAIN X 10000					NET FLUX DOWN X 10000				
$b = 0.03125$										
$\tau = 0.0$	10072	10229	10359	10400	10405	9981	9940	9906	9895	9894
$\tau = 0.01562$	9415	9695	9921	9992	10000	9739	9816	9874	9892	9894
$\tau = 0.03125$	8932	9252	9507	9586	9595	9509	9698	9844	9889	9894
$b = 0.06250$										
$\tau = 0.0$	10105	10346	10560	10631	10639	9968	9892	9824	9802	9799
$\tau = 0.03125$	8993	9462	9858	9986	10000	9493	9646	9761	9796	9799
$\tau = 0.06250$	8229	8762	9204	9345	9361	9063	9418	9701	9789	9799
$b = 0.12500$										
$\tau = 0.0$	10142	10495	10841	10962	10976	9948	9815	9682	9635	9630
$\tau = 0.06250$	8309	9063	9744	9974	10000	9039	9331	9555	9622	9630
$\tau = 0.12500$	7165	8005	8749	8996	9024	8267	8904	9439	9610	9630
$b = 0.25000$										
$\tau = 0.0$	10177	10664	11211	11422	11447	9924	9706	9449	9348	9336
$\tau = 0.12500$	7257	8399	9540	9952	10000	8233	8770	9192	9322	9336
$\tau = 0.25000$	5673	6890	8081	8504	8553	6948	8005	8970	9298	9336
$b = 0.50000$										
$\tau = 0.0$	10203	10826	11669	12040	12086	9902	9574	9094	8875	8848
$\tau = 0.25000$	5761	7345	9175	9911	10000	6909	7823	8582	8821	8848
$\tau = 0.50000$	3821	5358	7128	7829	7914	5024	6556	8171	8776	8848
$b = 1.00000$										
$\tau = 0.0$	10216	10948	12183	12843	12931	9889	9454	8616	8144	8080
$\tau = 0.50000$	3887	5801	8529	9832	10000	4990	6348	7611	8032	8080
$\tau = 1.00000$	1943	3489	5816	6927	7069	2758	4513	6885	7947	8080
$b = 2.00000$										
$\tau = 0.0$	10219	11009	12675	13836	14009	9885	9383	8089	7108	6960
$\tau = 1.00000$	1976	3823	7419	9676	10000	2738	4335	6185	6879	6960
$\tau = 2.00000$	595	1646	4124	5756	5991	910	2241	5018	6720	6960
$b = 4.00000$										
$\tau = 0.0$	10219	11023	13020	14955	15303	9884	9364	7684	5840	5499
$\tau = 2.00000$	605	1813	5631	9346	10000	904	2144	4324	5369	5499
$\tau = 4.00000$	71	420	2230	4318	4697	115	594	2762	5086	5499
$b = 8.000$										
$\tau = 0.0$	10219	11024	13147	15989	16683	9884	9363	7527	4629	3891
$\tau = 4.000$	72	463	3213	8590	10000	115	569	2301	3686	3891
$\tau = 8.000$	1	32	694	2728	3317	2	46	865	3220	3891
$b = 16.000$										
$\tau = 0.0$	10219	11024	13160	16625	17906	9884	9363	7510	3877	2457
$\tau = 8.000$	1	35	1022	6858	10000	2	44	711	2135	2457
$\tau = 16.000$	0	0	69	1262	2094	0	0	86	1491	2457
$b = 32.000$										
$\tau = 0.0$	10219	11024	13161	16804	18794	9884	9363	7510	3665	1414
$\tau = 16.000$	0	0	102	3790	10000	0	0	71	938	1414
$\tau = 32.000$	0	0	1	307	1206	0	0	1	362	1414
$b = \infty$										
$\tau = 0.0$	10219	11024	13161	16816	20000	9884	9363	7510	3652	0

TABLE 41 (continued)  
 $g = 0.875$ , Incidence from  $\mu_0 = 0.1$

$a =$	0.20	0.60	0.90	0.99	1.00	0.20	0.60	0.90	0.99	1.00
POINT DIRECTION GAIN X 10000						NET FLUX DOWN X 10000				
$b = 0.03125$										
$\tau = 0.0$	10167	10550	10888	10999	11011	9869	9564	9290	9199	9189
$\tau = 0.01562$	8862	9544	10123	10309	10331	8680	8934	9125	9182	9189
$\tau = 0.03125$	7630	8318	8895	9080	9101	7649	8374	8976	9167	9189
$b = 0.06250$										
$\tau = 0.0$	10224	10772	11300	11483	11504	9791	9261	8734	8548	8527
$\tau = 0.03125$	7759	8792	9733	10050	10086	7551	8033	8402	8514	8527
$\tau = 0.06250$	5767	6730	7601	7893	7926	5869	7061	8130	8486	8527
$b = 0.12500$										
$\tau = 0.0$	10268	10981	11749	12036	12070	9709	8887	7950	7589	7547
$\tau = 0.06250$	5897	7264	8641	9137	9195	5752	6610	7305	7522	7547
$\tau = 0.12500$	3291	4386	5510	5918	5966	3510	5167	6863	7475	7547
$b = 0.25000$										
$\tau = 0.0$	10290	11115	12115	12525	12574	9656	8573	7119	6492	6415
$\tau = 0.12500$	3379	4815	6493	7161	7242	3418	4744	5961	6369	6415
$\tau = 0.25000$	1106	1991	3127	3599	3657	1381	3134	5377	6303	6415
$b = 0.50000$										
$\tau = 0.0$	10294	11163	12320	12842	12908	9641	8423	6510	5567	5445
$\tau = 0.25000$	1137	2197	3765	4498	4591	1345	2894	4685	5365	5445
$\tau = 0.50000$	171	634	1510	1964	2023	362	1675	4075	5289	5445
$b = 1.00000$										
$\tau = 0.0$	10295	11174	12416	13032	13113	9639	8379	6142	4857	4680
$\tau = 0.50000$	175	693	1835	2522	2617	357	1587	3627	4563	4680
$\tau = 1.00000$	23	203	785	1194	1253	99	835	3019	4475	4680
$b = 2.00000$										
$\tau = 0.0$	10295	11176	12464	13168	13267	9639	8367	5913	4237	3984
$\tau = 1.00000$	23	218	964	1600	1699	98	804	2704	3833	3984
$\tau = 2.00000$	3	60	417	789	851	21	330	2050	3716	3984
$b = 4.00000$										
$\tau = 0.0$	10295	11176	12486	13278	13399	9639	8366	5787	3658	3286
$\tau = 2.00000$	4	64	520	1134	1251	21	321	1833	3099	3286
$\tau = 4.00000$	0	12	199	537	606	2	80	1154	2933	3286
$b = 8.0000$										
$\tau = 0.0$	10295	11176	12494	13371	13528	9639	8365	5739	3122	2552
$\tau = 4.0000$	0	13	252	864	1026	2	78	1027	2326	2552
$\tau = 8.0000$	0	1	70	355	439	0	7	439	2080	2552
$b = 16.0000$										
$\tau = 0.0$	10295	11176	12495	13440	13656	9639	8365	5731	2708	1800
$\tau = 8.0000$	0	1	89	673	941	0	7	390	1534	1800
$\tau = 16.0000$	0	0	11	198	305	0	0	72	1182	1800
$b = 32.0000$										
$\tau = 0.0$	10295	11176	12495	13472	13769	9639	8365	5731	2520	1136
$\tau = 16.0000$	0	0	14	444	926	0	0	64	815	1137
$\tau = 32.0000$	0	0	0	71	193	0	0	2	423	1137
$b = \infty$										
$\tau = 0.0$	10295	11176	12495	13477	13961	9639	8365	5731	2492	0

TABLE 41 (continued)  
 $g = 0.875$ , Incidence from  $\mu_0 = 1.0$

	$\alpha = 0.20$	$0.60$	$0.90$	$0.99$	$1.00$	$0.20$	$0.60$	$0.90$	$0.99$	$1.00$
	POINT DIRECTION GAIN X 10000					NET FLUX DOWN X 10000				
$b = 0.03125$										
$\tau = 0.0$	10010	10031	10050	10056	10056	9998	9995	9992	9991	9991
$\tau = 0.01562$	9890	9982	10054	10076	10079	9874	9932	9976	9989	9991
$\tau = 0.03125$	9766	9919	10037	10073	10077	9751	9870	9960	9988	9991
$b = 0.06250$										
$\tau = 0.0$	10015	10052	10086	10097	10099	9997	9990	9984	9982	9981
$\tau = 0.03125$	9776	9953	10094	10139	10144	9749	9865	9952	9978	9981
$\tau = 0.06250$	9534	9827	10058	10130	10138	9508	9741	9921	9975	9981
$b = 0.12500$										
$\tau = 0.0$	10024	10084	10147	10170	10173	9994	9981	9967	9963	9962
$\tau = 0.06250$	9550	9884	10164	10254	10265	9505	9731	9904	9956	9962
$\tau = 0.12500$	9082	9633	10086	10230	10246	9039	9487	9841	9950	9962
$b = 0.25000$										
$\tau = 0.0$	10033	10131	10250	10299	10305	9991	9965	9936	9924	9923
$\tau = 0.12500$	9104	9728	10280	10468	10489	9034	9468	9807	9911	9923
$\tau = 0.25000$	8233	9233	10111	10402	10436	8168	8993	9679	9898	9923
$b = 0.50000$										
$\tau = 0.0$	10043	10190	10417	10528	10542	9986	9941	9875	9843	9840
$\tau = 0.25000$	8262	9378	10465	10865	10913	8160	8960	9612	9817	9839
$\tau = 0.50000$	6749	8433	10092	10689	10759	6663	8068	9354	9789	9839
$b = 1.00000$										
$\tau = 0.0$	10051	10253	10678	10943	10980	9982	9910	9762	9673	9660
$\tau = 0.50000$	6780	8631	10723	11611	11722	6653	8017	9222	9615	9660
$\tau = 1.00000$	4513	6938	9893	11123	11275	4422	6458	8701	9558	9660
$b = 2.00000$										
$\tau = 0.0$	10053	10299	11048	11706	11812	9980	9884	9578	9309	9267
$\tau = 1.00000$	4538	7161	10960	12996	13279	4414	6393	8456	9183	9266
$\tau = 2.00000$	1994	4546	9134	11619	11954	1933	4067	7432	9056	9266
$b = 4.00000$										
$\tau = 0.0$	10054	10317	11462	13063	13384	9980	9872	9343	8583	8431
$\tau = 2.00000$	2006	4724	10702	15374	16153	1929	4012	7040	8285	8431
$\tau = 4.00000$	378	1809	7060	11613	12353	362	1539	5212	8001	8431
$b = 8.000$										
$\tau = 0.0$	10054	10319	11735	15088	16029	9980	9871	9174	7416	6919
$\tau = 4.000$	381	1887	8731	18304	20503	361	1514	4775	6681	6919
$\tau = 8.000$	13	243	3448	9793	11278	12	197	2335	6081	6919
$b = 16.000$										
$\tau = 0.0$	10054	10319	11795	17057	19390	9980	9871	9136	6247	4944
$\tau = 8.000$	13	255	4387	18644	24299	12	193	2088	4540	4945
$\tau = 16.000$	0	3	629	5885	8360	0	3	410	3521	4945
$b = 32.000$										
$\tau = 0.0$	10054	10319	11797	17993	22476	9980	9871	9134	5688	3123
$\tau = 16.000$	0	4	805	13191	25394	0	3	364	2429	3124
$\tau = 32.000$	0	0	18	2116	5294	0	0	12	1263	3125
$b = \infty$										
$\tau = 0.0$	10054	10319	11797	18135	27771	9980	9871	9134	5603	0

[illegible]

TABLE 41 (continued)  
 $g = 0.875$ , Incidence from Lambert Surface (U)

$\alpha =$	0.20	0.60	0.90	0.99	1.00	0.20	0.60	0.90	0.99	1.00
	POINT DIRECTION GAIN X 10000					NET FLUX DOWN X 10000				
$b = 0.03125$										
$\tau = 0.0$	10054	10178	10286	10321	10325	9989	9965	9944	9938	9937
$\tau = 0.01562$	9411	9689	9919	9992	10000	9747	9841	9913	9934	9937
$\tau = 0.03125$	8944	9293	9576	9665	9675	9518	9723	9882	9931	9937
$b = 0.06250$										
$\tau = 0.0$	10075	10258	10433	10493	10500	9982	9939	9897	9883	9881
$\tau = 0.03125$	8987	9450	9852	9985	10000	9509	9693	9834	9876	9881
$\tau = 0.06250$	8247	8829	9322	9481	9500	9079	9465	9774	9870	9881
$b = 0.12500$										
$\tau = 0.0$	10096	10354	10632	10736	10749	9972	9897	9816	9785	9781
$\tau = 0.06250$	8299	9040	9733	9972	10000	9066	9417	9689	9772	9781
$\tau = 0.12500$	7190	8105	8937	9219	9251	8293	8988	9572	9760	9781
$b = 0.25000$										
$\tau = 0.0$	10115	10456	10888	11070	11093	9961	9840	9682	9615	9606
$\tau = 0.12500$	7245	8365	9518	9949	10000	8276	8915	9429	9588	9606
$\tau = 0.25000$	5705	7026	8363	8850	8907	6990	8147	9204	9565	9606
$b = 0.50000$										
$\tau = 0.0$	10128	10548	11199	11519	11561	9950	9773	9478	9328	9309
$\tau = 0.25000$	5753	7308	9141	9906	10000	6971	8049	8977	9275	9309
$\tau = 0.50000$	3857	5528	7523	8340	8439	5082	6771	8558	9229	9309
$b = 1.00000$										
$\tau = 0.0$	10134	10615	11544	12109	12188	9944	9712	9197	8868	8821
$\tau = 0.50000$	3891	5788	8491	9825	10000	5065	6662	8223	8760	8821
$\tau = 1.00000$	1976	3678	6332	7642	7812	2819	4796	7476	8671	8821
$b = 2.00000$										
$\tau = 0.0$	10135	10647	11876	12857	13012	9942	9676	8874	8172	8059
$\tau = 1.00000$	1992	3867	7419	9672	10000	2810	4703	7039	7951	8059
$\tau = 2.00000$	617	1818	4743	6704	6988	952	2525	5814	7784	8059
$b = 4.00000$										
$\tau = 0.0$	10135	10655	12123	13756	14066	9942	9666	8596	7217	6947
$\tau = 2.00000$	621	1912	5777	9372	10000	949	2472	5344	6768	6947
$\tau = 4.00000$	77	518	2864	5471	5934	127	760	3623	6463	6947
$b = 8.000$										
$\tau = 0.0$	10135	10656	12236	14713	15339	9942	9665	8458	6116	5494
$\tau = 4.000$	77	544	3601	8762	10000	127	744	3258	5215	5494
$\tau = 8.000$	2	51	1133	3937	4661	3	77	1461	4690	5495
$b = 16.000$										
$\tau = 0.0$	10135	10656	12256	15492	16705	9942	9665	8433	5191	3889
$\tau = 8.000$	2	53	1447	7478	10001	3	76	1299	3471	3889
$\tau = 16.000$	0	1	189	2244	3295	0	1	245	2678	3890
$b = 32.000$										
$\tau = 0.0$	10135	10656	12256	15848	17920	9942	9665	8432	4766	2455
$\tau = 16.000$	0	1	242	5027	10002	0	1	218	1847	2456
$\tau = 32.000$	0	0	5	804	2082	0	0	7	960	2457
$b = \infty$										
$\tau = 0.0$	10135	10656	12256	15903	20000	9942	9665	8432	4701	1410

## 14   Results for Other Phase Functions, Finite Layers

### 14.1 SIMILARITY RELATIONS

#### 14.1.1 Derivation, Alternatives

We have met simple versions of the similarity relations in earlier sections, namely, for  $b = \infty$  (Section 12.2) and for  $a = 1$  (Section 13.2). We shall now discuss the general relations.

The problem is posed as follows. Suppose we have a thick slab, with optical thickness  $b$ , and with the scattering law at each point characterized by albedo  $a$  and asymmetry factor  $g$ . Is it possible to choose a slab with isotropic scattering ( $g = 0$ ), with a different optical thickness  $b_0$  and a different albedo  $a_0$  in such a manner that the reflection and transmission functions in the new situation closely resemble those in the earlier problem?

The practical significance of this problem is great, considering the many numerical data available for isotropic scattering (Chapters 8–9) and the amount of effort that can be saved if not every detail of the computation has to be repeated when a different scattering law is assumed. The similarity problem was first posed in this form during discussions in 1967 at a Symposium in Tucson and solved by van de Hulst and Grossman (1968) in the following manner.

Consider an unbounded medium. A diffusion stream through the unbounded medium is attenuated as  $\exp(-k\tau)$ , where  $k$  is the diffusion exponent. The first obvious relation to ensure similarity is

$$k\tau = k_0\tau_0 \quad (1)$$



A thick slab has a diffusion domain in which essentially these same formulas hold. Hence the ratio  $b_0/b$  should be the same as  $\tau_0/\tau$  so that

$$\tau/\tau_0 = b/b_0 = k_0/k \quad (2)$$

We have one further parameter to choose. This is used to make the shape of the diffusion pattern  $P(u)$  similar in the two cases compared. The normalization is arbitrary, but we can keep the weighted average value of  $u$  in the diffusion pattern, i.e., the factor (Display 5.2)

$$y = (1 - a)/k = (1 - a_0)/k_0 = y_0 \quad (3)$$

constant. The graph of  $y$  for the Henyey–Greenstein functions given in Fig. 12.6 may be used to match the proper numbers. Equations (2) and (3) can be combined into

$$\tau/\tau_0 = b/b_0 = k_0/k = (1 - a_0)/(1 - a) \quad (4)$$

The choice that leads to Eq. (4) is not unique. In that respect, the similarity relations resemble the problem of mapping the spherical earth on a plane map: there are many possibilities, each of which leaves a certain distortion. The merits of the various methods for different purposes can be explained, but the choice remains a matter of taste.

A first alternative is to require that  $D/y$ , instead of  $y$ , be invariant. By Display 5.2, this gives, instead of Eq. (4),

$$\tau/\tau_0 = b/b_0 = k_0/k = 1/(1 - ag) \quad (5)$$

A second alternative, to be explained presently, is to employ Eq. (2) and

$$1 - a_0 = (1 - a)/(1 - ag) \quad (6)$$

which follows from a simple combination of Eqs. (4) and (5).

We shall now discuss the merits of these possibilities. There is no logical reason why Eq. (5) should be better than Eq. (4), or conversely. The practical application of either of these forms requires that the transcendental function  $k(a, g)$  be available before the value of  $a_0$  which matches the combination  $(a, g)$  can be computed. This problem does not exist if Eq. (6) is chosen. We feel that Eq. (6) can be generally recommended as the better and easier choice for the following reasons:

(a) It is not necessary to compute  $k(a, g)$  before  $a_0$  is found, and in dealing with semi-infinite atmospheres the computation of  $k$  can be avoided altogether.

(b) Tests made on a key quantity,  $URU$  for  $b = \infty$ , show an almost perfect similarity on the basis of Eq. (6). See Fig. 12.5.

(c) Other tests showed that Eqs. (4) and (5) tended to give deviations from the true value to opposite sides. Equation (6) represents—in a sense—a choice

just between Eqs. (4) and (5). This can be seen as follows:

In Eq. (4), the invariant quantity is  $(1 - a)\sqrt{3}/k$ .

In Eq. (5), the invariant quantity is  $k/(1 - ag)\sqrt{3}$ .

In Eq. (6), the invariant quantity is  $s = [(1 - a)/(1 - ag)]^{1/2}$ .

$s$  is the geometric average between the quantities on the preceding lines. Each of the three quantities just mentioned has an expansion in  $k$ , by the equations of Chapter 5, of the form

$$k/(1 - g)\sqrt{3} + O(k^3)$$

which confirms that the three possibilities coincide if  $a$  is close to 1. The coefficients of  $k^3$  and higher terms differ.

### 14.1.2 Special Cases, Simple Versions

A first special case arises if we test the similarity principle on a set of problems in which an arbitrary peak of exact forward scattering is added to a given phase function with a given albedo. The derivation given in Section 14.1.3 shows that in this set *each* of the similarity rules, Eqs. (4), (5), and (6), is exactly fulfilled. This is gratifying as a logical test, but also shows that this exercise cannot serve to indicate which of these three choices is to be preferred.

A second special case is nearly conservative scattering ( $a$  near 1,  $k$  small). Then it usually does not pay to go through the actual computation of the function  $k(a, g)$ . It is simpler to neglect terms in  $k^3$  so that  $k = [3(1 - g)(1 - a)]^{1/2}$ , after which we find that each of the three formulas above leads to

$$\tau/\tau_0 = b/b_0 = k_0/k = 1/(1 - g) = (1 - a_0)/(1 - a) \quad (7)$$

Third, in the conservative case the same relation remains valid with  $a = a_0 = 1$ , so that

$$\tau/\tau_0 = b/b_0 = 1/(1 - g) \quad (8)$$

It is then sufficient to remember that  $b_0 = b(1 - g)$ , the reduced optical thickness, must be kept invariant. In this simple form the similarity relation has been known at least since the early work on neutron scattering about 1940. See remarks to that effect made by Davison (1957, Eqs. 17.25 and 17.26) or Stokes and DeMarcus (1971). The remark that this similarity is exact in the addition of a forward peak was also made by Davison (1957, footnote p. 241).

Another way of looking at the similarity relations is that they permit us (with fair accuracy) to treat certain functions as if the number of independent variables is one less than it actually is. This is summarized in some detail in Display 14.1. The escape function follows the same statements as the reflection function against a semi-infinite slab.

**DISPLAY 14.1**

## Simple Special Cases of Similarity Relations

Quantity	Actual number of variables	Reduced number of variables	Recommended equation	Examples
Internal intensity	4 ( $a, b, g, \tau$ )	3 ( $a_0, b_0, \tau_0$ )	Eqs. (6) + (2)	—
Reflection function	3 ( $a, b, g$ )	2 ( $a_0, b_0$ )	Eqs. (6) + (2)	—
Reflection against nonconservative, semi-infinite slab	2 ( $a, g$ )	1 ( $a_0$ )	Eq. (6)	Section 12.2
Reflection against finite conservative layer	2 ( $b, g$ )	1 ( $b_0$ )	Eq. (8)	Section 13.2
Reflection against conservative semi-infinite slab	1 ( $g$ )	0	—	Section 12.1

In each of the examples where two variables are reduced to one, we can take the invariant quantity as abscissa of a graph and find that the two-dimensional grid of points virtually collapses into one curve. A striking example is shown in Fig. 12.5.

Since we shall not return to the internal radiation field in later sections, attention is drawn here to Fig. 9.15 which shows this radiation field in a number of examples side by side with the approximately similar isotropic case. These examples were selected from available computer runs without optimizing the similarity fully. Yet the curves left and right look sufficiently alike to make them interchangeable for many practical purposes. This means that for such purposes the similarity rules are a reliable guide.

**14.1.3 Addition of a Forward Peak**

Scattering in the exact forward direction is no scattering at all. Hence, if in any problem we add the formal assumption that a certain amount of scattering occurs in the exact forward direction, this must make no difference in the results. In this way we can define two situations with different  $b$ ,  $a$ , and  $g$ , which are strictly equivalent. Since equivalence is stronger than similarity, we should hope that two equivalent situations obey the similarity rule stated earlier. This we shall now check.

Inside an atmosphere formed by real scatterers and characterized by the values  $b'$ ,  $a'$ ,  $g'$ ,  $k'$ , we sprinkle a well mixed medium of fictitious conservative

forward scatterers, characterized by the values  $b'' = 1$ ,  $a'' = 1$ ,  $g'' = 1$ ,  $k'' = 0$ . We then obtain the following depths for extinction = absorption + scattering.

$$\text{total extinction depth: } b = b' + b''$$

$$\text{total absorption depth: } b(1 - a) = b'(1 - a')$$

$$\text{total scattering depth: } ba = b'a' + b''$$

Taking only the forward component of the last relation we have

$$\langle \cos \alpha \rangle \text{ times scattering depth: } bag = b'a'g' + b''$$

Finally, the attenuation suffered by the total flux in the diffusion domain (a description valid if the depth is very large) is

$$\text{diffusion depth: } bk = b'k'$$

Combination of these various equations easily leads to

$$b/b' = (1 - a')/(1 - a) = a'(1 - g')/a(1 - g) = k'/k$$

which agrees with each of the rules stated in Section 14.1.1.

The preceding transformation is presented in the form of a logical test, but has practical applications as well. The actual scattering pattern of particles large compared to the wavelength has a diffraction peak, which, though not infinitely sharp, is very strongly concentrated around the forward direction. The necessity to include this peak can be very bothersome in numerical calculations, because it greatly increases the number of Legendre functions which have to be retained in the expansion of the phase function (Section 15.3.5). A practical consequence of the result just derived is that we can simply omit the diffraction peak, provided it is sharp, and provided we attach to the remaining phase function the appropriately adjusted values of  $a'$  and  $g'$ . The same conclusion has been reached by Hansen (1969).

A second practical application may be made, even if we do not bother about the existence of a diffraction peak. Say a result is sought for a phase function with a certain  $g'$  and  $a'$ , and we wish to make use of tables (e.g., this book or van de Hulst, 1968) available only for a somewhat different asymmetry factor  $g$ . We may then, by arbitrarily adding or subtracting a fictitious forward peak, quite easily transform to this value  $g$ . After transforming  $a'$  to  $a$  and  $b'$  to  $b$ , we can then obtain the result from the existing tables by interpolation in  $a$  and  $b$ .

## 14.2 TRUNCATION TESTS

Logically, the next step is to compute accurate results for situations which should be similar by the equations in the preceding section, and to see how well the numerical values match. Having done so for semi-infinite atmospheres in

Sections 12.1 and 12.2, we had hoped to find equally useful data for finite slabs in the published literature. The harvest was disappointing, for many authors stop when they have derived the formulas; others present numerical results only in the form of a few sample curves; still others use methods that plainly lack the accuracy necessary for these comparisons.

New computer runs of the same format as used for the other tables in this book, but for different phase functions, would have provided excellent material for this comparison. However, the comparisons which were available (see below) left no doubt that within a *practical* accuracy of a few percent the similarity laws can be trusted, so a *practical* reason for such additional computer runs did not exist.

We shall in this section compare situations in which the basic parameters  $a$ ,  $g$ , and  $b$  are equal, and only the coefficients  $\omega_2$  and higher in the Legendre expansion of the phase function are different. If these higher coefficients are all 0, we say that the phase function is truncated; so what we really do in the present section is to examine the influence of truncation.

The results are presented in the order of increasing  $g$ .

#### 14.2.1 Scattering with $g = 0$

Two symmetric scattering laws may be compared with isotropic scattering (I).

(P) The Rayleigh phase function, number 5 of Display 10.1, has received this name because the intensity pattern of single scattering of incident unpolarized light is the same as for Rayleigh scattering; this phase function does not occur in nature.

(R) Rayleigh scattering is physical scattering by induced dipole radiation. If the incident light is natural, the scattered light is 100% linearly polarized at right angles and has a smaller degree of linear polarization at other angles (see further Chapter 16).

Table 43 shows comparisons made for conservative scattering. The first quantity is the reflection function for perpendicular incidence and emergence. For very small slab thickness, where single scattering predominates, Rayleigh phase function and Rayleigh scattering are both stronger than isotropic scattering by about a factor of 1.5, which is the ratio of the phase functions for this angle ( $180^\circ$ ). For thicker layers, the ratio approaches 1; the difference creeps to 0.03 for moderate layers and to 0.045 for very thick layers. The differences between the first and second columns are about equal to those between the second and third column. In Fig. 14.1 we have plotted  $R(1, 1)$  on a large scale against  $(b + 1.42)^{-1}$ . On the basis of the comparisons in Table 30 (Section 12.1.2), we knew already that the value  $2q_\infty = 1.42$  may be taken equal. There is no doubt that the value of  $R(1, 1)$ , correct to about 0.1 %, may be read from these straight lines for any

TABLE 43

Comparison of Reflection Functions for  $q = 0, a = 1^a$

$b$	$R(1, 1)$			$UR(1)$			$URU$				
	$I$	$P$	$R$	$I$	$P$	$R$	$D$	$I$	$P$	$R$	$D$
$\frac{1}{32}$	0.00813	0.01176	—	0.01539	0.01539	—	0.01538	0.02914	0.02914	—	—
$\frac{1}{16}$	0.01662	0.02347	—	0.03032	0.03032	—	0.03030	0.05544	0.05545	—	—
0.125	0.03414	0.04651	—	0.05894	0.05892	—	0.05882	0.10220	0.10223	—	—
0.25	0.07009	0.09078	0.09781	0.11171	0.11161	0.11160	0.11111	0.17976	0.17985	0.1798	0.1813
0.5	0.1412	0.1718	—	0.2025	0.2022	—	0.2000	0.2958	0.2961	—	0.2988
1	0.2694	0.3075	0.3385	0.3413	0.3405	0.3402	0.3333	0.4466	0.4469	0.4469	0.4507
2	0.4598	0.5005	—	0.5175	0.5162	—	0.5000	0.6099	0.6102	0.6102	0.6137
4	0.6685	0.7102	0.7527	0.6909	0.6898	0.6889	0.6667	0.7540	0.7541	0.7542	0.7563
8	0.8326	0.8754	—	0.8218	0.8211	—	0.8000	0.8585	0.8585	—	0.8594
16	0.9356	0.9793	1.0243	0.9036	0.9032	0.9028	0.8889	0.9235	0.9235	0.9235	0.9238
32	0.9937	1.0378	—	0.9498	0.9495	—	0.9412	0.9601	0.9601	—	—
$\infty$	1.0569	1.1016	1.1471	1	1	1	1	1	1	1	1
First order	0.1250	0.1875	0.1875								
Higher order	0.9319	0.9141	0.9596								
Source	$b$	$b$	$c$	$b$	$b, d$	$c$	$e$	$b$	$f$	$c, g$	$e$

<sup>a</sup>  $I$  is isotropic scattering,  $P$ , the Rayleigh phase function,  $R$ , Rayleigh scattering, and  $D$ , Double peak.  
<sup>b</sup> Based on computations by K. Grossman.  
<sup>c</sup> Based on computations by J. Hovenier and J. Hansen.  
<sup>d</sup> Values for  $b = 4^{-3-4+6}$  in Kattawar *et al.* (1973) check well.  
<sup>e</sup> Based on integration of  $UR(\mu)$  from source  $b$ .  
<sup>f</sup> Hand integrated by data calculated from Sekera and Kahle (1966).  
<sup>g</sup> Supplemented by data calculated from Sekera and Kahle (1966).

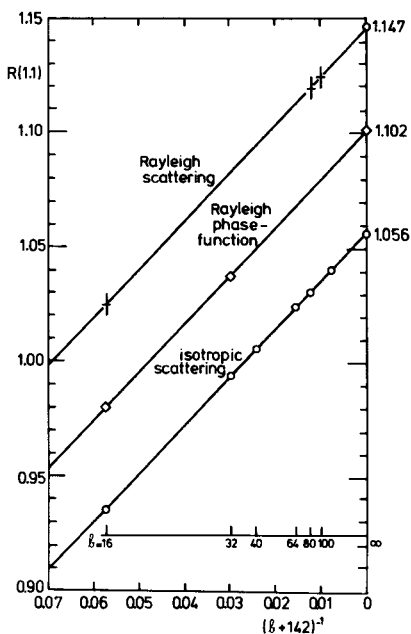


Fig. 14.1. Reflection with  $\mu = \mu_0 = 1$  against thick layers with three forms of conservative scattering.

value of  $b \geq 15$ . The values reached at  $b = \infty$  are accurately known. In the notation of Chandrasekhar (1950) these are the following:

Rayleigh phase function (Chandrasekhar, 1950, pp. 248, 261)

$$R(1, 1) = \frac{1}{64}\psi^2(1) + \frac{1}{8}\varphi^2(1) = 1.10163$$

Rayleigh scattering (Chandrasekhar, 1950, p. 145)

$$R(1, 1) = \frac{3}{4}\varphi(1)H_r(1) = \frac{3}{8}\chi(1)H_r(1) = 1.14709$$

As we have explained with another example in Table 31 (Section 12.2.2), the differences arise largely from the low-order scattering. Table 43 shows that the subtraction of the first-order scattering reduces the difference between  $R(1, 1)$  in Rayleigh scattering and isotropic scattering from 9 to 3%.

Differences of this magnitude have completely vanished in the albedo values, which are also shown in Table 43. These are albedo for perpendicular incidence  $UR(1)$  and spherical albedo  $URU$ . Rayleigh phase function differs from isotropic scattering by 0.3% at most in  $UR(1)$  and by 0.07% at most in  $URU$ . The initial data for this table came from graphs presented by Kahle (1968a, Fig. 12; 1968b, Figs. 4 and 9). Later, Dr. Hovenier gave me a number of accurate values for Rayleigh scattering computed by Dr. Hansen and himself. Plots of the differences between corresponding columns of Table 43 are shown in Fig. 14.2. The

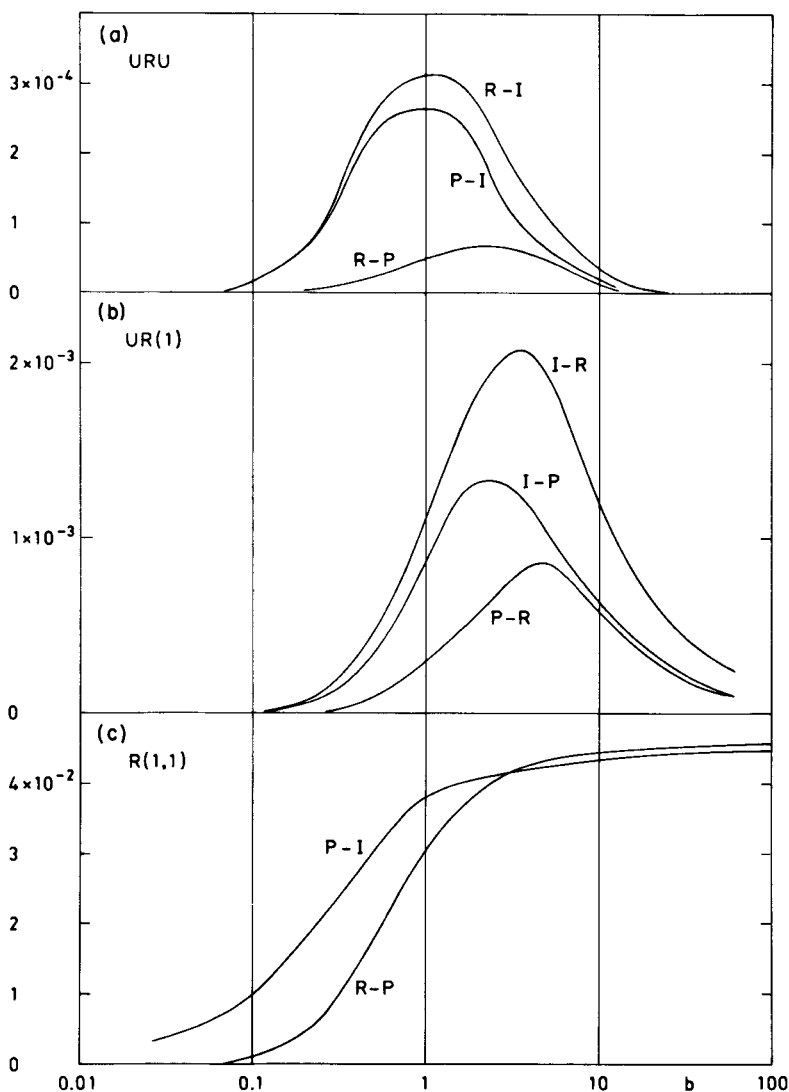


**Fig. 14.2.** The reflection differences between three forms of conservative scattering,  $I$  (isotropic),  $P$  (Rayleigh phase function), and  $R$  (Rayleigh scattering) are shown for slabs of varying thickness  $b$ . They are of the order of 1% in (c) the reflection function itself but substantially lower in (b) the plane albedo and (a) spherical albedo.



parts for  $b \geq 8$  match quite well the thick-layer formulas (Section 5.3), where the differences arise (to a small degree) from the difference in the extrapolation length  $q_0$  and (to a larger degree) from the different values of the escape function  $K(1)$ . The actual values of these quantities are in Table 30 in Section 12.1.2. Also the few numbers given by Kagiwada *et al.* (1968), when divided by  $\pi$  to give our flux values, are in perfect agreement with the corresponding numbers in Table 43 and Fig. 14.2.

It may be stressed again that the differences shown in Fig. 14.2 have mainly an academic importance. For practical purposes, the differences, at least in parts (a) and (b), are zero, and the three assumed scattering laws give the same result. It is curious to note that the values of  $UR(1)$  for the two other scattering laws may also be treated as those for isotropic scattering in Fig. 9.3. This results in two curves, which on the scale of that drawing are indistinguishable from the curve shown, the limits at  $b = \infty$  being 1.0671 and 1.0682 for scattering laws  $P$  and  $R$ , respectively.

Just for fun we have added to Table 43 two columns labeled double peak ( $D$ ) which refer to a phase function consisting of equal peaks of exact forward and exact backward scattering. This is function no. 23 of Display 10.1 with  $g = 0$ . The formulas referring to this phase function are in column 5 of Display 14.2. Since this highly schematic phase function has  $\omega_0 = 1, \omega_1 = 0, \omega_2 = 5, \omega_3 = 0$ , etc., and the Rayleigh phase function has  $\omega_2 = 0.5$ , we should expect that its results shows deviations from the isotropic results just about ten times bigger than the deviations shown by the results for the Rayleigh phase function. This order of magnitude is confirmed by the numbers, although the actual ratios vary considerably with  $b$ . This game is not entirely devoid of practical interest. There may be problems or circumstances, for instance with different geometries, where an exact treatment by means of the functions  $P$  and  $R$  would be extremely time consuming. It may then be useful to do the computation for isotropic scattering ( $I$ ) and for the very simple function ( $D$ ), and then to argue that we cannot be far wrong if we cut the overshoot back by a factor of 10 and adopt  $0.9(I) + 0.1(D)$  as the most likely answer.

#### 14.2.2 Scattering with $g = \frac{1}{3}$

A comparison between the values of  $UR(\mu)$  and  $UT(\mu)$  for three phase functions with  $g = \frac{1}{3}$  is found in a number of figures in Evans *et al.* (1965). These are the curves marked  $F = 0.75$  in their notation. Although different symbols are plotted for these three phase functions, the authors decided that one curve through these symbols suffices, thus illustrating the practical validity of the similarity principle. Plotting in these same graphs the accurate values for the Henyey–Greenstein phase function with  $g = \frac{1}{3}$ , i.e., a fourth phase function with the same  $g$  values, we find close agreement at small  $\mu_0$  and differences up to 0.02 in  $UR(1)$  (their Fig. 8) and up to 0.05 in  $UT(1)$  (their Fig. 9), both for  $b = 1, a = 0.9$ . The

**TABLE 44**  
Truncation Differences for a Finite, Nonconservative Layer with  $g = \frac{1}{3}$ <sup>a</sup>

	Reflection function			Transmission function		
	$N = 1$	H-G scattering	Difference	$N = 1$	H-G scattering	Difference
$\mu = 0$	0.679	0.708	-0.029	0.239	0.250	-0.011
0.1	0.660	0.678	-0.028	0.314	0.325	-0.011
0.5	0.424	0.428	-0.004	0.415	0.435	-0.020
0.9	0.270	0.267	+0.003	0.380	0.362	+0.018
1	0.239	0.239	0.000	0.368	0.338	+0.030
Integrals: $U$	0.366	0.366	0.000	0.528	0.530	-0.002
$N$	0.444	0.451	-0.007	0.515	0.524	-0.009

<sup>a</sup> For all numbers:  $b = 1$ ,  $a = 0.95$ ,  $g = \frac{1}{3}$ ,  $\mu_0 = 0.5$ .

fact that these differences are systematic and were found also in similar checks we made for  $g = 0$  against figures in the same paper, suggests that inaccuracy of their method, rather than inaccuracies in plotting or reading are to blame.

The smallness of these differences detracts nothing from the value of this paper for engineering purposes. If an error of a few percent does not count, the similarity principle is perfect and we can safely use either the curves in their paper or any of the tables and graphs presented in this book.

A check with higher precision is shown in Table 44, where we compare the reflection and transmission functions for  $b = 1$ ,  $a = 0.95$ ,  $g = \frac{1}{3}$ . The first phase function is linearly anisotropic scattering ( $N = 1$ ), and the data were made available by Dr. Kaper (Kaper *et al.*, 1970). The second phase function is Henyey-Greenstein scattering, and the data were obtained by Dr. Grossman at the NASA Institute for Space Studies, New York, N.Y.

The differences shown in Table 44 entirely fit the expectations. The actual reflection and transmission functions show differences up to 0.03, i.e. 8%. A large part of this difference is contained in the first-order terms. For instance, in  $T(\frac{1}{3}, 1)$  the first-order term for isotropic scattering with albedo 0.95 is 0.11046. Multiplication with the first phase function  $\Phi(0.5) = 1.5$  gives 0.16575, and multiplication with the second phase function  $\Phi(0.5) = 1.2959$  gives 0.14314. The difference of 0.023 explains most of the difference 0.030 seen in Table 44.

### 14.2.3 Scattering with Larger $g$ values

The literature is full of calculations in which more or less realistic phase functions for water clouds, with or without diffraction peak, have been used as a basis for the scattering calculations. The  $g$  values are in the range 0.7-0.9.

Almost invariably, either the method of calculation or the method of presentation leaves uncertainties so great that comparisons reliable to 1%, as required here, cannot be made.

A review (van de Hulst, 1968) showed differences up to 8% when reflection for the Henyey–Greenstein phase function with  $g = 0.50$  was compared with the corresponding quantity for a phase function truncated to  $N = 2$ . Differences up to 10% were seen between the Henyey–Greenstein results and Weinman's computation (1968) for a water cloud, which in turn agreed within 2% with Twomey *et al.* (1967) for the same situation. The check of the albedos  $UR$  against Weinman's gave an agreement within a fraction of a percent, thus confirming that the similarity relations hold better for these quantities. Differences of 5–10% were found with Irvine (1968) and up to 27% with Plass and Kattawar (1968). Many of these differences may be real and just show that similarity relations cannot be trusted if very accurate results are required.

The results of one test with a range of  $g$  values from 0 to 1 is shown in Fig. 14.3. For fixed values  $b = 1$ ,  $a = 0.95$ ,  $\mu_0 = 0.50$ , this figure shows how the main characteristics of the radiation field vary if the phase function varies from isotropic to completely forward scattering. The drawn curves refer to Henyey–Greenstein scattering as reported in Chapter 13. The dotted curves refer to set 12 of Display 10.1, for which computations had been made by Kaper and Veninga using the Case method. Figure 14.3a shows the net flux down, at top, midlayer, and bottom, which is called the net current in the nuclear scattering terminology. Figure 14.3b shows the point–direction gain, which is  $\mu_0$  times the scalar density.

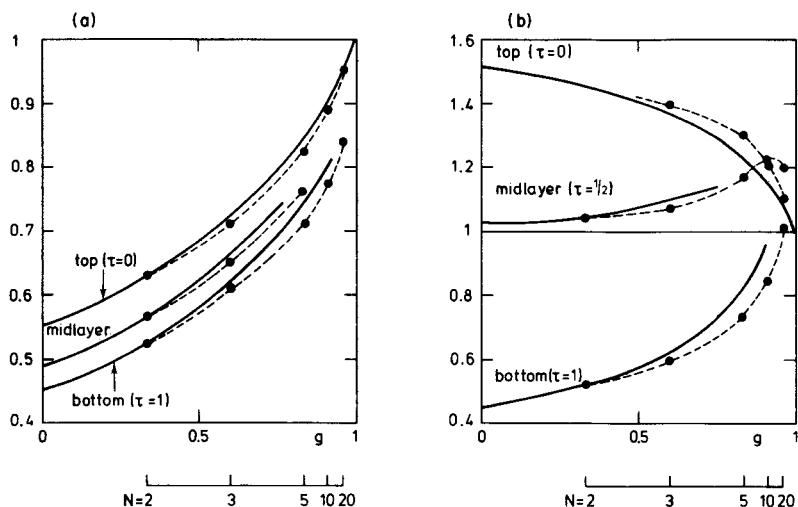


**Fig. 14.3.** Test to show the sensitivity of (a) net flux down (or net current) and (b) point-direction gain (or scalar density) to different assumptions about the phase function. Drawn curves: Henyey–Greenstein scattering;  $\bullet$  and dotted curves: phase function from set 12 of Display 10.1. For all curves:  $b = 1$ ,  $a = 0.95$ ,  $\mu_0 = 0.50$ .

We have plotted these curves on a common  $g$  scale using the formula  $g = N/(N + 2)$  for set 12. A somewhat better agreement could have been reached if the point  $N = 10$ , for instance, would have been plotted at  $g = 0.86$  instead of  $g = 0.91$ . This confirms the real differences between the two assumed sets of scattering laws, which were also apparent in Fig. 10.2.

### 14.3 STRICTLY FORWARD AND BACKWARD SCATTERING

It is sometimes useful to have ready formulas for strictly forward scattering ( $g = 1$ ) or strictly backward scattering ( $g = -1$ ) or for a combination of these (phase function 27 in Display 10.1). Such formulas are briefly derived here. Even though physically nothing happens upon the event of a scattering in the forward direction, we can nominally define the probability for such an event.

Let optical depth  $\tau$ , albedo  $a$ , asymmetry factor  $g$ , and cosine of angle with normal  $u$  be defined as usual. The total probability that an event occurs to a photon traveling in the direction  $u$  over a depth  $d\tau$  is  $d\tau/|u|$ . This probability is composed as follows:

- Probability  $p d\tau/|u|$ , with  $p = \frac{1}{2}a(1 + g)$ , for a forward scattering;
- Probability  $q d\tau/|u|$ , with  $q = \frac{1}{2}a(1 - g)$ , for a backward scattering;
- Probability  $(1 - a) d\tau/u$  for absorption;
- Sum:  $1 - a + p + q = 1$ .

A flux 1 incident in the direction  $(\mu_0, \varphi_0)$  on top of a slab with optical thickness  $b$  creates a radiation field which is composed exclusively of radiation along this direction (down) or along the opposite direction (up). Let  $D(\tau)$  be the flux down and  $A(\tau)$  the flux up, then the equation of radiative transfer is simply

$$\begin{aligned}\mu_0 dD/d\tau &= -D + pD + qA \\ -\mu_0 dA/d\tau &= -A + pA + qD\end{aligned}$$

with the boundary conditions  $D(0) = 1$ ,  $A(b) = 0$ .

The solution for  $a < 1$  can be found by introducing

$$\begin{aligned}z &= [(1 - p)^2 - q^2]^{1/2} = [(1 - a)(1 - ag)]^{1/2} \\ u &= z\tau/\mu_0, \quad u_1 = zb/\mu_0\end{aligned}$$

$$W = e^{u_1 - u}, \quad B = e^{u_1}, \quad C = [(1 - p + z)B - (1 - p - z)B^{-1}]^{-1}$$

and has the form

$$\begin{aligned}D &= [(1 - p + z)W - (1 - p - z)W^{-1}]C \\ A &= q(W - W^{-1})C\end{aligned}$$

**DISPLAY 14.2** Reflection and Transmission by Finite Layers with Double-Peak Phase Function

(1)	(2)	(3)	(4)	(5)	(6)	(7)
$g$ arbitrary	$g = 1$	$g = 0$	$g = -1$			
$a < 1$	$a = 1$	$a < 1$	$a < 1$	$a = 1$	$a < 1$	$a = 1$
General:						
$p$	$\frac{1}{2}a(1 + g)$	$1 - q$	$\frac{1}{2}a$	$\frac{1}{2}$	0	0
$q$	$\frac{1}{2}a(1 - g)$	$q = \frac{1}{2}(1 - g)$	$\frac{1}{2}a$	$\frac{1}{2}$	$a$	1
$z$	$[(1 - p)^2 - q^2]^{1/2}$	0	$(1 - a)^{1/2}$	0	$(1 - a^2)^{1/2}$	0
Finite slab thickness $b$ :						
$B$	$e^{zb/\mu_0}$	1	$e^{(1-a)^{1/2}b/\mu_0}$	1	$e^{(1-a^2)^{1/2}b/\mu_0}$	1
$C$	$[(1 - p + z)B - (1 - p - z)B^{-1}]^{-1}$	$\infty$	as column (1)	$\infty$	$[(1 + z)B - (1 - z)B^{-1}]^{-1}$	$\infty$
${}^a UR = r(\mu_0)$	$qC(B - B^{-1})$	$\frac{bq}{\mu_0 + bq}$	as column (1)	$\frac{\frac{1}{2}b}{\mu_0 + \frac{1}{2}b}$	$aC(B - B^{-1})$	$\frac{b}{\mu_0 + b}$
${}^a UT = t(\mu_0)$	$2zC$	$\frac{\mu_0}{\mu_0 + bq}$	as column (1)	$\frac{\mu_0}{\mu_0 + \frac{1}{2}b}$	$2(1 - a^2)^{1/2}C$	$\frac{\mu_0}{\mu_0 + b}$
$URU$	$b$	$2x - 2x^2 \ln(1 + x^{-1})$	$b$	as column (2) ( $x = \frac{1}{2}b$ )	$b$	as column (2) ( $x = b$ )
$UTU$	$b$	$(x = bq)$	$2E_3[(1 - a)b]$	$b$	$b$	$1 - URU$
Semi-infinite medium ( $b = \infty$ )						
$UR = URU$	$\frac{1 - p - z^c}{q}$	1	$1 - \frac{1}{2}a - (1 - a)^{1/2}$	1	$\frac{1}{a} - \left(\frac{1}{a^2} - 1\right)^{1/2}$	1

<sup>a</sup> For all columns:  $R(\mu, \mu_0) = r(\mu_0) \delta(\mu - \mu_0)/2\mu_0$ ,  $NR = r(\mu_0)/2\mu_0$ , and similarly for transmission.

<sup>b</sup> Integration gives complicated formula. <sup>c</sup> See equivalent forms in text.

which leads to the values at the boundaries:

$$\text{Reflected fraction of flux } UR = r(\mu_0) = A(0) = q(B - B^{-1})C$$

$$\text{Transmitted fraction of flux } UT = t(\mu_0) = D(b) = 2zC$$

Since everything happens along one path, the geometry of the cloud or scattering medium does not really matter. Therefore, the results just found depend only on the actual pathlength  $b/\mu_0$ .

These results have been entered into Display 14.2 for a variety of assumptions for  $g$  and  $a$ . The transition to the conservative case is straightforward and leads to very simple formulas. In columns where the integration was easy, the bi-moment  $URU$  has also been entered.

In the particular case of a semi-infinite atmosphere,  $UR$  is independent of  $\mu_0$  and hence equal to  $URU$ . The resulting value is best known in the literature in the form (not valid if  $q = 0$ )

$$UR = URU = \alpha - \beta = 1/(\alpha + \beta)$$

where

$$\alpha = (1 - p)/q, \quad \beta = z/q.$$

The most frequent use of these equations in the literature is as a two-stream approximation to the actual scattering process. They have been rederived dozens of times since Schuster (1905) and have found a wide application. In particular, the Kubelka-Munk equations, which are identical in form to the expression for  $UR$  in Display 14.2, have been used very extensively by generations of research workers on paints and solid surfaces (see further Section 20.2.1).

What we have presented here is not an approximation but an *exact result* for a double-peaked phase function, and as such it is also presented in more recent literature (Kattawar and Plass, 1973). This makes it possible to use these results, along with results for different phase functions, in finding the dependence of certain quantities on the precise scattering pattern.

For instance, results for fully forward scattering [column (3)] and fully backward phase functions [columns (6) and (7)] have been used in several earlier figures to provide the end points in graphs where results for the Henyey-Greenstein functions were plotted against  $g$ .

Another example is the conservative phase function in column (5), which consists of equal peaks forward and backward. It describes the simplest type of random walk process in a two-stream theory and shows, compared to the Rayleigh phase function, a roughly ten times exaggerated deviation from isotropic scattering. For that reason some numerical values were given in Table 43 (Section 14.2.1).

Finally, as a double check we wish to see if the equations just derived obey the transformation rules set forth in Section 14.1.3 for the addition of a forward peak. Adding a forward peak of arbitrary strength to the phase function assumed here keeps the phase function in the same class, but all parameters change. Let

the parameters in the old situation be written with primes and those in the new situation without primes. The transformation rule given in Section 14.1.3 can now be extended, using the definitions of  $z$ ,  $u_1$ ,  $B$ ,  $C$ , given above, to read:

$$\frac{b}{b'} = \frac{1 - a'}{1 - a} = \frac{a'(1 - g')}{a(1 - g)} = \frac{q'}{q} = \frac{1 - p'}{1 - p} = \frac{z'}{z} = \frac{C}{C'}$$

The quantities  $B$ ,  $UR$ , and  $UT$ , as given in Display 14.2, remain invariant under this transformation, which completes the check.

## REFERENCES

- Chandrasekhar, S. (1950). "Radiative Transfer." Oxford Univ. Press (Clarendon), London and New York. Also Dover, New York, 1960.
- Davison, B. (1957). "Neutron Transport Theory." Oxford Univ. Press (Clarendon), London and New York.
- Evans, L. B., Chu, C. M., and Churchill, S. W. (1965). *J. Heat Transfer* **87**, 381.
- Hansen, J. E. (1969). *J. Atmos. Sci.* **26**, 478.
- Irvine, W. M. (1968). *Astrophys. J.* **152**, 823.
- Kagiwada, H. H., Kalaba, R. E., and Segerblom, R. (1968). *J. Comput. Phys.* **3**, 159.
- Kahle, A. B. (1968a). Rand Corporation Memo. RM-5620-PR.
- Kahle, A. B. (1968b). *Astrophys. J.* **151**, 637.
- Kaper, H. G., Shultis, J. K., and Veninga, J. G. (1970). *J. Comput. Phys.* **6**, 288.
- Kattawar, G. W., and Plass, G. N. (1973). *J. Quant. Spectrosc. Radiat. Transfer* **13**, 1065.
- Kattawar, G. W., Plass, G. N., and Catchings, F. E. (1973). *Appl. Opt.* **12**, 1071.
- Plass, G. N., and Kattawar, G. W. (1968). *Appl. Opt.* **7**, 361.
- Schuster, A. (1905). *Astrophys. J.* **21**, 1.
- Sekera, Z., and Kahle, A. B. (1966). Rand Corporation Rep. R-452-PR.
- Stokes, R. A., and DeMarcus, W. C. (1971). *Icarus* **14**, 307.
- Twomey, S., Jacobowitz, H., and Howell, H. B. (1970). *J. Atmos. Sci.* **24**, 70.
- van de Hulst, H. C. (1968). *J. Comput. Phys.* **3**, 291.
- van de Hulst, H. C., and Grossman, K. (1968). In "The Atmospheres of Venus and Mars" (J. C. Brandt and M. B. McElroy, eds.), p. 35. Gordon and Breach, New York.
- Weinman, J. A. (1968). *Icarus* **9**, 67.

## 15 ☐ Polarization and Azimuth-Dependent Terms

### 15.1 THE FORMALISM

#### 15.1.1 Key Concepts

The combination of two quite different topics in one chapter heading may seem puzzling. The simple fact is that if we should treat these two topics separately, the story would become too repetitious. Combining them is in the interest of conciseness and clarity, provided we keep some key points in mind.

Virtually all results presented in the earlier chapters of this book refer to *unpolarized* radiation fields with *rotational symmetry* around the direction perpendicular to the atmosphere or slab. The radiation field at any depth was fully characterized by the intensity  $I(\theta)$ , where  $\theta$  is the angle of the direction of propagation with the (downward) normal. Two generalizations are now required.

Polarization:	replace $I(\theta)$ by $I(\theta), Q(\theta), U(\theta), V(\theta)$ or, written differently, $I_i(\theta), i = 1-4$ , which are the four Stokes parameters
Azimuth dependence:	replace $I(\theta)$ by $I(\theta, \varphi)$ or, upon Fourier analysis, by $I_i^m(\theta), m = 0, 1, \dots \infty$
Polarization and azimuth dependence combined:	replace $I(\theta)$ by $I_i(\theta, \varphi)$ or, upon Fourier analysis, by $I_i^m(\theta), i = 1-4, m = 0, 1, \dots \infty$



The two new assumptions introduce rather similar complications into the multiple scattering problems. This is readily seen if we look at the conceptually simplest method of solving them, namely, the method of successive orders (Section 4.3). In one half step described there, the local source function is found from the local intensity. This involves a reshuffling of the distribution in  $\theta$  and in  $\varphi$  as well as a new state of polarization. With either new assumption, this half step must be redone because a new specification of the local scattering process is necessary. The other half step, finding local intensity from the values of the source function along the line of sight, maintains the direction  $(\theta, \varphi)$  as well as the state of polarization. No new formulas are needed in that half step; the other Stokes parameters are integrated, just like the intensity, over optical depth  $\tau$ . Here we have introduced the assumption that the extinction coefficient per unit length in the cloud is independent of direction and of the state of polarization, which is very plausible in most natural circumstances. This assumption would not be correct, e.g., for a cloud of oriented crystals.

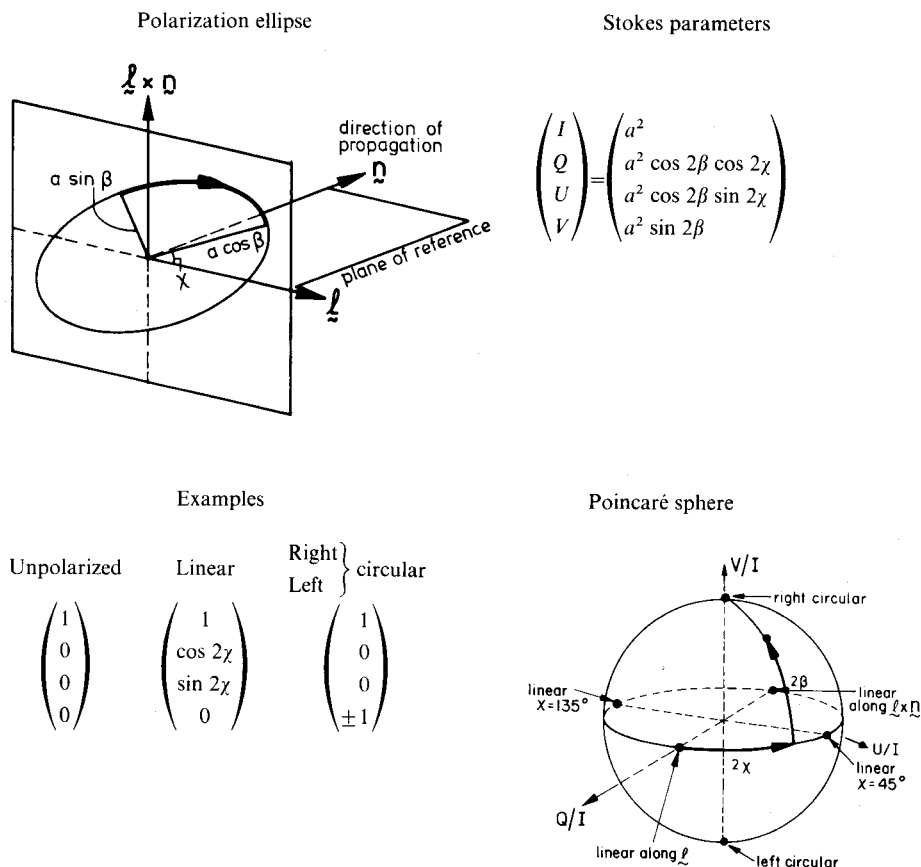
A difference should also be noted. We shall presently see that the Fourier analysis leads to strictly separable transfer problems, one for each value of  $m$ . The problem for  $m = 0$ , referring to the azimuth-independent terms, has been treated exhaustively in earlier chapters. All results (numerical or analytical) presented there *can be used without change*, as the  $m = 0$  contributions in a complete theory. However, there is no such theorem to separate the transfer problems for different states of polarization. For instance, the Rayleigh phase function, which is the traditional name for Rayleigh scattering with the polarization neglected, is only a nice practice example for Rayleigh scattering. Solutions of radiative transfer problems obtained by means of this phase function (Sections 14.2.1 and 16.2.2, end) are an approximation to, but not an exact term in the correct result for full Rayleigh scattering, not even if we should be interested in computing only the total intensity.

Finally, please note that there exists no *logical* reason why the two problems discussed in this chapter should always be combined. Problems with polarization exist also in the azimuth-independent terms, e.g., the pattern in the diffusion domain (Section 15.2.3), or the Milne problem for a Rayleigh-scattering atmosphere (Section 16.3.2). Azimuth dependent problems can quite well be formulated in the absence of any polarized radiation, as in Sections 15.3 and 15.4.

### 15.1.2 Stokes Parameters, The Phase Matrix

We summarize briefly the use of the 4 Stokes parameters to describe the intensity and state of polarization of any beam of light. Details and worked examples may be found in many textbooks.

The complete state of polarization of a beam of light traveling in a certain direction can be described by completing the intensity  $I$  with three further real

**DISPLAY 15.1**Representation of Polarized Light<sup>a</sup><sup>a</sup> Wavy underscore indicates vector quantities.

quantities of the same physical dimension:  $Q$ ,  $U$ , and  $V$  (see Display 15.1). They are defined with respect to a plane of reference chosen through the direction of propagation. The quantities  $U$  and  $Q$  together describe the magnitude and orientation of the linearly polarized component, and  $V$  describes the circularly polarized component. The quantities  $I$ ,  $(U^2 + Q^2)^{1/2}$ , and  $V$  are invariant to a rotation of the plane of reference. The ratio  $(U^2 + Q^2 + V^2)^{1/2}/I$  is the degree of polarization. If the degree of polarization has its maximum value, 1, the beam is said to be fully polarized. The quantities  $U/I$ ,  $Q/I$ ,  $V/I$  as rectangular coordinates then define a point on the unit sphere, which is called the Poincaré sphere. Points

inside this sphere correspond to partially polarized light. Natural (i.e., unpolarized) light has  $U = Q = V = 0$  and is represented by the center of the Poincaré sphere.

We shall further assume as known that we can treat the set of parameters  $I, Q, U, V$  as a four-vector and can write it as  $I_1, I_2, I_3, I_4$ , or briefly as  $\mathbf{I}$ ; and further that any operation on the beam by an instrument designed to analyze the beam and measure the strength of the component with a specific polarization can be described as multiplying this four-vector with another four-vector  $D_1, D_2, D_3, D_4$  (or briefly  $\mathbf{D}$ ), characterizing the detection properties of that particular instrument. An instrument with  $D_2 = D_3 = D_4 = 0$  measures total intensity, irrespective of the state of polarization of the beam.

After this brief review of a simple and convenient tool, let us see how concepts introduced earlier in this book must be completed in order to take into account the full polarization properties. The phase function  $\Phi(\cos \alpha)$  used earlier was a function of the angle  $\alpha$  between the direction  $(u', \varphi')$  in which the radiation enters a volume element and the direction  $(u, \varphi)$  in which it is scattered. We must now specify the intensity and state of polarization of the scattered light for any intensity and state of polarization of the incident light. This means that the one function has to be replaced by a  $4 \times 4$  matrix.

The precise form of this matrix depends on the two planes of reference chosen for the incident and scattered radiation. It has the simplest form if the scattering plane, i.e., the plane through the directions of propagation of incident and scattered radiation, is taken as the common plane of reference for both. This leads to the scattering matrix  $\mathbf{F}$  defined in Section 15.1.4.

This choice is not convenient in radiative transfer. It is then useful to work exclusively with planes of reference through the direction of propagation and the normal to the atmosphere. If we consider a scattering event with an arbitrary direction of incidence and an arbitrary direction of scattering, this new choice makes the planes of reference for incident and scattered beams different from each other and from the scattering plane. As a consequence, the phase matrix  $\mathbf{Z}$  with this new choice of reference planes is found from the scattering matrix  $\mathbf{F}$  by a pre- and postmultiplication by a rotation matrix. The equations are given in Section 15.1.4.

The absence of polarization assumed in earlier chapters is formally equivalent to taking  $Z_{ik} = 0$  for all elements different from  $Z_{11}$ . This has the following physical meaning. The index  $k$  refers to the polarization of the incident light. Setting the phase matrix components with  $k \neq 1$  equal to 0 means that the polarization of the incident light is assumed to be irrelevant; only its intensity counts. The index  $i$  refers to the polarization of the scattered light. Setting the components with  $i \neq 1$  equal to 0 means that we define the scattered radiation to be unpolarized (natural light, zero-degree polarization). Both assumptions would be fairly well fulfilled by chalk dust. The matrix elements other than  $Z_{11}$  are still relatively small for quartz dust, large water drops, etc. They are substantial for scattering by molecules or by very small drops.

The one element of the phase matrix that is nonzero in problems without polarization is the phase function  $Z_{11}$ . We have (cf. Display 4.4 or Section 15.1.4):

$$\begin{aligned} aZ_{11} &= a\Phi(\cos \alpha) = \sum_{n=0}^N \omega_n P_n(\cos \alpha) \\ &= \sum_{n=0}^N \omega_n P_n(u)P_n(u') + 2 \sum_{m=1}^N \sum_{n=m}^N c_n^m P_n^m(u)P_n^m(u') \cos m(\varphi - \varphi') \end{aligned}$$

Its azimuth-independent part,  $aZ_{11}^0$ , the first term of the Fourier expansion, is the redistribution function  $h(u, v)$ .

The operator  $U$  used extensively throughout this book (not to be confused with the Stokes parameter  $U = I_3$ ) should, in problems with polarization, be completed to the four-vector

$$\mathbf{U} = (U, 0, 0, 0)$$

This holds true for both physical meanings in which the operator  $U$  appears (cf. Sections 5.1 or 7.1.1). The following brief explanation may suffice. If  $U$  is used to specify an incident radiation field, it means such a radiation field as would be produced, e.g., by an emitting blackbody. This is unpolarized by definition. The same  $U$  would represent the radiation diffusely reflected from a perfectly white surface following Lambert's law, for which it is again consistent to assume absence of polarization. If, on the other hand,  $U$  is applied as an operator to the emergent radiation, it corresponds to the instruction: measure the light flux emerging from the surface. The 3 zeros then mean that only the first Stokes parameter counts and that in taking the flux, the three other parameters are irrelevant.

Very similar reasoning goes to show that the operator  $U$  makes physical sense only when applied to the azimuth independent component ( $m = 0$ ) of the radiation field.

The conclusion just reached for the operator  $U$  can be drawn on much the same grounds also for the operator  $N$ .

The Stokes parameters are not the only way to represent arbitrarily polarized light. In principle, any independent set of linear combinations of the Stokes parameters will do as well. The advantages and disadvantages of several such sets were discussed by Kuščer and Ribarič (1959) and by Sekera (1966). Transformation formulas between some sets were written out by Abhyankar and Fymat (1969).

One set, the CP representation, which has complex elements based on circular polarization, has the interesting property that the matrix is diagonal. This makes the CP representation, in combination with generalized spherical functions (Gel'fand *et al.*, 1963; cf. also James, 1976) the most elegant means to express the phase matrix. This method has been worked out in equations and numerical examples by Herman and co-workers (Herman 1965, 1970; Herman and Lenoble 1968) and independently by Domke (1973, 1974a,b).

Whether this representation also leads to faster or more convenient numerical computation remains to be seen. At any rate, we have chosen not to use the CP representation in this book. The expansions of the elements of the phase matrix in Sections 10.3.1 and 10.3.2 show that with a little more algebra the representation by means of the traditional Stokes parameters and associated Legendre functions offers a feasible alternative. The same remark holds true for the problem of expressing intensity and polarization of the radiation pattern in the diffusion domain (Section 15.2.3).

### 15.1.3 Fourier Analysis in Azimuth

Fourier analysis in the azimuth angle is simple in principle but leads to problems of notation which have fooled some authors and, presumably, more readers. Perhaps the danger of confusion is least if we spell out separately the formulas for the two situations we most need:

1. *Local scattering* at any depth inside a medium, symbolically represented by the equation  $\mathbf{J} = \mathbf{Z}\mathbf{I}$ , where  $\mathbf{I}$  is the intensity,  $\mathbf{Z}$  the phase matrix, and  $\mathbf{J}$  the source function. Full specification is given in Section 15.1.4.

2. *Diffuse reflection* against a slab of any thickness, symbolically represented by  $\mathbf{E} = \mathbf{R}\mathbf{I}$ , where  $\mathbf{I}$  is the incident radiation,  $\mathbf{R}$  the reflection matrix, and  $\mathbf{E}$  the diffusely reflected radiation. Full specifications are given in Section 15.1.5.

We recall that situation 1 occurs in the method of successive orders and in the traditional treatment by means of the equation of transfer. Situation 2 occurs in the doubling method. Combinations of 1 and 2 occur in Ambartsumian's method and in the theory for thick layers (Chapter 5).

Before presenting the equations, we mention three details which might lead to confusion if not specially pointed out.

(a) All equations are given for arbitrarily polarized light in agreement with the specifications given in Section 15.1.2. In order to retrieve the corresponding equations in the absence of polarization, simply take  $i = 1$ ,  $k = 1$  everywhere and ignore terms with other  $i, k$ .

(b) We make slightly restrictive symmetry assumptions both on the radiation fields treated and on the phase matrix. The radiation field is taken strictly symmetric with respect to a vertical plane. By measuring the azimuth from this plane we obtain *cosines only* in the Fourier expansion of some components and *sines only* in the Fourier expansion of other components. Without this symmetry assumption, the notation would be even more cumbersome and the equations longer, but basically nothing new would be added. The mildly restrictive assumption made about the phase matrix is specified in Section 15.1.4.

(c) In the definitions to follow, the terms with  $m = 0$  are written separately. This permits the introduction, in the definition of the Fourier coefficients of  $\mathbf{Z}$  and  $\mathbf{R}$ , of a factor of 2 for  $m \neq 0$ . This agrees with the choice made in Section

6.3.1 and avoids the appearance of the factor  $2 - \delta_{0,m}$  (which is 1 for  $m = 0$  and 2 for  $m \neq 0$ ) in later equations.

#### 15.1.4 Local Scattering Law

The scattered radiation emerging in any direction from a volume element was earlier called the source function. We shall use the same name for the four-vector describing the scattered polarized radiation from a volume element. It is a function of direction, and its form is determined by the radiation field to which this volume element is exposed and by the local scattering process.

We wish to formulate the local scattering process under rather general conditions and then subject all functions involved to Fourier analysis in azimuth. This requires a rather careful preparation; it is necessary to watch especially the symmetry of the various components. Hovenier (1969) has derived this symmetry by an elegant discussion of transformation properties. A good discussion is also found in Hansen and Travis (1974). The explicit expressions written here for the various matrices, show the symmetry properties directly.

The directions are represented in Fig. 15.1 as points on the unit sphere.  $N$  is the direction perpendicular to the slab, for which  $\theta = 0$ ,  $u = \cos \theta = 1$ . We consider a scattering process in which light is diverted from its initial direction  $P'$  to its final direction  $P$ . These two directions are specified by the direction cosines  $\cos \theta' = u'$ ,  $\cos \theta = u$  and by the azimuth angles  $\varphi'$  and  $\varphi$ . The scattering angle is  $\alpha$ . By spherical geometry we have

$$\cos \alpha = \cos \theta \cos \theta' + \sin \theta \sin \theta' \cos(\varphi' - \varphi)$$

$$\cos i' = (\cos \theta - \cos \theta' \cos \alpha) / \sin \theta' \sin \alpha, \quad \sin i' = \sin \theta \sin(\varphi' - \varphi) / \sin \alpha$$

$$\cos i = (\cos \theta' - \cos \theta \cos \alpha) / \sin \theta \sin \alpha, \quad \sin i = \sin \theta' \sin(\varphi' - \varphi) / \sin \alpha$$

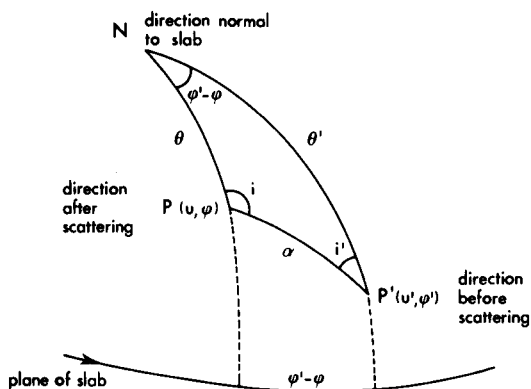


Fig. 15.1. Angles used in referring local scattering matrix to planes of reference through normal.

The phase matrix serves to convert the Stokes parameters of the incident light expressed with  $NP'$  as plane of reference into the Stokes parameters of the scattered light expressed with  $NP$  as plane of reference. This requires three steps:

Rotate plane of reference through  $i'$  from  $NP'$  to  $PP'$ , matrix  $L'$ .

Apply scattering matrix  $F$ .

Rotate plane of reference through  $i$  from  $PP'$  to  $NP$ , matrix  $L$ .

The combined operation is expressed by the phase matrix

$$\mathbf{Z} = \mathbf{L} \cdot \mathbf{F} \cdot \mathbf{L}'$$

in which the factors are (e.g., Chandrasekhar, 1950; Hovenier, 1969)

$$\mathbf{L}' = \begin{pmatrix} 1 & 0 & 0 & 0 \\ 0 & C' & -S' & 0 \\ 0 & S' & C' & 0 \\ 0 & 0 & 0 & 1 \end{pmatrix}, \quad \mathbf{F} = \begin{pmatrix} a_1 & b_1 & 0 & 0 \\ b_1 & a_2 & 0 & 0 \\ 0 & 0 & a_3 & b_2 \\ 0 & 0 & -b_2 & a_4 \end{pmatrix}, \quad \mathbf{L} = \begin{pmatrix} 1 & 0 & 0 & 0 \\ 0 & C & -S & 0 \\ 0 & S & C & 0 \\ 0 & 0 & 0 & 1 \end{pmatrix}$$

Here  $C' = \cos 2i'$ ,  $S' = \sin 2i'$ ,  $C = \cos 2i$ ,  $S = \sin 2i$ , and  $a_1, a_2, a_3, a_4, b_1, b_2$ , are six functions of  $\alpha$  that depend on the size and nature of the scattering particles. This form of  $F$  is not the most general one, but it is valid for rather wide assumptions (see van de Hulst, 1957). For instance, an assembly of randomly oriented symmetric particles has this form of scattering matrix; a cloud of water drops with any size distribution also has an  $F$  of this form.

Straight matrix multiplication gives

$$\mathbf{Z} = \begin{pmatrix} \boxed{\begin{matrix} a_1 & b_1 C' \\ Cb_1 & Ca_2 C' - Sa_3 S' \end{matrix}} & \boxed{\begin{matrix} -b_1 S' & 0 \\ -Ca_2 S' - Sa_3 C' & -Sb_2 \end{matrix}} \\ \boxed{\begin{matrix} Sb_1 & Sa_2 C' + Ca_3 S' \\ 0 & -b_2 S' \end{matrix}} & \boxed{\begin{matrix} -Sa_2 S' + Ca_3 C' & Cb_2 \\ -b_2 C' & a_4 \end{matrix}} \end{pmatrix}$$

Now the azimuth dependence can be examined. Keep  $\theta$  and  $\theta'$  fixed and consider all quantities in the preceding formulas as functions of  $\varphi - \varphi'$ . We readily see that

$\cos \theta$ , and hence  $\theta$ ,  $\sin \theta$ ,  
 $a_1, a_2, a_3, a_4, b_1, b_2$ ,  
 $\cos i, \cos i', C, C'$ , and  
 components of  $\mathbf{Z}$  outside the boxes

} are even functions of  $\varphi - \varphi'$ .

$\sin i, \sin i', S, S'$ , and

components of  $\mathbf{Z}$  inside the boxes

} are odd functions of  $\varphi - \varphi'$ .

The even functions give, upon Fourier analysis, a sum of cosines, in which the term  $m = 0$  is the azimuth-independent term. The odd functions give a sum of sines. We shall distinguish this property in the notation by giving the odd components of  $\mathbf{Z}$  a tilde ( $\tilde{Z}_{ik}$ ); the Fourier coefficients of the odd components will be distinguished in the same manner ( $\tilde{Z}_{ik}^m$ ). The even components and its coefficients will be written without a special mark. The resulting Fourier expansions are the following:

Even components  $Z_{ik}$  (outside boxes):

$$Z_{ik}(u, u', \varphi, \varphi') = Z_{ik}^0(u, u') + 2 \sum_{m=1}^{\infty} Z_{ik}^m(u, u') \cos m(\varphi - \varphi')$$

Odd components  $Z_{ik}$  (inside boxes):

$$\tilde{Z}_{ik}(u, u', \varphi, \varphi') = 2 \sum_{m=1}^{\infty} \tilde{Z}_{ik}^m(u, u') \sin m(\varphi - \varphi')$$

This completes the formal derivation of the phase matrix  $\mathbf{Z}$ , and we are now ready to write the detailed form of the local scattering equation.

It is evidently possible to do this for arbitrary incident radiation fields. However, this would spoil the symmetry and force us to use cosines *and* sines in the expansions of the same components, which we prefer to avoid. We therefore continue to use the assumption (Section 15.1.3) that the radiation field is symmetric with respect to the plane  $\varphi = 0$ . If this is true for the incident radiation, it is true after any number of scatterings and also for the entire intensity and the entire source function. More general formulas can be written down (Hansen, 1971), but nothing essential is thereby added.

The correct formulation of this symmetry can be found by a thought experiment. We mark the components of  $I(u, \varphi)$  and  $J(u, \varphi)$  which are odd in  $\varphi$  with a tilde and leave the even functions in  $\varphi$  unmarked. Let a slab be exposed to unpolarized radiation incident along one direction in the  $\varphi = 0$  plane (or with any intensity distribution symmetric with respect to this plane). Then we obtain by successive application of the phase matrix  $\mathbf{Z}$  the following four-vectors for intensity and source function. Note that they are written here as row vectors though actually they are used as column vectors.

$$\text{Unscattered radiation: } I_{\text{order } 0} = (I_1, 0, 0, 0)$$

$$J_{\text{order } 1} = (J_1, J_2, \tilde{J}_3, 0) \quad I_{\text{order } 1} = (I_1, I_2, \tilde{I}_3, 0)$$

$$J_{\text{order } 2} = (J_1, J_2, \tilde{J}_3, \tilde{J}_4) \quad I_{\text{order } 2} = (I_1, I_2, \tilde{I}_3, \tilde{I}_4)$$

All higher orders, as order 2

Sum of all orders, as order 2

This shows that generally, the first scattering leads to linear polarization, and two successive scatterings, to elliptical polarization, but only in directions outside the plane  $\varphi = 0$ .



Knowing the symmetry, we now define the Fourier coefficients by

$$i = 1, 2 \begin{cases} I_i(u, \varphi) = I_i^0(u) + 2 \sum_{m=1}^{\infty} I_i^m(u) \cos m\varphi \\ J_i(u, \varphi) = J_i^0(u) + 2 \sum_{m=1}^{\infty} J_i^m(u) \cos m\varphi \end{cases}$$

$$i = 3, 4 \begin{cases} \tilde{I}_i(u, \varphi) = 2 \sum_{m=1}^{\infty} \tilde{I}_i^m(u) \sin m\varphi \\ \tilde{J}_i(u, \varphi) = 2 \sum_{m=1}^{\infty} \tilde{J}_i^m(u) \sin m\varphi \end{cases}$$

The full local-scattering equation reads

$$\mathbf{J}(u, \varphi) = \frac{1}{4\pi} \int_{-1}^1 du' \int_0^{2\pi} d\varphi' \mathbf{Z}(u, \varphi; u', \varphi') \mathbf{I}(u', \varphi')$$

Inserting the Fourier expansions of the components of  $\mathbf{Z}$  and  $\mathbf{I}$  defined above we obtain  $\varphi'$  integrations, which are readily performed, and the components of the source matrix become:

$$J_1^0(u) = \frac{1}{2} \int_{-1}^1 du' (Z_{11}^0 I_1^0 + Z_{12}^0 I_2^0)$$

$$J_2^0(u) = \frac{1}{2} \int_{-1}^1 du' (Z_{21}^0 I_1^0 + Z_{22}^0 I_2^0)$$

$$J_1^m(u) = \frac{1}{2} \int_{-1}^1 du' (Z_{11}^m I_1^m + Z_{12}^m I_2^m - \tilde{Z}_{13}^m \tilde{I}_3^m - \tilde{Z}_{14}^m \tilde{I}_4^m)$$

$$J_2^m(u) = \frac{1}{2} \int_{-1}^1 du' (Z_{21}^m I_1^m + Z_{22}^m I_2^m - \tilde{Z}_{23}^m \tilde{I}_3^m - \tilde{Z}_{24}^m \tilde{I}_4^m)$$

$$\tilde{J}_3^m(u) = \frac{1}{2} \int_{-1}^1 du' (\tilde{Z}_{31}^m I_1^m + \tilde{Z}_{32}^m I_2^m + Z_{33}^m \tilde{I}_3^m + Z_{34}^m \tilde{I}_4^m)$$

$$\tilde{J}_4^m(u) = \frac{1}{2} \int_{-1}^1 du' (\tilde{Z}_{41}^m I_1^m + \tilde{Z}_{42}^m I_2^m + Z_{43}^m \tilde{I}_3^m + \tilde{Z}_{44}^m \tilde{I}_4^m)$$

in which  $m \geq 1$  and the arguments  $(u, u')$  with  $Z$  and  $u'$  with  $I$  have been omitted for brevity.

The first of these 6 equations, with  $I_2^0 = 0$ , is identical to the local scattering equation in the absence of polarization (Section 4.3):

$$J(u) = \frac{1}{2} \int_{-1}^1 h(u, u') I(u') du'$$

The full set of 6 equations forms the generalization of this redistribution equation to the case of arbitrary polarization, under the symmetry assumptions we have made.

It may be useful to point out that the coupling between the linear and circularly polarized components arises entirely from the element  $b_2$  in  $\mathbf{F}$ . The values of  $b_2$  are generally quite small (van de Hulst, 1957, p. 36) and there are circumstances in which no great harm is done by neglecting it altogether. This causes the considerable simplification that the fourth Stokes parameter is completely uncoupled from the first three. It is then justified to conduct the entire calculation with three-vectors and  $3 \times 3$  matrices and to leave the circularly polarized component to a separate and relatively simple computation. Rayleigh scattering rigorously has  $b_2 = 0$ . Hence the separation just described is a correct separation for Rayleigh scattering. An example in which  $b_2$  is not neglected but used for diagnostic means is mentioned in Section 19.2.2.

### 15.1.5 Diffuse Reflection and Transmission

The symbolic form of expressing the diffuse reflection is

$$E = RI$$

where  $I$  is the incident (downward) radiation,  $R$  the reflection function, and  $E$  the reflected (upward emerging) radiation. Under the assumptions in most earlier chapters this was a brief notation for

$$E(\mu) = \int_0^1 R(\mu, \mu_0) I(\mu_0) 2\mu_0 d\mu_0$$

With azimuth dependence and arbitrarily polarized light this must instead be read as a brief notation for

$$\mathbf{E}(\mu, \varphi) = \int_0^1 2\mu_0 d\mu_0 \int_0^{2\pi} (2\pi)^{-1} d\varphi_0 \mathbf{R}(\mu, \varphi; \mu_0, \varphi_0) \mathbf{I}(\mu_0, \varphi_0)$$

where  $\mathbf{E}$  and  $\mathbf{I}$  are four-vectors and  $\mathbf{R}$  a  $4 \times 4$  matrix.

Evidently, this equation is different from the local scattering equation, discussed in Section 15.1.4, by the different symbols and by the limits (0, 1) of the  $\mu_0$  integration. Also, the physical meaning is different, for  $\mathbf{R}$  is a property of the entire slab, including the effect of a great many scattering events in succession, whereas  $\mathbf{Z}$  was a property of a small volume element.

Yet there is also an intimate connection. In the limit of a very thin layer,  $\mathbf{R}$  consists exclusively of the once-scattered light. If  $d\tau \ll 1$  is the optical thickness, we have

$$\mathbf{R}(\mu, \varphi; \mu_0, \varphi_0) = (d\tau/4\mu\mu_0) \mathbf{Z}(\mu, \varphi; -\mu_0, \varphi_0)$$

The components of  $\mathbf{R}$  thus have the same symmetry properties with respect to  $\varphi - \varphi_0$  as the components of  $\mathbf{Z}$  have with respect to  $\varphi - \varphi'$ . It is obvious that since this is true for thin layers, it must remain true for layers of arbitrary thickness. A formal proof may be constructed on the basis of the method of successive orders, making use of the fact that  $\mathbf{Z}^n$  has the same symmetry properties as  $\mathbf{Z}$ .

In complete analogy with the preceding section, we may now write at once the specification of the equation  $E = RI$  in terms of Fourier coefficients. Write:

$$I_i(\mu_0, \varphi_0) = I_i^0(\mu_0) + \sum_{m=1}^{\infty} I_i^m(\mu_0) \cos m\varphi_0 \quad (i = 1, 2)$$

$$\tilde{I}_i(\mu_0, \varphi_0) = \sum_{m=1}^{\infty} \tilde{I}_i^m(\mu_0) \sin m\varphi_0 \quad (i = 3, 4)$$

$$E_i(\mu, \varphi) = E_i^0(\mu) + \sum_{m=1}^{\infty} E_i^m(\mu) \cos m\varphi \quad (i = 1, 2)$$

$$\tilde{E}_i(\mu, \varphi) = \sum_{m=1}^{\infty} \tilde{E}_i^m(\mu) \sin m\varphi \quad (i = 3, 4)$$

$$R_{ik}(\mu, \varphi; \mu_0, \varphi_0) = R_{ik}^0(\mu, \mu_0) + 2 \sum_{m=1}^{\infty} R_{ik}^m(\mu, \mu_0) \cos m(\varphi - \varphi_0) \quad (\text{unboxed})$$

$$\tilde{R}_{ik}(\mu, \varphi; \mu_0, \varphi_0) = 2 \sum_{m=1}^{\infty} \tilde{R}_{ik}^m(\mu, \mu_0) \sin m(\varphi - \varphi_0) \quad (\text{boxed})$$

Omitting the arguments  $\mu$  and  $\mu_0$ , we then have:

$$E_1^0 = \int_0^1 2\mu_0 d\mu_0 (R_{11}^0 I_1^0 + R_{12}^0 I_2^0), \quad \text{similarly } E_2^0$$

$$E_1^m = \int_0^1 2\mu_0 d\mu_0 (R_{11}^m I_1^m + R_{12}^m I_2^m - \tilde{R}_{13}^m \tilde{I}_3^m - \tilde{R}_{14}^m \tilde{I}_4^m), \quad \text{similarly } E_2^m$$

$$\tilde{E}_3^m = \int_0^1 2\mu_0 d\mu_0 (\tilde{R}_{31}^m I_1^m + \tilde{R}_{32}^m I_2^m + R_{33}^m \tilde{I}_3^m + R_{34}^m \tilde{I}_4^m), \quad \text{similarly } \tilde{E}_4^m$$

The transmission matrix  $\mathbf{T}$  obeys exactly the same equations. In each of the equations above we only have to replace  $\mathbf{R}$  by  $\mathbf{T}$  in order to find the Stokes parameters of  $\mathbf{D} = \mathbf{T}\mathbf{I}$ , the (downward) radiation emerging from the bottom of the slab, and their Fourier components.

The zero-order transmission, describing the direct, unscattered radiation, deserves special mention. It leaves the state of polarization intact and reduces the four Stokes parameters of the incident radiation in the same proportion by the factor  $\exp(-b/\mu_0)$ . The formal equation is

$$T_{ik, \text{order } 0}(\mu, \varphi; \mu_0, \varphi_0) = e^{-b/\mu_0} (2\mu_0)^{-1} \delta(\mu - \mu_0) 2\pi \delta(\varphi - \varphi_0) \delta_{ik}$$

which, upon Fourier analysis, yields

$$T_{ik, \text{order } 0}^m(\mu, \mu_0) = e^{-b/\mu_0} (2\mu_0)^{-1} \delta(\mu - \mu_0) \delta_{ik}$$

Please note the danger of confusing different meanings of the word "order." Above it is used in the sense that order  $n$  is the number of successive scatterings in the slab; zero-order means no scattering. An equally common usage is to call  $m$  (the coefficient of  $\varphi$ ) the order in the Fourier expansion. This is something entirely different. Compare Fig. 15.2, where both are used.

One more trap connected with symmetry matters should be pointed out. In formulating the adding method for dissimilar layers in Section 4.5.2, we carefully distinguished between the reflection up from the lower layer and the reflection down from the upper layer. We also added the statement that this difference could be ignored in the doubling method, i.e., in adding identical layers. We now have to warn that the last statement is correct only in the absence of polarization. The correct formulation for reflection involving polarization may be derived as follows.

At some step of the doubling method, let the radiation coming from the bottom half layer have the Stokes parameters  $I, Q, U, V$  each being a function of  $\theta$  ( $\theta > 90^\circ$ , so  $\cos \theta < 0$ ) and of  $\varphi$ . These parameters have been found by the reflection formulas for the half layer, expressed with a convention of the sense in which to measure  $\varphi$ . This same radiation approaches the top layer. If we now wish to apply again the same reflection formulas, we must choose proper conventions for that reflection. This means that we must look at the drawing upside down and, consequently, that the sign convention of  $\varphi$  has to be inverted. In this new convention (with the symmetry assumptions we have made about the radiation field), the Stokes parameters of the same radiation are  $I, Q, -U, -V$ . Only with these parameters can we apply the same reflection matrix and find the Stokes parameters of the reflected (downward) radiation, still in the "upside down" convention. This has to be inverted again, and the next reflection follows.

The formal expression of the physical discussion is that we must insert the mirror matrix

$$\mathbf{M} = \begin{pmatrix} 1 & 0 & 0 & 0 \\ 0 & 1 & 0 & 0 \\ 0 & 0 & -1 & 0 \\ 0 & 0 & 0 & -1 \end{pmatrix}$$

between any two reflections at the interface. The successive operations thus become

$$\mathbf{R} \mathbf{M} \mathbf{R} \mathbf{M} \mathbf{R} \mathbf{M} \mathbf{R}, \text{ etc.}$$

Alternatively, we may reach the same result by never changing the direction in which  $\varphi$  is counted. The succession of operations is then

$$\mathbf{R} \mathbf{R}^* \mathbf{R} \mathbf{R}^* \mathbf{R}, \text{ etc.}$$

where  $\mathbf{R}$  is the matrix for reflection from the top and

$$\mathbf{R}^* = \mathbf{M} \mathbf{R} \mathbf{M}$$

is the matrix for reflection from the bottom of a (half) layer.

This distinction was not mentioned in Chandrasekhar's book (1950). It was duly pointed out by Hovenier (1969) and correctly applied in later doubling work by Hansen, Hovenier, and others (references in Section 18.1.5). The error of neglecting it was again made by Howell and Jacobowitz (1970), which led to numerically incorrect results, as pointed out by Hansen (1971) and corrected by Jacobowitz and Howell (1971).

## 15.2 SOME RESULTS

Having prepared the tools in Section 15.1, we shall devote the remaining sections of this chapter to resulting formulas for specific cases and to numerical samples. It is not necessary to spread this material over different chapters, like we did for unpolarized phase functions in Chapters 11–14, for the simple reason that fewer accurate computations have been made and published. However, the thorough work done by many authors on Rayleigh scattering will be reviewed separately (Chapter 16).

### 15.2.1 Formal Use of Earlier Equations

The basic equations describing the local scattering law (derived in Section 15.1.4) and the reflection and transmission by a slab (derived in Section 15.1.5) were not available in earlier chapters. One might fear, therefore, that the equations by which multiple scattering problems can be solved (in any method) would have to be completely reconstructed with these new building stones. This fear is not correct, for the new equations are *new translations* of symbolic equations used before. Any earlier solution derived by, and expressed in these symbolic forms can be used without change; only the translation changes. This holds true in particular for all of Chapter 5. The very attractive prospect thus is that we do not have to redo completely such relatively complex problems as doubling, the theory for very thick layers, asymptotic fitting, and various eigenvalue problems. We shall now see how this concept works out and, in particular, how the former results have to be translated into a form which takes full account of polarization and azimuth dependence. We shall also make reference to work by other authors who have not used this “translation trick” but have presented lengthy derivations from scratch, with the same results.

### 15.2.2 Doubling Method

The symbolic equations for the adding method are found in Section 4.5.2. The first four equations of the first experiment in Display 4.6 are all we need. Adding identical layers, i.e., performing a proper doubling, means that double primes (") can be replaced by single primes ('). Then  $\mathbf{R}'$  and  $\mathbf{T}'$  are reflection and

transmission matrices by the half layer with incidence from the top;  $\mathbf{R}^{*}$  and  $\mathbf{T}^{*}$  are the corresponding matrices for incidence from the bottom. They can be found from the relations (Section 15.1.5)

$$\mathbf{R}^{*} = \mathbf{M}\mathbf{R}'\mathbf{M}, \quad \mathbf{T}^{*} = \mathbf{M}\mathbf{T}'\mathbf{M}$$

or also by simply replacing  $\varphi - \varphi_0$  by  $\varphi_0 - \varphi$ .

For the purpose of computer programming, it is useful to single out from  $\mathbf{T}'$  and  $\mathbf{T}^{*}$  the zero-order term, which refers to direct transmission and which was written explicitly in Section 4.5.2. The full translation formulas of Display 4.7 now read (Hansen, 1971):

$$\mathbf{D}_{\text{diff}} = \mathbf{T}'_{\text{diff}} + e^{-b'/\mu_0} \mathbf{S} + \mathbf{S}\mathbf{T}'_{\text{diff}}$$

$$\mathbf{A}_{\text{diff}} = e^{-b'/\mu_0} \mathbf{R}' + \mathbf{R}'\mathbf{D}_{\text{diff}}$$

$$\mathbf{R} = \mathbf{R}' + e^{-b'/\mu} \mathbf{A}_{\text{diff}} + \mathbf{T}^{*}_{\text{diff}} \mathbf{A}$$

$$\mathbf{T}_{\text{diff}} = e^{-b'/\mu} \mathbf{D}_{\text{diff}} + e^{-b'/\mu_0} \mathbf{T}'_{\text{diff}} + \mathbf{T}'_{\text{diff}} \mathbf{D}_{\text{diff}}$$

This completes the treatment of the doubling method for full azimuth dependence and for arbitrary polarization. The availability of this method made it possible to solve the outstanding problem of the Venus polarization (Section 18.1.5) and many problems of polarized light in the earth's atmosphere.

The effect of a ground surface under a cloudy atmosphere, treated in Section 4.5.4, is another application of the adding method. Therefore, even if the reflection from the ground surface is sensitive to the polarization of the incident light, e.g., an ocean surface, the translation formulas from Section 15.1.5 suffice.

### 15.2.3 Diffusion Pattern and Exponent

Let us first recall the physical picture: the medium consists of randomly oriented scatterers that have mirror symmetry in the sense defined in Section 15.1.4. Radiation is incident on the top surface from a certain direction  $(\theta_0, \varphi_0)$ . The radiation field set up inside the medium by multiple scattering is a complicated affair, necessitating in its description the use of all Stokes parameters and of azimuth dependent terms.

Deep inside the medium, the radiation field becomes much simpler. In natural daylight under a heavily overcast sky, it is impossible even to guess the sun's azimuth because the brightness of the sky from zenith to horizon looks the same in all azimuths. This situation from daily experience does *not* exactly illustrate the radiation field in a diffusion domain, because it is modified by the presence of ground reflection. But if we imagine looking from a balloon gondola into a very thick cloud layer, or into water from an observing point some 50 m under the ocean surface (Section 20.4.1), we have good, natural illustrations of a diffusion domain. The brightness and polarization distribution over all angles, up and down, in such a domain is azimuth-independent.

Under the symmetry assumptions made, neither elliptical polarization, nor linear polarization vibrating under an odd angle with the normal plane can be maintained in the diffusion domain. Only natural (unpolarized) light or linear polarization parallel or perpendicular to the normal plane is eligible. In summary: the radiation field must be confined to

$m = 0$ : azimuth independence and  
Stokes parameters  $I$  and  $Q$  (with  $U = V = 0$ )

This makes it possible in the following discussion to omit the third and fourth Stokes parameter and to write only two-vectors and  $2 \times 2$  matrices.

Mathematically, the radiation field in the diffusion domain is a solution of the homogeneous transfer equation for nonconservative scattering. This solution has the form

$$\mathbf{I}(\tau, u) = S\mathbf{P}(u)e^{-k\tau}$$

where  $k$ , the diffusion exponent, is a positive constant  $< 1$ , both  $\mathbf{I}$  and  $\mathbf{P}$  are two-vectors representing the two first Stokes parameters ( $I$ ,  $Q$ ), and  $S$  is an arbitrary coefficient defining the strength of the diffusion stream.

Before we discuss methods for finding the exponent  $k$  and the pattern  $\mathbf{P}(u)$ , let us look at what we have discarded. The omitted terms, which count strongly near the top surface, but whose exponents in the  $\tau$  dependence make them numerically insignificant in the diffusion domain, are of the following types:

(1) All azimuth-dependent terms; solutions corresponding to discrete eigenvalues in the azimuth-dependent terms are briefly discussed in Section 15.3.2.

(2) All singular eigenvalue solutions (with  $k > 1$ ) in the azimuth independent terms.

(3) Any higher discrete eigenvalue solutions (with larger values of  $k$  than the main solution) in the azimuth-independent terms.

(4) Any solution in the azimuth-independent terms having an antisymmetric form in the CP representation, i.e., having  $I = 0$ ,  $Q = 0$ , but  $U \neq 0$ ,  $V \neq 0$ . Such solutions can be ignored under the symmetry assumptions we have made, but under more general assumptions (which, e.g., lead to birefringence or dichroism in the bulk medium) the main solution contains also an antisymmetric part.

It is possible, as in the unpolarized case (Section 6.5), not to discard the other solutions but to include them into a fully exact solution by means of singular eigenvalue expansions. This task has been performed by Domke (1975a,b, 1976).

The solution for the diffusion domain with an arbitrary phase matrix has been worked out by Kuščer and Ribarič (1959), by Herman (1965), and by Domke (1974b). All start with the CP representation of polarized light together with generalized spherical functions, but find it useful in the course of the deriva-

tion to switch to two-vectors representing the Stokes parameters  $I$  and  $Q$ . Having prepared the ground in Section 10.3 by representing the phase matrix at once in the  $(I, Q)$  presentation with ordinary (associated) Legendre functions, we can directly write the result in this form. A detailed comparison with Domke (1974b) showed that his results can be transformed into ours, but that the final form and the derivation given below are simpler than his. As a key to the comparison we note that

$$\mathbf{P}^l(\mu) = \begin{bmatrix} c_l P_l^2(\mu) & 0 \\ 0 & P_l(\mu) \end{bmatrix} \quad \text{and} \quad \xi^l = \begin{bmatrix} c_l^{-1} f_l \\ g_l \end{bmatrix}$$

where the left-hand members are in Domke's notation, where

$$c_l = -[(l+2)(l+1)(l-1)]^{1/2}$$

and the symbols in the top lines should be replaced by 0 for  $l = 0$  or 1.

We may now proceed with the derivation. The basic integral equation can be written at once by translating the corresponding equation for unpolarized scattering (Eq. 12 in Section 5.2.2) as explained in Section 15.2.1. It has the form:

$$(1 - ku)\mathbf{P}(u) = \frac{1}{2} \int_{-1}^1 \mathbf{Z}^0(u, u') \mathbf{P}(u') du'$$

Here  $\mathbf{P}(u)$  is the two-vector to be determined together with the eigenvalue  $k$  and  $\mathbf{Z}^0(u, u')$  is the given  $2 \times 2$  matrix which equals a submatrix of the azimuth-independent part of the phase matrix  $\mathbf{Z}$ . This may be written (Section 15.1.4) as

$$\mathbf{Z}^0(u, u') = \frac{1}{2\pi} \int_0^{2\pi} d\varphi \begin{bmatrix} a_1(v) & b_1(v) \cos 2i' \\ b_1(v) \cos 2i & a_2(v) \cos 2i \cos 2i' - a_3(v) \sin 2i \sin 2i' \end{bmatrix}$$

where  $v = uu' + (1 - u^2)^{1/2}(1 - u'^2)^{1/2} \cos \varphi$ , and  $i$  and  $i'$  are as defined in Fig. 15.1 (Section 5.1.4). The expansions of each of the matrix elements, derived in Sections 10.3.1–10.3.3, make it possible to write this in the form

$$\mathbf{Z}^0(u, u') = \begin{bmatrix} \sum_{n=0}^{\infty} \omega_n P_n(u) P_n(u') & \sum_{n=2}^{\infty} \beta_n P_n(u) P_n^2(u') \\ \sum_{n=2}^{\infty} \beta_n P_n^2(u) P_n(u') & \sum_{n=2}^{\infty} \varepsilon_n P_n^2(u) P_n^2(u') \end{bmatrix}$$

where the upper indices 2 indicate associated Legendre functions of order 2. The three sets of coefficients describe the properties of the scattering particles. For an assembly of spherical particles they may be obtained in principle from the Mie theory as sketched in Section 10.3.

The obvious form of the expansion of  $\mathbf{P}(u)$  to match the given form of  $\mathbf{Z}^0(u, u')$  is

$$\mathbf{P}(u) = \begin{bmatrix} \sum_{n=0}^{\infty} (2n+1) g_n P_n(u) \\ \sum_{n=2}^{\infty} (2n+1) \frac{(n-2)!}{(n+2)!} f_n P_n^2(u) \end{bmatrix} \quad (1)$$



Orthogonality relations of the Legendre polynomials then reduce the integral equation to

$$(1 - ku)\mathbf{P}(u) = \left[ \sum_{n=0}^{\infty} (\omega_n g_n + \beta_n f_n) P_n(u) \right] \quad (2)$$

Before we can equate coefficients at both sides we must eliminate  $uP_n(u)$  and  $uP_n^2(u)$  by the familiar recursion formulas

$$(2n + 1)uP_n(u) = (n + 1)P_{n+1}(u) + nP_{n-1}(u)$$

$$(2n + 1)uP_n^2(u) = (n - 1)P_{n+1}^2(u) + (n + 2)P_{n-1}^2(u)$$

Equations (1) and (2) are equivalent to Eqs. (1a) and (1b) (Section 6.2.3) for scattering without polarization. These equations are retrieved if we put  $\beta_n = \varepsilon_n = f_n = 0$ . The two recurrence relations for  $g_n$  and  $f_n$ , coupled by the coefficients  $\beta_n$ , replace the one recurrence relation for  $g_n(\gamma)$ ,  $\gamma = k^{-1}$ , discussed in Sections 6.2.2 and 6.2.3. In solving from these equations for  $k$  and for the coefficients  $g_n$  and  $f_n$  we have a number of options like we had in the absence of polarization. The discussion in Sections 6.2.3, 12.3.1, and 12.3.2 can be easily generalized, so the following results may be given without much explanation. In any of these options, the diffusion pattern may be obtained from Eqs. (1) or (2) after the coefficients have been computed.

The normalization is determined by the choice  $g_0 = 1$ . The two recurrence relations yield all higher coefficients if we choose at the start the two constants  $k$  and  $f_2$ . The choice is correct only if it leads to  $g_n \rightarrow 0$  and  $f_n \rightarrow 0$  for  $n \rightarrow \infty$ . This criterion should suffice to determine  $k$  and  $f_2$ . Presumably it can be made into a very convenient computer procedure, for any (slightly) wrong choice will make  $g_n, f_n$ , or both “explode” if  $n \rightarrow \infty$ . The proof of this statement may be constructed in exact analogy to Section 12.3.1. If  $\omega_n, \beta_n$ , and  $\varepsilon_n$  are all 0 for  $n > N$ , then  $f_n$  for  $n > N$  must be a linear combination of the associated Legendre functions  $P_n^2(u)$  and  $Q_n^2(u)$ , just as  $g_n$  is a linear combination of  $P_n(u)$  and  $Q_n(u)$ .

An alternative way to obtain the correct values of  $k$  and  $f_2$  is based on two transcendental equations containing sums over  $n$ . This method, recommended by Kuščer and Ribarič (1959), may be most useful if the expansion coefficients  $\omega_n, \beta_n$ , and  $\varepsilon_n$  go to 0 quite rapidly, entirely as argued in Section 6.2.3.

If absorption is weak, i.e., if  $h_0 = 1 - \omega_0$  is small, the exponent  $k$  becomes small. Writing

$$h_n = (2n + 1) - \omega_n, \quad h'_n = (2n + 1) - c_n^2 \varepsilon_n$$

$$q_n = c_n \beta_n, \quad c_n = -[(n + 2)!/(n - 2)!]^{1/2}$$

we simply find the power expansions in  $h_0$

$$k^2 = h_0 h_1 - 4h_0^2 h_1 h'_2 (h_2 h'_2 - q_2^2)^{-1} + O(h_0^3)$$

$$f_2 = 2h_0 c_2 q_2 (h_2 h'_2 - q_2^2)^{-1} + O(h_0^2)$$

**TABLE 45**  
Diffusion Pattern Based on Mie Scattering<sup>a</sup>

Assumed scattering law	Diffusion exponent $k$	Forward/back ratio in diffusion pattern	Degree of polarization under 90° in diffusion pattern
Mie scattering by monodisperse spheres with $m = 1.20$ , $x = 3^b$	0.4100	29.25	7.4 %
Same phase function with neglect of polarization <sup>b</sup>	0.4103	29.50	0
(i.e., relative error of)	(+0.1 %)	(+0.9 %)	—
Henyey–Greenstein function, unpolarized, with correct value of asymmetry $g = 0.786^c$	0.4028	28.4	0
(i.e., relative error of)	(−2.3 %)	(−3 %)	—

<sup>a</sup> All data in this example refer to albedo  $\omega_0 = 0.8$ .

<sup>b</sup> Herman (1970, plus added private communication).

<sup>c</sup> Interpolated from Tables 23 and 25; central column uncertain.

These equations are derived both by Kuščer and Ribarič (1959, Eq. 13) and by Domke (1974b, Eqs. 55, 56). The transformation to the more practical expansions with  $k$  as the independent variable, equivalent to the expansions in Sections 12.3.1 and 12.3.2, is left to the reader.

Published numerical data to illustrate the results of this section seem to be few. Herman (1965) derived the formulas to obtain the 3 sets of coefficients for the symmetric solution, as well as the 3 sets of coefficients for the asymmetric solution from the Mie theory. The same author later (Herman, 1970) gave numerical examples. His notation, apart from a constant, is  $\beta_l$  for  $\omega_n$ ,  $\gamma_l$  for  $\beta_n$ , and  $\alpha_l$  for  $\varepsilon_n$ . One concrete example based on these data and checked (private correspondence) by Dr. Herman is presented in Table 45. It refers to Mie scattering by monodisperse spheres with refractive index  $m = 1.20$  and size parameter  $x = 3$ , with an arbitrarily assumed albedo  $a = 0.8$ . The comparison shows that the value of the diffusion exponent and the form of the diffusion pattern are hardly affected at all if polarization is neglected. Simple Henyey–Greenstein scattering gives results that deviate more strongly but may still be fully acceptable in many practical problems. Further numerical examples are in Kattawar and Plass (1976).

Domke (1974b) illustrates the expansion in the nearly conservative case by assuming a phase matrix which is a linear combination of Rayleigh scattering (factor  $c$ ) and isotropic scattering (factor  $1 - c$ ). His result (Eq. 60) contains

several misprints and should (in our notation) be replaced by

$$\mathbf{P}(u) = \{1 + 3^{1/2}(1-a)^{1/2}u + (1-a)(3u^2 - 1)\} \begin{bmatrix} 1 \\ 0 \end{bmatrix} \\ + (1-a) \frac{c}{10-7c} \begin{bmatrix} 3u^2 - 1 \\ -3(1-u^2) \end{bmatrix} + O\{(1-a)^{3/2}\}$$

and the corresponding exponent is

$$k = 3^{1/2}(1-a)^{1/2}\{1 - \frac{4}{3}(1-a)(5-3c)/(10-7c) + O[(1-a)^2]\}$$

Finally, *conservative scattering* ( $\omega_0 = 1$ ) leads again to much simpler equations. In this case  $k = 0$  and the general solution for  $\mathbf{I}(\tau, u)$  is a linear function of  $\tau$  and  $u$ . It is easily verified that

$$\frac{1}{2} \int_{-1}^1 \mathbf{Z}^0(u, u') \begin{pmatrix} 1 \\ 0 \end{pmatrix} du' = \begin{pmatrix} \omega_0 \\ 0 \end{pmatrix} = \begin{pmatrix} a \\ 0 \end{pmatrix}$$

and

$$\frac{1}{2} \int_{-1}^1 \mathbf{Z}^0(u, u') \begin{pmatrix} u' \\ 0 \end{pmatrix} du' = \begin{pmatrix} u\omega_1/3 \\ 0 \end{pmatrix} = \begin{pmatrix} agu \\ 0 \end{pmatrix}$$

are the generalization of Eqs. 2 in Section 5.1. The solution derived in shorthand notation in Chapter 5 can therefore be used unchanged. This means that the *unpolarized* solution, which was presented in Section 6.2.1 for conservative scattering in the absence of polarization, *also* holds for conservative scattering with polarization. Written fully:

$$\mathbf{I}(\tau, u) = \begin{pmatrix} A - \frac{3}{4}F(1-g)\tau + \frac{3}{4}Fu \\ 0 \end{pmatrix}$$

Here  $A$  is an arbitrary isotropic radiation field and  $\frac{3}{4}Fu$  an intensity component proportional to  $u = \cos \theta$ , which provides the net flux  $\pi F$  in the positive  $\tau$  and  $u$  direction. Both the isotropic and the asymmetric part are unpolarized. Only the coefficients  $\omega_0 = 1$  and  $\omega_1 = 3g$  enter into these equations. All higher coefficients ( $\omega_2, \omega_3, \dots; \beta_2, \beta_3, \dots; \varepsilon_2, \varepsilon_3, \dots$ ) are irrelevant.

### 15.2.4 Thick Layers and Asymptotic Fitting

We may now summarize the changes necessary to make all equations of Chapter 5 applicable to scattering with polarization. Since this "translation job" has been sufficiently prepared in the preceding pages, we present the full translation rules in Display 15.2 without further comments. These rules may be found particularly helpful in applying the equations for thick layers (Section 5.3) and of asymptotic fitting (Section 5.6).

**DISPLAY 15.2**

Translation of General Thick-Layer Theory into Equations Valid for Arbitrary Scattering with Polarization

Without polarization arbitrary phase function	With polarization arbitrary phase matrix
Phase function $\times$ albedo $a\Phi(v)$ , $v = \cos \alpha$	Four functions $a_1(v)$ , $b_1(v)$ , $a_2(v)$ , $a_3(v)$ , of which the first one is $a\Phi(v)$ , plus two additional functions $b_2(v)$ , $a_4(v)$ , which do not enter into the thick-layer theory
Redistribution function $h(u, v)$	Azimuth-independent part of phase matrix $\mathbf{Z}^0(u, u')$ , only $2 \times 2$ part needed in thick-layer theory
Legendre coefficients $\omega_n$ of phase function and redistribution function	Coefficients of phase matrix $\omega_n$ , $\beta_n$ , $\epsilon_n$ ; see Sections 10.3, 15.2.3
Albedo $a = \omega_0$	Albedo $a = \omega_0$
Asymmetry factor $g = \omega_1/3a$	Asymmetry factor $g = \omega_1/3a$
Diffusion constant $k$	Diffusion constant $k$
Diffusion pattern $P(u)$	Diffusion pattern $\mathbf{P}(u)$ , a 2-vector; see Section 15.2.3
Expansion coefficients $g_n$ of diffusion pattern	Two sets of expansion coefficients $g_n, f_n$ of diffusion pattern, see Section 15.2.3
Moments of diffusion pattern 1, $y$ , $D$ (Display 5.2)	Moments of diffusion pattern $\begin{pmatrix} 1 \\ 0 \end{pmatrix}$ , $\begin{pmatrix} y \\ 0 \end{pmatrix}$ , $\begin{pmatrix} D \\ 0 \end{pmatrix}$
Functions $N = 1/2\mu$ , $U = 1$ , $W = \mu$	Two-vectors $\mathbf{N} = \begin{pmatrix} N \\ 0 \end{pmatrix}$ , $\mathbf{U} = \begin{pmatrix} U \\ 0 \end{pmatrix}$ , $\mathbf{W} = \begin{pmatrix} W \\ 0 \end{pmatrix}$
Reflection function, azimuth-independent part $R(\mu, \mu_0)$	Reflection matrix ( $4 \times 4$ ), azimuth-independent part $\mathbf{R}^0(\mu, \mu_0)$
Transmission function, azimuth-independent part $T(\mu, \mu_0)$	Transmission matrix ( $4 \times 4$ ), azimuth-independent part $\mathbf{T}^0(\mu, \mu_0)$
Escape function $K(\mu)$	Escape function $\mathbf{K}(\mu)$ , a 2-vector
Further scalars $l, m, q$ (extrapolation length), $b, f$	Further scalars $l, m, q$ (extrapolation length), $b, f$

## 15.3 SUCCESSIVE SCATTERING IN THE AZIMUTH-DEPENDENT TERMS

15.3.1 The  $m$ - $n$  Plane

The method of successive orders of scattering (Section 4.3) is always simple in concept, but whether it is practical depends on the rate of convergence. This is particularly true for the azimuth independent terms ( $m = 0$ ) discussed in earlier chapters. We shall find in the present section that convergence is always fast for  $m \geq 1$ . The situation may be summarized as shown in the accompanying tabulation.

		Convergence	For details refer to
azimuth-independent:	if $b \ll 1$ , any $a$	fast	Figs. 4.2, 7.2, 13.10 Sections 5.4.2, 12.4
	if $a \ll 1$ , any $b$	fast	
	other	moderate	
	if $a \rightarrow 1$ , and $b \rightarrow \infty$	very slow	
azimuth-dependent:	$m \geq 1$ any $a$ , any $b$	fast	this section

The following subsections deal with certain details in the successive scattering method applied to arbitrary  $m \neq 0$ . After a brief interlude devoted to the diffusion solution (Section 15.3.2), we discuss the ratio of successive terms (effective albedo, Section 15.3.3), the exact value of the first-order term (Section 15.3.4), the number of terms required (Section 15.3.5), and a numerical example (Section 15.3.6).

Much of what is presented in this section has for years been common knowledge among those who make practical computations in this field. Published accounts are scarce. Useful references are Hansen and Pollack (1970), Anikonov (1974), and the papers cited in Section 15.3.5.

The Fourier terms in azimuth lead to strictly separate transfer problems for each Fourier order  $m$  (Section 15.1.3). Each of these can in principle be solved by separately computing the contributions after  $n$  successive scattering events. Imagine that in a specific problem such a computation is performed and that all terms  $(m, n)$  whose contribution falls below a certain limit (e.g.,  $10^{-4}$ ) are neglected. The terms to be retained are then arranged as sketched in Fig. 15.2.

Before demonstrating this by a practical example (Section 15.3.6), let us look at the consequences of this arrangement.

*Consequence 1:* If we are interested in the net effect of many successive scatterings (and this is what is loosely meant by the word diffusion), we are practically limited to the  $m = 0$  term, which is the azimuth independent part.

*Consequence 2:* If we are interested in the fine detail in the angular distribution in azimuth, we have to go to large  $m$ , and this permits us practically to consider single scattering only ( $n = 1$ ), or single scattering with a slight correction for terms of higher orders.

*Consequence 3:* If we require a full and accurate result, a method which blindly finds all terms within a given rectangle  $n \leq N$ ,  $m \leq M$  is extremely wasteful. More economically, and more elegantly, we can use shortcuts. For instance, take one strip for small  $m$ , all  $n$ , and a second strip for small  $n$ , all  $m$ , and then correct for the common terms which have been taken double. The practical ways to carry this out are left to the ingenuity of the reader.

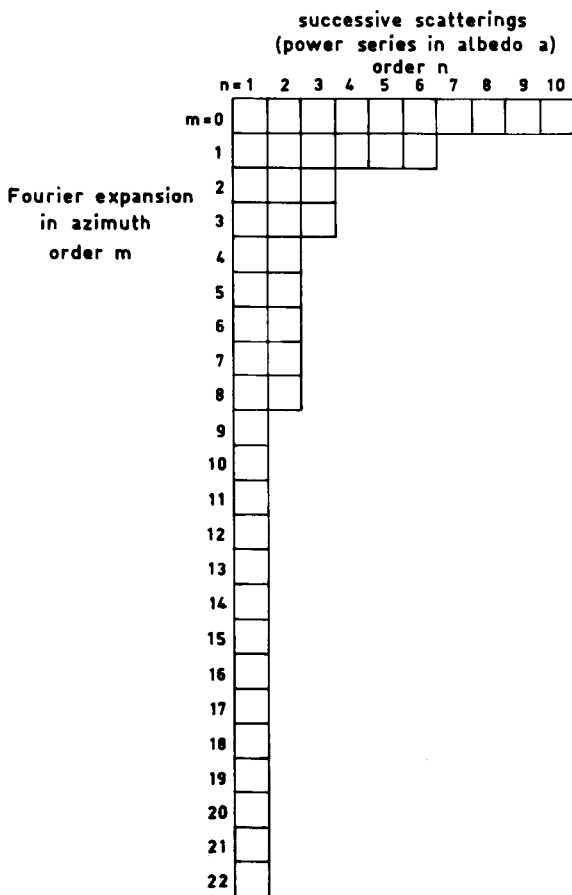


Fig. 15.2. Schematic diagram showing the terms in the double expansion necessary to describe azimuth-dependent reflection or transmission.

### 15.3.2 Diffusion Solution for the Azimuth-Dependent Terms

Earlier in this book we have seen that the diffusion formulation is useful when the successive scattering method is slowly convergent, i.e., for  $a$  near 1.

The reverse is also true: diffusion is bad if successive scattering is good. This is the situation for the azimuth dependent terms. The low effective albedo (Section 15.2.3) causes a strong damping. This means that the value of  $k$  is too large to make a diffusion solution attractive for numerical work.

This statement does not contradict the fact that, formally, in an unbounded medium diffusion solutions exist which are azimuth dependent and have an intensity of the form

$$I(\tau, u, \varphi) = e^{-k\tau} P^m(u) \cos m\varphi$$

For simplicity, the formulation is given for scattering without polarization. The integral equation and the characteristic equation keep the same form as in Section 6.2 provided we replace  $h(u, u')$  by the form given in Display 4.4,

$$h^m(u, u') = \sum_{j=m}^N \omega_j \frac{(j-m)!}{(j+m)!} P_j^m(u) P_j^m(u')$$

and define  $\Psi^{(m)}(\mu)$  as in Display 6.2. The eigenfunction then has the form

$$P^m(u) = \sum_{j=m}^{\infty} (2j+1) \frac{(j-m)!}{(j+m)!} g_j^{(m)}(k^{-1}) P_j^m(u)$$

where  $g_j^{(m)}$  is the polynomial defined in Display 6.2. A more complete treatment and numerical results are in Dlugach and Yanovitskii (1977).

### 15.3.3 Effective Albedo

Suppose absence of polarization. We then have from Section 15.1.4

$$J^m(u) = \frac{1}{2} \int_{-1}^1 h^m(u, u') I^m(u') du' \quad (m = 0, 1, \dots)$$

for the relation between the local intensity  $I$  and the local source function  $J$ , both in the  $m$ th Fourier component. Making expansions in associated Legendre functions

$$I^m(u) = \sum_{j=m}^{\infty} A_j^m P_j^m(u)$$

$$J^m(u) = \sum_{j=m}^{\infty} B_j^m P_j^m(u)$$

and using the form of  $h^m$  stated above, we find that the local scattering process is described by the extremely simple equation

$$B_j^m = \frac{\omega_j}{2j+1} A_j^m$$

The leading term, defining the simplest possible form that the radiation field can take for each  $m$ , is defined by  $j = m$ :

$$B_m^m = \frac{\omega_m}{2m + 1} A_m^m$$

The physical interpretation of this equation for  $m = 0$  is well known:  $A_0^0$  is proportional to the total incident radiation intercepted by an elementary volume, and  $B_0^0$  to the total radiation which leaves the same volume after having been scattered; the ratio  $\omega_0$  is the (local) albedo. By analogy we may therefore call  $\omega_m/(2m + 1)$  the *effective albedo* for the  $m$ th Fourier term.

In any practical phase function, except the complete forward or the complete backward peak (cf. Display 10.1), the value of the effective albedo  $\omega_m/(2m + 1)$  approaches 0 (or becomes exactly 0) as  $m \rightarrow \infty$ . This is the justification for drawing the diagram in Fig. 15.2 with successively shorter lines as  $m$  increases, until a long tail is left in which only single scattering counts.

The simplest possible solution cited above corresponds to the following physics. If we have sources homogeneously embedded in an infinite medium, giving in zero order a source function with the radiation pattern  $P_m^m(u)$ , then this pattern in direction and the homogeneity in depth persist through all orders ( $n$ ) of successive scattering, in each of which we would have

$$I_n(u) = J_n(u) = \frac{\omega_m}{2m + 1} I_{n-1}(u)$$

The sum of all orders then converges as a geometric series in which the effective albedo is the ratio.

The next question is What happens with less artificial assumptions, i.e., if we start with an arbitrary radiation field? Then we have a linear combination of many such fields. Let all  $\omega_j$  be nonnegative and let  $\omega_k/(2k + 1)$  be the largest among the numbers  $\omega_j/(2j + 1)$ ,  $j = m, m + 1, m + 2$ , etc. Then, after many successive scatterings, the ratio between terms of successive order will be  $\omega_k/(2k + 1)$ , and this may be called the effective albedo. Quite often  $k = m$ , so that we confirm our earlier guess. But it is conceivable that  $\omega_m$  happens to be zero or very small for the phase function at hand, in which case one of the next coefficients takes over.

All of this has been reasoned for an unbounded medium, but the same result holds for a semiinfinite atmosphere, simply because the high-order radiation penetrates so deeply that the presence of a boundary becomes a minor perturbation.

A more formal proof of the statement that the ratio of the orders in the reflection function approaches the limit

$$R_n^m(\mu, \mu_0)/R_{n-1}^m(\mu, \mu_0) \rightarrow \omega_k/(2k + 1) \quad \text{for } n \rightarrow \infty$$

can be constructed along the following lines. The reflection function in the  $m$ th Fourier term against a semi-infinite medium can be expressed in an  $H$  function,



defined in terms of a characteristic function  $\Psi$  defined in Display 6.2. If  $\omega_j = ab_j$ , as assumed in dealing with an analogous asymptotic problem in Section 12.3.2,  $\Psi$  is a nonlinear function of  $a$ . Let  $k$  be defined as above; then, as  $a$  gradually increases, the first value at which  $\int_0^1 2\Psi(\mu) d\mu = 1$  is, by an expression given in Section 6.2.2, seen to occur when  $h_k = 0$ , i.e., when  $a = a_1 = (2k + 1)/b_k$ . With that value of  $a$  we would have the situation equivalent to conservative scattering, in which the ratio between successive terms goes to 1 (Section 12.4). Hence, with an arbitrary value of  $a$  the ratio of successive terms goes to  $a/a_1 = ab_k/(2k + 1) = \omega_k/(2k + 1)$ , which we set out to prove.

An eigenvalue problem in successive scattering of the azimuth dependent terms can be formulated for finite layers, as we did for  $m = 0$  in Sections 7.4.1 and 13.4. For  $b \rightarrow \infty$  this eigenvalue should approach the effective albedo derived above.

For a phase matrix, i.e., in the presence of polarization, the derivation of an effective albedo requires more care, but the basic conclusion that the convergence becomes faster for higher  $m$  remains. Let us discuss only the azimuth-independent case ( $m = 0$ ), for which the full expression of the phase matrix is available in Section 15.2.3. We seek a solution of the equation

$$a_{\text{eff}} \mathbf{I}(u) = \frac{1}{2} \int_{-1}^1 \mathbf{Z}^0(u, u') \mathbf{I}(u') du'$$

Two simple solutions in which the radiation is unpolarized can be read from equations given in Section 15.2.3, namely

- (1) intensity  $\begin{pmatrix} 1 \\ 0 \end{pmatrix}$ , effective albedo  $\omega_0 = a$
- (2) intensity  $\begin{pmatrix} u \\ 0 \end{pmatrix}$ , effective albedo  $\frac{1}{3}\omega_1 = ag$

The simplest solution in which the intensity is polarized is of the form

- (3) intensity  $\begin{pmatrix} P_2(u) \\ xP_2^2(u) \end{pmatrix}$ , effective albedo  $a_{\text{eff}}$

The two values of  $x$  and the two corresponding values  $a_{\text{eff}}$  follow from the two equations

$$\begin{aligned} \omega_2 + 24\beta_2 x &= 5a_{\text{eff}} \\ \beta_2 + 24\epsilon_2 x &= 5xa_{\text{eff}} \end{aligned}$$

Numerical examples would be necessary to explore the significance of these solutions.

#### 15.3.4 The Exact First-Order Reflection and Transmission

First-order scattering ( $n = 1$ ) has the distinction that the scattering angle  $\alpha$  and the scattering plane are completely fixed if the direction of incidence ( $\mu_0, \varphi_0$ )

and the direction of emergence ( $u, \varphi$ ) are given. This means that in an atmosphere illuminated from a certain direction and observed from a certain direction, scattering occurs at each point under the same angle and with the same degree of polarization.

This observation leads to the simple rule: first-order diffuse reflection or diffuse transmission by a layer of any depth  $b$  is obtained by multiplying the result for isotropic scattering (Display 9.1) by the phase function  $\Phi(\cos \alpha)$  in the absence of polarization, or by the phase matrix  $\mathbf{Z}(u, \varphi; -\mu_0, \varphi_0)$  in the presence of polarization. Here  $u = +\mu$  for reflection and  $u = -\mu$  for transmission. This takes care of the entire column  $n = 1$ , all  $m$  in Fig. 15.2. It is possible to split  $\mathbf{Z}$  into its Fourier components with different  $m$ , as explained in Section 15.1.4; but this is not at all necessary, for usually the next step would be to make the Fourier synthesis again. In fact, Fourier analysis may make a simple situation look complicated, as an example for Rayleigh scattering (Table 54, Section 16.3.4) shows.

The moments and bimoments of the first-order reflection and transmission *cannot* be found in this easy way. The integrals from which they must be found contain exponential factors *and* the phase function in the integrand. Numerical integration is usually called for.

### 15.3.5 Number of Terms Required

How many terms are required in the expansions to reach a certain accuracy? We shall deal with unpolarized phase functions only and skip the trivial practice examples in which the phase function has a finite expansion of  $N + 1$  terms ( $N = 0, 1, 2$ ). The practical question is where to cut off the series in order to be assured of a certain accuracy, e.g., 3 or 5 figures. A general answer to this question cannot be given, but useful hints can be gathered both from computer experience and from an analysis of the asymptotic behavior of the terms. All answers compiled below must be read, give or take a few terms. We have tried to quote numbers of terms necessary for 5-figure accuracy; 4 or 5 terms less may be sufficient for 1% accuracy.

The data presented below, in particular under (B) and (C), are usefully complemented by the discussion and examples for *all* elements of the phase matrix given by Hansen and Travis (1974).

A distinction should be made between three types of expansions discussed under (A), (B), and (C) below.

#### (A) LEGENDRE EXPANSION OF THE PHASE FUNCTION

The Mie theory of scattering by spherical particles gives rise to two series defining complex amplitudes, from which four quadratic, real combinations can be made that enter into the scattering matrix for generally polarized light (van de Hulst, 1957). Dave (1970) has discussed the expansions of all four of these real combinations. Our discussion is confined to the phase function.

The expansions of the complex amplitudes in terms of functions related to the Legendre functions require a little over  $x$  terms, where  $x = 2\pi a/\lambda$  is the ratio of circumference to wavelength. This is a consequence of the localization principle which attributes the term with suffix  $n$  to a ray passing at a distance  $n\lambda/2\pi$  from the center. Terms with  $n > x$  correspond to rays missing the sphere (van de Hulst, 1957). In squaring to obtain the phase function, the required number of terms goes up to  $2x +$  a few. The expansion in Legendre functions thus obtained is discussed in Section 10.3.1. The tables by Clark *et al.* (1957) for  $m = 1.33$  show that the terms drop to the 1% level near  $2x + 4$  and to the  $10^{-5}$  level near  $2x + 9$ .

This is not the complete story. The many lobes which form the Mie pattern shift rapidly with size and/or wavelength. Exceptions to this statement are the diffraction peak near  $\alpha = 0^\circ$ , the glory peak near  $\alpha = 180^\circ$ , and the rainbow peaks. If we choose to ignore those exceptions, a polydisperse collection of drops must have a much smoother pattern and, therefore, a much shorter expansion than a monodisperse collection. From indirect evidence we estimate that about 20 or 30 Legendre terms should suffice to describe the smoothed pattern for water drops, independently of their size.

The justification for this easygoing attitude is that the most important of these features, the forward peak, can be reduced or removed almost without penalty if we take care to maintain the similarity (Section 14.1.2). The glory and the rainbow can be taken into account rigorously, if desired, in the first-order scattering (Section 15.3.4) and are washed out by the very nature of the scattering process in the higher-order terms. Why should one carry along a hundred extra terms that will not affect the results noticeably?

## (B) FOURIER EXPANSION OF THE PHASE FUNCTION

The expansion (Section 15.1.4, without polarization)

$$Z(u, u', \varphi, \varphi') = Z^0(u, u') + 2 \sum_{m=1}^{\infty} Z^m(u, u') \cos m(\varphi - \varphi')$$

is a simple consequence of the Legendre expansion discussed under (A). A cutoff of the number of terms in (A) leads to the same cutoff in (B). Dave (1970) presents some detailed empirical data on the number of terms  $N(u, u')$  required in (B) to reach 5-figure accuracy. We may summarize and interpret as follows.

If  $u = u' = 0$ , the plane of scattering is the equatorial (horizontal) plane and the scattering angle  $\alpha$  covers the full range ( $0^\circ, 180^\circ$ ). Hence

$$N(0, 0) = 2x + 10$$

If either  $u$  or  $u'$  is 1, the factor  $(1 - u^2)^{m/2}$  in the associate Legendre polynomial  $P_n^m(u)$  makes all but the first term vanish. Hence

$$N(1, u') = N(u, 1) = 1$$

At intermediate values a distinction must be made between the results for monodisperse and heterodisperse clouds. We find that the results of Dave's paper dealing with single drops, or monodisperse clouds, are fairly well represented by

$$N(u, u') = 2x \sin \theta + C$$

Here  $\theta$  is the smallest of the two angles defined by  $u = \cos \theta_1$ ,  $u' = \cos \theta_2$ . The constant  $C$  is 9 or 10 for 5-figure accuracy and 5 or 6 for 3-figure accuracy over the range  $10^\circ$ – $90^\circ$ , but must drop to 1 at  $0^\circ$ .

A heterodisperse cloud (Dave and Gazdag, 1970) has a smoother pattern. The diffraction peak near  $\alpha = 0^\circ$  can make itself felt only if  $|\theta_1 - \theta_2|$  is small. On the top of this peak, the number of required terms shown in their Fig. 1 may be represented by  $A \sin \theta + 10$ , where  $A$  varies from 60 to  $\sim 90$ , not unlike the values of  $2x$  of the largest drops actually present in the distribution. A slightly lower peak shows up near  $\theta_1 + \theta_2 = 180^\circ$ . If we keep clear of these peaks by about  $20^\circ$ , the number of terms is substantially smaller and fits reasonably well the expression

$$N(u, u') = 25 \sin \theta$$

where again  $\theta$  is the smallest of  $\theta_1$  and  $\theta_2$ .

The conclusion is that unless we wish to represent minute details, it is a waste of time to go to 300 terms (as some authors have done). Often 30 or 50 terms in the expansion suffice for high-accuracy results.

### (C) FOURIER EXPANSION OF THE REFLECTION AND TRANSMISSION FUNCTION

In these series, in which the function  $R^m(\mu, \mu_0, b)$  and  $T^m(\mu, \mu_0, b)$  appear as coefficients in the  $m$ th order terms (Section 15.1.5), the optical thickness  $b$  enters as yet another parameter. We shall avoid another detailed discussion, but simply state a few rules.

If  $b$  is rather small, i.e., for an optically thin layer, the effect that near-grazing rays go through a much longer path makes the functions peaked for small values of  $\mu$  and  $\mu_0$ . This does not, however, affect the number of terms in the Fourier expansion in  $\varphi$ .

In grazing incidence and reflection ( $\mu = \mu_0 = 0$ ) the way in which the reflection function depends on  $\varphi$  is an exact replica of the single-scattering phase function. This is a classical theorem I recall from Minnaert's lectures about 1941. The ratio of total reflected intensity to first-order reflected intensity simply goes to 1 in this limit (compare Table 38, Section 13.1). Hence, in this case the number of terms required in (C) is the same as stated in (B).

If at least one of the angles is well removed from the grazing directions, the number of necessary terms drops considerably. It becomes 1 (the azimuth independent term) if either  $\mu$  or  $\mu_0$  are 1. A rule of thumb for the intermediate angles, as in (B), is that the number of terms goes as  $\sin \theta = (1 - \mu^2)^{1/2}$  or  $(1 - \mu_0^2)^{1/2}$ , whichever is smallest.

## 15.3.6 A Numerical Example

The preceding discussion may be made less abstract by referring to a numerical example (Table 46). The atmosphere is taken semi-infinite with Henyey-Greenstein scattering,  $g = 0.5$ . The sums over  $n$  (next to last column) are taken with  $a = 1$ . Values for arbitrary  $a$  can be obtained by an extra factor  $a^n$  in the columns  $n = 1, 2$ , etc. All numbers refer to  $R(\frac{1}{2}, \frac{1}{2}, 180^\circ)$ . The factor 2 in the lines  $m \geq 1$  and the factor  $\cos m\varphi = \pm 1$  on all lines have already been introduced so that the sums (bottom line) are found by a direct summation along each column. The total sum 0.8512 is the reflection function sought. This function multiplied by  $\mu = 0.5$  is entered as one point in the brightness distribution of a planet in opposition (Fig. 18.7b).

The accuracy of these numbers, particularly on the lines  $m = 1$  and  $m = 2$ , is not guaranteed for  $n \geq 2$ , because the table was added as an afterthought from available but not entirely suitable machine output.

The following checks may be made.

1. The table has the form of Fig. 15.2. The form is sensitive to the value of  $\mu$ . For  $\mu = 0$ , only the first column remains. For  $\mu = 1$ , only the top line remains.
2. The number of necessary terms on the line  $m = 0$  is enormous. Its sum is 7.64 times the first-order term (Table 38). The convergence on this line may be analyzed by the method of Section 12.4.
3. The numbers on the lines  $m \geq 1$  converge approximately as geometric series with a ratio tending to the effective albedo  $g^m$  (Section 15.3.3). However, this approach does not give a good estimate of the  $n = 2$  term from the  $n = 1$  term.

TABLE 46

Numerical Example of Full Separation into Orders of Successive Scattering ( $n$ )  
and Orders of Fourier Expansion in Azimuth ( $m$ ).

	$n = 1$	$n = 2$	$n = 3$	$n = 4$	$n = 5$	$n = 6$	Sum, for $a = 1$		Ratio
							$n = 7-\infty$	$n = 1-\infty$	
$m = 0$	1338	1164	877	659	509	405	5272	10224	1
$m = 1$	-1047	-600	-270	-116	-50	-22	-18	-2123	$\frac{1}{2}$
$m = 2$	348	128	32	8	2	1	—	519	$\frac{1}{4}$
$m = 3$	-108	-26	-4	—	—	—	—	-138	$\frac{1}{8}$
$m = 4$	33	5	—	—	—	—	—	38	$\frac{1}{16}$
$m = 5$	-10	—	—	—	—	—	—	-10	—
$m = 6$	3	—	—	—	—	—	—	3	—
$m = 7$	-1	—	—	—	—	—	—	-1	—
Sum, $m = 0-7$	556	671	635	551	461	384	5254	8512	

<sup>a</sup> The function so separated is  $10^4 R(\frac{1}{2}, \frac{1}{2}, \varphi_0 + 180^\circ, \varphi_0)$ , i.e., the reflection function in opposition with  $\mu = \mu_0 = \frac{1}{2}$ , for a semi-infinite atmosphere with Henyey-Greenstein phase function with  $g = 0.5$ .

4. The column  $n = 1$  contains 8 terms to reach 4-figure accuracy. This is much smaller than the rough estimate of  $25 \sin \theta = 22$  terms for 5-figure accuracy (Section 15.3.5). This is due to the particularly smooth form of the Henyey–Greenstein function: the factor  $g^7$  in  $\omega_7 = 15g^7$  accounts for 2 extra decimal places.

5. The sum of the column  $n = 1$  should be

$$[1/4(\mu + \mu_0)]\Phi(-1) = \frac{1}{4} \times \frac{2}{9} = 0.0556$$

This is based on the rule explained in Section 15.3.4. The first factor is the value of  $R_1(\mu, \mu_0)$  for isotropic scattering (Display 8.1 with  $H(\mu) = 1$ , or Display 9.1 with  $b = \infty$ ). The second factor is the phase function for straight backscatter,  $\cos \alpha = -1$  (Display 10.1).

6. If we omit the minus signs in the column  $n = 1$ , we obtain the sum 0.2888, which should be  $R_1(\frac{1}{2}, \frac{1}{2}, 0^\circ) = \frac{1}{4}\Phi(0.5) = 0.2887$ , corresponding to  $\alpha = 60^\circ$ . If we omit the terms with odd  $m$  and give the terms with even  $m$  alternate signs, the same column gives the sum 0.1020, which should be  $R_1(\frac{1}{2}, \frac{1}{2}, 90^\circ) = \frac{1}{4}\Phi(-0.25) = 0.1020$ ; here  $\alpha = 104^\circ$ .

7. The number at  $n = 1, m = 1$  is  $\frac{1}{4}h(0.5, -0.5) = \frac{1}{4} \times (0.5353) = 0.1338$  (entry from Table 22, Section 11.1).

We do not expect the reader to check all 11 references to other sections in the preceding lines. These references may be useful if the reader gets entangled in a definition, a factor of 2, or a plus or minus sign.

## 15.4 BEHAVIOR OF FOURIER TERMS FOR LARGE $m$ ; A PRACTICE EXAMPLE

### 15.4.1 The Data

This section contains an elaboration of results very briefly reported by van de Hulst (1971). Related topics with numerical examples have been discussed by Anikonov (1974) and Kolesov (1974). A detailed comparison has not been made.

It was thought useful to have one concrete example of the manner in which the terms decrease as  $m$  goes up. For this purpose we used data kindly made available by Dr. J. Hansen. The numerical values of  $R^m(\mu, \mu)$  and  $T^m(\mu, \mu)$  were computed for  $m = 0-16$ , five values of  $\mu$ , all with  $\mu = \mu_0$ . The scattering pattern was the Henyey–Greenstein function (no polarization):  $g = 0.5$  with  $a = 0.01, 0.1, 0.9$ , and  $1$ ;  $g = 0.875$  with  $a = 0.9$  and  $1$ . The total layer thickness was  $b = \frac{1}{4}, \frac{1}{2}, 1 \dots 32$ .

We first write

$$R^m(\mu, \mu_0) = [a/4(\mu + \mu_0)](1 - e^{-b/\mu - b/\mu_0})h^m(-\mu, \mu_0)X^m(\mu, \mu_0)$$

$$T_{\text{diff}}^m(\mu, \mu_0) = [a/4(\mu_0 - \mu)](e^{-b/\mu_0} - e^{-b/\mu})h^m(\mu, \mu_0)Y^m(\mu, \mu_0), \quad \mu \neq \mu_0$$

$$T_{\text{diff}}^m(\mu, \mu) = (ab/4\mu^2)e^{-b/\mu}h^m(\mu, \mu)Y^m(\mu, \mu), \quad \mu = \mu_0$$

thus expressing the reflection and transmission functions as the exact forms for first-order (single) scattering multiplied by empirical correction factors  $X^m$  and  $Y^m$ . The functions  $h^m(u, u')$  are defined in Display 4.4. Compare also Section 15.1.

Table 47 shows a representative example, with  $g = \frac{1}{2}$ ,  $m = 3$ ,  $\mu = \mu_0 = \frac{1}{2}$ , which gives  $h^3(-\frac{1}{2}, \frac{1}{2}) = 0.02163$ ,  $h^3(\frac{1}{2}, \frac{1}{2}) = 0.2935$ . The correction factors depend on  $a$  and  $b$  and reach their maximum values at  $a = 1$ ,  $b = \infty$ . Even there the corrections for higher-order scattering are only 27 % in reflection and 35 % in transmission.

For comparison, Table 47 also shows the ratios (total to first-order reflection) at  $\mu = \mu_0 = 0.5$  for isotropic azimuth-independent scattering with  $a = 0.4$ . This was chosen among lists available for many values of  $a$  (Table 13, Section 9.1.2) for its resemblance to the numbers in the first column. Note that the value 0.4 is low, but not as low as the effective albedo  $\omega_m/(2m + 1) = a^m = 0.125$  defined in Section 15.3.3. This shows that the effective albedo cannot serve in a direct numerical comparison with isotropic scattering.

Let us now concentrate on reflection by fairly thick layers ( $b = 2-\infty$ ). If each order of successive scattering would be lower by a factor  $a\eta^m(\mu, \mu_0)$  than the

TABLE 47  
Azimuth-Dependent Term  $R^3$  of the Reflection Function and Ratios of Full Quantity to First-Order Part for Reflection  $X^3$  and Transmission  $Y^3$  <sup>a</sup>

$g = 0.5, m = 3$						(For comparison) $g = 0, m = 0$
		$a = 1$	0.9	0.1	0.01	$a = 0.4$
$2R^3(0.5, 0.5)$	$b = 0.25$	0.00795	0.00705	0.000694	0.0000684	—
	0.5	0.01142	0.01007	0.000954	0.0000937	—
	1	0.01339	0.01177	0.001086	0.0001064	—
	2	0.01374	0.01207	0.001106	0.0001083	—
	$4-\infty$	0.01375	0.01208	0.001107	0.0001084	—
$X^3(0.5, 0.5)$	$b = 0.25$	1.163	1.146	1.015	1.002	1.13
	0.5	1.222	1.197	1.020	1.002	1.20
	1	1.261	1.232	1.023	1.002	1.27
	2	1.271	1.240	1.023	1.002	1.30
	$4-\infty$	1.272	1.241	1.024	1.002	1.30
$Y^3(0.5, 0.5)$	$b = 0.25$	1.029	1.026	1.003	1.000	—
	0.5	1.051	1.045	1.005	1.001	—
	1	1.088	1.078	1.008	1.001	—
	2	1.161	1.146	1.015	1.002	—
	4	1.353	1.310	1.029	1.003	—

<sup>a</sup> The example refers to Henyey–Greenstein scattering with  $g = 0.5$ ,  $\mu = \mu_0 = 0.5$ .

TABLE 48  
Empirical Ratios  $\eta^m(\mu, \mu)$  between Successive Orders of Scattering

		$\cos^{-1} \mu$				
		88°	80°	60°	30°	0°
$g = 0.5$	$m = 1$	0.09	0.24	0.51	0.69	—
	$m = 3$	0.02	0.07	0.21	0.40	—
	$m = 6$	0.004	0.011	0.037	—	—
	$m = 9$	0.001	0.002	0.013	—	—
$g = 0.875$	$m = 6$	0.31	0.50	0.72	0.85	—
	$m = 9$	0.13	0.43	0.67	—	—
	$m = 12$	0.090	—	—	—	—
	$m = 15$	0.063	—	—	—	—
	$m = 18$	0.045	—	—	—	—

preceding one, the sum would form a geometric series and we should have

$$X^m(\mu, \mu_0) = [1 - a\eta^m(\mu, \mu_0)]^{-1}$$

The actual values fit this equation fairly well. Table 48 shows the  $\eta$  values obtained in this manner from the computed  $X$  values. Those for  $g = 0.5$  are fairly accurate because data were available for four values of  $a$ . The values for  $g = 0.875$  are less accurate. Dashes in the table mean that the computation was not made or failed to give a meaningful answer.

Inspection of Table 48 strongly suggests that  $\eta$  goes to zero for all values of  $g$  and  $\mu$  if  $m \rightarrow \infty$ . This is indeed what we set out to demonstrate, for vanishing  $\eta$  means that  $X^m$  is 1 and that the first order is at once the sum of all orders. The effect is strongest for the less peaked phase function ( $g = 0.5$ ) and for the near-grazing angles ( $\mu = \cos 88^\circ$ ). This we should expect because the general theorem states that grazing reflection should have  $\eta = 0$  strictly.

A tentative practical conclusion from Table 48 is that any errors made by omitting the correction factors  $X^m$  and  $Y^m$  altogether fall below 1% for  $m \geq 12$  when  $g = 0.5$  and for  $m \geq 30$  or 50 when  $g = 0.875$ .

15.4.2 Asymptotic Behavior of  $h^m(u, u')$

With the correction factors  $X^m$  and  $Y^m$  out of the way, the equations still contain the function  $h^m(u, u')$ . At first sight nothing much can be said about the behavior of this factor with increasing  $m$ . Direct computation in the example ( $m = 3$ ) discussed in Table 47 from the expansion given in Display 4.4 requires about six terms ( $n = 3$  to  $n = 8$ ) with oscillating signs and none of these is dominant.

The numerical results, however, give a pleasant surprise. If the reflection function is plotted on a logarithmic scale against  $m$  (Fig. 15.3), the dots fall on



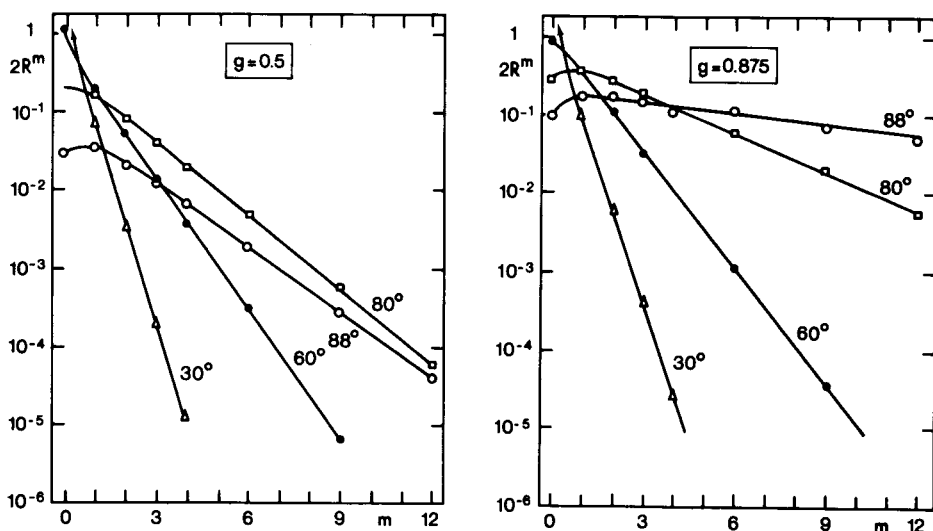


Fig. 15.3. Separate terms in the Fourier expansion in azimuth of the reflection function of a semi-infinite atmosphere for  $\mu = \mu_0 = \cos \theta$ . Two values of the asymmetry parameter  $g$  and 4 values of  $\theta$  have been adopted. The curves for  $m \geq 2$  essentially represent single scattering.

almost straight lines for  $m \geq 3$  for both values of  $g$  and for all angles considered. This, if theoretically understood, could lead to a substantial reduction in machine time. As expected, the steeper angles of incidence and emergence give rise to the steeper drop with increasing  $m$ . Also, the drop is not quite as steep for  $g = 0.875$  as it is for  $g = 0.5$ .

Clearly, Fig. 15.3 essentially represents the behavior of the factors  $h^m(u, u')$ , for the correction factors  $(1 - \eta^m)^{-1}$  remain small (although not negligible) on the scale of these figures. Table 49 shows this factor isolated in one particular

TABLE 49

Sample Values of the Azimuth-Dependent  
Terms of the Henyey-Greenstein Phase  
Function for  $g = 0.5$

$m$	Reflection $h^m(-\frac{1}{2}, \frac{1}{2})$	Transmission $h^m(\frac{1}{2}, \frac{1}{2})$
0	0.5353	1.643
1	0.2095	1.030
2	0.0695	0.566
3	0.0216	0.294
6	0.000554	0.0355
9	0.0000127	0.00389
12		0.000408
15		0.0000412

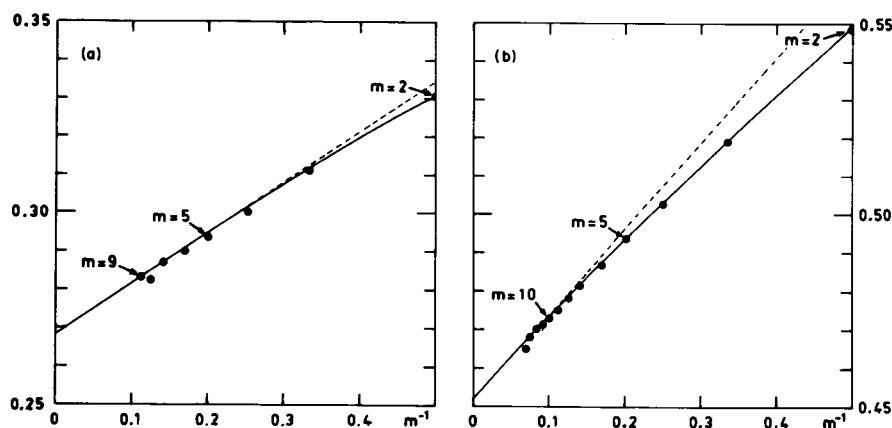


Fig. 15.4. Comparison of empirical ratios of successive terms in the azimuth expansion (●) with predicted asymptotic behavior (---). The example refers to (a) reflection and (b) transmission for  $g = 0.5$ ,  $\mu = \mu_0 = 0.5$ .

example,  $g = 0.5$ , with  $u = -\frac{1}{2}$ ,  $u' = +\frac{1}{2}$  (applicable to reflection) and  $u = u' = \frac{1}{2}$  (applicable to transmission). The accuracy should be a fraction of a percent. Values in the top line ( $m = 0$ ) were taken from Table 22 (Section 11.1). The ratios between successive terms are shown in Fig. 15.4. These ratios are not constant, as Fig. 15.3 might suggest, but drop slowly with increasing  $m$  and fit an empirical formula of the type

$$h^m/h^{m-1} = C + D/m$$

where  $h^m$ ,  $C$ , and  $D$  all depend on  $g$ ,  $u$ , and  $u'$ .

A general derivation of the asymptotic behavior of  $h^m(u, u')$  for an arbitrary phase function is not available. However, a solution was found for the particular phase function employed. This method may also work for other phase functions. In the Henyey–Greenstein phase function

$$\Phi(g, \cos \alpha) = (1 - g^2)/(1 + g^2 - 2g \cos \alpha)^{3/2}$$

we replace  $\cos \alpha$  by

$$\cos \alpha = uu' + (1 - u^2)^{1/2}(1 - u'^2)^{1/2} \cos(\varphi - \varphi')$$

and put  $\varphi' = 0$ . It is then seen that a similar form appears, in which  $\varphi$  takes the place of  $\alpha$ . Some algebra shows that the substitutions

$$\begin{aligned} c &= 1 + g^2 - 2guu', & d &= 2g(1 - u^2)^{1/2}(1 - u'^2)^{1/2} \\ r &= [c - (c^2 - d^2)^{1/2}]/d \\ s &= c/(1 + r^2) = d/2r, & f &= (1 - g^2)/(1 - r^2) \end{aligned} \quad (3)$$

give

$$\Phi(g, \cos \alpha) = fs^{-3/2}\Phi(r, \cos \varphi)$$

The Fourier expansion of this function still is not simple, for we know (van de Hulst and Davis, 1961) that already the zero-order coefficient leads to an elliptic integral. However, the expansion in terms of Legendre functions is well known:

$$\Phi(g, \cos \alpha) = fs^{-3/2} \sum_{n=0}^{\infty} (2n+1)r^n P_n(\cos \varphi)$$

Each Legendre function of order  $n$  is expressible in a finite sum, the terms of which are proportional to  $\cos m\varphi$  with  $m = n, n-2, n-4$ , etc., down to  $m = 1$  or 0. On rearranging these terms in the form prescribed by Display 4.4:

$$a\Phi(g, \cos \alpha) = h_0(u, u') + 2 \sum_{m=1}^{\infty} h^m(u, u') \cos m\varphi$$

we find that the function  $2h^m(u, u')$  consists of an infinite series, the terms of which correspond to  $n = m, m+2, m+4$ , etc. This series for  $m \neq 0, a = 1$  is

$$h^m(u, v) = \frac{3 \cdot 5 \cdots (2m+1)}{2 \cdot 4 \cdots 2m} \frac{fr^m}{s^{3/2}} \times \left[ 1 + \frac{2m+5}{2m+2} \left( \frac{r^2}{2} \right) + \frac{(2m+3)(2m+9)}{(2m+2)(2m+4)} \left( \frac{r^2}{2} \right)^2 + \cdots \right] \quad (4)$$

The form in brackets essentially converges as a geometric series with ratio  $r^2/2$ . The quantity plotted in Fig. 15.4 may on this basis be developed in powers of  $m^{-1}$ . The result is

$$\frac{h^m(u, u')}{h^{m-1}(u, u')} = r \left( 1 + \frac{1}{2m} - \frac{k}{m^2} + \cdots \right) \quad (5)$$

with

$$k = \frac{3}{4}r^2(1 - \frac{1}{2}r^2)$$

Table 50, still referring to the example of Table 49 and Fig. 15.4, shows that these equations lead rapidly to accurate results. The columns headed "theoretical" contain the numbers computed with the three written terms of Eq. (5). The curvature of the graphs in Fig. 15.4 is hardly visible because the coefficient  $k$  is so small. Evidently, terms omitted in Eq. (5) are so small that they do not affect the third decimal except in the ratio  $h^0/h^1$ .

The function  $h^m(u, u')$  itself can be similarly expressed by using Wallis' formula (Abramowitz and Stegun, 1965, p. 258) in Eq. (4). The result up to terms of the order  $m^{-1}$  is

$$h^m(u, u') = (4m/\pi)^{1/2} [fr^m/s^{3/2}(1 - \frac{1}{2}r^2)][1 + (k + \frac{3}{8})m^{-1} + \cdots]$$

TABLE 50  
Empirical and Theoretical Ratios  $h^m/h^{m+1}$  between Successive Terms of the Fourier Expansion in One Example

	Reflection $g = \frac{1}{2}, u = \frac{1}{2}, u' = -\frac{1}{2}$		Transmission $g = \frac{1}{2}, u = \frac{1}{2}, u' = \frac{1}{2}$	
	Empirical	Theory, Eq. (5)	Empirical	Theory, Eq. (5)
$m = 1$	0.391	0.388	0.627	0.615
2	0.332	0.332	0.549	0.549
5	0.294	0.294	0.494	0.494
10	0.281	0.281	0.473	0.473
$\infty$	—	0.268	—	0.451
Constants used	$r = 2 - \sqrt{3} = 0.2680$ $k = 0.0519$		$r = (4 - \sqrt{7})/3 = 0.4514$ $k = 0.1373$	

As a check, this equation for transmission,  $m = 12$ , gives  $4.04 \times 10^{-4}$  which differs by only 1% from the value given in Table 49.

Corresponding results for different angles of incidence and reflection, still for the Henyey–Greenstein scattering function, are given in Table 51. The lines marked “empirical” for each  $g$  give the slopes roughly read from Fig. 15.3. The lines marked “theoretical,  $m = \infty$ ” for each  $g$  give the values of  $r$  computed from Eq. (3) for  $u = -u' = \mu$ . The theoretical values for  $m = 5$  are, by two terms of Eq. (5), 10% larger. Both agree well with the empirical values. The remaining differences may be ascribed chiefly to the fact that in this comparison the factor  $X^m$  is  $(1 - \eta)^{-1}$  in the empirical values ( $a = 1$ ), but is absent in the theoretical value (corresponding to  $a = 0$ ).

TABLE 51  
Factors<sup>a</sup> by Which  $R^m(\mu, \mu)$  Drops for  $\Delta m = +1$

		$\cos^{-1} \mu$ $\mu^2$	0° 1	30° 0.75	60° 0.25	80° 0.03	88°–90° 0
$g = 0.5$	Empirical	(Fig. 15.3)	—	0.053	0.28	0.49	0.53
		in $m$ range	—	(1–4)	(2–9)	(2–12)	(2–12)
	Theoretical (Eq. 5)	at $m = 5$	0	0.069	0.29	0.50	0.55
		at $m = \infty$	0	0.063	0.27	0.46	0.50
$g = 0.875$	Empirical	(Fig. 15.3)	—	0.062	0.32	0.67	0.88
		in $m$ range	—	(1–4)	(2–9)	(2–12)	(2–12)
	Theoretical (Eq. 5)	at $m = 5$	0	0.079	0.36	0.74	0.97
		at $m = \infty$	0	0.071	0.33	0.67	0.88

<sup>a</sup> The numbers are based on Henyey–Greenstein phase functions with two values of  $g$ .

Although the numerical examples treated in this section all refer to  $|u'| = |u|$ , the equations given are equally useful for unequal values of  $|u|$  and  $|u'|$ . The limits are simple: If either  $u$  or  $u' = 1$ ,  $r = 0$ ; if  $u = u' = 0$ ,  $r = g$ ; and if  $g \rightarrow 1$ ,  $r \rightarrow 1$ .

## REFERENCES

- Abhyankar, K. D., and Fymat, A. L. (1969). **10**, 1935.
- Abramowitz, M., and Stegun, I. A. (1965). "Handbook of Mathematical Functions." Dover, New York.
- Anikonov, A. S. (1974). *Astrofizika* **10**, 227 [English transl.: **10**, 138].
- Chandrasekhar, S. (1950). "Radiative Transfer." Oxford Univ. Press (Clarendon), London and New York. Also Dover, New York, 1960.
- Clark, G. C., Chu, C. M., and Churchill, S. W. (1957). *J. Opt. Soc. Am.* **47**, 81.
- Dave, J. V. (1970). *Appl. Opt.* **9**, 1888.
- Dave, J. V., and Gazdag, J. (1970). *Appl. Opt.* **9**, 1457.
- Dlugach, J. M., and Yanovitskii, E. G. (1977). *Fiz. Atmosf. Okeana* **13**, 699 [English transl.: *Izv. Atm. Ocean. Phys.* **13**, 473 (1978)].
- Domke, H. (1973). *Gerlands Beitr. Geophys.* **82**, 482.
- Domke, H. (1974a). *Astrophys. Space Sci.* **29**, 379.
- Domke, H. (1974b). *Astrofizika* **10**, 205 [English transl.: **10**, 125 (1975)].
- Domke, H. (1975a). *J. Quant. Spectrosc. Radiat. Transfer* **15**, 669.
- Domke, H. (1975b). *J. Quant. Spectrosc. Radiat. Transfer* **15**, 681.
- Domke, H. (1976). *J. Quant. Spectrosc. Radiat. Transfer* **16**, 973.
- Gel'fand, I. M., Minlos, R. A., and Shapiro, Z. Ya. (1963). "Representation of the Rotation and Lorentz Groups and Their Applications." Pergamon, Oxford.
- Hansen, J. E. (1971). *J. Atmos. Sci.* **28**, 120.
- Hansen, J. E., and Pollack, J. B. (1970). *J. Atmos. Sci.* **27**, 265.
- Hansen, J. E., and Travis, L. D. (1974). *Space Sci. Rev.* **16**, 527.
- Herman, M. (1965). *C. R. Acad. Sci. Paris* **260**, 468.
- Herman, M. (1970). *Nouv. Rev. Opt. Appl.* **1**, 171.
- Herman, M., and Lenoble, J. (1968). *J. Quant. Spectrosc. Radiat. Transfer* **8**, 355.
- Hovenier, J. W. (1969). *J. Atmos. Sci.* **26**, 488.
- Howell, H. B., and Jacobowitz, H. (1970). *J. Atmos. Sci.* **27**, 1195.
- Jacobowitz, H., and Howell, H. B. (1971). *J. Atmos. Sci.* **28**, 1301.
- James, R. W. (1976). *Phil. Trans. R. Soc. A* **281**, 195.
- Kattawar, G. W., and Plass, G. N. (1976). *Appl. Opt.* **15**, 3166.
- Kolesov, A. K. (1974). *Tr. Astrophys. Obs. Leningrad Univ.* **30**, 3 (Russian).
- Kušćer, I., and Ribarić, M. (1959). *Opt. Acta* **6**, 42.
- Sekera, Z. (1966). *J. Opt. Soc. Am.* **56**, 1732.
- van de Hulst, H. C. (1957). "Light Scattering by Small Particles." Wiley, New York. Also Dover, New York, 1981.
- van de Hulst, H. C. (1971). *J. Quant. Spectrosc. Radiat. Transfer* **11**, 785.
- van de Hulst, H. C., and Davis, M. M. (1961). *Proc. Kon. Nederl. Akad. Wetensch. Amsterdam* **B64**, 220.

## 16 Rayleigh Scattering

### 16.1 THE PHASE MATRIX

#### 16.1.1 Assumptions

Rayleigh scattering is the name given to radiation from the electric dipoles induced by the incident radiation in any type of small particles (molecules, small drops, etc.). For the sake of simple terminology, we limit this name to particles of isotropic polarizability. Sometimes for clarity we call it “pure” Rayleigh scattering. Thomson scattering by free electrons differs from Rayleigh scattering only by the wavelength dependence. For the purposes of this book it is the same as Rayleigh scattering.

If light is incident from one direction and unpolarized, the confinement of the induced dipoles to the plane perpendicular to the direction of incidence makes the backward and forward scattering twice as strong (and unpolarized) as the perpendicularly scattered intensity (which is linearly polarized, perpendicular to the scattering plane). Figure 16.1 shows this familiar pattern. Pure Rayleigh scattering is conservative ( $a = 1$ ).

Many authors, challenged by the blue sky or by the intricate mathematics, have for a century devoted their efforts to solving transfer problems with the Rayleigh scattering law. Full solutions have been obtained by quite a variety of methods. We shall not review these methods but only the results. First, we list a few *deviating assumptions* that are often made.

(a) Omitting the polarization and taking the envelope of Fig. 16.1 defines Rayleigh’s phase function (Display 10.1, No. 5); it has no physical significance

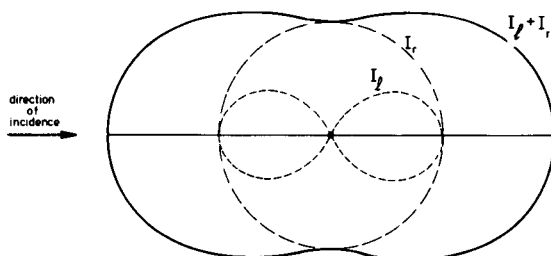


**Fig. 16.1.** Angular pattern of Rayleigh scattering for incident natural light. The intensities of each linearly polarized component are also shown:  $I_r$ , electric vector perpendicular to scattering plane;  $I_p$ , electric vector parallel to scattering plane.

but is a much used practice example. Note that some authors do not even make the distinction with actual Rayleigh scattering. This makes their numerical results misleading.

(b) Nonconservative Rayleigh scattering describes the properties of a medium in which a Rayleigh scattering component and an absorbing component are mixed.

(c) A linear combination of conservative isotropic scattering and pure Rayleigh scattering is not only a good practice example but also represents (except for circular polarization) the net effect of scattering by randomly oriented particles whose polarizability is described by a tensor with unequal components. Air shows this effect mildly (see Section 10.2.1). The full formulation is given under (e).

(d) An arbitrary linear combination of Rayleigh and isotropic scattering, with arbitrary albedo  $a$ , combines the preceding cases. Its phase matrix (Bond and Siewert, 1971) has the form

$$\mathbf{S} = ac\mathbf{R} + a(1 - c)\mathbf{O}$$

where  $\mathbf{R}$  is the phase matrix for pure Rayleigh scattering and  $\mathbf{O}$  that for unpolarized isotropic scattering.

(e) Computing the net scattering matrix resulting from randomly oriented particles with an arbitrary polarizability tensor is a classical problem (Chandrasekhar, 1950; van de Hulst, 1957; Gnedin *et al.* 1973; Hansen and Travis, 1974). The normalized scattering matrix is

$$\mathbf{F} = \frac{1 - \delta}{1 + \frac{1}{2}\delta} \begin{pmatrix} \text{scattering matrix} \\ \text{of pure} \\ \text{Rayleigh} \\ \text{scattering} \end{pmatrix} + \frac{\frac{3}{2}\delta}{1 + \frac{1}{2}\delta} \begin{pmatrix} 1 & 0 & 0 & 0 \\ 0 & 0 & 0 & 0 \\ 0 & 0 & 0 & 0 \\ 0 & 0 & 0 & -\cos \alpha \end{pmatrix}$$

where  $\delta$  is the traditional depolarization factor, which is the  $I_l/I_r$  ratio<sup>†</sup> of light scattered under  $90^\circ$  if the incident light is unpolarized. The first matrix is spelled out in Section 16.1.2. The second matrix may be equated to isotropic, unpolarized scattering in any problem where the element  $F_{44}$ , referring to circular polarization, does not enter. The extreme value  $\delta = 0.5$ , corresponding to particles that can be polarized along one axis, thus gives rise to a mixture of 40% pure Rayleigh scattering and 60% isotropic scattering.

### 16.1.2 Choice of the Set of Parameters to Describe Intensity and Polarization

It has been customary, for historical reasons, to treat Rayleigh scattering with the set of parameters  $\mathbf{I}_\Delta = (I_l, I_r, U, V)$  rather than with the Stokes parameters  $\mathbf{I} = (I, Q, U, V)$ , which we generally prefer to use. The symbol  $\Delta$  is a warning sign that this is *not* the set to which the formulations of Chapter 15 are directly applicable. The transformations  $I = I_l + I_r$  and  $Q = I_l - I_r$  are simple, and any result expressed in one set can be translated into the same result expressed in the other set by

$$\mathbf{I} = \mathbf{A}\mathbf{I}_\Delta, \quad \mathbf{I}_\Delta = \mathbf{A}^{-1}\mathbf{I}$$

with

$$\mathbf{A} = \begin{pmatrix} 1 & 1 & 0 & 0 \\ 1 & -1 & 0 & 0 \\ 0 & 0 & 1 & 0 \\ 0 & 0 & 0 & 1 \end{pmatrix}, \quad \mathbf{A}^{-1} = \begin{pmatrix} \frac{1}{2} & \frac{1}{2} & 0 & 0 \\ \frac{1}{2} & -\frac{1}{2} & 0 & 0 \\ 0 & 0 & 1 & 0 \\ 0 & 0 & 0 & 1 \end{pmatrix}$$

A matrix multiplication  $\mathbf{K} = \mathbf{Z}\mathbf{I}$  is equivalent to  $\mathbf{K}_\Delta = \mathbf{Z}_\Delta\mathbf{I}_\Delta$  if the vectors  $\mathbf{K}$  and  $\mathbf{I}$  are transformed as above and if the matrix is transformed as

$$\mathbf{Z} = \mathbf{A}\mathbf{Z}_\Delta\mathbf{A}^{-1}, \quad \mathbf{Z}_\Delta = \mathbf{A}^{-1}\mathbf{Z}\mathbf{A}$$

It often happens that for symmetry regions we can disregard the third and fourth Stokes parameters and work with two-vectors and  $2 \times 2$  matrices. We note that in that case  $\mathbf{A}^{-1} = \frac{1}{2}\mathbf{A}$ .

Yet another representation, in which the rotation matrices (Section 15.1.4) assume a simple form, is the CP representation (Kuščer and Ribarič, 1959).

$$\begin{pmatrix} I_2 \\ I_0 \\ I_{-0} \\ I_{-2} \end{pmatrix} = \begin{pmatrix} \frac{1}{2}(Q - iU) \\ \frac{1}{2}(I - V) \\ \frac{1}{2}(I + V) \\ \frac{1}{2}(Q + iU) \end{pmatrix} = \frac{1}{2} \begin{pmatrix} 0 & 1 & -i & 0 \\ 1 & 0 & 0 & -1 \\ 1 & 0 & 0 & 1 \\ 0 & 1 & i & 0 \end{pmatrix} \begin{pmatrix} I \\ Q \\ U \\ V \end{pmatrix}$$

but we shall not use this set.

<sup>†</sup> The subscripts l and r were adopted by Chandrasekhar and used by many others to stand for the last letters of parallel and perpendicular, respectively.



It is, of course, also possible to include frequency dependence and to go all the way back to the Born-Wolf coherency matrix (e.g., Sekera, 1966c; Abhyankar and Fymat, 1969). This does not simplify matters.

The scattering matrix (with the scattering plane as the plane of reference; cf. Section 15.1.2) is

$$\mathbf{F} = \frac{3}{4} \begin{pmatrix} 1 + \cos^2 \alpha & 1 - \cos^2 \alpha & 0 & 0 \\ 1 - \cos^2 \alpha & 1 + \cos^2 \alpha & 0 & 0 \\ 0 & 0 & 2 \cos \alpha & 0 \\ 0 & 0 & 0 & 2 \cos \alpha \end{pmatrix}$$

The azimuth-independent part of the Rayleigh-scattering phase matrix in the two most common representations is

$$\mathbf{Z}_{\Delta}^0(u, u') = \frac{3}{4} \begin{pmatrix} u^2 u'^2 + 2(1 - u^2)(1 - u'^2) & u^2 & 0 & 0 \\ & u'^2 & 1 & 0 & 0 \\ & 0 & 0 & 0 & 0 \\ & 0 & 0 & 0 & 2uu' \end{pmatrix}$$

$$\mathbf{Z}^0(u, u') = \frac{3}{8} \begin{pmatrix} 3 - u^2 - u'^2 + 3u^2 u'^2 & (1 - 3u^2)(1 - u'^2) & 0 & 0 \\ (1 - u^2)(1 - 3u'^2) & 3(1 - u^2)(1 - u'^2) & 0 & 0 \\ 0 & 0 & 0 & 0 \\ 0 & 0 & 0 & 4uu' \end{pmatrix}$$

### 16.1.3 Factorization

We now disregard the third and fourth Stokes parameters and denote the remaining  $2 \times 2$  matrices by the same symbols as before. Burniston and Siewert (1970) remark that for an arbitrary mixture of isotropic and Rayleigh scattering, as described in Section 16.1.1(d), it is possible to write the  $2 \times 2$  phase matrix as

$$\mathbf{Z}_{\Delta}^0(u, u') = a \mathbf{Q}_{\Delta}(u) \mathbf{Q}_{\Delta}^T(u')$$

where T denotes the transposed matrix and

$$\mathbf{Q}_{\Delta}(u) = \frac{3}{2(c+2)^{1/2}} \begin{pmatrix} cu^2 + \frac{2}{3}(1-c) & (2c)^{1/2}(1-u^2) \\ \frac{1}{3}(c+2) & 0 \end{pmatrix}$$

This decomposition has advantages in solving Rayleigh scattering problems by means of the eigenvalue method. The linearity of  $\mathbf{Z}_{\Delta}$  in  $c$ , though not evident, is still there.

The rules in the preceding subsection define uniquely the corresponding factorization in the  $(IQUV)$  system, namely

$$\mathbf{Z}(u, u') = a\mathbf{Q}(u)\mathbf{Q}^T(u')$$

with

$$\mathbf{Q}(u) = \frac{1}{2}\mathbf{A}\mathbf{Q}_\Delta(u)\mathbf{A}$$

We shall write the limiting cases in both systems. For isotropic scattering ( $c = 0$ ), we have

$$\mathbf{Q}(u) = \frac{1}{\sqrt{2}} \begin{pmatrix} 1 & 1 \\ 0 & 0 \end{pmatrix}, \quad \mathbf{Q}_\Delta(u) = \frac{1}{\sqrt{2}} \begin{pmatrix} 1 & 0 \\ 1 & 0 \end{pmatrix}$$

For Rayleigh scattering ( $c = 1$ ) we obtain

$$\mathbf{Q}(u) = \frac{\sqrt{3}}{4} \begin{pmatrix} s + v\sqrt{2} & s - v\sqrt{2} \\ (-1 + \sqrt{2})v & (-1 - \sqrt{2})v \end{pmatrix}, \quad \mathbf{Q}_\Delta(u) = \frac{\sqrt{3}}{2} \begin{pmatrix} u^2 & v\sqrt{2} \\ 1 & 0 \end{pmatrix}$$

where  $s = 1 + u^2$ ,  $v = 1 - u^2$ .

This particular factorization for Rayleigh scattering has been introduced by Sekera (1963), but it is not the only possible one. The following lemma (which we have not found stated in the literature) may be easily proven:

If a phase matrix can be factorized as

$$\mathbf{Z}(u, u') = \mathbf{Q}(u)\mathbf{Q}^T(u')$$

then it can also be factorized as

$$\mathbf{Z}(u, u') = \mathbf{Q}^*(u)\mathbf{Q}^{*T}(u')$$

where

$$\mathbf{Q}^*(u) = \mathbf{Q}(u)\mathbf{F}$$

and  $\mathbf{F}$  is any matrix, independent of  $u$  and  $u'$ , satisfying

$$\mathbf{F}\mathbf{F}^T = \mathbf{1} \quad (\text{unit matrix})$$

Eligible choices for the matrix  $\mathbf{F}$  are, for instance,

$$\mathbf{F} = \begin{pmatrix} 1 & 0 \\ 0 & -1 \end{pmatrix}, \quad \begin{pmatrix} 0 & 1 \\ 1 & 0 \end{pmatrix}, \quad \begin{pmatrix} 0 & -1 \\ 1 & 0 \end{pmatrix}, \quad \text{or} \quad \frac{1}{\sqrt{2}} \begin{pmatrix} 1 & -1 \\ 1 & 1 \end{pmatrix}$$

A different factorization for Rayleigh scattering, which is recommended by Sekera (1966a) for use with the  $(IQUV)$  representation, has

$$\mathbf{Q}(u) = \frac{\sqrt{3}}{2} \begin{pmatrix} v & s/\sqrt{2} \\ v & -v/\sqrt{2} \end{pmatrix}$$

It is easily verified that this form reduces to the previous one upon applying the last form of  $\mathbf{F}$  given above.

These examples should suffice. Please note that a certain amount of confusion may arise from the original Sekera (1966a) memorandum for two reasons:

- (1) He did not state the unique method by which a factorization in one system of representing polarization may be translated into a factorization in another system, but instead made ad hoc factorizations in a number of different systems.
- (2) He noted the nonuniqueness but did not state the method of constructing new factorizations by means of a matrix  $F$ .

## 16.2 EXACT SOLUTIONS

About 1940, the diffuse reflection and transmission by a Rayleigh scattering atmosphere of arbitrary thickness still formed a big unsolved problem. It was solved completely by Chandrasekhar. Others followed, either providing further numerical detail, or presenting alternative derivations. Still others made generalizations to related scattering laws.

We shall not attempt a complete review of these solutions. The basic principles have been explained in Chapters 4 and 15. Our aim, as in the earlier chapters of this book, is to present a selection of results with emphasis on the numerical data. These examples may help (a) to find a quick way into the literature, and (b) to obtain a physical understanding of some apparently strange results. We begin with a bibliography of exact solutions.

### 16.2.1 Derivations

Chandrasekhar (1950) derives for conservative Rayleigh scattering the intensity and polarization of the light reflected from or emitted by a semi-infinite atmosphere and the same quantities for reflection and transmission by a finite layer. The same topic simplified by a factorization procedure is treated by Sekera (1966b). Mullikin (1966) derives from scratch the complete internal and external radiation field including asymptotic formulas for large  $b$ . The same end is reached by a solution based on singular eigenfunction expansion by Shieh and Siewert (1969). A clear review explaining the main methods of solution to that date is in Mullikin (1969).

Since then, Adams and Kattawar (1970) have used the invariant embedding approach and Plass *et al.* (1973a) have worked out the solution by the matrix operator theory. Domke (1971a,b), by a method based on Sobolev's work, first solved the reflection and escape problem for semi-infinite atmosphere and then treated reflection and transmission by a finite Rayleigh scattering atmosphere. Both papers also give the solution for an arbitrary distribution of primary sources.

The many derivations dealing with the Rayleigh phase function [unpolarized, Section 16.1.1(a)] will not be reviewed separately because they form a simple application of the theory for general phase functions (Chapter 6).

Formulas for radiative transfer based on nonconservative Rayleigh scattering [Section 16.1.1(b)] were derived by Sekera (1963), Abhyankar and Fymat (1970), and Schnatz and Siewert (1970, 1971).

Transfer with a mixture of isotropic and Rayleigh scattering was treated by Lenoble (1970), Burniston and Siewert (1970), and Bond and Siewert (1971), all for the semi-infinite atmosphere. A faster way of computing the  $H$  matrices was given by Kriese and Siewert (1971).

### 16.2.2 Tables

The amount of effort spent in producing numerical tables relating to radiative transfer by Rayleigh scattering and its variations has been enormous. For reference, brief characteristics of the tables that have come to our attention are listed, but chances are that the list is not complete.

#### RAYLEIGH SCATTERING, $H$ FUNCTIONS

The  $H$  functions and 4 derived functions for conservative Rayleigh scattering,  $b = \infty$ , are in Chandrasekhar and Breen (1947) and in Chandrasekhar's book (1950). The corresponding functions for finite layers with  $b = 0.05$  (0.05) 0.25, 0.50, 1 are in Chandrasekhar and Elbert (1954), and for  $b = 0.15, 0.25, 0.5, 0.7, 1, 2, 4, 8, 16, 100$  in Sekera and Kahle (1966), repeated in Kahle (1977).

The  $H$  functions for Rayleigh scattering with absorption,  $b = \infty$ , are given by Lenoble (1970) for  $\mu = 0$  (0.05) 1 and  $a = 0.2, 0.4, 0.6, 0.7, 0.8, 0.9, 0.925, 0.95$  (0.01) 0.99, and by Abhyankar and Fymat (1971) for  $\mu = 0$  (0.01) 1 and  $a = 0$  (0.1) 0.6 (0.05) 0.8 (0.025) 0.9 (0.01) 0.98 (0.005) 0.995 (0.001) 0.999. These last tables include also four  $N$  functions and the zero-order moments with respect to  $\mu$ .

#### RAYLEIGH SCATTERING, REFLECTION, AND TRANSMISSION

Intensities, polarization, and phase angle of the light reflected from finite layers ( $b = 0.02, 0.05, 0.10, 0.15, 0.25, 0.50, 1$ ) are given in about 500 pages of tables by Coulson *et al.* (1960). The errors in these tables stay below 2 units in the fourth digit. Illustrations based on these tables have been discussed by Sekera (1957) and Coulson (1959a). Corresponding pictures of the radiation reflected from a spherical planet (Sekera and Viezee, 1971) are discussed in Section 16.3.3.

The work that was meant to complement these tables toward thicker layers up to  $b = 10$  (Dave and Walker, 1966, with added graphs and a table in Dave and Farukawa, 1966) was later shown to be unreliable for  $b = 10$ , with errors

greater than 10% in the transmitted flux. Many graphs showing reflection and transmission for the  $b$  values from 0.15 to 100 are given by Kahle (1968a). The reflected and transmitted flux (integrals with our operator  $U$ ) are presented separately (Kahle, 1968b). A comprehensive account appeared much later (Kahle, 1977). The transmission function for perpendicular incidence and ten values of  $b$  is given graphically by Kattawar *et al.* (1976), unfortunately on too small a scale.

Chandrasekhar's formulas and  $H$  functions must have been used many times to compute the reflected intensity and polarization for  $b = \infty$ , but the published literature shows a gap here, except for an occasional small-scale graph. The numerical results given in Section 16.3.3 are intended to fill this gap somewhat.

### RAYLEIGH SCATTERING, MILNE PROBLEM

Numerical results relevant to the escape problem (Milne problem) for conservative and nonconservative Rayleigh scattering are referred to in Section 16.3.2.

### MIXED RAYLEIGH SCATTERING AND ISOTROPIC SCATTERING

We refer to the phase matrix as written in Section 16.1.1(d). Four  $H$  functions for the conservative case ( $a = 1$ ) with degrees of polarization, extrapolated end points, and reflected flux values are given by Bond and Siewert (1971) for  $c = 0.4$  (0.2) 1 and  $\mu = 0$  (0.1) 1.

### RAYLEIGH PHASE FUNCTION

In radiative transfer by the Rayleigh phase function, polarization is absent, and the examples given in Section 14.2.1 show that the intensity differences with actual Rayleigh scattering are considerable. In fact, isotropic scattering is not much worse as an approximation. For that reason, the effort spent on tables based on the Rayleigh phase function is grossly overdone. The  $H$  functions for the conservative case ( $a = 1$ ) are in Chandrasekhar (1950). The  $H$  functions for  $a = 0.2, 0.4, 0.6, 0.7, 0.8, 0.9, 0.925, 0.95$  (0.01) 1, and the coefficients for the Busbridge polynomials are given by Lenoble (1970). For finite and infinite layers,  $X$  and  $Y$  functions and 4 related functions with the arguments  $b = 0.2$  (0.2) 1 (0.5) 3, 4, 5, 10, 20,  $\infty$ , and  $a = 0.3, 0.5, 0.7, 0.8, 0.9, 0.95, 0.98, 0.99, 0.995, 0.999, 1$  are given by Sweigart (1970).

The values of  $aK(a, \mu)$  where  $K(a, \mu)$  is the escape function (solution of Milne problem) for the Rayleigh phase function are given in Table 2 of Dlugach and Yanovitskii (1974) for  $a = 0.7, 0.8, 0.9, 0.95, 0.98, 0.99, 0.995, 0.999, 1$ .

Much graphical material and a few tables are given by Plass *et al.* (1973a) for reflected and transmitted intensities and by Plass *et al.* (1973b) for the interior radiation field. Both papers deal with the Rayleigh phase function, although the title says Rayleigh scattering. The table in Plass *et al.* (1973a) gives  $\pi^{-1}R(1, \mu_0)$ ,

in agreement with Fig. 14.1. The same confusion of terminology occurs in Canosa and Penafiel (1973), who used the Rayleigh phase function and tabulate the “net flux,” which in our notation reads  $\mu_0 \pi UT(\mu_0)$ , for  $b = 1$  and 16, both with  $a = 1$ .

16.3 SOME RESULTS FOR A SEMI-INFINITE ATMOSPHERE

The literature on Rayleigh scattering shows the expected pattern: problems dealing with a semi-infinite atmosphere have been treated more elaborately than problems with finite layers, for the simple reason that there is one parameter less ( $b = \infty$ ). We shall review the two classical problems, the Milne problem (escape function) and the diffuse reflection problem, in Sections 16.3.2–4. They are preceded by a brief review of the functions needed in the exact solutions and followed by some numerical examples for nonconservative Rayleigh scattering (Section 16.3.5).

16.3.1 Characteristic Functions and *H* Functions

Conservative Rayleigh scattering ( $a = 1$ ) in a semi-infinite atmosphere ( $b = \infty$ ) leads to five *H* functions, each defined in terms of its own characteristic function  $\Psi(\mu)$  by the familiar nonlinear equation

$$H(\mu) = 1 + \mu H(\mu) \int_0^1 \frac{\Psi(x)H(x) \, dx}{\mu + x}$$

Table 52 shows some data pertaining to these five functions. We refer to them by the Mullikin index. The first two (5, 4) suffice to express the intensity and linear polarization of the azimuth-independent term. The next two (1, 2) refer to the Fourier terms in azimuth with  $m = 1$  and 2. The last one (3) refers to circular polarization, Stokes parameter *V*, which is fully separable from the

TABLE 52  
Characteristic Functions and *H* Functions for Conservative Rayleigh Scattering

Notation (Chandrasekhar)	Index (Mullikin)	Characteristic function $\Psi(\mu)$	$\Psi$ -norm	<i>H</i> function		Moment $\alpha_0$	Discrete <i>k</i> value
				<i>H</i> (1)	<i>H</i> ( $\frac{1}{2}$ )		
$H_1$	5	$\frac{3}{8}(1 - \mu^2)$	1	3.4695	2.3146	2.2977	0
$H_r$	4	$\frac{3}{8}(1 - \mu^2)$	0.5	1.2780	1.2167	1.1974	none
$H^{(1)}$	1	$\frac{3}{8}(1 - \mu^2)(1 + 2\mu^2)$	0.7	1.4659	1.3373	1.3093	0.9148
$H^{(2)}$	2	$\frac{3}{16}(1 + \mu^2)^2$	0.7	1.3963	1.2702	1.2497	0.7410
$H_v$	3	$\frac{3}{4}\mu^2$	0.3	1.2036	1.1365	1.1258 <sup>a</sup>	0.8528

<sup>a</sup> Found by new integration.

rest. The “ $\Psi$ -norm” is defined as  $\int_0^1 2\Psi(\mu) d\mu$  and may in a very loose sense be regarded as another effective albedo, because this norm must be  $\leq 1$ .

The values of  $H(\mu)$  are given for  $\mu = 1$  and  $\mu = \frac{1}{2}$  in order to help locate them in the literature (cited in Section 16.2). They are indeed larger for larger  $\Psi$ -norm, and so is the zero-order moment  $\alpha_0 = \int_0^1 H(\mu) d\mu$ . For all five,  $H(0) = 1$ .

All discrete solutions  $k$  of the characteristic equation

$$\int_0^1 \frac{2\Psi(\mu) d\mu}{1 - k^2\mu^2} = 1$$

(Mullikin, 1966; Domke, 1971a) are given in the last column. They play an essential role in the exact solution by Mullikin’s method and can probably all be interpreted in terms of a diffusion solution in an unbounded medium. The magnitude of the discrete  $k$  value does not have an apparent relation to the  $\Psi$ -norm except that  $k = 0$  if  $\Psi$ -norm = 1.

One consequence of these numbers should be pointed out because it helps us to visualize the situation deep inside a thick atmosphere. The azimuth-dependent parts and the elliptical polarization are damped out almost as rapidly as the direct intensity of a light ray penetrating the atmosphere, because their  $k$  values are close to 1. The only solution persisting at large depth then is the almost trivial diffusion solution in which the intensity is unpolarized, independent of azimuth, linear in optical depth, and linear in  $\cos \theta = u$ . This solution was written out for arbitrary laws without polarization in Section 6.2.1 and was proven to exist also for an arbitrary scattering law with polarization in Section 15.2.3.

### 16.3.2 The Milne Problem; Escape Function

The problem of escape of a constant net flux from a Rayleigh-scattering atmosphere has been solved by Chandrasekhar, and our only task is to copy the result in a form consistent with the general theory of Chapter 5 and Section 15.2.1, because this form of writing at once gives access to a number of further cross checks and relations.

We use Mullikin’s upper indices 1–5 (see Table 52) and Chandrasekhar’s notation  $q$  and  $c$ . The escape function, which is a two-vector, is, in the  $I_1 I_r$  notation:

$$\mathbf{K}_{\Delta}(\mu) = \begin{pmatrix} K_1(\mu) \\ K_r(\mu) \end{pmatrix} = \begin{pmatrix} (3/8\sqrt{2})qH^{(5)}(\mu) \\ (3/8\sqrt{2})(\mu + c)H^{(4)}(\mu) \end{pmatrix}$$

i.e., in the  $IQ$  notation:

$$\mathbf{K}(\mu) = \begin{pmatrix} K(\mu) \\ -pK(\mu) \end{pmatrix} = \begin{pmatrix} (3/8\sqrt{2})[qH^{(5)}(\mu) + (\mu + c)H^{(4)}(\mu)] \\ (3/8\sqrt{2})[qH^{(5)}(\mu) - (\mu + c)H^{(4)}(\mu)] \end{pmatrix}$$

where  $q = 0.68989$ ,  $c = 0.87294$ . These and some other parameters are given in 9 decimals by Bond and Siewert (1967).

TABLE 53  
Solution of Escape Problem for Rayleigh  
Scattering<sup>a</sup>

$\mu$	$K_i(\mu)$	$K_r(\mu)$	$K(\mu)$	$p$
0	0.18294	0.23147	0.41441	0.1171
0.1	0.24247	0.28150	0.52397	0.0745
0.2	0.29057	0.32381	0.61439	0.0541
0.3	0.33599	0.36429	0.70029	0.0404
0.4	0.38010	0.40388	0.78398	0.0303
0.5	0.42343	0.44294	0.86637	0.0225
0.6	0.46624	0.48165	0.94789	0.0163
0.7	0.50869	0.52013	1.02882	0.0111
0.8	0.55087	0.55844	1.10931	0.0068
0.9	0.59286	0.59661	1.18947	0.0032
1.0	0.63469	0.63469	1.26938	0

<sup>a</sup>  $KN = 0.86118$ ,  $KU = 1.00000$ , and  $KW = q_\infty = 0.71215$  is the extrapolation length.

Table 53 gives an excerpt from a longer table given in Chandrasekhar's book (his Table 24) together with some derived constants. The values of  $KU = 1$  and of  $KN = 3(q\alpha_0 + cA_0 + A_1)/8\sqrt{2}$  follow from the numbers given in Chandrasekhar's Table 23.

Note that in any oblique direction the escaping radiation is polarized perpendicularly to the normal plane ( $I_r > I_1$ ,  $p > 0$ ). The maximum polarization, reached at grazing escape, is 11.7%.

The theory just cited gives the external radiation field, including the extrapolation length  $q_\infty$ . It is possible to describe the internal radiation field in close analogy to the solution for isotropic scattering by two Hopf functions  $q_1(\tau)$  and  $q_2(\tau)$ . Both functions reach the value  $q_\infty$  for  $\tau \rightarrow \infty$  and are calculated by Domke (1971a).

16.3.3 Diffuse Reflection

The reflection matrix derived by Chandrasekhar is given in Display 16.1. The triangles ( $\blacktriangle$ ) serve as a reminder that the matrix is in the  $(I_1, I_r, U, V)$  notation and that the transformations of Section 16.1.2 are necessary to get it into the  $(I, Q, U, V)$  form. No further simplification is generally possible. The appearance of sine and cosine in the azimuth-dependent terms is as predicted in Section 15.1.5.

16.3.4 Diffuse Reflection in the Principal Plane

The number of independent variables in Display 16.1 is 3, i.e.,  $\mu$ ,  $\mu_0$ , and  $\varphi - \varphi_0$ . In order to narrow it down still further, let us consider the situation



## DISPLAY 16.1

Diffuse Reflection against a Rayleigh-Scattering Semi-Infinite Atmosphere

$$R_{\Delta}(\mu, \mu_0, \varphi, \varphi_0) = \begin{vmatrix} \boxed{\begin{matrix} R_{11} & R_{12} \\ R_{21} & R_{22} \end{matrix}} & \boxed{\begin{matrix} R_{13} \\ R_{23} \end{matrix}} & 0 \\ \boxed{\begin{matrix} R_{31} & R_{32} \end{matrix}} & \boxed{R_{33}} & 0 \\ 0 & 0 & 0 & \boxed{R_{44}} \end{vmatrix}$$

with

$$\begin{aligned} \boxed{\begin{matrix} R_{11} & R_{12} \\ R_{21} & R_{22} \end{matrix}}_{\Delta} &= \frac{3}{16(\mu + \mu_0)} \left[ \begin{pmatrix} 2[1 - c(\mu + \mu_0) + \mu\mu_0]H^{(5)}(\mu)H^{(5)}(\mu_0) & q(\mu + \mu_0)H^{(5)}(\mu)H^{(4)}(\mu_0) \\ q(\mu + \mu_0)H^{(4)}(\mu)H^{(5)}(\mu_0) & [1 + c(\mu + \mu_0) + \mu\mu_0]H^{(4)}(\mu)H^{(4)}(\mu_0) \end{pmatrix} \right. \\ &+ \begin{pmatrix} -4\mu\mu_0 & 0 \\ 0 & 0 \end{pmatrix} (1 - \mu^2)^{1/2} (1 - \mu_0^2)^{1/2} H^{(1)}(\mu)H^{(1)}(\mu_0) \cos(\varphi - \varphi_0) \\ &\left. + \begin{pmatrix} \mu^2\mu_0^2 & -\mu^2 \\ -\mu_0^2 & 1 \end{pmatrix} H^{(2)}(\mu)H^{(2)}(\mu_0) \cos 2(\varphi - \varphi_0) \right] \end{aligned}$$

$$\begin{aligned} \boxed{\begin{matrix} R_{13} \\ R_{23} \end{matrix}}_{\Delta} &= \frac{3}{16(\mu + \mu_0)} \left[ \begin{pmatrix} -2\mu \\ 0 \end{pmatrix} (1 - \mu^2)^{1/2} (1 - \mu_0^2)^{1/2} H^{(1)}(\mu)H^{(1)}(\mu_0) \sin(\varphi - \varphi_0) \right. \\ &\left. + \begin{pmatrix} \mu^2\mu_0 \\ -\mu_0 \end{pmatrix} H^{(2)}(\mu)H^{(2)}(\mu_0) \sin 2(\varphi - \varphi_0) \right] \end{aligned}$$

$\boxed{\begin{matrix} R_{31} & R_{32} \end{matrix}}_{\Delta}$  is the same, transposed, and with  $\mu$  and  $\mu_0$  interchanged.

$$\boxed{R_{33}} = [3/16(\mu + \mu_0)] [(1 - \mu^2)^{1/2} (1 - \mu_0^2)^{1/2} H^{(1)}(\mu)H^{(1)}(\mu_0) \cos(\varphi - \varphi_0) - \mu\mu_0 H^{(2)}(\mu)H^{(2)}(\mu_0) \cos 2(\varphi - \varphi_0)]$$

$$\boxed{R_{44}} = [3/8(\mu + \mu_0)] [-\mu\mu_0 H^{(3)}(\mu)H^{(3)}(\mu_0) + (1 - \mu^2)^{1/2} (1 - \mu_0^2)^{1/2} H^{(4)}(\mu)H^{(4)}(\mu_0) \cos(\varphi - \varphi_0)]$$

in the principal plane, defined by  $\varphi - \varphi_0 = 0$  or  $180^\circ$ . In this situation exclusively, it is useful to keep  $\theta_0 > 0$  and to measure the angle of emergence from  $-90^\circ$  (grazing) through  $0^\circ$  (normal) to  $+90^\circ$  (grazing). We call  $\theta$  positive for  $\varphi - \varphi_0 = 180^\circ$ . Thus light reflected straight back into the direction from where it came (opposition) has positive  $\theta$ . We further write

$$\begin{aligned} \mu_0 &= \cos \theta_0 & \mu &= \cos \theta \\ \sigma_0 &= \sin \theta_0 & \sigma &= \sin \theta \\ \text{scattering angle:} & & \alpha &= \pi - |\theta - \theta_0| \end{aligned}$$

Furthermore we shall now assume that the incident light is unpolarized, which makes the Stokes parameters of the diffusely reflected light in the principal plane equal to

$$\begin{pmatrix} R_1 + R_r \\ R_1 - R_r \\ 0 \\ 0 \end{pmatrix}$$

with

$$R_1(\theta, \theta_0) = [3/32(\mu + \mu_0)]\{2[1 + \mu\mu_0 - c(\mu + \mu_0)]H^{(5)}(\mu)H^{(5)}(\mu_0) + q(\mu + \mu_0)H^{(5)}(\mu)H^{(4)}(\mu_0) + 4\mu\mu_0\sigma\sigma_0H^{(1)}(\mu)H^{(1)}(\mu_0) - \mu^2\sigma_0^2H^{(2)}(\mu)H^{(2)}(\mu_0)\}$$

$$R_r(\theta, \theta_0) = [3/32(\mu + \mu_0)]\{[1 + \mu\mu_0 + c(\mu + \mu_0)]H^{(4)}(\mu)H^{(4)}(\mu_0) + q(\mu + \mu_0)H^{(4)}(\mu)H^{(5)}(\mu_0) + \sigma_0^2H^{(2)}(\mu)H^{(2)}(\mu_0)\}$$

As a first numerical illustration we show in Table 54 the results for opposition ( $\theta = \theta_0$ ). This table serves three purposes.

(a) It has direct astronomical significance, for the tabulated function is  $\mu R(\mu, \mu, 180^\circ)$ , which is the (local) brightness of a planet covered with a thick Rayleigh atmosphere, seen at opposition. The planet Neptune approximately fits this description. The brightness is normalized to the brightness 1 that would be displayed by a white Lambert surface seen face-on at the same position. At the center of the disk, this brightness is exceeded by 15%. The projected distance from the center of the disk is  $\sigma \times$  radius of disk.

(b) For comparison the table shows the results that would be obtained for two different scattering laws: isotropic scattering I and Rayleigh phase function P. Compare Table 43 in Section 14.2.1.

(c) The table also shows the separate Fourier terms which make up these results. This may serve as a check, but hardly aids our understanding. Already for single scattering, Fourier analysis in azimuth performed on the reflection function for oblique incidence is not easily visualized.

For further illustration, Fig. 16.2 shows the degree of polarization of light diffusely reflected in the principal plane. It is simply based on inserting numbers into the equations for  $R_1$  and  $R_r$  presented above. A number of interesting features may be seen in this figure and the companion Figs. 16.4–16.6.

1. The angle under which the light emerges (viewing angle  $\theta$ ) covers the angles  $-90^\circ$ – $+90^\circ$ . By an obvious generalization of the definitions we could also make  $\theta_0$  go from  $-90$  to  $+90^\circ$ . The polarization then does not change if the sign of both  $\theta$  and  $\theta_0$  is inverted, so the contour map is symmetric with respect to the origin (normal incidence and reflection). This made it unnecessary to draw the entire square.

TABLE 54 Brightness of Planet in Opposition<sup>a</sup>

	Isotropic scattering (I)	Rayleigh phase function (P)	Rayleigh scattering (R)				Differences	
			l	r	l - r	l + r	p = (r - l)/(r + l)	(P - I) (R - P)
$\mu = 1$ , perpendicular incidence and reflection, center of disk								
$m = 0$ , Total	1.0569	1.1016	0.5735	0.5735	0.0000	1.1471	0	0.0447 0.0456
$\mu = 0.9$								
$m = 0$	0.9320	0.9515	0.4744	0.4947	-0.0202	0.9691	-	-
$m = 1$	0	0.0307	0.0603	0	0.0603	0.0603	-	-
$m = 2$	0	0.0018	-0.0137	0.0169	-0.0305	0.0032	-	-
Total $\mu R$	0.9320	0.9840	0.5210	0.5116	+0.0096	1.0326	-0.0093	0.0520 0.0486
$\mu = 0.5$								
$m = 0$	0.5064	0.5123	0.2805	0.2384	0.0421	0.5188	-	-
$m = 1$	0	0.0369	0.0629	0	0.0629	0.0629	-	-
$m = 2$	0	0.0282	-0.0142	0.0567	-0.0709	0.0425	-	-
Total $\mu R$	0.5064	0.5775	0.3292	0.2951	+0.0341	0.6242	-0.0546	0.0711 0.0467
$\mu = 0.1$								
$m = 0$	0.1945	0.2150	0.1469	0.0755	0.0715	0.2224	-	-
$m = 1$	0	0.0019	0.0023	0	0.0023	0.0023	-	-
$m = 2$	0	0.0475	-0.0005	0.0548	-0.0553	0.0542	-	-
Total $\mu R$	0.1945	0.2644	0.1487	0.1302	0.0185	0.2789	-0.0665	0.0699 0.0145
$\mu = 0$ , grazing incidence and reflection, limb of disk								
$m = 0$	0.1250	0.1406	0.0938	0.0469	0.0469	0.1406	-	-
$m = 1$	0	0	0	0	0	0	-	-
$m = 2$	0	0.0469	0	0.0469	-0.0469	0.0469	-	-
Total $\mu R$	0.1250	0.1875	0.0938	0.0938	0	0.1875	0	0.0625 0

<sup>a</sup> The tabulated function is  $\mu R(\mu, \mu, 180^\circ)$  for  $a = 1, b = \infty$ .

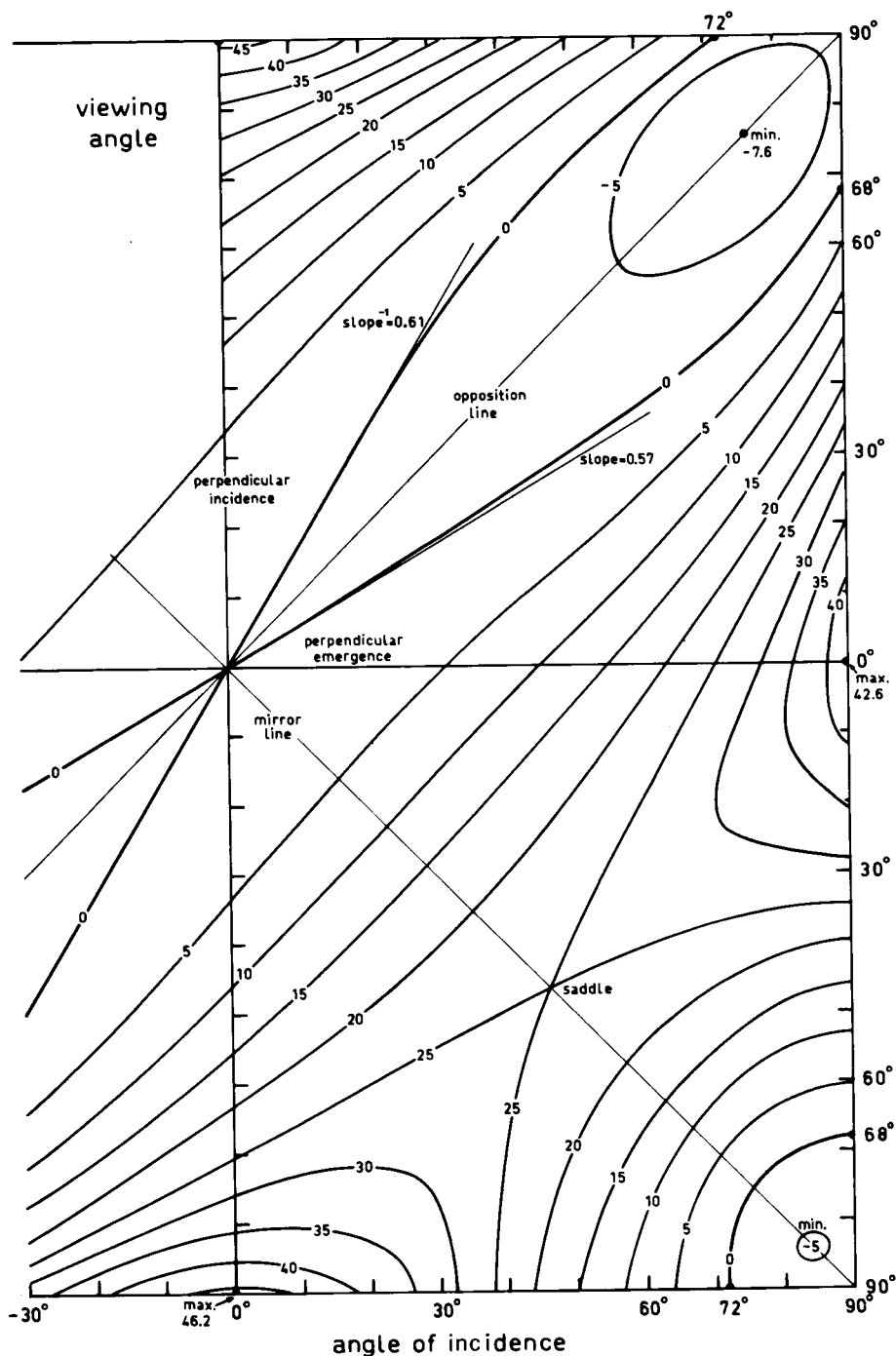


Fig. 16.2. Radiation diffusely reflected from an infinitely deep Rayleigh atmosphere in the principal plane, i.e., in directions of view coplanar with the direction of illumination and the normal to the atmosphere. Numbers with each curve show percentage polarization with a sign as explained in text.

2. If only single scattering were present, the lines of equal polarization would be the straight lines of equal scattering angle. One of these, the line  $\alpha = 180^\circ$ , is drawn and marked "opposition line." It corresponds to zero degree of polarization of the single scattering. The other lines of equal  $\alpha$  are parallel to this diagonal. The line  $\alpha = 90^\circ$  corresponds to 100% polarization of the single scattering. Broadly, zero polarization indeed occurs near the main diagonal,  $\alpha = 180^\circ$ , and again near  $\alpha = 0^\circ$ . A ridge of maximum polarization, 25–46%, occurs along the  $\alpha = 90^\circ$  line. The finer details are due to multiple scattering.

3. Any point on the other diagonal marked "mirror reflection" corresponds to a direction of reflection as would be obtained by specular reflection against a mirror or ocean surface. This diagonal only resembles a line of symmetry, for the figure is not exactly symmetric. The lack of symmetry in the pair of variables  $\mu, \mu_0$  is also seen in the formulas. The reciprocal problem to finding the intensity of a polarized reflected component for incident natural light is finding the total intensity of the reflected light for incident polarized light. This is different from the problem posed here. Hence the reciprocity principle, though still valid, is of no help in this particular problem. Compare Hovenier (1970).

4. Near all corners negative polarization is seen, i.e., in contrast to the situation for single Rayleigh scattering, the  $l$  component parallel to the principal plane dominates. This can be understood as follows. At these points single scattering is almost unpolarized. The two points of successive scattering which give the second-order contribution must both be close to the surface because of the grazing incidence and emergence. Hence the path between these points must be mainly parallel to the surface. The extreme possibilities are either that the path is along the directions of incidence and emergence, in which case the second-order scattering is unpolarized (Fig. 16.3a), or it can go across these directions, in which case the  $l$  component dominates (Fig. 16.3b).

5. Cross sections along the two diagonals of Fig. 16.2 are shown in Fig. 16.4. The opposition curve has direct significance in showing the degree of

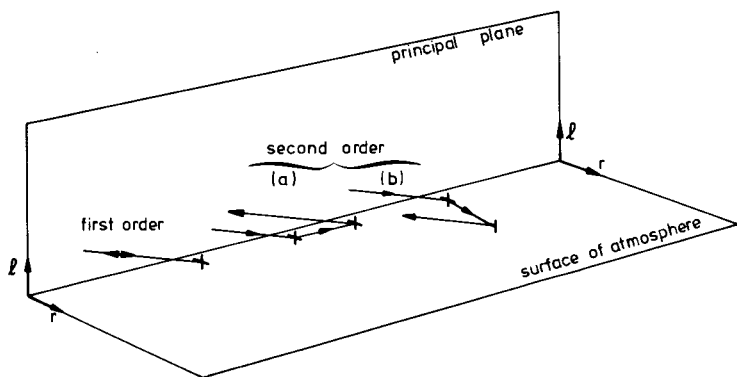


Fig. 16.3. Qualitative explanation of the occurrence of net negative polarization (predominance of the component with electric vector parallel to the principal plane) for near-grazing incidence and reflection.

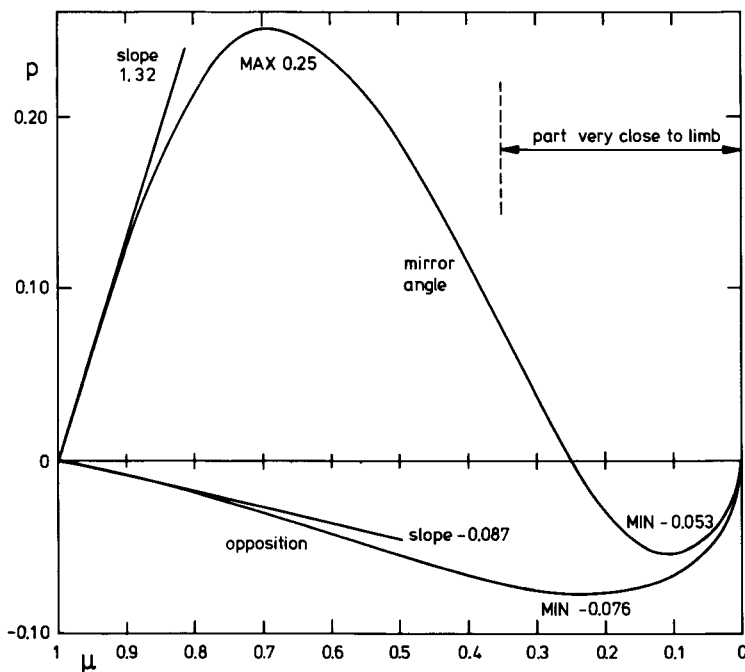


Fig. 16.4. Cross sections through Fig. 16.2 along the two diagonals.

polarization of the light reflected at opposition from any part of the disk of a planet covered with a Rayleigh atmosphere. Note, however, that the projected distance from the center of the disk is  $\sigma$ , not  $\mu$ . The dotted line near  $\mu = 0.35$  corresponds to  $\sigma = 0.94$ ; it is in practice virtually impossible to make reliable measurements as close to the limb as that. Each point on the other diagonal corresponds to the symmetry point of a planetary crescent, which is readily accessible to observation.

6. All 4 sides of a quarter-square of Fig. 16.2 are shown in Fig. 16.5. They do not require further explanation, except that the near symmetry in the variables  $\mu$  and  $\mu_0$  is again striking.

7. In several of these figures, slopes are drawn corresponding to the linear behavior in  $1 - \mu$  and  $1 - \mu_0$  near the point corresponding to perpendicular incidence and reflection. These slopes have been obtained by inserting the linear approximations

$$H^{(5)}(\mu) = 3.4695 - 2.285(1 - \mu)$$

$$H^{(4)}(\mu) = 1.2780 - 0.083(1 - \mu)$$

$$H^{(1)}(\mu) = 1.4659 - 0.187(1 - \mu)$$

$$H^{(2)}(\mu) = 1.3963 - 0.190(1 - \mu)$$

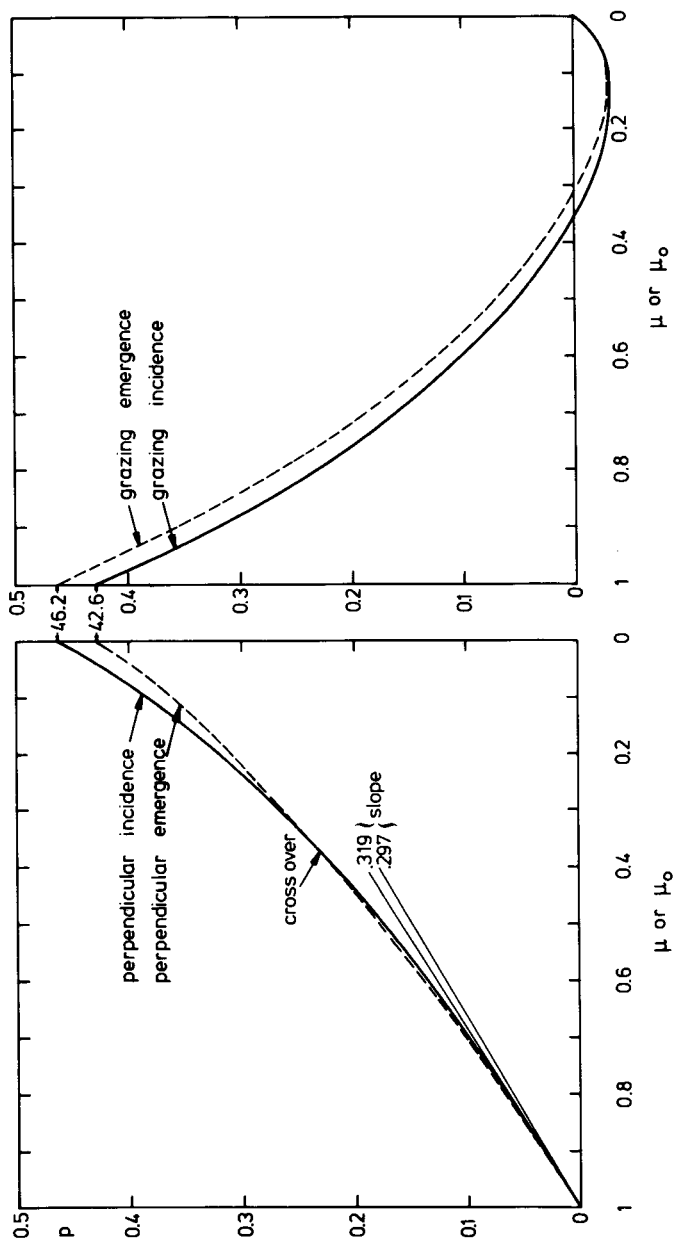


Fig. 16.5. Cross sections through Fig. 16.2 along all 4 sides of a quarter-square. The directions of incidence and emergence can almost, but not quite be interchanged.

into the exact formulas. The tangents to the two zero-polarization curves in the center point of Fig. 16.2 with their slopes 0.57 and  $(0.61)^{-1}$  are very nearly, but not exactly symmetric with respect to the two diagonals.

8. One other saddle point, two minima, and two maxima are shown in Fig. 16.2. The precise location of the saddle point and second minimum may be a little off the mirror diagonal.

9. Cross sections through Fig. 16.2 along a vertical line, i.e., for a fixed angle of incidence, are found in various places in the literature (Chandrasekhar, 1950; van de Hulst, 1949) and in Fig. 16.7 below.

10. A cut through Fig. 16.2 along a line parallel to the opposition line is shown in Fig. 16.6. It corresponds to the distribution of polarization that should be observed along the equator of a planet  $10^\circ$  away from the opposition point. The resemblance to the exact opposition curve in Fig. 16.4 is clearly seen. It is also striking that there is an almost exact symmetry with respect to the mirror

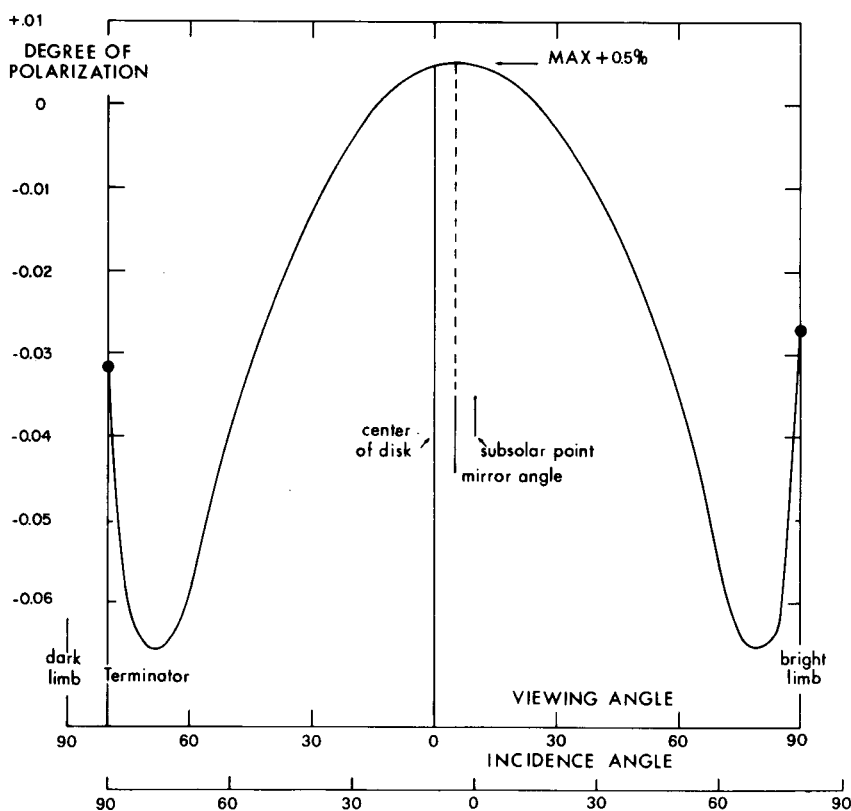


**Fig. 16.6.** This cross section through Fig. 16.2, along a line shifted  $10^\circ$  away from the opposition diagonal, corresponds to a planet seen with a phase angle of  $10^\circ$ . The curve shows the degree of polarization along the great circle of the planet which contains the subearth and subsun points.



angle, although the form of the exact equations would hardly lead us to expect this. Note again that the abscissa is *not* the projected distance from the center of the disk; anything beyond viewing angle  $70^\circ$  will in practice fade into the limb.

### 16.3.5 Nonconservative Rayleigh Scattering

A number of applications, e.g., absorption lines and planetary albedo, make it desirable to have accurate information on the diffuse reflection by semi-infinite atmospheres in which the Rayleigh scattering occurs with an albedo  $a < 1$ . The numerical illustration presented in Fig. 16.7 refers to a semi-infinite atmosphere and is based on the results of Abhyankar and Fymat (1970). It shows intensity and polarization of the light diffusely reflected in the principal plane when light is incident  $60^\circ$  from the normal. Note that in the conservative case ( $a = 1$ )  $R_1 + R_r$  is somewhat over 1 in some directions and a little under 1 in other directions, showing that broadly speaking, the deviation from a white Lambert surface is not enormous. Note also that the polarization curve for  $a = 1$ ,

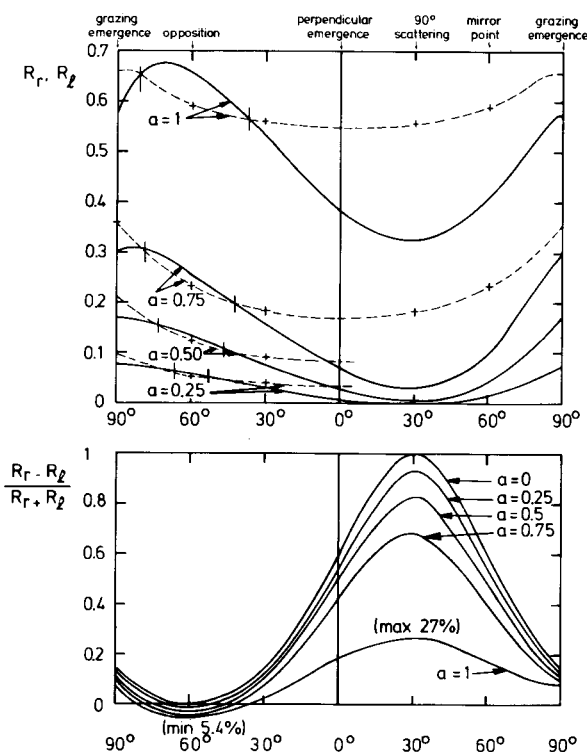


**Fig. 16.7.** Intensity and polarization of light diffusely reflected in the principal plane from a semi-infinite atmosphere with Rayleigh scattering and absorption, illuminated under  $60^\circ$  from the zenith. The albedo for single scattering  $a$  is varied from 0 to 1.

passing through a minimum of  $-5.4\%$  and a maximum of  $+27\%$ , constitutes another cross section of Fig. 16.2. The polarization curve in the limit  $a = 0$  simply shows the polarization by single Rayleigh scattering, which reaches  $100\%$  at a  $90^\circ$  scattering angle.

Small deviations from conservative scattering, such as are responsible for weak spectral lines, require  $a$  values close to 1, e.g., in the range from 0.95 up. Interpolation from the present numerical data would be mostly guesswork, and a quick way to find the behavior near  $a = 1$  from the Abyankhar-Fymat equations is not seen.

Fortunately, here it is possible to use the general theory of Chapter 5, which has been made applicable to scattering with polarization by the translation rules in Display 15.2. The matrix form of Eq. (35) in Section 5.4.1 reads

$$\mathbf{R} = \mathbf{R}_0 - [4k/3(1 - g)]\mathbf{K}_0 \cdot \mathbf{K}_0 + \dots$$

Here the asymmetry factor  $g$  is 0 for Rayleigh scattering, so that from Eq. (30) in the same section we have  $k = t\sqrt{3} + \dots$  with  $t$  defined by  $a = 1 - t^2$  and dots denoting higher powers. Furthermore, we know the escape function  $\mathbf{K}_0$  for  $\mu = 0.5$  or  $\mu_0 = 0.5$  from Section 16.3.2. Upon substitution, we then obtain in the  $(I, Q)$  notation

$$\mathbf{R}(t) = \mathbf{R}(0) - \frac{4}{\sqrt{3}} t \begin{pmatrix} 0.8664 \\ -0.0195 \end{pmatrix} \cdot (0.8664 \quad -0.0195) + \dots$$

For incident natural light this becomes

$$\mathbf{R}(t) \begin{pmatrix} 1 \\ 0 \end{pmatrix} = \mathbf{R}(0) \begin{pmatrix} 1 \\ 0 \end{pmatrix} - t \begin{pmatrix} 1.733 \\ -0.039 \end{pmatrix} + \dots$$

which, in combination with the values for  $a = 1$ ,  $t = 0$  already known gives the starting values and slopes near  $t = 0$  as follows:

$$R_i + R_r = 1.248 - 1.733t$$

$$R_i - R_r = 0.068 - 0.039t$$

$$R_i = 0.658 - 0.886t$$

$$R_r = 0.590 - 0.847t$$

$$p = \frac{(R_r - R_i)}{(R_r + R_i)} = -0.0545 - 0.0443t$$

In Fig. 16.8 the points obtained from Abhyankar's and Fymat's tables have been plotted against  $t$ . For convenience, all reflection values have been divided by  $a$ . This makes a nicer picture but does not affect the slopes at  $t = 0$ . It is clear that these slopes are an essential help in drawing smooth free-hand curves

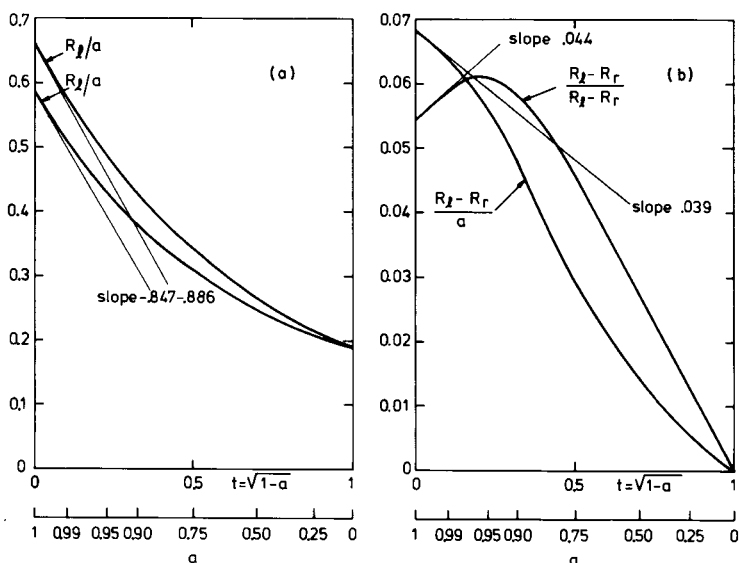


**Fig. 16.8.** Polarization of light reflected into the precise backward direction against a semi-infinite Rayleigh atmosphere viewed and illuminated at  $60^\circ$  with the normal. (a) Reflected intensities in the separate directions of linear polarization plotted against single-scattering albedo  $a$ . (b) Difference of the quantities in (a) and degree of polarization.

through the computed points. The values for any albedo value  $a$  between 0.75 and 1 may be read from these curves with about 1% accuracy.

The degree of polarization has an upward slope; this is found by a straight division of  $R_l - R_r$  by  $R_l + R_r$ . It shows that the impression given by Fig. 16.7 that the polarization of  $-5.4\%$  at opposition goes uniformly to 0 when  $a$  goes from 1 to 0 is wrong. An extreme value of  $-6.1\%$  is reached near  $a = 0.95$ .

The appearance of this maximum was so surprising that the author felt it necessary to gain further insight by an explicit computation of some terms of low order. The expectation was that the polarization of the  $n$ th order would decrease rapidly with increasing  $n$  because the random directions of the  $n - 1$  light paths between the  $n$  positions where scattering occurs will tend to spoil the nice geometry necessary for a strong polarization effect. It now turns out (Table 55) that the strongest (negative) polarization of about  $15\%$  occurs near  $n = 4$ . This corresponds to the maximum *net* polarization near  $a = 0.95$  shown in Fig. 16.8. The last column, to be compared with the column  $R_l + R_r$ , gives the values for isotropic scattering  $\mu = \mu_0 = \frac{1}{2}$  from Table 12.

The origin of the numbers in Table 55 is as follows: first order: exact values, trivial; second order: exact values but by no means trivial. The recommended method is to use the general expressions for the second-order terms, derived for arbitrary phase matrices by Hovenier (1971). For a check the author also made

TABLE 55

Contributions of Terms of Different Order to the Polarization of a Semi-Infinite Rayleigh Atmosphere Seen at Opposition with  $\mu_0 = \frac{1}{2}$

Number of successive scatterings $n$	$R_i$	$R_r$	$R_i - R_r$	$R_i + R_r$	$-p$	$R$ (isotropic)
1	0.188	0.188	0	0.375	0	0.250
2	0.101	0.085	0.016	0.186	0.086	0.137
3	0.064	0.049	0.015	0.113	0.133	0.087
4	(0.04)	(0.03)	(0.01)	(0.07)	(0.14)	—
$\infty$	0	0	0	0	0.022	0
Sum 1-3 for $a = 1$	0.353	0.322	0.031	0.674	0.046	0.474
Sum 4- $\infty$ for $a = 1$	0.305	0.268	0.037	0.566	0.065	0.539
Sum 1- $\infty$ for $a = 1$	0.658	0.590	0.068	1.248	0.054	1.013

a probabilistic computation from scratch. Performing the integration over the two scattering depths  $\tau_1$  and  $\tau_2$ , we arrive at the term for double isotropic scattering

$$R_2(\mu, \mu, 180^\circ) = \frac{1}{8} \int_0^1 \frac{dx}{\mu + x} = \frac{1}{8} \ln(1 + \mu^{-1})$$

Here  $x$  is the direction cosine (taken positive) of the path between the two scattering positions. To make this formula suitable for double Rayleigh scattering, we must put into the integrand the proper factors depending on  $x$  and  $\varphi$  and average over  $\varphi$  before the integration over  $x$  is carried out. The spherical geometry is too tedious to be repeated. For instance, the resulting difference for  $\mu = \frac{1}{2}$  is

$$\begin{aligned} (R_i - R_r)_2 &= \frac{9}{64} \times \frac{3}{128} \int_0^1 \frac{-15x^4 - 42x^2 + 17}{x + \frac{1}{2}} dx \\ &= \frac{9}{64} \times \frac{3}{128} \left( -\frac{5}{4} + \frac{89}{16} \ln 3 \right) = 0.01602 \end{aligned}$$

Further in Table 55, the lines for  $n = 3$  and  $n = 4$  and an independent check on  $n = 2$  were obtained by graphical extrapolation of the differences in the Abhyankar and Fymat tables for  $a = \frac{1}{4}, \frac{1}{2}$ , and  $\frac{3}{4}$ . Finally, the polarization of the very high-order terms must approach that of the escape function, which was given in Section 16.3.2 and is 2.2% for  $\mu = 0.5$ .

This practice example may be worked out in many ways as the need arises. In particular we note the possibility of obtaining asymptotic equations for the terms of very high order along the lines of Section 12.4.

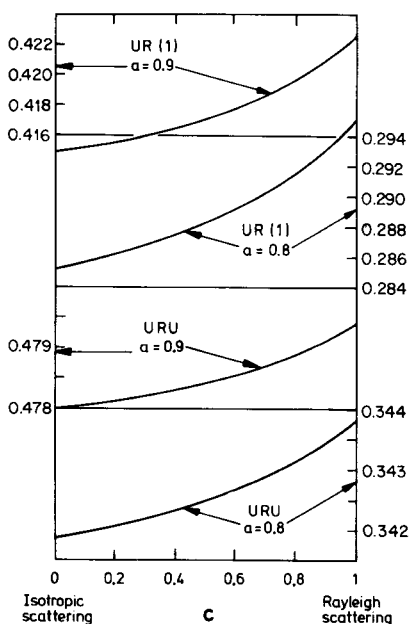


**Fig. 16.9.** Sample results for the fraction of incident flux reflected against a semi-infinite atmosphere with a mixture of Rayleigh scattering and isotropic scattering.

As a final illustration, we present in Fig. 16.9 the reflected flux values for a mixture of isotropic scattering and Rayleigh scattering, as defined in Section 16.1.1. The direction of incidence is either perpendicular to the atmosphere (1) or isotropic (*U*). The numbers for  $c = 0.4, 0.6, 0.8$ , and 1 were taken from Bond and Siewert (1971); those for  $c = 0$ , from Table 12. The very slight dependence on  $c$  is entirely in line with the experience in similar comparisons made in Section 14.2.1.

The escape problem for Rayleigh scattering with absorption has application to the emission characteristics of several astronomical objects. Harrington (1969) tabulates the intensity and polarization of the escaping radiation for an albedo  $a = \frac{5}{6}$  at all optical depths. A comparison is made with the situation for  $a = 1$  (our Table 53) and for a model in which  $a$  varies with depth as  $(1 + \tau)^{-1}$ . Gnedin *et al.* (1973) present the results of more extensive computations for a range of  $a$  values in three graphs.

Deep inside a medium with nonconservative Rayleigh scattering, we find for any albedo  $a$  a fixed diffusion exponent  $k$  and a fixed diffusion pattern in which the radiance and polarization are functions of the angle with the direction of propagation. The general theory is in Section 15.2.3. Tables are given by Kattawar and Plass (1976). They show that the  $k(a)$  relation for the Rayleigh phase function (scalar theory) is about halfway between the corresponding relations for Rayleigh scattering (matrix theory) and isotropic scattering.

## 16.4 RAYLEIGH SCATTERING IN ATMOSPHERES OF FINITE DEPTH

The exact solutions for finite values of  $b$  have been referred to in Section 16.2. The additional variable  $b$  leads to even longer formulas than those quoted for  $b = \infty$  in Display 16.1, but no really new complications occur. Just as in isotropic scattering, each of the  $H$  functions defined in Table 52 is replaced by an  $X$  and  $Y$  function if we pass from infinite to finite layers. We shall not quote these formulas, but pass immediately to examples and comments without claiming completeness.

### 16.4.1 Polarization of the Blue Sky

One of the phenomena that fascinated the 19th and early 20th century scientists was the appearance of points of zero polarization along the sun's vertical circle. They are even called by famous names: Arago, Brewster, Babinet. In most regions along the sun's vertical polarization is positive, i.e., vibration is perpendicular to the vertical, and in some regions negative, i.e., vibration is parallel to the vertical. The neutral points separate these regions. Dorno extended the same definitions to other verticals and made painstaking measurements to determine the entire neutral curve on the sky. The curves computed by Chandrasekhar and Elbert (1954), of which Fig. 16.10 gives only one example for clarity, match these observations fairly well.

The relevance of these curves is not as great as it seems. Outside the sun's vertical, the plane of polarization generally makes an oblique angle, and the information whether  $I_1$  or  $I_r$  is larger has little interest unless the third Stokes parameter  $U$  is also determined. The zenith in Fig. 16.10 is not really a singular point, for at  $37^\circ$  from the sun, the first-order scattering with its characteristic polarization perpendicular to the sun's vertical fully dominates. Only by the choice of the plane of reference, is this same polarization registered as positive or negative with neutral directions at azimuth  $\pm 45^\circ$  from the sun's vertical.

When the sun sinks toward the horizon, the stretch of negative polarization sinks with it until the Brewster point sets. At the same moment, a third neutral point, the Arago point, rises at the opposite end. When the sun has finally reached the horizon, the Arago point has risen to the same height as the Babinet point, and the entire picture has become symmetric. Figure 16.11 (Sekera, 1957) shows the location of these three points as functions of solar zenith distance for three assumed values of the optical thickness  $b$ . Dots mark the points corresponding to Fig. 16.10.

Sekera has computed the influence of diffuse ground reflection on the neutral points in the same paper.

What happens to the neutral points when  $b$  increases still further is not immediately apparent. Since we observe diffusely transmitted light, we know for sure that for very large  $b$  the polarization pattern should finally agree in each



vertical, independent of the sun's elevation, with the solution of the Milne problem (Section 16.3.2) in which no neutral points occur at all. Further information is in eight figures of Kattawar *et al.* (1976), where the dependence on  $b$  is fully computed.

Extensive tables by Coulson *et al.* (1960) give complete information including the Stokes parameter  $U$  and the orientation of the plane of polarization for a set of atmospheres from  $b = 0.02$  to  $b = 1$ . These tables would have been even more useful if some tables of the moments had been added. Maps of the sky showing the orientation of the plane of polarization are given by Sekera (1957), Fig. 8, and by Coulson (1959a), Fig. 12.

### 16.4.2 Polarization of a Rayleigh Atmosphere Seen from Outside

A second set of examples based on the same calculations deals with the reflection from a planetary atmosphere seen from outside. The main characteristics were discussed with many illustrations by Coulson (1959a,b). Figure 16.12 presents a selection of the maps drawn by Sekera and Viezee (1961). They show for four assumed situations at (a)–(d) the intensity and (e)–(h) the degree and direction of polarization. The observer is over point  $E$ ; the sun, over point  $S$ . All illustrations selected here refer to thickness  $b = 1$ . The intensity plotted is (in our notation)  $\mu_0 R$ , which is the intensity seen by the observer expressed in a unit defined by a perfectly white Lambert surface facing the sun.

In (a), (b), (e), and (f) the scattering angle is  $180-16.3^\circ$ , which corresponds to  $\cos \alpha = 0.96$ . At this angle the polarization of single scattering, 4.1%, is small enough to be dominated at both ends of the principal plane by negative polarization from higher order, so that two neutral points occur. The scattering angle in (c), (d), (g), and (h),  $180-36.9^\circ$ , corresponding to  $\cos \alpha = 0.80$ , gives 22.0% polarization by single scattering, so that neutral points do not occur.

Each map for a dark planetary surface ( $A = 0$ ) is accompanied by a map for a moderately bright Lambert surface ( $A = 0.25$ ) under the atmosphere. The surface seen through the atmosphere is expected to increase the intensity and decrease the polarization, which is exactly what the maps show. The numbers in each intensity map at points corresponding to an interchange of  $\mu$  and  $\mu_0$  may be checked by means of the reciprocity principle. Such a check is not possible on the polarization maps (cf. Section 18.2).

The reflected fraction of the incident flux (from the atmosphere and underlying ground surface combined) has the form

$$UR(\mu_0) = 1 - \gamma(\mu_0)(1 - A)/(1 - sA)$$

where  $A$  is the albedo of the ground surface (following Lambert's law),  $s = URU$ ,  $\gamma(\mu_0) = UT(\mu_0) = \frac{1}{2}[\gamma_1(\mu_0) + \gamma_r(\mu_0)]$ , and  $\mu_0$  is the cosine of the zenith angle of the sun. For an assumed optical thickness  $b = 0.144$  (valid for the earth's



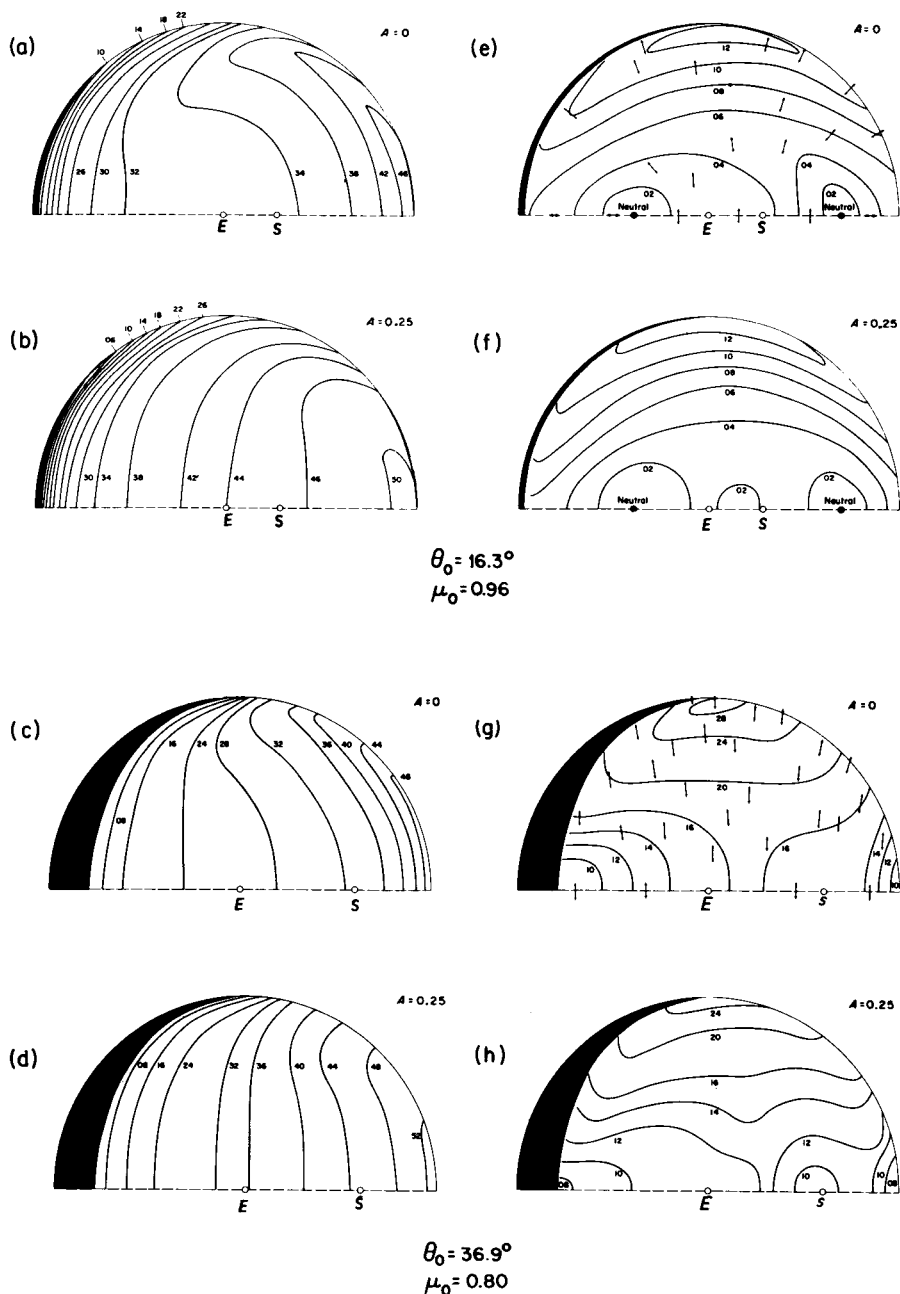


**Fig. 16.12.** Intensity (a)–(d) and degree and direction of polarization (e)–(h) of the light reflected from a planet covered by a Rayleigh scattering atmosphere with optical thickness 1. Each combination of two values of the phase angle and two values of the ground albedo is shown. S is the subsun point; E the subearth point (adapted from Sekera and Viezee, 1961).

TABLE 56  
Reflected Fractions of Flux by a Rayleigh Atmosphere with  
Optical Thickness  $b = 0.144$

$\mu_0$	$\gamma_t$	$\gamma_r$	$\gamma$	$A = 0$ $UR$	$A = 0.25$ $UR$
0	0.387	0.420	0.404	0.596	0.688
0.02	0.445	0.423	0.434	0.566	0.665
0.1	0.607	0.601	0.604	0.396	0.534
0.4	0.848	0.847	0.847	0.153	0.346
1	0.933	0.933	0.933	0.067	0.280
$U$	—	—	0.885	0.115	0.317

atmosphere in green light at 500 nm) the numbers in Table 56 are obtained. These match, with differences of about 1 unit in the third decimal, the values tabulated by Coulson (1959a). The values of  $\gamma_t$ ,  $\gamma_r$ , and  $s$  were interpolated from Chandrasekhar and Elbert. More accurate values, if needed, can be obtained in the manner explained in Section 14.2.1 (Table 43 and Fig. 14.2). The last line of Table 56 shows the corresponding values for the incidence  $U$ , i.e.,  $2 \times$  moments of order 1 of the function of  $\mu_0$  tabulated in that column.

The value of  $URU$ , which is 0.115 in this example, can be taken for other wavelengths from Table 43 and then integrated with the solar energy spectrum as weighting function to find the albedo of the earth's atmosphere as a whole (without aerosols and ground surface). This is a shorter route than to integrate first over the wavelengths and only then take the  $U$  moment. The resulting albedo is nearly 7%.

Toward the violet and ultraviolet, larger values of  $b$  occur. The same is true in visual light at the polar regions of Jupiter and on the entire planet Uranus. Problems for these larger  $b$  values may be solved by a variety of computing methods:

- (a) From the equations in Display 16.1, using recent tables cited in Section 16.2.2. This still requires a fair number of substitutions before the result is ready.
- (b) A separate numerical solution as chosen by Herman and Browning (1965) or Kattawar *et al.* (1976).
- (c) An exact asymptotic treatment for large  $b$  as worked out in great detail by Mullikin (1966), but the long formulas still make it quite a task to arrive at practical numbers.
- (d) Since experience with isotropic scattering has shown (Fig. 9.3) that in certain problems graphical interpolation between  $b = 1$  and  $b$  near  $\infty$  is quite feasible, we may try the same with Rayleigh scattering. Such a method is illustrated in Fig. 16.13.

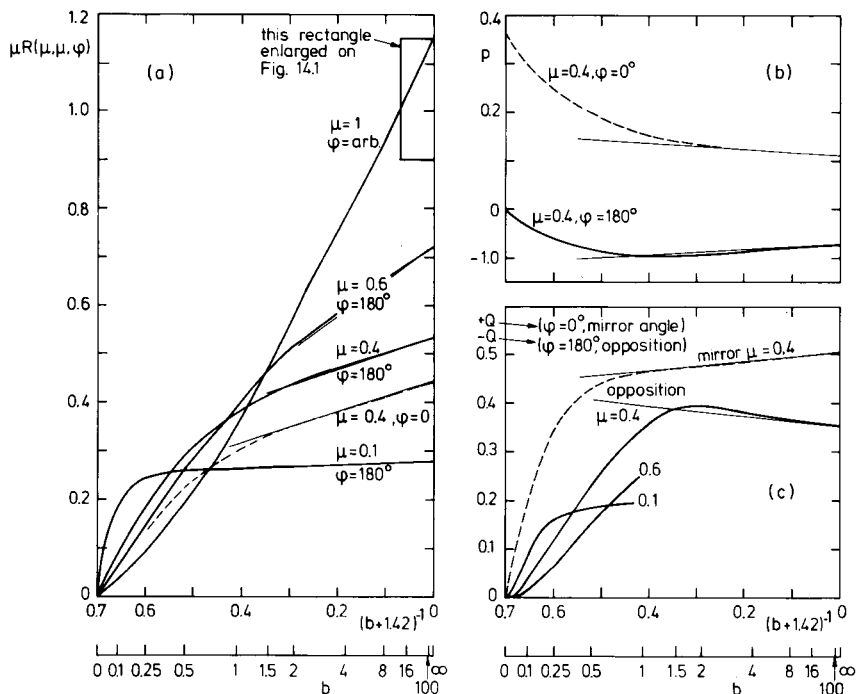


**Fig. 16.13.** Intensity (a), second Stokes parameter (c), and degree of polarization (b) of radiation diffusely reflected from a flat Rayleigh atmosphere of finite optical thickness  $b$ . The asymptotic approach to straight tangents for  $b \rightarrow \infty$  is demonstrated. In each example, equal zenith angles of incidence and emergence ( $\mu = \mu_0$ ) and two values of the azimuth corresponding to the opposition and the mirror directions have been chosen.

Assuming atmospheres with pure, conservative Rayleigh scattering without ground reflection, we seek the reflection function  $R(b, \mu, \mu_0, \varphi)$  for a given point of the planet ( $\mu, \mu_0, \varphi$ ) as a function of  $b$ . The intensity  $\mu_0 R$ , degree of polarization  $p$ , and Stokes parameters  $Q$  and  $U$  can be taken directly from the Coulson tables for  $b \leq 1$ . They have been plotted in Fig. 16.13 against a linear  $(b + 1.42)^{-1}$  scale. In each example shown,  $\mu = \mu_0$  and  $\varphi = 0$  or  $180^\circ$ .

In the vectorially written asymptotic equation

$$\mathbf{R}(b) = \mathbf{R}(\infty) - 4\mathbf{K} \cdot \mathbf{K}/3(b + 2q)$$

we can now substitute  $\mathbf{R}(\infty)$  from Section 16.3.3 and  $\mathbf{K}$  from Table 53. For instance,  $\mu = 0.4$  gives

$$K_1 = 0.380, \quad K_r = 0.404, \quad K_r - K_1 = 0.024, \quad K_r + K_1 = 0.784,$$

and

$$q = 0.712.$$

Incident natural light requires a postmultiplication by the vector  $\begin{pmatrix} 1 \\ 1 \end{pmatrix}$  so that we obtain

$$I(b) = \mu R(b; \mu, \mu, \varphi) = \mu R(\infty; \mu, \mu, \varphi) - 4\mu[K_r(\mu) + K_l(\mu)]^2/3(b + 2q) \\ = 0.446 - 0.328/(b + 1.42) \quad \text{for} \quad \mu = 0.4, \quad \varphi = 0^\circ$$

or

$$= 0.533 - 0.328/(b + 1.42) \quad \text{for} \quad \mu = 0.4, \quad \varphi = 180^\circ$$

$$Q(b) = \mu p R(b; \mu, \mu, \varphi) \\ = \mu p R(\infty; \mu, \mu, \varphi) - 4\mu[K_r(\mu) - K_l(\mu)][K_r(\mu) + K_l(\mu)]/3(b + 2q) \\ = +0.0508 - 0.0100/(b + 1.42) \quad \text{for} \quad \mu = 0.4, \quad \varphi = 0^\circ$$

or

$$= -0.0353 - 0.0100/(b + 1.42) \quad \text{for} \quad \mu = 0.4, \quad \varphi = 180^\circ$$

The ratio is the degree of polarization, which, for the principal plane, may be defined with a sign (Section 16.3.4). By straight division we find

$$p(b) = +0.114 + 0.061/(b + 1.42) \quad \text{for} \quad \mu = 0.4, \quad \varphi = 0^\circ \\ = -0.066 - 0.060/(b + 1.42) \quad \text{for} \quad \mu = 0.4, \quad \varphi = 180^\circ$$

Note that the curve for  $\mu = 1$  in Fig. 16.13 repeats in a small rectangle the data shown in Fig. 14.1. The asymptotic values of  $p$  for  $b = \infty$  may be read from Fig. 16.4. It is not certain that the smooth transition from the points for  $b \leq 1$  to the asymptotes has been sketched in correctly, but only a minor uncertainty is left. Points read from the curves published by Herman and Browning (1965) for  $\varphi = 0^\circ$  at  $b = 2$  and  $b = 4$  fit quite well. The curves for  $\varphi = 180^\circ$ , corresponding to opposition, will be discussed in connection with the polarization of Jupiter's polar caps (Fig. 18.9).

Note also the different behavior near  $b = 0$ . At  $\mu_0 = \mu = 0.4$ ,  $\varphi = 0$ , the actual scattering angle is nonzero with cosine  $2(0.4)^2 - 1 = -0.68$  and  $p = 0.368$ . At opposition,  $\varphi = 180^\circ$ , the scattering angle is 0 so that  $p$  starts at 0, and  $Q$  starts with a quadratic rise in  $b$  because it arises only from second and higher order scattering (Section 16.4.3).

### 16.4.3 Polarization in the Separate Orders

An instructive example in which the polarization of the various orders of scattering can be seen is given in Fig. 16.14. It is based on computations made by Dr. P. Bosma (unpublished). The end points of the curves in the  $I, Q$  plane correspond to the intensity  $\mu_0 R(\mu, \varphi, \mu_0, 0)$  reflected from an atmosphere of thickness  $b$  and  $a = 1$ .

Also shown are the terms up to order three. They are added as vectors, and the terms of still higher order are sketched in as a curve. We have plotted in

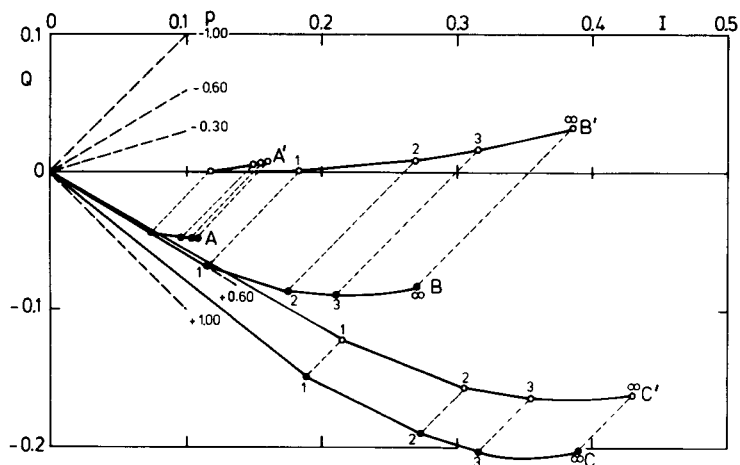


**Fig. 16.14.** The radiation reflected from a conservative Rayleigh atmosphere is broken down into the contributions from successive scattering orders, plotted and added as vectors in the  $I$ - $Q$  plane. The directional specifications are

A: $b = 0.25$ , $\mu_0 = 0.5$ , $\mu = 0.5$ , $\varphi = 0$	A': same with $\varphi = 180^\circ$
B: $b = 1$ , $\mu_0 = 0.5$ , $\mu = 0.5$ , $\varphi = 0$	B': same with $\varphi = 180^\circ$
C: $b = 1$ , $\mu_0 = 0.9$ , $\mu = 0.1$ , $\varphi = 0$	C': same with $\varphi = 180^\circ$

Fig. 16.15 a further case D from a table presented by Dave and Walker (1964), which gives the orders up to  $n = 15$ . These computations are all based on iteration of the auxiliary equation of the source function, further details of which are presented by Dave (1964) and by Dave and Walker (1966).

Take, for example, curve B of Fig. 16.14. The light comes in at  $60^\circ$  with the vertical and is reflected at the other side at  $60^\circ$  with the vertical so that the scattering angle is  $120^\circ$ , and single scattering has 60% polarization. The intensity of this term is

$$I_1 = \frac{3}{4}(1 + \frac{1}{4})\mu_0 R_{\text{isotr}} = 0.9375 \times 0.1227 = 0.1152$$

Double scattering, to be added to this, is a little more than half the first term, and still positively polarized but less strongly so. This continues. The ratio between successive terms of order  $n + 1$  and  $n$  approaches a constant, which Dave and Walker (1966) found to be 0.639. This may be compared with the value 0.619 for  $b = 1$  in isotropic scattering (Table 4, Section 7.4.1). The polarization of the separate terms continues to decrease until it becomes negative, which makes the curve curl slightly up. It reaches a final value, which is estimated from the graph as  $-25\%$ .

The other curves A, A', B', C, C' in Fig. 16.14 and D in Fig. 16.15 behave similarly. They all curl up; they all show the geometric progression of the steps towards the end. The final slope corresponds to negative polarization in all cases except D, where it must be 0 because we look at the zenith. The final slope

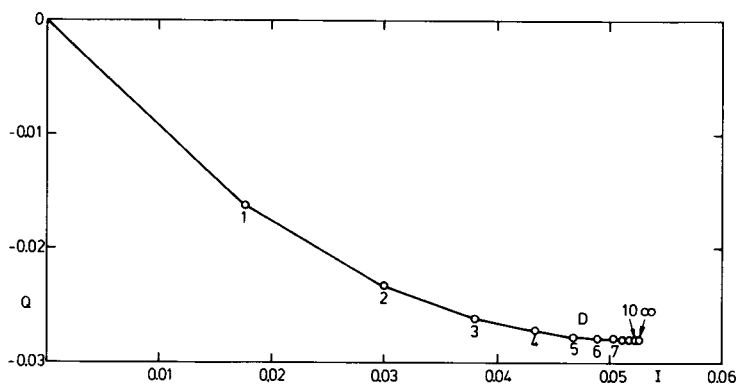


Fig. 16. 15. Contributions of successive scattering shown in the same way as in Fig. 16.14 for one further set of assumptions. D:  $b = 1$ ,  $\mu_0 = 0.2$ ,  $\mu = 1$

corresponds to the degree of polarization of the intensity emitted in the eigenvalue solution. Hence it cannot depend on  $\varphi$  and must be the same in A as in A', in B as in B', and C as in C'. The final ratio between successive terms depends on  $b$  only and must have the same value 0.639 in B, B', C, C', and D.

It would be possible to follow up the problems suggested by these figures by a precise solution of the eigenvalue problem. This would yield both the final slopes of the curves and the final ratios of the geometric series. Higher terms in the asymptotic expansions for large  $n$  could be obtained from a discussion (analytical or numerical) of the solution for  $a$  near 1. One thing is clearly shown by these figures and confirms a conclusion which we also reached for  $b = \infty$  (Table 55): The approximation made in some earlier work that the polarization of the higher order terms is negligible is too rough.

#### 16.4.4 Polarization of the Zenith Sky

As an example of how to deal with thick Rayleigh atmospheres, we pose the following problem. We wish to make an accurate graph, covering all  $b$ , of the *degree of polarization* at the zenith when the sun is  $30^\circ$  above the horizon. The following solution of this problem has a bit of everything: interpolation from published tables or graphs, additional computations, numerical checks, and physical verifications. This treatment is by no means recommended as the best, but we think it may be typical for the normal situation in which a research scientist feels he cannot spend weeks, yet is not content with guesswork.

The degree of polarization is the ratio between the polarized part of the intensity and the total intensity. It is wise to make graphs of these two functions, and not only of their ratio. These function are

$$\mu_0 T(\mu, \mu_0) = \mu_0(T_1 + T_r)$$

$$\mu_0 pT(\mu, \mu_0) = \mu_0(T_r - T_1)$$

We put  $\mu = 1$ ,  $\mu_0 = 0.5$ ; the total depth  $b$  will be varied, and the albedo for single scattering will be  $a = 1$ . The ground is supposed to be dark ( $A = 0$ ).

At the zenith, any vertical plane may be taken as plane of reference in defining the Stokes parameters; we choose the vertical plane containing the sun, defined by  $\varphi = 0$ . Since the scattering angle is  $\alpha = 120^\circ$ , the polarization seen at the zenith is  $(1 - \cos^2 \alpha)/(1 + \cos^2 \alpha) = 60\%$  for thin layers, in which single scattering dominates. Very thick layers will still let a fair amount of radiation diffuse through, but in the diffusion process the information about the position of the sun will be lost, so that looking to the zenith at the bottom of the atmosphere, no plane can be preferred, and  $p$  must become 0.

The references in Section 16.2.2 show that up to  $b = 1$ , intensity and polarization are available in tables (Coulson *et al.*, 1960). They require nonlinear interpolation because of the large steps in  $\mu_0$ . Beyond  $b = 1$ , we can make use of the recipes and tables of auxiliary functions by Sekera and Kahle (1966) or Kahle (1977). The formulas are fairly complicated; not less than sixteen values must be taken from these tables to obtain (after the necessary multiplications, additions, etc.) the intensity and polarization in the zenith at one  $b$ , one  $\mu_0$ . This can easily be done on a desk computer. Even so, we feel safer with some direct physical checks, mainly to make sure that we do not misinterpret the notations or definitions. Checks can be found at both extremes (small  $b$  and large  $b$ ).

First look at the total (diffuse) intensity. Since we know that conservative scattering at large  $b$  gives expressions with  $b + 2q_0$  in the denominator, we choose  $(b + 2q_0)^{-1}$  with  $2q_0 = 1.424$  as abscissa. This incidentally solves the problem of mapping the set of values  $b = 0 - \infty$  on a finite scale. Complete curves are drawn in Fig. 16.16 for  $b \leq 1$  from the Coulson tables for all  $\mu_0$  adopted there. For larger  $b$  they are copied from figures presented by Kahle (1968b) for  $\mu_0 = 0.1, 0.6$ , and 1.

We see that the upper curve ( $\mu_0 = 1$ ) and lower curve ( $\mu_0 = 0.1$ ) differ by a factor of 2 for very small  $b$  but by a factor over 20 for  $b > 8$ . Both results can be checked from basic physics. For  $b \ll 1$ , the atmosphere is so transparent that the air molecules stand in the same sunshine, whether the sun is high or low, so the factor  $\mu_0$  cancels out. In isotropic scattering, all curves would therefore come to the same tangent, which follows from  $\mu_0 T(\mu, \mu_0) = b/4\mu$ , so that the slope for  $\mu = 1$  would be  $\frac{1}{4}$ . The Rayleigh scattering pattern increases the coefficient to  $\frac{3}{8}$  if  $\mu_0 = 1$  and decreases it to  $\frac{3}{16}$  if  $\mu_0 = 0$ . These tangents have been drawn in and match the curves well.

In thick layers, the factor  $\mu_0$  comes in fully, for it determines how much of the radiation falls on a fixed area of the top surface of the atmosphere. This would make a factor of 10 between  $\mu_0 = 1$  and  $\mu_0 = 0.1$ . Part of this radiation leaks through to the bottom surface, and the difference is enhanced because steep incidence gives a better injection into the diffusion domain. The result is that the zenith brightness at large  $b$  is 24 times brighter for  $\mu_0 = 1$  than for  $\mu_0 = 0.1$ .

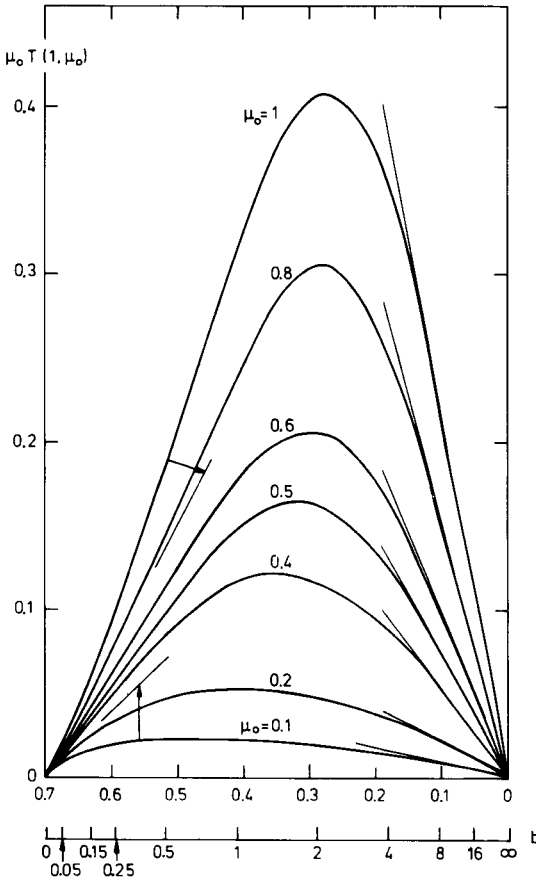


**Fig. 16.16.** Intensity of the zenith sky observed from the bottom of a pure Rayleigh atmosphere of varying optical thickness  $b$  with solar altitude varying from overhead ( $\mu_0 = 1$ ) to near the horizon ( $\mu_0 = 0.1$ ).

The full quantitative result follows easily from Section 5.4.3, Eq. 45, which reads, with  $g = 0$ :

$$T(\mu, \mu_0) = 4K_0(\mu)K_0(\mu_0)/3(b + 2q_0)$$

The corresponding tangents, with the numbers  $K(\mu)$  given in Table 53, have been drawn in Fig. 16.16. As expected from similar experience with isotropic scattering, the curves match the tangents quite well from  $b = 6$  up. The tangents obviously give more reliable values, at  $b = 8, 16$ , and  $100$ , than can be read with limited accuracy from Kahle's graphs. It now is clear that in order to obtain a complete smooth curve for  $\mu_0 = 0.5$ , two more points (for  $b = 2$  and  $b = 4$ ) computed the long way suffice, and this is what we did.



The polarization is perpendicular to the vertical through the sun when  $b$  is small, and we expect this to remain true for all  $b$ . Choosing this vertical as the plane of reference, we must have at the zenith

$$I_1 = \mu_0 T(1, \mu_0)^{\frac{1}{2}}(1 - p)$$

$$I_r = \mu_0 T(1, \mu_0)^{\frac{1}{2}}(1 + p)$$

where  $p$  is the degree of polarization. We find the terms containing  $p$  in the Kahle and Sekera tables as the second-order Fourier component in azimuth, for, if the plane of reference is chosen under an odd angle  $\varphi$  with the sun's vertical, this term appears as the set of Stokes parameters

$$\begin{pmatrix} I_1 \\ I_r \\ U \end{pmatrix} = \begin{pmatrix} -\frac{1}{2} \cos 2\varphi \\ \frac{1}{2} \cos 2\varphi \\ \sin 2\varphi \end{pmatrix} p \mu_0 T(1, \mu_0)$$

with

$$p \mu_0 T(1, \mu_0) = \frac{3}{16} \mu_0 (1 + \mu_0) [X_2(\mu_0) Y_2(1) - X_2(1) Y_2(\mu_0)]$$

Sekera and Kahle correctly interpret this dependence on  $\varphi$ , but their comment that this occurs "for physical reasons" is misleading. Rather, it is a mathematical disguise caused by our insistence to rotate the plane of reference, which creates the impression of a singularity, while in reality everything near the zenith is as smooth as can be. We have computed this function for all values of  $b$  in the SK tables and plotted it in Fig. 16.17a. The same scale of abscissas has been chosen as in Fig. 16.16 to allow easy comparison. The tangent at small  $b$  is  $\frac{9}{64}b$  and corresponds to 60% polarization.

The behavior at large  $b$  we can guess, because these  $X$  and  $Y$  functions have been defined by a characteristic function for which Table 52 gives the discrete  $k$  value  $k = 0.7410$ . Hence there should be a diffusion domain in which the pattern is repeated and the polarized part of the intensity decreases with optical depth as  $\exp(-0.741\tau)$ . Consequently, the transmission through a layer of thickness  $b \gg 1$  should be proportional to  $\exp(-0.741b)$ . We checked this in Fig. 16.17 by multiplying the numerical values from the Sekera-Kahle tables by the factor  $\exp(+0.741b)$ . The result is fully satisfactory. At  $b = 8$ , the value of  $\mu_0 p T$  is reduced to  $6.6 \times 10^{-4}$ , and at  $b = 16$ , to  $1.83 \times 10^{-6}$ , too small to be seen in the figure, but the product with the exponential factor nicely reaches a finite limit near 0.27.

Figure 16.17b shows as a full-drawn curve the polarization, which is the ratio of the quantity plotted in Fig. 16.17a to that found in Fig. 16.16. The result is as expected. At  $b = 1$  the degree of polarization has dropped to 37%, at  $b = 4$ , to 9%, and beyond  $b = 10$  it vanishes. This completes the practice problem.

What happens if we reverse the situation and ask for the polarization of the sky at  $30^\circ$  over the horizon when the sun is in the zenith? The transmission function  $T(\mu, \mu_0)$  itself is symmetric in  $\mu$  and  $\mu_0$ . Therefore, except for a factor of

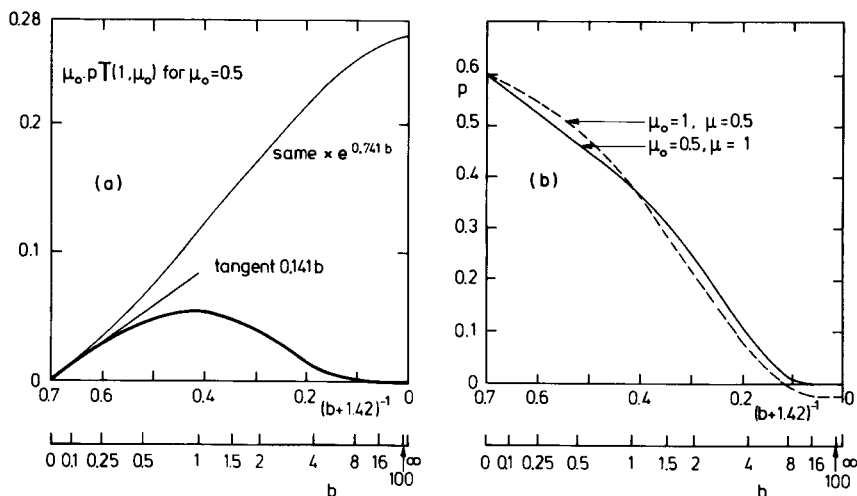


Fig. 16.17. Polarization of transmitted light. (a) Linearly polarized part of the zenith sky radiance in a pure Rayleigh atmosphere of varying optical thickness  $b$  and solar zenith angle  $60^\circ$ . The thin curve shows the asymptotic behavior. (b) The full drawn curve shows the degree of polarization corresponding to (a). The dashed curve shows the degree of polarization with  $\mu$  and  $\mu_0$  interchanged.

2 due to the factor  $\mu_0$ , we can again use Fig. 16.16. The polarization possesses only near symmetry, to which we already referred in discussing Figs. 16.2 and 16.5. The calculation from the SK tables is entirely different from the preceding one because now we are confined to the azimuth-independent term. Yet the  $p'$  curve thus obtained and shown as a dashed curve in Fig. 16.17b is rather similar to the  $p$  curve. There is an overshoot of about  $2\frac{1}{2}\%$  near  $b = \frac{1}{2}$ , a crossover near  $b = 1$ , and an undershoot by  $2-2\frac{1}{2}\%$  for  $b > 2$ . The polarization becomes negative beyond  $b \sim 7$  and finishes for very thick layers at the constant value  $-2.25\%$ , known from the solution of the escape problem (Table 53).

This near symmetry does not mean a failure of the reciprocity theorem. It is perfectly possible to describe situations with polarization that are reciprocal and to apply to those situations the reciprocity theorem (Sections 3.4.1 and 18.2); but the two experiments to which the curves in Fig. 16.17 refer are *not* reciprocal in that sense.

Calculations of the type just sketched, but with absorption included, are necessary for finding the amount of ozone from the zenith sky polarization. See Herman and Yarger (1965) for an example.

## REFERENCES

- Abhyankar, K. D., and Fymat, A. L. (1969). *J. Math. Phys.* **10**, 1935.  
 Abhyankar, K. D., and Fymat, A. L. (1970). *Astron. Astrophys.* **4**, 101; erratum, **5**, 491.  
 Abhyankar, K. D., and Fymat, A. L. (1971). *Astrophys. J. Suppl.* **23**, 35.

- Adams, C. N., and Kattawar, G. W. (1970). *J. Quant. Spectrosc. Radiat. Transfer* **10**, 341.
- Bond, G. R., and Siewert, C. E. (1967). *Astrophys. J.* **150**, 357.
- Bond, G. R., and Siewert, C. E. (1971). *Astrophys. J.* **164**, 97.
- Burniston, E. E., and Siewert, C. E. (1970). *J. Math. Phys.* **11**, 3416.
- Canosa, J. R., and Penafiel, H. R. (1973). *J. Quant. Spectrosc. Radiat. Transfer* **13**, 21.
- Chandrasekhar, S. (1950). "Radiative Transfer." Oxford Univ. Press (Clarendon), London and New York. Also Dover, New York, 1960.
- Chandrasekhar, S., and Breen, F. H. (1947). *Astrophys. J.* **105**, 435.
- Chandrasekhar, S., and Elbert, D. D. (1954). *Trans. Am. Phil. Soc.* **44**, 643.
- Coulson, K. L. (1959a). *Planet. Space Sci.* **1**, 265.
- Coulson, K. L. (1959b). *Planet. Space Sci.* **1**, 277.
- Coulson, K. L., Dave, J. V., and Sekera, Z. (1960). "Tables Related to Radiation Emerging from a Planetary Atmosphere with Rayleigh Scattering." Univ. of California Press, Berkeley, California.
- Dave, J. V. (1964). *J. Opt. Soc. Am.* **54**, 307.
- Dave, J. V., and Furukawa, P. M. (1966). *J. Opt. Soc. Am.* **56**, 394.
- Dave, J. V., and Walker, W. H. (1964). Paper presented at *Int. Radiat. Symp. Leningrad, August*.
- Dave, J. V., and Walker, W. H. (1966). *Astrophys. J.* **144**, 798.
- Dlugach, J. M., and Yanovitskii, E. G. (1974). *Icarus* **22**, 66.
- Domke, H. (1971a). *Astron. Zh.* **48**, 341 [English transl.: *Sov. Astron. AJ* **15**, 266].
- Domke, H. (1971b). *Astron. Zh.* **48**, 777 [English transl.: *Sov. Astron. AJ* **15**, 616].
- Gnedin, Yu. N., Dolginov, A. Z., Potashnik, E. L., and Silant'ev, N. A. (1973). *Sov. Astron. AJ* **16**, 809.
- Hansen, J. E., and Travis, L. D. (1974). *Space Sci. Rev.* **16**, 527.
- Harrington, J. P. (1969). *Astrophys. Lett.* **3**, 165.
- Herman, B. M., and Browning, S. R. (1965). *J. Atmos. Sci.* **22**, 559.
- Herman, B. M., and Yarger, D. N. (1965). *J. Atmos. Sci.* **22**, 644.
- Hovenier, J. W. (1970). *Astron. Astrophys.* **7**, 86.
- Hovenier, J. W. (1971). *Astron. Astrophys.* **13**, 7.
- Kahle, A. B. (1968a). *J. Geophys. Res.* **73**, 7511.
- Kahle, A. B. (1968b). *Astrophys. J.* **151**, 637.
- Kahle, A. B. (1977). A Solution of the Rayleigh Scattering Problem for Plane-parallel Atmospheres of Large Optical Thickness, Rand paper series P-5795. The Rand Corporation, Santa Monica, California.
- Kattawar, G. W., and Plass, G. N. (1976). *Appl. Opt.* **15**, 3166.
- Kattawar, G. W., Plass, G. N., and Hitzfelder, S. J. (1976). *Appl. Opt.* **15**, 632.
- Kriese, D. T., and Siewert, C. E. (1971). *Astrophys. J.* **164**, 389.
- Kuščer, I., and Ribarič, M. (1959). *Opt. Acta* **6**, 42.
- Lenoble, J. (1970). *J. Quant. Spectrosc. Radiat. Transfer* **10**, 533.
- Mullikin, T. W. (1966). *Astrophys. J.* **145**, 886.
- Mullikin, T. W. (1969). *SIAM-AMS Proc.* **1**, 3.
- Plass, G. N., Kattawar, G. W., and Catchings, F. E. (1973a). *Appl. Opt.* **12**, 314.
- Plass, G. N., Kattawar, G. W., and Binstock, J. (1973b). *J. Quant. Spectrosc. Radiat. Transfer* **13**, 1081.
- Schnatz, T. W., and Siewert, C. E. (1970). *J. Math. Phys.* **11**, 2733.
- Schnatz, T. W., and Siewert, C. E. (1971). *Mon. Notices. R. Astron. Soc.* **152**, 491.
- Sekera, Z. (1957). *Handb. Phys.* **48**, 288.
- Sekera, Z. (1963). Rand Corporation Memo. R-413-PR.
- Sekera, Z. (1966a). Rand Corporation Memo. RM-4951-PR.
- Sekera, Z. (1966b). Rand Corporation Memo. RM-5056-PR.
- Sekera, Z. (1966c). *J. Opt. Soc. Am.* **56**, 1732.
- Sekera, Z., and Kahle, A. B. (1966). Rand Corporation Rep. R-452-PR.

- Sekera, Z., and Viezee, W. (1961). Rand Corporation Rep. R-389-PR.
- Shieh, P. S., and Siewert, C. E. (1969). *Astrophys. J.* **155**, 265.
- Sweigart, A. V. (1970). *Astrophys. J. Suppl.* **22**, 1.
- van de Hulst, H. C. (1949). In "The Atmospheres of the Earth and Planets" (G. P. Kuiper, ed.). Univ. Press, Chicago, p. 49.
- van de Hulst, H. C. (1957). "Light Scattering by Small Particles." Wiley, New York. Also Dover, New York, 1981.

## **Part IV ○ SAMPLE APPLICATIONS**

## 17 Photon Optical Paths and Absorption Lines

### 17.1 GENERAL THEORY

#### 17.1.1 Why Photon Path Statistics?

An astronomer tends to associate photon optical paths directly with absorption lines. The equivalent width of an absorption line grows with the path length covered. This dependence is not linear but shows some form of saturation made visible in the curve of growth. Conversely, astronomers are used to the fact that the observed equivalent width of an absorption line can be taken as a measure of the average path length, provided the curve of growth is known or can be constructed empirically.

Multiple scattering adds a fundamental difficulty to this familiar situation. A long (average) optical path may mean that the light has covered a long path through a deep atmosphere; but it may equally well arise from a zigzag of many short tracks traveled in a much thinner atmosphere with multiple scattering. To distinguish between these extremes, or to determine that the situation is intermediate, is a question of great practical importance in planetary spectroscopy.

A scientist in a different field may react differently to the key word "photon path." A lidar expert, for instance, will be immediately aware of the fact that photon path is, apart from a constant factor, equivalent to echo delay time. Therefore, he likes to interpret the echo time at once geometrically and find the distance at which the backscatter occurred. This interpretation is usually correct. However, in lidar reflection on clouds the long path may again be due to a zigzag path arising from multiple scattering, and the conversion of echo time to place of scattering becomes far more complex.

In both examples a quantitative theory must start with a reliable computation of the distribution of photon optical paths in certain standard situations. Such computations are discussed first. In Section 17.3 we then apply this knowledge to absorption lines seen in diffuse reflection against a cloudy atmosphere.

If the full photon path distribution has been computed, we can also construct the response to an instantaneous pulse of radiation, or to radiation with an arbitrary distribution in time. For that reason, the problems discussed in this chapter are often found under the heading “nonstationary (or time-dependent) problems of radiative transfer.”

Apart from the time delay incurred on the path between two scattering centers, there may be a time delay (with a certain probability function) at each scattering center. This occurs, e.g., in situations where instead of scattering we must read absorption and subsequent reemission. An excellent guide to the literature where both these delays are taken into account is Nagirner’s (1974) review. We shall further assume instantaneous scattering.

### 17.1.2 An Equivalence Theorem

Since the optical path appears in an exponential factor, it is obvious that photon path statistics may be related to Laplace transforms. We shall omit a historical discussion of who has pursued this idea and in what precise form. Our references go back to Irvine (1964). Nagirner (1974) traces the literature back to a paper by Fock in 1926.

We shall now derive an equivalence theorem from which it is possible to express the photon path distribution exactly as the inverse Laplace transform of a function known from the solution of the stationary transfer problem.

Imagine the space between the scattering centers pervaded by a homogeneous medium of which we can vary the absorption. We assume a well mixed atmosphere, in which the gross properties do not change with height. The equivalence theorem states that it does not matter whether the constituents doing the scattering and those doing the absorption are identical. We can imagine them as fully separate, with one constituent (haze) providing conservative scattering at discrete centers and the other constituent (gas) providing absorption along the full light paths between scattering events. We can also imagine that part or all of the absorption occurs in the scattering particles. Generally, some of the absorption may occur in the haze particles, expressed by a single-scattering albedo  $a < 1$ , and some may occur in the gas, expressed by an exponential in the path length. The words haze and gas merely serve as an aid in visualizing the situation; they might also have been called agent 1 and agent 2.

The purpose of this thought experiment is to save computing time. A good many numerical and analytical results are available in the literature and in earlier chapters of this book for well mixed atmospheres consisting of nonconservative scatterers in a clear medium. With the proper equivalence rule, these

same results can be used to answer questions about a well mixed atmosphere with scattering and/or absorbing haze particles embedded in an absorbing gas. The extension to inhomogeneous layers should be obvious and will not be spelled out.

Suppose we wish to compute a measurable quantity  $I$  anywhere in the atmosphere. By inert parameters, we mean the variables which define the quantity sought but do not change in different equivalent situations. These inert parameters will not be written. They are, for instance,  $b$ , the optical thickness of the haze layer;  $g$ , the asymmetry factor, and possible further parameters characterizing the phase function;  $\mu_0$ , cosine of angle of incidence; and  $(u, \varphi)$ , cosine and azimuth angle defining the direction in which the intensity is measured.

The quantity  $I$  in the following formulas may be the specific intensity itself, but it may also be an integral (moment or bimoment) over  $\mu_0$  or  $\mu$ , or both. Other quantities, like the intensity reflected from a layer with a diffusely reflecting ground surface, can be treated by the same formalism.

It is easiest to conceive that the computation of  $I$  has been performed by the Monte Carlo technique, so that the history of every event contributing to  $I$  is known. In particular, a photon contained in  $I$  may have been scattered  $n$  times by a haze particle and have traveled a total optical path  $\lambda$  through the layer. Here  $n = 0, 1, 2, \dots$  and  $\lambda = 0 - \infty$  are definite numbers. In the absence of any absorption, it is then possible to write the following equations:

*Without gas and haze absorption*

$$I = \sum_{n=0}^{\infty} I_n = \sum_{n=0}^{\infty} I_n \int_0^{\infty} p_n(\lambda) d\lambda \quad (1)$$

Here  $p_n(\lambda)$  signifies the normalized probability distribution of the optical path length  $\lambda$  among the photons that contribute to  $I$  and have been scattered  $n$  times.

It is also possible to refrain from counting the number of scattering events and to define  $p(\lambda)$  as the normalized probability distribution of the optical path length  $\lambda$  among all photons contributing to  $I$ . Then, instead of Eq. (1), we have

$$I = I \int_0^{\infty} p(\lambda) d\lambda \quad (2)$$

Now we change the model assumptions by introducing absorption in the haze and in the gas. Let  $l$  be the geometrical path length and  $h$  the geometrical layer thickness (both in centimeters); and  $\sigma$  the scattering coefficient of haze,  $\kappa$  the absorption coefficient of haze, and  $\kappa_v$  the absorption coefficient of gas at some frequency  $\nu$  inside an absorption line or band (all in reciprocal centimeters). Then the dimensionless quantities entering into the problem are the albedo of haze particles  $a = \sigma/(\sigma + \kappa)$ , the optical thickness outside the absorption band  $b = h(\sigma + \kappa)$ , the optical path outside the absorption band  $\lambda = l(\sigma + \kappa)$ , the optical path at frequency  $\nu$  inside the absorption band  $\lambda_v = l(\sigma + \kappa + \kappa_v) = \lambda(1 + \gamma_v)$ , and the ratio of gas absorption to haze extinction at



frequency  $\nu$ ,  $\gamma_\nu = \kappa_\nu/(\sigma + \kappa)$ . With these new assumptions the quantity sought can be written at once as in Eq. (3).

*With gas and haze absorption*

$$I_\nu(a, \gamma_\nu) = \sum_{n=0}^{\infty} I_n a^n \int_0^{\infty} p_n(\lambda) e^{-\gamma_\nu \lambda} d\lambda \quad (3)$$

Here  $I_n$  and  $p_n(\lambda)$  are the functions introduced in Eq. (1). Two modifications are made in order to go from Eq. (1) to Eq. (3). First, the absorption in the haze particle is expressed by a factor  $a$  ( $< 1$ ) per scattering event. Note that  $b$  has been kept constant, so that with decreasing  $a$  the absorption  $\kappa$  increases, and the scattering  $\sigma$  decreases. Secondly, the factor

$$e^{-\kappa_\nu l} = e^{-\gamma_\nu \lambda}$$

expresses the gas absorption. Similarly, Eq. (2) is modified to

$$I_\nu(a, \gamma_\nu) = I(a, 0) \int_0^{\infty} p(a, \lambda) e^{-\gamma_\nu \lambda} d\lambda \quad (4)$$

It is important to note that Eq. (3), which is essentially the formulation used in several papers by Irvine (1964, 1966, 1967), has a hybrid form. There is no compelling reason to treat the absorption by the gas and by the haze differently. In fact, the total extinction factor  $\exp(-\lambda_\nu)$  has one part,  $\exp(-\lambda)$ , hidden in the factor  $I_n p_n(\lambda)$ , and a second part  $\exp(-\lambda \gamma_\nu)$  written explicitly. This unequal treatment serves to formulate the equivalence theorem.

In Eqs. (1) and (3), promote the optical thickness  $b$  of the haze layer to a written variable and, if applicable, also the optical depth  $\tau$  at which the quantity  $I$  is measured. Further, drop the index  $\nu$  of  $\gamma_\nu$  and  $I_\nu$ . The quantity in Eq. (3) is now written as  $I(a, b, \tau, \gamma)$  and we adopt the notation  $I(a, b, \tau)$  for  $I(a, b, \tau, 0)$ . Equations (3) and (4) with the new notation become

$$\begin{aligned} I(a, b, \tau, \gamma) &= \sum_n I_n(b, \tau) a^n \int_0^{\infty} p_n(b, \tau, \lambda) e^{-\gamma \lambda} d\lambda \\ &= I(a, b, \tau) \int_0^{\infty} p(a, b, \tau, \lambda) e^{-\gamma \lambda} d\lambda \end{aligned} \quad (5)$$

and because of the normalization of  $p_n(b, \tau, \lambda)$ :

$$I(a, b, \tau) = \sum_n I_n(b, \tau) a^n \quad (6)$$

We now observe that for physical reasons the result should not change if we choose to incorporate  $\kappa_\nu$  with  $\kappa$ . The definitions introduced above then yield a new optical thickness  $b' = b(1 + \gamma)$ , a new optical depth  $\tau' = \tau(1 + \gamma)$ , and a new albedo  $a' = a(1 + \gamma)^{-1}$ , and the equivalence theorem is

$$I(a, b, \tau, \gamma) = I(a', b', \tau') \quad (7)$$

The first use of this equivalence theorem is that any problem concerning a haze atmosphere, conservative or nonconservative, pervaded by an absorbing gas can be replaced by an equivalent problem in which the space between the haze particles is clear and the specifications have been changed from  $(a, b, \tau)$  to  $(a', b', \tau')$ . The new problem has exactly the same answer as the old. This statement is quite independent of the particular forms [Eqs. (3) and (5)] in which we have expressed the quantity  $I(a, b, \tau, \gamma)$ . Any (correct) method by which this quantity can be computed or measured is permitted.

The second use of the equivalence theorem is in finding the probability distribution of photon paths by means of an inverse Laplace transform (Display 17.1).

## 17.2 PHOTON OPTICAL PATHS

### 17.2.1 Path Length Distribution and Mean Path Length

Equation (3) from Section 17.1.2 permits us, in combination with the equivalence theorem [Eq. (5)], to compute the path-length distribution and the mean path length in a turbid atmosphere. Clearly, the distribution of the path lengths  $\lambda$  of the photons which contribute to a chosen quantity  $I(a, b, \tau)$  depends on the unwritten parameters  $\mu_0, \mu, g$ , etc., as well as on  $a, b$ , and  $\tau$ . Equation (5) has the form of a sum over all orders and an integral over all path lengths. We can, as we wish, invert one of these processes or both. By making the Taylor expansion in  $a$  we obtain the terms corresponding to each order of scattering  $n$ . By inverting the Laplace transform in  $\lambda$  we obtain the path-length distribution  $p_n(\lambda)$  or  $p(\lambda)$ .

If we desire, we may at the same time obtain any moment of this distribution. The mean path length

$$\langle \lambda \rangle = \int_0^{\infty} \lambda p(\lambda) d\lambda$$

is the most important one.

We have spelled out in Display 17.1 a comprehensive formulation in the form of a procedure for a computing program. Each line can be separately verified from Eqs. (5), (6), and (7) of the preceding section. A good number of cross checks can be made. The most important checks are given in lines 12 and 13. We leave the detailed verification to the reader but point out a few details.

The fact that the mean path lengths  $\langle \lambda \rangle$  (and higher moments) can be obtained by differentiation is most readily seen from Eq. (4) of Section 17.1.2, without first performing the inverse Laplace transform.

An important point is that the Taylor expansion (line 7) uses the values of  $I(a, b)$  on a cut through the  $(a, b)$  plane along which  $b$  is constant, but the inverse Laplace transform uses the values on a cut along which the haze scattering thickness  $ba = b'a'$  is constant. This is the parameter which does not change if

**DISPLAY 17.1****Determination of Path-Length Distribution and Mean Path Length**

Line	Equation
Preparation	
1	Define $I(a, b, \tau)$ . Choose values of the unwritten parameters ( $\mu_0, \mu, g$ , and possibly others).
2	Find $I(a, b, \tau)$ in table or formula by any acceptable method.
3	Adopt notation for inverse Laplace transform: $F(\lambda) = L^{-1}[f(\gamma)]$ defines the function satisfying $f(\gamma) = \int_0^\infty F(\lambda)e^{-\gamma\lambda} d\lambda$ .
Scattering orders combined	
4	$p(a, b, \tau, \lambda) = L^{-1}\{I[a/(1 + \gamma), b(1 + \gamma), \tau(1 + \gamma)]/I(a, b, \tau)\}$
5	$\langle \lambda(a, b, \tau) \rangle = \partial \ln I(a, b, \tau) / \partial \ln a - \partial \ln I(a, b, \tau) / \partial \ln b - \partial \ln I(a, b, \tau) / \partial \ln \tau$
6	In special case $b = \infty, \tau = 0$ : $\langle \lambda(a, \infty, 0) \rangle = d \ln I(a) / d \ln a$
Scattering orders separate	
7	$I_n(b, \tau) = (n!)^{-1} [\partial^n I(a, b, \tau) / \partial a^n]_{a=0}$
8	$p_n(b, \tau, \lambda) = L^{-1}\{I_n[b(1 + \gamma), \tau(1 + \gamma)] / (1 + \gamma)^n I_n(b, \tau)\}$
9	$\langle \lambda_n(b, \tau) \rangle = n - \frac{\partial \ln I_n(b, \tau)}{\partial \ln b} - \frac{\partial \ln I_n(b, \tau)}{\partial \ln \tau}$
	In special case $b = \infty, \tau = 0, n \geq 1$ :
10	$p_n(\infty, 0, \lambda) = \lambda^{n-1} e^{-\lambda} / (n-1)!$
11	$\langle \lambda_n(\infty, 0) \rangle = n$
Relations to be used as checks	
12	$p(a, b, \tau, \lambda) I(a, b, \tau) = \sum_{n=0}^{\infty} p_n(b, \tau, \lambda) a^n I_n(b, \tau)$
13	$\langle \lambda(a, b, \tau) \rangle I(a, b, \tau) = \sum_{n=0}^{\infty} \langle \lambda_n(b, \tau) \rangle a^n I_n(b, \tau)$

we vary the frequency through an absorption line. Since  $\tau'$  varies as  $b'$ , the ratio  $\tau/b$  is constant. This makes it possible to write line 9 alternatively as

$$\langle \lambda_n(b, \tau) \rangle = n - b [\partial \ln I_n(b', \tau/b) / \partial b']_{b=b'}$$

where  $I_n$  must be considered as a function of  $b'$  and  $\tau/b$ .

In diffusely reflected light, the zero-order term is absent, and the sums start with  $n = 1$ .

If the quantity considered is the diffusely reflected intensity against a semi-infinite atmosphere ( $b = \infty, \tau = 0$ ), or one of its moments or bimoments, the

Taylor expansion and the inverse Laplace transform are made from the same function of one variable  $I(a)$ . This leads to the significant simplification that on line 8 we have to take the inverse Laplace transform of the function  $(1 + \gamma)^{-n}$ , which is the universal form for  $p_n(\lambda)$  shown on line 10. This form can be substituted in line 12, but no further simplification is possible because  $p(a, \lambda)$  still is dependent on the set of numbers  $I_n$ . A further consequence is that either line 5 or line 13 reduces to the simple equation for the mean path length on line 6.

### 17.2.2 Results: Semi-Infinite Atmospheres

In the particular case of diffuse reflection against a semi-infinite atmosphere, it is attractive to use the fact that  $p_n(\lambda)$  has a very simple form and to employ lines 10 and 12 of Display 17.1 to find  $p(\lambda)$  for all scattering orders combined. The numbers  $I_n$  may be found for a number of examples in Table 34 (Section 12.4.2) and for  $n = 1-3$  also in Table 12 (Section 9.1.1). In 18 examples, both with isotropic and anisotropic scattering, the values of  $4\mu\mu_0 I_n$  for  $n = 1-50$  are given by Uesugi *et al.* (1971). The authors have indicated that there are some misprints in Tables 2 and 3. The summing can be done numerically, or by employing series expansions appropriate to small or large values of  $\lambda$ .

We shall present one example in some detail. Consider diffuse reflection with perpendicular incidence and perpendicular emergence ( $\mu = \mu_0 = 1$ ) against an isotropically scattering conservative atmosphere,  $a = 1$ . Numerical values are found in Table 57, and a graph is shown in Fig. 17.1. Here  $I = 1.05692$ , which is the infinite sum of  $I_1 = 0.12500$ ,  $I_2 = 0.08664$ , etc.

First, for small  $\lambda$  we may simply expand as shown in the accompanying tabulation.

$I_1 p_1(\lambda)$	$= 0.12500e^{-\lambda}$	$= 0.12500 - 0.12500\lambda + 0.06250\lambda^2 + \dots$	
$I_2 p_2(\lambda)$	$= 0.08664\lambda e^{-\lambda}$	$=$	$+ 0.08664\lambda - 0.08664\lambda^2 + \dots$
$I_3 p_3(\lambda)$	$= 0.06527\lambda^2 e^{-\lambda}/2 =$		$+ 0.03264\lambda^2 + \dots$
Sum is $I p(\lambda)$		$= 0.12500 - 0.03836\lambda + 0.00850\lambda^2 + \dots$	
Hence $p(\lambda)$		$= 0.11827 - 0.03629\lambda + 0.00804\lambda^2 + \dots$	(8)

Convergence is fast. The quadratic approximation leaves an error which rises to 1.4% at  $\lambda = 1$ . Use of an expansion of this type with many more terms for large  $\lambda$  is possible but not very attractive.

Second, an asymptotic expansion for large  $\lambda$  may be derived by noting that only high orders (near  $n = \lambda$ ) contribute effectively to the  $p(\lambda)$  for large values of  $\lambda$ . Hence, in computing  $p(\lambda)$  for large values of  $\lambda$ , it suffices to use the asymptotic form of  $I_n$  for large  $n$ . This is (Section 12.4.2)

$$I_n = r(n + c)^{-3/2}[1 + sn^{-2} + O(n^{-3})]$$

TABLE 57

Path-Length Distribution for Reflection Against Semi-Infinite Atmosphere with Conservative, Isotropic Scattering, Perpendicular Incidence and Reflection ( $b = \infty, a = 1, \mu = \mu_0 = 1$ )

(1)	(2)	(3)	(4)	(5)	(6)	(7)
				Asymptotic expression for large $\lambda$		
	Quadratic expansion in $\lambda$ Section 17.2.2 Eq. (8)	Successive scattering	Padé approximation $N = 7$ Fouquart	With correction factor Section 17.2.2 Eq. (9)	Main term of Eq. (9)	Correction factor exact
$\lambda$	$p(\lambda)$ approx.	$p(\lambda)$	$p(\lambda)$	$p(\lambda)$ approx	$I_{\lambda+1}/I$	$C$
0	0.11827	0.11827	—	—	0.11827	1.000
0.1	0.11472	—	0.11471	—	—	—
0.2	0.11133	—	0.11132	—	—	—
0.4	0.10504	—	0.10496	—	—	—
0.5	0.10214	0.10196	0.10198	—	—	—
1	0.09002	0.08876	0.08876	—	0.08198	1.083
2	—	0.06902	0.06900	—	0.06175	1.118
4	—	0.04544	0.04542	—	0.04007	1.134
5	—	0.03813	0.03809	—	0.03366	1.132
10	—	0.01948	0.01943	0.01984	0.01760	1.104
20	—	0.00855	0.00855	0.00860	0.00799	1.070
40	—	0.00340	0.00341	0.00341	0.00327	1.042
50	—	0.00249	0.00247	0.00250	0.00242	1.034
80	—	0.00128	0.00129	0.00128	0.00125	1.022
100	—	—	0.00095	0.00093	0.00091	1.018
200	—	—	—	0.000337	0.000334	1.009
400	—	—	—	0.000120	0.000120	1.005
500	—	—	—	0.000086	0.000086	1.004
1000	—	—	—	0.000031	0.000031	1.002

where in our numerical example  $r = 1.033$ ,  $c = 3.76$ , and  $s = 4.9$  (read from Fig. 12.16). Inserting this form in line 12 of Display 17.1, we obtain, for  $a = 1$ ,

$$p(\lambda) = r \sum_{n=1}^{\infty} p_n(\lambda)(n + c)^{-3/2}[1 + sn^{-2} + \cdots]$$

It is not even necessary to replace the sum by an integral, for exact sums of powers of  $n$  over the Poisson distribution  $p_n(\lambda)$  (Display 17.1, line 10) can be used. Writing the sum of any function  $f_n$  as

$$\{f_n\} = \sum_{n=1}^{\infty} f_n p_n(\lambda)$$

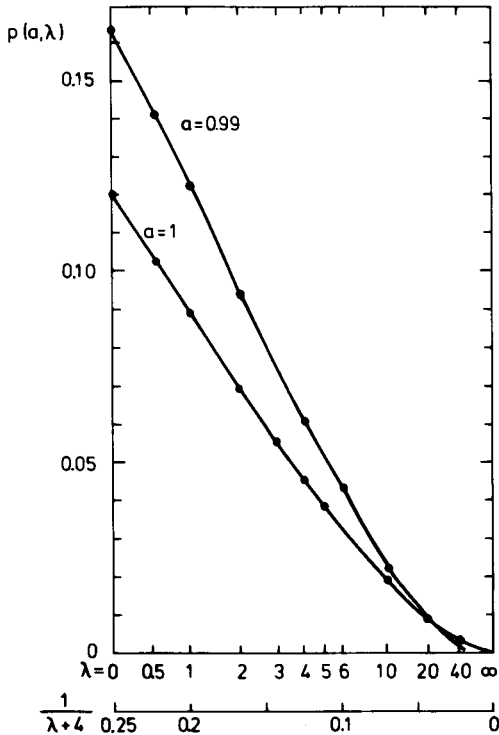


Fig. 17.1. Path-length probability distribution for perpendicular reflection against an isotropically scattering semi-infinite atmosphere. The distributions shown for  $a = 1$  and  $a = 0.99$  are both normalized to 1.

and using  $x = n - (\lambda + 1)$ , we have

$$\begin{aligned} \{n - 1\} &= \lambda, & \{(n - 1)(n - 2)\} &= \lambda^2, \\ \{x\} &= 0, & \{x^2\} &= \lambda, & \{x^3\} &= \lambda, & \{x^4\} &= 3\lambda^2 + \lambda + 1 \end{aligned}$$

The summation can now be performed and gives

$$p(\lambda) = (r/Iy^{3/2})[1 + \frac{15}{8}y^{-1} + O(y^{-2})]$$

where  $y = \lambda + 1 + c$ . If  $\lambda$  is an integer, this may be put into the even simpler form

$$p(\lambda) = I_{\lambda+1}C/I, \quad \text{with } C = 1 + \frac{15}{8}y^{-1} + O(y^{-2}) \tag{9}$$

Third, we look at available numerical values. Two other authors have presented relevant numbers or graphs. A comparison is made in Table 57. Column (2) gives the result of Eq. (8). Column (3) shows results newly computed by direct summation over  $n$ . At  $\lambda = 4$ , terms until  $n = 10$ , inclusive, are needed to achieve good accuracy. Numbers in this column have been supplemented from

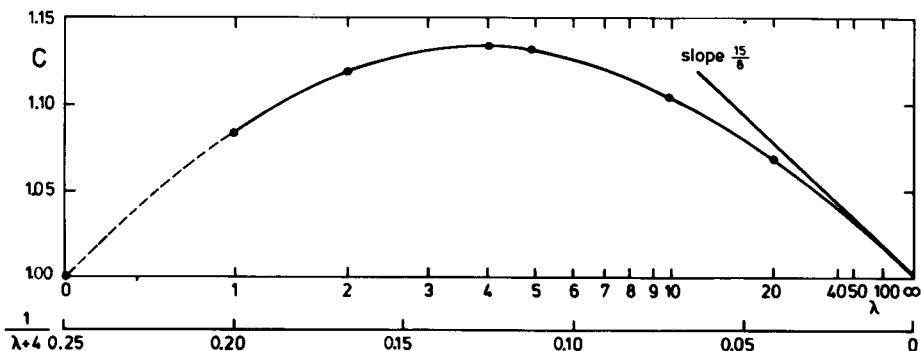


Fig. 17.2. Correction factor  $C$  necessary to find the correct path-length probability distribution for the example worked out in Table 57.

$\lambda = 5$  on with numbers made available by Irvine from the data on which the curves in Appleby and Irvine (1973) are based. Column (4) shows data made available by Fouquart, obtained by a method based on Padé approximation (Fouquart, 1974). Column (6) gives the simplest asymptotic formula consisting of Eq. (9) above, with  $C = 1$ . This is not very good because its errors drop below 1% only for  $\lambda > 170$ . Column (5) gives the much better approximation with  $C = 1 + \frac{15}{8}\lambda^{-1}$ , in which the 1% error limit is reached near  $\lambda = 15$ . The exact values of  $C$ , computed as the ratio between the values in columns (4) and (6), are given in the last column and are also presented in Fig. 17.2. The factor  $C$  introduces a correction that never exceeds 13.4% over the entire range.

The numbers in columns (5)–(7) for  $\lambda > 50$ , where other data were not accurate or not available, have been obtained directly from the asymptotic formula. Note that the average path  $\langle \lambda \rangle$  is infinite in this example. Fouquart's approximation in column (5) gave instead  $\langle \lambda \rangle = 432$ .

Turning now to the path length distribution for nonconservative scattering (but still for diffuse reflection against a semi-infinite atmosphere), we find that no new computational effort is necessary. The factor  $a^n$  appearing in line 12 of Display 17.1 can be combined with the factor  $\lambda^{n-1}$  in the Poisson distribution. The result is

$$p(a, \lambda) = a[I(1)/I(a)]e^{(a-1)\lambda}p(1, a\lambda)$$

which reduces the problem to the path-length distribution for conservative scattering derived above. The corrections are: (a) an added exponential factor cutting down the probability of longer path lengths and (b) a renormalization. We feel that this derivation is simpler than given by Uesugi and Irvine (1970a). The same result may also be obtained from the inverse Laplace transform on line 4 of Display 17.1. For an illustration, Fig. 17.1 shows the curve for  $a = 0.99$ . It may seem surprising that both probability distributions shown in Fig. 17.1 are normalized to 1. The explanation is that roughly 40% of the probability for  $a = 1$

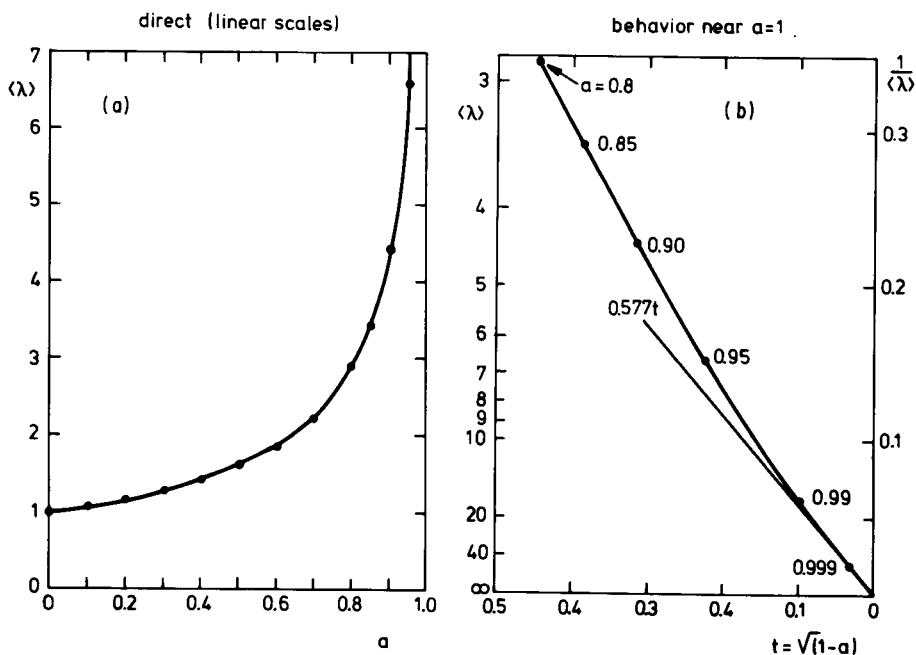


Fig. 17.3. Average photon path length for normal incidence and reflection from a semi-infinite atmosphere with isotropic scattering. The variation with single-scattering albedo  $a$  is shown for small and intermediate values (a) and for  $a$  close to 1 (b).

is in the tail beyond  $\lambda = 20$ . The strong reduction in this tail when we go to  $a = 0.99$  is compensated for by the higher probability at small  $\lambda$ .

The average path length  $\langle\lambda\rangle$  is finite for any  $a < 1$ . Figure 17.3 shows the values of  $\langle\lambda\rangle$  corresponding to normal incidence and reflection from an isotropically scattering atmosphere of infinite depth. The expression for small  $a$  is

$$\langle\lambda\rangle = 1 + 0.693a + \dots$$

The asymptotic expressions for  $a$  near 1, with  $t = (1 - a)^{1/2}$ ,  $dt/da = -2/t$ , are the following:

$$R = 1.057 - 3.661t + 7.84t^2 + \dots \quad (\text{Table 34})$$

$$dR/da = 1.831t^{-1} - 7.84 + \dots$$

$$1/\langle\lambda\rangle = 0.577t + 0.473t^2 + \dots$$

$$\langle\lambda\rangle = 1.732t^{-1} - 1.42 + \dots$$

This completes the numerical example. All of these results may be derived in a variety of ways and may easily be generalized to other angles of incidence and reflection and to other phase functions. For instance, Nagirner (1974) cites



several authors who have derived an asymptotic equation (his Eq. 15) that in our notation reads

$$R(1, \infty, \mu, \mu_0)p(1, \infty, \mu, \mu_0, \lambda) = 2K(1, \mu)K(1, \mu_0)/[3(1 - g)\pi]^{1/2}\lambda^{3/2}$$

valid for  $a = 1$ ,  $b = \infty$ , arbitrary  $\mu$  and  $\mu_0$ , arbitrary phase function, and  $\lambda \gg 1$ . This equation is readily found from  $Ip(\lambda) = ry^{-3/2}$  (see above) by equating  $I$  to  $R(\mu, \mu_0)$  and  $y$  to  $\lambda$ , and by finding  $r = -F_1(4\pi A)^{-1/2}$  according to Display 12.2, using the expansions [Eqs. (30) and (35)] of Section 5.4.1. Use pencil and paper! The equation thus derived is cruder in two ways than the example treated above, namely by the neglect of the term  $1 + c$  in  $y$  and of the term  $\propto y^{-1}$  within square brackets.

Uesugi and Irvine (1970a) derive  $\langle \lambda \rangle$  essentially by using lines 11 and 13 of Display 17.1. They present a table of  $\langle \lambda \rangle$  for isotropic scattering, various angles of incidence and emergence, and a range of albedo values. A more direct method is to use line 6 of Display 17.1, which in isotropic scattering reduces to

$$\langle \lambda \rangle = 1 + [a/H(a, \mu)] \partial H(a, \mu)/\partial a + [a/H(a, \mu_0)] \partial H(a, \mu_0)/\partial a$$

where  $H(a, \mu)$  is the familiar  $H$  function (Section 8.3.1). Accurate values of the derivatives are readily obtained from the expansions in powers of  $a - a_0$  presented by Stibbs and Weir (1959).

Finding  $\langle \lambda \rangle$  for anisotropic phase functions generally requires a new computation. It should be noted, however, that in the particular case ( $b = \infty, \tau = 0$ ) considered here, in virtue of the relations (13) and (11) of Display 17.1, we have

$$\langle \lambda \rangle = \langle n \rangle$$

where the average path at the left side is taken without regard to the number of scatterings, and the average number of scatterings at the right side is taken without regard to the path length. The same relation may be verified by differentiating an arbitrary power expansion in  $a$  according to Display 17.1, line 6.

Near-conservative scattering gives asymptotically

$$\begin{aligned} \langle \lambda \rangle = \langle n \rangle &= 2K(1, \mu)K(1, \mu_0)/R(1, \mu, \mu_0)[3(1 - g)(1 - a)]^{1/2} \\ &= C/2(1 - a)^{1/2} \end{aligned}$$

an equation also cited in Display 17.2, block 3.

The full run of  $\langle n \rangle$  from  $a = 0$  to  $a = 0.999$  is shown for three phase functions in Fig. 4 of Uesugi and Irvine (1969).

### 17.2.3 Results: Finite Slabs, Separate Orders

If tabulated values of the reflection or transmission function are available, generally, a double interpolation is necessary before the photon path-length distribution can be found by means of the inverse Laplace transforms (Display 17.1, line 4). Similarly, finding the average path length  $\langle \lambda \rangle$  requires differentia-

tions with respect to  $a$  and  $b$ . The corresponding computation for the intensity at an internal point requires a third differentiation with respect to  $\tau$ . It is possible but tedious to perform these operations with fair accuracy from the tables presented elsewhere in this book.

Relatively few of such results are available in the published literature. Before presenting a selection of those results some more items of theory will be mentioned.

(a) *Exact results for  $n = 1$  and 2.* Irvine (1964) has developed exact expressions of  $p_1(\lambda)$  and  $p_2(\lambda)$  and of  $\langle\lambda_1\rangle$  and  $\langle\lambda_2\rangle$  for the reflection and transmission functions of homogeneous slabs. The equations are valid for an arbitrary phase function, but his illustrations all refer to isotropic scattering and so do ours.

(b) *The dispersion.* This item and the next are applicable both to  $p_n(\lambda)$  and to  $p(a, \lambda)$ . The dispersion  $\sigma$  of any distribution function  $p(\lambda)$  is defined as the root-mean-square deviation from the mean value  $\langle\lambda\rangle$ . If the equation defining  $p(\lambda)$  is

$$p(\lambda) = L^{-1}[F(1 + \gamma)/F(1)]$$

we can find  $\langle\lambda\rangle$  and  $\sigma$  and any higher moments of  $p(\lambda)$  by writing out the Laplace transform, differentiating  $i$  times under the integral, and then putting  $\gamma = 0$ . The results are as follows:

$$i = 0: \quad \text{normalization } 1$$

$$i = 1: \quad \langle\lambda\rangle = -d(\ln F)/d\gamma$$

$$i = 2: \quad \sigma^2 = \langle\lambda^2\rangle - \langle\lambda\rangle^2 = d^2(\ln F)/d\gamma^2$$

Insertion of the specific forms of  $F$  found in Display 17.1 gives for  $\langle\lambda(a)\rangle$  and  $\langle\lambda_n\rangle$  the expressions on lines 5 and 9. With omission of  $\tau$  as an independent variable for simplicity, the corresponding dispersion values become

$$\sigma^2(a) = 2a \partial L/\partial a + a^2 \partial^2 L/\partial a^2 - 2ab \partial^2 L/\partial a \partial b + b^2 \partial^2 L/\partial b^2$$

and

$$\sigma_n^2 = n + b^2 \partial^2 \ln I_n(b)/\partial b^2$$

with  $L = \ln I(a, b)$ .

(c) *Approximation by a standard curve.* If we modify the function  $F(1 + \gamma)$ , keeping its value and its first and second derivatives at  $\gamma = 0$  intact, the inverse Laplace transform will be replaced by a modified distribution with the correct mean value and dispersion. A convenient standard form is

$$p(\lambda) = [m/\Gamma(k)](m\lambda)^{k-1}e^{-m\lambda}, \quad F(1 + \gamma) = 1/(1 + \gamma/m)^k$$

If  $\langle\lambda\rangle$  and  $\sigma$  are known, the two constants must be adapted by choosing

$$m = \langle\lambda\rangle/\sigma^2, \quad k = m\langle\lambda\rangle = m^2\sigma^2$$

The maximum of this standard curve does not coincide with the mean but falls at  $\langle\lambda\rangle - 1/m$ .

(d) *Formulas for finite  $b$ , large  $n$ .* For any finite  $b$ , if we let  $n$  become large enough, a point is reached beyond which any further step in the method of successive scattering in practice amounts to a multiplication by the largest eigenvalue  $\eta_1$ . This is reached sooner (i.e., for smaller  $n$ ) if  $b$  is small. The theory has been fully presented for isotropic scattering in Section 7.4, but the principle is the same for anisotropic scattering.

A straight application of the preceding equations to values of  $n$  beyond this point gives

$$\begin{aligned} I_n &= C_1(b)[\eta_1(b)]^{n-1} \\ \langle\lambda\rangle &= n - b[d \ln C_1/db + (n-1) d \ln \eta_1/db] \\ \sigma^2 &= n + b^2[d^2 \ln C_1/db^2 + (n-1) d^2 \ln \eta_1/db^2] \end{aligned}$$

These equations show that  $\langle\lambda\rangle$  approaches for  $n \rightarrow \infty$  a straight asymptote  $A + Bn$ , where the constants  $A$  and  $B$  are known. The same constants appear in the final intercept and slope if we plot  $\langle\lambda\rangle/n$  against  $1/n$  or against  $1/(n+c)$ , where  $c$  is arbitrary. The behavior of  $\sigma^2$  is similar, with different values of the constants.

As a first illustration, Fig. 17.4 shows the values of  $\langle\lambda\rangle/n$  for normal diffuse reflection  $\mu_0 = \mu = 1$  against an isotropically scattering atmosphere. The entire range of  $n$  values from  $n = 0$  to  $\infty$  is represented for a set of chosen  $b$  values. The values for  $n = 1$  were obtained from the exact expressions. Those for  $n = 2$  and 3 were obtained by numerical differentiation of the values of the separate terms in Table 12 (Section 9.1.1). The tangent (intercept and slope) at  $n = \infty$  follows from the theory just given under (d). For instance, at  $b = 1$ , the theory of Section 7.4.2 gives the numerical values  $C_1 = 0.0967$  and  $dC_1/db = 0.014$ , whereas from Table 4 (Section 7.4.1), we may read and find by differentiation  $\eta_1 = 0.619$  and  $d\eta_1/db = 0.248 \pm 0.003$ . The derived values

$$A = -(b/C_1) dC_1/db + (b/\eta_1) d\eta_1/db = -0.14 + 0.40 = 0.26$$

and

$$B = 1 - (b/\eta_1) d\eta_1/db = 0.599$$

appear as slope and intercept in the curve  $b = 1$  in Fig. 17.4.

In making this drawing, with the several numerical differentiations involved, we have not reached quite the accuracy we wished. Yet an immediate estimate of  $\langle\lambda_n\rangle$  may be made from this graph within some 5% for any  $a$  and any  $b$ . Similar graphs may be constructed for different values of  $\mu$  and  $\mu_0$ .

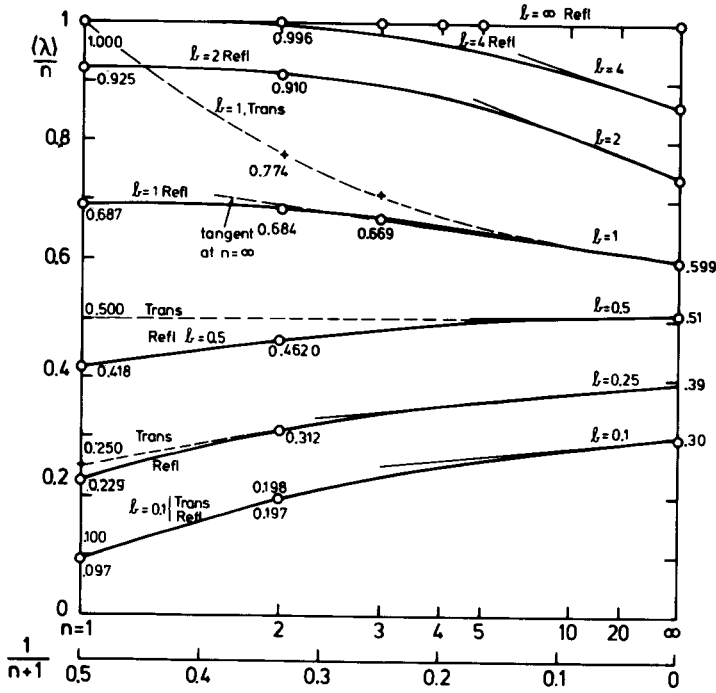


Fig. 17.4. Average photon path length per scattering event computed separately for any number of successive scattering events  $n$  for reflection against or transmission by an isotropically scattering slab; normal incidence and reflection, optical thickness  $b$ .

Whenever  $n$  is large enough to make the term based on the first eigenfunction dominant [see (d), above], the reflection and transmission terms become equal. This is shown in Fig. 17.4 by the reflection and transmission curves approaching the same tangent.

For a further illustration, Fig. 17.5 shows the value of  $\sigma^2/n$ , this time for  $b = 1$  only, in a presentation entirely analogous to Fig. 17.4. In computing the tangent at  $n^{-1} = 0$ , we have used the following numbers based on numerical differentiation:  $d^2 \ln \eta_1/db^2 = -0.576$ ,  $d^2 \ln C_1/db^2 = -0.89$ , intercept  $B = 0.424$ , and slope  $A = -0.31$ .

Finally, we show in Fig. 17.6 one example of the actual probability distributions  $p_n(\lambda)$ , again referring to the working example  $b = 1$ ,  $\mu = \mu_0 = 1$ , isotropic scattering. The exact distribution functions for  $n = 1$  and  $n = 2$  according to Irvine's formulas have been drawn. In the same drawing we show adapted standard curves (see item (c) above) with the correct mean and dispersion, which for  $n > 3$  may be read from Figs. 17.4 and 17.5. The numbers are

$$\begin{aligned} n = 2: \quad & \langle \lambda \rangle = 1.37, \quad \sigma^2 = 0.65, \quad m = 2.10, \quad k = 2.88, \quad \lambda_{\max} = 0.89 \\ n = 5: \quad & \langle \lambda \rangle = 3.23, \quad \sigma^2 = 1.87, \quad m = 1.73, \quad k = 5.60, \quad \lambda_{\max} = 2.66 \end{aligned}$$

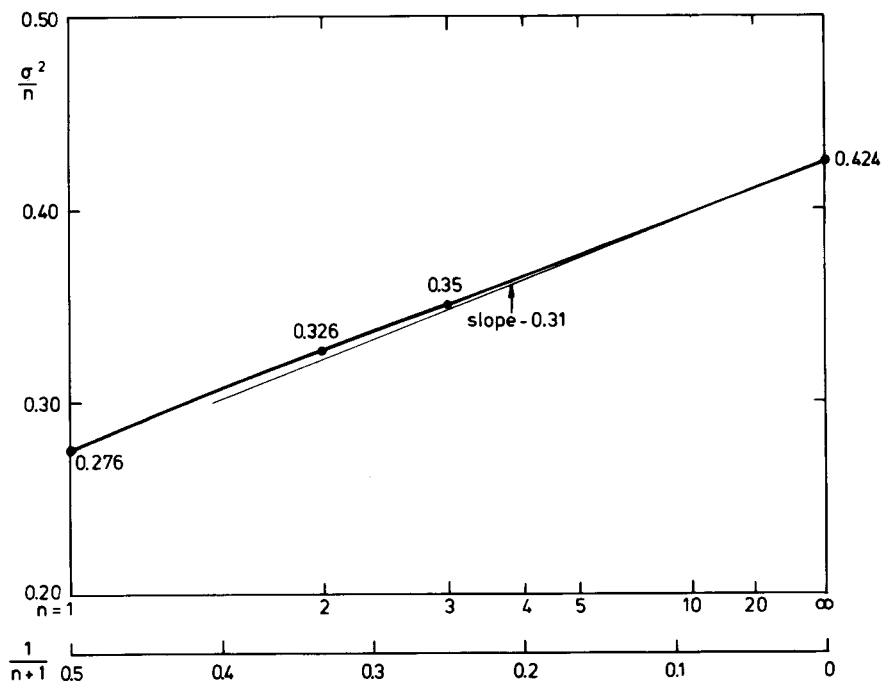


Fig. 17.5. Variance of photon path length about the average, per scattering event, computed separately for any number of successive scattering events  $n$ . Assumptions: optical thickness  $b = 1$ , perpendicular incidence and reflection, isotropic scattering.

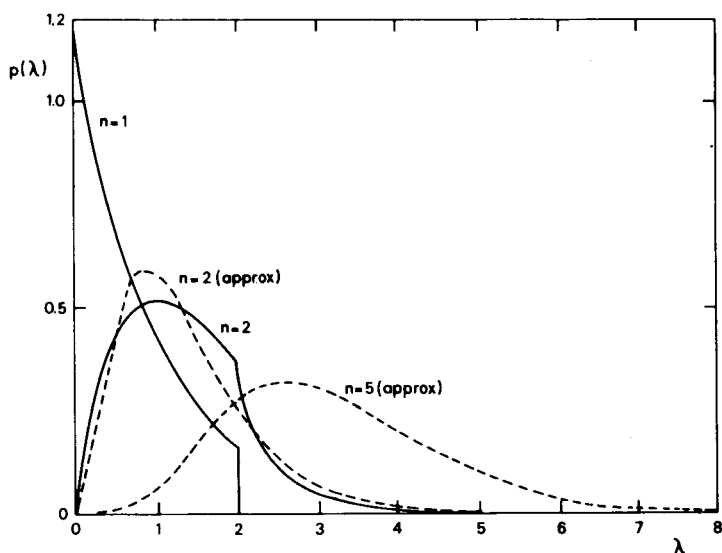


Fig. 17.6. Path-length distribution of radiation diffusely reflected back in vertical direction after  $n$  scattering events from a slab of isotropically scattering particles of optical thickness 1 exposed to vertical illumination. The curves, known exactly for small  $n$ , rapidly approach the asymptotic form.

The fact that the standard curve is a fairly good approximation to the exact curve already for  $n = 2$  suggests that for  $n \geq 3$  the exact curves (which are not available) will be almost indistinguishable from the adapted standard curves.

### 17.2.4 Results: Finite Slabs, Combined Orders

If the reflection or transmission at all values of  $a$  has been computed numerically or analytically by any of the methods discussed earlier (Chapters 9, 13, or 14), the probability distribution of the photon paths  $\lambda$  follows directly from an inverse Laplace transform (Display 17.1, line 4) and the mean path  $\langle \lambda \rangle$ , from a differentiation (line 5). We present two examples.

(a) *Thick layers.* Ivanov and Gutsabash (1974) have worked out the probability distributions for reflection and transmission starting from the asymptotic formulas for thick layers (Sections 5.3, 5.5 of this book). The results, rewritten in a notation consistent with ours, are

$$\begin{aligned} \text{reflection: } p_R(1, b, \lambda) &= p_R(1, \infty, \lambda) \\ &\quad - [4K(1, \mu)K(1, \mu_0)/3(1 - g)(b + 2q_0)] \\ &\quad \times (1/\lambda_d)R_\delta(\lambda/\lambda_d) \end{aligned}$$

$$\begin{aligned} \text{transmission: } p_T(1, b, \lambda) &= [4K(1, \mu)K(1, \mu_0)/3(1 - g)(b + 2q_0)] \\ &\quad \times (1/\lambda_d)T_\delta(\lambda/\lambda_d) \end{aligned}$$

where  $p_R(1, \infty, \lambda)$  is the path-length distribution in reflection for a semi-infinite conservative atmosphere (which is given by Ivanov and Gutsabash only in the limit  $\lambda \gg 1$ , but has been discussed in more detail in Section 17.2.2). Further

$$\begin{aligned} \lambda_d &= 3(1 - g)(b + 2q_0)^2 \\ R_\delta(x) &= \frac{2}{\pi^{1/2}x^{5/2}} \sum_{j=1}^{\infty} \left[ j^2 - \frac{x}{2} \right] e^{-j^2/x} \\ T_\delta(x) &= \frac{2}{\pi^{1/2}x^{5/2}} \sum_{j=1}^{\infty} \left[ \left( j - \frac{1}{2} \right)^2 - \frac{x}{2} \right] e^{-(j-1/2)^2/x} \end{aligned}$$

Figure 17.7 shows a graph of these functions.

(b) *An example with isotropic scattering.* As a further illustration we present one example over the full range of  $b$  with its limiting cases.

Figure 17.8 shows the average path length  $\langle \lambda \rangle$  for normal reflection against a slab with conservative isotropic scattering,  $\mu = \mu_0 = 1$ ,  $a = 1$ . Since  $\langle \lambda \rangle$  increases approximately as  $b$ , we have plotted the proportionality factor. Irvine (1964) conjectured from a few computed points that this factor would go to  $\sim 1.7$  for  $b \rightarrow \infty$ . The actual points were found in various ways by numerical differentiation of available data (Table 12) according to line 5 of Display 17.1.

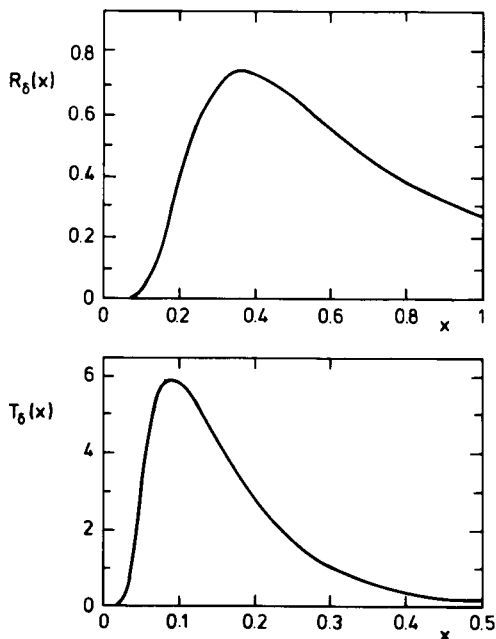


**Fig. 17.7.** Auxiliary functions appearing in the asymptotic forms of the photon path probability distributions for very thick layers with arbitrary anisotropic phase function (from Ivanov and Gutsabash, 1974).

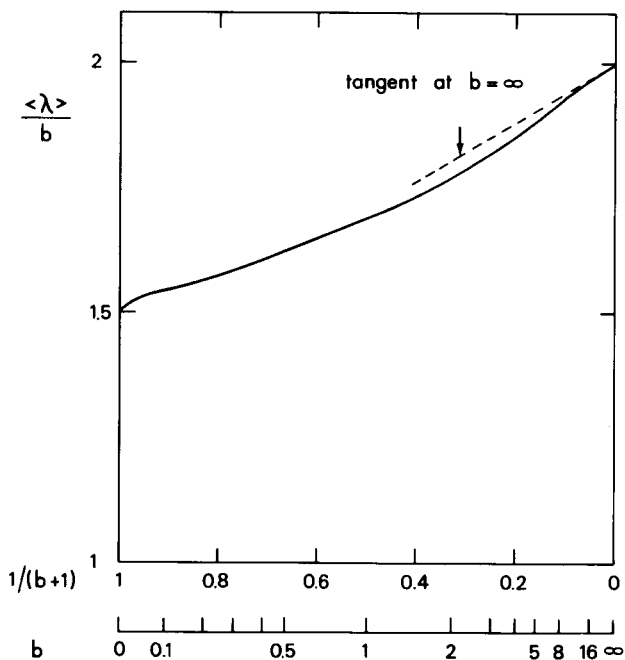


**Fig. 17.8.** Average photon path divided by slab thickness for perpendicular reflection against a slab with conservative isotropic scattering.

They show that the factor rises from 1.5 at  $b = 0$  to 2.0 at  $b = \infty$ . The fact that two differentiations are necessary may have introduced errors of the order of 0.01–0.02 in  $\langle \lambda \rangle / b$ . Yet various checks on the theory for small and large  $b$  suggest that the somewhat strange curve (with two inflection points and a cross-over point of the tangent at  $b = \infty$ ) is correct.

The limit 1.5 at  $b = 0$  in Fig. 17.8 appears to be an exception to the rule that simple results can be simply derived. I have found no other way than a brute-force expansion. From line 5 in Display 17.1 we find for arbitrary  $b$

$$\langle \lambda \rangle / b = (1/bR)(\partial R / \partial a)_{a=1} - (1/R)(\partial R / \partial b) \quad (10)$$

Both terms diverge logarithmically for  $b \rightarrow 0$ . Although  $b$  is very small, single scattering alone does not do the trick. We may, for instance, start from the geometric series approximation

$$R(a, b, \mu, \mu_0) = aR_1(b, \mu, \mu_0) / [1 - a\eta_1(b)]$$

where from Section 9.1.2

$$R_1(b, \mu, \mu_0) = [1/4(\mu + \mu_0)](1 - e^{-b/\mu - b/\mu_0})$$

and from Section 7.4.1

$$\eta_1(b) \approx (-\tfrac{1}{2}l + \tfrac{3}{4})b + \tfrac{1}{8}b^2 + \dots, \quad \text{with} \quad l = \ln b + 0.577.$$

The result for  $\mu = \mu_0 = 1$ ,  $a = 1$  becomes

$$(1/b)(\partial R / \partial a)_{a=1} = [1/4(1 - \eta_1)^2](1 - b + \tfrac{2}{3}b^2 \dots)$$

$$\partial R / \partial b = [1/4(1 - \eta_1)^2][1 - \tfrac{5}{2}b + (\eta_1 b + \tfrac{8}{3}b^2) + \dots]$$

Taking the difference and dividing by  $R = b/4(1 - \eta_1)$ , we finally obtain

$$\langle \lambda \rangle / b = \tfrac{3}{2} + \tfrac{1}{2}(\eta_1 - b)$$

This derivation is spelled out because to the author it was not trivial. It can easily be extended to transmission, to other  $\mu, \mu_0$ , to  $a \neq 1$ , and presumably also to anisotropic scattering.

The asymptotic behavior for large  $b$  again requires care. In “the nasty corner” near  $a = 1$ ,  $b = \infty$  (Section 5.4.2, Eq. 41; also Fig. 19.11) we cannot at once simplify the quantity  $f = \exp[-k(a)(b + 2q)]$  introduced in Section 5.3, Eq. 24. With the specifications for isotropic scattering (Display 8.1) and  $t = (1 - a)^{1/2}$  we thus have

$$R(a, b, \mu, \mu_0) = R(1, \infty, \mu, \mu_0)[1 - (\mu + \mu_0)3^{1/2}t(1 + f^2)/(1 - f^2) + \dots]$$

After transforming this for  $b^2(1 - a) \ll 1$  to

$$R(a, b, \mu, \mu_0) = R(1, \infty, \mu, \mu_0)\{1 - (\mu + \mu_0)(b + 2q)^{-1}[1 + b^2t^2 + \dots]\}$$

we find that in Eq. (1) above, the second term vanishes and the first term goes, for  $a \rightarrow 1$ ,  $b \rightarrow \infty$ , to

$$\langle \lambda \rangle / b = \mu + \mu_0$$

which confirms the limit 2 in the practice example.



## 17.3 ABSORPTION LINES IN DIFFUSE REFLECTION

## 17.3.1 Equivalent Width, Curve of Growth

Consider a well mixed atmosphere consisting of gas and embedded larger particles (haze). Let one of the gas components have an absorption line, in which over a narrow range of frequencies  $\nu$  the absorption coefficient of the gas has an added term  $\kappa_\nu$ . This term varies from 0, through a certain maximum  $\kappa_0$  at the line center, and back to 0. The entire line is supposed to be narrow enough to treat the otherwise existing scattering and absorption coefficients of gas and haze combined as constants over the entire line width. These are referred to as the continuum absorption coefficient  $\kappa$ , and the continuum scattering coefficient  $\sigma$ .

We shall simplify the terminology by now excluding any continuum absorption by the gas as well as any scattering by the gas. This does not mean that these quantities are neglected; they can simply be included in the absorption and scattering by the haze particles, as we have already done in Section 17.1.2.

We shall limit the discussion to absorption lines seen in diffuse reflection. Other problems, e.g., absorption lines seen if we observe the sun or any integrated part of the sky from inside a hazy atmosphere, can be treated in the same fashion. Clearly, the most restrictive assumption we make is the assumption of homogeneity, which is made throughout this book. This will never be true in practice, since the mixing ratio gas/haze or the broadening function of the spectral line, or most probably both, will change with height in the atmosphere. Ad hoc treatments are therefore necessary in any practical problem. The relations presented below serve to explain the main features and may be used as checks.

We continue to write the measured quantity, which is now specified as the reflection function  $R$ , as  $I$ .

The relative depression at any frequency in the line is (Fig. 17.9)

$$d(\nu) = (I_c - I_\nu)/I_c$$

Its graph as a function of  $\nu$  is called the line profile and its integral over  $\nu$ , the equivalent width:

$$W = \int d(\nu) d\nu$$

The integral must be extended over the full region of  $\nu$  in which the depression is noticeable. By writing

$$\kappa_\nu = f(\nu)\kappa_0$$

and varying  $\kappa_0$  but not  $f(\nu)$ , we can vary the strength of the absorption line. Since, generally,  $I_\nu$  is a nonlinear function of  $\kappa_\nu$ , the line profile will not have the same shape as the absorption coefficient profile  $f(\nu)$ . As a consequence, the equivalent

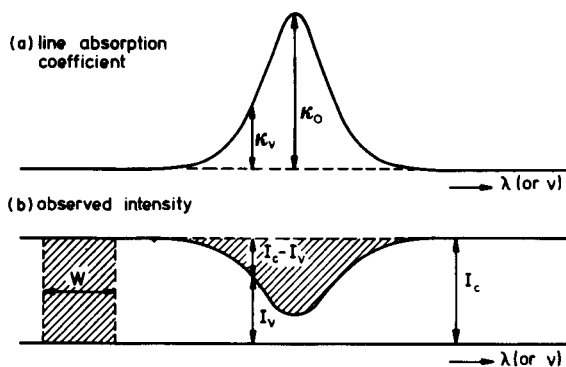


Fig. 17.9. Notations used in deriving equivalent width  $W$  of an absorption line.

width will not, generally, be proportional to the inherent absorption line strength  $\kappa_0$ . The graphical representation of  $W$  as a function of  $\kappa_0$  is called the curve of growth. This curve of growth is an important concept in the interpretation of absorption lines in astrophysics, because it makes it possible to go from the most readily measured quantity  $W$  to the inherently important quantity  $\kappa_0$ , which in turn permits conclusions about composition, etc.

### 17.3.2 A Systematic Review for Homogeneous Layers

The literature on this subject shows a somewhat piecemeal development, dictated by the needs as they arose in the practical interpretation of planetary spectra. By the time details of the vertical distribution were included in the model, it seemed that nothing useful could be done besides a big computer program. We believe, however, that the intermediate problem based on fully homogeneous models still merits a systematic review. This problem—though simple in principle—shows already a ramification of special cases that is at first sight bewildering. Since these special cases recur, *mutatis mutandis*, in inhomogeneous models, it is helpful to study their interrelations first under the simple assumption of homogeneity.

All relevant equations have been brought together in Display 17.2. The special cases that lead to simple but rigorous formulas are listed without specifying in advance the form, or the asymmetry factor, of the phase function.

*Block 1* shows the general situation. Scattering may be conservative or non-conservative, the atmosphere finite or infinite, the case described in block 2 being the only exception. The equivalent width observed in diffuse reflection can be generally expressed in the value  $W(l)$  that would be measured in a straight absorption tank of length  $l$  filled with this gas.

The corresponding specifications for a line with a damping profile (Lorentz shape) are given in the right column. The curve of growth for a single path  $l$

**DISPLAY 17.2**

Equations for the Equivalent Width of an Absorption Line Seen in Diffuse Reflection against a Semi-Infinite Atmosphere

	Line absorption coefficient $\kappa_v$ has arbitrary shape, with maximum $\kappa_0$ at $v = v_0$ , strength $S = \int \kappa_v dv$	Lorentz line shape $\kappa_v = S\alpha/\pi[(v - v_0)^2 + \alpha^2]$ $2\alpha$ is the full width at half maximum
<b>Block 1</b>		
Continuum optical path; $\lambda$ has arbitrary probability distribution $p(\lambda)$ (with exception of divergent case, block 2).	General: $W = \int_0^\infty p(\lambda)W(l) d\lambda$ $l = \lambda/(\sigma + \kappa)$ $W(l)$ is the equivalent width on straight path of length $l$ .  Weak lines ( $\kappa_0 \ll 1$ ), linear law $W(l) = Sl$ $W = S\langle\lambda\rangle/(\sigma + \kappa)$ $\langle\lambda\rangle = \int_0^\infty p(\lambda)\lambda d\lambda$ is the mean path length  Strong lines ( $\kappa_0 \gg 1$ ) behavior depends on form of line wings.	General as left column, with $W(l) = 2\pi\alpha F(z)$ $z = Sl/2\pi\alpha$ $F(z) = ze^{-z^2}[I_0(z) + I_1(z)]$ $I_n(z)$ is the modified Bessel function of first kind.  Weak lines ( $z \ll 1$ ), linear law as left column, $F(z) = z$ .  Strong lines ( $z \gg 1$ ) as above, with $F(z) = (2z/\pi)^{1/2}$ $W(l) = (4\alpha Sl)^{1/2}$ $W = [4\alpha S\langle\lambda\rangle/(\kappa + \sigma)]^{1/2}$ $\langle\lambda\rangle = \langle\lambda^{1/2}\rangle^2 = [\int_0^\infty p(\lambda)\lambda^{1/2} d\lambda]^2$ is the square mean root path length.
<b>Block 2</b>		
Reflection against semi-infinite, conservative atmosphere ( $b = \infty$ , $a = 1$ ). Other specifications $\mu$ , $\mu_0$ , $g$ , etc., are arbitrary.	$\langle\lambda\rangle = \infty$ (diverges) Weak lines ( $\kappa_0 \ll \sigma$ ) reach no linear part $W = C(\beta S/\sigma)^{1/2}$ $C(\mu_0, \mu, g)$ $= 4K(\mu)K(\mu_0)/R(\mu, \mu_0)[3(1 - g)]^{1/2}$ $\beta$ is defined by $\int \kappa_v^{1/2} dv = (S\beta)^{1/2}$ Strong lines ( $\kappa_0 \gg \sigma$ ) behavior depends on form of line in wings.	$\langle\lambda\rangle$ and $\langle\lambda\rangle$ diverge General Weak lines } $W = \infty$ , throughout. Strong lines }
<b>Block 3<sup>a</sup></b>		
Reflection against semi-infinite, nearly conservative atmosphere ( $b = \infty$ , $0 \leq 1 - a \leq 1$ ). Other specifications $\mu$ , $\mu_0$ , $g$ , etc., are arbitrary.	$\gamma_0 = \kappa_0/(\kappa + \sigma)$ , finite $\beta$ Very faint lines ( $\gamma_0 \ll 1 - a \ll 1$ ) as block 1, weak lines, linear law. $\langle\lambda\rangle = C/2(1 - a)^{1/2}$ with $C$ from block 2. Weak lines ( $1 - a \ll \gamma_0 \ll 1$ ) as block 2, weak lines, square root law.  Strong lines ( $1 - a \ll 1 \ll \gamma_0$ ) as block 2, strong lines, form depends on wings.	$\beta$ is not finite for Lorentz line Very faint lines as left column, linear law.  Weak lines approximate form as block 2 with $\beta = (4\alpha/\pi)[1 + \text{arc sinh } x_1]^2$ $x_1 = (\kappa_0/4\kappa)^{1/2}$  Strong lines as block 1, strong lines. Square root law.

<sup>a</sup> For distinction of three cases, see Fig. 17.10.

has the classical Ladenburg-Reiche form going from a linear to a square root part. In this case it is necessary to introduce the square mean root path length  $\langle\langle\lambda\rangle\rangle$ , which was first used by Fouquart and Lenoble (1973) under the name  $\lambda_{\text{effective}}$ . Its general definition in terms of  $p(\lambda)$  is given in Display 17.2.

Block 2 describes the exceptional case in which the continuum reflects 100% of the incident radiation because  $b = \infty$ ,  $a = 1$ . A very small absorption in the gas then gives a disproportionate drop in the reflection. This was first noted by van de Hulst (1949). By Eqs. (30) and (35) of Section 5.4, the "depression" defined above becomes

$$d(\nu) = C(1 - a)^{1/2} + \text{higher orders in } (1 - a)^{1/2}$$

with  $C$  as shown in Display 17.2.

This square root law in  $1 - a$  at one frequency leads in the curve of growth to a square root law in  $S$  for *weak* lines. The coefficient introduced here has the character of an effective line width. It must be of the order of  $S/\kappa_0$ , but it may also diverge because of extended wings, as in the case of a Lorentz profile.

Block 3, dealing with nearly conservative atmospheres, is of great practical value because an albedo of cloud particles about 0.999 is not uncommon. Here the interesting situation arises that *three* cases must be distinguished, a fact first established by Chamberlain (1970). This is caused by the fact that the depression at one frequency inside the line depends on two essential parameters, which (in the notation introduced in Section 17.1.2) are

$$\gamma = \text{line absorption coeff at } \nu / \text{extinction coeff in continuum} = \kappa_\nu / (\kappa + \sigma)$$

$$q = \text{line absorption coeff at } \nu / \text{absorption coeff in continuum} = \kappa_\nu / \kappa$$

All possible combinations of  $\gamma$  and  $q$  can be depicted in a plane, as we have done in Fig. 17.10a. In wandering through the frequencies in the line, only the (common) numerator changes, and the ratio  $\gamma/q = 1 - a$ , where  $a$  is the continuum albedo, remains constant. Hence we move on a line with unit slope. One such line, corresponding to  $a = 0.99$ , has been heavily drawn. It is cut in two places by the dash-dot dividing lines on which either  $\gamma$  or  $q$  is 1. Thus three domains are defined, in which we can hope to arrive at simple formulas. This division always exists if  $a$  is close to 1, which is the practical situation. In particular: in domain I,  $\gamma$  is well below  $1 - a$ ; in domain II,  $\gamma$  is between  $1 - a$  and 1; and in domain III,  $\gamma$  is well above 1. In the limit  $a = 1$ , only domains II and III remain.

The entire spectral line can be similarly classified according to the domain in which we find the deepest point (where the line absorption coefficient is  $\kappa_0$ ). This classification is summarized in Fig. 17.10b.

Having explained these distinctions, we return to the formulas in Display 17.2, block 3. For finite  $\beta$  (i.e., wings less pronounced than damping wings) we need only find  $\langle\lambda\rangle$ . From

$$R = R_c[1 - C(1 - a)^{1/2} + \dots]$$

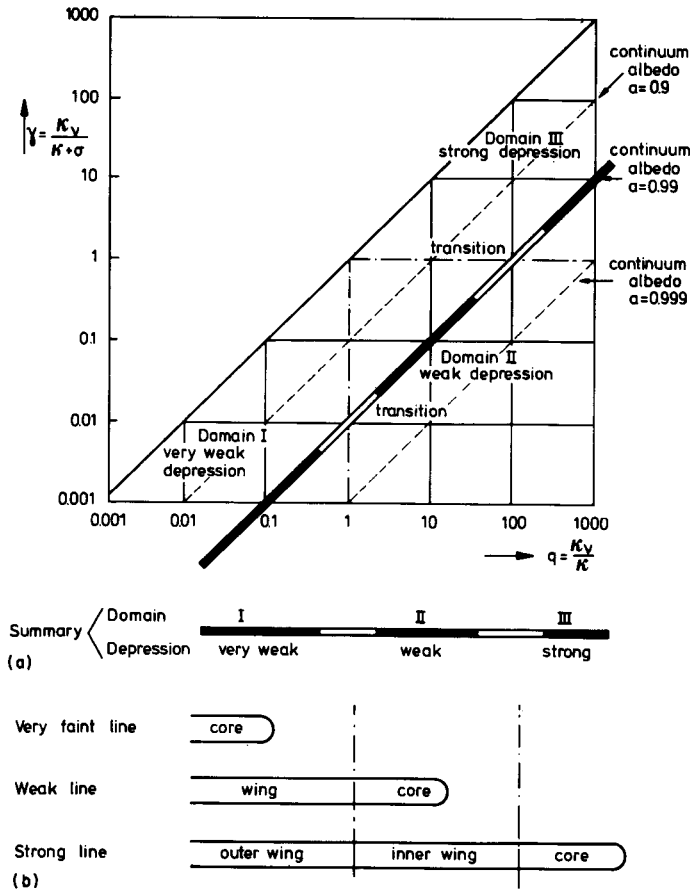


**Fig. 17.10.** Distinction of limiting cases in deriving the equivalent width of an absorption line seen in diffuse reflection against an atmosphere with nearly conservative scattering in the continuum. Two transition lines, at  $q = 1$  and at  $\gamma = 1$ , define three domains. (a) Depression at one frequency; (b) entire line. Consult text for further explanation.

we proceed by means of Display 17.1, line 5, and readily find the equation given. The weak and strong lines in this column behave as in block 2.

The situation is different in the presence of damping wings, which make the  $\beta$  defined in block 2 infinite. The “weak” lines in the right column of block 3 must then form a transition between the linear law for very faint lines and the square root law for strong lines. The approximate form is obtained by assuming that the line–core formula (depression in Domain II) and the line–wing formula (depression in Domain I) are both valid all the way to the frequency where their values match. This happens at

$$\nu - \nu_0 = \pm (\kappa_0/4\kappa)^{1/2} \alpha = \pm x_1 \alpha$$

An elementary integration then gives for the equivalent width of the two wings combined

$$W_{\text{wings}} = 2C\alpha(\kappa_0/\sigma)^{1/2}$$

and for  $W_{\text{core}}$  the same expression with the extra factor

$$\text{arc sinh } x_1 = \ln [x_1 + (x_1^2 + 1)^{1/2}]$$

This is well above 1 but not extremely so. For instance,  $\kappa_0/\kappa = 25$  gives  $x_1 = 2.5$ ,  $\text{arc sinh } x_1 = 1.647$ , so that in this fairly extreme example the core has only 1.65 times the equivalent width of the wings. Anyhow, there is a slow (logarithmic) increase in the coefficient of the square root law. The simplest way to express this is to write the result again in the form of block 2;  $\beta$  then assumes the form given in block 3.

Although the results presented in Display 17.2 are more complete (in terms of the general phase function) than those presented in the published literature, they form by no means a ready program for computing the curve of growth. The transitions from one domain to another have not been treated, the Ladenburg-Reiche function  $F(z)$  being the only exception. Additional numerical work or approximation formulas will generally be needed to remedy this defect.

A good example of such a treatment, valid for isotropic scattering, is Chamberlain's 1970 paper, in which he consistently employs the approximation

$$H(a, \mu) = H(1, \mu) / \{1 + \mu[3(1 - a)]^{1/2}\}$$

for the  $H$  function, which has no errors exceeding 6% over the whole range of  $\mu$  and  $a$  (Chamberlain and McElroy, 1966).

Another procedure, if  $b = \infty$ , is to write  $I$  as the sum of its orders  $I_n$  (Uesugi and Irvine, 1970b). The universal form of  $p_n(\lambda)$  from line 10 is Display 17.1 then leads to certain simplifications. In particular, Fouquart and Lenoble (1973) have shown that the integrals containing the Ladenburg-Reiche function  $F(z)$  in the integrand can be expressed in terms of associated Legendre polynomials. The summation over the orders must be performed numerically, but known asymptotic behavior (Section 12.4.1) permits the sum  $n = N - \infty$  to be replaced by an integral expressible in the exponential integral. The reader is referred to the original paper for details.

We have resisted the temptation to add to Display 17.2 yet another block referring to finite atmospheres. The distinction of many cases would teach us nothing essentially new. In the limit of thick layers we approach the formulas already given. For thinner layers, with the presence of a diffusely reflecting bottom surface, we approach the situation in which  $W$  is essentially  $W(l)$ , where  $l$  is the unique path  $l = h(\mu^{-1} + \mu_0^{-1})$  where  $h$  is the geometric depth of the atmosphere.

### 17.3.3 Inferences from the Curve of Growth

The curve of growth is usually constructed from observational data, and its shape then reveals certain properties of the atmosphere. A proper warning is always: Don't jump to conclusions. This is particularly true in the diffuse reflection problem just described. For instance, in Display 17.2 two situations occur in which the curve of growth follows a square root law ( $W \sim S^{1/2}$ ). These situations (block 1, last column; block 2, first column) have nothing in common. The square root law arises for completely different reasons. Such a coincidence may warn us that it is generally hazardous to infer physical properties from a mere inspection of the curve of growth.

Examples of general studies, that might be applied to any planetary atmosphere, are in Lenoble (1966) and Chamberlain (1970). The general theory has been reviewed in Section 17.3.2. The actual history has been, however, that the theoretical developments have followed the demands posed by particular observations. This is illustrated in detail for the Venus absorption lines in Section 18.5.2.

A problem related to the curve of growth occurs when the spectrum contains many absorption lines that cannot be measured separately by the spectrograph employed. It is not necessary then to take recourse to one of the various models of band structure that have been worked out in the literature. Quite generally, it is possible to lump the lines together in order to construct the actual curve of growth (Arking and Grossman, 1972).

### REFERENCES

- Appleby, J. F., and Irvine, W. M. (1973). *Astrophys. J.* **183**, 337.  
 Arking, A., and Grossman, K. (1972). *J. Atmos. Sci.* **29**, 937.  
 Chamberlain, J. W. (1970). *Astrophys. J.* **159**, 137.  
 Chamberlain, J. W., and McElroy, M. B. (1966). *Astrophys. J.* **144**, 1148.  
 Fouquart, Y. (1974). In "Exploration of the Solar System" (A. Woszczyk and C. Iwaniszewska, eds.), I. A. U. Symp. 65, p. 171. Reidel, Dordrecht, The Netherlands.  
 Fouquart, Y., and Lenoble, J. (1973). *J. Quant. Spectrosc. Radiat. Transfer* **13**, 447.  
 Irvine, W. M. (1964). *Bull. Astron. Inst. Neth.* **17**, 266.  
 Irvine, W. M. (1966). *Astrophys. J.* **144**, 1140.  
 Irvine, W. M. (1967). *Astrophys. J.* **147**, 1193.  
 Ivanov, V. V., and Gutsabash, S. D. (1974). *Fiz. Atmos. Okeana* **10**, 851.  
 Lenoble, J. (1966). *J. Quant. Spectrosc. Radiat. Transfer* **8**, 64.  
 Nagirner, D. I. (1974). *Astrofizika* **10**, 445 [English transl.: *Astrophysics* **10**, 274 (1976)].  
 Stibbs, D. W. N., and Weir, R. E. (1959). *Mon. Not. R. Astron. Soc.* **119**, 512.  
 Uesugi, A., and Irvine, W. M. (1969). *J. Atmos. Sci.* **26**, 973.  
 Uesugi, A., and Irvine, W. M. (1970a). *Astrophys. J.* **159**, 127.  
 Uesugi, A., and Irvine, W. M. (1970b). *Astrophys. J.* **161**, 243.  
 Uesugi, A., Irvine, W. M., and Kawata, Y. (1971). *J. Quant. Spectrosc. Radiat. Transfer* **11**, 797.  
 van de Hulst, H. C. (1949). In "The Atmosphere of the Earth and Planets" (G. P. Kuiper, ed.). Univ. of Chicago Press, Chicago, Illinois.

## 18 Planets

Many of the techniques and numerical results presented in the preceding chapters have been developed with a view to interpreting observational data on the planets.

The sun has only nine planets, none of which correspond to a simple model. This disparity between model and reality has always been clear but has been demonstrated most strikingly by the close ups of Mars and Jupiter from space probes. Yet when specific phenomena are studied, the need continually arises for comparisons or checks based on certain simplified models. It is in this vein that the following calculations for a “model planet” must be understood.

For the same reason we refrain from a systematic review of the properties of the individual planets. A somewhat satisfactory treatment, in which the subject of light scattering would play at most a subordinate role, is far beyond the scope of this book.

### 18.1 INTEGRATION OVER THE PLANET'S DISK

#### 18.1.1 Phase Function of a Planet

Many observations refer to the radiation coming from the entire visible part of the planet, i.e., from the entire disk. Until 1940 instruments that permitted with satisfactory photometric accuracy a distinction between different parts of the planet's disk were rarely used. This situation has been greatly improved by observations both from spacecraft and by means of more powerful ground-based instruments. Still, in many routine observations and often in polarimetry



DISPLAY 18.1

The Planetary Phase Function

1. Step-by-step construction

Total flux emitted by sun	$4\pi S$	
Emitted by sun per steradian	$S$	
Arriving near planet per unit area	$S/r^2$	
Falling on a unit area of the planet's surface	$\mu_0 S/r^2$	
Reflected from a unit area of the planet's surface per steradian if Lambert's law were valid	$\mu_0 \mu S/\pi r^2$	
Reflected from a unit area of the actual planet's surface per steradian	$\mu_0 \mu SR(\mu, \mu_0, \varphi)/\pi r^2$	
Reflected from entire planet per steradian	$(S/\pi r^2) \int \mu \mu_0 R(\mu, \mu_0, \varphi) dO$	
Arriving from planet per unit area at earth	$(S/\pi r^2 \Delta^2) \int \mu \mu_0 R(\mu, \mu_0, \varphi) dO$	(1)
Arriving from sun per unit area at earth	$S/r_1^2$	(2)
Ratio of observed flux densities planet/sun	$(r_1^2/\pi r^2 \Delta^2) \int \mu \mu_0 R(\mu, \mu_0, \varphi) dO$	(1)/(2)
Difference of astronomical magnitude planet-sun	$-2.5^{10} \log[\text{ratio (1)/(2)}]$	
Sunlight intercepted by entire planet	$\pi b^2 S/r^2$	
If all of this were scattered isotropically we should receive per unit area at earth	$b^2 S/4r^2 \Delta^2$	(3)
Phase function $\times$ albedo of entire planet	$(4/\pi b^2) \int \mu \mu_0 R(\mu, \mu_0, \varphi) dO = F(\alpha)$	(1)/(3)

2. Derived and traditional quantities

Spherical albedo = Bond albedo	$A^* = \frac{1}{2} \int_0^\pi F(\alpha) \sin \alpha d\alpha = pq$
Geometric albedo	$p = \frac{1}{4} F(180^\circ)$
Phase integral	$q = 2 \int_0^\pi [F(\alpha)/F(180^\circ)] \sin \alpha d\alpha$

3. Comparison of planet with one particle

	Phase function	Albedo	Product
Any scattering particle (notation of Chapter 10)	$\Phi(\cos \alpha)$	$a$	$a\Phi(\cos \alpha)$
Any planet (notation of Chapter 18)	$F(\alpha)/A^*$	$A^*$	$F(\alpha)$

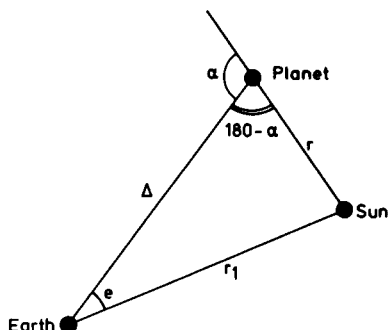


**Fig. 18.1.** Distances and angles in planetary observation;  $\alpha$  is the scattering angle,  $180 - \alpha$  the phase angle (standard astronomical term),  $e$  the elongation (standard astronomical term).

and spectrophotometry, the observer is content to obtain integrated-disk measurements. A similar integration of the diffusely reflected radiation over the planet's disk is then required in the model computations. This task involves simple geometry only, but it proves to be tedious, both in analytic and in numerical integrations.

In order to obtain the right factors, it appears best to follow definitions step by step (Display 18.1). The large-scale geometry in the sun-earth-planet triangle is shown in Fig. 18.1. Note that the phase angle (most widely used) is the supplement of the scattering angle (which we use).

All quantities in Display 18.1 are per unit time in a chosen (narrow or wide) frequency interval and may be expressed in arbitrary (luminosity or energy) units.

The ratios (1)/(2) and (1)/(3) are independent of the choice of units. The ratio (1)/(2) corresponds to the classical practice of measuring the magnitude difference between the planet and the sun. Size and distances enter into this comparison. Often  $r$  and  $\Delta$  are already replaced by  $r_1 = 1$  astronomical unit, before the observations are published. The ratio (1)/(3) =  $F(\alpha)$  is of direct theoretical interest, for it yields the phase function of the planet regarded as one big "particle." Note, however, the difference in notation spelled out in Section 3 of Display 18.1.

Section 2 of Display 18.1 defines three quantities with their traditional names (Harris, 1961; Tomasko, 1976). We return to the spherical albedo in Section 18.1.2. The geometric albedo  $p$  is the directly measurable quantity for a planet in opposition. The factor  $\frac{1}{4}$  arises from the traditional choice of a flat white disk for reference. Not separately named is the ratio  $F(\alpha)/F(180)$ , which is the classical phase function normalized to 1 at opposition. Integration of this function over all phase angles as shown gives the phase integral  $q$ , and the product  $pq$  gives again  $A^*$ .

Our aim in this section is to derive  $F(\alpha)$  of the entire planet if the reflecting properties of each part of its surface (or cloud cover) are known. This requires

an integration over the disk. The result is independent of the size of the planet. We have three options in performing this integration.

#### OPTION (1): BY PLANETARY COORDINATES

With this choice the element  $dO$  is simple and so are the integration limits. Introduce longitude  $\zeta$  and colatitude  $\eta$  as shown in Fig. 18.2. We follow Horak (1950) with the only difference in notation being that  $\alpha$  has been replaced by  $180 - \alpha$ . Express  $\mu$ ,  $\mu_0$ , and  $\varphi$  in these coordinates by spherical geometry. We find

$$0 \leq \alpha \leq \pi, \quad 0 \leq \eta \leq \pi, \quad \pi/2 - \alpha \leq \zeta \leq \pi/2$$

$$\cos \beta = -\cos(\alpha + \zeta) \sin \eta, \quad \cos \theta = \cos \zeta \sin \eta$$

$$\cos \varphi = (\cos \beta \cos \theta + \cos \alpha) / \sin \beta \sin \theta, \quad \sin \varphi = \sin \alpha \cos \eta / \sin \beta \sin \theta$$

$$dO/b^2 = \sin \eta \, d\eta \, d\zeta$$

and with these formulas the integral in Display 18.1 can be computed.

#### OPTION (2): BY THE ANGLES $\beta$ AND $\theta$

In each half segment (north and south of the equator) the point  $P$  is uniquely defined by  $\beta$  and  $\theta$ . With these coordinates the integrand has a simpler form and the element  $dO$  is simply  $dO = b^2 \, d\beta \, d\theta \sin \varphi$ . However, the limits in the  $\beta$ ,  $\theta$  plane are not simple.

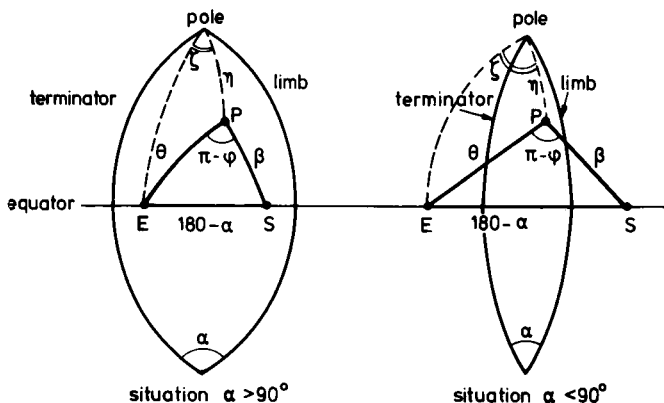


**Fig. 18.2.** Planet illuminated by sun. The visible, illuminated segment of the planet's surface is shown. The same drawing represents the surface of the unit sphere, where distances are angles.  $P$  is an arbitrary point,  $S$  the subsolar point,  $E$  the subearth point, i.e., the center of disk,  $SE = 180 - \alpha$  the phase angle,  $\alpha$  the scattering angle for first-order scattering sun-planet-earth,  $\varphi$  the azimuth angle of local diffuse reflection.  $\cos \beta = \cos PS = \mu_0$  is the cosine of angle of incidence.  $\cos \theta = \cos PE = \mu$  is the cosine of angle of emergence. Terminator = shadow limit,  $90^\circ$  from  $S$ , equation  $\mu_0 = 0$ . Limb = viewing limit,  $90^\circ$  from  $E$ , equation  $\mu = 0$ .

## COMPARISON OF OPTIONS (1) AND (2)

A point in favor of option (2) seems to be that  $F(\alpha)$  has the form

$$F(\alpha) = \int_0^1 d\mu \int_0^1 d\mu_0 W(\alpha, \mu, \mu_0) R[\mu, \mu_0, \varphi(\alpha, \mu, \mu_0)]$$

where the weighting function  $W$  could be tabulated or programmed once, to be used with various assumptions about the reflection function  $R$ . However, the form is not particularly convenient, nor does Fourier analysis in  $\varphi$  lead to significant simplifications.

In numerical tests Hovenier and Hansen (private communication) did not find a clear advantage of one of the options (1) or (2). They used Horak's equations because these were readily available.

Option (3) is based on the determination of the expansion of  $F(\alpha)$  in terms of Legendre functions. To my knowledge it has not been used in practical computation, but it may well have certain advantages over options (1) and (2). Its derivation (Section 18.1.3) is best preceded by the discussion of spherical albedo.

## 18.1.2 Spherical Albedo

The function  $F(\alpha)$  is known for the outer planets over a limited range of  $\alpha$  near  $180^\circ$  ( $\pi - \alpha$  near 0). For Venus and Mercury it can be measured over the full range. On the assumption of spherical symmetry of the planet, the knowledge of the full phase function can be used to find the total fraction of incident light reflected in all directions together. This is the Bond albedo or spherical albedo  $A^*$ . Following the definitions of Display 18.1, we have

$$A^* = \frac{1}{2} \int_0^\pi F(\alpha) \sin \alpha d\alpha$$

There has been a misconception (Horak, 1950; Harris, 1961) that the  $A^*$  for a model planet can be obtained only by computing  $F(\alpha)$  first. Instead, we may equally well take the simpler route:

$$A^* = URU = \int_0^1 \int_0^1 R(\mu, \mu_0) 4\mu\mu_0 d\mu d\mu_0$$

where

$$R(\mu, \mu_0) = \frac{1}{2\pi} \int_0^{2\pi} R(\mu, \mu_0, \varphi) d\varphi$$

Numerical values have already been given for many assumptions in earlier chapters. We also refer to Fig. 12.5.

An elegant "physical" proof that  $A^* = URU$  is the following (van de Hulst, 1974).  $A^*$  is defined as the fraction of incident flux reflected from the entire

planet upon illumination from one direction (the sun). This fraction will not change if we put yet another sun in the sky, nor if we cover (as a mathematical exercise) the sky with suns. Each area of the planet is then exposed to uniform illumination. The fraction of incident flux reflected from this area, and hence for the entire planet, is  $URU$  by definition. The clearest explanation in the earlier literature is by Russell (1916).

Three integrations are thus necessary to go from  $R(\mu, \mu_0, \varphi)$  to  $A^*$ . One route is to first make the two integrations (over  $\varphi$  and  $\mu$ ) which lead to the plane albedo

$$UR(\mu_0) = \int_0^1 R(\mu, \mu_0) 2\mu d\mu$$

and then to proceed by integration over  $\mu_0$  to find  $A^*$ . The alternative route is to make the first integrations over two coordinates on the planet for finding  $F(\alpha)$  and then to make the final integration over  $\alpha$  in order to find  $A^*$  as defined above. This route corresponds to the traditional formula  $A^* = pq$  (see Display 18.1).

### 18.1.3 Other Integrals over the Phase Function

Represent the integration domain just described by a cubic box in a three-space with coordinates  $\mu^2$ ,  $\mu_0^2$ , and  $\varphi/\pi$ , each going from 0 to 1. To each point in this box belongs a value of  $R(\mu, \mu_0, \varphi)$  and a value of  $\alpha$ . The values  $\alpha = \text{const}$  are found on closed surfaces and for curiosity some of them are sketched in Fig. 18.3; they contract into a point at  $\alpha = 0^\circ$  and into a line at  $\alpha = 180^\circ$ .

From the expressions just derived, we see that  $A^*$  is the integral of  $R(\mu, \mu_0, \varphi)$  over the box, and  $\frac{1}{2} \sin \alpha F(\alpha) d\alpha$  the integral of  $R(\mu, \mu_0, \varphi)$  over the volume of the box enclosed between the surfaces  $\alpha$  and  $\alpha + d\alpha$ . (The same result may be derived from the definition in Display 18.1.)

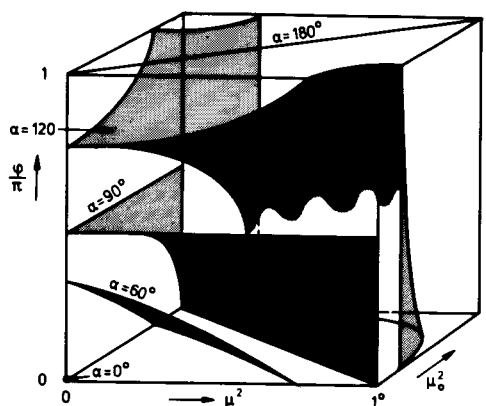


Fig. 18.3. Integration box for planetary reflection.

Now consider the integral over the box

$$\begin{aligned} C_n &= \frac{1}{2} \int_0^\pi P_n(\cos \alpha) F(\alpha) \sin \alpha \, d\alpha \\ &= \int_0^1 \int_0^1 \int_0^1 P_n(\cos \alpha) R(\mu, \mu_0, \varphi) \, d(\mu^2) \, d(\mu_0^2) \, d(\varphi/\pi) \end{aligned}$$

which differs from the integral defining  $A^*$  by the insertion of the  $n$ th order Legendre polynomial  $P_n(\cos \alpha)$ . By the addition theorem for Legendre functions we have (signs based on definitions in Fig. 18.2)

$$(-1)^n P_n(\cos \alpha) = P_n(\mu) P_n(\mu_0) + 2 \sum_{m=1}^n (-1)^m \frac{(n-m)!}{(n+m)!} P_n^m(\mu) P_n^m(\mu_0) \cos m\varphi$$

Further we use the Fourier expansion of  $R(\mu, \mu_0, \varphi)$  given in Section 15.1.5. The periodic terms in  $\varphi$  cancel out upon integration and we are left with the (apparently new) relation:

$$\begin{aligned} C_n &= (-1)^n \int_0^1 \int_0^1 P_n(\mu) P_n(\mu_0) R(\mu, \mu_0) A \mu \mu_0 \, d\mu \, d\mu_0 \\ &\quad + 2 \sum_{m=1}^n (-1)^{n-m} \frac{(n-m)!}{(n+m)!} \int_0^1 \int_0^1 P_n^m(\mu) P_n^m(\mu_0) R^m(\mu, \mu_0) A \mu \mu_0 \, d\mu \, d\mu_0 \end{aligned}$$

where  $C_0 = A^*$ , the spherical albedo.

OPTION (3): FINDING  $F(\alpha)$  VIA  $C_n$

An attractive third way of computing the phase function  $F(\alpha)$  of the planet now appears: Compute  $C_n$  by means of the equation just given; then find

$$F(\alpha) = \sum_{n=0}^{\infty} (2n+1) C_n P_n(\cos \alpha)$$

In this method no awkward geometry enters; the main burden of the computation is in finding  $C_n$ . An advantage may be that the relations between certain details in the phase function of the planet and certain details in the reflection function, or the scattering pattern of the individual atmospheric particles, become more transparent.

### 18.1.4 Simple Examples of Planetary Phase Functions

#### A. WHITE PLANET FOLLOWING LAMBERT'S LAW

Consider a planet whose surface at each point behaves like a perfectly white diffusely reflecting surface according to Lambert's law. This example has much wider use than for planets alone. Randomly oriented white particles of convex

form (e.g., chalk dust) have in the mean the same scattering pattern. Direct integration gives

$$R(\mu, \mu_0) = 1, \quad R^m(\mu, \mu_0) = 0 \quad \text{for } m \geq 1$$

$$F(\alpha) = (8/3\pi)(\sin \alpha - \alpha \cos \alpha)$$

This equation may be two centuries old; it used to be given with argument  $\pi - \alpha$  (Schoenberg, 1929). The first expansion coefficients, found either by direct integration from the given form of  $F(\alpha)$ , or from  $C_n = (-1)^n [\int_0^1 P_n(\mu) 2\mu d\mu]^2$  are  $A^* = C_0 = 1$  (spherical albedo);  $C_1 = -\frac{4}{9}$ ,  $C_2 = \frac{1}{16}$ ,  $C_3 = 0$ ,  $C_4 = \frac{1}{576}$ , ... Note that backscattering predominates, because the planet in its "full" phase is brighter than when it is seen as a crescent. Accordingly, the asymmetry factor  $g = \langle \cos \alpha \rangle = C_1 = -\frac{4}{9}$  has a negative value. The fraction of the radiation scattered into the backward hemisphere is  $\frac{5}{6}$ . Numerical values are in Table 58.

Lambert's law assumed here is not a bad approximation of a sandy or rocky surface. For that reason the "bare" planets and satellites, i.e., the moon, Mercury, and the asteroids, have a phase curve somewhat similar to that of a white sphere. The most striking differences are the following:

- (1) an albedo much smaller than 1.
- (2) an even more enhanced peak at opposition. This "opposition effect" is often ascribed to crevices in the surface, although aerosols may also produce such an effect (Mead, 1970).
- (3) a small amount of polarization.

#### B. NEARLY BLACK PLANET (LOMMEL-SEELIGER LAW)

Consider a planet fully covered with a homogeneous, optically thick atmosphere. Assume isotropic scattering with an albedo  $a \ll 1$ . Then higher powers of  $a$  may be neglected. The planet looks almost black, and its phase function may be computed from the first-order reflection only:

$$R(\mu, \mu_0) = a/4(\mu + \mu_0)$$

This equation is obtained from Display 9.1, with  $b = \infty$ , or from Display 8.1, with  $H(a, \mu) = 1$ . Without any justification it has often been assumed (a century ago) that this dependence of  $\mu$  and  $\mu_0$  might still be correct for arbitrary values of  $a$ . The reflection law thus defined is known as the law of Lommel-Seeliger. This law is only of historical interest, except in the limit of very small  $a$ , where it corresponds to a physically consistent but rarely needed model.

The phase function of the planet, corresponding to this law according to the theory in Sections 18.1.1 and 18.1.2, is found in the classical astrophysical literature (Schoenberg, 1929, pp. 63–65 and Table VIa). Transcribed into our notation:

$$F(\alpha) = \frac{a}{2} \left[ 1 + \frac{\cos^2(\alpha/2)}{\sin(\alpha/2)} \ln \tan \frac{\pi - \alpha}{4} \right]$$

A computation of the expansion coefficients starting from  $F(\alpha)$  is tedious. More easily we may use the exact expressions in terms of bimoments of the reflection function given for arbitrary  $a$  in the example which follows. For  $a \ll 1$  (Lommel-Seeliger law) they reduce to  $F$  functions (Sections 2.5 and 8.4). The exact results are

$$C_0 = \frac{2}{3}a(1 - \ln 2), \quad C_1 = \frac{1}{3}a(1 - 2 \ln 2), \quad \text{etc.}$$

Numerical values are given in Table 58. As a curiosity we add that Blättner's (1972) quantity  $p(\varphi)$  corresponds to our  $F(\alpha)/4\pi C_0$ , and that his numerically determined factor 0.61104 accurately matches the exact value  $3/[16(1 - \ln 2)]$ .

#### C. PLANET COVERED WITH A THICK, ISOTROPICALLY SCATTERING ATMOSPHERE

This is an obvious practice problem, but very few numerical results are found in the literature. Horak (1950) gives for  $a = 0.95$  and  $a = 0.975$  a list of values of  $j(\alpha)/F$ , which upon multiplication by  $4/\pi$  give  $F(\alpha)$ . Hansen (private communication) has checked the values for  $a = 0.95$  with a finer mesh in the numerical integration and finds that many of Horak's values are too high by 0.2–0.1%. The same difference is found by a direct integration of the value for opposition

$$F(180^\circ) = a \int_0^1 H^2(a, \mu) \mu \, d\mu$$

The numerical integration can be eased by subtracting out  $H_{\text{approx}}^2(a, \mu)$  using a linear or quadratic approximation representing  $H(a, \mu)$  well for  $\mu$  near 1, for which Table 7 (Section 8.3.1) gives the necessary data. Talley and Horak (1956) present a crude computation for  $a = 1$ . The best data available to the author are collected in Table 58.

The first coefficients of the expansion of  $F(\alpha)$  in spherical harmonics may be taken for arbitrary  $a$  from Table 9 (Section 8.4). By the definitions of that section we have

$$\begin{aligned} C_0 &= URU = o_{11} \\ C_1 &= -\frac{4}{3}o_{22} \\ C_2 &= \frac{1}{4}(o_{11} - 3o_{13} + \frac{9}{4}o_{33}) \\ C_3 &= -o_{22} + 2o_{24} - o_{44} \end{aligned}$$

#### D. THICK ATMOSPHERE WITH LINEARLY ANISOTROPIC SCATTERING

For a few numerical examples, see again Horak (1950) and Harris (1961, Tables 24 and 25).

#### E. PLANET COVERED WITH A RAYLEIGH SCATTERING ATMOSPHERE

Tables showing intensity and polarization as a function of phase angle, computed by numerical integration over the disk and supported by checks from



TABLE 58  
Phase Function of "Model Planets"

		$F(\alpha)$ for thick atmosphere, isotropic scattering						
		$a \ll 1$ (Lommel-- Seeliger)	$a = 0.8$	$a = 0.95$	$a = 0.975$	$a = 0.99$	$a = 1$	
$\alpha$	$F(\alpha)$ for white sphere (Lambert)							
Opposition or inferior conjunction (full planet)								
180	2.667	0.5000 <i>a</i>	0.871	1.569	1.85	2.138	2.759	
170	2.628	0.4881 <i>a</i>	—	—	—	—	2.710	
160	2.518	0.4627 <i>a</i>	—	1.467	1.77	—	2.58	
150	2.349	0.4296 <i>a</i>	—	—	—	—	—	
140	2.134	0.3920 <i>a</i>	—	1.233	1.45	—	2.16	
130	1.888	0.3516 <i>a</i>	—	—	—	—	—	
120	1.624	0.3100 <i>a</i>	—	0.944	1.11	—	1.58	
110	1.355	0.2682 <i>a</i>	—	—	—	—	—	
100	1.093	0.2275 <i>a</i>	—	0.652	0.76	—	1.07	
90	0.8488	0.1884 <i>a</i>	—	—	—	—	—	
80	0.6302	0.1518 <i>a</i>	—	0.398	0.46	—	0.619	
70	0.4430	0.1181 <i>a</i>	—	—	—	—	—	
60	0.2907	0.0880 <i>a</i>	—	0.202	0.23	—	0.294	
50	0.1741	0.0604 <i>a</i>	—	—	—	—	—	
40	0.0917	0.0400 <i>a</i>	—	0.078	0.09	—	0.102	
30	0.0395	0.0226 <i>a</i>	—	—	—	—	—	
20	0.0119	0.0101 <i>a</i>	—	0.015	—	—	0.0179	
10	0.0015	0.0027 <i>a</i>	—	—	—	—	—	
Superior conjunction (crescent phase)								
0	0	0	0	0	0	0	0	

Expansion coefficients	$C_0$	1	0.2046a	0.3419	0.5967	0.695	0.7946	1
	$C_1$	-0.4444	-0.0773a	-0.1384	-0.2521	-0.298	-0.3458	-0.4472
	$C_2$	+0.0625	+0.0072a	—	—	—	—	+0.0705
	$C_3$	0	-0.0018a	—	—	—	—	-0.0042
	$C_4$	+0.0017	+0.0006a	—	—	—	—	+0.0021
Asymmetry $g = C_1/C_0$		-0.444	-0.378	-0.405	-0.422	-0.428	-0.435	-0.447
Normalized opposition value $4/q = F(180)/C_0$		2.667	2.444	2.548	2.629	2.660	2.691	2.759
Geometrical albedo $p = \frac{1}{4} F(180)$		0.667	0.125a	0.218	0.392	0.462	0.534	0.690
Phase integral $q = C_0/p$		1.500	1.637	1.570	1.521	1.504	1.486	1.450

Monte Carlo computation, are given by Kattawar and Adams (1971) for optical thickness 0.2, 0.5, 1, 5, and 10 and various values of the ground albedo.

#### F. INTERCOMPARISON

We list in Table 58 the available numbers and also the asymmetry parameter  $g = C_1/C_0$  of the model planet, considered as one scattering particle. The fact that the light reflected from the planet is much stronger in opposition (full phase) than in the crescent phase leads to a negative  $g$  near  $-0.4$  in each example. The differences are as expected: the Lommel-Seeliger law has a relative bias in favor of grazing angles and hence the smallest asymmetry.

There is a trend toward increasing asymmetry with increasing  $a$ . The same trend is recognized in the normalized opposition values shown in the last line of Table 58.

#### 18.1.5 Venus Phase Curve and Polarization

Venus can be observed over nearly the full range of phase angles  $0-180^\circ$ . Suppose we have for a planet complete, well calibrated integrated disk measurements, which means that the function  $F(\alpha)$  of the planet is known. Suppose further that the planet is covered with a very thick, homogeneous cloud cover. Does the observed function  $F(\alpha)$  then completely determine the (average) albedo  $a$  for single scattering and phase function  $\Phi(\alpha)$  of the cloud particles? This academic question must probably be answered with yes. For the part of  $F$  that arises from first-order scattering would, if it were known separately, certainly give the answer, because it is directly proportional to  $\Phi$ . The higher order contributions must vary too weakly with variations in the adopted  $\Phi$  to spoil this determination. Similarly, if polarization is involved, the observed polarization curve of the planet certainly determines the (average) polarization properties of the cloud particles uniquely.

The problem thus defined requires model fitting of some kind for its actual solution. It has proved practical to divide the problem into three steps:

- (i) to match the spherical albedo  $A^*$ ,
- (ii) to match the phase curve  $F(\alpha)$  disregarding polarization, and
- (iii) to match the polarization curve.

The reason for separating the first point is that the similarity law on the spherical albedo is so nearly perfect that we cannot hope to infer the values of  $a$  and  $g$  separately from  $A^*$  alone. Instead, the observed  $A^*$  defines a curve in the  $(a, g)$  domain on each point of which the match is good (Fig. 12.5). Recent writers have used this knowledge to find at once with any trial particle phase function the  $a$  to be adopted. This saves time, because it reduces the number of tries necessary.

TABLE 59

Constants Necessary to Match the Observed Spherical Albedo and Polarization Curve of the Planet Venus Assuming a Homogeneous, Semi-Infinite Atmosphere<sup>a</sup>

Wavelength	Refractive index $n$	Asymmetry factor $g$	Observed spherical albedo $A^*$	Derived single-scattering albedo $a$
Infrared 990 nm	1.43	0.715	0.90	0.99941
Yellow 550 nm	1.44	0.718	0.87	0.99897
Ultraviolet 365 nm	1.46	0.761	0.55	0.98427

<sup>a</sup> Hansen and Hovenier, 1974

Hansen and Hovenier (1974) use the simpler relation

$$1 - a = (1 - a^{\text{iso}})(1 - g)$$

which dates back to earlier work and which is a good approximation if  $a$  is near 1 (cf. Section 14.1.1). Here  $a^{\text{iso}}$  is the value of single-scattering albedo that would have to be adopted to match the observed  $A^*$  by isotropic scattering. Table 59 shows their final numbers. Here the particle size and refractive index, and hence  $g$ , follow essentially from the polarization (see below), and the  $a$  then follows from the observed  $A^*$  as explained above. This approximation to  $a$  differs little from the value found by the formula in Section 12.2.3. The last decimal of  $a$  is hardly significant. The assumed distribution function of particle radii  $r$  was

$$n(r) = \text{const } r^{(1-3b)/b} e^{-r/cb}$$

with fitted values  $c = 1.05 \mu\text{m}$ ,  $b = 0.07$ . It is interesting to compare the values given in Table 59 with those given in the older literature. See reviews by Arking and Potter (1968), Hansen and Hovenier (1974), and Sobolev (1975, Chapter 10). The adopted values of  $g$  vary widely and so do the values of  $a$ , but when collected in a graph the  $(a, g)$  combinations for each wavelength nicely follow the curve  $A^* = \text{const}$ .

The separation between steps (ii) (phase function) and (iii) (polarization) again has a practical reason. The phase function is observed by means of photometry under varying twilight conditions and without a suitable object of comparison so that it is hard to reach an accuracy of a few percent. The polarization can be measured with far greater accuracy. Errors smaller than 0.1 % in the degree of polarization have been standard practice since the pioneer measurements by Lyot, which started more than fifty years ago. For a good review of observations and interpretation see Coffeen and Hansen (1973).

The polarization (in single scattering) carries a clear signature of particle size and of particle refractive index, as is explained in detail by Hansen and Travis (1974), and is well illustrated by the example shown in Fig. 10.4.

For these reasons the most demanding job is to find a model that matches the observed polarization curve. If this job is completed, it remains to verify

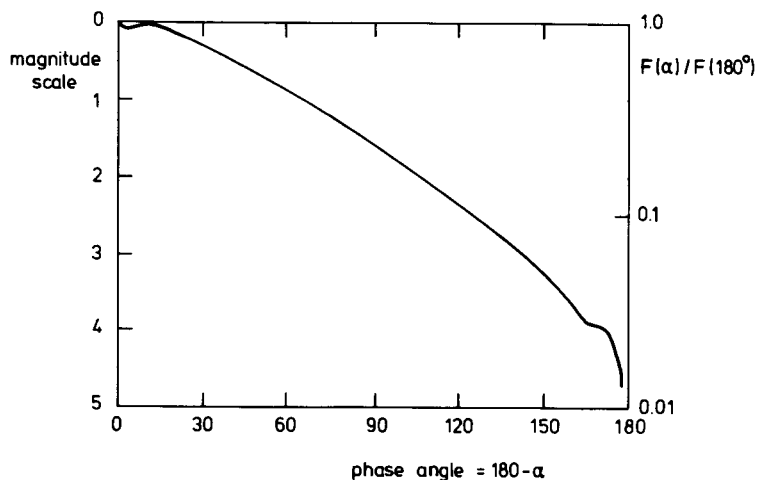


**Fig. 18.4.** Computed phase function of Venus corresponding to the best fit to the polarization measurements (from Hansen and Travis, 1974, Fig. 25 or 27).

that the phase function of the planet following from this model does not come into conflict with the observed phase function. In the work of Hansen and Hovenier (1974) this check came out so well that it was not documented separately. The phase curve corresponding to their finally adopted model (Hansen and Travis, 1974) is reproduced in Fig. 18.4. We shall report further only on the polarization.

Lyot (1929) interpreted his Venus measurements by means of two simplifying assumptions: All polarization is due to single scattering, and the intensity ratio of total scattering to first-order scattering is about a factor 3. Both assumptions were extremely crude and did not do justice to the accuracy of the observations. For instance, it can be seen from Table 38 (Section 13.1) that the ratio of total to first-order scattering is not at all constant. The first real progress was made by Hovenier (1971) and Hansen (1971a), who independently applied the doubling method, computed the azimuth-dependent terms, and performed the integration over the disk to reach a model computation with the required accuracy of better than 0.1%. This method led to the provisional conclusion (Hansen and Arking, 1971) that the refractive index of the cloud particles for visual light must be very close to 1.45. Since then many further models were computed in a joint effort. Details of the method are given by Hansen and Hovenier (1971). In a comprehensive discussion of the observational material at all wavelengths, Hansen and Hovenier (1974) conclude that the particles are spherical, remarkably homogeneous in size, with refractive index ranging from 1.43 in the near infrared to 1.46 in the near ultraviolet, and that they probably consist of a concentrated solution of  $\text{H}_2\text{SO}_4$ . Figure 18.5 shows as an example the sensitivity to size; the best fit with the size distribution cited earlier in this section was obtained with  $c = 1.05 \mu\text{m}$ ,  $b = 0.07$ .

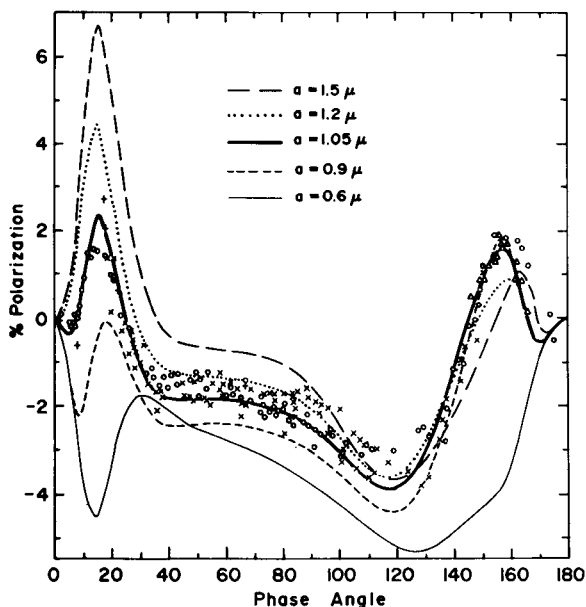


Fig. 18.5. Polarization of sunlight reflected by Venus in the visual wavelength region. Separate symbols show observations from four authors. The different theoretical curves show the influence of the effective radius in the assumed size distribution. All are for refractive index, 1.44,  $\lambda = 0.55 \mu\text{m}$ , and include a Rayleigh contribution (from Hansen and Hovenier, 1974).

Hansen and Hovenier (1974) also include Rayleigh scattering in their model calculations. Because of the  $\lambda^{-4}$  dependence, this is most noticeable towards the ultraviolet. Assuming for convenience a homogeneous mixing of cloud particles and gas, they find that the ratio of extinction by Rayleigh scattering to extinction by cloud particles is 0.045 at  $0.365 \mu\text{m}$ . With a plausible vertical structure of the atmosphere this leads them to a pressure of  $50 \pm 25$  mbars at  $\tau = 1$ , i.e., near the cloud tops. This means that we see only very high cloud layers in the Venus atmosphere. Further observations, including those at other wavelengths, are reviewed by Coffeen and Hansen (1973). The polarization in the ultraviolet is more variable than at visual wavelengths. This is probably connected with the existence of variable “ultraviolet markings,” which may be nothing but variations in cloud height.

Although the work just described is excellent, it leaves us in one respect dissatisfied. Lyot's assumption of attributing the polarization exclusively to single scattering was elegant but too crude. Hansen and Hovenier's method is accurate but can only be performed with a huge amount of computer time. Is there not between these extremes some other method that combines relative simplicity with sufficient accuracy?

The present answer to this question is negative. For instance, the method advocated by Sobolev (1968, 1975) may estimate the magnitude of the higher order scattering more exactly than Lyot's, but still has no guaranteed accuracy.

On the other side a number of avenues to cut short the full doubling have been explored or are still open, with no guarantee that any of these leads to real savings in programming or computing time. We mention four of these:

(a) Hovenier (1971) noticed that while the polarization of second and third order scattering was by no means zero, the successive orders in the Stokes parameter  $Q$  converged much more rapidly than those of the intensity. His "novel approximation" consists of computing at least two orders of  $Q$  and finding the sum, on the assumption that the remaining terms form a geometric series with the ratio  $Q_2/Q_1$ . Hansen and Travis (1974) showed that the same method applied to four computed terms yielded accuracies of 0.2% or better. No theoretical basis for this approximation has been found.

(b) The rapid convergence is reminiscent of the rapid convergence we noticed in the azimuth-dependent terms in the absence of polarization (see Section 15.1.1 and Fig. 15.2). Exploring this analogy might lead to better insight.

(c) The CP representation of polarized light has been explored for theoretical work (see explanation and references in Section 15.1.2) but hardly at all for practical numerical computations. Dr. Hovenier pointed out to me that an analogy exists between the CP representation in dealing with polarized phase matrices and the Legendre function expansion in dealing with unpolarized phase functions. Systematic use of this expansion with a realistic phase matrix is thus likely to require an effort out of proportion with the results, in analogy with the final conclusion of Section 6.1.

(d) More directly appealing to our physical understanding is the following consideration. We may arbitrarily write the Venus particle phase matrix as the sum of an unpolarized strongly forward-directed phase function and a polarized phase matrix with a less elongated diagram. The second-order light then contains many photons which have suffered one minor deviation by the first part and a major deviation by the second part (in this or the reverse order). If we schematically replace the first part by a forward peak—and the examples in Chapters 12 and 14 show that this usually leads to similar results—this second-order contribution would have exactly the same polarization pattern as the first order. This probably explains why the actual second order shows a similar polarization curve as the first order and perhaps it gives a clue to their ratio. Hansen (1971b) worked out a method of this type. He concluded that it was no more work than the first-order approximation, clearly better but still not accurate enough for most purposes.

## 18.2 PRACTICAL USE OF THE RECIPROCITY PRINCIPLE

In a famous paper Minnaert (1941; see also Minnaert, 1961) called attention to the practical use of the reciprocity principle in planetary photometry. This topic, which applies equally well to bare planets as to planets covered with a

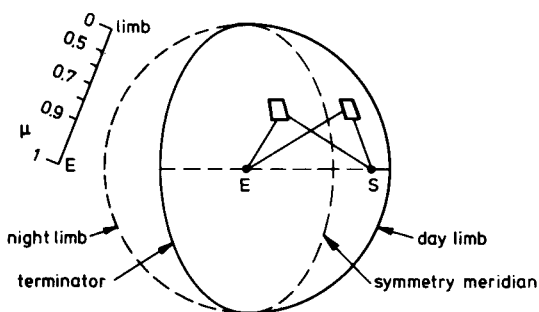


**Fig. 18.6.** Reciprocity in planetary observation. The visible and illuminated segment of the planet has symmetry around the symmetry meridian, with  $S$  and  $E$  in symmetric positions. The two drawn rectangles on the face of the planet are equally large and in symmetric positions and carry by diffuse reflection the same flux from the sun to the earth. The rectangle which is seen narrower has a proportionally larger brightness. The scale of  $\mu$  (cosine of viewing angle) can be fitted along any radius from  $E$ .

thin or thick atmosphere, must precede any discussion of the light distribution across the planet's disk.

The visible hemisphere has at its center the sub-earth point  $E$ . The illuminated hemisphere has at its center the sub-sun point  $S$ . These hemispheres overlap in a symmetric segment on the planet's surface, bounded at one side by the limb and at the other side by the terminator (Fig. 18.2). The meridian which cuts it into halves will be called the symmetry meridian.

The projection of this segment, as seen on the face of the planetary disk, is not symmetric (Fig. 18.6). Let the points  $A$  and  $B$  have symmetric positions (in space) with respect to the symmetry meridian, and let the radiance observed at these points (in any photometric system) be  $I_A$  and  $I_B$ . Let the cosines of the viewing direction with the normal at these points be  $\mu_A$  and  $\mu_B$ . Then, if the surface properties in  $A$  and  $B$  are the same, on the basis of the reciprocity principle:

$$I_A \mu_A = I_B \mu_B$$

The most attractive derivation goes back to fundamentals. Place an isotropic (unpolarized) point source at the sun and an isotropic (total-intensity) detector at the earth. The flux carried from one to the other through a certain area near  $A$  will remain the same if source and detector are interchanged. Then rotate by  $180^\circ$  and assume symmetry about the equator. The conclusion then is that the flux carried from sun to earth through the rectangle near  $A$  is the same as carried through the rectangle near  $B$ . The projected areas are in the proportion  $\mu_A/\mu_B$ . Hence the surface brightness, or specific intensity, obeys the stated relation.

In an alternate, more formal derivation we call the flux from the sun arriving per unit area near the planet  $\pi$ . We then have by definition (Chapter 1; Section 18.1.1):

$$I_A = \mu_B R(\mu_A, \mu_B, \varphi), \quad I_B = \mu_A R(\mu_B, \mu_A, \varphi)$$



where the angle  $\varphi$  is the same in magnitude and sign. We must then argue that

$$R(\mu_A, \mu_B, \varphi) = R(\mu_B, \mu_A, -\varphi) = R(\mu_B, \mu_A, \varphi)$$

The first equal sign expresses the reciprocity principle (Section 3.4.1). The second equal sign involves a symmetry assumption, which is normally fulfilled.

The function of this principle in planetary photometry is that it is possible to find four points (two above and two below the equator) where the photometry may be directly compared. Only physical differences between those points, e.g., arising from different surface materials or from daily or seasonal changes in the atmosphere, can spoil the relation.

Minnaert proceeds to show that several of the empirical photometric laws suggested in the literature violate the reciprocity principle. He suggests trying a new empirical relation

$$I\mu = \text{const} (\mu\mu_0)^k$$

which obeys the reciprocity rule and has since been successfully applied to describe photometric data on the moon, Mars, Jupiter, and Saturn (see further Section 18.3.1). The plots of  $\log(I\mu)$  against  $\log(\mu\mu_0)$ , from which the constant  $k$  may be read as the slope, are known as "Minnaert plots." The Lambert law has  $k = 1$ .

The reciprocity principle cannot, strictly, be used in this form for checking the degree of polarization. Since measuring the polarization requires putting a polarizer in the beam near the earth, the strictly reciprocal experiment requires putting a polarizer in the beam near the sun, which is impossible. Compare Section 3.4.1 and Hovenier (1969, 1970) for the full symmetry relations for polarized light. Notwithstanding, we may in practice expect that the degrees of polarization of the radiation received from  $A$  and from  $B$  are *very nearly* the same. That this is so is demonstrated for a thick atmosphere with Rayleigh scattering by the examples presented in Section 16.3.4. There is no reason to expect that it would fail to be true for other phase matrices. Compare Kawabata and Hansen (1975).

The symmetry relations for circular polarization are contained in the papers of Hovenier just cited. Sazonov (1972) also derives the conditions under which circular polarization of the reflected radiation may occur and puts them in the form of two symmetry relations, the polar effect and the opposition effect. The scanty observations yet available seem to obey these relations. Although Sazonov does not refer to the older literature, his recommendation about the use of these relations is quite similar to Minnaert's recommendation about the use of Helmholtz's reciprocity principle. If the observation of a planet should violate one of these relations, this would demonstrate that one of the assumptions is not fulfilled. Conservatively, this might mean that the atmospheric conditions at the reciprocal sites are not identical. Sazonov jumps instead to the conclusion that the assumption about the absence of magneto-optic molecules in surface or atmospheres would not be fulfilled and, since such molecules are usually associated with life, that this would be a simple way to detect a sign of life on a planet.

## 18.3 A PLANET IN OPPOSITION

## 18.3.1 Intensity Distribution on Disk

The outer planets can be observed from earth only near opposition. Opposition occurs when the planet and the sun, as seen from the earth, have longitudes that differ by  $180^\circ$ . If the latitudes were also equal and opposite, we would have the situation of "precise opposition," in which the light source (the sun) and the observer (the earth) are seen from the planet in exactly the same direction. The observed intensity is then a function of  $\mu$ , the cosine of the angle of incidence, only, and is generally expressed by

$$I(\mu) = \mu R(\mu, \mu, 180^\circ)$$

We shall in this section examine some properties valid for this ideal case of precise opposition.

The intensity  $I(\mu)$  is observed at a fraction  $(1 - \mu^2)^{1/2}$  of the planet's radius from the center. By practical limitations the outer 5% of the disk radius near the limb cannot be observed accurately, which makes the range of values  $\mu = 0 - 0.31$  unobservable.

Figure 18.7 gives a number of sample curves for this brightness distribution, all computed for very thick atmospheres. Unit intensity corresponds to the intensity of a perfectly white disk held at the position of the planet, perpendicular to the direction from sun and earth. The computation for isotropic scattering

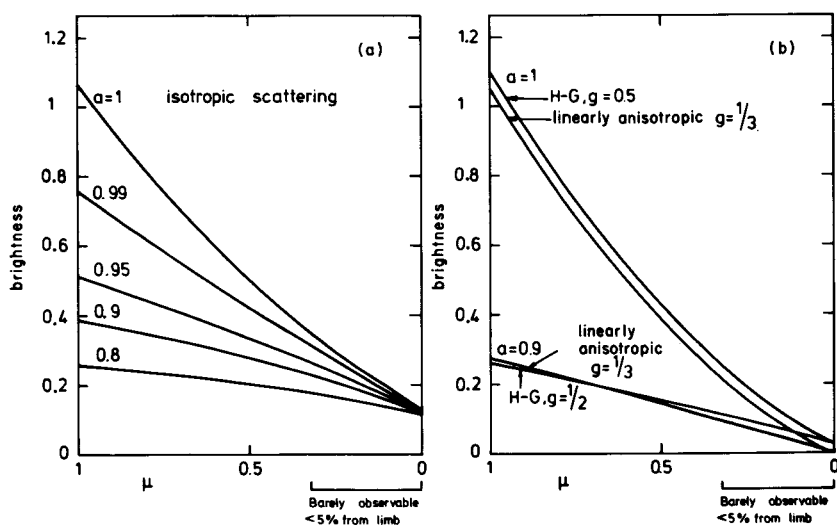


Fig. 18.7. Brightness distribution on disk of a planet in opposition. The plotted function is  $\mu R(\mu, \mu, 180^\circ)$  for various assumptions about phase function and single-scattering albedo.

(a) requires no comment. The curves can be understood by observing that first-order scattering contributes the value  $0.125a$ , independent of  $\mu$ . This is all we see at the limb, where  $\mu = 0$ . Multiple scattering raises predominantly the center values, until at  $a = 1$  the center of the disk is rather similar to the standard white disk, and, in fact 5.7% brighter.

A similar trend is seen in Fig. 18.7b. Here the single-scattering contribution is much smaller. For H-G scattering with  $g = 0.5$  it is  $0.125 \times 0.222 = 0.028$ , and it is even zero (in opposition) for the phase function  $1 + \cos \alpha$ . This difference persists in the sum of all orders if  $a = 0.9$ . However, at  $a = 1.0$  the high-order scattering slightly overcompensates this difference and raises the anisotropic results a little above the isotropic results, except with the linearly anisotropic phase function.

The computation of these curves requires the inclusion of the azimuth-dependent terms. The situation is simple only at the two limits (cf. Sections 15.3.1 and 15.3.6):

center,  $\mu = 1$ , azimuth-independent term only;  
limb,  $\mu = 0$ , single scattering only.

The equations for linearly anisotropic scattering are given in detail in Chandrasekhar's book. The points at  $\mu = 0.5$  on the  $g = 0.5$  curves for Henyey-Greenstein scattering are fully explained in Section 15.3.6. Additional values for many more phase functions, namely Rayleigh phase functions and Henyey-Greenstein function with  $g = 0, 0.5, 0.75, 0.8, 0.85, 0.9$  and for single scattering albedos  $a = 0.7, 0.8, 0.9, 0.95, 0.98, 0.99, 0.995, 0.999$ , and 1 are presented in three-decimal tables by Dlugach and Yanovitskii (1974). It is necessary to multiply their function  $r(\mu)$  with their reflection coefficient of the center of the disk to obtain the function which is plotted in Fig. 18.7. The agreement is excellent. The values in Table 3 of Anikonov (1974) also agree well.

For a further check note that the geometric albedo  $p$  defined in Display 18.1 and tabulated in Table 58 can be obtained from the curves of Fig. 18.7 by integration:

$$p = \frac{1}{4}F(180^\circ) = \int_0^1 2\mu^2 R(\mu, \mu, 180^\circ) d\mu = \int_0^1 I(\mu) 2\mu d\mu$$

In single scattering:

$$p_{\text{single}} = \frac{1}{4}F_1(180^\circ) = \frac{1}{8}a\Phi(180^\circ)$$

An important point in judging these curves is that in the azimuth-dependent terms the single scattering is always dominant (Section 15.3.1). Consequently, similarity rules are not valid for these terms. As a further consequence, the observed brightness distribution still contains a fair clue to the phase function. However, detailed information about the phase function cannot be obtained. Since (in the observable range of  $\mu$ ) differences from straight lines are minor, it is

futile to expect that more than two parameters (e.g.,  $a$  and  $g$ ) can be determined from such observations.

A particular method for obtaining two such parameters which has gained some popularity, is to make Minnaert plots (cf. Section 18.2). It can be applied to photometric data taken at any part of the disk and does not require exact opposition. The exponent  $k$  in the relation

$$\mu I = \text{const} \cdot (\mu\mu_0)^k$$

is determined empirically from a plot of  $\log(\mu I)$  against  $\log(\mu\mu_0)$ . Usually a fair match is obtained over the range of abscissae (0 to  $\sim -0.6$ ) over which good data are available. Values of  $k$  may range from 1.1 down to 0.6 and the practical accuracy is about  $\pm 0.1$ . See values obtained on Mars (Binder and Jones, 1972, Pleskot and Kieffer, 1977), on Jupiter and Saturn (Binder and McCarthy, 1973), and on Jupiter (Wattson *et al.*, 1976).

The values of  $k$  may also be obtained from theoretical models. Figure 18.8 shows the values corresponding to the distributions of Fig. 18.7. Since  $\mu = \mu_0 = 0.5$  gives the abscissa  $-0.6$  in the Minnaert plot, we have defined  $k$  by  $k = \log[2I(1)/I(0.5)]/\log 4$ . Values read from Figs. 9 and 11 of Binder and McCarthy (1973), which agree quite well with ours, were also used. A more complete set of values was constructed from the tables of Dlugach and Yanovitskii (1974) by Teifel (1976).

Some conclusions from this figure are the following: (a) values of  $k$  both above and below 1 occur; (b)  $k$  drops substantially when the albedo becomes  $< 1$  and

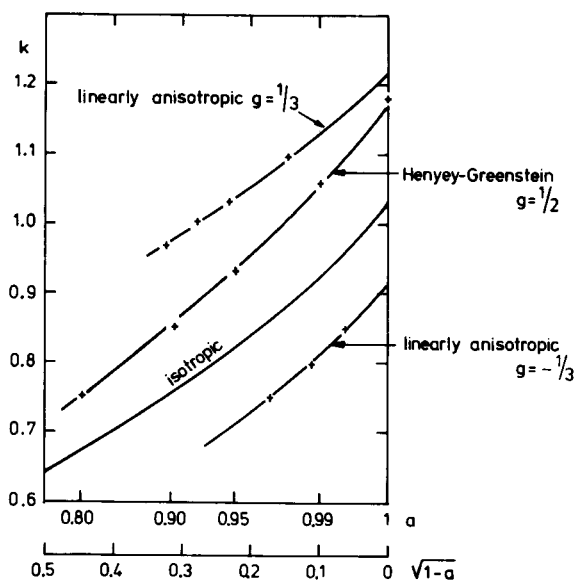


Fig. 18.8. Exponent of Minnaert plot for model atmospheres.

the relation is approximately linear in  $\sqrt{(1-a)}$ ; (c)  $k$  rises when more forward scattering is introduced and is not only sensitive to the asymmetry factor  $g$ , but also to higher expansion coefficients of the phase function, as shown by the fact that the points for the Henyey–Greenstein function with  $g = \frac{1}{2}$  fall even below those for linearly anisotropic scattering with  $g = \frac{1}{3}$ .

The practical use of such plots (Binder and McCarthy, 1973) is that the exponent  $k$  and the geometric albedo  $p$  form a set of two “observed,” parameters which for practical purposes suffices to describe the photometric data in a particular wavelength band. The theoretical calculations described above may then serve to calibrate  $k$  and  $p$  against two parameters describing the single scattering, e.g., the albedo  $a$  and the asymmetry factor  $g$ . This may not be the final answer to all questions, but it certainly is a sensible approach.

Barkstrom (1973) has remarked that the Minnaert plots for low values of the single-scattering albedo  $a$  can be made to resemble a straight line much better if the abscissa is chosen to be  $\log[\mu\mu_0/(\mu + \mu_0)]$ . This was demonstrated to be so for isotropic scattering and presumably is true also for anisotropic scattering. Such a Minnaert–Barkstrom plot has (near  $\mu = \mu_0 = 1$ ) a tangent with a slope that is twice the slope of the corresponding Minnaert plot. If only points with  $\mu = \mu_0$  are plotted, the entire curve remains the same, with the abscissa compressed by a factor 2. If  $a \rightarrow 0$ , the slope of the Minnaert plot goes to  $\frac{1}{2}$ , and that of the Minnaert–Barkstrom plot to 1.

The Minnaert plots are based on a rough empirical formula, which is not likely to suffice if accurate data, not near opposition, are available. Kattawar and Young (1977) conclude, indeed, that they cannot match the Mariner Mars isophotes obtained at  $60^\circ$  phase angle by a Minnaert function, but need a Mie scattering model.

A rough orientation about the actual values of the geometric albedo is provided by Table 60. The classical review paper is by Harris (1961). Continuous updating is necessary. We have used data obtained or reviewed for all planets by Wamsteker (1973); for Jupiter by Axel (1972), Duysinx and Henrist

TABLE 60  
Geometric Albedo  $p$  of the Major Planets and Titan<sup>a</sup>

Wavelength range ( $\mu\text{m}$ )	Jupiter	Saturn	Uranus	Neptune	Titan
0.8–1.1	0.10–0.40	—	0.03–0.20	0.05–0.10	—
0.6–0.8	0.30–0.52	—	0.07–0.45	0.20–0.25	0.21–0.37
0.4–0.6	0.36–0.45	0.46	0.40–0.63	0.50	0.12–0.31
0.3–0.4	0.26–0.32	0.21–0.32	0.48–0.59	0.58–0.62	0.06–0.12
0.25–0.3	0.25–0.28	—	—	—	—
0.20–0.25	0.15–0.25	—	—	—	—
0.17–0.20	0.05–0.20	—	—	—	—

<sup>a</sup> Rough orientation only.

(1973), Tomasko (1976); for Uranus by Prinn and Lewis (1973); and for Titan by Danielson *et al.* (1973), Younkin (1974), and Hunten (1974).

The ranges of  $p$  shown in the table are mostly real, as revealed by narrow-band spectrophotometry. It is necessary in serious work to turn to the original papers. Even so, the rough list shows several features clearly: Jupiter is red, Uranus and Neptune more bluish, undoubtedly due to Rayleigh scattering in the atmosphere. Since we must multiply  $p$  by the geometric factor  $q \approx 1.5$  (Table 58) in order to obtain the spherical albedo, we see that in the wavelength range in which they show the highest albedo, these planets reflect 70–90% of the incident light.

In order to convert these data (or better ones!) into estimates of the properties of individually scattering particles by the conversion  $(k, p) \rightarrow (a, g)$  sketched above, we need a theoretical grid consisting of two sets of curves (Binder and McCarthy, 1973). Information on the construction of the curves  $k = \text{const}$  on the  $(a, g)$  plane has already been given. The curves  $p = \text{const}$  can be constructed similarly or plotted directly from Table 21 of Dlugach and Yanovitskii (1974). The alternative of using  $A^* = pq$  (Display 18.1), where  $A^*$  can be very accurately expressed in a closed formula for any  $a$  and  $g$  (Fig. 12.5) and  $q$  is about 1.50 (Table 58), is not accurate enough, because Fig. 3 of Dlugach and Yanovitskii (1974) shows that the variations in  $q$  are not negligible.

Although not presented in the same form, the method of converting limb-darkening curves measured at different latitudes into single-scattering albedo on the assumption of isotropic scattering (Pilcher and Kunkle, 1976; Tomasko, 1976) is basically a variant of the conversion procedure described above.

The problems of the theoretical explanation of such measurements can be further illustrated by examining an example. Belton *et al.* (1971) discussed the then available values of geometrical albedo for Uranus, with emphasis on its spectral change. They were content to make three drastic simplifications in the calculations:

(a) isotropic scattering. This may cause an error of 9%. This error can now be easily cut down, either by using the correct phase functions, or by referring to existing tables or to the similarity principle.

(b) replacement of  $H$  function by a linear function in  $\mu$ . This causes an error smaller than 2%.

(c) replacement of the albedo, which decreases with increasing depth  $\tau$  as  $a = a(0) \cdot \exp(-\eta\tau)$ , by the constant albedo  $a_{\text{eff}}$ , which Belton *et al.* solve from

$$\tau_{\text{eff}} = 1/2[3(1 - a_{\text{eff}})]^{1/2}, \quad a_{\text{eff}} = a(0)e^{-\eta\tau_{\text{eff}}}$$

as recommended by Chamberlain and McElroy (1966). The error introduced is about 10%. Direct improvement could only be obtained by a full numerical computation for an atmosphere in which  $a$  varies with depth; but it is also possible that a similarity principle for such atmospheres, to which Chamberlain and McElroy's article gives a first approach, may be more systematically developed.

The next significant progress in the observational data was the high-resolution photometry of the Uranus disk by Danielson *et al.* (1972) obtained with Stratoscope II. In essence, these data may be interpreted by fitting them to model curves as shown in Fig. 18.7. However, since the point spread function (half-maximum diameter =  $0.15''$ ) still is not negligibly narrow compared to the planet's disk (diameter  $4''$ ), the authors chose to make the comparison with convolved limb-darkening curves. It should not be surprising that in spite of the accuracy obtained in the photometry, only a crude distinction between different models could be made.

Four models with roughly the correct geometrical albedo were compared: A thick Rayleigh scattering atmosphere (with  $1 - a = 0.05$ ) has too little limb darkening, and a thick Henyey–Greenstein scattering atmosphere (with  $1 - a = 0.002$ ) has too much limb darkening. A finite Rayleigh scattering layer with  $b = 0.5$ ,  $a = 1$  over a Lambert surface with  $A = 0.75$  gives roughly the correct match, but even a bare Lambert surface gives a nearly acceptable curve. In recent years more and more physics has been put into the models. See Danielson (1977) and the references cited there.

### 18.3.2 Polarization near Jupiter's Poles and Limb

The strong polarization near Jupiter's limbs was discovered as a prominent feature in Lyot's measurements fifty years ago. It arises from Rayleigh scattering by gas above the clouds. The fact that it is stronger near the poles, where it reaches some 6%, than near the equatorial limbs, where it reaches about 1% in visible light, must be due to a lower effective cloud level or a thinner upper cloud structure near the poles, leaving a thicker molecular atmosphere within clear view. Variations with time must be caused by varying cloud heights or by variations in aerosol content. See review by Coffeen and Hansen (1973).

The fact that the observed light has the electric vector predominantly in a radial direction can be understood from the fact that second and higher order Rayleigh scattering contributes most strongly. First-order scattering at exact opposition has zero polarization. Model computations are explained in Sections 16.3.4–16.3.5 (Fig. 16.3 and Table 55). With the sign convention adopted there the polarization is called negative. The theoretical polarization curve goes to 0 again at the very limb, where only first-order scattering remains; but this decrease starts very close to the limb. For instance, in a pure Rayleigh scattering atmosphere with  $b = \infty$ , the strongest polarization of  $-7.6\%$  occurs at  $\mu = 0.24$  (Fig. 16.4), which corresponds to  $(1 - \mu^2)^{1/2} = 0.971$ . This is about  $0.7''$  from the limb and can be observed only under very good seeing conditions.

Precise model computations are necessary to check whether the explanations suggested above are quantitatively correct. Gehrels *et al.* (1969) have made such computations in order to compare their and other observers' data with a set of models. Clearly, the quantity to be varied is the optical depth  $b$  above the cloud

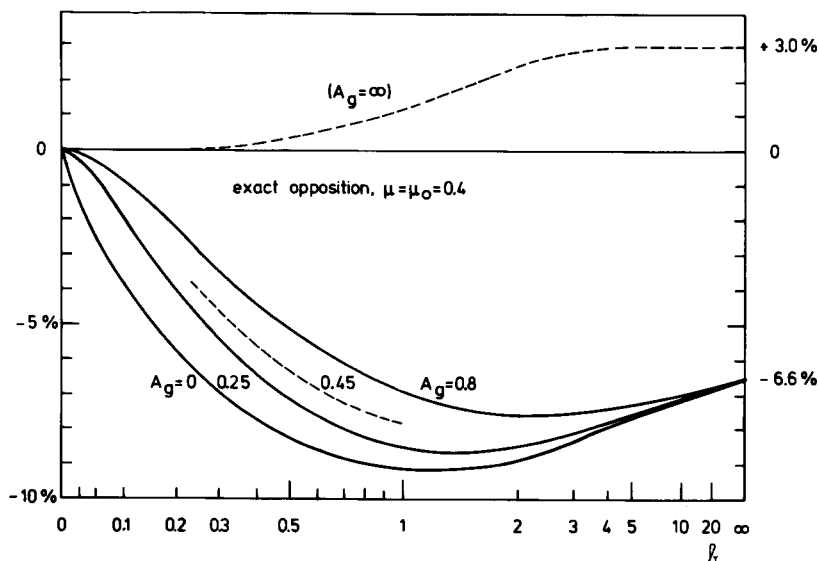


Fig. 18.9. Polarization of one point on the disk of a planet covered by a finite Rayleigh atmosphere. Exact opposition is assumed and the point is close to the limb at 0.91 radii from the center. The optical thickness  $b$  and the ground albedo  $A_g$  are varied.

deck, but if  $b$  is finite, a certain amount of diffuse reflection straight from the cloud deck gets through and, therefore, we must also vary  $A_g$ , the albedo of this deck, that is, if we don't want to make fancier assumptions (Section 18.4.1) about this deck than that its reflection is unpolarized and may be approximated by Lambert's law.

Figure 18.9 shows how the polarization in this simple model varies with  $b$  and  $A_g$ . The curves were newly computed from the exact equations with the help of the tables of Sekera and Kahle (1966). In the range  $b \leq 1$  they match the results tabulated by Coulson *et al.* (1960). For curiosity, we have also plotted the polarization of the radiation that would emerge if the only source of light were a luminous unpolarized ground surface shining by Lambert's law. This polarization is positive and reaches, at  $b = \infty$ , the value of 3.0% found in Table 53. This curve is shown in Fig. 18.9 with the appropriate label  $A_g = \infty$ .

It may seem puzzling, at first, that all curves of Fig. 18.9 show that keeping  $A_g$  fixed and varying the optical depth  $b$ , the polarization goes through an extreme value near  $b = 1$ . This occurs even if the ground is dark. This intrinsic effect of a finite atmosphere arises from the fact that the strongest negative polarization (in opposition) comes from light that has been scattered a few times in succession. Table 55 (Section 16.3.5) shows that this extremum is near  $-14\%$  for  $b = \infty$ ,  $n = 3-4$ . The net polarization of all orders combined must be small at small  $b$  because single scattering is so strong. At large  $b$  the orders higher than



4, which again have smaller polarization, depress the net result. This makes a maximum value of some 9% at intermediate  $b$  altogether plausible.

The observed value, in the Jupiter polar regions at  $\mu = 0.4$ , is on the average  $-5.6\%$ , well below the value of  $-6.6\%$  computed for  $b = \infty$ . This means that we definitely must go to the small  $b$  side of the maximum before we can find a match. The result is not very sensitive to the assumed  $A_g$  value. Gehrels *et al.* take  $A_g = 0.45$  and conclude that  $b = 0.34$  gives the best match to Lyot's 1924 opposition data.

As an added assurance that the correct side of the maximum has been chosen, we can examine the polarization at one  $\mu$  as a function of wave length. The  $\lambda^{-4}$  law produces a wide range of  $b$ , so we have an entire curve to match. The north-polar observations of 1960 and 1963 so discussed by Gehrels *et al.* show indeed a curve with a maximum in  $|p|$ . At the same time, the south polar curve did not show a pronounced maximum.

The east and west limbs show a similar effect but of a much smaller magnitude. Gehrels *et al.* give a typical value  $b = 0.05 \pm 0.02$  at the equator against  $b = 0.4$  for the south and 0.6 for the north pole, at  $\lambda = 0.56 \mu\text{m}$ .

Outside opposition, up to the maximum phase angle of  $11^\circ$  for earth-based observations, the theoretical picture is much the same. The big difference is that the entire curve shifts due to the polarization in the single-scattering term. This single scattering enhances the polarization at the poles, but reduces it (makes it less negative) at the equator limbs. This is illustrated for  $b = \infty$  by the model curve of Fig. 16.6. The same model shows that near-symmetry should exist with respect to the point midway between the center of the disk and the subsolar point. The measurements of polarization over the entire disk (Hall and Riley, 1968) appear to confirm this expectation.

It remains to be discussed how the polarization near the center of the disk varies with phase angle. The study which Loskutov (1971) devotes to this problem is simplistic in not taking multiple scattering in the atmosphere into account. In another respect it is more refined than the treatment above because it represents the clouds as a thick deck of ammonia droplets (refractive index 1.38, average value of  $2\pi a/\lambda = 3$  or 3.5). Taking the geometric albedo of the cloud deck as 0.59, he finds that the run of polarization with wavelength can be represented approximately by the cloud deck alone, but that a somewhat better match to the observations is obtained with a Rayleigh-scattering atmosphere of  $b = 0.1$ –0.2.

The preceding write-up was completed before the Jupiter fly-by of Pioneer 10 in December 1973. The polarimeter results, referring to phase angle  $103^\circ$ , scattering angle  $\alpha = 77^\circ$  show, as expected, strong positive polarization of the order of 8% arising from first-order Rayleigh scattering. A very preliminary analysis was made by Coffeen (1974). A fuller discussion from the same team (Baker *et al.*, 1975) led to values of  $b$  ranging in blue light from 0.10 in the equatorial regions to 0.29 and 0.36 in the polar regions (latitudes  $+71^\circ$  and  $-60^\circ$ ). See also summaries by Teifel (1976) and Tomasko (1976).

The discussion presented above for Jupiter may be repeated in a similar vein for Saturn and Uranus, but the greater distance makes it more difficult on those planets to make measurements at various  $\mu$ .

## 18.4 PARTIALLY TRANSPARENT ATMOSPHERES

### 18.4.1 Various Assumptions about the "Ground"

It is convenient to introduce distinctive terms:

*Transparent atmosphere:* A fair proportion of the incident sunlight reaches the ground directly, and some details on the ground are visible to an outside observer.

*Translucent atmosphere:* A fair proportion of the incident sunlight reaches the ground, but only as diffuse radiation. An outside observer sees no sharp surface detail but can—in principle—recognize extended dark and bright surface areas as diffuse patches.

*Opaque atmosphere:* Virtually no light reaches the ground. The ground properties are irrelevant to an outside observer.

In the present section we shall deal with transparent and translucent atmospheres.

Under the usual assumptions of horizontal homogeneity of both the atmosphere and the ground, adding the ground to the finite atmosphere is a straightforward application of the adding method. This method, in its general matrix formulation (Section 4.5.2) leads to an infinite series in which each successive term has an extra factor  $R_g R^{*}$  representing another reflection against the ground and one (from below) against the atmosphere. If both  $R_g$  and  $R^{*}$  depend on azimuth, the azimuth dependence is different in each term of this series. Fourier expansion in  $\varphi$  then leads to series representing the different Fourier orders  $m$ , converging with different rapidity. Similarly, if *both* factors have a nontrivial dependence on polarization, the successive terms in the series have different states of polarization.

If, however, the ground *or* the atmosphere reflects light independently of  $\varphi$ , only the series with  $m = 0$  remains. Similarly, if ground reflection or atmospheric scattering completely depolarizes the light, the adding method may be limited to the intensity, ignoring the other Stokes parameters. The series are very rapidly convergent (Section 13.4) except in the very rare case in which both the atmosphere *and* the ground have the property that they reflect virtually all of the incident light.

We shall now discuss some sets of assumptions that lead to simplifications or to otherwise interesting results. Further illustrations are scattered in the literature (e.g., Coulson *et al.*, 1966).

### A. LAMBERT GROUND SURFACE

A ground reflecting by Lambert's law with albedo  $A_g$  has the reflection law in the usual notation:  $R_g(\mu, \mu_0, \varphi) = A_g$  (a constant)  
in the vector notation (Section 5.1)  $R_g = A_g U \cdot U$

This is independent of azimuth. The series in the adding method becomes an exact geometric series with ratio  $A^*A_g$ , where  $A^* = UR_{\text{atm}}U$ . Light incident on the top of the atmosphere is reflected by the combination of atmosphere plus ground according to the reflection function

$$R(\mu, \mu_0, \varphi) = R_{\text{atm}}(\mu, \mu_0, \varphi) + [A_g/(1 - A_g A^*)]t_{\text{atm}}(\mu)t_{\text{atm}}(\mu_0)$$

where  $t_{\text{atm}}(\mu) = T_{\text{atm}}U$  (Section 4.5.4).

This result contains no assumption about the thickness of the atmosphere. It represents thin and thick atmospheres, as well as any intermediate case. In thin atmospheres the second term dominates. It is the ground reflection modified by a factor somewhat less than 1. In thick atmospheres, the first term due to atmospheric scattering dominates and the second term is a small correction.

The distinction between transparent and translucent atmospheres, with which we started this section, is not visible in this equation because by definition  $T_{\text{atm}}$  includes the direct *and* the diffuse transmission. Equations valid for inhomogeneous atmospheres and for the internal radiation field are given in Section 4.5.4.

### B. SPECULAR REFLECTION: WATER SURFACE BELOW ATMOSPHERE

The literature contains many elaborate derivations of the equations valid in the presence of a specularly reflecting bottom surface. The list, which is probably incomplete, includes Casti *et al.* (1969, 1970, 1973), Sobolev (1975, Section 4.5), Ueno and Mukai (1973), Plass *et al.* (1973), Ueno (1974), and Kat-tawar (1974). These derivations may be replaced by a simple application of the adding method. The following explanation ought to be self-sufficient, but more formal discussions along the same lines are available in the papers cited. It is necessary to keep the azimuth dependence in the equation, i.e., to include all Fourier components. The most direct way is to formulate the reflection by the mirror surface as

$$R_g(\mu, \mu_0, \varphi) = r(\mu)[\delta(\mu - \mu_0)/2\mu]2\pi \delta(\varphi - \varphi_0)$$

where  $\delta$  denotes Dirac's delta function, and  $r(\mu)$  is the intensity reflection coefficient for incidence and reflection under angle  $\arccos \mu$ .

If desired, polarization may be included by a matrix formulation. For the normalization, compare the representation of directly transmitted light (Section 15.1.5). The azimuth  $\varphi$  (after reflection) equals  $\varphi_0$  (before reflection) because the projection of the light path on the mirror surface continues in the same direction

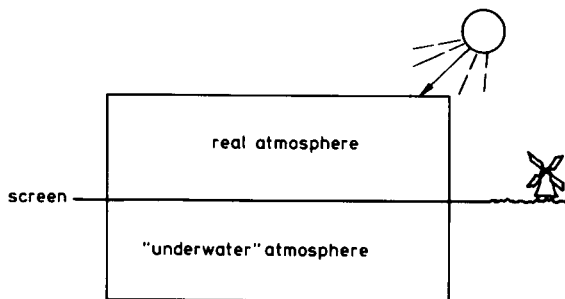


Fig. 18.10. Conceptual image for treating scattering in an atmosphere over a reflecting sea surface.

and no change in the definition of  $\varphi$  is made upon reflection. The rest is a straightforward substitution, in which any "multiplication" with the matrix  $R_{\text{atm}}$  is the usual integration over the variables  $\mu_0$  and  $\varphi_0$ , and in which any multiplication with the matrix  $R_g$  is a real multiplication by the factor  $r(\mu)$ . We shall not write the complete result.

An alternative approach, that avoids the use of  $\delta$  functions but draws more heavily on visualization, can be elegantly taken as follows. Imagine the atmosphere with all its properties actually reflected in the mirror to form what we shall call the "underwater atmosphere" (Fig. 18.10). If reflection should occur without loss,  $r(\mu) = 1$ , the calculation just becomes one step in the doubling method. However, we should not forget at the end to reflect the underwater atmosphere again on the real one. The combined result then reads

$$R_{\text{comb}}(\mu, \mu_0, \varphi; b) = R(\mu, \mu_0, \varphi; 2b) + T(\mu, \mu_0, \varphi; 2b)$$

The second term contains the directly reflected light as a singular part. Any other reflection law can be included in this concept as due to an absorbing screen between the two halves. The screen may be taken into the top half as a factor  $r(\mu)$  of its transmission law or into the underwater half as a factor  $r(\mu_0)$  of its transmission. In any case, the adding method has to be used, even if  $r(\mu)$  is a constant other than 1. Finally, the two halves have to be folded together again.

The academic discussion above says nothing about the waves, air bubbles, and spray, which characterize the real air-sea interface and also greatly affect the play of light. For those topics the reader may refer to Preisendorfer (1971, 1976).

### C. ATMOSPHERE ABOVE A CLOUD DECK

The correct treatment of a homogeneous atmosphere above a thick cloud deck calls again for the adding method and generally permits no shortcuts. Here, an interesting possibility arises. The cloud deck is itself a semi-infinite atmosphere with specified particle albedo  $a$  and phase function  $\Phi(\cos \alpha)$ , which

usually differs from those of the atmosphere on top. We know from Chapter 12 that such semi-infinite atmospheres show striking similarities for widely different phase functions. This means that the cloud deck *may* have a reflection function very similar to that of a semi-infinite atmosphere with the same properties as the atmosphere on top. We shall then say that the atmosphere and cloud deck are “matched.” Logically, the combination of an atmosphere with a matched cloud deck again yields the reflection function of the semi-infinite atmosphere. In this “matched” situation it is impossible to obtain the depth of the atmosphere on top from photometric investigations. However, spectroscopic evidence on molecules in the overlying atmosphere can be used for that purpose, for a match in the continuous spectrum creates a mismatch at any frequency inside the absorption line.

#### D. TRANSLUCENT ATMOSPHERE ABOVE ARBITRARY GROUND

A translucent atmosphere is thick enough to damp out all azimuth-dependent terms in the transmission function. We then have the familiar situation of days of heavy overcast, in which a fair amount of light reaches the earth's surface but the distribution of this light does not tell us the position of the sun in the sky. The formulas relevant to a translucent atmosphere without ground surface (Section 5.3) are in matrix notation:

$$R_{\text{atm}} = R - cf K \cdot K, \quad T_{\text{atm}} = c K \cdot K$$

where  $R$  is the reflection function and  $K$  the escape function for a semi-infinite atmosphere,  $c = mf/l(1 - f^2)$ , and  $m$ ,  $f$ , and  $l$  have the meaning defined in Sections 5.1 and 5.3. We may combine this with a ground surface with an arbitrary reflection function  $R_g$  and find for the combination:

$$R_{\text{comb}} = R_{\text{atm}} + T_{\text{atm}} R_g [1 + R_{\text{atm}} R_g + (R_{\text{atm}} R_g)^2 + \cdots] T_{\text{atm}}$$

Somewhat disappointingly, no further simplification is possible with these general assumptions, except that we see at once that the result has the form

$$R_{\text{comb}} = R_{\text{atm}} - d K \cdot K$$

in which  $d$  is a constant that may be expressed as  $cf$  minus a series of integrals that involve the functions  $R_{\text{atm}}$ ,  $R_g$ , and  $K$ .

#### E. TRANSLUCENT ATMOSPHERE OVER LAMBERT SURFACE

The result for the combined assumptions (A) and (D) is simply the result just stated, with

$$d = cf - \frac{A_g c^2 (KU)^2}{1 - A_g [A^*(\infty) - cf (KU)^2]}$$

An equivalent form is

$$d = cf \frac{1 - A_g A^*(\infty) - A_g (m/l) (KU)^2}{1 - A_g A^*(\infty) + A_g cf (KU)^2}$$

The normal situation is that the ground albedo is not strong enough to compensate for the fact that the atmosphere is not infinitely deep. In this situation the constant  $d$  is positive. The opposite situation (negative  $d$ ) occurs if  $A_g$  is high enough and certainly if  $A_g = 1$ . The cross-over occurs at the intermediate value

$$A_g(\text{matched}) = [A^*(\infty) + (m/l)(KU)^2]^{-1}$$

Numerical illustrations are given in Section 18.4.2.

#### F. TRANSLUCENT ATMOSPHERE OVER IDENTICAL ATMOSPHERE

We now combine assumptions (C) and (D) and wish to check whether we recover the reflection function of a semi-infinite atmosphere  $R$ , if we specify that  $R_g = R$ , so that the total combination is the homogeneous semi-infinite atmosphere. Surprisingly, the algebra is not obvious. Define the number

$$x = KR[1 + (R_{\text{atm}}R) + (R_{\text{atm}}R)^2 + \cdots]K$$

Equations (5) and (6) of Section 5.2.2, transposed, lead to

$$KR = m^{-1}Q(1 - RR)$$

Substitution into the preceding equation gives, after multiplication and subtraction,

$$\begin{aligned} x &= m^{-1}QK - m^{-1}QcfK \cdot KR[1 + (R_{\text{atm}}R) + (R_{\text{atm}}R)^2 + \cdots]K \\ &= l/m - lcfx/m \end{aligned}$$

Solution of this linear equation and further substitutions give

$$x = (l/m)(1 - f^2) = f/c$$

The main check is now straightforward:

$$\begin{aligned} R_{\text{comb}} &= R - cfK \cdot K + cK \cdot KR[1 + (R_{\text{atm}}R) + \cdots]cK \cdot K \\ &= R + (-cf + c^2x)K \cdot K = R \end{aligned}$$

#### 18.4.2 Contrast of Surface Markings

Suppose we have a planetary surface showing surface detail in the form of brighter and darker markings. Sharp details can be seen only in light that suffers no scattering from the surface to the observer. This directly transmitted fraction is  $\exp(-b/\mu)$ , where  $\mu$  is the cosine of the angle with the normal and  $b$  the total optical depth.

Larger dark or bright areas may still "shine through" in multiply scattered light. The brightness of a sufficiently extended area, as seen from outside, is given for Lambert surface reflection by Section 4.5.4 or 18.4.1(a). Its dependence on the two main parameters is shown for a particular example in Fig. 18.11. This example is based on Henyey-Greenstein scattering with  $g = 0.5$ , albedo

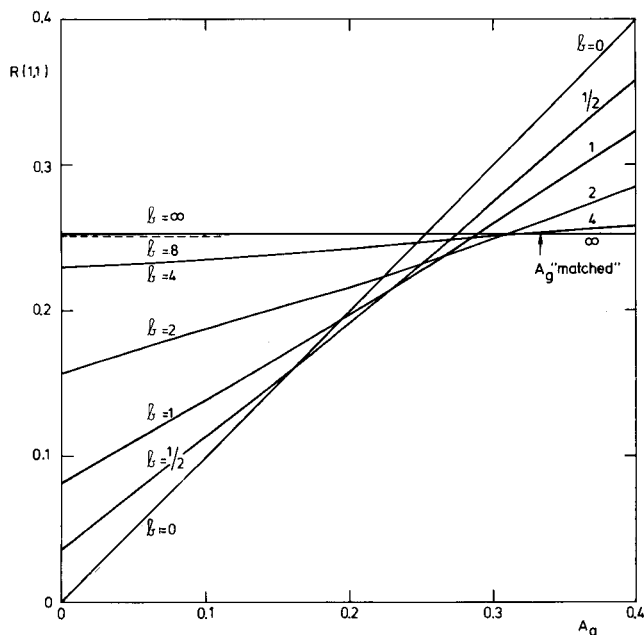


**Fig. 18.11.** Influence of optical depth and ground albedo on reflected intensity. Henyey-Greenstein scattering with  $g = 0.5$  and albedo 0.9 has been used. The reflection function for  $\mu = \mu_0 = 1$  is plotted.

$a = 0.9$  and gives the reflection for perpendicular incidence and emergence,  $\mu = \mu_0 = 1$ . For any fixed total optical thickness  $b$ , the brightness increases almost linearly with the ground albedo  $A_g$ . This increase is slower for thick atmospheres and absent for  $b = \infty$ , because the ground then has no influence. At any fixed  $A_g$ , the brightness does not vary uniformly with  $b$ . A dark ground, e.g.,  $A_g < 0.1$ , is gradually masked by the brighter atmosphere. At intermediate  $A_g$  values (roughly  $0.20 < A_g < 0.30$ ), the combined  $R$  first decreases, then increases with growing  $b$ . For  $A_g > 0.334$ , the combined  $R$  decreases with increasing  $b$  all the way. The number 0.334 is the value  $A_{g, \text{matched}}$  [Section 18.4.1(e)] for this example. In Fig. 18.11 the curves  $b = \text{const}$  for large  $b$  pivot about this point.

Let us now look at the contrast between two extended areas seen side by side. A thin haze or cloud layer overlying both areas and illuminated by the sun greatly reduces the apparent contrast as seen from outside. This is the reason why contrasts seen on the Mars surface during “clearings” of the blue haze cannot be seen when the haze is there. Also the dramatic reduction of all surface detail by the great dust storm during the first weeks of observation of Mars 9 in 1971 was due to this effect.

A practice example (van de Hulst, 1971), inspired somewhat by the actual markings, is shown in Fig. 18.12. We have selected two regions seen near the center of the disk at opposition ( $\mu = \mu_0 = 1$ ). The bright region (brightness plotted as abscissa) has  $A_g = 0.25$  and the dark region (brightness plotted as ordinate) has  $A_g = 0.05$ . The two diagrams correspond to two scattering laws: isotropic scattering and Henyey–Greenstein function with  $g = 0.5$ .

Inside each diagram the single scattering albedo  $a$  and the optical depth  $b$  of the haze layer are varied. If the haze has completely cleared ( $b = 0$ ), we see the full contrast ratio 5; if it is completely dense ( $b = \infty$ ), the contrast ratio is 1. Somewhat surprisingly, we find that the contrast ratio at intermediate values depends strongly on  $b$ , but very little on  $a$ . Separate photometry of the dark and bright markings would in practice be necessary to determine  $a$ . Although the similarity rules cannot be expected to give a precise answer in this application, where the optical depths are small, the two diagrams are strikingly similar, with the curves of constant  $b$  and of constant  $a$  shifted approximately as predicted by the similarity rules. The curvature, which is striking in the curve  $a = 0.9$  in the lower figure, can be explained by referring to Fig. 18.11.

Evidently, calculations of this kind for different assumptions of the ground albedo and reflection law, different haze scattering patterns, and different directions of incidence and reflection are needed before such curves can be used as a firm basis for interpreting the observational data.

Before leaving this subject, the warning should be repeated that elegant curves based on a simple model are hardly ever the final answer. The actual contrast of the Mars surface areas may be dependent as much on minute changes in surface composition as on changes in the atmosphere (Pollack and Sagan, 1969).

The assumption was made above that the areas were sufficiently extended to make calculations for infinitely extended areas applicable. This assumption is not terribly restrictive in applications to Mars but may be quite unrealistic in certain observations of contrasts on the Earth surface. The dependence of the contrast degradation on horizontal extent, as well as references to earlier work on terrestrial applications, may be taken from Odell and Weinman (1975).

### 18.4.3 Examples of Internal Radiation Field

If the radiation field inside an atmosphere without ground surface has been computed, it is simple, by the equations of Section 4.5.4, to find the internal radiation field for the same atmosphere with added Lambert ground surface.

One example is shown in Fig. 18.13. It is based on a conservative atmosphere with optical thickness  $b = 1$ , isotropic scattering, and perpendicular incidence. The adopted ground reflection is  $A_g = 0.2$ . A discontinuity in the intensity at  $u = 0$ , where the direction changes from slightly up to slightly down, exists at the very top and bottom. At the top ( $\tau = 0$ ) the intensity jumps from zero (down)



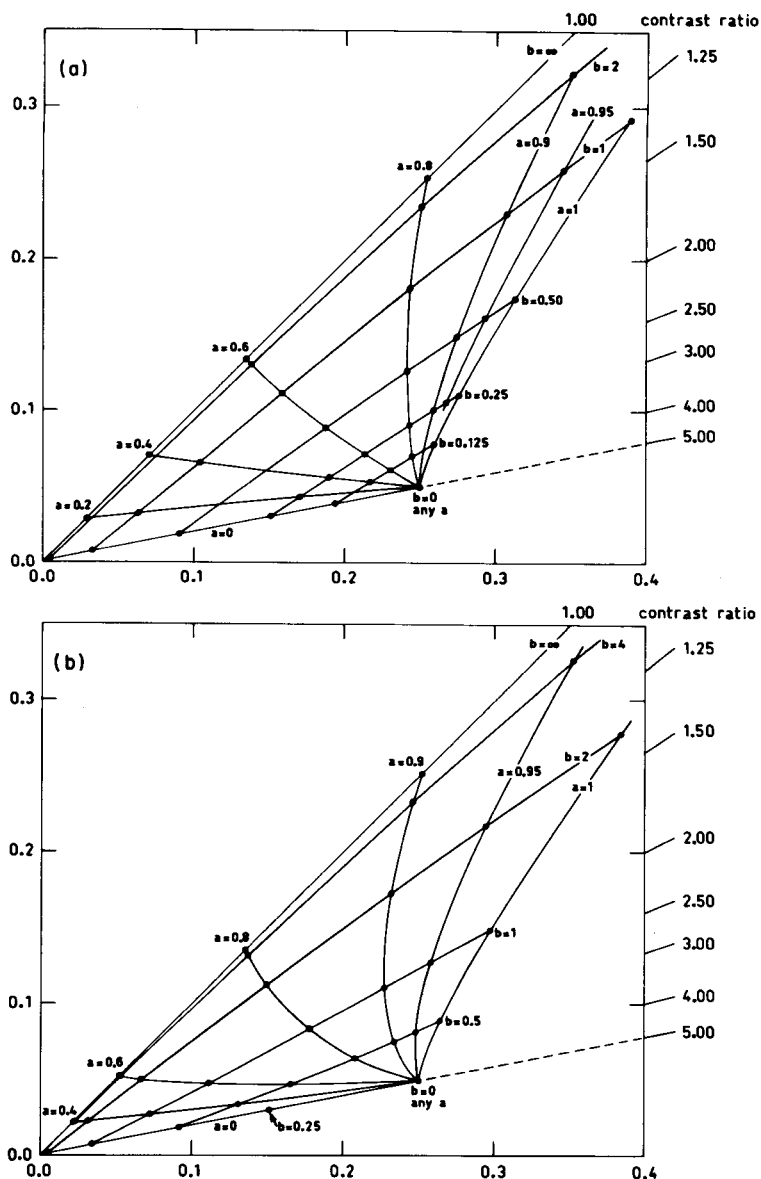
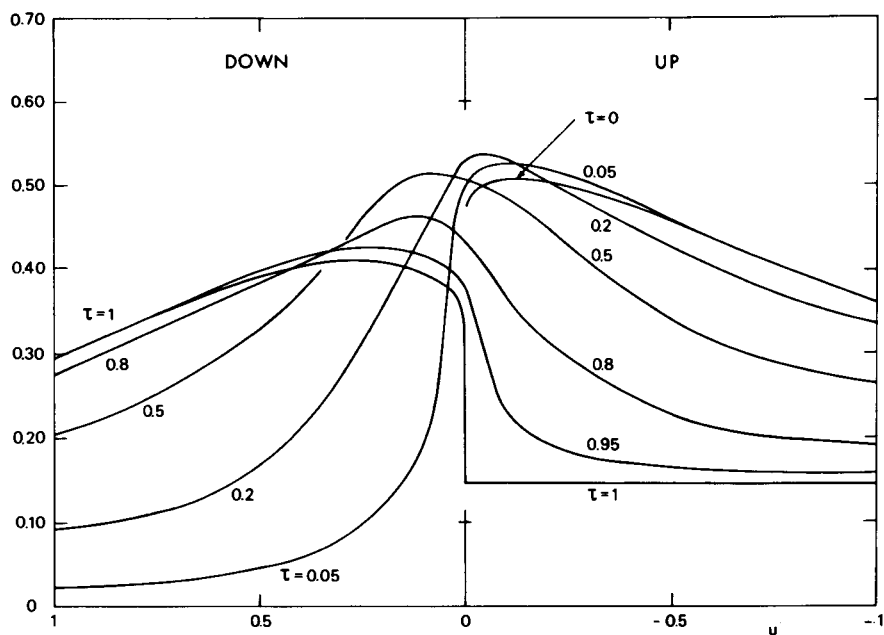


Fig. 18.12. Reduction of contrast of two extended areas near the center of a planetary disk. The two coordinates are the brightness of a light area with  $A_g = 0.25$  and a dark area with  $A_g = 0.05$ . The overlying atmosphere or haze is characterized by optical depth  $b$ , single-scattering albedo  $a$ , and asymmetry factor  $g$  of the phase function.  $\mu = \mu_0 = 1$ . (a) Isotropic scattering, and (b)  $g = 0.5$ .



**Fig. 18.13.** Example of distribution of diffuse light intensity at various depths inside a finite atmosphere. Perpendicular incidence ( $\mu_0 = 1$ ), and isotropic, conservative scattering ( $g = 0$ ,  $a = 1$ ) has been assumed. The atmosphere of total thickness 1 is backed by a ground surface with diffuse reflection coefficient  $A_g = 0.20$ . Abscissa  $u$  is the cosine of the angle with downward normal.

to 0.474 (up). For  $A_g = 0.5$  this would be 0.541. The intensity at the bottom jumps from 0.145 (up) to 0.352 (down). The corresponding numbers for  $A = 0.5$  are 0.424 and 0.562. The intensity radiated away from the bottom thus is smaller than  $A_g$ , the value it would have in the same illumination without atmosphere. Close to the top ( $\tau = 0.05$ ) the curve has become continuous, and the downward radiation shows an approximate proportionality to  $u^{-1}$ . A similar dependence is shown in the upward radiation near the bottom ( $\tau = 0.95$ ). The curves for intermediate  $\tau$  values require no comments. A similar illustration for  $A_g = 0.50$  is shown in Fig. 1 of Grant and Hunt (1968), with a logarithmic intensity scale.

What is an extremely simple practice example here must be repeated in greater detail and with more variation in the models, when it comes to computing the response of a probe lowered into the atmosphere. Such computations are necessary both in retrospect, in the interpretation of measured data, and in advance, in optimizing the design of the instrument to be flown. An example serving both purposes is discussed in Section 18.6.

An example of how to use the radiation field in the terrestrial atmosphere to infer information on ground reflectivity over large areas is mentioned in Section 19.1.2.

## 18.5 INTERPRETATION OF PLANETARY ABSORPTION SPECTRA

### 18.5.1 Method and General Theory

In spite of the new opportunity of direct access by means of space probes, spectra taken from the earth still form the basic material on which our knowledge of the planetary atmospheres is based. The development of Fourier spectroscopy appears to have removed almost all technical limitations on obtaining spectra of the highest quality (Connes *et al.*, 1969).

The main burden then falls on the interpretation. If the planet would have a nonscattering atmosphere above a diffusely reflecting ground, the light path would be unambiguous: down through the atmosphere from the sun to the ground and back up again from the ground toward the earth. Even in this simple limit the interpretation of the spectra is complicated by the fact that composition, mixing ratios, excitation temperature, and all line-broadening parameters may vary along this path. If, however, the atmosphere is hazy or contains partially transparent cloud layers, the enormous complication is added that light comes to the earth along many different paths. A good treatment requires that the statistics of these paths be taken into full account. These two complications, the physical one due to stratification and the geometrical one due to path statistics by multiple scattering, make the interpretation of planetary spectra almost intractable. Yet these spectra are our prime source of information on the composition of the planetary atmospheres.

The ideal method is to adopt a model with all the complications one can think of and patiently grind out a "synthetic spectrum." If this fits, it *may* be the correct model; if it does not fit, try another one. This is the only method without a logical objection but it is extremely slow. Actual planetary science works by partial shortcuts in which the order is reversed. The aim is to arrange the observed data in such a manner that a direct inference of certain physical parameters becomes possible. Such methods are never completely foolproof but are extremely useful when applied in the domain where their rationale is valid. The inference of pressures from line broadening or of abundances from a curve of growth are good examples of such direct techniques of limited validity.

The aim set for this book is to present the geometrical complications in a sufficiently systematic manner so that the reader may judge for himself which approximations or asymptotic forms are eligible for a direct method. The presentation given in Section 17.3 may help in selecting a good method for the problem at hand. As an illustration we review in the next section the manner in which several generations of planetary scientists have struggled with one particular problem.

### 18.5.2 The Venus Absorption Lines: A Case History

The following pages give a historical review of the Venus absorption lines with an emphasis on the models for interpretation that accompanied each

advance in the observations. A fine review dealing also with the observations themselves was given by Young (1972).

The situation around 1948 is clearly seen from the symposium report "The Atmospheres of the Earth and Planets" (Kuiper, 1949; revised edition, 1952). Four papers are relevant to the Venus absorption lines.

Dunham (1949) tells of the discovery in 1932 of the strongest CO<sub>2</sub> bands in the Venus spectrum with heads at 7820 and 7883 Å by means of the Mt. Wilson coude spectrograph. It seems incredible to a present-day reader that it took then the good luck of a batch of extra sensitive photographic plates and exposures of 2 and 4 hr to observe them at all.

Very soon the first rough attempts were made to reproduce these bands by a folded light path in a pipe filled with CO<sub>2</sub>. The strength could roughly be matched with a light path of  $40 \text{ m} \times 10 \text{ atm} = 400 \text{ m atm}$ . It was obvious that the pressure was too high, the path too short, and the product unreliable. In the same symposium Herzberg (1949) deals with more refined laboratory experiments with multiple-folded light paths. He reaches a match with  $2000 \text{ m} \times 1 \text{ atm} = 2000 \text{ m atm}$ . In the meantime the invention of the lead sulfide cell had greatly improved the observing technique and Kuiper (1949) already shows fifteen CO<sub>2</sub> bands in the 1.0–1.7 μm wavelength region. Herzberg warns that for many of those the match is reached for much smaller products of light path times pressure. He also shows evidence that if this product is kept constant, the line strength increases with increasing pressure.

The usual interpretation of these experiments was that the light path thus determined corresponds to twice the path length above the reflecting layer. This interpretation was put in doubt by van de Hulst (1949) who showed that the interpretation would be basically different if the gas and the cloud particles were well mixed. Chandrasekhar's series of articles on radiative transfer, which was preparatory to his book of 1950, was then almost complete and it was not difficult to extract the information needed in the planetary reflection problem. In particular, it was clear that if the continuum outside the absorption lines is formed by perfect scattering ( $a = 1$ ) from a semi-infinite atmosphere, then any small absorption works out as a reduction of the reflected intensity proportional to the *square root* of the absorption strength  $(1 - a)$ . This means a far stronger effect than linear absorption. That this effect must have great consequences both for the observed line strength and line shape was obvious. The theory behind this simple rule is now available in far greater detail and for far more general assumptions (Display 17.2).

The first clue to the question of which of the possible models was closer to the truth was obtained by Chamberlain and Kuiper (1956). In a series of measurements of the CO<sub>2</sub> band at 8689 Å over a range of phase angles they found that the band strength markedly increased with increasing phase angle. Here "phase angle" is used in the traditional sense as the supplement to the scattering angle. Thus, when Venus is seen fully illuminated (near superior conjunction, small phase angle) the band is strong and when Venus is seen as a crescent (near inferior conjunction) the band is weak. This is exactly opposite of what would be

expected from a simple path up and down towards a reflection layer and is *prima facie* evidence that particle scattering plays a major role.

In the next ten years other Venus problems demanded much attention but this one seems to have been temporarily stagnant. The theory was available in principle but much sorting out would be necessary before it could serve as a reliable tool for the interpretation of good observational data. Great strides in this direction were made by Chamberlain and McElroy (1966) and by Belton, Hunten, Gray, and others in the years that followed. Good summaries of the situation at that time are available (Chamberlain, 1970; Hunten, 1971; Young, 1972).

The theoretical problem of what absorption lines to expect from a well mixed scattering and absorbing atmosphere is complicated but not difficult. A systematic summary (without the historical perspective) is in Display 17.2. For instance, if we look in Display 17.2 under the assumptions of block 2 at the equivalent width of a weak line of arbitrary shape, we recover immediately (a) the proportionality with the square root of the line strength (1949), and (b) the decrease in equivalent width if more nearly grazing angles of incidence and reflection are involved, i.e., at larger phase angles (1956). The reason is that the reflection function  $R(\mu, \mu_0)$  is rather insensitive to  $\mu$ , but the escape function  $K(\mu)$  drops by a large factor if  $\mu$  varies from 0 to 1 (Fig. 11.2).

The early interpretations were usually made with isotropic scattering, with or without a statement validating the results for more general single-scattering phase functions by the similarity relations. Hansen (1969) showed, however, that the phase effect in the equivalent widths of absorption lines cannot be obtained accurately by similarity. A more detailed follow-up (Whitehill and Hansen, 1973) recommends that the single-scattering phase function known from the polarization studies (Section 18.1.5) be used. Their models show that the equivalent width of a line may very well go through a maximum if the Venus phase varies from 0 to 180°. They also suggested that line profiles (if available at all) are a better test than the phase effect, which may be affected by variations in time during the synodic period of the planet.

In the meantime, it was obvious to anyone that in the long run it would be very unsatisfactory to have only two extreme models: one with a sharply defined reflection layer and another conceived as a fully mixed scattering and absorption atmosphere. Sooner or later more realistic models with multiple layers, or a continuous variation of properties, would have to be treated. Here two attitudes were possible: invest all your hopes in a large computer, or keep looking for means that permit a simple visualization and shorter methods of calculation.

An example of the second philosophy is the idea (van de Hulst and Irvine, 1962) of basing the calculation on the distribution function of photon optical paths in the continuum. Irvine pursued this problem in quite a number of papers with different co-workers and largely solved it. Parallel developments in the same subject were being made by Sobolev and his co-workers. The literature

does not show much evidence of interaction between these groups but the author's observation is that the contacts at various occasions have been strong enough to ensure that no valuable results were missed. A systematic treatment of these problems is given in Chapter 17.

As is normal with newly developed methods, the optical path statistics was first tried out on known test cases. In fact, all of Chapter 17 deals with the usual homogeneous (well mixed) atmospheres that are the almost exclusive topic of this book. Irvine (1975) still states that "results at present are limited to homogeneous atmospheres." The models considered by Young and Kattawar (1976, 1977) do not deviate far from this assumption. Yet, we are getting close to the real problem. The knowledge of the statistics of the light paths, how many photons penetrate deeply, and what their average penetration is may be taken as the core of the interpretation of absorption lines formed by nonhomogeneous atmospheres. With this basic philosophy, a new attack at the interpretation of the Venus absorption lines was made by Fouquart (1974, 1975), and Buriez *et al.* (1979).

Since the analysis by Fouquart goes beyond the assumption of Section 17.3, we must be more elaborate in the explanation. The essence of Fouquart's method is given in a notation consistent with Chapter 17. The new concept introduced by Fouquart is "penetration depth." The most convenient way to visualize this concept is to think of a Monte Carlo calculation in which a very large number of photons enters the atmosphere from a particular direction, and the precise path of each is registered. Having selected all photons that contribute to a certain result (for example, those that emerge from the top in a certain direction), we can interrogate the register about their individual properties. In Chapter 17 we have dealt with only two properties:  $\lambda$ , the total optical path length, and  $n$ , the number of scattering events on the path. Fouquart's penetration depth, which we shall call  $q$ , is a third property and is simply defined as the optical depth of the deepest scattering event on the path.

If we know the statistics of  $q$  for a semi-infinite atmosphere, we know it for layers of any thickness  $b$ ; for in a layer with thickness  $b$ , paths with  $q > b$  do not exist and the statistics of the paths with  $q < b$  is identical to that for  $b = \infty$ , for these photons have never been deep enough to see whether the atmosphere extends below the level  $\tau = b$  or not.

Fouquart first explores the combined statistics of  $q$  and  $\lambda$  in a homogeneous atmosphere. Let the usual parameters  $a$ ,  $g$ ,  $\mu_0$ , and  $\mu$  be fixed and only  $a$  written. Suppose we know (by any method explained in previous chapters) the reflected intensity  $R(a, b)$  and the corresponding probability distribution of the path lengths  $p(a, b, \lambda)$ , normalized as usual to integral 1. Since the penetration depth for  $\lambda < 2b$  cannot possibly be larger than  $b$ , the relation

$$p(a, b, \lambda)R(a, b) = p(a, \infty, \lambda)R(a, \infty) \quad \text{if } \lambda < 2b$$

must hold. Fouquart exploits this by defining a renormalized distribution

$$f(a, b, \lambda) = [R(a, b)/R(a, \infty)]p(a, b, \lambda)$$

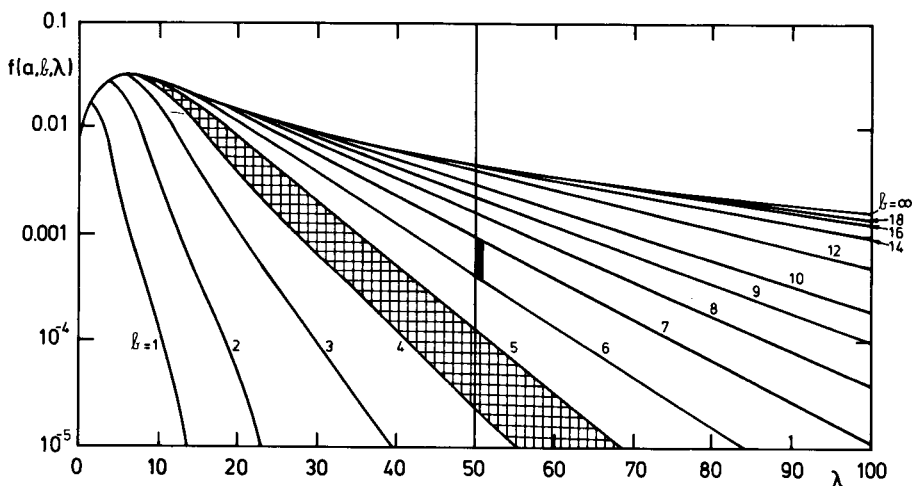


**Fig. 18.14.** Division of photon light paths by total optical length  $\lambda$  and by deepest point reached (penetration depth)  $b$ . This diagram refers to photons reflected perpendicularly ( $\mu = \mu_0 = 1$ ) from a semi-infinite cloud layer of Mie particles with  $x = 2$ ,  $m = 1.33$ ,  $a = 0.999$  (adapted from Fouquart, 1975). See further explanation in text.

for which the relation takes the even simpler form:

$$f(a, b, \lambda) = p(a, \infty, \lambda) \quad \text{if } \lambda < 2b$$

Figure 18.14 shows an example worked out by Fouquart. It refers to perpendicular reflection ( $\mu = \mu_0 = 1$ ) on an atmosphere of which the scatterers are characterized by a Mie scattering pattern with size parameter  $x = 2$  and refractive index  $m = 1.33$  and by an albedo  $a = 0.999$ . The figure shows the curves of  $f(a, b, \lambda)$  against  $\lambda$  for all integer values of  $b$  from 1 to 13. They all coincide from  $\lambda = 2b$  downward with the top curve, which is  $p(a, \infty, \lambda)$ .

We may now inspect these curves with the knowledge that  $b$  may be equated to the penetration depth  $q$  and extract a number of interesting data. First, if the figure were redrawn with a linear  $f$  scale and with the  $\lambda$  scale extending all the way to infinity, the area contained between two chosen  $\lambda$  lines and two chosen  $b$  curves equals the fraction of light paths, in reflection against a semi-infinite atmosphere, that satisfy the simultaneous conditions that  $\lambda$  and  $q$  are between these chosen boundaries. The black parallelogram in Fig. 18.14 marks the fraction contained in the intervals  $\lambda = 50-51$ ,  $q = 6-7$ ; the magnitude of this fraction, read from the figure, is  $5 \times 10^{-4}$ .

Second, we can see the distribution of paths  $\lambda$  belonging to a given penetration depth  $q$ . For instance, the cross-hatched area between the curves  $b = 4$  and  $b = 5$  signifies all paths reaching a penetration depth in the interval  $q = 4-5$ . Its total area is 0.079 and its distribution of path lengths normalized to total area 1 is shown in Fig. 18.15. The maximum is reached at  $\lambda = 16$ . The median at  $\lambda = 18$  and the lines at  $\lambda = 11.5$  and 31 cutting 10% wings from each

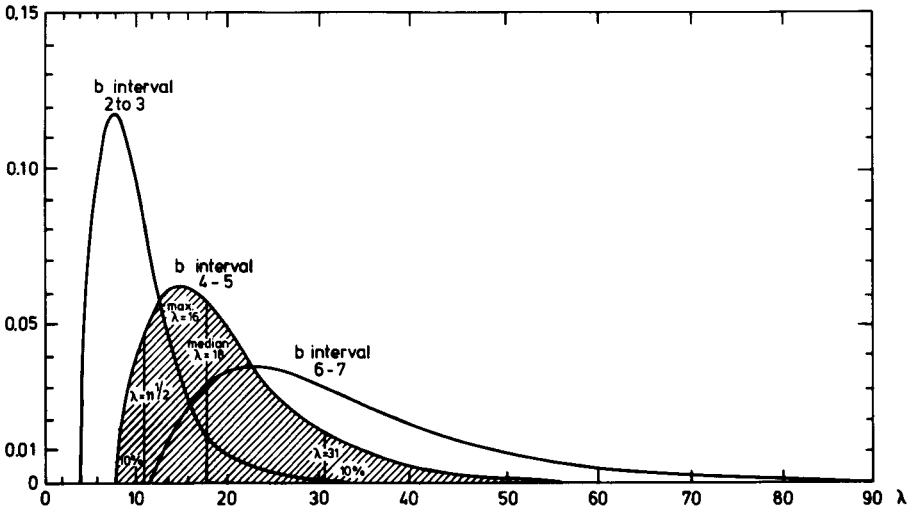


Fig. 18.15. Distribution of photon light paths for tracks reaching a penetration depth in a given interval. The assumptions are the same as in Fig. 18.14. The shaded area corresponds to the shaded area in that figure (from Fouquart, 1975).

side are also drawn in. The corresponding curves for two different  $b$  intervals complete the figure.

Finally, we can make a vertical cross section through Fig. 18.14, which displays how the penetration depths are distributed among photons that have all covered the same path length  $\lambda$ . Fouquart's curve for  $\lambda = 50$  is shown in Fig. 18.16. It has a maximum near  $q = 8.5$ , a median near  $q = 8.9$ , and the 10% area wings are limited by  $q = 6.0$  and  $q = 12.4$ . In the same figure the curves for  $\lambda = 12$  and  $\lambda = 87$  are also shown. Note that the curve for  $\lambda = 12$  reaches 0 at the

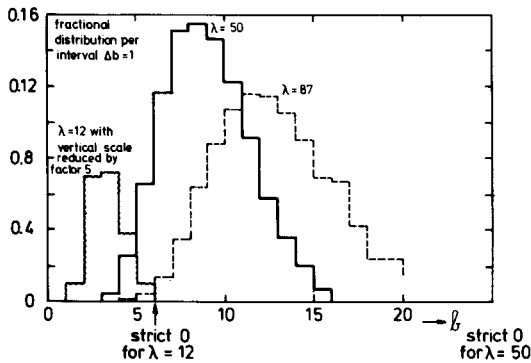


Fig. 18.16. Distribution of penetration depths for tracks with a given total length. The assumptions are again as in Fig. 18.14. Area under each step curve is 1 (from Fouquart, 1975).



maximum possible  $q = \frac{1}{2}\lambda$ . The other distributions are practically zero long before they reach this point.

For a numerical check, we can retrieve the fraction in the black parallelogram in Fig. 18.14 in two ways. First, at  $\lambda = 50$  in the curve  $b = 6-7$  of Fig. 18.15 we read a probability 0.009; multiplying this with the total  $b = 6-7$  fraction, which is 0.053 (not separately presented) we obtain the result 0.0005. Second, at  $b = 6-7$  on the curve  $\lambda = 50$  in Fig. 18.16 we read a fraction 0.117. This fraction of the total at  $\lambda = 50$ , which is 0.0043 as read from the top curve of Fig. 18.14, is again 0.0005.

The main points which are brought out by this analysis are the following: (a) These curves can be constructed with relative ease, and (b) both the  $\lambda$  distribution for fixed  $q$  (Fig. 18.15) and the  $q$  distribution for fixed  $\lambda$  (Fig. 18.16) are fairly narrow. Generally,  $\lambda$  and  $q$  go together with a spread of some 40%. This may hardly seem interesting to a theorist, but a practical physicist knows that many probing methods in science have to be content with such wide "filters," and that quite accurate results may then be obtained if the filter characteristics are properly known and used.

After preparing this added tool we may now return to the absorption lines seen in reflection from an inhomogeneous atmosphere. The absorption is caused by the factor  $\exp(-\gamma_v \lambda)$  as explained in detail in Section 17.1. Hence each absorption line, or part of an absorption line (core, wing, etc.), is most sensitive to a particular range of continuum path lengths  $\lambda$ . We have just seen that in turn, each range of  $\lambda$  corresponds roughly to a particular range of penetration depths  $q$ . This means that the method just explained opens the possibility to state (with good numerical accuracy, though with some spread) *at what depth the lines are formed*.

The adjustment of an initially homogeneous model by changing the properties of certain layers responsible for certain lines should now be easy. This is in essence what Fouquart does. The precise technique is hardly interesting since most research workers may wish to choose their own device. In any case, until more experience has been gained, it would be well to use the method suggested above only in an exploratory fashion. The final check should be made with some more elaborate "exact" method, for which enough possibilities are available. The paper by Sato *et al.* (1977) is a fine example.

### 18.5.3 Absorption Seen by an Omnidirectional Probe

This section is a brief nostalgic record of a conversation held in the late Dr. Nordberg's office at the Nasa Goddard Space Flight Center on 10 September 1962. This conversation led me to resume research on scattering in planetary atmospheres which I had dropped some 14 years before and became the reason for working on this book, which took about the same number of years to complete.

The issue was simple. Under consideration was the idea of lowering a probe into the Mars atmosphere in order to measure the presence of any absorption lines in the near infrared by looking directly into the sun. Since it seemed impossible to equip such a probe with a pointing system, a probe registering the radiation in all downward directions was considered. The question was whether such a probe, which registers the sky together with the sun, can still detect the presence of absorption lines.

Dr. Hanel remarked that this was the same problem as for a Paetzold probe to measure ozone in the earth's atmosphere. I said that for simple assumptions the answers would be in the literature and produced a few days later a table based on Chandrasekhar and Elbert (1952).

The conclusion was that for a rough determination of the presence and strength of any absorption line, the measurements of sun plus sky can serve as well as the sun measurements alone. Yet the length of time it had taken to dig these data from the literature was disappointing. The wish to have data more readily available for a wider set of assumptions became the guiding principle of this book.

Table 61 presents for isotropic scattering the original sample table with somewhat more accurate numbers taken from Table 12 (Section 9.1.1) and double checked with the formula of Display 9.1 and the  $Y$  function tabulated by Carlstedt and Mullikin (1966). The assumptions are no ground reflection and pure scattering with optical depth  $b = 0.5$  outside the absorption band. Inside

TABLE 61  
Readings of Omnidirectional Probe at Bottom of Atmosphere<sup>a</sup>

	$\mu_0 \simeq 1$ (sun at zenith)		$\mu_0 = 0.5$ (sun 30° above horizon)		$\mu_0 = 0.1$ (sun close to horizon)	
	Reference band <sup>b</sup>	Absorption band <sup>c</sup>	Reference band <sup>b</sup>	Absorption band <sup>c</sup>	Reference band <sup>b</sup>	Absorption band <sup>c</sup>
Isotropic scattering ( $g = 0$ )						
Sun + sky	1.0538	0.5274	0.7090	0.2272	0.0865	0.0119
Sun only	0.6065	0.3679	0.3679	0.1353	0.0067	0.0000
Sky only	0.4473	0.1595	0.3411	0.0919	0.0798	0.0119
Moderately forward scattering ( $g = 0.5$ )						
Sun + sky	1.1644	0.6109 <sup>d</sup>	0.8327	0.2689 <sup>d</sup>	0.1056	0.0136 <sup>d</sup>
Sun only	0.6065	0.3679	0.3679	0.1353	0.0067	0.0000
Sky only	0.5579	0.2430 <sup>d</sup>	0.4648	0.1336 <sup>d</sup>	0.0989	0.0136 <sup>d</sup>

<sup>a</sup> The given numbers are  $2\mu_0 NT(\mu_0)$ .  
<sup>b</sup> Reference band:  $b = 0.5, a = 1$ .  
<sup>c</sup> Absorption band:  $b = 1, a = 0.5$ .  
<sup>d</sup> Found by interpolation, last digits uncertain.

the absorption band the optical depth is assumed to be doubled. The corresponding numbers for moderate forward scattering with  $g = 0.5$  have now been added from Table 35 (Section 13.1). The original conclusion holds for both sets of data.

## 18.6 THERMAL EMISSION OF THE PLANETS

The title suggests an extremely vast subject, tied in with the energy balance, atmospheric and surface chemistry, and atmospheric dynamics of the planets. See, e.g., Kondratiev and Moskalenko (1977) for a recent review. This section has a far more modest aim. It intends to show by a few chosen examples which results obtained in earlier chapters of this book are relevant to this problem.

We direct our attention mostly to the planet Venus, which by its very thick atmosphere has posed the biggest puzzles. Very briefly, the prominent observed facts are the following.

(1) Thermal emission in the 8–13  $\mu\text{m}$  window corresponds to a blackbody temperature near 240 K.

(2) In the same band the emission from the planet shows a pronounced limb darkening.

(3) the temperature increases somewhat, to about 280 K, if we go to the longer waves around 100 and 350  $\mu\text{m}$ .

(4) The actual temperature deep in the atmosphere is much higher, going up to some 700 K. This has first been inferred from radio astronomy and was later confirmed by space probes entering the atmosphere.

### A. AN ISOTHERMAL NONBLACKBODY

One way to explain the limb darkening is to regard the emission as coming from a scattering and absorbing atmosphere of large optical thickness (a cloud deck) that is approximately isothermal. The intensity emitted in direction  $\mu$  (cosine of angle with normal) is then, by Kirchhoff's law,

$$I(\mu) = B(T) \cdot \alpha(\mu)$$

where  $B(T)$  is the blackbody intensity of a body at temperature  $T$ . The dependence on wavelength is present in all factors but not written. Further,  $\alpha(\mu)$  is the absorbed fraction for radiation incident from direction  $\mu$ . In the present case, for very thick layers, this absorbed fraction is simply the nonreflected fraction. Hence in the notation of earlier chapters

$$\alpha(\mu) = 1 - UR(\mu)$$

where  $UR(\mu)$  is the reflected fraction given for many phase functions in earlier chapters. Goody (1964), who first proposed this simple explanation, remarks

that for isotropic scattering this takes a simple form (Section 8.4) which at once gives

$$I(\mu) = B(T)(1 - a)^{1/2}H(a, \mu)$$

The form of the limb-darkening curve  $H(a, \mu)$  matches the observations well for  $a = 0.85$ – $0.9$ , but this also means that  $T$  must be raised to 280 K in order to match the absolute value.

Clearly, such a match is not unique but may also be made on the assumption of a different phase function. Goody gives an example with linearly anisotropic scattering. For arbitrary phase functions, by the equations of Section 5.4.1, we have

$$UR(\mu) = 1 - [4k/3(1 - g)]K(1, \mu) + O(k^2)$$

where  $K(1, \mu)$  is the escape function for conservative scattering. Hence, in any case, for  $a \rightarrow 1$  the limb darkening becomes identical to that expected from an atmosphere with a deep-seated internal heat source (Sections 5.5 and 11.2). This is exactly as we should expect since in this limit the superficial layers contribute very little to the total emission.

The fully opposite situation occurs if  $a$  is zero. This means that incident radiation would *not* be reflected, so  $UR(\mu) = 0$ , and that the planet is truly an isothermal blackbody with  $I(\mu) = B(T)$ , showing no limb darkening. The emission by the planet Jupiter comes close to this situation, because the equivalent blackbody temperature over the observable part of the disk is extremely flat (Murray and Wildey, 1963). The data now available at  $8.4 \mu\text{m}$  (Orton, 1975) and at 20 and  $45 \mu\text{m}$  (Orton, 1976) require a more detailed discussion in terms of local variations and vertical temperature structure.

## B. A BLACK NONISOTHERMAL BODY

An alternative, even simpler explanation of the limb darkening is obtained by assuming that no scattering occurs at all. The planet then is black in the sense that any incident radiation would be fully absorbed. The simplest assumption is that each layer of optical depth  $\tau$  radiates black body radiation  $B(T)$  appropriate to the temperature  $T(\tau)$  present at that depth. This determines the composite function  $B[T(\tau)] = B'(\tau)$ , and the emitted intensity emerging in direction  $\mu$  is

$$I(\mu) = \int_0^\infty B'(\tau) e^{-\tau/\mu} d\tau/\mu$$

This is the normal situation in stellar atmospheres. The limb ( $\mu \rightarrow 0$ ) is darker because the radiation emerging in those directions comes mostly from the superficial, cooler layers. The observations leave no doubt that the temperature of the Venus atmosphere rises steadily when we penetrate towards deeper layers. Therefore the present explanation must be essentially correct and explanation A, though elegant, is mostly useless.

The theory just presented must be completed by a computation of the function  $T(\tau)$ , which results from the energy balance in the atmosphere. This question has a precise, though nontrivial answer under the following set of assumptions: original source of energy is deep-seated (essentially at  $\tau \rightarrow \infty$ ); energy exchange occurs only by radiation; absorption is grey ( $\tau$  independent of wavelength). The answer then is that  $T^4$  is proportional to the function  $\tau + q(\tau)$ , which was displayed in Fig. 8.12 and which in rough estimates is often replaced by the straight-line Eddington approximation  $\tau + \frac{2}{3}$ .

The reason why the curve from Fig. 8.12 is applicable is that the net effect of all absorption and emission processes is that no energy can get lost. Hence the intensity integrated over all wavelengths behaves as if it diffuses through a medium subject only to isotropic scattering with albedo 1.

As soon as any of these assumptions is dropped, it becomes necessary to consider the full balance of energy gains and losses at each layer before the function  $T(\tau)$  at any wavelength can be constructed. Such computations, with or without the label "greenhouse effect," have been performed in many variations, but they usually lead into details that are not interesting in the context of this book.

An interesting variation on the simplest set of assumptions is an atmosphere (or thick cloud layer) with nonzero scattering in the infrared. Let the scattering be again "grey" in the sense that both the albedo  $a$  and the phase function  $\Phi(\cos \alpha)$  are independent of  $\lambda$  through the IR (infrared) range and let the primary energy source again be deep-seated, and the energy be transported exclusively by radiation. The radiation intensity in the entire IR region may then be lumped together. Since energy is conserved, this combined intensity emerges from the atmosphere as in the problem of an emerging constant net flux (Sections 5.2.1 and 11.2) in which the albedo is 1 and the appropriate phase function is (Samuelson, 1967)

$$\Phi'(\cos \alpha) = 1 - a + a\Phi(\cos \alpha)$$

This means that, e.g., the limb darkening of the *combined* IR radiation for all practical purposes can be read directly from the top curves in Fig. 11.2. It also means that the actual temperature  $T$  in the atmosphere establishes itself so that  $\pi^{-1}\sigma T^4$  (where  $\sigma$  is the Stefan-Boltzmann constant) equals the source density in this equivalent problem. Having thus established the temperature distribution with depth, it is necessary to go back to the original problem with absorption *and* scattering in order to find the emerging intensity at each wavelength.

### C. MORE COMPLEX MODELS

Models A and B are relatively simple. In all other situations, e.g., with different means of energy transport, more elaborate calculations are called for. Now that the models for the greenhouse effect are well in hand mathematically (Samuelson, 1968; Shultis and Kaper, 1969), it has also become clear that the

TABLE 62  
Absorption of Sunlight in Venus Atmosphere

Height above Venus ground	Layer	Downward visual radiation observed from Venera 8 at $\mu_0 \approx 0.10$	Absorbed percentage of visual radiative energy incident on entire planet <sup>a</sup>		Specification of parameters of different layers					
			Model I	Model II	Model I			Model II		
					<i>g</i>	<i>a</i>	<i>b</i>	<i>g</i>	<i>a</i>	<i>b</i>
Outside		100 (= $W_0$ ) <sup>b</sup>	9.98	0	0	0.997565	18.9	0	1	8.4
48 km	Layer 1 (visible cloud layer)									
35 km	Layer 2	18	0	8.62	0	0.999999	561	0	0.97328	4.4
0 km	Layer 3	7	0	0	0	0.999999	517	--	--	0
	Ground	2	0.02	1.38	Ground albedo = 0.995			Ground albedo = 0.6		

<sup>a</sup> This corresponds to incidence  $U$  in our notation.

<sup>b</sup> Put here arbitrarily at 100; the actual value is 55 W/m<sup>2</sup>.

actual temperature on Venus depends strongly also on dynamical processes in the atmosphere. Yet, with the advent of more complicated models, the need to assess the influence of the radiative effects will remain and the demand for quick and reliable methods to do so may even increase. We hope that some answers to this demand may be found in this book.

As an example, we copy in Table 62 the essential data on two models (a three-layer and a two-layer model) which Lacis and Hansen (1974) fitted to the Venera 8 sunlight measurements. These models are based on isotropic scattering ( $g = 0$ ) because a corresponding match with a different value of  $g$  can easily be made by means of the similarity rules (Section 14.1). Both models have been chosen to give a visual planetary albedo of 90% and both match the observations. This shows that the downward visual radiation measured in one situation is *not* sufficient to determine in what layer the energy of the nonreflected 10% of the incident visual radiation is deposited.

In either model the top layer, which is the visible cloud layer, is translucent in the sense defined in Section 18.4.1. This means that in spite of the large optical depth of this layer, enough radiation trickles through so that the reflectivity of the atmosphere plus ground below this top layer do matter in the final result. The models represent extremes, as skillfully explained by Lacis and Hansen.

With reference to Section 18.4.1(d) and (e), model I is an extreme case of a negative  $d$  value. A semi-infinite layer with the value of  $a$  assumed for the top layer would reflect 89.3% (value of  $URU$ ); by assuming the finite optical depth  $b = 18.9$  this is reduced to 88.6% in the absence of a bottom surface. The equations are in Section 5.3. The crucial factor is  $f$ , which in this case is  $f = 0.176$  ( $k = 0.0854$ ,  $l = 0.886$ ). By adding a "bottom" with 100% reflectivity, this difference is overcompensated, and the  $URU$  of the combination goes up to 90.0%.

In model II the layers below the top layer do all the absorbing, and the top layer has a linear gradient in  $\tau$  as is necessary in a thick layer with conservative scattering (cf. examples in Sections 8.6.2 and 9.5). Between models I and II lies the model in which the layers below layer 1 have the "matched reflectivity"  $A_g = 0.9$ .

Lacis and Hansen correctly take the point of view that separate calculations for anisotropic scattering are not necessary because in layers of such thickness it is sufficient to rely on the similarity rules. Evidently the same results are reached by inserting the numbers appropriate to the adopted anisotropic phase function into the equations quoted from Sections 5.3 and 18.4.1.

## REFERENCES

- Anikonov, A. S. (1974). *Astrofizika* 10, 227 [English transl.: *Astrophysics* 10, 138 (1975)].  
 Arking, A., and Potter, J. (1968). *J. Atmos. Sci.* 25, 617.  
 Axel, L. (1972). *Astrophys. J.* 173, 451.  
 Baker, A. L., et al. (1975). *Science* 188, 468.

- Barkstrom, B. R. (1973). *J. Geophys. Res.* **78**, 6370.
- Belton, M. J. S., McElroy, M. B., and Price, M. J. (1971). *Astrophys. J.* **164**, 191.
- Binder, A. B., and Jones, J. C. (1972). *J. Geophys.* **77**, 3005.
- Binder, A. B., and McCarthy, D. W. (1973). *Astron. J.* **78**, 939.
- Blättner, W. (1972). *Beitr. Phys. Atmos.* **45**, 20.
- Buriez, J. C., Fouquart, Y., and Fymat, A. L. (1979). *Astrophys. J.* **230**, 590.
- Carlstedt, J. L., and Mullikin, T. W. (1966). *Astrophys. J. Suppl.* **12**, 449.
- Casti, J. L., Kalaba, R., and Ueno, S. (1969). *J. Quant. Spectrosc. Radiat. Transfer* **9**, 537.
- Casti, J. L., Kalaba, R., and Ueno, S. (1970). *J. Quant. Spectrosc. Radiat. Transfer* **10**, 1119.
- Casti, J. L., Kagiwada, H., and Kalaba, R. (1973). *J. Quant. Spectrosc. Radiat. Transfer* **13**, 267.
- Chamberlain, J. W. (1970). *Astrophys. J.* **159**, 137.
- Chamberlain, J. W., and Kuiper, G. P. (1956). *Astrophys. J.* **124**, 399.
- Chamberlain, J. W., and McElroy, M. B. (1966). *Astrophys. J.* **144**, 1148.
- Chandrasekhar, S., and Elbert, D. (1952). *Astrophys. J.* **115**, 244.
- Coffeen, D. L. (1974). *J. Geophys. Res.* **79**, 3645.
- Coffeen, D. L., and Hansen, J. E. (1973). In "Planets, Stars and Nebulae Studied with Photopolarimetry" (T. Gehrels, ed.), p. 518. Univ. of Arizona Press, Tucson, Arizona.
- Connes, P., Connes, J., and Maillard, J. P. (1969). "Atlas des spectres infrarouges de Venus, Mars, Jupiter et Saturne." Ed. du Centre National de la Recherche Scientifique, Paris.
- Coulson, K. L., Dave, J. V., and Sekera, Z. (1960). "Tables Related to Radiation Emerging from a Planetary Atmosphere with Rayleigh Scattering." Univ. of California Press, Berkeley, California.
- Coulson, K. L., Gray, E. L., and Bouricius, G. M. B. (1966). *Icarus* **5**, 139.
- Danielson, R. E. (1977). *Icarus* **30**, 462.
- Danielson, R. E., Tomasko, M., and Savage, B. (1972). *Astrophys. J.* **178**, 887.
- Danielson, R. E., Caldwell, J. J., and Larach, D. R. (1973). *Icarus* **20**, 437.
- Dlugach, J. M., and Yanovitskii, E. G. (1974). *Icarus* **22**, 66.
- Dunham, Th. (1949). In "The Atmospheres of the Earth and Planets," (G. P. Kuiper, ed.) Chapter 11. Univ. of Chicago Press, Chicago, Illinois.
- Duysinx, R., and Henrist, M. (1973). In "Exploration of the Solar System" (A. Woszczyk and C. Iwaniszewska, eds.), I. A. U. Symp. 65, p. 351. Reidel, Dordrecht, The Netherlands.
- Fouquart, Y. (1974). *J. Quant. Spectrosc. Radiat. Transfer* **14**, 497.
- Fouquart, Y. (1975). Ph.D. Thesis, Univ. de Lille, Lille, France.
- Gehrels, T., Hermans, B. M., and Owen, T. (1969). *Astron. J.* **74**, 190.
- Goody, R. (1964). *Icarus* **3**, 98.
- Grant, I. P., and Hunt, G. E. (1968). *Icarus* **9**, 526.
- Hall, J. S., and Riley, L. A. (1968). *Lowell Observatory Bull.* **7**, 83.
- Hansen, J. E. (1969). *Astrophys. J.* **158**, 337.
- Hansen, J. E. (1971a). *J. Atmos. Sci.* **28**, 120.
- Hansen, J. E. (1971b). *J. Atmos. Sci.* **28**, 1400.
- Hansen, J. E., and Arking, A. (1971). *Sci.* **171**, 669.
- Hansen, J. E., and Hovenier, J. W. (1971). *J. Quant. Spectrosc. Radiat. Transfer* **11**, 809.
- Hansen, J. E., and Hovenier, J. W. (1974). *J. Atmos. Sci.* **31**, 1137.
- Hansen, J. E., and Travis, L. D. (1974). *Space Sci. Rev.* **16**, 527.
- Harris, D. L. (1961). In "The Solar System" (G. P. Kuiper and B. M. Middlehurst, eds.), Vol. III, Planets and Satellites, p. 272. Univ. of Chicago Press, Chicago, Illinois.
- Herzberg, G. (1949). In "The Atmospheres of the Earth and Planets," (G. P. Kuiper, ed.) Chapter 13. Univ. of Chicago Press, Chicago, Illinois.
- Horak, H. G. (1950). *Astrophys. J.* **112**, 445.
- Hovenier, J. W. (1969). *J. Atmos. Sci.* **26**, 488.
- Hovenier, J. W. (1970). *Astron. Astrophys.* **7**, 86.
- Hovenier, J. W. (1971). *Astron. Astrophys.* **13**, 7.



- Hunten, D. M. (1971). *Space Sci. Rev.* **12**, 539.
- Hunten, D. M. (ed.) (1974). The Atmosphere of Titan, a workshop held at Ames Research Center, NASA Report SP-340.
- Irvine, W. M. (1975). *Icarus* **25**, 175.
- Kattawar, G. W. (1974). *J. Quant. Spectrosc. Radiat. Transfer* **14**, 157.
- Kattawar, G. W., and Adams, C. N. (1971). *Astrophys. J.* **167**, 183.
- Kattawar, G. W., and Young, A. T. (1977). *Icarus* **30**, 367.
- Kawabata, K., and Hansen, J. E. (1975). *J. Atmos. Sci.* **32**, 1133.
- Kondratiev, K. Ya, and Moskalenko, N. I. (1977). "Teplovoe Isluchenie Planet." Gidrometeoizdat, Leningrad.
- Kuiper, G. P. (1949). "The Atmospheres of the Earth and Planets." Univ. of Chicago Press, Chicago, Illinois.
- Lacis, A. A., and Hansen, J. E. (1974). *Science* **184**, 979.
- Loskutov, V. M. (1971). *Astron. Zh.* **48**, 1046 [English transl.: *Sov. Astron. AJ* **15**, 828].
- Lyot, B. (1929). *Ann. Observ. Paris (Meudon)* **8**.
- Mead, J. L. (1970). *Icarus* **13**, 82.
- Minnaert, M. (1941). *Astrophys. J.* **93**, 403.
- Minnaert, M. (1961). In "The Solar System" (G. P. Kuiper and B. M. Middlehurst, eds.), Vol. III, Planets and Satellites, p. 213. Univ. of Chicago Press, Chicago, Illinois.
- Murray, B. C., and Wildey, R. L. (1963). *Astrophys. J.* **137**, 692.
- Odell, A. P., and Weinman, J. A. (1975). *J. Geophys. Res.* **80**, 5035.
- Orton, G. S. (1975). *Icarus* **26**, 142.
- Orton, G. S. (1976). In "Jupiter, Studies of the Interior, Atmosphere, Magnetosphere and Satellites" (T. Gehrels, ed.), p. 206. Univ. of Arizona Press, Tucson, Arizona.
- Pilcher, C. P., and Kunkle, T. D. (1976). *Icarus* **27**, 407.
- Plass, G. N., Kattawar, G. W., and Catchings, F. E. (1973). *Appl. Opt.* **12**, 314.
- Pleskot, L. K., and Kieffer, H. H. (1977). *Icarus* **30**, 341.
- Pollack, J. B., and Sagan, C. (1969). *Space Sci. Rev.* **9**, 243.
- Preisendorfer, S. (1971). *J. Quant. Spectrosc. Radiat. Transfer* **11**, 723.
- Preisendorfer, S. (1976). "Hydrologic Optics," 6 Volumes, U.S. Dept. of Commerce, NOAA Environmental Research Laboratories, Honolulu, Hawaii. In particular Vol. 6, Chapter 12.
- Prinn, R. G., and Lewis, J. S. (1973). *Astrophys. J.* **179**, 333.
- Russell, H. N. (1916). *Astrophys. J.* **43**, 173.
- Samuelson, R. E. (1967). *Astrophys. J.* **147**, 810.
- Samuelson, R. E. (1968). *J. Atmos. Sci.* **25**, 634.
- Sato, M., Kawabata, K., and Hansen, J. E. (1977). *Astrophys. J.* **216**, 947.
- Sazonov, V. N. (1972). *Astron. Zh.* **49**, 833 [English transl.: *Sov. Astron. AJ* **16**, 678 (1973)].
- Schoenberg, E. (1929). *Handb. Astrophys.* **II**, 1.
- Sekera, Z., and Kahle, A. B. (1966). Rand Corporation Rep. R-452-PR. Santa Monica, California.
- Shultis, J. K., and Kaper, H. G. (1969). *Astron. Astrophys.* **3**, 110.
- Sobolev, V. V. (1968). *Astron. Zh.* **45**, 169.
- Sobolev, V. V. (1975). "Light Scattering in Planetary Atmospheres." Pergamon, Oxford (Original Russian, 1972).
- Talley, R. L., and Horak, H. G. (1956). *Astrophys. J.* **123**, 176.
- Teifel, V. G. (1976). In "Jupiter, Studies of the Interior, Atmosphere, Magnetosphere and Satellites" (T. Gehrels, ed.), p. 441. Univ. Arizona Press, Tucson, Arizona.
- Tomasko, M. G. (1976). In "Jupiter, Studies of the Interior, Atmosphere, Magnetosphere and Satellites" (T. Gehrels, ed.), p. 486. Univ. Arizona Press, Tucson, Arizona.
- Ueno, S. (1974). *Astrophys. Space Sci.* **30**, 27.
- Ueno, S., and Mukai, S. (1973). *J. Quant. Spectrosc. Radiat. Transfer* **13**, 1261.
- van de Hulst, H. C. (1949). In "The Atmospheres of the Earth and Planets," (G. P. Kuiper, ed.) Chapter 3. Univ. of Chicago Press, Chicago, Illinois.

- van de Hulst, H. C. (1971). In "Planetary Atmospheres" (C. Sagan *et al.*, eds.), I. A. U. Symp. 40, p. 177. Reidel, Dordrecht, The Netherlands.
- van de Hulst, H. C. (1974). *Astron. Astrophys.* **35**, 209.
- van de Hulst, H. C., and Irvine, W. M. (1962). La physique des planètes, *Congr. Colloq. Univ. Liège* **24**, 78.
- Wamsteker, W. (1973). *Astrophys. J.* **184**, 1007.
- Wattson, R. B., Rappaport, S. A., and Frederick, E. E. (1976). *Icarus* **27**, 417.
- Whitehill, L. P., and Hansen, J. E. (1973). *Icarus* **20**, 146.
- Young, L. D. G. (1972). *Icarus* **17**, 632.
- Young, L. D. G., and Kattawar, G. W. (1976). *Icarus* **29**, 483.
- Young, L. D. G., and Kattawar, G. W. (1977). *Icarus* **30**, 360.
- Younkin, R. L. (1974). *Icarus* **21**, 219.

## 19 ☐ Scattered Light in the Earth's Atmosphere

### CHOICE OF TOPICS

Anybody who spends a day browsing through journals on atmospheric physics must be impressed by the progress of the last decades. This is certainly the vivid impression of the author, who wrote a review on light scattering in atmospheres many years ago (van de Hulst, 1949a). In many centers one generation of research workers after the other has helped to advance our knowledge of the physical and optical properties of the atmosphere and its embedded aerosols. We must be content in this book to cite only some chosen examples. They serve to illustrate which calculations from the earlier chapters may be profitably used in discussing problems of the earth's atmosphere.

The first motivation for studying atmospheric scattering is the wish to understand: People have been intrigued for ages by the rainbow, the blue sky, the twilight colors, and the darkness under a thick cloud layer. Added motivations of a more practical nature often guide this curiosity to attack particular problems. This guidance may be concealed and noticeable only to the attentive reader, or it may be prominently displayed in a coordinated attack on some practical problem.

Some practical problems are monitoring pollution, weather prediction, weather modification, including rain making, visibility near airports or seaports, and remote sensing from satellites.

The choice of topics in what follows is somewhat arbitrary. We hope that their variety does some justice to the wide scope of the subject.

## 19.1 LOOKING AT THE DAYLIGHT SKY

## 19.1.1 The Obvious Codes

Just what can we infer by looking at the brightness distribution of the daylight sky? Instruments are not required for a first examination. We refer to Minnaert's "Light and Colour in the Open Air" (1940) for an inspired account of *all* that is to be seen. In the present section we stick to the questions that have some bearing on multiple scattering and optical depth.

First there is the obvious color code:

*Blue* indicates molecules or very finely divided aerosol. Any particle that has a polarizability independent of wavelength ( $\lambda$ ) scatters as  $\lambda^{-4}$  in the range of wavelength much larger than its size, thus causing the blue color of the sky and the blueish haze in the landscape.

*White* indicates clouds consisting of any type of particles large compared to the wavelength and with albedo close to 1.

*Black* (usually gray or a less intense white) indicates that the cloud or cloud layer is so thick that a small absorption in each drop (i.e., albedo not quite 1) makes itself strongly felt in the final intensity.

*Red*, usually near sunrise or sunset, indicates that we see light scattered from clouds after the illuminating sunlight has already covered a long extinction path through clear air.

In directions close to the sun we see the blue sky gradually change into the white "aureole," the brightness of which rapidly increases upon approach to the sun. Here aerosol particles of moderate and large size reveal themselves by their extremely strong forward scattering.

## 19.1.2 The Zenith-Horizon Brightness Ratio

The brightness distribution of the sky, although not as spectacular as its colors, has its own striking clues. The clear sky is brightest at the horizon; the overcast sky is brightest near the zenith. This statement is correct regardless of the sun's altitude and is predicted for any scattering diagram. Basically, the sky near the horizon must be bright for an optically thin atmosphere because the light path is long. It is proportional to  $\sec z = 1/\mu$ , where  $z$  is the angle from the zenith and  $\mu = \cos z$ . The sky near the zenith must be brighter if we look at it from under an optically thick atmosphere because its transmission becomes proportional to the escape function  $K(\mu)$ , which is always largest for  $\mu = 1$ .

Figure 19.1 shows an illustrative example. At both sides of the figure we have taken conservative scattering ( $a = 1$ ), placed the sun at  $30^\circ$  above the horizon ( $\mu_0 = 0.5$ ), and averaged over azimuth. The plotted function is the transmission function  $T(1, b, \mu, \mu_0)$  divided by its value for  $\mu = 1$ . Values of  $T$  for isotropic

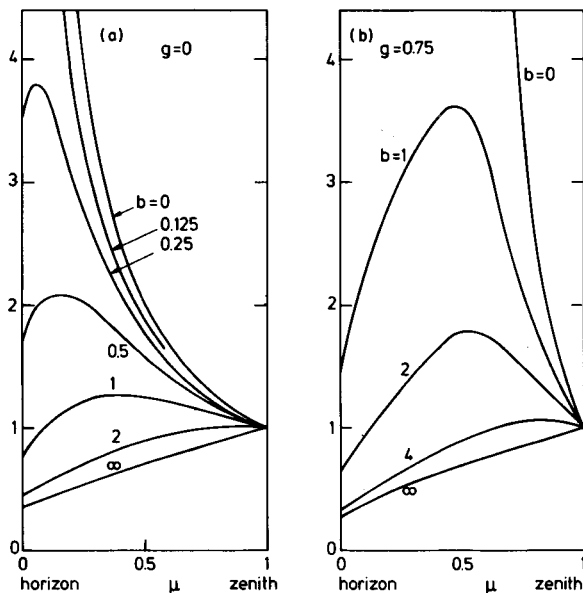


Fig. 19.1. Relative brightness distribution from horizon to zenith as seen below the atmosphere. The diffuse sky brightness, averaged over azimuth, is plotted;  $\mu_0 = 0.5$ , no ground reflection.

scattering were read from Table 12 (Section 9.1.1). The curve for  $b = 0$  is simply  $1/\mu$ ; the curve for  $b = \infty$  is  $K(1, \mu)/K(1, 1) = H(1, \mu)/H(1, 1)$ , with  $H$  taken from Table 7 (Section 8.3.1). Figure 19.1b is based on Henyey–Greenstein scattering with  $g = 0.75$ , which is a fair approximation to scattering by water drops. Here the curves for  $b = 1, 2$ , and  $4$ , are based on Table 35 (Section 13.1) and the curve for  $b = \infty$ , on Table 26 (Section 11.2). The curve for  $b = 0$  gives  $\mu^{-1}h(\mu, 0.5)$ , where  $h(u, v)$  is the redistribution function. Its values for  $g = 0.75$ , which are not shown in Table 22 (Section 11.1), were taken from a small table by van de Hulst and Davis (1961). All curves for  $b \leq 2$  in this part of the figure show that the sky brightness is enhanced near the actual altitude of the sun ( $\mu = 0.5$ ), even though the averaging over azimuth has reduced the contrast. This bias vanishes for thicker cloud layers, where neither the azimuth nor the altitude of the sun can be inferred from the brightness distribution observed below the cloud deck (Section 19.2.2).

We have used the colloquial term “brightness” in this explanation. The old-fashioned astrophysicist may replace it by “surface brightness,” those used to modern terminology by “radiance” or “luminance.” Refinements of these curves can be made in many ways: use more precise scattering diagram, add polarization, compute azimuth-dependent terms, introduce albedo  $< 1$ , add ground reflection, introduce vertical inhomogeneity, or introduce curvature of the earth. Each of these additions increases the complexity, but the problem remains manageable. See references in Section 19.2.2. To venture beyond that and study

also the play of light in a sky with broken clouds would seem a problem fit not for a computer but for a fantasy on a lazy summer day. Yet such problems have been studied for practical purposes; see the brief review in Section 20.1.3.

In Shifrin's work (Shifrin and Kozhaev, 1972), we came across an interesting practical application involving the ground albedo. Shifrin notes that the brightness distribution of a 100% overcast sky depends strongly on the percentage of the ground covered by snow, and suggests that this dependence may be used to monitor the average snow cover in a wide area from one observing site. The method is based on measurements of the sky brightness at 10 azimuths and at zenith angles 0, 20, 40, 60, and 80°. A plot of the azimuth average against  $\mu$  is approximated by a straight line

$$\sigma(\mu) = \text{const}(1 + \frac{3}{2}\eta\mu)$$

from which  $\eta$  is found. The effective ground albedo then follows from another approximate relation

$$A = (1 - \eta)/(1 + \eta), \quad \text{equivalent to} \quad \eta = (1 - A)/(1 + A)$$

Finally, the percentage of snow cover  $q$  is obtained from

$$q = (A - A_{\text{soil}})/(A_{\text{snow}} - A_{\text{soil}}), \quad \text{equivalent to} \quad A = qA_{\text{snow}} + (1 - q)A_{\text{soil}}$$

A typical value for fresh snow averaged over the visual wavelengths is  $A_{\text{snow}} = 0.70$  (with actual values from 0.60 to 0.85). The value assumed for humid soil is  $A_{\text{soil}} = 0.10$ . With these values, a measured  $A = 0.40$  gives  $q = 0.5$ . The estimated accuracy is about 0.04 in  $\eta$ , leading to a relative error of 12% in  $A$  and of about 20% in  $q$ . The values and the accuracy were confirmed by aerial surveys made on the same days.

Let us now examine the basis of this method. Clearly, it cannot be exact, for the brightness of the transmitted light is not linear in  $\mu$ . However, in two limits it is approximately correct. If  $A = 0$  and the cloud deck is opaque, we simply see the escape function (Fig. 11.2), which, for atmospheric albedo  $a = 1$ , agrees approximately with  $\eta = 1$  (see below). In the other extreme, if  $A = 1$  and again  $a = 1$ , we have the situation deep inside an (atmospheric + ground) combination without losses, in which an exactly isotropic radiation field prevails. For arbitrary  $A$  and Lambert reflection, we have assumptions identical to case (e) in Section 18.4.1, but we now need the downward radiation field at the ground. Employing Eqs. (20) and (21) of Section 5.3, and the notation of Section 18.4.1, except for the omission of the index  $g$  for ground, we readily find

$$T_{\text{comb}} = cK \cdot \left\{ K + \frac{A(KU)[UR_{\infty} - cf(KU)K]}{1 - A[UR_{\infty}U - cf(KU)^2]} \right\} \quad (1)$$

If the atmosphere is conservative ( $a = 1$ ), further simplifications result. The remaining vectors are then  $K$  and  $UR = U$ , and the constants become  $KU = 1$ ,

$UR_{\infty}U = 1$ , and  $c = cf = \frac{4}{3}/(b + 2q_0)(1 - g)$ , where  $b$  is the total optical depth and  $q_0$  the extrapolation length. After some reduction, the result for  $a = 1$  is

$$T_{\text{comb}} = cK \cdot [(1 - A)K + AU]/(1 - A + Ac) \quad (2)$$

Returning to standard notation we must write the front factor  $K$  as  $K(\mu_0)$ , the second factor  $K$  as  $K(\mu)$ , and  $U$  as 1. The relative brightness distribution is expressed by the numerator. If we choose the linear approximation  $K(\mu) = 0.50 + 0.75\mu$ , we then obtain precisely Shifrin's formula with  $\eta = (1 - A)/(1 + A)$ . However, examination of Fig. 11.2 shows that a more precise fit is obtained by  $K(\mu) = 0.46 + 0.80\mu$ , which gives  $\eta = 1.16(1 - A)/(1 + 1.18A)$ . There is virtually no dependence on phase function.

Although the correction thus found is hardly worth mentioning, the derivation has revealed that the assumption  $a = 1$  enters critically at various stages. To answer any doubts we can proceed from Eq. (1) by substituting the expressions for *nearly* conservative scattering from Section 5.4.1, neglecting higher powers of the diffusion exponent  $k$ . After a tedious reduction, we then find the comforting result that linear correction factors in  $k$  remain only in the front factor but cancel out in the part that expresses the dependence on  $\mu$ . Hence Shifrin's method may also be used under a slightly absorbing cloud deck.

### 19.1.3 How Dark Is It under a Cloud Deck?

The absolute value of the illumination below a cloud deck reveals a property of the scattering particles without instrumentation. We repeat here with a newly chosen numerical example an argument first made by Piotrowski (1955, 1956). Piotrowski points out that a cloud deck of isotropic scatterers, e.g., with total optical thickness  $b = 8$ , on which the sun shines from above with cosine zenith angle  $\mu_0$ , would let a fraction (in our notation)  $UT(\mu_0)$  of the solar radiation reach the ground.

The asymptotic Eq. (45) in Section 5.4.3 for conservative scattering gives

$$UT(\mu_0) = \frac{4}{3}K(\mu_0)/(1 - g)(b + 2q_0)$$

With  $\mu_0 = 0.7$ , i.e., solar altitude about  $45^\circ$ , we have  $K(0.7) = 1.03$  (Fig. 11.2), and with  $g = 0$ ,  $2q_0 = 1.42$  we obtain  $UT(\mu_0) = 0.146$ . For simplicity no reflection from the ground has been added. For a check we may read the exact value 0.14549 from Table 12 (Section 9.1.1). Hence in this example the illumination of a flat surface is only 15% of what it would have been under direct sunlight. Any amateur photographer knows that this corresponds to a fairly heavy cloud deck. Now Piotrowski asks whether under the same assumptions the sun's disk would still be visible through the clouds. To answer this question we observe that in the units of Table 12 the sky brightness at the place where the sun should be is 0.150. The units are such that  $\mu_0\Omega B = 1$ , where  $\Omega = 0.68 \times 10^{-4}$  is the solid angle subtended by the solar disk and  $B$  is the brightness of the unocculted

solar disk, which in this example becomes  $B = (\mu_0 \Omega)^{-1} = 2.10 \times 10^4$ . However, the clouds reduce this direct image by the factor

$$\exp(-b/\mu_0) = \exp(-11.43) = 1.09 \times 10^{-5}$$

so that in the adopted units the brightness of the direct solar image seen through the clouds is 0.23. This makes it still clearly visible over the brightness 0.15 of the diffuse sky (the actual sum 0.38 is seen at the position of the disk).

Clearly, we have encountered a paradox: the common experience is that a reduction of the general illumination to 15% corresponds to a heavy overcast through which we cannot discern the sun's disk. This does not match the calculation that the sun's disk should still be clearly visible. Piotrowski points out that this paradox is *prima facie* evidence for the fact that the scattering diagram of the cloud particles is *not* isotropic. Since  $(1 - g)q_0$  is virtually a constant (Section 12.1.2), the denominator of the asymptotic formula cited above may be written as  $(1 - g)b + 0.71$ . Hence, with an asymmetry parameter  $g = 0.8$ , we have simply to multiply  $b$  by 5 in order to leave the diffuse radiation virtually unchanged from the preceding example. This raises the total optical thickness of the cloud deck to 40 and the reduction factor of the direct solar image is now  $10^{-25}$ , which makes the sun's disk utterly invisible and completely resolves the paradox.

#### 19.1.4 How Much Higher Order Scattering Is There in the Clear Sky?

We shall presently see (Section 19.1.5) that the aureole in a clear sky can be explained to good accuracy by single scattering. At wider angles, farther than  $10^\circ$  from the sun, multiple scattering gradually assumes more significance. For a pure Rayleigh sky (in which there is no aureole) details are cited in Chapter 16. Aerosols were included in calculations of this type by de Bary and Bullrich (1964a,b) with elaborate computations of intensity and polarization, all based on a Junge distribution of aerosol particle sizes. In a separate paper, de Bary (1964) summarized the results of these calculations and compared them with measurements made at Los Angeles. The method was approximative. Ten years later, with faster computers available and with a new iteration technique developed by Eschelbach (1971), she repeated these calculations with full accuracy and in greater detail (de Bary, 1973; de Bary and Eschelbach, 1974). The assumed particle refractive index is  $1.5 - 0.01i$  or  $1.5 - 0.02i$ ; the ground albedo, 0 or 0.25. The altitude of the sun is  $24^\circ$  in the first paper and is varied in the second one. Ranges of values are considered for wavelength from 450 to 650 nm, angle from sun from  $10^\circ$  up, and turbidity  $T$  from 2 to 6.

The results, of which Fig. 19.2 presents an illustration, show the expected trends. At  $10^\circ$  from the sun primary scattering still accounts for over 90% of the total radiance. This percentage decreases as the angle increases, as the wavelength decreases, and as the turbidity increases. At the highest assumed



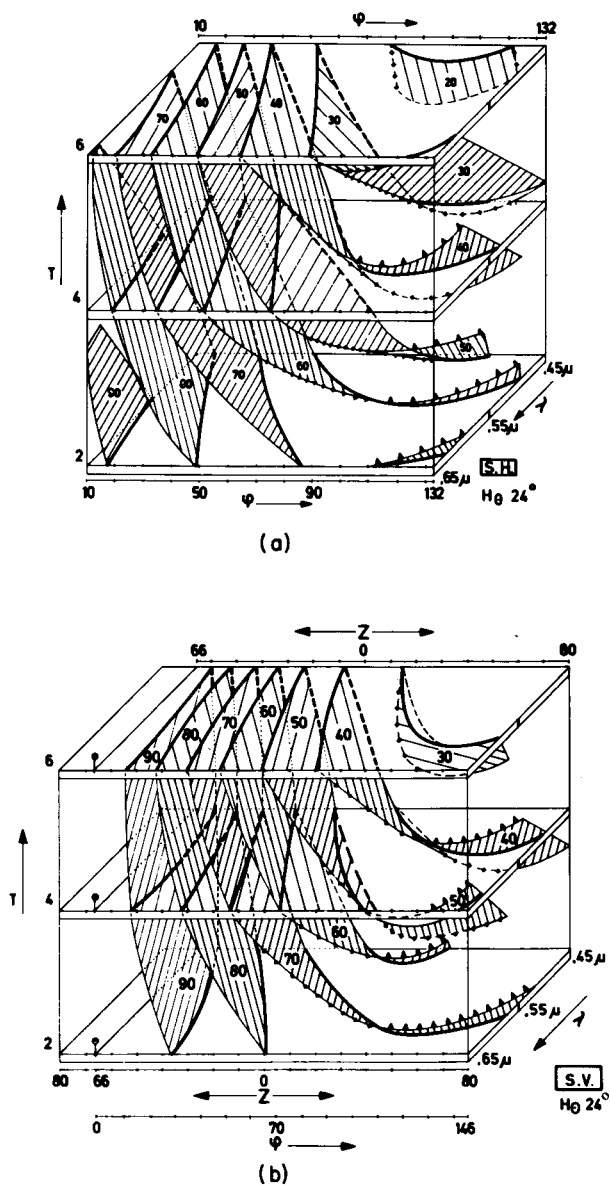


**Fig. 19.2.** Percentage primary scattering in the sky brightness. Sun's elevation  $24^\circ$ . (a) Along horizontal circle through sun; (b) along vertical circle through sun. Aerosol refractive index  $m = 1.5$ . Variable quantities: wavelength  $\lambda$ , turbidity  $T$ , angle from sun  $\phi$ , angle from zenith  $Z$  (from de Bary, 1973).

turbidity  $T = 6$  in directions far from the sun, typical percentage values for primary scattering are  $\sim 20\%$  in the blue and  $\sim 30\%$  in the red. A confirmation may be cited from Table 3 of Green *et al.* (1972). At  $\lambda = 550$  nm they assume Rayleigh optical depth 0.096 and particle optical depth 0.182 and find that the secondary scattering at  $2^\circ$  from the sun is  $0.2\%$  of the primary scattering and that the  $1\%$  level is reached at  $12\text{--}20^\circ$  from the sun.

Even with a turbidity 6, the total optical depth of the atmosphere at 550 nm is  $6 \times 0.10 = 0.60$ , small enough to render multiple scattering calculations relatively easy. In Section 19.1.6 we discuss a problem dealing with much thicker layers.

A quite different situation also prevails in the middle ultraviolet, i.e., the wavelength range 300–340 nm, where the ozone absorption sets in. The dose of radiation in this range is directly related to skin cancer incidence and for that reason has been studied elaborately. Typically, the Rayleigh optical depth at 315 nm may be put at 1, the ozone absorption optical depth at 0.5, and the aerosol scattering optical depth again at 0.5. In this situation,  $10^\circ$  from the sun only half the radiance is due to single scattering (Shettle and Green, 1974; Furman *et al.*, 1976), and in solar radiometry care should be exercised not to include too large a portion of the aureole (Sutherland *et al.*, 1975).

### 19.1.5 The Aureole

Where most of us live, even on a bright sunny day, there is a fair amount of turbidity in the air. This manifests itself most clearly if we try to look close to the sun. The sky color changes gradually from blue to intense white and its brightness continually increases until we arrive at the solar disk itself, which is again brighter by an enormous factor.

This bright area of sky around the sun is called the aureole. Its evident explanation is small-angle (near-forward) scattering by aerosol particles. Statistically, larger particles contribute to the smaller scattering angles and smaller particles to the larger scattering angles. This occurs in almost inverse proportion, because the scattering at those angles is almost exclusively described by diffraction around the particle, which does not depend on particle composition (Section 10.2.2). Hence, accurate measurement of the brightness distribution in the aureole is a potentially powerful method of determining the size distribution function of the aerosol particles.

Consistent with the purpose of this book, we do not try to review all the variations that have been observed with geographical location, altitude of the observatory above sea level, and weather situation. Van de Hulst (1949a) mentioned three sets of measurements; Eiden (1968) mentions four more recent sets besides his own. Grether *et al.* (1976, 1979) report on routine measurements from several sites. Deepak (1975, p. 265) describes a photographic observing technique and inversion procedures.

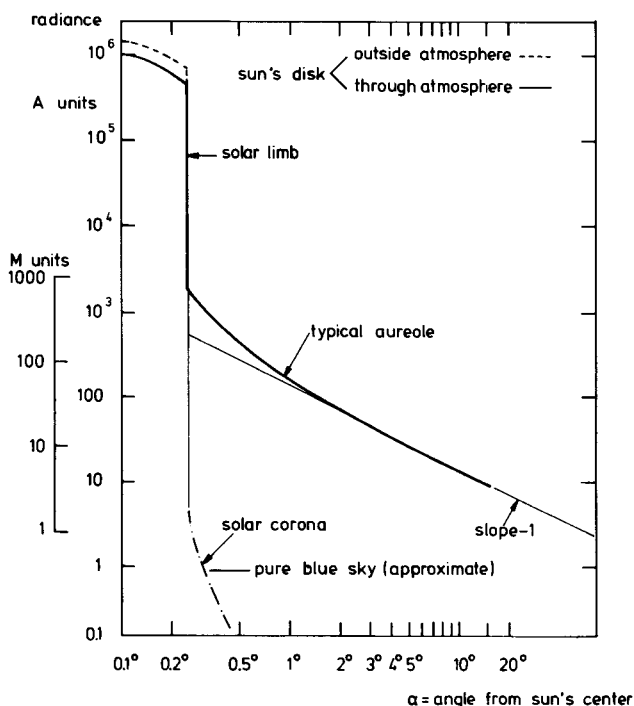


Fig. 19.3. Radiance values of aureole under typical conditions compared to sun's disk and corona and to the Rayleigh blue sky.

For a typical example we adopt: wavelength 550 nm, station near sea level, molecular optical depth of atmosphere:  $\tau_{\text{mol}} = 0.1$ , turbidity  $T = \tau_{\text{total}}/\tau_{\text{mol}} = 3$ , total optical depth of atmosphere due to aerosol and molecules  $\tau_{\text{total}} = 0.3$ , and sun's altitude above horizon  $30^\circ$ , so  $\sec Z = 2$ .

Figure 19.3 presents the typical aureole radiance observed under these circumstances (Eiden, 1968, Fig. 6b). In this figure the radiance on a logarithmic scale has been plotted against the angle from the center of the sun's disk, again on a logarithmic scale. In order to facilitate the theoretical discussion, we have referred the radiance to the average radiance of the sun's disk. The conversion requires some care. Near 550 nm the spectral radiance of the sun, averaged over the disk, is in conventional astrophysical units:

$$F = 2.8 \times 10^{14} \text{ erg cm}^{-3} \text{ sec}^{-1} \text{ sr}^{-1}$$

where  $\text{cm}^{-3}$  is to be read as "per (centimeter)<sup>2</sup> (area) and per centimeter (wavelength band)." If we call this  $10^6$  A units, then we have defined the scale at the left side of Fig. 19.3. Eiden (1968) and other meteorologists express the spectral

radiance in units which we shall term

$$1 \text{ M unit} = 10^{-3} \text{ cal min}^{-1} \text{ cm}^{-2} (100 \text{ \AA})^{-1} \text{ sr}^{-1}$$

With the proper conversion factors, at the adopted wavelength, this gives:  $1 \text{ M unit} = 2.5 \text{ A units}$ , and this defines the second scale of Fig. 19.3.

Figure 19.3 illustrates a number of familiar points. First, the aureole completely drowns the solar corona, which arises from scattering by electrons around the sun and by dust particles in interplanetary space. Second, the aureole drowns by a factor of the order of 100 (at  $1^\circ$ )–10 (at  $15^\circ$ ) the molecular scattering, which, at wider angles, causes the blue sky. These ratios depend strongly on wavelength and weather conditions. Third, the sun's limb stands out sharply by a drop in radiance of the order 1000. That it is a gradual transition when seen on the scale of fractions of seconds of arc (owing to the structure of the sun's atmosphere and to "seeing" in the earth's atmosphere) is irrelevant in the present context.

It is possible to infer from Fig. 19.3, even before the physical discussion in terms of aerosol scattering, that the inner aureole consists almost exclusively of directly scattered sunlight (primary scattering). The reasoning is as follows. An aerosol particle near the bottom of the earth's atmosphere is exposed (1) to direct sunlight and (2) to the aureole radiance, exactly as shown in Fig. 19.3. If part (1) is scattered, it creates primary scattering. If part (2) is scattered, it creates multiple scattering, both parts being strongly peaked towards the direction of the sun and hence contributing to the total aureole. The ratio is found by simple integration over solid angle, which leads to the following integrals (in A units times degrees squared): direct sunlight integrated radiance  $= \pi(\frac{1}{4})^2 10^6 = 62,000\pi$ ; aureole radiance integrated between angles  $\alpha_1$  and  $\alpha_2$ , by an approximation formula (see Fig. 19.3),

$$\int_{\alpha_1}^{\alpha_2} \left( \frac{125}{\alpha} \right) 2\pi\alpha \, d\alpha = 250\pi(\alpha_2 - \alpha_1) = 2500\pi$$

where we have arbitrarily put  $\alpha_2$  at  $10^\circ$  and neglected  $\alpha_1$ . The ratio of these two numbers shows that multiple scattering would contribute about 4% of the aureole's radiance, if all aerosol particles were exposed to this illumination. In fact the aerosol particles higher up along the path see a clearer sky, and the actual ratio is more likely to be 2%.

If the integration were extended over the full sky, the sky radiation due both to aerosols and to molecular scattering enters in much closer competition with the direct sunlight, as indeed we should expect from the total optical depth of 0.3. Hence there must be a nonnegligible radiance arising from multiple scattering all over the sky. This part, discussed in Section 19.1.4, is not peaked near the sun, and hence contributes hardly anything to the aureole inside  $10^\circ$ .

Having established that only primary scattering is involved, we may turn to the interpretation in terms of a distribution of particle sizes. This subject will be resumed in Section 19.2.3.

### 19.1.6 The Hazy Sun

Several years ago Prof. F. W. Went of Reno, Nevada informed me by letter that at exceptional times the sun's disk does not have a sharp limb. I referred this information to Prof. M. Minnaert of Utrecht, Holland, who confirmed that the phenomenon existed but did not know an explanation, although for many decades he had made an intensive study of the phenomena of natural atmospheric optics (Minnaert, 1937, 1940, 1953).

At first sight such a phenomenon seems impossible. The discussion in the preceding section leaves only two possibilities. Either the sun's disk is not visible at all because the contrast with the surrounding sky is too low (which occurs roughly at cloud decks with optical depth  $b/\mu \geq 14$ ), or the sun's direct image, weakened by a factor  $\sim 10^{-5}$ , still shines through the clouds, retaining its appearance and its sharp limb. This is indeed common experience: skippers for many centuries have made a sextant fix for determining the altitude of the sun's upper or lower limb as easily through clouds as in a clear sky. The same, with the radiance a factor  $10^6$  lower, holds true for the moon seen at night through cloud veils.

How then can we explain the hazy sun? The only explanation appears to be that we do not in fact see the unscattered solar image, but rather light that has suffered so many scattering events by extremely small angles that the net result is a hazy image or a kind of composite "aureole" that resembles the direct image. This at once implies that the possibility of only single scattering (as in the normal aureole) must be ruled out, for the optical depth which is large enough to render the direct image invisible would also render the image formed by single scattering events invisible.

The following estimate does not claim precision but serves to show that an explanation of this type is quantitatively possible. The true cross section of intensity along a solar diameter has a width about  $30'$  and some limb darkening. Estimate that the equivalent Gaussian profile has a full width at half maximum (FWHM) of  $25'$ . Suppose the hazy sun has also a Gaussian cross section with  $\text{FWHM} = 35'$ . The ratio  $35'/25'$  is  $\sqrt{2}$ , so the broadening profile of effectively  $n$  scattering events must also be Gaussian with  $\text{FWHM} = 25'$ . The precise theory of such multiple small-angle scattering is reviewed in Section 20.5.2 but is of no consequence here.

Next, we use the fact (Section 10.2.2) that particles large compared to the wavelength have equal cross sections for small-angle scattering (caused by diffraction) and for wide-angle scattering plus absorption. Since our attention is focused on the "aureole," which virtually coincides with the solar image, and assuming we have only such large particles, any scattering event gives the probability  $\frac{1}{2}$  that the photon is retained and the probability  $\frac{1}{2}$  that it is lost from the hazy image. Hence, if  $b$  is the total optical depth through which the sun is seen, the direct (sharp) solar image is reduced in intensity by a factor  $e^{-b}$ , but the

hazy image only by a factor  $e^{-b/2}$ . The situation may therefore occur that the sharp image is rendered invisible while the hazy image is not. A practical value might be  $e^{-b/2} = 10^{-3}$ ,  $e^{-b} = 10^{-6}$ ,  $b = 14$ . Then, very roughly, the average number of scattering events  $n$  contributing to the hazy image is also 14, and the scattering profile, i.e., the diffraction pattern corresponding to one such event, must have  $\text{FWHM} = 25'/\sqrt{14} = 7'$ . For droplets of a single size this corresponds to a diameter of  $0.3 \text{ mm} = 300 \mu\text{m}$ . In the more realistic case of a size distribution, using the rule quoted in the discussion of the aureole, we would obtain an effective particle diameter  $2r = 10/0.055 = 180 \mu\text{m}$ .

These provisional estimates suggested that the hazy sun can be explained if (a) the optical thickness of the clouds is just right, and (b) the cloud is strongly loaded with large particles. Minnaert (in 1970), before his death, commented in correspondence that he agreed with the computation but was not convinced. The explanation might hold for altostratus clouds, but why would not nimbostratus, from which we know it rains, and fog also show the hazy sun?

New and more objective information has since become available. From continuous scans of the solar image and aureole, Dr. Arlon Hunt (private communication; Grether *et al.*, 1976, 1979) found several examples of this behavior. He concludes that the hazy-sun phenomenon is not common and occurs in the presence of dense cirrus or cirrostratus clouds. The suggestion that nonsphericity of the ice particles is an essential factor in the explanation does not seem to offer good prospects, for it has been shown (van de Hulst, 1957) that randomly oriented cylinders, for instance, form a diffraction pattern that is strikingly similar to that of spheres.

However, another puzzle appears from the observations: the hazy sun sometimes has a disk radiance only a factor 30 below its clear-sky value. This would halve the  $b$  and  $n$  estimated above and require particle sizes larger by a factor  $\sqrt{2}$ . Perhaps such large ice particles occur, or perhaps transparent ice particles with plane-parallel faces are an exception to the rule that in any scattering event half the radiation is lost from the hazy image. Further studies are necessary.

## 19.2 THE NATURAL AEROSOLS

### 19.2.1 General Properties

Ever since Rayleigh's explanation of the blue sky by molecular scattering a century ago, it has been evident that such a pure molecular atmosphere is a rare exception. Particles with sizes of the order of the wavelength of light are far more effective scattering agents per unit mass. Hence, even if such particles represent a negligible fraction by weight, they may dominate the scattering properties of

the atmosphere and they often do. Such particles are called aerosols. A much used ratio is

$$\text{turbidity } T = \frac{\text{attenuation by molecules + aerosols}}{\text{attenuation by molecules alone}}$$

A value of  $T = 3$  or 6 somewhere in the visual spectrum is quite common, even on days on which the sky would be called clear by normal standards.

Aerosol particles have a wide variety of origin and a corresponding variety in their distribution with altitude and with size. Typical man-made aerosols are those due to industrial pollution and to the combined output of many house stoves. The natural aerosols are often specified as maritime or continental, but this division is not foolproof, for drops of concentrated salt solutions of marine origin are found over all continents and dust blown from the Sahara at times dominates the aerosol at the other side of the Atlantic Ocean. Forest fires have a short-lived but sometimes spectacular effect. The stratosphere contains a layer near 20 km height that is always present but in the course of decades varies in importance in close correlation with volcanic eruptions.

This book is not the place to go into further detail. See McCartney (1976) for review and bibliography. The preceding sketch suffices to suggest the great practical and theoretical interest in monitoring the natural aerosols. From the many methods of diagnosing their composition and size distribution, we have made a somewhat arbitrary selection to be discussed in Sections 19.2.2–19.2.4.

What is the best method for determining the composition, size distribution, and altitude distribution of atmospheric aerosols or cloud particles? The answer to this question depends on how often, how accurately, and how cheaply one wishes to obtain the answer. The method of direct collection at different atmospheric levels and study under the electron microscopic stands apart as a method which is neither easy nor cheap. In order for the results to be useful at all it is necessary to control precisely the relative humidity (Hänel, 1972a, b; 1976).

In the matter of altitude distribution the methods reviewed in Sections 19.2.2–19.2.4 have nothing special to offer. If we dismiss *in situ* measurements as too cumbersome, it is necessary to isolate a known volume for close study. It is important to keep this volume small. This helps to guarantee the absence of higher order scattering and thus leads to a simpler interpretation, but it also makes the quantity to be measured so small that errors may creep in. In the practical compromise some secondary scattering may still be present.

Isolation of the volume to be studied can be done in two ways. In the purely geometrical way (Fig. 19.4) part of the volume illuminated by a collimated beam (e.g., a searchlight) is observed by the collimated beam of a telescope. The searchlight and telescope must be some distance apart. The scattering volume is then defined as the overlap of the two beams, crosshatched in Fig. 19.4.

The alternative way to isolate a small volume is to use the accurate time of return of an emitted pulse. This is the method of lidar sensing. A precision of

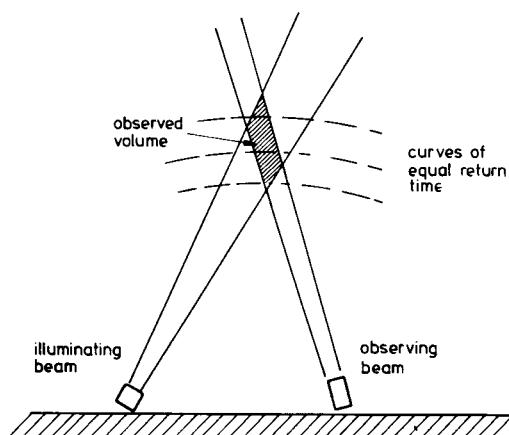


Fig. 19.4. Principle of selecting a volume of air by crossed beams and/or by lidar echo return time.

$10 \text{ nsec} = 10^{-8} \text{ sec}$  corresponds to 3 m in the double distance. Practical considerations of intensity, price, and ease of operation rather than technological limitations determine the actual choice. Again, by choosing proper dimensions we may in most circumstances (but not in all) interpret the return signals in terms of single scattering. In lidar returns from clouds, multiple scattering is a serious complication (Section 19.3.1).

The two principles of isolation can be combined by placing the lidar transmitter and receiver some distance apart (bistatic lidar).

In the matter of size distribution, all methods suffer from the problem that any measurement in nature refers to a mixture of particles of all sizes. Hence the interpretation always requires the solution of an integral equation, where the function to be determined is the size distribution law. The dilemma is then to choose between two classes of methods:

(a) to construct a *ready-made atlas* (library, catalog) of models based on some assumed size distribution laws with a few free parameters. Good judgment should then be used in finding the curve which best fits the measurements. The disadvantages of this method are that some bias may be introduced by the first assumptions and also that there is some waste in producing models that are not finally used.

(b) to use a formal *inversion procedure* from which the size distribution can be determined seemingly without bias. Such integral equations are unstable in that the inversion procedure gives nonsense if we try to get more detail in the solution than is warranted by the accuracy of the measurements. Hence, any practical inversion method has built-in restraints to avoid this instability, and these restraints mean in practice that the number of parameters actually free is seriously restricted, as in method (a).



I generally prefer the simple method (a) for the same reason that I am content with buying a ready-made suit instead of one tailored to measure: The deviation from perfect fit is small and the price difference great.

The properties of some size distributions that are often used for this purpose are shown in Display 19.1. Since each of these forms is simple, it is futile to trace who used them first. For instance, this author used the power-law distribution in an astronomical problem well before it was introduced by Junge into meteorology (see Section 19.2.4). The log-normal distribution becomes a symmetric Gaussian when the transformation to  $\log r$  is made, but on the  $r$ -scale it is nearly symmetric only for  $t \ll 1$ . The gamma distribution again is classical. Deirmendjian (1969) calls his generalization (number 3 in the list) a "modified gamma distribution," and by Zuev (1974) it is attributed to Shifrin (1955). The simplest distribution (number 5) has been very widely used in the literature as "Deirmendjian's haze," but Zuev (1974) cites it from Khrgian and Mazin (1952).

The number of free parameters in these functions is 3, 2, or 1, as shown, apart from the factor that may be added to adjust the total number of particles. In some problems the lower or upper limits of the Junge distribution or both are unimportant, but the assumption that this is always so can lead to wrong conclusions.

In each of the distributions the average value  $\bar{r}$  is larger than the mode  $r_{\max}$  at which  $f(r)$  reaches its maximum value.

The suitability of the three methods for the determination of composition (refractive index) and size may be characterized as follows:

wide angle scattering and polarization (Section 19.2.2): quite sensitive, in selected ranges of angles, to both composition and size.

aureole or small angle scattering (Section 19.2.3): permits direct size determination, unsensitive to composition.

wavelength dependence of extinction (Section 19.2.4): usually no unique determination of both size *and* refractive index but rather sensitive to the product size  $\times$  (refractive index  $- 1$ ).

## 19.2.2 Wide Angle Scattering and Polarization

In this section we consider the natural situation of sunlight scattered by the entire atmosphere. The scattered radiation is intense and easily measurable, but it is affected by a large proportion of higher order scattering and is therefore difficult to interpret uniquely.

The studies made on planets (Coffeen and Hansen, 1973; Hansen and Travis, 1974; cf. also Fig. 18.5) show that the polarization more completely than the radiance retains the signature of particle composition and size. For that reason we concentrate on polarization. This problem has been elaborately studied for a planetary atmosphere or cloud layer seen from outside. Polarization observations made inside the atmosphere should be equally telling. By deBary's

DISPLAY 19.1

Some Common Size-Distribution Laws

Brief name	Functional form normalized to $\int_0^\infty f(r) dr = 1$	Free parameters	Derived quantities		
			Mode, $r_{\max}$	Average $\bar{r}$	Dispersion $\sigma^2$
1. Junge distribution	$f(r) = \begin{cases} Cr^{-p} & \text{for } r_1 < r < r_2 \\ 0 & \text{outside this range} \end{cases}$ $C = (p - 1)(r_1^{-p+1} - r_2^{-p+1})^{-1}$	$p, r_1, r_2$ ( $p > 0$ )	$r_1$ (if $p > 0$ )	Not of interest	Not of interest
2. Log-normal distribution	$f(r) = \frac{\exp\{-t/4 - [\ln(r/a)]^2/t\}}{a(\pi t)^{1/2}}$	$a, t$ ( $t > 0$ )	$a$	$ae^{3t/4}$	$a^2(e^{2t} - e^{1.5t})$
3. Deirmendjian distribution	$f(r) = Cr^\alpha \exp(-br^\gamma)$ $C = \gamma b^{(\alpha+1)/\gamma} / \Gamma[(\alpha+1)/\gamma]$	$\alpha, \gamma, b$	$(\alpha/b\gamma)^{1/\gamma}$	$b^{-1/\gamma} \frac{\Gamma(\frac{\alpha+2}{\gamma})}{\Gamma(\frac{\alpha+1}{\gamma})}$	$b^{-2/\gamma} \left\{ \frac{\Gamma(\frac{\alpha+3}{\gamma})}{\Gamma(\frac{\alpha+1}{\gamma})} - \left[ \frac{\Gamma(\frac{\alpha+2}{\gamma})}{\Gamma(\frac{\alpha+1}{\gamma})} \right]^2 \right\}$
4. Gamma distribution = number 3 with $\gamma = 1$	$f(r) = Cr^{\alpha} \exp(-br)$ $C = b^{\alpha+1} / \Gamma(\alpha+1)$	$\alpha, b$	$\alpha/b$	$(\alpha+1)/b$	$(\alpha+1)/b^2$
5. Standard haze distribution = number 4 with $\alpha = 2$	$f(r) = Cr^2 \exp(-br)$ $C = \frac{1}{2}b^3$	$b$	$2/b$	$3/b$	$3/b^2$

computations (Section 19.1.4) the fraction of higher order scattering is substantial but not overwhelming, and since high-order scattering will not really show the typical features of the polarization diagram, we may use the same graph presented by Coffeen and Hansen to select from them the scattering angles where the most typical clues to refractive index and/or size may be found.

Many detailed studies corroborate the sensitivity of polarization measurements to the presence of aerosol particles. Soon after the Krakatoa eruption in 1883, Cornu observed a striking drop of the maximum sky polarization from 75 to 48% (Coulson, 1971), and in 1889 he reported that changes of weather often preceded by a drop in polarization (Shifrin, 1951). A modern study emphasizing on the wavelength dependence of polarization is presented by Ge (1962).

Kuriyan *et al.* (1974b) systematically explore the accuracy by which model parameters (optical depth, refractive index, effective radius) of the aerosol can be inferred from measurements of polarization and intensity of the scattered light. They find—in agreement with the experience of Hansen and Hovenier (private communication)—that trying to determine more than two parameters of the distribution (in essence: effective radius and spread) is asking too much. They recommend, in fact, to stick always to a distribution of the haze type (line type Display 19.1).

Further examples of the distribution of intensity and polarization over the full sky for models based on realistic mixtures of aerosols and Rayleigh scattering may be found in Tanaka (1971a, b, c) and Yamamoto and Tanaka (1971). The maximum (linear) polarization is always found in the prime vertical at  $90^\circ$  from the sun; but the value of the degree of polarization at this maximum as a function of solar elevation and wavelength still gives a strange collection of graphs if model calculations of all authors are combined.

A recent set of papers (Kattawar *et al.*, 1976; Plass *et al.*, 1976; Hitzfelder *et al.*, 1976) offers further comparison material. The first two of these papers document with thirty-eight graphs and many tables the radiance and polarization reflected from and transmitted by an atmosphere of total optical thickness from  $2^{-9}$  to  $2^{+10}$ . Here either Rayleigh scattering or Deirmendjian's container model haze  $L$  model is assumed. This complements earlier work on the maritime haze  $M$  model by Kattawar *et al.* (1973). In the third paper Hitzfelder *et al.* (1976) assume a combination of Rayleigh scattering and haze  $L$  with a realistic vertical structure.

The typical differences between a sky with and without pollution (smog) are well illustrated by Coulson (1971).

The neutral points, where the degree of polarization in the clear sky goes through zero, have intrigued all generations who have studied sky polarization. Their shift by the presence of an aerosol layer was studied by Kano (1968). Both the Kattawar and the Coulson paper just cited contain additional information about the shift of these neutral points by the presence of haze and on the appearance of a new class of neutral points. The position of maximum polarization and the value of that maximum are also well documented.

A word may now be said about the fourth Stokes parameter, which indicates the ellipticity of the polarization. The ellipticity is due to secondary scattering, for by the Mie theory natural (unpolarized) incident light gives linear polarization after one scattering, and this gives elliptical polarization after another scattering unless symmetry reasons forbid it. These symmetry reasons make the elliptical polarization zero in the sun's vertical.

Eiden (1971, see also Bullrich *et al.* 1974, Fig. 7) concludes for air loaded with a realistic amount of aerosol particles that the degree of ellipticity reaches a peak at scattering angles  $\sim 140^\circ$ , and that the position of this peak can very well be used to find the complex index of refraction of the aerosol particles. Kawata and Hansen's analysis (1976) also includes elliptical polarization. Further material is found in Plass *et al.* (1976).

If special attention is given to the sky radiance near the horizon, or to situations with the sun near the horizon, the plane-slab formulas are no longer valid. Rather than a formal treatment in terms of spherical geometry (cf. Section 20.1.1), most authors prefer to use simple corrections to include the effects of the curvature of the earth. The total mass along the outward light path from an observation point at distance  $R + h$  from the earth's center, along a straight line which makes an angle  $z$  with the observer's zenith direction, in an atmosphere with constant scale height  $H$  is not proportional to  $\sec z = 1/\mu$ , but to the Chapman function  $\text{Ch}(\chi, z)$  with  $\chi = (R + h)/H$ . Tables are in Wilkes (1954) or McCartney (1976), but the numbers in the accompanying tabulation suffice to show that corrections of several percent are required from  $15^\circ$  above the horizon. The value  $\chi = 800$  is roughly correct for an observer in the troposphere.

$z$	$\text{Ch}(800, z)$	$\text{Ch}(\infty, z) = \sec z$	Ratio
0–60°	—	—	1.000
70°	2.90	2.92	1.006
75°	3.80	3.86	1.017
80°	5.55	5.76	1.038
85°	10.1	11.5	1.132
88°	18.7	28.7	1.53
90°	35.5	$\infty$	$\infty$
92°	96.8	—	—

An even simpler function that works well to replace  $\sec z$  (Green and Martin, 1966; Green *et al.*, 1974) is

$$\sec(z, y) = (1 - \sin^2 \theta/q)^{-1/2}, \quad q = (1 + y/R)^2$$

where  $R$  is the earth's radius and  $y$  the effective altitude of the scattering species.

What we have said about aerosol and haze may *mutatis mutandis* be applied to clouds. A great variety of methods and interpretations may be found scattered in the literature. For instance, Coffeen and Hansen (1972, 1973) describe an infrared polarimeter developed for airborne remote sensing of cloud particle

sizes and shapes. The instrument measures linear polarization over the range 1.1–3.5  $\mu\text{m}$  with a 1.5° field of view. The “cloudbow” is very striking and many other features, several of which are size dependent, make it possible to determine mean sizes. Cloud systems were found with mean particle radii as small as 5  $\mu\text{m}$ , and as large as 30  $\mu\text{m}$ . Tropical cirrus clouds show a quite different polarization curve, which makes it easy to distinguish water clouds from ice clouds. Sassen *et al.* (1977) have employed clouds created in a laboratory chamber in order to find the most sensitive criteria for this distinction.

If we are under a heavy cloud deck that receives sunlight from above, the transmitted radiation will generally be independent of azimuth and distributed with  $\mu = \cos \theta$  proportional to the escape function  $K(\mu)$ , which has quite similar forms for different phase functions (Fig. 19.1, lower curves). To complement the description given in Section 19.1.2, we may find from Table 26 (Section 11.2) that the radiance drops from the zenith to 30° above the horizon by a factor

$$\frac{K(0.5)}{K(1)} = \begin{cases} 0.684 & \text{for } g = 0.75, \quad a = 1 \\ 0.683 & \text{for } g = 0.875, \quad a = 1 \end{cases}$$

The measurements mentioned by Coulson (1971) under a stratus cloud in Los Angeles give the measured value 0.73 (read from his Fig. 13), in fair agreement with the theoretical values. The empirical formula of Moon and Spencer (1942), in which the sky radiance is proportional to  $1 + 2 \cos \theta$ , gives  $\frac{2}{3} = 0.67$  for this ratio. The measurements reported by Ambartsumian (1943) gave 3.0 for the average zenith/horizon ratio, again in good agreement with this empirical formula.

### 19.2.3 Size Distribution from the Aureole

The radiance distribution in the aureole was described in Section 19.1.5 (Fig. 19.3). Scattering at these small angles consists mostly of diffraction, which arises from the geometric blocking of the light beam and is thus determined by the shape and size of the particle but not by its composition. Hence, the aureole contains no strong clues to particle refractive index or composition. Since each spherical particle has the same diffraction pattern, with angular width inversely proportional to particle size, the radiance distribution in the aureole is tied to the size distribution by a simple integral equation, which can be solved.

The policy point of choosing between model fits or formal inversion procedures has been explained in Section 19.2.1. We review a few simple models.

*Model 1.* Let the number of particles per unit volume with radii between  $r$  and  $r + dr$  be  $n(r)$ . Van de Hulst (1947), in studying the inner zodiacal light, which is nothing but an “aureole” formed by the interplanetary dust, showed that a power law

$$n(r) = \text{const} \cdot r^{-p}$$

leads with Fraunhofer diffraction at small scattering angles  $\alpha$  to a power law in the aureole radiance:

$$F(\alpha) = \text{const} \cdot \alpha^{-q}, \quad \text{with } q = 5 - p$$

The integral over sizes is convergent at both ends (0 and  $\infty$ ) if  $2 < p < 5$  and hence  $3 > q > 0$ . The assumption made by Junge (1952), and since then much used in the meteorological literature, that

$$n(r) dr = \text{const} \cdot r^{-\gamma} d(\log r)$$

is the same assumption with  $p = \gamma + 1$ , so that the exponent in the aureole radiance law is  $q = 4 - \gamma$ .

It is customary to limit the Junge law by lower and upper cutoff radii  $r_1$  and  $r_2$ , in which  $r_1$  is usually taken at  $0.04 \mu\text{m}$ , and  $r_2$  at 10, 30, or  $150 \mu\text{m}$ . One or the other cutoffs is necessary if  $q$  is outside the range 0–3. The usually observed exponent is near  $q = 1$  (Fig. 19.3), which means that we can forget about the cutoff and find at once  $\gamma = 3$ . The particles most effectively contributing to the radiance at angle  $\alpha$  (in degrees) have a radius  $r = 5/\alpha$  (in microns). So the value  $\gamma = 3$  just derived should refer to the range  $r = 0.5\text{--}5 \mu\text{m}$ . This is indeed what Eiden's more elaborate calculations show.

Eiden (1968) goes in several ways beyond this very simple theory. In particular he discusses a range of wavelengths, the effects of variations in the cutoffs, and the effect (noticeable at wider angles) of reflection and refraction by the particles. He also finds that a single exponent often does not suffice, but that  $\gamma$  may be a little larger in the range  $r = 0.1\text{--}1 \mu\text{m}$ . A detailed review would lead too far from the main theme of this book.

*Model 2.* The necessity of introducing cutoffs can be entirely avoided by adopting a size distribution law that properly converges at small and large  $r$ . Kuriyan and Sekera (1974) show that the size distribution law listed in Display 19.1 as form 5, "standard haze," with one parameter  $b$ , when combined with the Fraunhofer diffraction law at small angles is amenable to analytical integration. The resulting intensity distribution normalized to 1 at  $\theta = 0^\circ$  is the hypergeometric function

$$I(\theta) = {}_3F_2\left(\frac{3}{2}, \frac{7}{2}, 4; 2, 3; -z\right)$$

where  $\theta$  is the scattering angle in radians,  $\theta \ll 1$ ,  $z = (2\theta k/b)^2$ ,  $k = 2\pi/\lambda$ ,

$${}_3F_2(p_1, p_2, p_3; q_1, q_2; z) = \sum_{n=0}^{\infty} \frac{(p_1, n)(p_2, n)(p_3, n)}{(q_1, n)(q_2, n)} \frac{z^n}{n!}$$

and

$$(p, n) = p(p+1)(p+2) \cdots (p+n-1)$$

A graph of this function (not shown by Kuriyan and Sekera) is shown in Fig. 19.5. Although the expansion given above converges only for  $z \leq 1$ , the function

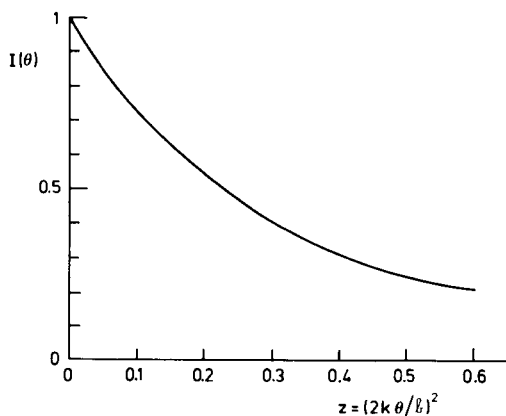


**Fig. 19.5.** Brightness distribution in near-forward scattering (diffraction peak) when averaged over the "standard haze" size distribution.

can be extended and tails off for large  $z$  into the normal intensity pattern  $\sim \theta^{-3}$  for a diffraction pattern but without the separate rings that are typical for monodisperse particles (cf. van de Hulst, 1957, Section 8.3).

Such an integration, while elegant, is not of great use since a computer evaluation of the values of the hypergeometric function is necessary anyhow. Many users may prefer a lengthier, more direct integration. Kuriyan and Sekera show in the same paper that if the Fraunhofer diffraction pattern is replaced by the Rayleigh-Gans pattern ("soft" particles, Born approximation), another hypergeometric function appears, but now in a form that can be converted into an algebraic expression (same  $z$ , same  $k$ , same condition, same size distribution):

$$I(\theta) = {}_3F_2\left(2, \frac{9}{2}, 5; \frac{5}{2}, 4; -z\right) = (3z^3 + 16z^2 + 35z + 70)/70(1 + z)^5$$

As an alternative to the simple model fits we have formal inversion procedures, many of which have been assessed in Deepak (1977). A practical method of inverting aureole radiances in the range from 1 to 20° from the sun is discussed by Twitty (1975). Here we are already outside the angles of pure diffraction theory. Twitty *et al.* (1976) show the practical results obtained by this method in interpreting airborne aureole measurements.

### 19.2.4 Inversion of the Extinction Curve

By extinction curve we understand the graph which shows the optical depth of the atmosphere, or of a chosen atmospheric layer, as a function of inverse wavelength. The extinction curve for particles of one kind and size has a typical shape with a maximum and additional humps (Fig. 10.3). In a mixture of particles of different sizes and refractive indices many such curves are superposed. The net effect of this superposition is the observed extinction curve, usually with one

broad maximum. The problem of inferring from this curve the distribution function of sizes and refractive indices is again an inversion problem of an integral equation.

Let  $r$  be the drop radius,  $\lambda$  the wavelength,  $k = 2\pi/\lambda$ ,  $x = kr = 2\pi r/\lambda$ , and let  $n(r) dr$  be the number of droplets per centimeter<sup>3</sup> with radii between  $r$  and  $r + dr$ . Assume that all drops have the same refractive index  $m = n - in'$ , where the imaginary part  $n'$  is 0 for nonabsorbing particles. The Mie theory gives the efficiency factor for extinction  $Q(m, x)$ . The cross section per unit volume, which is also the attenuation factor per unit length, is

$$C(\lambda) = \int_0^\infty n(r)Q(m, x)\pi r^2 dr$$

This quantity depends on  $\lambda$  both through  $m$  and through  $x$ , but often the variation of  $m$  with  $\lambda$  is so small that it may be neglected. In that case a plot of  $C$  against  $x$  for fixed  $m$  gives at once a plot of the extinction against  $\lambda^{-1}$ , except for the proper scale factors.

In trying to find  $n(r)$  from  $C(\lambda)$ , a fitting procedure to a collection of assumed model distributions often suffices. However, the present trend in the literature of determining aerosol size distribution from extinction curves is clearly towards more formal inversion procedures. This is justified only if rather accurate measurements are available. We mention a few typical studies in which one or the other philosophy is followed.

1. Van de Hulst (1949b) obtained a collection of accurate extinction curves based on seven assumed size distributions and three assumptions about the refractive index:  $m = 1.33$ ,  $m = 1 + \varepsilon$ ,  $m = 1 + \varepsilon - i\varepsilon \tan 15^\circ$ , where  $\varepsilon$  is any small, real number. He writes  $n(r) \propto f(r/r_1)$ , where  $f(u)$  has an assumed form and  $r_1$  is a scale factor to be chosen later. Further he writes  $Q(m, x) = E(m, \rho)$ , where  $\rho = 2x(m - 1) = 4\pi r(m - 1)/\lambda$ . Let  $\rho_1 = 4\pi r_1(m - 1)/\lambda$ . Then the efficiency factor for extinction by the polydisperse medium is

$$Q(\rho_1) = \int_0^\infty E(m, u\rho_1)f(u)u^2 du \bigg/ \int_0^\infty f(u)u^2 du$$

in which the denominator is proportional to the total geometric cross section.

The Mie theory shows that in the limit of "soft" particles, i.e., if  $x \gg 1$ ,  $2x(m - 1) \ll 1$ , the radius  $r$  and refractive index  $m$  enter into the final result *only* through the combination  $\rho$ . Hence in this limit—and for actual aerosols in fair approximation—it is fundamentally impossible to infer the size and refractive index separately from the inversion.

In the limit of soft, nonabsorbing particles the integration can be made analytically, with the results shown in Display 19.2, where

$$\text{Ci}(a) = - \int_a^\infty (\cos x/x) dx$$



**DISPLAY 19.2**

Model Distributions of Radii and Resulting Extinction Curves

Model	$f(u)$	Expression for $Q(\rho_1)$	
(a)	Peak: $\delta(u - 1)$	$2 - 4a^{-1} \sin a + 4a^{-2}(1 - \cos a)$	$a = \rho_1$
(b)	$\begin{cases} u^{-1} & u < 1 \\ 0 & u > 1 \end{cases}$	$2 + 8a^{-2}(-1 + \cos a + \gamma + \ln a - \text{Ci } a)$	$a = \rho_1$
(c)	$\begin{cases} 1 & u < 1 \\ 0 & u > 1 \end{cases}$	$2 + 12a^{-2}(1 - \cos a) - 24a^{-3} \sin a$	$a = \rho_1$
(d)	$\begin{cases} u & u < 1 \\ 0 & u > 1 \end{cases}$	$2 + 8a^{-2}(1 + 2 \cos a) - 48a^{-3} \sin a + 48a^{-4}(1 - \cos a)$	$a = \rho_1$
(e)	$\begin{cases} 0 & u < \frac{1}{2} \\ u^{-5} & u > \frac{1}{2} \end{cases}$	$2 - a^2 \text{Ci } a + a \sin a - \cos a - 2a^{-1} \sin a + 2a^{-2}(1 - \cos a)$	$a = \frac{1}{2}\rho_1$
(f)	$\exp(-4u)$ , all $u$	$2 + 2(1 + a^2)^{-1} - 4(1 + a^2)^{-2}$	$a = \frac{1}{4}\rho_1$
(g)	$\exp(-2.75u^3)$ , all $u$	no analytic expression	—
(h)	$\propto u^{-p}$ , all $u$ $3 < p < 4$	$\sim \rho_1^{3-p}$	—

(cosine integral) and  $\gamma = 0.5772$  (Euler's constant). The numerical distribution (g) from the original paper may be replaced by an exponential, as shown, but it does not lead to a simple analytic extinction curve. Distribution (h) is discussed separately below.

Each of the extinction curves thus found starts from 0, increases proportionally to  $\rho^2$ , reaches via an inflexion point (maximum slope) the first maximum, and finally goes asymptotically to 2 for  $\rho \rightarrow \infty$ . Since the curves would look very much alike when drawn on full scale, we copy in Fig. 19.6 the gradient curves showing  $dQ/d\rho_1$  against  $\rho_1$ . Numerical data on the position of inflexion point and first maximum shown in Table 63 may help one appreciate the small differences. In the broader size distributions, in particular distribution (f), the maximum is only a little above 2 and displaced towards a relatively large value of  $\rho$ .

As expected, the variation caused by a change in the real part of the refractive index (from A to B) are small. The imaginary part of the refractive index (from B to C) has a clearer effect. Hence  $n'$  may be inferred with greater precision from measurements than  $n$ , a finding confirmed by recent studies cited below.

The discovery that analytical integration of the soft-particle extinction curve over simple size distributions is possible appears to have been made many times. Zuev (1974) cites a list of papers by Tvogorov, Shifrin, and others, mostly from the period 1960–1965. Box and McKellar (1977) perform the integration by noting that the original curve can be represented by a Struve function. This fact was mentioned not for soft spheres but for soft cylinders by van de Hulst (1951).

2. A power-law size distribution  $n(r) \sim r^{-p}$ , which is the same as a Junge distribution  $dN/d(\log r) \sim r^{-\gamma}$ ,  $\gamma = p - 1$  over the full range  $r = 0 - \infty$  does not

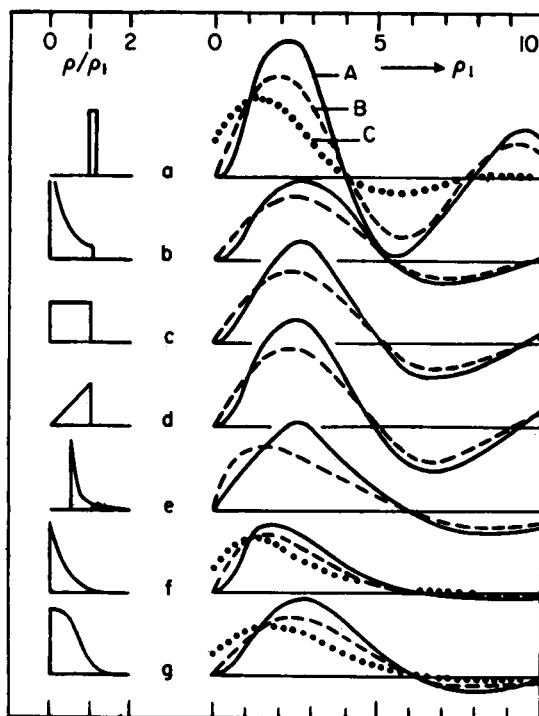


**Fig. 19.6.** Extinction gradients  $dQ/d\rho_1$  against  $\rho_1$  for seven assumed size distributions and three assumptions for the refractive index: (A)  $m = 1.33$ ; (B)  $m = 1 + \varepsilon$ ; (C)  $m = 1 + \varepsilon - i\varepsilon \tan 15^\circ$ . The first zero point corresponds to maximum extinction (from van de Hulst, 1949b).

give a convergent integral for the geometric cross section, nor for the total volume. Yet, since the efficiency factor starts linearly with  $x$  (absorption proportional to volume) if  $n' \neq 0$ , and more slowly if  $n' = 0$ , the total extinction is expressed by a convergent integral if  $3 < p < 4$ . The  $\lambda$  dependence is then as  $\lambda^{-\alpha}$  with  $\alpha = p - 3 = \gamma - 2$  with the restraint that  $0 < \alpha < 1$ .

Such a power law means that if  $\log(\text{attenuation})$  is plotted against  $\log(\text{wavelength})$ , a straight line appears with slope  $-\alpha$ . In the meteorological literature since 1951 this is known as Ångström's law (McCartney, 1976). If this extinction law is seen to be valid over a substantial range of  $\lambda$ , we may infer from the analysis above that a power-law size distribution with  $\gamma = \alpha + 2$  holds over a substantial range of  $r$ .

This very simple relationship is hardly ever the full story, so it is used mostly as a reference law only (e.g., Quenzel, 1970). If the measurements cover only a factor 2 in wavelength (from 400 to 800 nm) it would seem an overstatement to call this law "meaningful and sufficient to use as a cross-check" (DeLuisi *et al.*, 1976). These authors find from the first GAARS (Global Atmospheric Aerosol and Radiation Study) field test certain days on which the extinction is neutral:

TABLE 63

First Maximum and First Inflection Point of Extinction Curves for Some Polydisperse Media<sup>a</sup>

Distribution function	(A) $m = 1.33$		(B) $m = 1 + \varepsilon$		(C) $m = 1 + \varepsilon - i\varepsilon \tan 15^\circ$	
	Inflection point	Maximum	Inflection point	Maximum	Inflection point	Maximum
a	2.2	4.1	2.0	4.1	1.3	4.0
	2.07	3.90	1.60	3.17	1.00	2.46
	0.84	0	0.61	0	0.47	0
b	2.8	5.4	2.4	5.5	—	—
	1.61	3.07	1.16	2.56	—	—
	0.50	0	0.38	0	—	—
c	2.7	5.0	2.4	5.1	—	—
	1.80	3.37	1.37	2.80	—	—
	0.62	0	0.45	0	—	—
d	2.5	4.8	2.2	5.0	—	—
	1.80	3.56	1.32	2.92	—	—
	0.64	0	0.48	0	—	—
e	2.7	6.0	1.5	6.0	—	—
	1.72	3.29	0.84	2.69	—	—
	0.53	0	0.37	0	—	—
f	1.7	7.2	1.7	6.9	1.3	9.0
	0.72	2.50	0.82	2.25	0.70	2.09
	0.41	0	0.36	0	0.32	0
g	2.8	6.2	2.5	6.1	1.7	7.0
	1.47	3.10	1.15	2.55	0.80	2.18
	0.46	0	0.35	0	0.30	0
h	None	None	None	None	None	None

<sup>a</sup> The distribution functions are defined in Display 19.2. The three numbers in each box are from top to bottom: position  $\rho_1$ , extinction value  $Q(\rho_1)$ , half slope  $\frac{1}{2}dQ/d\rho_1$ .

$\alpha = 0$ ,  $\gamma = 2$ , and other days in which there is a distinct reddening:  $\alpha = 0.6$ ,  $\gamma = 2.6$ , signifying the presence of fewer large particles. Generally,  $\alpha$  is a convenient quantity for characterizing optical air quality in studies where the possible correlation with weather or pollution is examined (Frantzen, private communication).

3. The possibilities of formal inversion procedures for obtaining the size distribution from the extinction law without bias have been explored by many authors. For reviews, see Fymat (1976) and papers by Twomey, Rodgers, and others in Deepak (1977). In the soft-particle limit the inversion procedure can be carried out by means of Mellin transforms both for nonabsorbing particles

(Shifrin and Perelman, 1963, 1964) and for absorbing particles (Perelman and Punina, 1969). Heintzenberg (1975) developed and used an inversion method based on a size distribution consisting of a number of log-normal distributions. In applying these procedures to actual data the stability problem (Section 19.2.1) always appears in some form.

4. A practical approach has been adopted by Kuriyan *et al.* (1974a). They varied the parameter  $b$  of the Deirmendjian distribution (No. 5 in Display 19.1) and also the real part  $n$  and the imaginary part  $n'$  of the refractive index. The theoretical extinction curves thus obtained were made more realistic by adding some noise. Reading these curves at six wavelength intervals (the precise number was not critical) they could empirically test with what precision each of the parameters could be retrieved from measurements with a given accuracy. Their results may be summarized as shown in the accompanying tabulation.

Photometric data available in	Error range of inferred parameters		
	$\Delta b/b$	$\Delta n$	$\Delta n'$
4 significant figures	0.005	0.01	0.005
3 significant figures	0.01	0.04	0.02
2 significant figures	0.1	0.15	0.04

## 19.3 LIDAR REFLECTION FROM CLOUDS

### 19.3.1 Multiple Scattering Contribution

Lidar (in early papers called laser radar) is a particular form of active remote sensing. Let us briefly explain the terminology. "Sensing" refers to an instrumented quantitative measurement of certain properties and "remote" means that the instrument is not *in situ* but far away.

The great majority of remote sensing methods are passive: the instrument picks up the radiation that by natural causes happens to be emitted, reflected, or scattered from the object under study. All of classical astronomy, including the study of planetary atmospheres (Chapter 18), is thus based on remote sensing. Passive remote sensing of the earth's surface and atmosphere has been developed in many directions. See, for instance, the handbook compiled by Derr (1972).

In active remote sensing a signal (mostly a short pulse of radiation) is sent by the instrument to the object, and the backscattered signal is picked up and analyzed. Radar, based on the reflection of radio waves, is the best known example. When it became possible to do the same with light, using laser beams, soon the term *lidar* was invented and became generally used.

Lidar has now become a well established technique used on a regular basis for routine observations and permitting many refinements for special research purposes. A good review, discussing the various ways in which the *single-scattering* lidar equation may be put to use, was given by Collis *et al.* (1974). Basically, the time of the lidar echo tells the position of the scattering particles, and the intensity of the echo tells something about the concentration, modified both by individual backscatter properties and by attenuation along the (double) path.

No such clear conclusions are possible if multiple scattering enters. The normal way to cope with this problem is to suppress multiple scattering. This can be done by making the reception cone, from which the receiver can pick up the returned signal, narrow enough. This effect can be qualitatively understood as follows. The primary scattering centers are all within the extremely narrow laser beam. Potential secondary scattering centers are spread evenly in and around it up to distances of the order of a mean free path. By making the reception cone narrower and narrower, the number of secondary scattering centers that actually takes part is proportionally reduced, but the primary scattering remains constant. Precise calculations for the chosen geometry, e.g., by means of the Monte Carlo method, must be made in order to find out the quantitative influence of multiple scattering. Customary values of the diameter of the reception cone range from  $2 \text{ mrad} = 7'$  (minutes of arc) to  $5 \text{ mrad} = 17'$ . With the higher of these values, multiple scattering is found to be negligible in lidar reflection from clear air or haze but fairly strong in echoes from fog or clouds.

We now go into some detail on the multiple scattering contribution in lidar return signals from clouds. Results cited in earlier chapters of this book deal with uncollimated beams thus are *not* directly relevant to this problem. After early attempts by means of geometric methods (references in papers cited below), most authors, e.g., Blättner *et al.* (1974), Kunkel and Weinman (1976), have used Monte Carlo methods. A faster way may not exist. Even if one should wish to obtain the path-length distribution from inverse Laplace transform of a function  $I(a)$ , as explained in Section 17.2.1, he would, in this particular geometry, still be advised to use Monte Carlo methods to obtain  $I(a)$  first. It is then simplest to use immediately the path-length information available in the calculation. Presumably, the same Monte Carlo calculation may be used to better advantage by using both direct statistics and inverse Laplace transform.

An analytical method, which has been shown to work remarkably well, is the method based on replacing the phase function by some 5 to 7 Gauss functions peaked partly in the forward direction and partly in the backward direction (Weinman *et al.* 1975; Weinman 1976). The approximation of small-angle scattering is used throughout so that successive scattering by the component Gauss functions leads again to a Gaussian distribution in angle around either the forward or the backward direction. All possibilities are added in a Neumann series. The same method has been applied to analyzing the spread of delay times in forward transmission (Weinman and Shipley, 1972; see also Section 20.4.2).

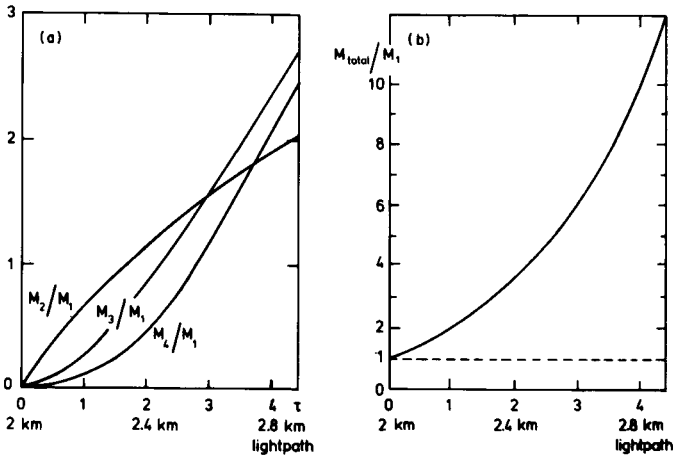


**Fig. 19.7.** Model calculation referring to lidar reflection from a cloud. (a) Multiple scattering contributions due to orders 2, 3, and 4; (b) the ratio of total to single-scattering signal (adapted from Weinman, 1976).

A remarkable result of these studies is that the *back-scattered* signal is rather sensitive to the assumed shape of the *forward* peak, a point noted earlier by Weinman and Ueyoshi (1969).

A selected example for one case that is rather fully documented by Weinman (1976) is shown in Fig. 19.7. Here the phase function of Deirmendjian's Cloud C-1 model at 700 nm has been used. The cloud base is at 1 km from the lidar and the attenuation length in the cloud is 0.1 km, so that single scattering at an optical depth  $\tau$  above the cloud base corresponds to a total light path of  $2 + 0.2\tau$  km. Both scales are shown. Figure 19.7a gives as a function of light path the ratios between the signal  $M_n$  arising from  $n = 2, 3$ , or 4 successive scatterings to the signal  $M_1$  arising from single scattering. In Fig. 19.7b all contributions, including those for  $n > 4$ , have been added to form  $M_{\text{total}} = \sum_{m=1}^{\infty} M_m$ , and the ratio to  $M_1$  is shown. These results are for a 5 mrad reception cone. Weinman also gives results for cones of 1 and 10 mrad half angle. The presence of multiple scattering increases the signal over the single-scattering return by a factor  $M_{\text{total}}/M_1$ . This can formally be written as an apparent change of the attenuation factor  $\exp(-2\tau)$  into

$$(M_{\text{total}}/M_1) \exp(-2\tau) = \exp[-2\tau(1 - \bar{F})]$$

Figure 19.7b has been constructed from the values of  $\bar{F}$  given in Weinman's paper.

The lidar problem just described is rather remote from the problems of extended illumination treated in this book. In order to establish the link, it would be interesting to study the following theoretical problem. Take a homogeneous cloud specified by the usual parameters  $b$ ,  $a$ ,  $g$ , and illuminate it perpendicularly upwards with a sharp laser beam. Then compute the radiation

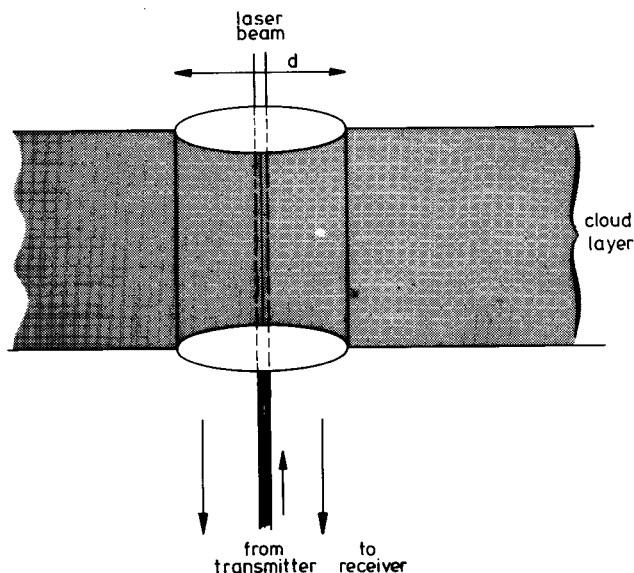


Fig. 19.8. Conceptual sketch of lidar return from a column of varying diameter.

scattered straight down per unit solid angle from a cylindrical column with diameter  $d$ , which has the laser beam as axis (Fig. 19.8). The integrated pulse strength, regardless of echo time, then has a specific ratio

$$R(d) = \frac{\text{total returned signal}}{\text{signal returned by single scattering}}$$

which must rise from  $R(0) = 1$  to a high value  $R(\infty)$  which is reached as soon as  $d$  is large enough to enclose practically all of the returned signal in the reception column. The limit  $R(\infty)$  is a number we know already from the theory for uncollimated beams. We read from Table 13 (Section 9.1.2) for isotropic scattering and Table 38 (Section 13.1) for Henyey–Greenstein phase functions the typical values ( $\mu = \mu_0 = 1$ ,  $a = 1$ ,  $b = \infty$ ):

$$\begin{array}{cccc} R(\infty) = & 8.46 & 17.86 & 39.42 & 109.52 \\ \text{for } g = 0 & & 0.25 & 0.50 & 0.75 \end{array}$$

Water drops have a relatively larger backscatter than a Henyey–Greenstein phase function, but the value of  $R(\infty)$  will at least be of the order of 50.

These numbers refer to the signals integrated over all echo times. Since lidar records give signal strength versus echo time, the data above should still be differentiated according to echo time. This can be done by the general theory of the statistics of light paths given in Display 17.1. Since the speed of light  $c$  is constant, the echo time is simply  $t = lc$ , where  $l$  is the geometric light path.

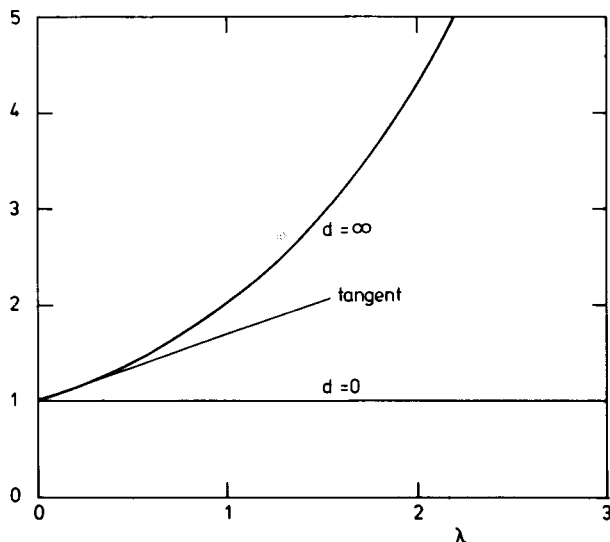


Fig. 19.9. Ratio of total to single scattering versus light path  $\lambda$  (convertible to lidar echo time  $t$ ) in a theoretical situation with isotropic scattering,  $b = \infty$ ,  $a = 1$ ,  $\mu = \mu_0 = 1$ , and variable diameter  $d$  of the reception column.

As a practice example we present in Fig. 19.9 the curve for a semi-infinite cloud with isotropic scattering ( $b = \infty$ ,  $a = 1$ ,  $g = 0$ ,  $\mu = \mu_0 = 1$ ). The path-length distribution for this situation has already been discussed in Section 17.2.2, Table 57. The total echo with optical path  $\lambda$  is proportional to

$$p(\lambda)I_{\text{tot}} = \sum_{n=1}^{\infty} p_n(\lambda)I_n = \sum_{n=1}^{\infty} \frac{\lambda^{n-1} e^{-\lambda}}{(n-1)!} I_n$$

This must be divided by the corresponding single-scattering echo with optical path  $\lambda$

$$p_1(\lambda)I_1 = \frac{1}{8}e^{-\lambda}$$

The ratio is

$$R(\infty) = \left( \frac{\text{total echo}}{\text{single-scattering echo}} \right)_{\text{at path } \lambda} = 8 \sum_{n=1}^{\infty} \frac{\lambda^{n-1}}{(n-1)!} I_n$$

The resulting curve, shown in Fig. 19.9, initially rises as  $1 + 0.693\lambda$  and continues to rise faster and faster, eventually as  $8.26e^{\lambda}(\lambda + 4.76)^{-3/2}$ . The same equations with different values of  $I_n$  hold for anisotropic scattering.

This practice example shows that for an infinitely wide reception beam ( $d = \infty$ ), it is relatively simple to deduce the exact influence of any order of scattering. Unfortunately, this information has little practical value. The curves for  $d = \infty$  would become relevant only if the reception cone at cloud level had a width of several mean free paths, i.e., at least 100 m. In practice a reception cone



of 5 mrad width projects on a cloud deck at 1 km height a circle of only 5 m diameter. As we can see in Fig. 19.7, this very much smaller value of  $d$  serves to reduce the ratio  $R(d)$  to a more acceptable value. Qualitatively, the curves in the two figures are quite similar.

### 19.3.2 Depolarization

In actual lidar studies of clouds, the problem of multiple scattering has been tied from the beginning to the problem of depolarization. Single backscatter of a linearly polarized pulse from a spherical particle occurs with the same linear polarization. Hence in this ideal situation the crosspolarized return signal should be 0. In actual measurements it is not. The depolarization ratio  $\delta$  is defined as

$$\delta = P_{\perp}/P_{\parallel}$$

where  $P_{\perp}$  is the power received with the receiver polarization perpendicular to the transmitter polarization, and  $P_{\parallel}$  the corresponding power with parallel polarization.

A nonzero  $\delta$  may have either of two explanations:

- (a) the particles are nonspherical, e.g., ice crystals, or
- (b) double or higher order scattering occurs.

Fortunately, the distinction between these two explanations does not have to come only from theory. The typical situation encountered in simply structured clouds is sketched in Fig. 19.10, which compiles information from various figures presented by Pal and Carswell (1973). The depolarization ratios observed on cumulus clouds (drops) and cirrus clouds (ice crystals) fall in the same range but their variation with depth is different. In both figures the signal returned from near the cloud base should represent single scattering only, which checks with a zero  $\delta$  for drops and a nonzero  $\delta$  for crystals. The changes with depth represent the multiple scattering influence.

A sketch of the separate strength of the parallel and perpendicular echo signals is shown in the bottom part of Fig. 19.10. The parallel echo rises fast to a peak at 50 m penetration depth, which corresponds to  $100 \text{ m} = \sim 1.6$  mean free paths. The perpendicular echo (which has been plotted on a twice larger vertical scale) reaches a broad maximum around 80 m depth. This behavior is consistently seen in simply structured water clouds. The numbers in Table 64 were read from the figures presented by Balin *et al.* (1975). This shows that the behavior in optical depth does not vary much and that the Pal-Carswell example with a reasonable estimate  $\sigma = 16 \text{ km}^{-1}$ , mean free path  $\sigma^{-1} = 63 \text{ m}$ , coincides with the average data of Balin *et al.* (1975).

The situation is not always so simple. McNeil and Carswell (1975) review the statistical experience about the  $\delta$  values in red and blue over several years.

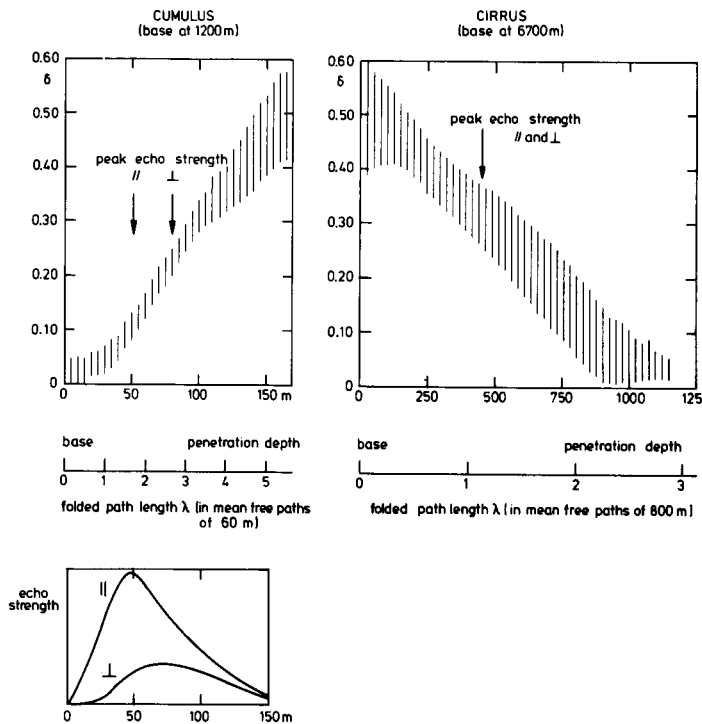


Fig. 19.10. Depolarization ratio  $\delta$  and depth of peak echo strength observed in a typical cumulus and cirrus cloud (adapted from data in various figures in Pal and Carswell, 1973).

TABLE 64  
Characteristics of Lidar Echoes from Simply Structured Water Clouds

Attenuation coefficient	Depolarization $\delta = 0.20$ is reached at	Displacement between peak echo in // and $\perp$ components	Reference
$\sigma(\text{km}^{-1})$	Penetration depth $L(\text{km})$ Optical depth $\sigma L$	$\Delta L(\text{km}^{-1})$ $\sigma \Delta L$	
8	0.14 1.1	0.07 0.6	Balin <i>et al.</i> (1975)
16	0.08 1.3	0.03 0.5	Balin <i>et al.</i> (1975)
33	0.05 1.6	0.01 0.35	Balin <i>et al.</i> (1975)
16 <sup>a</sup>	0.075 1.2	0.03 0.5	Pal and Carswell (1973)

<sup>a</sup> Guess.

Contrary to the suggestion in Fig. 19.10, they find that in cirrus clouds the depolarization ratio often stays constant with penetration depth at a value  $\delta = 0.3\text{--}0.4$ . In rare cases values of  $\delta > 1$  have been observed, which must be due to preferred orientation of the ice crystals.

## 19.4 ELEMENTS OF THE EARTH RADIATION BUDGET

### 19.4.1 The Need for Parametrization

The climate and any factors that affect it are of vital interest to mankind. This justifies a huge effort in measurements, matched by an equally extensive set of physical, dynamical, and statistical calculations. These factors may be natural or man-made. Very rarely they may be traced to a distinct event. An example is the Mt. Agung volcanic eruption of 1963, which introduced aerosols into the stratosphere causing, one or two years later, a global climate perturbation making the stratosphere at 60 mbar warmer by  $0.5^\circ$ , and the tropical stratosphere cooler by about  $5^\circ$  (Hansen *et al.*, 1978).

Clearly, scattering and absorption by clouds and aerosols should enter as very important factors into the calculations. The fact that at many times and places more than half of the solar radiation is reflected back into space from the cloud tops must severely affect the radiation budget.

The radiation reaching the ground arrives partly as direct (solar) radiation, partly as diffuse radiation. Typically, on a summer day at moderate latitudes, the total amount integrated over a clear day may be  $30 \text{ MJ/m}^2$  (megajoules per square meter), of which 10% is diffuse radiation. On a partially cloudy day, it may be  $20 \text{ MJ/m}^2$ , of which half is diffuse (Buyco and Namkoong, 1977), and on a gloomy day only diffuse radiation comes through and the total may be  $5 \text{ MJ/m}^2$ .

Clouds may also affect the measurements. For instance, data obtained from remote sensing may be wrongly interpreted if absence (or unrealistic properties) of clouds and/or aerosols is assumed.

The question is how to take these annoying but real complications into account. Partial answers under a variety of idealized circumstances may be found in the preceding chapters. For instance, the fraction of the incident energy diffusely reflected from a plane-parallel cloud layer is in the notation of this book called  $UR$ . It depends at any wavelength on four variables:  $\mu_0$ , the cosine of the zenith angle of the sun,  $b$ , the optical thickness of the cloud,  $a$ , the single-scattering albedo,  $g$ , the asymmetry factor of the phase function, and to less extent also on further parameters specifying the phase function. The dependence of  $UR$  on these variables may be read from many tables and graphs in Chapters 8, 9, and 11–14.

Since each of the variables  $b$ ,  $a$ , and  $g$  is a function of wavelength, even within the narrow domain of a spectral line, the calculations should in principle be performed separately for each wavelength. An integration over wavelength then yields a suitable quantity to enter into the radiation budget. Integrations over separate absorption lines are reviewed (in a different context) in Section 17.3.

The problem of replacing the effect of a complicated absorption band pattern by a few well chosen parameters is another problem with a long history. It is treated in many textbooks, but its practical details are fairly remote from the main topic of this book. Let it suffice to state that the mathematical basis for any such band model is exponential sum fitting, a procedure extensively discussed by Hunt and Grant (1969), Arking and Grossman (1972), Wiscombe and Evans (1977), Quenzel *et al.* (1978), and others.

The standard problem of determining  $UR$  thus requires four parameters at least. Strictly the number four is too little, for this problem does not at all include other geometries such as broken or billowing clouds. Yet the practical model makers in dynamic climatology or weather prediction find four parameters a lot. They greatly prefer simpler but nonexact answers, in which fewer parameters suffice. It is imperative to look for such answers in order to avoid an undue fraction of the computation effort (and cost) going into a side problem. The problem of finding such fair approximations with few parameters is the problem of *parametrization*.

The "best choice" of parametrization involves a trade-off between factors of accuracy and economy, which must be judged in the context of a practical situation. For that reason a general recommendation cannot be given. What we do, in fact, is to supply building bricks that may or may not be found useful.

The similarity rules (Section 14.1) show a simple way to suppress the parameter  $g$ . Since these rules have asymptotic validity for thick layers, it is advisable to check them by means of sample calculations. It may then turn out that not this parametrization but a somewhat different one is more suitable for the problem at hand.

The problem of how best to parametrize the effect of a broken cloud deck still appears to be unsolved. However, it was recognized at the 1976 radiation meeting of IAMAP (International Association of Meteorology and Atmospheric Physics) as a problem of importance; see references in Section 20.1.3. It is necessary to define the proportion of clear sky as a parameter, but already the question of how this proportion depends on the zenith angle is a nontrivial problem in geometrical probability. If we then come to multiple scattering calculation and wish to do a somewhat clean mathematical job, the complications multiply enormously, as the sample problem discussed in Section 20.1.3 shows. In practice this may be an invitation to return to extremely crude assumptions, such as the assumption that each of the fluxes can be written as  $c$  times the value for the uniform cloud case plus  $(1 - c)$  times the value for the clear-sky case, where  $c$  is the fractional cloud cover (Nack and Green, 1974).

### 19.4.2 Where Is the Energy Deposited?

The energy which is not returned into space is absorbed either in the ground or in the various constituents of the atmosphere (molecules, aerosols, cloud particles). In clear weather ground absorption dominates. In overcast weather calculations will have to show where most of the absorption takes place. We shall in this section recapitulate what answers are readily available and, in particular, how the balance works out for a thick cloud deck with nearly conservative scattering.

Answers for homogeneous slabs have been given in the preceding chapters. We refer in particular to Table 15 and Fig. 9.4 for isotropic scattering and to Table 39 and Fig. 13.4 for anisotropic scattering with asymmetry factors ranging up to  $g = 0.875$ . The distribution function of the heights or depths in the atmosphere, where the absorption takes place, is in principle available in two ways. Either subtraction in the tables of fluxes or multiplication by  $1 - a$  in the tables of point-direction gain gives the desired answer. See Tables 16, 17, and 41 and the numerical examples in Section 9.2. The gain is proportional to what is commonly called flux divergence or radiation divergence, and this again determines the local heating rate.

An example for a realistic atmosphere under clear conditions may be quoted from Eschelbach (1973a, b). At the wavelength  $\lambda = 450$  nm, with ground albedo 0.25, he finds that a clean Rayleigh atmosphere (turbidity  $T = 1$ ) gives

$$31\% \text{ refl. into space} + 0\% \text{ abs. in atm.} + 69\% \text{ abs. in ground} = 100\%$$

If nonabsorbing aerosols are added to make  $T = 4$ , the numbers change into

$$34\% \text{ refl. into space} + 0\% \text{ abs. in atm.} + 66\% \text{ abs. in ground} = 100\%$$

However, the actual aerosols are slightly absorbing, which has a strong effect. The reflection is even reduced instead of decreased, and the numbers become

$$30\% \text{ refl. into space} + 10\% \text{ abs. in atm.} + 60\% \text{ abs. in ground} = 100\%$$

Separate graphs in Eschelbach's papers specify the heating rates at various heights.

The effect of a small absorptivity of the scattering particles becomes even more pronounced if the atmosphere is optically thick, which is the normal situation for a cloud layer. We recall that the reflected fraction would be 100% if the optical thickness were infinite ( $b = \infty$ ) and the scattering were perfect ( $a = 1$ ). A deviation from either assumption produces a loss. The exact situation near  $b = \infty$ ,  $a = 1$  has puzzled so many research workers that we have earlier referred to this point as "the nasty corner" of the  $(a, b)$  domain. The full analysis of this problem for a homogeneous slab is given in Section 5.4.1. A practical formula for the reflected fraction is in Section 5.4.2. Because of its basic interest, we shall now work out this practice problem to show where the energy goes.

**Problem.** A very thick atmosphere (optical depth  $b \gg 1$ ) with nearly conservative scattering ( $1 - a \ll 1$ ) and an arbitrary phase function is at its top exposed to unidirectional radiation with angle  $\theta_0$  with the normal,  $\cos \theta_0 = \mu_0$ . Most of the incident flux is diffusely reflected, but some is lost by absorption within the atmosphere and some is lost by transmission into the ground, which we assume black. What is the ratio between these two kinds of losses?

**Answer.** The answer is contained in the equations for thick layers (Section 5.3). Write:

fraction of incident flux

absorbed in atmosphere:  $L_{\text{atm}}(\mu_0) = 1 - RU - TU$

fraction of incident flux

absorbed in ground:  $L_{\text{gr}}(\mu_0) = TU$

total loss:

$$L_{\text{atm}}(\mu_0) + L_{\text{gr}}(\mu_0) = 1 - RU$$

and introduce the notation  $t = (1 - a)^{1/2}$ ,  $s = (b + 2q)^{-1}$ , where  $q$  is the extrapolation length for conservative scattering. In two limits we have a simple proportionality:

If  $b = \infty$  ( $s = 0$ ), then  $L_{\text{gr}} = 0$  and  $L_{\text{atm}} \propto t$  for  $t \ll 1$

If  $a = 1$  ( $t = 0$ ), then  $L_{\text{atm}} = 0$  and  $L_{\text{gr}} \propto s$  for  $s \ll 1$

Yet, we may not simply add these two small losses if both  $t$  and  $s$  are nonzero. The physical reason for this fact is clear: small absorption losses in the atmosphere, in order to fully work out, need an atmosphere that is very thick; small penetration to the ground, in order to materialize, needs a scattering albedo very close to 1. Graphically this can be seen in Fig. 19.11. This figure happens to refer to isotropic scattering because it is an enlarged portion of the upper right-hand corner of Fig. 9.2. We shall soon see, however, that the shape of the curves is universal. A simple addition of the losses proportional to  $t$  and to  $s$  would mean that the equal-loss curves would be straight lines connecting the point on the horizontal boundary ( $t$  axis,  $L_{\text{atm}}$  only) with the point on the vertical boundary ( $s$  axis,  $L_{\text{gr}}$  only). The actual curves differ greatly from straight lines.

We shall now discuss the exact asymptotic forms in the corner domain  $s \ll 1$ ,  $t \ll 1$ . In the section cited we find

$$\left. \begin{array}{l} L_{\text{atm}} \\ L_{\text{gr}} \\ L_{\text{atm}} + L_{\text{gr}} \end{array} \right\} = \frac{4K(1, \mu_0)}{[3(1 - g)]^{1/2}} \left\{ \begin{array}{l} t(1 - f)/(1 + f) \\ t2f/(1 - f^2) \\ t(1 + f^2)/(1 - f^2) \end{array} \right.$$

The argument 1 of  $K$  refers to the conservative case ( $a = 1$ ) and

$$f = e^{-k(b+2q)} = e^{-[3(1-g)]^{1/2}t/s}$$

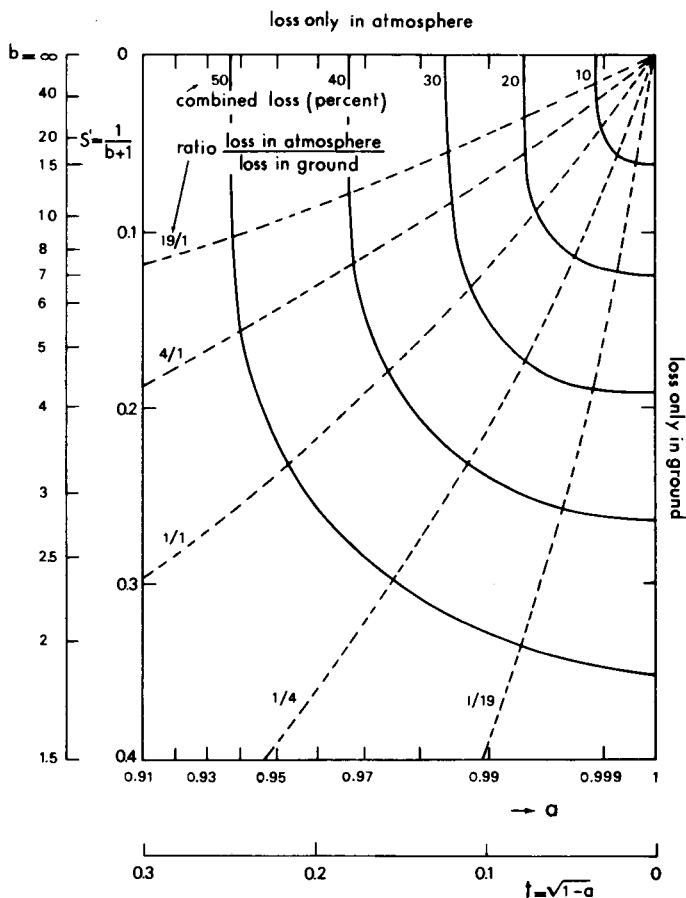


Fig. 19.11. Balance between losses due to finite depth and to nonperfect scattering. Heavy curves give the nonreflected fraction of incident flux, i.e., the combined loss. The data refer to a finite atmosphere of thickness  $b$  consisting of isotropically scattering particles with single scattering albedo  $a$  exposed to vertically incident radiation. See further explanation in text.

In isotropic scattering the common factor is replaced by  $H(1, \mu_0)$  (Display 8.1) and the results just found check with those in Display 9.2. The value of  $f$  cannot be further simplified because  $f$  ranges from the limit 0 for  $s = 0$  to 1 for  $t = 0$ . In the latter limit we may replace  $t/(1 - f)$  by  $s/[3(1 - g)]^{1/2}$ , thus retrieving the thick-layer formulas for conservative scattering.

The curves for constant loss in the  $t$ - $s$  plane, as shown in Fig. 19.11, can in the corner domain be represented simply by  $t(1 + f^2)/(1 - f^2) = \text{const}$ . The ratio between the two loss values is

$$n = (L_{\text{atm}}/L_{\text{gr}}) = (1 - f)^2/2f$$

from which we can solve  $f = n + 1 - [n(n + 2)]^{1/2}$  and subsequently  $t/s = (-\ln f)/[3(1 - g)]^{1/2}$ , which gives the slope of the tangent to any curve of constant ratio  $n$  in the corner of Fig. 19.11. These slopes are given in the accompanying tabulation.

$n = L_{\text{atm}}/L_{\text{gr}} = 0$	$\frac{1}{19}$	$\frac{1}{4}$	1	4	19	$\infty$
$f = 1$	0.6842	0.5000	0.2680	0.1010	0.0250	0
$(1 - g)^{1/2}t/s = 0$	0.219	0.400	0.760	1.324	2.130	$\infty$

Please note that in this problem, as in any typical thick-layer problem, the value of  $\mu_0$  and the choice of phase function enter only via the injection function  $K(1, \mu_0)$ . Since this is a common factor, the curves and ratios just discussed are universal for homogeneous cloud layers. Only the scale factors have to be adjusted. The actual illustration (Figs. 9.2 and 19.11) refers to perpendicular incidence and isotropic scattering.

Figure 19.11 also shows the practical limits of this asymptotic theory. These simple formulas give rather accurate results for any situation in which the total loss remains below 20%. This means, for isotropic scattering,  $a > 0.994$ ,  $b > 7$ . It is not important whether we plot  $s' = (b + 1)^{-1}$ , as done in the figure, or  $s = (b + 1.4)^{-1}$ .

A final warning: nobody should mistake the treatment of a simple model in the preceding pages for a treatment of energy deposition in the actual clouds. There is quite a literature over the past 10 years, of which this author is sure to have seen only a corner. Moreover, in the GARP (Global Atmospheric Research Program) international program and its various subprograms, a fine effort is made to solve the most crucial questions by a direct attack. Fairly complete treatments not directly connected with this effort are, e.g., in Feigelson (1973, 1978), Feigelson and Tsvang (1974), and Morcrette (1977).

Morcrette (see also Fouquart *et al.*, 1977) demonstrates the overriding importance of the liquid water content and shows an approximation method to take the vertical variation in liquid water content and drop size into account. He confirms the thin layer of strong cooling near the top of the cloud.

Grassl (1975) points out that the heating of a cloud by radiation in the visual domain is strongly increased by the absorbing aerosol particles, which are present both as condensation nuclei within water drops and suspended in air. For example, a nucleus with radius  $0.5 \mu\text{m}$  and imaginary part of the refractive index  $k = 0.02$  within a water drop of radius  $5 \mu\text{m}$  reduces its albedo for single scattering to  $a = 0.9978$ . The same value is correct for drops with the Deirmendjian C1 size distribution and leads for a cloud with optical thickness 32 (vertical incidence, no ground absorption) to 14% of the incident radiation being absorbed within the cloud. Addition of suspended aerosol particles makes  $a = 0.9963$  and increases the absorption to 22%.



## REFERENCES

- Ambartsumian, V. A. (1943). *Dokl. Akad. Nauk SSSR* **43**, 106.
- Arking, A., and Grossman, K. (1972). *J. Atmos. Sci.* **29**, 937.
- Balin, Yu. S., Zadde, G. O., Zuev, V. E., Matvienko, G. G., Samokhvalov, I. V., and Shamanaev, V. S. (1975). Preprint of paper presented at Int. Assoc. of Meteo and Atmos. Phys., Melbourne, Australia.
- Blättner, W. G., Collins, D. G., and Wells, M. B. (1974). Air Force Cambridge Research Laboratories, Bedford, Massachusetts, Report RRA T 7402.
- Box, M., and McKellar, B. H. J. (1977). *J. Opt. Soc.* **67**, 260 (abstract).
- Bullrich, K., Eiden, R., Eschelbach, G., Fischer, K., Hänel, G., and Heintzenberg, J. (1974). In *UCLA Int. Conf. Radiat. Remote Probing Atmos.* (J. G. Kuriyan, ed.), p. 135. Western Periodicals Co., North Hollywood, California.
- Buyco, E. H., Namkoong, D. (1977). Correlation of Total, Diffuse, and Direct Solar Radiation, NASA Tech. Memo. TM X-3422.
- Coffeen, D. L., and Hansen, J. E. (1972). *Proc. Int. Symp. Remote Sensing Environ.*, p. 515. Environm. Res. Institute, Ann Arbor, Michigan.
- Coffeen, D. L., and Hansen, J. E. (1973). In "Planets, Stars and Nebulae Studied with Photopolarimetry" (T. Gehrels, ed.), p. 518. Univ. of Arizona Press, Tucson, Arizona.
- Collis, R. T. H., Russell, P. B., Uthe, E. E., and Viezee, W. (1974). *UCLA Int. Conf. Radiat. Remote Probing Atmos.* (J. G. Kuriyan, ed.), p. 267. North Hollywood, California.
- Coulson, K. L. (1971). *J. Quant. Spectrosc. Radiat. Transfer* **11**, 739.
- de Bary, E. (1964). *Appl. Opt.* **3**, 1293.
- de Bary, E. (1973). *Beitr. Phys. Atmos.* **46**, 213.
- de Bary, E., and Bullrich, K. (1964a). *Optik* **21**, 199.
- de Bary, E., and Bullrich, K. (1964b). *Optik* **21**, 467.
- de Bary, E., and Eschelbach, G. (1974). *Tellus* **26**, 682.
- Deepak, A. (ed.) (1977). "Inversion Methods in Atmospheric Remote Sounding." Academic Press, New York.
- Deirmendjian, D. (1969). "Electromagnetic Scattering on Spherical Polydispersions." Elsevier, Amsterdam.
- DeLuisi, J. J., et al. (1976). Results of a Comprehensive Atmospheric Aerosol Radiation Experiment in Southwestern United States, part 1, preprint.
- Derr, V. E. (1972). Remote Sensing of the Troposphere. Univ. of Colorado, Boulder, Colorado.
- Eiden, R. (1968). *Tellus* **20**, 380.
- Eiden, R. (1971). *Appl. Opt.* **10**, 749.
- Eschelbach, G. (1971). *J. Quant. Spectrosc. Radiat. Transfer* **11**, 757.
- Eschelbach, G. (1973a). *Beitr. Phys. Atmos.* **46**, 249.
- Eschelbach, G. (1973b). *Ann. Géophys.* **29**, 329.
- Feigelson, E. M. (1973). Radiant Heat Transfer in a Cloudy Atmosphere. Israel Progr. for Sci. Translations, Jerusalem (orig. Russian: Gidrometeor. Izd. Leningrad, 1970).
- Feigelson, E. M. (1978). *Contr. Atmos. Phys.* **51**, 203.
- Feygelson, Ye. M., and Tsvang, L. R. (eds.) (1974). Heat Transfer in the Atmosphere. NASA Tech. Translation NASA TT F F-790, Washington, D.C. (orig. Russian: Nauka Press, Moscow, (1972).
- Fouquart, Y., Bonnel, B., and Morcrette, J. J. (1977). In *Proc. Symp. Radiat. Atmos.* (H.-J. Bolle, ed.), p. 483. Science Press, Princeton, New Jersey.
- Furman, D. R., Mo, T., and Green, A. E. S. (1976). *J. Atmos. Sci.* **33**, 537.
- Fymat, A. L. (1976). In "Optical Propagation in the Atmosphere," Agard Conf. Proc. No. 183. Agard, Neuilly.
- Gehrels, T. (1962). *J. Opt. Soc. Am.* **52**, 1164.
- Grassl, H. (1975). *Contr. Atmos. Phys.* **48**, 199.

- Green, A. E. S., and Martin, J. D. (1966). In "The Middle Ultraviolet; Its Science and Technology" (A. E. S. Green, ed.), Chapter 7. Wiley, New York.
- Green, A. E. S., Sawada, T., and Shettle, E. P. (1974). *Photochem. Photobiol.* **19**, 251.
- Green, A. E. S. *et al.* (1972). *J. Colloid Interface Sci.* **39**, 520.
- Grether, D. F., Hunt, A. J., and Wahlig, M. (1976). Lawrence Berkeley Labor. Report, LBL 5292.
- Grether, D. F., Evans, D., Hunt, A., and Wahlig, M. (1979) Lawrence Berkeley Labor. Report, LBL 9412.
- Hänel, G. (1972a). *Aerosol Sci.* **3**, 377.
- Hänel, G. (1972b). *Aerosol Sci.* **3**, 455.
- Hänel, G. (1976). *Adv. Geophys.* **19**, 74.
- Hansen, J. E., and Travis, L. D. (1974). *Space Sci. Rev.* **16**, 527.
- Hansen, J. E., Wei-Chung Wang, and Lacis, A. A. (1978). *Science* **199**, 1065.
- Heintzenberg, J. (1975). *J. Aerosol Sci.* **6**, 291.
- Hitzfelder, S. J., Plass, G. N., and Kattawar, G. W. (1976). *Appl. Opt.* **15**, 2489.
- Hunt, G., and Grant, I. (1969). *J. Atmos. Sci.* **26**, 963.
- Junge, C. E. (1952). *Ber. Deutsch. Wetterdienst U.S. Zone* **35**, 261.
- Kano, M. (1968). *J. Opt. Soc. Am.* **58**, 789.
- Kattawar, G. W., Plass, G. N., and Catchings, F. E. (1973). *Appl. Opt.* **12**, 1071.
- Kattawar, G. W., Plass, G. N., and Hitzfelder, S. J. (1976). *Appl. Opt.* **15**, 632.
- Kawata, Y. and Hansen, J. E. (1976). In "Jupiter, Studies of the Interior, Atmosphere, Magnetosphere and Satellites," (T. Gehrels, ed.), p. 516. Univ. of Arizona Press. Tucson, Arizona.
- Khragian, A. Kh., and Mazin, I. P. (1952). *Tr. Tsentralnoi Aerolog. Observ.* **7**, 56.
- Kunkel, K. E., and Weinmann, J. A. (1976). *J. Atmos. Sci.* **33**, 1772.
- Kuriyan, J. G., and Sekera, Z. (1974). *Q. J. R. Meteorol. Soc.* **100**, 67.
- Kuriyan, J. G., Phillips, D. H., and Chahine, M. T. (1974a). *J. Atmos. Sci.* **31**, 2233.
- Kuriyan, J. G., Phillips, D. H., and Willson, R. C. (1974b). *Q. J. R. Meteorol. Soc.* **100**, 665.
- McCartney, E. J. (1976). "Optics of the Atmosphere; Scattering by Molecules and Particles." Wiley, New York.
- McNeil, W. R., and Carswell, A. I. (1975). *Appl. Opt.* **12**, 2158.
- Minnaert, M. (1937). First printing of Minnaert (1953).
- Minnaert, M. (1940). "Light and Colour in the Open Air." Bell, London. Also Dover, New York (1954).
- Minnaert, M. (1953). "De natuurkunde van het vrije veld," Vol. I, Licht en kleur in het landschap. Thieme, Zutphen.
- Moon, P., and Spencer, D. E. (1942). *Illum. Eng.* **37**, 707.
- Morcrette, J. J. (1977). Calcul des flux infrarouges des tanx de refroidissement radiatif en atmosphère nuageuse. Thèse Univ. de Lille. Lille, France.
- Nack, M. L., and Green, A. E. S. (1974). *Appl. Opt.* **13**, 2405.
- Pal, S. R., and Carswell, A. I. (1973). *Appl. Opt.* **12**, 1530.
- Perelman, A. Ya, and Punina, V. A. (1969). *Pure Appl. Geophys. (PAGEOPH)* **74**, 92.
- Piotrowski, S. R. (1955). *Bull. Acad. Pol. Sci. Cl. III* **3**, 303.
- Piotrowski, S. R. (1956). *Acta Astron.* **6**, 61.
- Plass, G. N., Kattawar, G. W., and Hitzfelder, S. J. (1976). *Appl. Opt.* **15**, 1003.
- Quenzel, H. (1970). *J. Geophys. Res.* **75**, 2915.
- Quenzel, H., Bakau, S., and Koepke, P. (1978). *Contrib. Atmos. Phys.* **51**, 28.
- Sassen, K., Liou, K. N., and Hunter, S. (1977). Scattering of Polarized Laser Light by Water Droplet and Ice Crystal Clouds, Sci. Rep. I, Dept. Meteorology, Univ. of Utah. Salt Lake City, Utah.
- Shettle, E. P., and Green, A. E. S. (1974). *Appl. Opt.* **13**, 1567.
- Shifrin, K. S. (1951). Scattering of Light in a Turbid Medium (Russian) (NASA Tech. Translation TT F-477, April 1968).
- Shifrin, K. S. (1955). *Tr. Glavnoi Geofiz. Observ.* **46**, 5.

- Shifrin, K. S., and Kozhaev, D. A. (1972). "Optics of the Oceans and the Atmosphere" (K. S. Shifrin, ed.), pp. 210-222, Publ. NAUK, Leningrad (in Russian).
- Shifrin, K. S., and Perelman, A. Ya. (1963). *Opt. Spectrosc.* **15**, 285.
- Shifrin, K. S., and Perelman, A. Ya. (1964). *Pure Appl. Geophys. (PAGEOPH)* **58**, 208.
- Sutherland, R. A., McPeters, R. D., Findlay, G. B., and Green, A. E. S. (1975). *J. Atmos. Sci.* **32**, 427.
- Tanaka, M. (1971a). *J. Meteor. Soc. Jpn.* **49**, 296.
- Tanaka, M. (1971b). *J. Meteor. Soc. Jpn.* **49**, 321.
- Tanaka, M. (1971c). *J. Meteor. Soc. Jpn.* **49**, 333.
- Twitty, J. T. (1975). *J. Atmos. Sci.* **32**, 584.
- Twitty, J. T., Parent, R. J., Weinman, J. A., and Eloranta, E. W. (1976). *Appl. Opt.* **15**, 980.
- van de Hulst, H. C. (1947). *Astrophys. J.* **105**, 471.
- van de Hulst, H. C. (1949a). In "The Atmosphere of the Earth and Planets" (G. P. Kuiper, ed.). Univ. of Chicago Press, Chicago, Illinois.
- van de Hulst, H. C. (1949b). *Rech. Astron. Observ. Utrecht* **11**, part 2.
- van de Hulst, H. C. (1951). *Astrophys. J.* **112**, 1.
- van de Hulst, H. C. (1957). "Light Scattering by Small Particles." Wiley, New York. Also Dover, New York, 1980.
- van de Hulst, H. C., and Davis, M. M. (1961). *Proc. Kon. Nederl. Akad. Wetensch.* **B64**, 220.
- Weinman, J. A. (1976). *J. Atmos. Sci.* **33**, 1763.
- Weinman, J. A., and Shipley, S. T. (1972). *J. Geophys. Res.* **77**, 7123.
- Weinman, J. A., Twitty, J. T., Browning, S. R., and Herman, B. M. (1975). *J. Atmos. Sci.* **32**, 577.
- Weinman, J. A., and Ueyoshi, K. (1969). *J. Atmos. Sci.* **26**, 600.
- Wilkes, M. V. (1954). *Proc. Phys. Soc. London* **B67**, 304.
- Wiscombe, W. J., and Evans, J. W. (1977). *J. Comput. Phys.* **24**, 416.
- Yamamoto, G., and Tanaka, M. (1974). In *Int. Conf. Radiat. Remote Probing Atmos.*, UCLA (J. G. Kuriyan, ed.), p. 74. Western Periodicals C., North Hollywood, California.
- Zuev, V. E. (1974). "Propagation of Visible and Infrared Radiation in the Atmosphere." Wiley, New York (original Russian, 1970).

## 20 Miscellaneous Applications

### 20.1 OTHER GEOMETRIES

The aim of this book is to produce a collection of tables, graphs, and formulas referring to solutions of multiple scattering problems in *slab geometry*. Cloud layers in the atmospheres of the earth and planets are the leading example. Other layered structures are reviewed in Section 20.2. Problems referring to semi-infinite atmospheres (the half-space) or to unbounded media are simple limits of the slab problem. Optics of the deep sea (Section 20.4) is a fine natural example.

A vast multitude of problems remain in which the configuration of scatterers or sources has a different geometry. Each of these configurations would require a separate book, if numerical results were to be presented in detail similar to those for slabs. No attempt in that direction has been made. Some problems of interest are briefly reviewed in Sections 20.1.1–20.1.3. See also Lenoble (1978).

The Monte Carlo method can be directly applied to any configuration. However, the “constructive” methods of invariant embedding, adding, and doubling, can also be adapted to other geometries. The equations should be written with care, but by and large they are so obvious that papers without numerical results hardly seem worth printing. Asymptotic theory for other geometries remains relatively unexplored and deserves more attention.

For instance, Monte Carlo computations for small and moderate optical depths  $\tau$  may often be combined with available results for  $\tau = \infty$ ; for it should be possible to treat any face of a body of arbitrary shape in this limit as the face of a semi-infinite medium (i.e., half-space). This is but one example of a generally

recommendable "grafting" process (van de Hulst, 1977), in which two theories developed on different sets of assumptions are linked together in a domain of common validity.

### 20.1.1 Spherical and Miscellaneous Configurations

The two areas of research to which radiative transfer owes much of its original development are stellar atmospheres and nuclear reactor technology.

Stars are spherical. In most stellar atmospheres the mean free path is so small compared to the radius of the star that the plane-layer approximation suffices; but there are many astronomical objects with extended atmospheres or scattering halos in which the spherical geometry is essential.

To go to spherical geometry from plane geometry is more than a minor modification in the equation of transfer. In plane geometry we have used the facts that the total optical depth of a slab is the essential parameter and that the geometrical arrangement with height inside the slab is immaterial. For that reason it was permitted to apply the computations for a homogeneous slab to actual atmospheres in which the density drops exponentially with height. Similar transformations hold for cloud layers and for the galactic dust layer (Section 20.5.1).

No such equivalence exists in spherical geometry, for the slant angles along a straight path then vary with the geometric position. As a result, a spherical halo of homogeneous density or a scattering shell of finite thickness, both thought to be placed around a central star, produce different emerging radiation fields even if the phase function and the optical thickness along a radius are assumed equal. Conclusion: to tabulate and discuss a somewhat representative set of results in spherical geometry is an even larger job than to do so for a slab.

In planetary atmospheres the spherical geometry must be taken into account near the horizon, e.g., in twilight studies. This can often be done by a simple adjustment of the plane theory, as mentioned in Section 19.2.2. More generally, a computation based on the equation of transfer for spherical geometry should be made from scratch. The literature on such computations has been reviewed by Lenoble (1978) and in separate chapters of many of the standard textbooks cited in Chapter 1.

Nuclear reactors have practical shapes, which never resemble infinite slabs. Only in studying partial problems in reactor technology, e.g., the shielding power of scattering layers of a certain depth, have research workers in nuclear scattering tackled practice problems which are identical to those treated earlier in this book. The theoretical developments in this field in the postwar decades have reached great sophistication (e.g., Davison, 1957; Lewis, 1965). We have used some information that was readily available. An example is the relation between amplification factor and critical size, which (for slab geometry only) may be read from Fig. 13.12.

The terminology, of course, must be translated. It may suffice to mention the equivalences shown in the accompanying tabulation. A more extensive glossary given by Kourganoff (1963, Section 12) differs in detail.

Our terminology and notation			
Nuclear scattering terminology		At entry surface (top)	At other surface (bottom)
Directional flux	Reflection or transmission function	$R(\mu, \mu_0)$	$T(\mu, \mu_0)$
Net current	Net flux down	$1 - UR(\mu_0)$	$UT(\mu_0)$
Scalar density	$\mu_0^{-1} \times$ point-direction gain	$\mu_0^{-1} + 2NR(\mu_0)$	$2NT(\mu_0)$

These practice problems serve only for orientation. The actual design calculations clearly refer to geometries far outside the scope of this book.

20.1.2 Pencil Beams

Even if we maintain slab geometry for the configuration of scatterers, the sources of illumination may not satisfy the assumptions made in the standard problem described in Section 4.1.3. This happens in particular if the illumination comes from a narrow beam (as in the searchlight or lidar problem, Section 19.3), or from a point source of radiation in or near the slab (as in a reflection nebula, Section 20.5.1). In any such problem at least one independent variable is added to the arguments ( $a, g, b, \mu, \mu_0$ ) that we considered throughout this book. This means basically a new problem requiring a separate computation.

Nevertheless, the earlier results referring to illumination by an infinitely extended beam remain useful in problems of this class. It is possible to employ them as checks in the form of integrals of the resulting functions over the added variable. The derivation of such integral formulas, which probably would merit a wider exploitation than is found in the literature, appears easiest by means of thought experiments. For instance, many laser beams side by side provide a uniform illumination, or many stars side by side form an extended narrow source layer. To amplify this remark without numerical illustrations would be pretentious. The computation leading to Fig. 19.9 may be cited as an example of such an integral check, the integration there being taken over the imagined infinite width of the lidar reception cone.

The searchlight problem was first discussed in some detail by Chandrasekhar (1958). Subsequent developments are found in Hunt (1968), Rybicki (1971), Romanova (1971, 1973), and Becket *et al.* (1974). The practical emphasis is on the gradual spread of the light around an initially very narrow beam in a haze or fog, but most of the published numerical examples refer to the very unrealistic assumption of isotropic scattering.

The opposite extreme is the assumption of scattering under very small angles only. The measured deviations then result from many scattering events. The theory for this limit is well worked out. A summary and references are in Section 20.5.2.

In the lidar problem the emphasis is on the time spread and the polarization of the returned signal. References and a number of results are found in Section 19.3.

### 20.1.3 Broken and Towered Clouds

Any deviation from the assumption of a smooth stratiform cloud deck may profoundly affect the interpretation of photometric, polarimetric, or spectroscopic data on the diffuse radiation. This is as true for light reflected from a distant planet as for measurements in our own atmosphere. The actual variety of forms is infinite, and schematic representations can be made in many ways. Some models which have been considered are smooth slabs topped by rectangular towers, smooth slabs topped by infinitely long rectangular ridges, isolated clouds of cylindrical or cuboid form, and a broken cloud deck consisting of isolated clouds.

Problems of this type have been assessed as having "top priority" (Irvine, 1975) and being "largely unexplored" (Appleby and van Blerkom, 1975). The 1976 IAMAP (International Association of Meteorology and Atmospheric Physics) Symposium on radiation (Bolle, 1977) indeed contains 5 papers in this class (Barkstrom and Arduini, 1977; Aida, 1977; McKee and Klehr, 1977; Avaste and Vainikka, 1977; Davies and Weinman, 1977). Yet the impression is that the all-out effort necessary to master these problems is still lacking. Possibly, prospective authors have been discouraged by the bewildering variety of configurations. The papers that do exist face two distinct challenges:

(1) the astronomical (or meteorological) challenge of seeing how badly and in what sense the interpretation of the data, e.g., of the center-limb variation of an absorption line, is affected by the new assumptions.

(2) the applied mathematics challenge of solving the multiple scattering problem for a given simple model in a sufficiently complete and reliable manner. By "sufficient" we mean that more refined calculations should yield increased accuracy but no real surprises.

The present state of the art seems to be that the applied mathematics challenge has hardly been met at all but that the astronomers (and meteorologists), eager to interpret their data, have started to discuss them with whatever incomplete calculations are available. A good review with a dozen references is in Appleby and van Blerkom (1975). See also Lenoble (1978).

In treating a broken cloud deck the most naive way out is to assume that the reflection function can be described by  $c \times$  reflection function of solid cloud deck +  $(1 - c) \times$  reflection function of cloudless planet, where  $c$  is the frac-

tional cloud cover. In certain situations of relatively flat clouds sufficiently far apart, this zero-order approximation may make sense. It has been applied by Nack and Green (1974). If the clouds have a realistic vertical dimension and are not too far apart, there is not the slightest guarantee that this approximation is useful. Even the very first mathematical problem in that case, namely, how  $c$  depends on zenith angle (as exemplified by the fraction of time of *direct* sunshine at a point on the surface) is nontrivial. Some Russian papers referring to this situation have been reviewed by Niilisk and Ohvril (1978).

A review of empirical formulas would be out of place, unless they could be checked against reliable computations. The author has looked for at least one example where the applied mathematics challenge has been reasonably met, and this is discussed in the next few pages. The data, consisting of calculated numerical values *with* asymptotic behavior, are presented in Table 65. The material in this table is almost exclusively based on Monte Carlo computations for cuboid clouds by Davies and Weinman (1977), and Davies (1978), kindly made available before publication. I have obtained the numbers at the grid points of Table 65 by interpolation and extrapolation, in which the asymptotic values also served as a guide.

The configuration considered in this example is a homogeneous cuboid cloud. This is a cloud having a square base with side  $\tau_h$  and a height  $\tau_v$ , all measured in mean free paths. The scattering is supposed to be conservative and isotropic. The radiative energy entering vertically into the top square emerges in one of four ways: "up top," "down bottom," "up sides," or "down sides," where up and down refer to photons with an exit direction subtending an angle smaller or larger than  $90^\circ$  with the direction of incidence. The table shows percentage results for each of these parts separately, with sum 100, as well as the partial sums "up total" and "down total."

The arrangement of each section of Table 65 is the same. The three essential parameters are  $\tau_h$ ,  $\tau_v$ , and their ratio  $\tau_v/\tau_h$ . If one of these goes to 0 or to  $\infty$ , then at least one other must go to 0 or to  $\infty$ . Thus 6 asymptotic cases result, in each of which two parameters are 0 or  $\infty$ . It would be most elegant to arrange these asymptotic cases as sides of a hexagon, joining each other at "corners" where all three are 0 or  $\infty$ . Since typesetting is simpler in a rectangular grid, we have selected the method of Table 65, to which Fig. 20.1 gives the key.

Basically, this is still a hexagonal arrangement. In each of the 6 diagrams in Table 65, the center square refers to  $\tau_v = \tau_h = \tau_v/\tau_h = 1$ . Grouped around it are the numbers referring to cases in which these parameters step up or down by factors  $\sqrt{10} = 3.2$  at a time. In frames around it are the six asymptotic cases. Those for  $\tau_v/\tau_h = \text{const}$  are approached by staying on the same horizontal line, those for  $\tau_v = \text{const}$  are approached by staying in the same vertical column, and those for  $\tau_h = \text{const}$  are approached by staying on the same diagonal line from upper left to lower right. The 6 "corner" values, in which these 6 sides meet, have values 0, 50, or 100. Only two corner values (top right and bottom left) are shown in the table.



TABLE 65

Fate of Radiation Vertically Incident on Top of Cuboid Cloud with Isotropic Scattering<sup>a</sup>

$\tau_v =$										$\tau_v/\tau_h =$										$\tau_v =$												
$\infty$	—	10	3.2	1	0.32	0.1	—	0	$\infty$	$\infty$	—	10	3.2	1	0.32	0.1	—	0	$\infty$													
Up top										Down bottom																						
			0	0	0	0	0	→	0	$\infty$			0.005	4.1	37	73		90.5	→	100												
			13	5	1.6	<i>a</i>				↑	↑		0	0	0					↑												
100		27	13	5	1.6					0	10	0	0	0	0.01	5	38					100										
100		51	27	13	5	1.6					0	3.2	0	0	0	0.05	6	40	74					100								
100		72	51	27	13	5	1.6					0	1	0	0	0	1.3	8	46	76	92					100						
100		87	71	47	23	9	3.0	0	0	0.32	0	0	0	0	7.8	25	55	82	93	100	100											
100			81	58	30	12	3.9	0	0	0.1	0	0	13		32	61	84	94	100	100	100											
↓				0	0	0	0	0	↓	↓						100	100	100	100	100												
100	←	85	64	34	14	4.8					0	0	←	15		36	66	86	95.2													
Up sides										Down sides																						
			50	48	32	14	4.8	→	0	$\infty$			50	48	32	14		4.8	→	0												
			41	47	49	<i>b</i>				↑	↑		46	48	49	<i>c</i>				↑												
0		33	41	43	30					0	10	0	0	40	46	47	30					0										
0		21	33	38	27	12					0	3.2	0	28	40	43	28	12	12	0												
0		14	21	30	20	9	3.2	0	0	1	0	0	14	27	35	21	10	3.2	0													
0		6	9	13	11	5	1.8	0	0	0.32	0	0	7	12	15	11	4	1.8	0	0												
0			2	5	4	2	0.9	0	0	0.1	0	0	4		5	5	2	0.9	0	0												
↓				0	0	0	0	0	↓	↓						0	0	0	0	0												
0	←	0	0	0	0	0					0	0	←	0		0	0	0	0	0												
Up total										Down total																						
			50	48	32	14	4.8	→	0	$\infty$			50	52	68	86		95.2	→	100												
			54	52	51	<i>a + b = 1 - c</i>				↑	↑		46	48	49	<i>c</i>				↑												
100		60	54	48	32					0	10	0	0	40	46	52	68					100										
100		72	60	51	32	14					0	3.2	0	28	40	49	68	86					100									
100		86	72	57	33	14	4.8	0	0	1	0	0	14	28	43	67	86	95.2	100	100												
100		93	80	60	34	14	4.8	0	0	0.32	0	0	7	20	40	66	86	95.2	100	100	100											
100			83	63	34	14	4.8	0	0	0.1	0	0	17		37	65	86	95.2	100	100	100											
↓				0	0	0	0	0	↓	↓						100	100	100	100	100												
100	←	85	64	34	14	4.8					0	0	←	15		36	66	86	95.2													

<sup>a</sup> Based on computations by Davies and Weinman (1977).

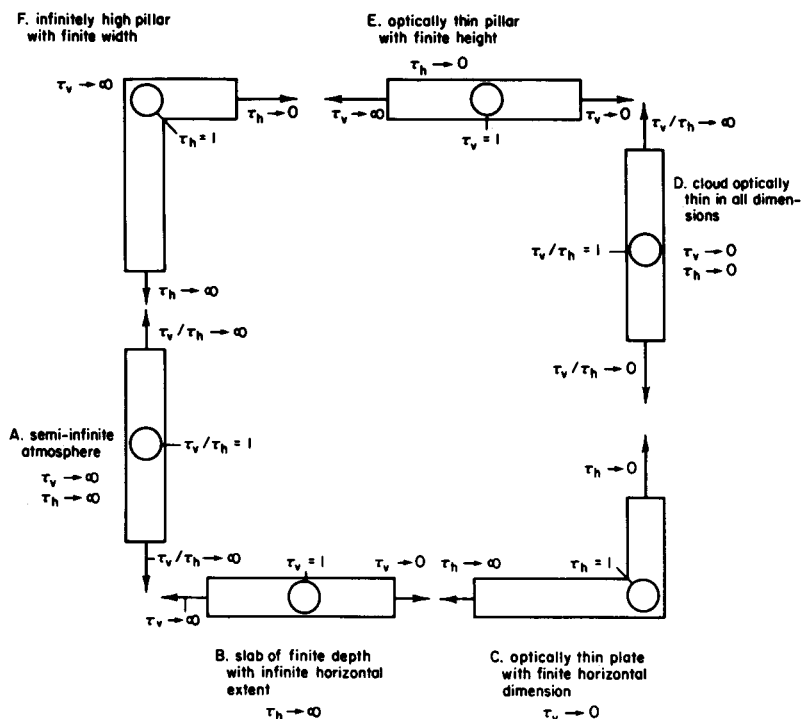


Fig. 20.1. Key to the arrangement of Table 65 on scattering by cuboid clouds. Frames A to F represent the six asymptotic cases; arrows point to the corners.

**Discussion.** The inner square of 22 numbers will not be discussed here. A full discussion, including a comparison with numbers calculated from a modified Eddington method, is in the original paper (Davies and Weinman, 1977). In our comments we shall concentrate on the 6 sides, going around the square counterclockwise, starting with the most familiar cases.

**A. Semi-infinite atmosphere.** If both  $\tau_h$  and  $\tau_v$  go to  $\infty$ , their ratio does not matter. The diffuse reflection from the top is 100% because the scattering has been assumed conservative.

**B. Slabs of finite depth.** The sides get nothing and the division between top (reflection) and bottom (transmission) is as described in detail in Section 9.2, Table 15.

**C. Thin plate with finite horizontal dimension.** In the limit of zero optical depth, 100% of the incident radiation emerges unscattered at the bottom. Near this limit, a fraction  $\tau_v \ll 1$  is initially stopped and scattered. Then, if  $\tau_h$  is not very small, geometric reasons alone cause hardly any radiation to escape through the sides. The top and bottom each take half of the scattered radiation, so that fraction up top is  $\frac{1}{2}\tau_v$ , fraction down bottom is  $1 - \frac{1}{2}\tau_v$ .

D. *Cloud optically thin in all dimensions.* Again there is 100% transparency in the strict limit. The scattered radiation equals  $\tau_v$  in first order and its distribution among top, sides, and bottom depends on the geometry. In a cube ( $\tau_v/\tau_h = 1$ ) each side receives an equal share so that fraction up top =  $\frac{1}{6}\tau_v$ , fraction down bottom =  $1 - \frac{5}{6}\tau_v$ , fraction up sides = fraction down sides =  $\frac{1}{3}\tau_v$ . Toward thin plates (corner DC) the top and bottom each take half of the scattered radiation, and towards thin pillars (corner DE) the sides take all, equally divided between up and down.

E. *Optically thin pillar with finite height.* In this limit, where  $\tau_h \rightarrow 0$ , only unscattered radiation in the amount  $e^{-\tau_v}$  manages to exit through the bottom face. The remainder exits by the sides, equally up and down.

F. *Infinitely high pillar with finite width.* Here  $\tau_v = \infty$  and  $\tau_h$  ranges through all values from 0 to  $\infty$ . This is the only side of the hexagon leading to numbers that are not trivial or well known. The total percentage 100 is divided into 3 parts. The values of these parts, which have been labeled  $a$ ,  $b$ , and  $c$  in Table 65, are based on a combination of theory and empirical extrapolation from  $\tau_v = 10$ . Small values of  $\tau_h$  present no problem. At intermediate and large values of  $\tau_h$ , the source density inside the long cylinder falls roughly as  $\exp(-kz)$  with optical depth  $z$  and also falls from the center to the side of the cylinder. Both effects are caused by the losses from the sides. We estimate  $k = 0.8$  at  $\tau_h = 3.2$  and  $k = 0.4$  at  $\tau_h = 10$ , but a precise theory is lacking. Radiation leaving the sides in a downward slanting direction has a somewhat larger intensity than radiation leaving the sides in an upward slanting direction, so  $c > b$ .

This completes the discussion of the asymptotic cases shown in Table 65 and Fig. 20.1 and also our treatment of one chosen example of isolated clouds. Clearly, this was not a full review but an attempt to show how complex the problem is if a somewhat satisfactory numerical treatment is requested. Independent computations on the same problem have been made by McKee and Cox (1974). The papers by Davies and Weinman (1977) and Davies (1978), on which the results above are based, also gives corresponding graphs for  $g = 0.86$  based on the Henyey-Greenstein phase function and for a different angle of incidence.

## 20.2 LAYERED STRUCTURES

### 20.2.1 Layers of Paint; the Kubelka-Munk Formulas

Solid materials consisting of a fine powder, or containing scattering and absorbing particles immersed in a medium, are found in our daily life in a wide variety. Pigments, paints, papers, textiles, synthetic plastics, and a simple layer of sand are obvious examples. Suspensions of various kinds, e.g., opal glass (air bubbles in glass), milk (fat globules in a watery solution), and mist (water drops in air) may be placed in the same class.

In many of these examples, the user of the industrial product may have specific wishes about the color and brightness of the product when applied in a layer of a certain thickness. The manufacturer responds to these wishes by making an effort to control composition, size, number, and mixing ratios of the particles in such a manner that the product fulfills the customer specifications. This requires (among other things) a theoretical insight into the relation between the particle properties and the bulk properties of the product. The theory needed is the theory of multiple scattering or radiative transfer.

An assumption made throughout this book, and in all usual theories, is that each particle has enough room to develop its own scattering diagram. This means that the particles should be in what in electromagnetic theory is called the far-field pattern of the neighboring particles. If the particles touch or nearly touch each other, this assumption is violated. For that reason most of the examples mentioned, with the exception of opal glass and mist, cannot be treated rigorously by the normal radiative transfer techniques. A mathematical physicist might at this point conclude that the problem is intractable, although this may not be the final word (see Goedecke, 1977), but someone with an industrial or experimental purpose is not so easily discouraged. He will conveniently ignore this difficulty and proceed anyhow.

Many authors, with somewhat different applications in mind, have independently tackled this problem in essentially the same manner. Kortüm (1969) lists 18 research papers between 1918 and 1950 in which the reflection and transmission of a layer of particulate material is discussed. The paper by Kubelka and Munk (1931) is often chosen for reference. The Kubelka-Munk (KM) solution is based on a two-stream approximation, which goes back to an idea first used in astrophysics (Schuster, 1905). This means that Kubelka and Munk, instead of solving the full transfer equation, are content to solve only for the stream up and the stream down, if the layer is thought to be horizontal. This necessarily involves some handwaving in writing the first equation. Although from there on everything is exactly solved, the solution remains an approximation to the three-dimensional transfer problem.

We quote the KM solution in the notation used by Kortüm (1969), except that we have replaced his  $a$  and  $b$  by  $\alpha$  and  $\beta$  in order to avoid confusion with our notation. Let  $K = 2 \times$  absorption coefficient per unit length,  $S = 2 \times$  coefficient for scattering into the backward hemisphere, again per unit length,  $\alpha = (S + K)/S$ , and  $\beta = \sqrt{\alpha^2 - 1}$ . The reflecting power of a layer of arbitrary depth  $d$  without reflecting back surface is, then, in two equivalent forms,

$$R_0 = (e^{2Sd\beta} - 1)/(R_\infty^{-1}e^{2Sd\beta} - R_\infty) = 1/[\alpha + \beta \coth(Sd\beta)]$$

Here  $\coth$  denotes the hyperbolic cotangent; and  $R_\infty$ , the value reached for very thick layers  $d = \infty$ , is given by

$$R_\infty = \alpha - \beta = 1/(\alpha + \beta)$$

Before examining the accuracy of these widely used formulas as approximations to the solution of realistic three-dimensional problems, we recall that they also describe the *exact* solution of a different problem, in which the phase function consists only of a forward and a backward peak. This problem was solved in Section 14.3. The assumption is that radiation impinges unidirectionally, under an angle of cosine  $\mu_0$  with the normal, on a flat layer with optical thickness  $b$ . The scattering is assumed to be either in the forward direction or in the backward direction, and some absorption is assumed to occur also. The albedo and the forward/backward ratio are characterized by the parameters  $a$  and  $g$ , or alternatively by the parameters  $p = \frac{1}{2}a(1 + g)$  and  $q = \frac{1}{2}a(1 - g)$ . Since the radiation never deviates from the forward and backward direction along the original path, only the total pathlength  $b/\mu_0$  occurs in the result. The reflecting power, i.e., the fraction of the incident radiation that is reflected from the layer under these assumptions, is given by  $UR$  in column 1 of Display 14.2. Without further comment we state that this result is identical to the KM expression for  $R_0$  given above, if we follow the translation rules shown in the accompanying enumeration. Here  $c$  is a proportionality constant depending on the choice of the unit of length.

KM	Sec. 14.3, arbitrary $g$	Sec. 14.3, $g = -1$
$S$	$q/c$	$a/c$
$K$	$(1 - p - q)/c$	$(1 - a)/c$
$S + K$	$(1 - p)/c$	$1/c$
$d$	$bc/\mu_0$	$bc/\mu_0$
$\alpha$	$(1 - p)/q$	$1/a$
$\beta$	$z/q$	$(1/a)\sqrt{1 - a^2}$
$\beta Sd$	$zb/\mu_0$	$(b/\mu_0)\sqrt{1 - a^2}$

The last column shows the expressions for pure backward scattering,  $g = -1$ . This is the proper choice if we wish to start (as in the KM derivation) from the concept that scattering into the forward hemisphere can be fully neglected. Under this particular assumption, the ratio between  $S$  and  $K$  is indeed as  $a$  to  $1 - a$ . We have already demonstrated in Section 14.3 the exact equivalence between the results for different  $g$  if the values of  $a$  and  $b$  are properly adjusted.

For conservative scattering the KM solution transforms into

$$R_0 = Sd/(Sd + 1), \quad R_\infty = 1$$

again in agreement with Display 14.2.

### 20.2.2 Layers of Paint; Accuracy Tests

The problem which Kubelka and Munk (and others) profess to solve in an approximate manner is "What fraction of the light is reflected from a diffuse surface exposed to incident radiation from all directions in a hemisphere?"

TABLE 66  
Accuracy Test of Kubelka–Munk Formula for Semi-Infinite Layer

Values of $URU$	Isotropic scattering (Section 8.4, Table 9)		Henye–Greenstein phase function (Section 12.2.2)	Linearly anisotropic scattering (Section 12.2.1)
	$a = 0.8, g = 0$	$a = 0.99, g = 0$	$a = 0.9, g = \frac{1}{3}$	$a = 0.9, g = \frac{1}{3}$
Exact	0.3419	0.7946	0.4090	0.4083
KM formula	0.3820	0.8182	0.4121	0.4020
Approx formula Section 12.2.3	0.3404	0.7945	0.4086	0.4086

This corresponds roughly to the situation in broad daylight or in a well lit room. Translated into the terminology of this book, the question is “How large is the bimoment  $URU$ ?” We have seen (Sections 12.2.3 and 18.1.2) that this quantity is also the spherical albedo for a planet. In earlier chapters and throughout the literature there is a wealth of accurate information about this quantity. Hence, there is no necessity to use the KM approximation at all; but for those who wish to, a few checks can readily be made.

(a) *A semi-infinite layer.* Some numerical comparisons with exact results quoted from earlier sections are shown in Table 66. The approximation formula from Section 12.2.3 remains well within a 1% error, but the error of the KM formula  $R_0 = \alpha - \beta$  varies from +11 to -1%. For isotropic scattering, by the translation rules just given we have put  $\alpha = (1 - \frac{1}{2}a)/\frac{1}{2}a = (2/a) - 1$ , which gives  $\beta = (2/a)(1 - a)^{1/2}$ . In the other two examples, which have the same combination  $(a, g)$  we have followed the procedure  $\alpha = (1 - af)/(a - af)$ , where  $f$ , the fraction scattered into the forward hemisphere taken from Display 10.1, was 0.7351 and 0.7500, respectively.

(b) *A finite layer.* The recommendation by KM is to take for  $d$  the actual thickness, measured perpendicularly to the layer, and for  $S$  twice the scattering coefficient per unit length, where only scattering into the backward hemisphere is counted, and scattering into the forward hemisphere is regarded as non-existent. We call this a recommendation because the reasoning behind it has an element of arbitrariness. The actual length along a slanting path is  $d/\mu$ , and by a plausible assumption about the radiation field we can argue that 2 is a fair average over the values of  $1/\mu$ .

We apply this procedure to a finite layer with isotropic scattering. The factor 2 in this test happens to compensate for the neglected scattering into the forward hemisphere, so that  $S$  is the actual scattering coefficient per unit length,  $k_{sca} = ak_{ext}$ , where  $k_{ext}$  is the extinction coefficient per unit length. We then find that  $Sd = ak_{ext}d = ab$ , where  $b$  is the optical thickness measured normally to the layer. Only numerical tests can show how well the approximation fits the exact results. In the two examples in Table 67 we find again differences up to

**TABLE 67**  
 Test of Kubelka–Munk Approximation for a Finite Layer with Isotropic Scattering

Optical depth normal to layer $b$	URU for isotropic scattering			
	$a = 1$		$a = 0.8$	
	Exact	KM approx	Exact	KM approx
0	0	0	0	0
0.25	0.1798	0.2000	0.1327	0.1519
0.5	0.2958	0.3333	0.2056	0.2401
1	0.4466	0.5000	0.2802	0.3261
2	0.6099	0.6667	0.3280	0.3728
4	0.7540	0.8000	0.3411	0.3817
$\infty$	1	1	0.3419	0.3820

and exceeding 10%, the KM approximation always giving too high values. Such comparisons may be extended at will from the tables available in earlier chapters.

(c) *Refinements.* The literature contains many further refinements of the KM formulas, most of which correspond to items already covered. First, there is anisotropic scattering by the individual particles. We would naturally turn to the similarity relations, but this is not necessary. They are already built in because we have demonstrated the strict observance of these relations by double-peaked phase functions with different  $g$  (Section 14.3).

Second, internal and external reflection against a glossy front surface is not included in the equations of this book. See Kortüm (1969) or the marine optics books cited in Section 20.4.

Third, there is the diffusely reflecting backlayer. The answer for an arbitrary diffuse reflection law is in Section 4.5.4. The much simpler equations obtained when Lambert reflection is specified are in Section 18.4.1. Clearly the formulas developed for this situation by the paint experts should be identical to those of the planet experts. Let  $R_g$  be reflectance of the backing;  $R_0$ , reflectance of the layer without backing;  $T_0$ , transmittance of the layer without backing; and  $R_\infty$ , reflectance of a semi-infinite layer, all symbols understood to mean bimoments URU or UTU. From Section 4.5.4 we obtain the reflectance of the layer with back surface combined:

$$R = R_0 + R_g T_0^2 / (1 - R_g R_0)$$

We now insert, with  $E = \exp(2Sd\beta)$

$$R_0 = (E - 1) / (R_\infty^{-1} E - R_\infty), \quad T_0 = (R_\infty^{-1} - R_\infty) E^{1/2} / (R_\infty^{-1} E - R_\infty)$$

of which the first equation was given earlier in this section, and the second is taken from the results in Section 14.3 by the same translation rules. After some algebra we obtain

$$R = [R_{\infty}^{-1}(R_g - R_{\infty}) - R_{\infty}(R_g - R_{\infty}^{-1})E]/[R_g - R_{\infty} - (R_g - R_{\infty}^{-1})E]$$

which is the form derived by Kubelka–Munk, so the test is complete.

Fourth, the situation of two layers with different properties on top of each other has been considered. The method devised for this case (Kubelka, 1954; Kortüm, 1969, p. 122) is the same as our adding method (Section 4.5.2). Because of the two-stream approximation it can be worked out in numbers rather than in matrices.

A wide variety of practical applications have been based on the KM approximation. In these applications, terms like “contrast ratio” and “hiding power” are defined and diagrams made for ready use. It is somewhat of a pity that all this work has been based on a rather crude approximation, so that it has not reached the sophistication obtained in the equivalent astronomical applications. For instance, diagrams like Fig. 18.12 showing the visibility of a bright or dark area through a planetary atmosphere are at once applicable to the visibility of a spot covered by a layer of paint. Before taking this comment too seriously, it should be kept in mind, however, (1) that a 10% accuracy is not bad in practice, and (2) that close packing of the particles makes any available transfer theory questionable anyhow.

### 20.2.3 “New Snow Fallen in Calm”

The brilliant reflection of sunlight from a snow pack and the penetration into its deeper layers are due to multiple scattering by the individual ice crystals. The individual scatterers are (as in layers of paint) too close together to expect the theory of the preceding chapters to be applicable. Nevertheless Barkstrom and Querfeld (1975) and Bohren and Barkstrom (1974) find excellent agreement between this theory and measurements from various sources.

We review these results briefly and tie them into the formulas and tables given earlier. The diffuse reflection from the top of the snow cover is clearly forward directed. Barkstrom and Querfeld use a phase function derived by the Mie theory for spheres with refractive index 1.20 (at 0.6  $\mu\text{m}$ ) and a size distribution with modal diameter 0.245  $\mu\text{m}$ . This phase function has asymmetry parameter  $g = 0.506$ , but higher order Legendre coefficients fall below those for Henyey–Greenstein scattering with  $g = 0.5$ , e.g.,  $\omega_2 = 1.02$  instead of 1.25. The reflection function  $R(\mu, \mu_0, \varphi)$  computed for a semi-infinite layer with this phase function and with individual scattering albedo  $a = 0.996$  shows a good match to the observed reflection from snow. The fact that both isotropic scattering (Barkstrom, 1972) and Henyey–Greenstein scattering fit less well agrees with the finding in Section 12.2.2 that in such a comparison the detailed form of



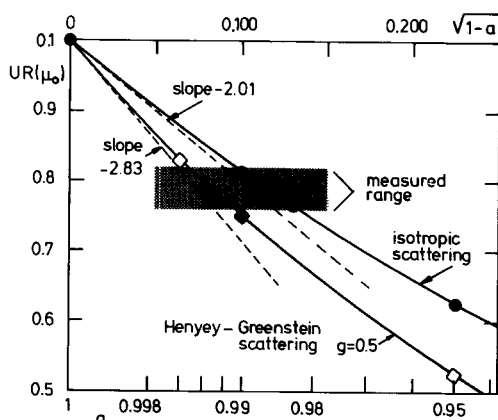


Fig. 20.2. Reflectance of fresh snow packs (grey area) compared with two curves based on multiple scattering theory;  $a$  is the single-scattering albedo.

the phase function is important. The agreement with the phase function of actual snow, with 1000 times larger grain size and refractive index 1.32, must be accidental.

In the comparisons shown below, this exact form is not important. Fresh snow packs studied in the Antarctic reflected for  $\mu_0 = 0.5$  some 76–82 % of the incident light. We have plotted in Fig. 20.2 the reflected flux  $UR(\mu_0)$  against  $(1 - a)^{1/2}$  because we may derive from Eqs. (30) and (35) in Section 5.4.1 that

$$UR(\mu_0) = 1 - 4[(1 - a)/3(1 - g)]^{1/2} K_0(\mu_0) + O(1 - a)$$

The slopes near  $a = 1$ , based on the values of  $K_0(\mu)$  in Table 26, have been drawn in, as well as the actual values of  $UR(\mu_0)$  given in Table 27. All Barkstrom's points lie exactly on these curves so, clearly, the Legendre coefficients  $\omega_2$  and beyond hardly matter, in agreement with tests shown in Section 12.2.2. His recommendation to adopt simply the  $a$  from isotropic scattering theory should not be followed.

The albedo for diffuse illumination, which we call spherical albedo, follows from the same formula with the factor  $K_0(\mu_0)$  omitted (Sections 5.4.1 and 12.2.3), and for  $a = 0.996$ ,  $g = 0.5$  becomes  $A = 0.81$ .

The tests in Chapter 12 suggest that the quantities characterizing the radiation field in deep layers again are insensitive to parameters other than  $a$  and  $g$ . For  $a = 0.996$ ,  $g = 0.5$  we find by the simplest approximation (Section 5.4.1, Eq. 30) that  $k = [3(1 - a)(1 - g)]^{1/2} = 1/12.9$ , while Barkstrom and Querfeld read from a graph that  $1/k = 13.1$ . This means that the sunlight seeps through the snow by multiple scattering in such a way that it requires a layer 13 times deeper to be attenuated by a given factor than does a narrow vertical beam of light. The actual distances depend on wavelength and on the density of the snow.

In one computed example a drop by a factor  $e$  took place in 6.9 and 0.53 cm, respectively. Thus

$$\frac{\text{flux extinction}}{\text{beam extinction}} = \frac{k}{1} = \frac{1}{13} = \frac{(6.9 \text{ cm})^{-1}}{(0.53 \text{ cm})^{-1}}$$

The absorption  $1 - a$  increases strongly towards longer wavelengths. It is roughly proportional to grain size because scattering is proportional to area and absorption to volume. Bohren and Barkstrom derive the relation  $1 - a = 0.84k_i d$ , where  $k_i$  is the absorption coefficient of bulk ice and  $d$  the diameter of the ice spheres. Numbers that fit the example just given would be  $d = 0.3 \text{ mm}$ ,  $k_i = (62 \text{ cm})^{-1}$ .

In layers deeper than  $\tau = 5$ , i.e., at more than 3 cm below the surface, we reach the diffusion domain, where the intensity distribution with angle is independent of depth and of angle of incidence. Tables are in Section 11.1. In the near-conservative approximation, we find from Section 5.4.1, Eq. (32) that

$$\frac{\text{upward flux}}{\text{downward flux}} = 1 - \frac{4k}{3(1 - g)} = 0.80$$

while Barkstrom and Querfeld find 0.815. The absolute intensity level depends strongly on the angle of incidence because it is proportional to  $\mu_0 K(\mu_0)$ . For instance, between  $\mu_0 = 0.995$  and  $\mu_0 = 0.122$  the ratio computed from Table 26 is 19.2, which matches the ratio that can be read from Barkstrom and Querfeld (1975), Fig. 5.

These checks show that for many purposes the simple model computations and formulas presented in earlier chapters serve surprisingly well to describe the optical properties of the basically far more complex scattering system of a layer of snow.

The preceding results hold for an extended area of snow, in uniform sunlight. In one particular experiment the sample was limited by a white cardboard cylinder of diameter 11 cm. Bohren and Barkstrom correctly remark that this is not at all wide enough to give the correct flux extinction coefficient. The losses at the sides cause a greater extinction; the authors state that even with a cardboard albedo of 0.83 the measured flux extinction may be a factor 3 too high. The geometry of the problem is very similar to that of the cuboid clouds of Davies and Weinman (Section 20.1.3), and the two results could probably be compared.

### 20.2.4 Plant Canopies

Another problem of evident economic interest is the penetration of sunlight into a densely grown cornfield, or any other plant canopy. Here we have even less reason than in the examples of the preceding sections to expect that the basic conditions of the scattering theory covered in this book are fulfilled. The leaves of plants are not randomly oriented; nor are they randomly placed, for

they try to catch light from clearings left above; nor are they in the “far field” of other leaves, as is already implied by using the word “clearing.”

Surprisingly, it has proved possible in spite of these theoretical objections to make good use of the radiative transfer formulas, if only to provide the framework for an ordered comparison and interpretation of various measurements (Weinman and Guetter, 1972). The canopy is not a homogeneous layer but has maximum extinction coefficient at half the highest stalk height. The maximum energy deposit occurs somewhat above this half height if the sun is overhead and rather near the top if the sun is low. In order to reproduce a set of measurements at  $1\ \mu\text{m}$  wavelength, Weinman and Guetter use a model consisting of three layers: the atmosphere, with optical thickness 0.08; the plant canopy, with optical thickness 3.1 and  $a = 0.98$ ,  $g = -0.44$ ; and the ground, with reflection coefficient 0.25. The plant parameters are in good accord with laboratory measurements. There is a poetic coincidence with the asymmetry  $g = -0.44$  in the phase function of a white planet (Section 18.1.4, Table 58).

### 20.3 HEAT TRANSFER; RADIATION HYDRODYNAMICS

Quite a number of problems in thermodynamics and fluid dynamics resemble the problems of multiple light scattering treated in this book. Some are even fully identical, though the solutions have been developed independently. It would be foolish to try to cover these problems in a brief section, but some indications and references may be given.

(a) Insulating layers of porous or fibrous material are of great technical importance. Williamson (1977) abstracts close to a hundred documents on cryogenic foam insulation alone and lists 400 more by title. Heat transfer through such layers in most practical applications occurs largely by conduction, but 5–20% of the heat may be transported by radiation. Description of the radiative part in terms of the two-stream approximation is good enough (Hamaker, 1947; Larkin and Churchill, 1959; Sections 14.3, 20.1, and 20.2.2 of this book.)

(b) Molecule paths in a very tenuous gas are in detailed analogy with photon paths in radiative transfer. A brief but good discussion is, e.g., in Probstein (1963). The optical thickness  $b$  of the slabs in our previous chapters corresponds to the ratio between geometric slab thickness and the molecular collision mean free path (Knudsen number). Numerical solutions made to find the heat transfer between walls of a different temperature as a function of  $b$  match those made in far greater detail in radiative transfer (Chapter 9 of this book). It is not clear whether the proposed term “radiation slip” caught on. The information that the constant  $K$  in the asymptotic formula is not  $\frac{2}{3}$  but 0.710 is lacking in Probstein’s article, and the reader may note that the lower curve of Fig. 9.3 permits a far more accurate comparison than a direct plot of the heat transfer rate against  $b$ .

(c) The electromagnetic wave propagation in a gas, fluid, or plasma, is influenced by the motions and inhomogeneities of the medium. This again is a highly developed field (e.g., Uscinski, 1977), where the practical demands of communication engineering and theoretical developments go side by side. We cannot enter this field. However, sometimes these problems may be treated as if they referred to multiple scattering by separate elements. For instance, Feinstein *et al.* (1972), applying Born's approximation to electromagnetic wave propagation in isotropic plasma turbulence, assume that the phase function is proportional to  $(1 + a^2 k^2)^{-11/6}$ , with  $k = 2k_0 \sin \frac{1}{2}\theta$ , where  $\theta$  is the scattering angle,  $a$  the scale size characterizing the turbulent spectrum, and  $k_0$  the incident wave number. The same function is proportional to  $(1 - b \cos \theta)^{-11/6}$  with  $b = 2a^2 k_0^2 / (1 + 2a^2 k_0^2)$ . The two curves shown in their Fig. 2 and presumably also their further calculations refer to  $2ak_0 = 3.69$  and  $6.75$ . By direct analytic integration the author found the corresponding values  $g = 0.68$  and  $0.84$  of the asymmetry parameter. These values may also be estimated by direct comparison with the Henyey–Greenstein phase functions given in Table 21. The labels  $ak_0 = 3.7$  and  $6.7$  (without factor 2) are not consistent. The solutions of the half-space problem derived for these strongly forward-directed phase functions by means of singular eigenfunction expansions should, by the findings of Section 12.1, closely resemble those tabulated for the Henyey–Greenstein functions in Chapter 11.

(d) At temperatures of the order of a million degrees, the momentum of the radiation in transfer reacts back on the fluid motion. The equations for such problems of radiation hydrodynamics have been set forth by Pomraming (1973). The same book contains useful chapters on other complications in transfer theory (refraction, dispersion, and Lorentz transformation).

## 20.4 LIGHT SCATTERING IN THE OCEANS

It takes little imagination to get a vision of the deep-blue light field in the depth of the oceans, with its solemn significance both for the living beings that are at home there and for man who ventures there as explorer. Light scattering by the water itself, by microorganisms, and by suspended mineral particles reduces the visibility. Typically, one attenuation length (length in which the intensity of a light beam is reduced to  $1/e$ ) may be 20 m in clear oceans, 5 m in coastal waters, and very much less in polluted waters. In ordinary daylight conditions objects can be sighted at 3–6 attenuation lengths. A self-luminous object in otherwise dark water may be visible to 15 or 20 attenuation lengths (Duntley, 1974).

Virtually all of the developments in multiple scattering made with a view to problems of atmospheres and clouds recur in the depth of the ocean. They have partly been quoted or adapted and partly derived from scratch with other notations and a different terminology. In addition, certain unique features occur,

e.g., the change of refractive index at the air-ocean interface. This requires a relatively simple adjustment of the boundary conditions if the sea surface is smooth; but in the normal situation with surface waves, it introduces another stochastic element into the problem (Plass *et al.*, 1976).

An introduction to the rapidly expanding literature may be gained from the following books: Jerlov and Steeman Nielsen (1974), Monin and Shifrin (1974), Jerlov (1976), and the six-volume work of Preisendorfer (1976), the first volume of which is written as "a self-contained short course on hydrologic optics."

We shall now show by a few examples which results in this book are of direct interest to marine optics.

### 20.4.1 Asymptotic Radiance

The light field deep under the sea surface offers a perfect example of what we have called a "diffusion domain." In conditions of natural illumination it has a diffusion stream going vertically down with a diffusion exponent and an angular pattern uniquely determined by the angular scattering pattern (phase function) of a small volume, all exactly as set forth in the general theory of Chapter 5.

Imagine an observer descending into the sea and measuring at a number of depths the way in which the radiance varies with direction. When he has descended 10 m the direct sunlight (unscattered radiation) will still be observable. At 30 m this may not be so, but the general radiance may still reveal whether the sun is high or low in the sky, or the sky overcast. Coming to 50 m or deeper, he finds that no such trace of the external situation is left in the radiance pattern that surrounds him. The light just comes generally from above; it has a pattern which is symmetric about the vertical and in which the radiance from the zenith may exceed the radiance from the nadir by a factor of the order of 200.

This pattern is called the *asymptotic radiance*. It does not change any further if he descends still deeper, but the radiance at all angles decreases in the proportion described by the exponential factor  $\exp(-k_J d)$ . Here  $d$  is the depth in meters and  $k_J$  (in  $\text{m}^{-1}$ ) is the asymptotic radiance attenuation coefficient (Jerlov, 1976). We have appended the J to distinguish Jerlov's notation from ours.

This  $k_J$  is generally smaller than the total attenuation coefficient  $c_J$  that is suffered by a beam and that consists of the scattering coefficient  $b_J$  and the absorption coefficient  $a_J$ :

$$c_J = a_J + b_J$$

By appropriate instrumentation, for which we refer to the books cited, it is possible to measure each of these quantities. The interrelation between these quantities should check with theory. Some information relevant to this check has been collected in Fig. 20.3. The abscissa is:

$$\text{single-scattering albedo } a = \frac{b_J}{c_J} \frac{\text{(beam) scattering coefficient}}{\text{(beam) attenuation coefficient}}$$

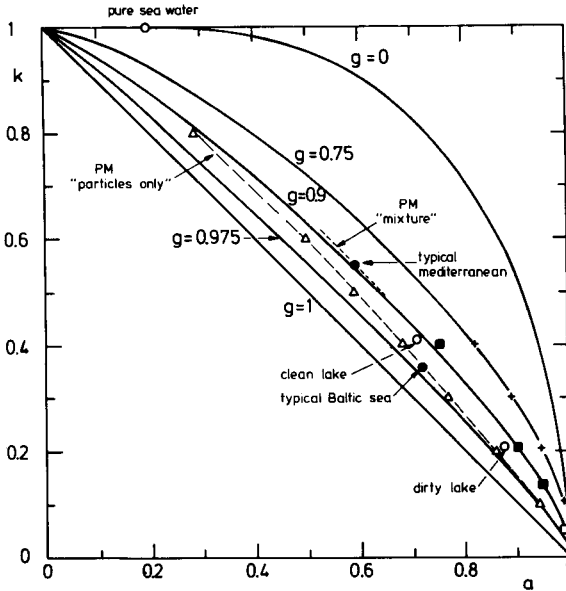


**Fig. 20.3.** The measured combination of diffusion exponent  $k$  and albedo for single scattering  $a$  in natural water bodies and in laboratory experiments are in good agreement with the theoretical curves for various scattering asymmetries  $g$ . +, blackened latex suspension;  $\square$ , milk;  $\blacksquare$ , blackened milk. See text for further detail.

where the terminology of this book is shown on the left and the marine optics terminology on the right. The ordinate, expressed likewise, is

$$\text{diffusion exponent } k = \frac{k_j}{c_j} \frac{\text{asymptotic radiance attenuation coefficient}}{\text{beam attenuation coefficient}}$$

Clearly, this situation in the deep sea is identical with the situation in a diffusion domain as described in Section 5.2.1 and in greater numerical and theoretical detail in Sections 11.1 and 12.3. In fact, the deep sea offers the finest natural example of such a diffusion domain.

Jerlov (1976) attributes the theoretical concept of asymptotic radiance to Shulejkin (1933). Preisendorfer (1976) ascribes the empirical discovery to Whitney (1941) and places the theoretical proof still later. In this book (Chapter 5) the existence of such a domain was postulated as an obvious fact and references, with no attempt at a real review, go back to 1942.

The numerical and analytical treatment in this book is probably more exhaustive than in the equivalent hydrological literature. The agreement illustrated by Fig. 20.3 is excellent.

First, Fig. 20.3 shows a few theoretical curves for Henyey–Greenstein scattering with asymmetry parameters  $g = 0$  (isotropic),  $g = 0.75$ ,  $g = 0.9$ ,

$g = 0.975$ , and  $g = 1$  (completely forward scattering). Three of these curves are shown, with inverted coordinates, in Figs. 12.13 and 12.14. Full numbers are in Table 23 (Section 11.1). Parts of two other theoretical curves which I have read from published graphs (Prieur and Morel, 1971), are dotted in. In the mixture these authors assumed a 10% admixture of molecular scattering to the scattering particles.

Shown as open circles are a number of points typical for experimental situations. Pure sea water, from which all particles are filtered out, has at 475 nm about 80% absorption and 20% scattering:

$$b_j = 3.6 \times 10^{-3} \text{ m}^{-1}, \quad c_j = 18 \times 10^{-3} \text{ m}^{-1}, \quad \text{so} \quad a = 0.20$$

which makes  $k$  indistinguishable from 1. Added particles in the sea cause mostly scattering, and little absorption, so more turbid waters like the Baltic Sea have a larger value of  $a$  than clear waters like the Mediterranean. Consequently the ratio  $k_j/c_j$  is smaller in the Baltic, although both  $k_j$  and  $c_j$  are higher than in the Mediterranean. The two "lake" situations, selected as typical for a wider set of measurements in the literature, show a similar difference. Presumably, in polluted waters, where the particulate material may be absorbing, the points will creep up the curve again.

Laboratory measurements of fine quality have been reported and compared with a refined theory by Herman and Lenoble (1968). Figure 20.3 includes the curve "blackened milk." Milk, presumably with albedo  $a$  very close to 1, and with a measured asymmetry parameter  $g = 0.906$ , was mixed with black paint, which is assumed to be fully absorbing. The curve coincides almost perfectly with our  $g = 0.90$  curve. The documentation is insufficient for determining whether the deviation towards the upper end is due to different values of the higher Legendre expansion coefficients of the phase function. A second set of experiments made with a solution of polyvinyl acetate spheres with measured value  $g = 0.762$  agrees very well both with the theoretical curve of Herman and Lenoble and with the Henyey-Greenstein curve for  $g = 0.75$ .

What can we learn from the measured form of the asymptotic radiance pattern? In principle, we may reconstruct from it the complete phase function, i.e., the pattern for single scattering. Formal inversion procedures to do this are given by Herman and Lenoble (1968) and by Zaneveld (1974). However, we may just as easily turn back to the theory of Section 6.2.1, where two important functions are expanded in Legendre functions as shown in the accompanying tabulation.

Function	Expansion coefficients
Phase function $\times$ albedo	$\omega_n$ , with $\omega_0 = a$
Diffusion pattern = asymptotic radiance pattern	$(2n + 1)g_n(\gamma)$

For brevity we further omit the argument  $\gamma = k^{-1}$ , which is constant in a given homogeneous water body. The interrelation taken from Display 6.2, with  $m = 0$ , is then

$$(2n + 1 - \omega_n)g_n = k[(n + 1)g_{n+1} + ng_{n-1}]$$

from which we may immediately solve

$$\omega_n = 2n + 1 - k[(n + 1)g_{n+1} + ng_{n-1}]/g_n$$

This is the desired inversion formula, from which  $\omega_n$  may be found if the asymptotic radiance pattern and hence all  $g_n$  are known. Note that  $g_0 = 1$ . It is necessary first to determine  $k$  from the vertical gradient.

The crucial question, however, is whether this is a well determined problem or another example of an inversion procedure that works well only if the starting data are perfectly accurate. The answer to this question depends on where the representative point in Fig. 20.3 lies. This can best be seen by considering two extremes.

At the lower end, where  $a \geq 0.85$  and  $k \leq 0.2$ , the coefficients  $g_n$  go rapidly to 0 for  $n \rightarrow \infty$ . This cannot be seen at once from the equation but was discussed at length in Section 6.2.3. Both these facts make the determination of  $\omega_n$  quite poor. We may at best obtain the first two coefficients

$$\omega_0 = a = 1 - kg_1$$

$$\omega_1 = 3ag = 3 - k(2g_2 + 1)/g_1$$

At the upper end, where  $a < 0.1$  and  $k$  is close to 1, all  $g_n$  approach 1. This means that the asymptotic radiance pattern is a narrow downward-directed peak. This can be physically understood from the fact that the attenuated radiation at this end is hardly reinforced by scattering, so at great depths the unscattered radiation is still important. Only the radiation which has the smallest exponent  $\tau/(\cos \theta)$  finally survives. This is radiation from the zenith,  $\theta = 0$ ,  $\mu = 1$ . In the limit where  $g_n = 1$ , the radiance distribution by Eq. (2) of Section 6.2.3 becomes the phase function multiplied by an extra factor  $(1 - ku)^{-1}$ . The extra factor is about 0.5 in the upward direction but is very large in the downward direction ( $u = 1$ ). The conclusion is that at this end the inversion is well determined, but another problem appears. The asymptotic radiance pattern itself is very hard to measure, because it establishes itself only at extreme optical depth due to the fact that the factors  $\exp(-\tau)$  and  $\exp(-k\tau)$  differ very little. Hence in this situation it is not a practical proposition to measure the asymptotic radiance pattern at all.

The upshot is that the possibility of determining by inversion more than the first few expansion coefficients of the phase function looks poor at both ends. Herman and Lenoble (1968) ran a test in which the first three coefficients  $\omega_1/\omega_0$ ,  $\omega_2/\omega_0$ , and  $\omega_3/\omega_0$  were kept fixed but the higher ones were varied at will. They could not detect differences in the asymptotic radiance pattern larger than 0.1 %.



### 20.4.2 Measurements at Moderate Depth

Aesthetic satisfaction is no criterion in practical research. Most measurements in hydrologic optics are not carried out in the asymptotic radiance field. They refer to the range of depths between the surface and the onset of the asymptotic domain. The formulas for this transition domain are less simple but not less tractable than those valid deeper down. We cite a few examples below.

First, we can obtain by simple integration of the equation of transfer over all directions a set of differential equations, exactly valid at any optical depth. Two of these are listed in Section 5.2.3 as Eq. (18). The first one expresses the conservation of energy: the net flux transported downward at any level decreases as the energy is locally absorbed. The corresponding equation in hydrologic optics is called Gershun's equation, dated 1936.

Since the terms, notations, and units are different, we shall in this case spell out the translation. What we have called net flux down ( $\pi F$ ) is proportional to downward irradiance minus upward irradiance  $E_d - E_u$  in Jerlov's notation. What we have called average intensity ( $E$  in Section 5.2.3,  $J$  in Chapters 7–9) is proportional to his scalar irradiance  $E_0$ . Jerlov's quantities are in watts per square meter, while the tables in this book give dimensionless numbers based on an assumed incident flux of  $\pi$  units on a unit area of the top of the atmosphere. If  $Q$  is the actual flux in watts per square meter onto the top of the atmosphere, we have

$$(E_d - E_u)_J = QF, \quad (E_0)_J = 4QE$$

Further,  $(a/c)_J = 1 - a$  and  $(c \, dz)_J = d\tau$ , so Gershun's equation  $d(E_d - E_u)/dz = -aE_0$  translates indeed into Eq. 18 of Section 5.2.3. The direct (unscattered) radiation is included at both sides and can be separated out if desired.

This is only the first of an infinite set of equations that can be obtained by multiplying both sides of the equation of transfer by  $P_n(u)$  and then integrating. The entire set provides, in principle, a method for finding the local albedo and phase function from the measured radiance at arbitrary optical depth. This requires the inversion procedure spelled out by Zaneveld (1974) and Jerlov (1976, p. 98). Presumably this procedure is subject to the same practical limitations discussed in Section 20.4.1.

Practical measurements at a given optical depth are often limited to certain characteristic quantities. The most important ones are

$$\text{reflectance } R = (E_u/E_d)_J$$

The name may sound strange to someone outside marine optics; this quantity is our upward flux divided by downward flux, in the adding method (Section 4.5) denoted by  $UA/UD$ .

$$\text{average cosine } \mu = [(E_d - E_u)/E_0]_J$$

$$\text{radiance attenuation coefficient } K = [d \ln(E_d - E_u)/dz]_J$$

Each of these is a well defined measurable quantity at all depths, reaching a known limit in the asymptotic domain. Detailed model computations are necessary to determine how they depend on optical depth  $\tau$  and on angle of incidence  $\theta_0$  outside the asymptotic domain. Such computations have been performed by many authors.

If a limited accuracy is all we need, simple approximation formulas suffice. A successful example in marine optics appears to be the quasi-single scattering approximation (Gordon, 1973; McCluney, 1974; Gordon and McCluney, 1975; Gordon *et al.*, 1975). The last paper shows by many tables and graphs based on Monte Carlo computations that the quasi-single scattering approximation often gives results near 1% accuracy. This is better than the tests of a different approximation shown in Tables 66 and 67 (Section 20.3.2). The difference may be in the fact that the actual underwater phase function is highly forward directed with only some backscatter and even less side scatter. Since a systematic presentation of approximative methods has not been included in this book, further discussion is left aside.

## 20.5 INTERSTELLAR SCATTERING

The scattering agents in astronomy range from electrons, atoms, and dust grains to rocks and entire planets. The few examples selected in this section have been chosen for their proximity to the main topic of this book. We did not wish to include examples where everything can be explained in terms of single scattering. This rules out the fascinating subject of the zodiacal light which arises from direct scattering of sunlight by interplanetary dust. We have also avoided examples with complex geometry. In such problems the answer invariably is to try a Monte Carlo computation (Section 20.1.1).

With these severe restrictions a number of relevant examples are left. We may owe this fact to the astronomers rather than to nature, because observations are always analyzed first in terms of simple models. There is nothing wrong, however, with this bias. Only by starting with simple models can we isolate the essential features and avoid overinterpretation.

### 20.5.1 Reflection Nebulae; Diffuse Galactic Radiation

The visual aspect of the Milky Way with its striking dark patches leaves no doubt that many of the interstellar dust clouds have optical depths exceeding unity. This means that light scattered by such clouds may have suffered more than one scattering in the cloud and, therefore, that the model computations of this book may be relevant.

The analysis of the interstellar extinction itself, with its dependence on wavelength and its dichroicity (interstellar polarization), has quite a history. A brief reference was made in Section 19.2.4. A recent review is found in Greenberg (1978).

The scattered light can be observed in two forms traditionally distinguished as follows: (a) Reflection nebulae show the light scattered from an individual cloud illuminated by one star. (b) The diffuse galactic radiation is scattered from the ensemble of clouds illuminated by the ensemble of stars.

Several hundreds of reflection nebulae have been cataloged and the brightest among them studied many times for color, brightness, and polarization. An extensive review, with the theory based exclusively on single scattering, is given by Vanysek (1969). The interpretation is often inconclusive. The main reason is that the geometry of the nebula and the position of the star with respect to the nebula are not given but must be guessed from the data. For instance, placing the star in front of, or a little way inside the cloud makes a huge difference in the relative color.

A recurring question is whether single scattering suffices or multiple scattering should be included and, if so, how much. Rather different approaches to this question are possible.

First, keys for a rapid assessment are found in Fig. 4.2 (domain of validity of single scattering) or in Table 13 in Section 9.1.2 and Table 38 in Section 13.1 (ratio of total to single scattering). These tables show a wide variation of parameters, including optical thickness, albedo, angle, and phase function (or asymmetry parameter); but they have the common drawback of referring to slab geometry in parallel illumination.

Second, in the actual situation, where the star is close to the face of the slab, the results just mentioned are valid as integral checks for the reason explained in Section 20.1.2. Computations made for a pencil beam would provide the complete results directly as follows. The problem of finding the radiance of a reflection nebula at a certain angle from the illuminating star is reciprocal to the problem of finding the total radiation density at the position of the star, if a fictitious pencil beam is sent from the earth into the cloud. Practical experience with this reversal does not seem to be available.

The third approach is to make Monte Carlo calculations for model reflection nebulae from scratch. This has been done by Roark *et al.* (1974) and in greater detail by Witt (1977a, b, c) and Witt and Oshel (1977). They show that if the star is close to the face of the dust slab, single scattering dominates in the vicinity of the star. The contribution of multiple scattering increases with increasing distance, so that the outward gradient is found far too steep if multiple scattering is neglected.

In a typical example Witt and Oshel (1977, Fig 1) present a model of the Merope reflection nebula (distance 126 parsec) consisting of a slab with optical thickness  $b = 3$  equal to the geometrical thickness 1 parsec. The star is slightly outside the front face at 0.05 parsec distance. At  $1600'' \approx 1$  parsec away from the star their data for  $a = 0.6$  give the ratio (in arbitrary units)

$$\frac{\text{total scattering}}{\text{first-order scattering}} = \frac{64}{21} = 3.0$$

Further,  $\langle n \rangle$ , the average number of scatterings as defined in Section 17.2.2, is 2.5. For conservative scattering ( $a = 1.0$ ) the corresponding numbers in the same situation would have been

$$\frac{\text{total scattering}}{\text{first-order scattering}} = \frac{615}{35} = 17.5$$

and  $\langle n \rangle = 9.5$ . Witt and Oshel express most of their results in terms of a quantity called the effective multiplicity  $m$ , defined (in our notation) by

$$m = \log[I(a)/I(1)]/\log a$$

Clearly  $m$  equals the average number of scatterings for some value of the albedo between  $a$  and 1. The number found for  $a = 0.6$  in the example quoted is  $m = 4.4$ .

By varying all parameters Witt arrives at a set of twenty-one tables and many figures, which suffice for a thorough discussion of ANS (Astronomical Netherlands Satellite) measurements of the Merope nebula (Andriesse *et al.*, 1977).

Yet such an impressive piece of work could have been made more useful for general purposes if it were set up from the start with a view to incorporating data available for parallelly illuminated slabs as integral checks and as limiting cases. For illustration, consider Fig. 4 of Witt and Oshel (1977), where the position of the star is varied and its effect on the effective multiplicity examined. The authors judge that  $m$  has reached a constant value between 2.5 and 3 when the star is 0.5 parsec or more from the front face. Interpolation of the tables in Section 13.1 for an infinitely extended slab with the proper specifications ( $b = 2$  and  $g = 0.7$ ) shows, however, that the perpendicular reflection  $R(1, 1)$  is 0.0321 for  $a = 0.7$  and 0.130 for  $a = 1$ . This gives  $m = \log(0.0321/0.130)/\log(0.7) = 3.9$ . A closer comparison cannot be made because the Monte Carlo computation refers to a finite disk, which is moreover tilted.

The dense, spherical clouds called "globules" deserve special mention. This is not the place to discuss their astronomical importance. The surface brightness of such a cloud and its variation from center to limb must contain clues to the albedo and phase function of the dust particles. Witt and Stephens (1974) addressed this problem by assuming that the globule was placed in an isotropic (galactic) radiation field. They made Monte Carlo computations for total optical depths  $\tau$  up to 10, assuming uniform density inside or a density varying as  $r^{-2}$ , with various values of the single-scattering albedo  $a$  and the asymmetry parameter  $g$  of the Henyey-Greenstein scattering phase function. Later, Fitzgerald *et al.* (1976) inferred for a particular nebula with some limb brightening that  $\tau = 16$ ,  $a = 0.70 \pm 0.08$ , and  $g = 0.70 \pm 0.03$ .

The general features are easily seen. For conservative scattering the intensity remains uniform and isotropic throughout the cloud, for any optical depth and any phase function. In this limit the cloud is invisible for lack of contrast with the sky. In the other limit,  $a = 0$ , the cloud is black against the bright sky, with only some light shining through if  $\tau$  is small. For intermediate values of  $a$  we must rely on the Monte Carlo computations if  $\tau$  has moderate

values. However, in the limit  $\tau \rightarrow \infty$  and uniform density we then approach the situation of a semi-infinite slab exposed to uniform radiation. This means that in the notation of this book the measured brightness is  $UR(\mu)$ . Numerical values for  $a = 0.5$ ,  $g = 0.7$ , taken by crude interpolation from Table 27 (Section 11.3) are  $UR(1) = 0.027$ ,  $UR(0.7) = 0.044$ , and  $UR(0.5) = 0.065$ . These values confirm the existence of limb brightening and match those given in Fig. 1 of Witt and Stephens quite well. They may be used for extrapolation to large  $\tau$  if ever the need for more accurate values arises.

In comparison with the light from individual reflection nebulae, the diffuse galactic light is more difficult to measure but easier to interpret, at least if we are willing to assume a highly stylized distribution of stars and of interstellar grains. The traditional model is to assume that the stars, as isotropic light sources, and the grains, as anisotropic scatterers, form a homogeneous slab extending infinitely in the  $x$  and  $y$  directions. The distribution of stars and grains in the  $z$  direction was usually taken to be the same, following Henyey and Greenstein (1941). The medium can then, for purposes of the calculation, be compressed into a slab of finite optical depth  $b$  filled homogeneously with sources and scatterers. This is the problem treated for isotropic scattering in Section 9.4.

The angular distribution for the radiance at a midlayer point (here: the earth) is found as a byproduct of the doubling method. This was explained for an arbitrary phase function in Section 4.5 and illustrated by a few examples with Henyey–Greenstein scattering in Fig. 9.15 and Table 40 (Section 13.3). Those examples are not directly relevant here, because they assume external illumination.

The corresponding problem with homogeneous internal sources was solved by van de Hulst and Davis (1961) and van de Hulst and de Jong (1969). Their conclusion is illustrated in Fig. 20.4. As long as the absolute level at galactic latitude  $30^\circ$  remains uncertain, a range of combinations of albedo  $a$  and anisotropy factor  $g$  all give virtually the same profile of radiance versus galactic latitude. Although much better observations had become available in the meantime (Witt, 1968), this meant that the interpretation remained ambiguous and gave at best a curve in the  $(a, g)$  plane at any wavelength. For subsequent observations, see, e.g., Mattila (1970) and Witt and Lillie (1973).

The assumption that stars and dust have the same  $z$  distribution is probably too rigid. Bastiaansen and van de Hulst (1977) showed a way to eliminate this assumption and still keep the problem simple. They replaced the stars at high- $z$  coordinates by layers of external sources at both sides of the dust layer. The added parameter is then  $F$ , the fraction of starlight homogeneously generated inside the dust layer ( $0 \leq F \leq 1$ ). Solutions of the transfer problem with internal sources only ( $F = 1$ ) and with external source layers only ( $F = 0$ ) were already available. Not very surprisingly, they found that very similar observable profiles are obtained if a change of  $F$  is accompanied by an appropriate adjustment in  $a$  and/or  $g$ .

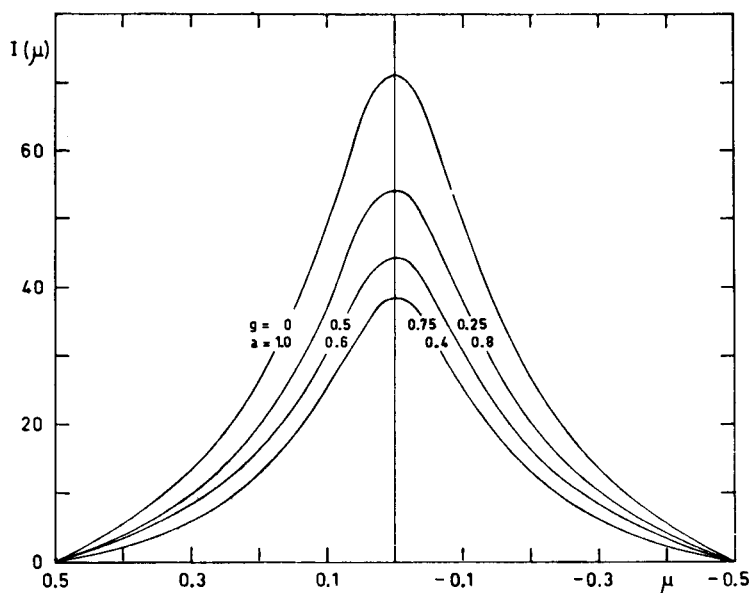


Fig. 20.4. The computed excess diffuse galactic light above its intensity at  $30^\circ$  galactic latitude is shown to follow similar curves for 4 different models (from van de Hulst and de Jong, 1969).

It is instructive to compare this method with a much earlier study by Kaplan and Pikelner (1963), who also pointed out that stars extend to larger  $z$  values than grains. They adopted a linearly anisotropic phase function, used Eddington's approximation, and made the very questionable approximation that the latitude distribution of starlight is the same at all distances  $z$  from the galactic plane. This distorts the model and does not lead to simple formulas. This comparison shows that approximations which translate the complex natural problem into a simple understandable model can be recommended, but that approximations which ease the mathematics but confuse the model should be avoided.

### 20.5.2 Multiple Small-Angle Scattering

Because of its very simple mathematical structure, this last topic has diverse applications to other fields, e.g., lidar propagation and ocean optics (see below). However, it has led to extensive studies aimed at astronomy: small angle x-ray scattering by interstellar dust and interstellar radio scintillation. We have chosen to present it in terms of x-ray scattering. Some references to other applications are given at the end.

The pattern for single scattering of x-rays depends by a simple theory (van de Hulst, 1957, Beeman *et al.*, 1957) on the shape, size, and composition of the

dust grain. Conversely, the measured scattering pattern yields information about size and shape. Averages over an assembly with different sizes, shapes, and orientations can be derived easily.

Suppose we observe a discrete x-ray source behind a sufficiently dense interstellar cloud. Since x-ray scattering occurs under quite small angles, the scattered radiation remains part of the blurred image, or halo, of the source, even after repeated scattering. If the source itself is sharp, an observer on earth measures the following intensities, relative to the unaffected intensity:

sharp image,

$$e^{-\tau_a - \tau_s}$$

integrated blurred image = halo,

$$e^{-\tau_a}(1 - e^{-\tau_s})$$

and integrated total image,

$$e^{-\tau_a}$$

Here  $\tau_a = (1 - a)\tau$  is the absorption optical depth,  $\tau_s = a\tau$  the scattering optical depth,  $\tau$  the total optical depth, and  $a$  the albedo. These simple equations may be written at once and correspond to column (3) of Display 14.2.

The angular intensity distribution within the halo was first computed for single scattering by Overbeck (1965). In practice this suffices if  $\tau_s < 0.2$ . Hence, estimating the visual extinction at 20 times the x-ray extinction near 1 keV or 13 Å (Martin, 1970), multiple x-ray scattering becomes significant only for sources with a visual obscuration exceeding 4 magnitudes.

Single scattering by a small angle  $\theta$  at midcourse along a path of length  $l$  introduces a detour of length  $l\theta^2/16$ , i.e., a time delay of  $l\theta^2/16c$ , where  $c$  is the velocity of light. The delay varies with scattering angle and with the position of the scattering particle. Therefore, a hypothetical source which emits a mathematically sharp pulse will in fact be observed with a pulse spread out in time.

In multiple scattering these two effects, the angular spread and the pulse delay and spread, remain intimately linked. As usual, not much of the specific pattern information is left in this multiple scattering process. In practice it suffices to retain only one parameter,  $4s$ , the mean square of the angular deviation per unit length. The problem thus is reduced to a random-walk problem, which can be solved exactly. The reader is referred to the literature for details (Williamson, 1972; Alcock and Hatchett, 1978; van de Hulst, 1980).

If the assumption is made that a homogeneous cloud of scattering particles occupies an arbitrary part of the line of sight between the source and observer, certain complicated geometrical factors appear in the formulas. They arise from scaling and from the fact that the correlations among angular displacement, linear displacement, and time delay must be taken into account.

In the simple situation in which the full distance  $l$  between the source and the earth is occupied by this medium, the arrival angle  $\varphi$  at the earth has the mean square value

$$\langle \varphi^2 \rangle = \frac{4}{3}sl$$

The x-rays from this source arrive at the earth with the average time delay  $\langle t \rangle = \frac{1}{3}sl^2/c$ , when averaged over all directions of arrival (i.e., over the entire halo). Here  $c$  is the velocity of light. At the exact center direction the delay is shorter, namely  $0.200sl^2/c$ , and at the angle  $1.75(sl)^{1/2}$ , where the halo intensity has dropped to 0.1 times the central intensity, the average delay has increased to  $0.814sl^2/c$ .

This is only one of many possible geometrical models. There may be one or several clouds of limited extent in the line of sight. The more realistic situation, in which the source, an x-ray pulsar, is not pulsed in time but has a narrow beam sweeping across the observer, may be similarly treated. In principle, we can thus see the scattered image move across the cloud, while it gradually brightens and dims again just as the beam of a lighthouse is observed through the haze.

All this is fine in theory, but reality is more complex. Not only may the sources have an intrinsic halo and beam structure, but the numbers should be in the observable range. The normal interstellar grains with sizes about  $0.1 \mu\text{m}$  at their average density in the galactic plane make  $4s$  of the order of  $10 (\text{arcmin})^2/\text{kpc}$ . This makes the halo observable but spreads the delay times over the order of days, which would preclude observing x-ray bursts from near the galactic center. Alcock and Hatchett (1978) remedy this problem by arbitrarily assuming 30 times larger grains of  $3 \mu\text{m}$ , which reduces  $s$  by a factor 1000 and shortens the burst tails to their observed duration of 10–200 seconds. At the same time, the optical depth becomes small so that single scattering suffices. This is certainly not the final answer.

The framework of the multiple scattering theory just sketched, based on only one parameter,  $s$ , is so simple that it finds very diverse applications. Exactly the same curve of pulse shape with exponential tail may be found reproduced in three different places: Williamson (1972) deals with multiple scattering of radio waves by electron density fluctuations in interstellar space (interstellar scintillation) and shows this pulse shape in his Fig. 7; Ivanov and Gutsabash (1974) deal with the asymptotic behavior of the propagation of a light pulse in the atmosphere and show this pulse shape in their Fig. 2 and Table 2; we have reproduced it as  $T_\beta(x)$  in Fig. 17.7; finally, Alcock and Hatchett (1978), dealing with x-ray scattering, show this shape as their Fig. 10. In each case it is the distribution function of delay times, if an omnidirectional source is observed through a medium with constant small-angle scattering coefficient  $s$ . The formula, except for scale factors, is the inverse Laplace transform of  $y/\sinh y$ .

We have mentioned only one of the possible pulse shapes. For instance, the pulses observed from a beamed source or observed at a particular direction within the scattered image (halo) have slightly different shapes, as the full theory shows.



We have touched here a tiny part of a wide set of problems. Astronomers have learned to live with the fact that the image of any distant source is dimmed and blurred by the intervening medium. When referred to the earth's atmosphere, the dimming is called "extinction" and the blurring is called "seeing." The blurred image is not constant in time and may in extreme cases even jump back and forth. Seeing also spoils observations with high time resolution: a sharp pulse is distorted into a wider, delayed pulse with an exponential tail.

It is now customary to use the same terms for media beyond the earth. Practical studies of interplanetary seeing at radio frequencies led to the discovery of pulsars. Interstellar extinction has long been recognized as grossly distorting our view of the galactic system before the advent of radio astronomy. The increase in apparent size of the radio source at the galactic nucleus, from 0.02" at 9 GHz to 0.5" at 1.7 GHz and 1.5" at 1.0 GHz, clearly arises from interstellar seeing (Davies *et al.*, 1976; Oort 1977).

The general subject of propagation in random media borders the subject matter of this book and has a huge literature of its own (see e.g., Fejer, 1953; Scheuer, 1968; Harris *et al.*, 1970; Uscinsky, 1977). Perhaps the finest applications of multiple small-angle scattering theory will finally be found in quite different fields, such as atmospheric or underwater propagation.

## REFERENCES

- Aida, M. (1977). *Proc. Symp. Rad. Atm.* p. 214. Science Press, Princeton, New Jersey.
- Alcock, C., and Hatchett, S. (1978). *Astrophys. J.* **222**, 456.
- Andriess, C. D., Piersma, Th.R., and Witt, A. N. (1977). *Astron. Astrophys.* **54**, 841.
- Appleby, J. F., and Van Blerkom, D. J. (1975). *Icarus* **24**, 51.
- Avaste, O. A., and Vanikka, G. M. (1977). *Proc. Symp. Rad. Atm.* p. 220. Science Press, Princeton, New Jersey.
- Barkstrom, B. R. (1972). *J. Glaciol.* **11**, 357.
- Barkstrom, B. R., and Arduini, R. F. (1977). *Proc. Symp. Rad. Atm.* p. 188. Science Press, Princeton, New Jersey.
- Barkstrom, B. R., and Querfeld, C. W. (1975). *J. Glaciol.* **14**, 107.
- Bastiaansen, P. A., and van de Hulst, H. C. (1977). *Astron. Astrophys.* **61**, 1.
- Beckett, P., Foster, P. J., Hutson, V., and Moss, R. L. (1974). *J. Quant. Spectrosc. Rad. Transfer* **14**, 1115.
- Beeman, W. W., Kaesberg, P., Webb, M. B., and Anderegg, J. W. (1957). *Handbuch Phys.* **32**, 321.
- Bohren, C. F., and Barkstrom, B. R. (1974). *J. Geophys. Res.* **79**, 4572.
- Bolle, H.-J. (1977). *Proc. Symp. Rad. Atmos.* Science Press, Princeton, New Jersey.
- Chandrasekhar, S. (1958). *Proc. Nat. Acad. Sci. U.S.* **44**, 933.
- Davies, R. (1978). *J. Atmos. Sci.* **35**, 1712.
- Davies, R., and Weinman, J. A. (1977). *Proc. Symp. Rad. Atm.* p. 225. Science Press, Princeton, New Jersey.
- Davies, R. D., Walsh, D., and Booth, R. S. (1976). *Mon. Notices R. Astron. Soc.* **177**, 319.
- Davison, B. (1957). "Neutron Transport Theory." Oxford Univ. Press (Clarendon), London and New York.
- Duntley, S. Q. (1974). In "Optical Aspects of Oceanography" (N. G. Jerlov and E. Steeman-Nielsen, eds.), p. 135. Academic Press, New York.

- Feinstein, D. L., Butler, F. E., Piech, K. R., and Leonard, A. (1972). *Phys. Fluids* **15**, 1641.
- Fejer, J. A. (1953). *Proc. R. Soc. London Ser. A* **220**, 455.
- FitzGerald, M. P., Stephens, T. C., and Witt, A. N. (1976). *Astrophys. J.* **208**, 709.
- Goedecke, G. H. (1977). *J. Opt. Soc. Am.* **67**, 1339.
- Gordon, H. R. (1973). *Appl. Opt.* **12**, 2803.
- Gordon, H. R., Brown, O. B., and Jacobs, M. M. (1975). *Appl. Opt.* **14**, 417.
- Gordon, H. R., and McCluney, W. R. (1975). *Appl. Opt.* **14**, 413.
- Greenberg, J. M. (1978). In "Cosmic Dust" (J. A. M. MacDonnell, ed.), pp. 187–294. Wiley, New York.
- Hamaker, H. C. (1947). *Philips Res. Rep.* **2**, 55, 103.
- Harris, D. E., Zeissig, G. A., and Lovelace, R. V. (1970). *Astron. Astrophys.* **8**, 98.
- Henry, L. G., and Greenstein, J. L. (1941). *Astrophys. J.* **93**, 70.
- Herman, M., and Lenoble, J. (1968). *J. Quant. Spectrosc. Rad. Transfer* **8**, 355.
- Hunt, G. E. (1968). *SIAM J. Appl. Math.* **16**, 228.
- Irvine, W. M. (1975). *Icarus* **25**, 175.
- Ivanov, V. V., and Gutsabash, S. D. (1974). *Fiz. Atmos. Okeana* **10**, 851.
- Jerlov, N. G. (1976). "Marine Optics." Elsevier, Amsterdam.
- Jerlov, N. G., and Steemann-Nielsen, E. (eds.) (1974). "Optical Aspects of Oceanography." Academic Press, New York.
- Kaplan, S. A., and Pikelner, S. B. (1963). "The Interstellar Medium," pp. 237–240. Moscow. English Translation, Harvard Univ. Press, Cambridge, Massachusetts, 1970, pp. 192–194.
- Kortüm, G. (1969). "Reflectance Spectroscopy." Springer, Berlin and New York.
- Kourganoff, V. (1963). "Basic Methods in Transfer Problems." Dover, New York.
- Kubelka, P. (1954). *J. Opt. Soc. Am.* **44**, 330.
- Kubelka, P., and Munk, F. (1931). *Z. Tech. Phys.* **12**, 593.
- Larkin, B. K., and Churchill, S. W. (1959). *Am. Inst. Chem. Eng. J.* **5**, 467.
- Lenoble, J. (1978). Standard Procedures to Compute Radiative Transfer in a Scattering Atmosphere, Vol. 3 (second draft): Review of Methods for Horizontally Inhomogeneous Atmospheres and Non Plane-Parallel Atmospheres. Radiation Commission, International Association of Meteorology and Atmospheric Physics (I.U.G.G.).
- Lewins, J. (1965). "Importance, The Adjoint Function." Pergamon, Oxford.
- Martin, P. G. (1970). *Mon. Notices R. Astron. Soc.* **149**, 221.
- Mattila, K. (1970). *Astron. Astrophys.* **9**, 53.
- McCluney, W. R. (1974). *Appl. Opt.* **13**, 2422.
- McKee, T. B., and Cox, S. K. (1974). *J. Atmos. Sci.* **31**, 1885.
- McKee, T. B., and Klehr, J. T. (1977). *Proc. Symp. Rad. Atm.* p. 217. Science Press, Princeton, New Jersey.
- Monin, A. S., and Shifrin, K. S. (ed.) (1974). "Hydrophysical and Hydrooptical Investigations in the Atlantic and the Pacific Oceans" (Russian) Izd. Nauk, Moscow.
- Nack, M. L., and Green, A. E. S. (1974). *Appl. Opt.* **13**, 2405.
- Niilisk, H. J., and Ohvrill, H. A. (1978). In Lenoble (1978).
- Oort, J. H. (1977). *Ann. Rev. Astron. Astrophys.* **15**, 295.
- Overbeck, J. W. (1965). *Astrophys. J.* **141**, 864.
- Plass, G. N., Kattawar, G. W., and Guinn, J. A. (1976). *Appl. Opt.* **15**, 3161.
- Pomraning, G. C. (1973). "Radiation Hydrodynamics," Pergamon, Oxford.
- Preisendorfer, R. W. (1976). "Hydrologic Optics," 6 Volumes. National Oceanic and Atmospheric Administration, Environmental Research Laboratories, Honolulu, Hawaii.
- Prieur, L., and Morel, A. (1971). *Cah. Océanogr.* **23**, 35.
- Probstein, R. F. (1963). *AIAA J.* **1**, 1202.
- Roark, T., Roark, B., and Collins, G. W. (1974). *Astrophys. J.* **190**, 67.
- Romanova, L. M. (1971). *Fiz. Atmos. Okean* **7**, 1153.
- Romanova, L. M. (1973). *Fiz. Atmos. Okean* **9**, 198.
- Rybicki, G. (1971). *J. Quant. Spectrosc. Rad. Transfer* **11**, 827.

- Scheuer, P. A. G. (1968). *Nature (London)* **218**, 920.
- Schuster, A. (1905). *Astrophys. J.* **21**, 1.
- Shulejkin, V. V. (1933). *Geofizika* **3**, 3.
- Uscinsky, B. J. (1977). "The Elements of Wave Propagation in Random Media." McGraw-Hill, New York.
- van de Hulst, H. C. (1957). "Light Scattering by Small Particles." Wiley, New York. Also Dover, New York, 1981.
- van de Hulst, H. C. (1977). In "Inversion Methods in Atmospheric Remote Sounding" (A. Deepak, ed.), p. 1. Academic Press, New York.
- van de Hulst, H. C. (1980). In preparation.
- van de Hulst, H. C., and Davis, M. M. (1961). *Proc. Koninkl. Akad. Wetenschappen B* **64**, 220.
- van de Hulst, H. C., and de Jong, T. (1969). *Physica* **41**, 151.
- Vanysek, V. (1969). *Vistas Astron.* **11**, 189.
- Weinman, J. A., and Guetter, P. J. (1972). *J. Appl. Meteorol.* **11**, 136.
- Whitney, L. V. (1941). *J. Mar. Res.* **4**, 122.
- Williamson, F. R. (1977). Cryogenic Foam Insulation. Abstracted publications, NASA Reference Publ. 1002.
- Williamson, I. P. (1972). *Mon. Notices R. Astron. Soc.* **157**, 55.
- Witt, A. N. (1968). *Astrophys. J.* **152**, 59.
- Witt, A. N. (1977a). *Astrophys. J. Suppl.* **35**, 1.
- Witt, A. N. (1977b). *Astrophys. J. Suppl.* **35**, 7.
- Witt, A. N. (1977c). *Astrophys. J. Suppl.* **35**, 21.
- Witt, A. N., and Lillie, C. F. (1973). *Astron. Astrophys.* **25**, 397.
- Witt, A. N., and Oshell, E. R. (1977). *Astrophys. J. Suppl.* **35**, 31.
- Witt, A. N., and Stephens, T. C. (1974). *Astron. J.* **79**, 948.
- Zaneveld, J. R. V. (1974). In "Optical Aspects of Oceanography" (N. G. Jerlov and E. Steemann-Nielsen, eds.), p. 121. Academic Press, New York.

## □ Index

### A

- Absorption, *see also* Loss  
  in atmosphere, 204, 684–687  
  with aerosol, 684  
  depth, 481  
  in ground, 204, 684–687  
  by particle, 18, 574–576  
  along path, 574–576  
  in tau interval, 205–206
- Absorption line, 36, 573  
  in diffuse reflection, 592–598  
  depth of formation, 640  
  homogeneous slab, 593–597  
  inhomogeneous atmosphere, 637, 640  
  square root law, 635  
  well-mixed atmosphere, 636  
  by omnidirectional probe, 640–642  
  profile, 592–597
- Absorption band, 575, 683  
  structure, 598
- Absorption coefficient, 592–595
- Accuracy, 519, 523  
  check, 203, 362
- Added layer, 70–71, 101, 174
- Adding ground surface, 625–629
- Adding method, 43, 54, 56–62, 625, 703  
  convergence, 57  
  with polarization, 62, 505
- Aerosol, 317, 661–675 *see also* Turbidity  
  altitude, 662  
  causing aureole, 651, 657–659  
  collection, 662  
  composition, 662  
  continental, 662  
  maritime, 662  
  natural, 661–675  
  origin, 662  
  refractive index, 664  
  size distribution, 657, 662  
    from aureole, 668–670  
    from extinction curve, 671–675  
    by inversion, 668, 670  
    by model fit, 668–670  
  wide angle scattering, 664, 666–668
- Air  
  phase function, 310–311  
  phase matrix, 532  
  polarization, 311, 532
- Air–sea interface, 627, 708
- Albedo, *see also* Plane albedo; Spherical albedo  
  critical, 225  
  effective, 516, 518, 524  
  geometric, 600–601  
  in reactor physics, 4  
  for single scattering, 3, 35, 303, 312  
  notation, 3  
  power expansion, 381, 383  
  transformation, 481
- Altostratus, 661

**A matrix**, 58–61  
 Henyey–Greenstein phase function, 462–464  
**Ambartsumian function**, 44, 99–102, 108, 119  
 as matrix, 102  
**Ambartsumian method**, 43, 50–54, 174  
**Amplitude**  
 complex, 21  
 transformation by scattering, 18–20  
**Angle with normal**, sign, 4  
**Ångström's law**, 673  
**Anisotropy**, *see* Asymmetry parameter  
**A.N.S.**, *see* Astronomical Netherlands Satellite  
**Antisymmetric solution**, 508  
**Approximation**, *see* specific methods  
**Arago point**, 555  
**Astronomical Netherlands Satellite**, 715  
**Asymmetry parameter**, 35, 68, 70, 79,  
 303–309, 312–314, 316–324, 372–373,  
 384–388  
 transformation, 481  
 water drop, 312–313  
**Asymptotic expression**, thick layer, 68–87  
 conservative, 81  
 isotropic scattering, 202  
**Asymptotic fitting**, 45, 82, 85–87, 93, 202–203,  
 335, 339, 362, 367  
**Asymptotic radiance**, 708–711  
 attenuation, 708–709  
 pattern, 710–711  
**Atmosphere**, with ground surface,  
 inhomogeneous, 64  
 internal radiation, 631–633  
 reflection function, 626–632  
**Attenuation length**, 707  
**Aureole**, 311, 651, 655, 657–661  
 measurement, 657–660, 670  
 multiple scattering, 659–661  
 radiance, 669–670  
 in ultraviolet, 657  
**Auxiliary equation**, 48, 49  
 for Rayleigh scattering, 562  
**Azimuth-dependent terms**, 90, 493–494,  
 498–505  
 effective albedo, 516–518

## B

**Babinet point**, 555  
**Backlayer**, diffusely reflecting, 702  
**Backscatter**, 305–307, 314  
 predominant, 403–404  
**Backward peak**, 307, 309, 368, 489–492

**Beam**  
 attenuation coefficient, 708–710  
 extinction coefficient, 705  
 scattering coefficient, 708, 710  
**Bessel function**, 388  
 modified, 594  
**Binomial expansion**, 109, *see also*  
 Characteristic binomial  
**Blackbody**, 25, 204, 497  
**Blackbody radiation**, 25  
**Blue sky**, 310–311, 531, 555–557, 651, 661  
**Bond albedo**, 600, 603, *see also* Spherical  
 albedo  
**Born approximation**, 670  
**Bottom boundary**, *see* Ground surface  
**Brewster point**, 555  
**Brightness**, 651, 652, *see also* Radiance  
**Busbridge polynomial**, 43, 91–92, 105,  
 108–113, 120

## C

**Case method**, 84, 118, 121–122, 335, 405  
**Chapman function**, 667  
**Characteristic binomial**, 94–95, 112  
**Characteristic equation**, 516  
 alternate form, 98  
 methods of solution, 96–99  
 multiple roots, 381, 383–388  
 roots, 96–98, 107  
**Characteristic function**, 43, 91, 94, 112,  
 119–120, 518  
 determination, 94  
 for four-term phase function, 356–357  
 integral check, 95  
 for small  $N$ , 96  
**Characteristic root**, 377–378  
**Circular polarization**, symmetry relations, 616  
**Cirrostratus**, 661  
**Cirrus**, 661, 680–682  
 polarization, 668  
**Clearing**, 706  
**Climate**, 682–683  
**Closely packed particles**, 699–703  
**Cloud**  
 atmospheric, 317  
 broken, 653, 683, 694–695  
 cooling, 687  
 cuboid, 694–698, 705  
 asymptotic case, 695–698  
 corner domain, 695–698  
 Henyey–Greenstein scattering, 698  
 isotropic scattering, 695–698

- heating, 687
  - heterodisperse, 521
  - isolated, 694–698
  - liquid water content, 687
  - model, 320, 322–324
  - monodisperse, 521
  - particle, remote sensing, 667
  - phase function, 315–317
  - polarization, 667
  - reflected energy, 682
  - terrestrial, 388
  - Cloudbow, 668
  - Cloud cover, fractional, 683, 695
  - Cloud deck, 651–652
    - opaque, 653–654
    - with overlying atmosphere, 627–630
    - radiance, 651–652, 668
    - reduction of illumination, 654–655
  - Cloud layer,
    - internal radiation field, 206
    - reflection function, weak loss, 80
  - Coastal water, 707
  - Coherency matrix, 23, 534
  - Computer time, 86
  - Condensed notation, *see* Shorthand notation
  - Conservative atmosphere, 188, 190
  - Conservative scattering, 38
  - Constraint, 103–104, 11, 663
  - Continued fraction, 380, 383
  - Continuum
    - absorption, 592, 595
    - albedo, 595–596
    - of eigenvalues, 159
    - extinction, 595
    - optical path, 594
    - scattering, 572
  - Contour integral, 159
  - Contrast ratio, 629–632, 703
  - Convergence, *see* specific methods
  - CP representation of polarized light, 497, 508, 533, 614
  - Critical albedo, 140, 233
  - Critical limit, 233
  - Critical size of reactor, 692
  - Cross section
    - for absorption, 25
    - for emission, 25
  - Cuboid, *see* Cloud, cuboid
  - Cumulus, 680–681
  - Curve of growth, 593–598, 634
    - slab with ground surface, 597
    - square root law, 594–598
  - Cylinder, randomly oriented, 661
- D**
- Damping profile, 593–596
  - Daylight sky, *see* Sky, daylight
  - Delta-Eddington approximation, 41
  - $\delta$  function, 309
  - Depolarization
    - of lidar echo, 680–682
    - of molecular scattering, 311, 533
  - Depression in absorption line, 592–596
  - Detailed balance, 16–17, 23, 27
    - in astrophysics, 17
    - inverse use, 17–18, 20
  - Detector
    - as four-vector, 496
    - reading, 133–135
    - reciprocity to source, 615
    - sensitivity, 130
  - Diffraction, 657, 660–661
    - anomalous, 315
    - Fraunhofer, 314
    - pattern, with size distribution, 669–670
    - peak, 312, 314, 322–323
      - omission, 481
  - Diffusion, *see also* specific phase function
    - approximation, 75–76, 159
      - improved, 76
    - coefficient, 75, 159
    - constant, 144
    - depth, 481
    - domain, 68, 70, 75–76, 82, 90, 92–93, 178–180, 183, 187–188, 198, 201, 209–213, 224, 478, 708–711
      - with polarization, 507–508, 512
    - equation, 159
    - exponent, 70, 78, 93, 708–709, 711
      - asymptotic expression, 152
      - check, 87
      - error by neglect of polarization, 511
      - higher root, 383
      - with polarization, 508–513
        - as variable, 78–80, 380–384, 386
    - inward, 394
    - length, 70, 93, 152, 377
    - mode, 70
    - nonconservative, 93
    - outward, 394
    - pattern, 109, 111, 478, 710
      - expansion, 384
      - forward/back ratio, 511
      - with polarization, 507–512
        - moments, 513
      - as vector, 69

- Diffusion (*cont.*)  
 solution, 121  
   azimuth-dependent terms, 515–517  
   conservative, 92  
   nonconservative, 93  
 stream, 70–77, 224, 339, 477  
   internal reflection, 71–72, 374–375  
   negative, 72, 80, 212, 374  
   from source layer, 83
- Direct experiment, 207
- Disk, *see* Planet; Sun
- Dispersion function, 97, 105–106
- D* matrix, 58–61  
   Henyey–Greenstein phase function, 462–464
- Double peak phase function  
   asymmetry factor, 489  
   flux, 490–491  
   reflection function, 483, 486, 490–491  
     bimoment, 491  
   semi-infinite medium, 490–491  
   transmission, 490–491
- Doubling method, 43, 45, 54–56, 209, 222, 396, 612, 691, 716  
   azimuth-dependent terms, 507  
   basis for asymptotic fitting, 85  
   convergence, 43, 63  
     Henyey–Greenstein phase function, 408–411  
     improved, 146  
     isotropic scattering, 232–234, 408–410  
   critical limit, 233–234  
   eigenvalue, 232–234, 408–411  
   from Milne equation, 146–148  
   with polarization, 505–507
- Dust, 496  
   from forest fire, 662  
   interplanetary, 659, 713  
   interstellar, 713  
   scattering pattern, 606  
   slab, 714
- E**
- Earth  
   atmosphere  
     albedo, 559  
     optical depth, 310  
     scattered light, 650–661, 664–668  
   radiation budget, 682–683
- Echo delay time, 573
- Eddington approximation, 76, 143, 370, 644, 717
- Eddington method, modified, 697
- E* function, *see* Exponential integral
- Eigenfunction  
   of diffusion equation, 74  
     Henyey–Greenstein phase function, 335, 337–338  
   expansion, 121, 132, 405  
     of Milne operator, 144  
   singular, 74, 159  
     as expansion term, 43, 121, 159, 222  
     with polarization, 122
- Eigenvalue, *see also* Doubling method, convergence  
   of anisotropic transfer equation, spectrum, 376–388  
   of diffusion equation, 74, 93  
     Henyey–Greenstein phase function, 333–336  
   discrete, 43, 93  
   in successive order method  
     Henyey–Greenstein phase function, 407–408  
     isotropic scattering, 233
- Electron as scatterer, 531
- Electron capture, 18
- Elliptical integral, 333
- Elongation, 601
- Embedding, *see* Invariant embedding
- Emergence, *see* Escape function;  
   Reflection; Transmission
- Emission, thermal, 18, 24  
   disk, 26  
   isothermal body, 642  
   nonisothermal body, 643–644  
   nontransparent sphere, 26  
   slab, 221  
     zero-order, 220–221
- Energy, *see also* Flux; Loss  
   deposition in cloud, 687  
   fate  
     asymptotic, 684–687  
     Henyey–Greenstein phase function, 400–402  
     isotropic scattering, 205–206  
   sink, 180
- Equator of planet, 602
- Equivalence, 480  
   theorem, 574–577
- Equivalent width, 573, 592–598
- Error  
   function, 160  
   integral, 393

propagation, 63  
 round-off, 86  
 Escape function, 72, 111–114, 116–117, 151,  
 339, 357–363, 486, 513, 668, *see also*  
 specific phase function  
 moment, 116–117  
   expansion, 80, 360–362  
 nearly conservative,  
   expansion, 79  
 reduction to  $H$  function, 91  
   conservative, 117  
   nonconservative, 115–116  
 similarity, 374, 479  
 as vector, 69  
 Escape probability, 181–182, 208, 213–217  
 isotropic scattering, 213–217, 220  
   one-sided, 213–217  
   two-sided, 213–214  
 slab, Henyey–Greenstein phase function,  
   405–406  
 Escape region, isotropic scattering, 179,  
   211–213  
 Euler's constant, 9, 672  
 Expansion, *see* Successive order  
 Exponential  
   integral, 8–10, 196, 597  
   asymptotic form, 9  
   differentiation, 9  
   expansion, 9  
   generalized, 10–11  
   sum fitting, 683  
 Extinction, *see also* Interstellar extinction  
   coefficient, 316  
   curve, 317  
     inversion, 670–675  
     maximum, 670–674  
     model fit, 671–674  
     polydisperse medium, 672–675  
   depth, 481  
 Extrapolated endpoint, 73  
 Extrapolation length, 72, 117, 174, 234, 409, 513,  
   685, *see also* Escape function  
 finite layer, 218  
 Hopf, 218  
 nearly conservative,  
   expansion, 79  
 nonconservative,  
   similarity, 374–376  
   reduced, 115, 357–363  
   similarity, 357–362  
 Extrapolation to large thickness,  
   201–203

## F

Far-field scattering pattern, 18–20, 699  
 $F$  function, 8, 11–13, 136, 187, 196  
   differentiation, 11  
   expansion, 13  
   numerical values, 12–13  
   recurrence, 11, 13  
   reduction, 11  
 Fluid motion with radiation, 707  
 Fluorescent scattering, 231  
 Flux  
   absorbed  
     Henyey–Greenstein phase function,  
       400–402, 456–461  
     isotropic scattering, 203–206, 218, 228,  
       282–290  
   from bottom of atmosphere, 64  
   directional, 693  
   divergence, 684  
   emerging, 81–82, 188, 190, 497  
   extinction coefficient, 705  
     in column of finite width, 705  
   net, 5, 75, 693, 712  
   in diffusion domain, 184  
   in slab, 488  
     conservative, 209, 282–290, 292–299  
     Henyey–Greenstein phase function,  
       405, 465–476  
     isotropic scattering, 205–206, 208, 292,  
       299  
   operator, 69  
   reflected, 81, 486–487  
     Henyey–Greenstein phase function,  
       400–405, 456–461  
     isotropic scattering, 174, 203–205,  
       228–230, 282–290  
   transmitted, 486–487  
     Henyey–Greenstein phase function,  
       400–401, 456–461  
     isotropic scattering, 201–205, 228,  
       282–290  
     zero order, 203, 282–290, 456–461  
 $F$  matrix, 21  
 Fog, 317, 661  
 Forward and backward peak, 700  
 Forward peak, 307, 309, 358–360, 489–492  
   addition, 362, 368–369, 479–481, 491–492  
   influencing lidar echo, 677  
 Forward scattering, 305–307, 403–405,  
   480  
 Four by four matrix, 496, 500, 503



Fourier expansion in azimuth, 493–494, 498,  
501–505, 514–515  
number of terms, 520–523  
ratio between orders, 525  
Rayleigh scattering, 519, 543–544  
Fourier spectroscopy, 634  
Fourier transform, 158  
Four-vector, 496–497, 503  
Fraunhofer diffraction, *see* Diffraction  
Fredholm integral equation, 110, 122, 162

## G

GAARS field test, 673  
Gain, *see also* Point-direction gain  
in antenna theory, 26  
arbitrary configuration, 26  
extended definition, 27  
upon scattering, 152  
Galactic light  
diffuse, 714, 716–717  
illuminating globule, 715  
Gamma size distribution, 664–665  
GARP, *see* Global Atmospheric Research  
Program  
Gaussian distribution, 159–161, 316  
Gaussian division, 43  
Gaussian quadrature, 226  
Generalized spherical function, 497, 508  
Geometric albedo  
for model atmosphere, 621  
of planet, 600–601, 618, 620–621  
Geometric factor, 609, 621  
Geometric series, 141, 591, 614  
Geometry different from slab, 486  
Gershun equation, 712  
G function, 8, 13–15, 136, 196  
expansion, 14, 228  
numerical values, 14–15  
recurrence, 14  
symmetry, 13  
Glass bead, 313  
Global Atmospheric Research Program, 687  
Globule, 715–716  
Glory, 312, 315–316, 322–324  
Glossy surface, 702  
Grafting of theories, 692  
Grazing reflection, 525  
on sphere, 313  
Greenhouse effect, 644

Green's function  
asymptotic expansion, 393  
factorization, 393  
Grey absorption, 644  
Ground surface below atmosphere, 35, 63–65,  
204, 507, 625–629

## H

Hailstone, 314, 316  
Half-space, 90, 691  
Halo, 314  
Haze, 666  
absorbing, 375  
model, 316–317, 320–322  
phase function, 311, 315–317  
size distribution, 664–665  
Heating rate, 684  
Heat transfer, 706–707  
through insulating layer, 706  
between walls, 706  
Heney–Greenstein phase function, 307–309,  
320–322, 331–332, *see also* Flux  
azimuth-dependent terms, 522–529  
characteristic equation, roots, 384–388  
in diffuse galactic light, 716–717  
diffusion  
exponent, 333–336, 367, 511, 709–710  
expansion, 335  
length, 333–336  
pattern, 335, 337–338  
escape function, 339–342, 367  
conservative, 358–361  
expansion coefficients, 308, 331  
extrapolation length,  
conservative, 340–341, 359–361, 376  
nonconservative, 340–341, 367, 376  
in globule, 715  
internal reflection coefficient, 374–375  
Kuščer polynomials, 378–379  
Legendre coefficients, 308, 331  
Minnaert plot, exponent, 619–620  
plane albedo, 367–369, 400–403  
point-direction gain, 405–406, 465–476  
moment, 405, 467–468, 471–472, 475–476  
rapid-guess formulas, 363–364  
reflection function, 367–368, 396–399,  
412–453, 486–487  
azimuth-dependent terms, 523–529  
asymptotic, 525–529  
ratio of total to first order, 524–525

bimoment, 339, 343–354, 398, 401,  
     403–405, 412–453, 701–702  
 first order, 399–400, 412–443  
 low order, 412–443  
 moment, 339, 345–354, 398, 412–453  
 nearly conservative, 391–392  
 in opposition, 617–618  
 ratio of total to first order, 397–399,  
     454–455, 678  
 semi-infinite atmosphere, 339, 342–354  
 slab with varying ground, 629–632  
 semi-infinite atmosphere, 339–354  
 similarity parameter, 478  
 slab, 396–476  
 spherical albedo,  
     semi-infinite atmosphere, 344, 367,  
         370–371  
     slab, 403–405  
 successive orders, convergence, 522–523  
 transmission function, 396–399, 412–453,  
     486–487, 652  
     azimuth-dependent terms, 523–529  
         asymptotic, 525–529  
         ratio of total to first order, 524–525  
     bimoment, 398, 412–453  
     low order, 412–443  
     moment, 398, 412–453, 487  
 truncation, 488  
 unbounded medium, 331–338  
*H* function, 43, 91, 104–108, *see also* specific  
     phase function  
 expansion, 108  
 explicit expression, 106–107  
 integral relation, 106–107  
 isotropic scattering, 162–169, 187, 203, 225,  
     584, 597, 621  
     in corner domains, 166  
     definition, 162  
     derivative, 165  
     near divergence, 167–168  
     expansion, 163–166  
     integral, 168  
     integral equation, 162  
     moments, 169–171  
         asymptotic form, 170–171  
         expansion, 169–171  
     numerical values, 163–164  
     representation  
         integral, 162  
         rational, 163  
     virtual angles, 166–169  
 moment, 108, 112

Hiding power, 703  
 Historical note, 54, 201  
 Hopf function, 163, 176, 183, 188, 190  
     for Rayleigh scattering, 541  
 Hopf solution, 140, 394  
 Hybrid formulation, 576  
 Hydrodynamics, 706–707  
 Hydrologic optics, 707–713  
     asymptotic domain, 708–711, 713  
 Hyperbolic function, 77, 699  
 Hypergeometric function, 669–670

## I

IAMAP, *see* International Association of  
     Meterology and Atmospheric Physics  
 Ice, 179  
     absorption coefficient, 705  
     cloud, 668  
     crystal, 314, 661  
 Importance, 28  
 Inferior conjunction, 608  
 Inhomogeneous atmosphere  
     by adding method, 58–61  
     reflection function, isotropic scattering,  
         52–53  
 Injection function, *see* Escape function  
 Injection region, isotropic scattering, 209,  
     211–212  
 Instability  
     in inversion procedure, 663  
     in recurrence, 377–380  
 Insulation by foam, 706  
 Integral check, 693, 715  
 Integral equation, *see also* Milne equation  
     for Ambartsumian functions  
         linear, 103–104, 109  
         nonlinear, 103–104  
     for diffusion, 72–73, 93, 376  
     eigenvalue, 377–378  
 Fredholm, 110, 122, 162  
     for *H* function, 91  
         linear, 105–107, 162  
         nonlinear, 105–106, 109, 162  
     for reflection and transmission, 99  
     for size distribution  
         inversion, 663  
         model fitting, 663  
     for Sobolev  $\Phi$  function, 118, 120, 138–139  
     for *X* and *Y* function  
         linear, 119  
         nonlinear, 52, 119, 224

- Integration
  - of  $H$  function, 607
  - over  $\tau$ , 135, 209
- Intensity, 5, 134, *see also* Radiance
  - at arbitrary depth, 69, 117–122
  - average
    - hemispherical, 69
    - at midlayer, 77
  - in diffusion domain, 97
  - as four-vector, 498
  - internal, 221–224
    - similarity, 480
  - local, 494
  - with polarization, 20, 493–495
  - specific, 5, 27
  - at surface, 82
  - transformation
    - by rotation, 22–23
    - by scattering, 20–22
- Interaction principle, 62
- Interference, 20
- Intermediate results, *use*, 40
- International Association of Meteorology and Atmospheric Physics, 683, 694
- Interpolation between small  $b$  and  $\infty$ 
  - isotropic scattering, 201–203
  - Rayleigh scattering, 559
- Interstellar dust, 713
- Interstellar extinction, 713, 718, 720
- Interstellar grain, 716, 719
- Interstellar polarization, 713
- Interstellar radio scintillation, 717, 719
- Invariance principle, 53, 73, 102, 162, 185
- Invariant embedding, 42, 53, 99, 102, 691
  - Rayleigh scattering, 536
- Inverse problem, 34, 36
- Inversion from radiance to phase function
  - asymptotic, 710–711
  - moderate depth, 712
- Irradiance, 5
  - downward, 712
  - scalar, 5, 712
  - upward, 712
  - vector, 5
- Isotropic scattering, *see also* specific functions
  - diffusion, 152
    - constant, 150, 152
    - exponent, 150, 152
  - emerging radiation, 183–190
  - escape function, 151, 358–362
  - with forward peak, 307
  - with homogeneous sources, 220–221
  - internal intensity, 221–224
  - Kuščer polynomials, 378–379
  - Minnaert plot, exponent, 619
  - plane albedo, 198–199, 483–486
  - phase matrix, factorization, 535
  - point-direction gain, 136, 138–139, 206–213, 216–218, 292–299
    - differential equation, 174
    - in diffusion domain, 175, 209–213
    - expansion, 175–176
    - integral, 186, 218–220
    - as matrix, 130, 136
    - moment, 136, 138–139, 174–182, 206–221, 292–299
      - differential equation, 227
      - integral, 220
      - zero order, 208
    - nearly conservative, 178–180
    - numerical values, 176–178, 207, 292–299
    - in semi-infinite atmosphere, 174–182
    - at surface, 175, 224
    - thick layer, 209–213
  - rapid-guess formulas, 362–364
  - reflection function, 151, 192–203, 222, 236–281, 398, 617–618
    - bimoment, 136, 172–174, 193–194, 202, 236–281
      - nearly conservative, 390–392
    - eigenfunction expansion, 145
    - first order, 194, 236–281
    - with ground, 631–632
    - as matrix, 130, 133–135
    - moment, 136, 172, 193–194, 200–202, 236–281
    - for  $\mu \rightarrow \infty$ , 219–220
    - numerical values, 236–281, 482–486, 543–544
    - ratio total to first order, 196–198
    - second order, 236–281
    - thick slab, 201–203, 482–486
    - third order, 236–281
  - specifications, 149–151, 185, 201, 209
  - spherical albedo, 198–199, 370, 483–486
  - successive orders, eigenvalue, 141–144, 586
  - thick layer, 198–203
  - transmission function, 192–203, 222–223, 651–652
    - bimoment, 136, 193, 195, 237–279
    - diagonal value, 195
    - diffuse, 130, 193, 195
    - eigenfunction expansion, 145
    - first order, 195, 237–279
    - as matrix, 130, 133–135
    - moment, 136, 193, 195, 200–202, 237–279

- numerical values, 237–279
- second order, 237–279
- thick slab, 200–203
- third order, 237–279
- zero-order, 193–196, 237–279
  - as matrix, 130
- Isotropic sector phase function, 307, 308
  - escape function, 358–361
  - extrapolation length, 376
  - internal reflection coefficient, 374–375
- J**
- Junge size distribution, 655, 664, 669, 672
- Jupiter
  - cloud level, 622, 624
  - geometric albedo, 620–621, 624
  - infrared limb darkening, 643
  - Minnaert plot, 616, 619
  - polarization, 559, 561, 622–624
- K**
- Kirchoff's law, 18
  - for blackbody, 25
  - for finite body, 24
  - for polarized light, 25–26
  - for surface, 32
  - for thin disk, 25
- KM *see* Kubelka–Munk formula
- K matrix, 57, 59
- Knudsen number, 706
- Kubelka–Munk formula, 491, 698–703
  - accuracy test, 700–702
  - conservative scattering, 700
  - finite layer, 699–702
- Kuščer polynomial, 91, 94–98, 120, 376
  - asymptotic expression, 377
  - convergence, 377–379
  - ratio of orders, 377–380
  - recurrence, 94–95, 377
- L**
- Ladenburg–Reiche function, 595, 597
- $\Lambda$  operator, 130
- Lambert law, 204, 497, 605, 608
- Lambert surface, 6, 468, 472, 476
  - below atmosphere, 623, 626
- Laplace transform, 574, 577, 585
  - inverse, 574, 577–579, 582, 584, 589, 676, 719
- Laser, 314
- Laser radar, 675
- Latex suspension, 709–710
- Legendre coefficient, 308, 317–324
  - high order, 703
- Legendre expansion, 482, 614, 710
  - example, 523
  - number of terms, 519–520
- Legendre function, 79, 528, 605
  - associated, 47, 94–95, 324, 498, 509–510, 516, 520
  - related function, 311, 325
  - of second kind, 98, 366, 379
- Legendre polynomial, 43, 89, 94–95, 109, 304, 317
  - associated, 325–328, 597
- Lidar, 573, 662–663, 693–694, 717
  - attenuation factor, 677
  - bistatic, 663
  - clouds, 573, 675–682
  - depolarization, 680–682
  - echo time, 663, 676
  - multiple scattering, 676–680
  - reception cone, 676–677, 679–680
  - return signal
    - function of reception column, 678–680
    - orders, 677
    - ratio of total to single scattering, 678–679
- Life on planet, 616
- Lighthouse, 719
- Limb, *see* Globule; Planet; Sun
- Line absorption, *see* Absorption
- Linearly anisotropic phase function, 89, 96–97, 121, 305–306
  - Busbridge polynomials, 364
  - characteristic equation, root, 365–367, 381–382
  - in diffuse galactic light, 717
  - diffusion exponent, 365–367
  - dispersion function, 366
  - escape function, 339, 358–359, 367
  - extrapolation length, 366–367
  - $H$  function, 364–366
    - derivative, 365–366
    - moment, 364–365
  - Kuščer polynomial, 378–379
  - Minnaert plot, exponent, 619–620
  - plane albedo, 368–369
  - reflection function, 486–487, 617–618
    - bimoment, 367, 701
    - moment, 367–368
  - spherical albedo, 367
  - transmission function, 486–487

Local scattering, 498–503, 506–516  
 Log-normal size distribution, 664–665, 675  
 Lommel-Seeliger law, 196, 606–610  
 Lorentz profile, 593–595  
 Loss, *see also* Absorption  
   in atmosphere, 77, 80, 685–687  
     weak absorption, 78, 80, 180  
   by finite depth, 80  
   in ground, 685–687  
   at large depth, 80  
   total, 685–687  
 Luminance, 652

## M

Magneto-optic activity, 616  
 Magnitude of planet, 600–601  
 Manufacturing control, 699  
 Marine optics, *see* Hydrologic optics  
 Mars  
   clearing, 630  
   haze, 630  
   isophotes, 620  
   Minnaert plot, 616, 619–620  
   surface changes, 631  
 Matching of cloud deck and atmosphere,  
   628–630, 646  
 Matrix, 128  
   dot product, 76, 145  
   inversion, 111, 146  
    $\mu\mu$ , 46, 68–69, 128, 130  
    $\mu\tau$ , 128, 130  
   operator theory, 62  
   partitioning, 146–148  
   product, 68–69, 128, 131, 172  
   singular, 69, 129–131  
    $\tau\mu$ , 128, 130  
    $\tau\tau$ , 128, 130  
   transfer method, 43, 62–63, 74  
   unit, 69, 535  
 Mellin transform, 674  
 Merope, reflection nebula, 714, 715  
 Metallic optical properties, 314  
 Method, *see also* specific methods  
   advantages, 42–44  
   of computation, 40  
   criteria, 39–44  
   of derivation, 39  
   discretization, 41, 43–44  
   drawbacks, 42–44  
   hybrid, 41, 45, 50  
   multistream, 44

  preferred, 45  
   probabilistic, 41  
   traditional, 90  
 Microwave, analog measurement, 314  
 Midlayer intensity, 43  
   in galaxy, 716  
   Henyey–Greenstein phase function, 223,  
     405, 462–464  
   isotropic scattering, 209, 223, 292–299, 405  
 Mie theory, 303, 304, 311–314, 317–320,  
   324–325, 509, 511, 519, 671, 703  
   absorbing sphere, 313–314  
   nonabsorbing sphere, 312–313  
   polarization, 312, 315  
   scattering pattern, 304, 311–312, 356, 638  
     amplitude, 324  
     asymmetry, 312–314, 316  
     lobe shift, 520  
 Milk, 698, 709–710  
   blackened, 709–710  
 Milky Way, 713  
 Millimeter wave, 317  
 Milne equation, 127–128, 131–132, 146  
   eigenfunctions, 140–144  
   eigenvalues, 140–144  
   generalized, 48, 49  
   homogeneous, 150, 152–153, 185  
   inhomogeneous, 153, 185  
   in matrix form, 131  
   solution, 131–132  
 Milne matrix, expansion, 145  
 Milne operator, 127–130, 134  
   eigenvalues, 140–144  
 Milne problem, 85, 90, 111–114, 169, 393  
 Minnaert–Barkstrom plot, 620  
 Minnaert plot, 616, 619–620  
 Mirror  
   angle, 545–546, 549  
   matrix, 505  
 Mist, 698–699  
 Mixing ratio, 592  
 Mode of propagation, 121, 333  
 Mode radius, 316, 322, 664–665  
 Model, use, 34–36, 713, 717  
 Molecule, 496  
   free path, 706  
 Moment, *see* specific function  
 Monte Carlo method, 44, 575, 610, 676, 691  
   cuboid cloud, 695–698  
   reflection nebula, 713–715  
 Multiple scattering, 34–35  
 $\mu$  vector, 64, 68–69, 128, 130, 172

## N

- Nasty corner of  $(a, b)$  domain, 81, 591, 684–687
- Natural light, 23, 28, 496, 508
- Nearly conservative scattering, 78–81, 388–389, *see also* specific phase functions
- Neptune, geometric albedo, 620–621
- Net current, 488, 693
- Net flux, *see* Flux
- Neumann series, 42, 132, 146–147, 676
- Neutron scattering, 79
- Nonasymptotic part, 159
- Nonspherical particle, 314–315
  - lidar echo, 680
- Nonstationary problem, 574
- Nonuniqueness, 381
- $N$  operator, 69, 497
- Normalization
  - of eigenfunction in diffusion, 74–75
  - of incident flux, 193
  - of  $\mu$  vector, 172
  - by other authors, 78, 85
  - of specular reflection function, 626
- Nuclear reactor, *see* Reactor

## O

- Ocean, *see also* Hydrologic optics
  - under atmosphere, 507
- Omnidirectional probe, 640–641
- Onsager relation, 17
- Opacity, 143
- Opal glass, 698–699
- Opaque atmosphere, 625
- Operator
  - defining moment, 69
  - on  $\mu$ , 130
  - on  $\tau$ , 128, 130
- Opposition, 608, 610
  - effect, 606
  - in circular polarization, 616
  - line, 545–546
- Optical depth, 68, 128
  - reduced, 396
  - transformation, 481
- Optical path, *see* Photon, path
- Optical thickness, 76, 575
  - reduced, 479
- Order, *see also* Successive order
  - in Fourier expansion, 505, 514–515, 522–529
  - of successive scattering, 505, 514–515, 522–523

- Orthogonality, 121, 326
  - half-range, 43, 121
- Overcast sky, 507
- Ozone, 567, 641, 657

## P

- Padé approximation, 580, 582
- Pactzold probe, 641
- Paint layer, 491, 698–703
  - covered spot, 703
  - reflecting power, 700
- Parametrization, 683
- Particulate material, 699
- Peak, *see also* Diffraction; Forward peak;
  - Transmission function, zero-order
  - downward, 711
- Pencil beam in inverse problem, 714
- Penetration depth, 637–640
  - statistics, 639–640
- Phase angle, 601
- Phase function, 5, 35, 70, 303–317, 496–497, *see also* specific phase functions
  - asymmetry, 70, 304
  - change of sign, 305
  - asymptotic radiance, 710–711
  - azimuth average, 70, 497
  - characteristics, 303
  - choice, 303, 310
  - elliptical, 308
  - expansion
    - Fourier, 520–521
    - in Legendre functions, 80–123, 304, 317–324, 481, 519–520
    - finite, 305–306, 356–357
  - family, 305, 308
  - integral, 70
    - forward part, 305–307, 309
  - inverse linear, 307, 308
  - of large body, 308
  - normalization, 5, 70, 304
  - singular, 308–309
  - of sphere, 303, 304
  - sum
    - of exponentials, 320–322
    - of Gauss functions, 676
- Phase integral of planet, 600–601
- Phase matrix, 494–498, 500–503, 513
  - azimuth-independent part, 324, 513
  - effective albedo, 518
  - expansion, 317, 324–329, 509
  - symmetry, 504

- Phase shift, 312, 317
- Photoionization, 18
- Photon
- exit angle, 695
  - path
    - geometrical, 575
    - mean, 388, 577–579, 583–587, 589–591
      - near-conservative scattering, 583–584
      - in separate order, 578
      - in transmission, 586–587
    - optical, 575
    - probability distribution, 577–582
      - asymptotic, 579–582, 588–590
      - dispersion, 585–588
      - exact, 585, 587–588
      - moment, 577
      - nonconservative, 582–584
      - semi-infinite atmosphere, 579–584, 589
      - in separate order, 578–580, 585, 587–588
      - slab, 584–585, 588
      - standard curve, 585–586, 588–589
    - root-mean-square, 388
    - square mean root, 594–595
    - statistics, 573–591, 634, 636–640
      - for fixed penetration depth, 638–639
      - inhomogeneous slab, 575
- Physical definition, 70–73
- Physical derivation, 54, 101, 179–180, 603–604
- Physical meaning
- of matrix and vector, 130
  - of matrix product, 68–69, 129, 174, 193
  - of Neumann series, 132
- Physical system, linear, 16
- Pillar scattering, 697–698
- Pioneer, 624
- Plane albedo, 4
- Eddington approximation, 370
  - similarity, 482–486
  - thick layer, 486
- Plane of reference, 20, 495–497, 499–500
- choice, 20, 555, 564, 566
  - rotation, 22–23, 495–497, 500
- Plane-parallel layer, *see* Slab
- Planet, 599–649, *see also* specific planets;
- Geometric albedo; Spherical albedo
  - absorption spectrum, 370, 372–374, 593, 634–640
  - brightness distribution, 615–618
  - flux, reflected, 600
  - full phase, 606, 608, 610
  - integration over disk, 35, 599–614
  - limb, 602, 615
    - darkening, 132
    - infrared, 221
  - model computation, 34–36, 599, 606–610, 621
  - with ground, 35, 198
  - with thick atmosphere, 607–609
  - nearly black, 606
  - in opposition, 132, 522, 543–544, 617–624
  - as particle, 600–601, 610
  - phase function, 599–610
    - asymmetry factor, 606–611
    - integral, 604–605
    - Legendre expansion, 605, 607, 609
    - in opposition, 607
  - polarization, 549, 557–563, 599, 610–614, 623–624
    - near-symmetry, 546–547, 616
  - with Rayleigh scattering,
    - diffuse reflection, 537, 557–561
    - finite depth, 623–624
    - polarization, 549, 557–563
    - surface reflection, 196
    - symmetry about equator, 615–616
    - thermal emission, 642–646
    - white, 605–606, 608–609
- Plant canopy, 705–706
- Plate scattering, 697–698
- Poincaré sphere, 495
- Point-direction gain, 4, 29, 37, 693, *see also*
- specific phase function
  - by adding method, 56–60
  - in Ambartsumian's method, 50
  - in arbitrary configuration, 4, 29
  - asymptotic, 84
  - with ground surface, 64
  - inhomogeneous slab, 32, 58–60
  - reciprocal definition, 29, 32, 56
  - at separation layer, 60, 488
  - at surface, 37, 488
- Poisson distribution, 580
- Polarizability, 531
- tensor, 314, 532
- Polarization, 5, 39, 493–513, *see also* Stokes
- parameter
  - circular, 495–496, 503
  - degree, 495
  - ellipse, 495
  - elliptical, 501
  - linear, 495–496, 501
  - partial, 496
  - reciprocity, 17–26, 30–31

- representation, 495–498, 533
    - CP, 324, 533
    - transformation, 497, 533
  - signature, 315
  - state, 494–496
  - Polluted water, 710
  - Polynomial, 151, *see also* Busbridge polynomial; Kušcer polynomial; Legendre polynomial; Sobolev polynomial
  - Polyvinyl acetate, 710
  - Power law size distribution, 664–665, 672–673
  - Propagation, *see* Diffusion; Random medium propagation
  - $\Psi$ -norm, 539–540
  - Pulse delay, 718–720
    - spread in time, 718–720
- Q**
- Quasi-single scattering approximation, 41, 713
- R**
- Radar, 675
  - Radiance, 5, 615, 652, *see also* Intensity
    - attenuation coefficient, 712
    - unit, 658–659
  - Radiation
    - density, 73, 84, 138
    - dose, 657
    - hydrodynamics, 706–707
    - pressure on sphere, 313–314
    - slip, 706
  - Radiative equilibrium, 152
  - Radiative transfer, historical note, 54
  - Radio wave scattering, 719–720
  - Rain, model, 316
  - Rainbow, 312, 315–316, 322–324
  - Random medium propagation, 720
  - Random orientation, 23, 500, 532, 605, 661
  - Random walk, 718
  - Rapid-guess formula, 83, 362–364
  - Rayleigh–Gans pattern, 670
  - Rayleigh phase function, 305–306, 311, 356, 494, 531–532
    - escape function, 362
    - exact solution, 537–538
    - $H$  function, 538
    - internal radiation field, 538
    - plane albedo, 483–486
    - reflection function, 482–486, 543–544, 618
    - spherical albedo, 370, 483–486
    - transmitted flux, 539
  - Rayleigh scattering, 305, 494, 503, 531–569
    - characteristic function, 539
    - diffusion domain, 566
      - exponent, 539–540, 554, 566
    - escape function, 358–359, 362, 540–541, 567
      - nonconservative, 554
    - exact solution, 536–538
    - with ground surface, 557–563
      - reflection function, 557–561
    - with isotropic scattering, 532, 537–538, 554
      - escape function, 358–359
      - phase matrix, 532, 534–536
    - $H$  function, 537, 539–540, 547
    - Milne problem, 356, 538, 540–541
    - of natural light, 531, 543, 561
    - nonconservative, 532, 537, 550–554
    - pattern, 531–532
    - phase matrix, 531–536
      - azimuth-independent part, 534
      - factorization, 534–536
    - plane albedo, 483–486, 538
    - on planet, 543–544, 557–563, 607, 610
    - polarization, 311, 531–533
      - near-symmetry, 543, 546–547, 567, 616
      - in principal plane, 541–549
        - orders, 546, 622
        - sign, 542, 546, 561
      - in zenith, 563–567
    - pure, 311, 531–533
    - reflection function, 482–486, 536–538, 541–543
      - Fourier terms, 519, 543–544
      - orders, 552–553, 561–563
      - in principal plane, 541–544
    - representation, 533
    - semi-infinite atmosphere, 540–550
    - slab, 555–567
      - asymptotic, 559–561
      - eigenvalues, 562–563
    - spherical albedo, 483–486
    - tables, 537–538
    - transmission function, 536–538, 564–567
  - Reactor, 28, 692–693
  - Reciprocity, 16–33, 59, 393
    - arbitrary configuration, 24–27
    - of detector and source, 135, 615
    - of escape and injection, 72
    - in  $F$  matrix, 21–22
    - in physical meaning, 17, 100, 135, 213
    - with polarization, 27, 546, 567, 616



- Reciprocity (*cont.*)  
 principle, 16–17, 85, 129  
 reflection function, 193, 614–616  
 slab, 30–31  
 surface, 30  
 transmission function, 193  
 use in photometry, 614–616
- Redistribution  
 equation, 503  
 over frequencies, 94  
 function, 49, 69, 497  
   Henyey–Greenstein phase function, 332–333, 397, 652  
   integral, 70  
   isotropic scattering, 150  
   matrix, 130, 131–134
- Reduction to  $H$  functions, 362
- Redundant parameter, 86
- Reference, *see* Plane of reference
- Reference band, 641
- Reflectance in hydrologic optics, 712
- Reflection, *see also* specific phase functions;  
   Plane albedo; Spherical albedo  
 coefficient, 202  
 of diffusion stream, 72  
 function, 5–6, 36–38, 51, 72, 102–103, 498  
   by atmosphere  
     over cloud, 627–629  
     over ground, 63, 64, 625–626, 628–629  
     over sea, 63, 626–627  
 bimoment, 80–81, 701  
   first order, 519  
 computation, 91, 118–120  
 first order, 367–368, 397, 484, 487, 518–519  
 Fourier expansion, 504–505, 521–523  
 high order terms, 388–393  
 inhomogeneous slab, 31, 58–59, 61  
 as matrix, 69  
 moment, 116–117, 519  
 nearly conservative, 79–80, 389–392  
 ratio of total to first order, 454–455, 521  
 reduced to  $H$  function, 91–92, 109, 115–117  
 similarity, 372–374, 480  
 thick layer, 82  
 matrix, 498, 503–506, 513  
 thin slab, 503–504  
 nebula, 693, 714–715  
   multiplicity, 715  
   ratio of total to first order, 714–715
- Remote sensing  
 active, 675–676  
 passive, 675
- Resolvent, 120
- Restraint, *see* Constraint
- Reverse experiment, 28–29, 32, 207
- Roadmap, 118–119
- Rotation matrix, 496, 500, 533
- S
- Saturn  
   geometric albedo, 620–621  
   Minnaert plot, 616, 619
- Scalar, 68
- Scalar density, 488, 693
- Scattering  
   angle, 499, 601  
   backward, 305, 307, 384, 489–491  
   coherent, 18–20  
   conservative, 78, 81–83  
   depth, 481  
   far-field, 18–20, 22  
   incoherent, 20, 27  
   local, 494, 499–503  
   matrix, 496, 500, 519
- Schwarzschild–Milne integral equation, 127
- Searchlight, 693–694
- Seasonal change, 616
- Sea water, 709–710
- Seeing, 720
- Semi-infinite atmosphere, 90, 355–376, 388–394
- Shell, scattering, 692
- Shorthand notation, 69–70, 128–130, 512
- Similarity, 303, 317  
   in diffusion pattern, 375  
   in escape function, 357–359  
   in extrapolation length, 374–376  
   not in azimuth-dependent terms, 618  
   parameter, 75, 369, 372, 479  
   in reflection function, 397–399  
   relation, 223–224, 477–481, 646, 683  
     accuracy, 482  
     alternatives, 478–479  
     conservative scattering, 355–362, 403–405, 408, 479  
     degenerated, 355  
     nonconservative, 364, 372–374, 477–479  
     for slab, 403–405, 477–481  
   in spherical albedo, 370–371  
   test, 370, 372–376  
     clouds, 487–489  
     by truncation, 366–369
- Single scattering albedo, *see* Albedo
- Singular eigenfunction expansion, 43, 67, 74, 90, 222

- with polarization, 508
- Rayleigh scattering, 536
- Size distribution, 664–665
  - of aerosol,
  - of drops, 315–316, 318, 320, 323
- Size parameter, 318–322
- Sky, *see also* Blue sky
  - clear fraction, 683
  - daylight, 310–311, 651–661
    - multiple scattering, 655–657
  - polarization, 557, 664, 666–668
    - elliptical, 667
    - with ground reflection, 555
  - neutral point, 555–557, 666
  - at zenith, 563–567
  - radiance, 664, 666–668
    - near horizon, 667
    - Rayleigh scattering, 564–565
    - single scattering fraction, 655–657
    - zenith–horizon ratio, 651–654
      - below clouds, 507, 651–652
      - with snow cover, 653–654
  - red, 651
  - white, 651
- Slab, *see also* specific phase function
  - inhomogeneous, reciprocity, 30–31
  - thick, asymptotic expression, 76–78
- Small-angle scattering, multiple, 660–661, 717–720
- Smog, 666
- Snow, 179
  - albedo, 653
  - cover, 653–654
  - flake, 314
  - pack, 703–705
    - reflectance, 703–704
- Sobolev method, 118–120
- Sobolev  $\Phi$  function, 138–139, 209, 220
- Sobolev polynomial, 43
- Sobouti function, 226–227, 230–231
- Soft particle, 670–673
- Solar radiation to ground, 654–655
- Source
  - homogeneous distribution, 218–221
  - layer
    - internal, 68, 83–84, 137–138, 213
    - isotropic scattering, 153–161, 206
    - unidirectional, 85
  - at surface, 32, 50, 129
  - in unbounded medium, 153–161
  - zero order, 48, 193
- Source function, 494, 499
  - asymptotic, 160–161
  - in diffusion domain, 97
  - expansion, 130
  - first order, 138
    - as four-vector, 498–499, 501
  - isotropic scattering, 133–137, 150, 179, 188, 190, 206, 209, 211–213, 222
    - orders, 137, 160–161
    - at surface, 193, 213
  - starting term, 48, 130, 134
  - total, 130, 138
- Source matrix, 502
- Spectral line, *see* Absorption line
- Specular reflection, 626–627
- Sphere, as scatterer, 311–314, 511
- Spherical albedo, 4, 26, *see also* specific phase function; Reflection, function, bimoment approximation, 369–371
  - expansion, 369–370
  - first order term, 370
  - of planet, 600–601, 603–611
  - ratio total to first order, 370, 454–455
  - similarity, 369–371, 482–486
  - of snow, 704
- Spherical geometry, 602, 692
  - approximation, 667
- Square mean root path length, 594–595
- Standard haze, size distribution, 665–666, 669
- Standard problem, 38–39
  - with polarization, 39
- Stellar atmosphere, 692
  - emission, 643
- Stokes parameter, 20–22, 316, 324, 493–498, 500, 503, 505, 533–535
- Stratoscope, 622
- Stratosphere, heating, 682
- Struve function, 672
- Subcritical domain, 198, 234
- Successive order
  - azimuth-dependent terms, 514–518, 522–530
  - Fourier components, 49
  - from invariance, 50
  - method, 42, 45–46, 67
    - convergence, 141, 393, 514–515
      - Henyey–Greenstein phase function, 406–408
      - isotropic scattering, 135–137, 141–142
      - semi-infinite atmosphere, 388–393
    - half-step, 47–49, 494
    - starting function, 48
- Sulfuric acid, 612
- Sun
  - corona, 658–659
  - disk, 129, 658
  - visibility through cloud, 654–655, 660–661

Sun (*cont.*)

- hazy, 660–661
- limb, 658

## Superior conjunction, 608

## Surface

- brightness, 615
- correction function, 183–187
- detail, visibility, 625, 629–632
- reflection, 6, 491, 606

## Symbolic equation, 506

Symmetry, *see also* Reciprocity

- assumption, 498, 501
- in azimuth, 499
- check, 17
- meridan, 615
- relation, 17
- rotational, 493

## Synthetic spectrum, 634

## T

 $\tau$  vector, 128, 130

## Taylor expansion, 577

## Terminator, 602, 615

## Thermodynamics

- equilibrium, 17
- nonequilibrium, 17

## Thickness, reduced, 405

## Thomson scattering, 531

## Thought experiment, 17, 99, 693

## Three by three matrix, 503

## Time delay

- along path, 573, 574
- upon scattering, 574

## Time dependent problem, 153

## Time-reversal, invariance, 17

## Titan, geometric albedo, 620–621

## Transfer equation, 41, 47–48, 75, 92–93, 127–128, 712

- anisotropic, 376–388
- boundary condition, 111
- formal solution, 48
- homogeneous, 508

## Transfer function, 2-point, 27–28, 33

## Transition region, 178–179, 209

## Translation

- of Kubelka–Munk formulas, 700
- of normalization, 78
- of symbolic formulas, 506, 512
- of terminology, 6
- nuclear scattering, 693

## Translucent atmosphere, 625–626, 628–629

- over identical atmosphere, 629
- over Lambert surface, 628–629

Transmission, 36–38, *see also* specific phase function

- by adding method, 61
- diffuse, 61, 503
- first order, 397, 487, 518–519
- moment, 519

## Transmission function, 6, 37, 102–103

- Fourier expansion, 504, 521–522
- inhomogeneous slab, 31, 58–59, 61
- as matrix, 69
- thick layer, 82, 654
- zero order, 37, 52, 55, 61

## Transmission matrix, 513

- zero order, 504

## Transparent atmosphere, 625–626

## Trial function, 410

## Truncation, 366–369, 481–487

## Turbidity, 315, 662

- affecting sky brightness, 655–658
- spectrum, 316

## Turbulent spectrum, 707

## Twilight, 692

## Two by two matrix, 508–509, 513, 533–536

## Two-stream approximation, 41, 309, 491, 699, 706

## Two-vector, 508–513, 540

## U

 $U$  matrix, 497

## Underwater atmosphere, 627

## Uniform incidence, 399, 401, 468, 472, 476

## Uniqueness, 74, 103, 105, 162, 224, 610

Unpolarized light, *see* Natural light $U$  operator, 497

## Uranus

- geometric albedo, 620–621
- limb darkening, 622
- model atmosphere, 622
- polarization, 559

 $U$  vector, 69

## V

## Variation principle, 132

Vector, *see*  $\mu$  vector;  $\tau$  vector; Shorthand notation

## Vector product, 68, 128

## Venera eight, 645–646

## Venus

- absorption line, 598, 634–636
- phase effect, 635–636
- atmosphere energy balance, 644–646
- carbon dioxide bands, 635

cloud  
 multiple layer, 645–646  
 particle, 611–613  
   refractive index, 612–613  
   size distribution, 611–613  
 pressure at top, 613  
 ground albedo, 645  
 infrared limb darkening, 642–643  
 phase function, 610–612  
 polarization, 196, 315, 507, 610–614  
   measurement, 611  
   Rayleigh scattering contribution, 613  
   in second order, 614  
   theory, 611–614  
 spherical albedo, 610–611  
 temperature, 642–646  
 thermal emission, 642–646  
 ultraviolet marking, 613  
 Virtual angle, 166, 181, 230–231  
 Visibility of object in water, 707  
 Volcanic eruption, 662, 666, 682

## W

Wallis formula, 390, 528  
 Water  
   cloud, 487–488, 500  
   drop,  
     asymmetry factor, 313  
     phase function, 315–321, 496  
 Wave propagation in turbulent medium,  
   707  
*W* vector, 69

## X

*X* function, 43–44, 91  
 isotropic scattering, 136, 139, 193, 208–210,  
   224–227  
   moment, 219, 225–230  
     expansion, 228  
     nonlinear relation, 232  
     numerical value, 225–227, 292–299  
 Rayleigh phase function, 538  
 Rayleigh scattering, 555, 566  
*X* ray  
 extinction, 718  
 halo, 718–719  
 pulsar, 719  
 scattering, 717

## Y

*Y* function, 43–44, 91  
 isotropic scattering, 136, 139, 193, 208–210,  
   224–227  
   contour diagram, 225–226  
   moment, 219, 225–230  
     expansion, 228  
     nonlinear relation, 232  
     numerical value, 225–227, 292–299  
     virtual angles, 225–226  
 Rayleigh phase function, 538  
 Rayleigh scattering, 555, 566

## Z

Zenith, *see* Sky  
 Zodiacal light, 668, 713

computations (Section 19.1.4) the fraction of higher order scattering is substantial but not overwhelming, and since high-order scattering will not really spoil the typical features of the polarization diagram, we may use the same graphs presented by Coffeen and Hansen to select from them the scattering angles where the most typical clues to refractive index and/or size may be found.

Many detailed studies corroborate the sensitivity of polarization measurements to the presence of aerosol particles. Soon after the Krakatoa eruption of 1883, Cornu observed a striking drop of the maximum sky polarization from 75 to 48 % (Coulson, 1971), and in 1889 he reported that changes of weather were often preceded by a drop in polarization (Shifrin, 1951). A modern study with emphasis on the wavelength dependence of polarization is presented by Gehrels (1962).

Kuriyan *et al.* (1974b) systematically explore the accuracy by which the model parameters (optical depth, refractive index, effective radius) of the aerosol can be inferred from measurements of polarization *and* intensity of the sky. They find—in agreement with the experience of Hansen and Hovenier (private communication)—that trying to determine more than two parameters of the size distribution (in essence: effective radius and spread) is asking too much. They recommend, in fact, to stick always to a distribution of the haze type (line 5 in Display 19.1).

Further examples of the distribution of intensity and polarization over the full sky for models based on realistic mixtures of aerosols and Rayleigh scattering may be found in Tanaka (1971a, b, c) and Yamamoto and Tanaka (1974). The maximum (linear) polarization is always found in the prime vertical about  $90^\circ$  from the sun; but the value of the degree of polarization at this maximum as a function of solar elevation and wavelength still gives a strange collection of graphs if model calculations of all authors are combined.

A recent set of papers (Kattawar *et al.*, 1976; Plass *et al.*, 1976; Hitzfelder *et al.*, 1976) offers further comparison material. The first two of these papers document with thirty-eight graphs and many tables the radiance and polarization reflected from and transmitted by an atmosphere of total optical thickness from  $2^{-9}$  to  $2^{+10}$ . Here either Rayleigh scattering or Deirmendjian's continental haze *L* model is assumed. This complements earlier work on the maritime haze *M* model by Kattawar *et al.* (1973). In the third paper Hitzfelder *et al.* (1976) assume a combination of Rayleigh scattering and haze *L* with a realistic vertical structure.

The typical differences between a sky with and without pollution (smog) are well illustrated by Coulson (1971).

The neutral points, where the degree of polarization in the clear sky goes through zero, have intrigued all generations who have studied sky polarization. Their shift by the presence of an aerosol layer was studied by Kano (1968). Both the Kattawar and the Coulson paper just cited contain additional information about the shift of these neutral points by the presence of haze and on the appearance of a new class of neutral points. The position of maximum polarization and the value of that maximum are also well documented.